frontiers | Research Topics

Interaction between coronavirus and hosts

Edited by
Yu Chen, You Zhou, Ke Xu and Guiqing Peng

Published in
Frontiers in Cellular and Infection Microbiology

ISSN 1664-8714
ISBN 978-2-8325-2681-1
DOI 10.3389/978-2-8325-2681-1

About Frontiers

Frontiers is more than just an open access publisher of scholarly articles: it is a pioneering approach to the world of academia, radically improving the way scholarly research is managed. The grand vision of Frontiers is a world where all people have an equal opportunity to seek, share and generate knowledge. Frontiers provides immediate and permanent online open access to all its publications, but this alone is not enough to realize our grand goals.

Frontiers journal series

The Frontiers journal series is a multi-tier and interdisciplinary set of open-access, online journals, promising a paradigm shift from the current review, selection and dissemination processes in academic publishing. All Frontiers journals are driven by researchers for researchers; therefore, they constitute a service to the scholarly community. At the same time, the *Frontiers journal series* operates on a revolutionary invention, the tiered publishing system, initially addressing specific communities of scholars, and gradually climbing up to broader public understanding, thus serving the interests of the lay society, too.

Dedication to quality

Each Frontiers article is a landmark of the highest quality, thanks to genuinely collaborative interactions between authors and review editors, who include some of the world's best academicians. Research must be certified by peers before entering a stream of knowledge that may eventually reach the public - and shape society; therefore, Frontiers only applies the most rigorous and unbiased reviews. Frontiers revolutionizes research publishing by freely delivering the most outstanding research, evaluated with no bias from both the academic and social point of view. By applying the most advanced information technologies, Frontiers is catapulting scholarly publishing into a new generation.

What are Frontiers Research Topics?

Frontiers Research Topics are very popular trademarks of the *Frontiers journals series*: they are collections of at least ten articles, all centered on a particular subject. With their unique mix of varied contributions from Original Research to Review Articles, Frontiers Research Topics unify the most influential researchers, the latest key findings and historical advances in a hot research area.

Find out more on how to host your own Frontiers Research Topic or contribute to one as an author by contacting the Frontiers editorial office: frontiersin.org/about/contact

Interaction between coronavirus and hosts

Topic editors

Yu Chen — Wuhan University, China

You Zhou — Cardiff University, United Kingdom

Ke Xu — Wuhan University, China

Guiqing Peng — Huazhong Agricultural University, China

Citation

Chen, Y., Zhou, Y., Xu, K., Peng, G., eds. (2023). *Interaction between coronavirus and hosts*. Lausanne: Frontiers Media SA. doi: 10.3389/978-2-8325-2681-1

Table of contents

frontiers in Cellular and Infection Microbiology

ORIGINAL RESEARCH
published: 16 December 2021
doi: 10.3389/fcimb.2021.792202

Earlier *In Vitro* Viral Production With SARS-CoV-2 Alpha Than With Beta, Gamma, B, or A.27 Variants

Samuel Lebourgeois[1]*, *Houssem Redha Chenane*[1], *Nadhira Houhou-Fidouh*[2], *Reyene Menidjel*[1], *Valentine Marie Ferré*[1,2], *Gilles Collin*[1,2], *Nabil Benmalek*[2], *Romain Coppée*[1], *Lucile Larrouy*[1,2], *Yazdan Yazdanpanah*[1,3], *Jean-François Timsit*[1,4], *Charlotte Charpentier*[1,2], *Diane Descamps*[1,2] and *Benoit Visseaux*[1,2]

[1] Université de Paris, Infection Antimicrobials Modelling Evolution (IAME), Institut National de la Santé et de la Recherche Médicale (INSERM), Paris, France, [2] Assistance Publique - Hôpitaux de Paris (AP-HP), University Hospital Bichat-Claude Bernard, Laboratoire de Virologie, Paris, France, [3] Assistance Publique - Hôpitaux de Paris (AP-HP), University Hospital Bichat-Claude Bernard, Maladies Infectieuses et Tropicales, Paris, France, [4] Assistance Publique - Hôpitaux de Paris (AP-HP), University Hospital Bichat-Claude Bernard, Réanimation Médicale et Infectieuses, Paris, France

OPEN ACCESS

Edited by:
Yu Chen,
Wuhan University, China

Reviewed by:
Fred David Mast,
Seattle Children's Research Institute, United States
Alberto Antonelli,
University of Florence, Florence, Italy

***Correspondence:**
Samuel Lebourgeois
Samuel.lebourgeois@inserm.fr

Specialty section:
This article was submitted to Virus and Host, a section of the journal Frontiers in Cellular and Infection Microbiology

Received: *09 October 2021*
Accepted: *23 November 2021*
Published: *16 December 2021*

Citation:
Lebourgeois S, Chenane HR, Houhou-Fidouh N, Menidjel R, Ferré VM, Collin G, Benmalek N, Coppée R, Larrouy L, Yazdanpanah Y, Timsit J-F, Charpentier C, Descamps D and Visseaux B (2021) Earlier In Vitro Viral Production With SARS-CoV-2 Alpha Than With Beta, Gamma, B, or A.27 Variants. Front. Cell. Infect. Microbiol. 11:792202. doi: 10.3389/fcimb.2021.792202

Since its emergence in China at the end of 2019, SARS-CoV-2 has rapidly spread across the world to become a global public health emergency. Since then, the pandemic has evolved with the large worldwide emergence of new variants, such as the Alpha (B.1.1.7 variant), Beta (B.1.351 variant), and Gamma (P.1 variant), and some other under investigation such as the A.27 in France. Many studies are focusing on antibody neutralisation changes according to the spike mutations, but to date, little is known regarding their respective replication capacities. In this work, we demonstrate that the Alpha variant provides an earlier replication *in vitro*, on Vero E6 and A549 cells, than Beta, Gamma, A.27, and historical lineages. This earlier replication was associated with higher infectious titres in cell-culture supernatants, in line with the higher viral loads observed among Alpha-infected patients. Interestingly, Beta and Gamma variants presented similar kinetic and viral load than the other non-Alpha-tested variants.

Keywords: alpha, SARS-CoV-2, variants, replication cycle, infectious titres

INTRODUCTION

In late 2019, severe acute respiratory syndrome coronavirus 2 (SARS-CoV-2), the etiological agent of coronavirus infectious disease 2019 (COVID-19), emerge worldwide. Following its rapid spread, SARS-CoV-2 was declared as pandemic by the World Health Organisation (WHO) on 11 March 2020 (Zhu et al., 2020). To date, COVID-19 has affected more than 200 countries with more than 250 million confirmed cases and more than 5 million deaths. SARS-CoV-2 infects the upper and lower respiratory tract, causing mild to severe respiratory syndromes (Harrison et al., 2020).

Since the beginning of these pandemic, several variants of SARS-CoV-2 have emerged. The first successful emergence was observed in March to April 2020 with the spread of the D614G mutation (Hodcroft et al., 2021). This mutation has been associated to higher viral loads and a better adhesion to the angiotensin-converting enzyme 2 (ACE2) cellular receptor (Korber et al., 2020). Since the late 2020, several new variants of concerns were identified. The Alpha variant, also known as the 20I/

501Y.V1 or B.1.1.7 variant, has been firstly detected in London in December 2020 and rapidly spreading across Europe and worldwide. This variant is associated to higher viral loads and higher number of deaths (Challen et al., 2021 Davies et al., 2021). It presents, over all its genome, a total of 14 amino-acid substitutions and 3 deletions including several mutations in the S-glycoprotein, mainly the Δ69/70 and Δ144 deletions and the N501Y. Outside the S-glycoprotein, the main characteristic mutations are relating to ORF1 (T1001I, A1708D, I2230T, and Δ3665-3677), ORF8 (Q27stop, R25I, K68stop, and Y73C), and nucleocapsid (D3L, R203K, G204R/P, and S235F) (Duerr et al., 2021). The Beta, also known as the B.1.351, 20H/501Y.V2 or South-African variant, has been firstly detected in South-Africa in December 2020 and has also already spread worldwide. This Beta variant was phylogenetically distinct from the three main lineages (B.1.1.54, B.1.1.56, and C.1) circulating widely in South Africa during the first epidemic wave (Tegally et al., 2021a). The Beta has shown two mutations on the S-glycoprotein, the N501Y, also characterised in the Alpha variant, and the E484K mutation actually known to confer the antibody resistance against SARS-CoV-2 (Tegally et al., 2021b). Outside the S-glycoprotein, two other mutations relating to ORF 1 (K1655N) and nucleocapsid (T205I) on the viral genome are mainly described (Tegally et al., 2020; Garcia-Beltran et al., 2021). Similarly, the Gamma variant, also known as the P.1, 20J/501Y.V3 or Brazilian variant, shows both N501Y and E484k mutations with the addition of the K417T. The Gamma variant is responsible of a large new outbreak in Brazil, causing high mortality, and is currently spreading in Americas and Europe (Buss et al., 2021). Outside the S-glycoprotein, the main described mutations are relating to ORF1 (S1188L, K1798G, Δ3675-3677, and E5666D), ORF8 (E92K and 28269–28273 insertion), and nucleocapsid (P80R, R203K, G204R/P) (Sun et al., 2021). Another variant of interest, the A.27 or 19B/501Y, has also been recently detected and is slowly spreading in France. It is characterised into the S-glycoprotein by the absence of the D614G mutation but the presence of L452R and N501Y mutations that could improve viral transmission. Outside the S-glycoprotein, several other mutations could be identified in the N gene (S202N), ORF1a (P286L, D2980G, P1000L), ORF3a (V50A), and ORF8(L84S) (Fourati et al., 2021).

If the urgency of specific immunoglobulins and vaccine development has prompted the international community to look deeply for serum neutralisation studies and impact of new variants (Chen et al., 2020; Weisblum et al., 2020), there is still too little data on their infectivity and replication cycle. Such data are indeed of importance to explain some of their pathogenic aspects such as higher viral load or mortality (Challen et al., 2021).

In this work, we sought to study the replicative capacity of a historical B strain along with Alpha, Beta, Gamma, and A.27 variants currently circulating in France and worldwide. Our experiments were conducted in the widely spread Vero E6 cell line model and confirmed in human A549 lung cell line expressing the ACE-2 receptor and TMPRSS2 coreceptor. We observed several differences in replication and infectious viral particle production rates, especially with the Alpha variant, that should play a part in its higher viral loads and death rates.

MATERIALS AND METHODS

Cell Lines and Viral Lineages

The Vero E6 cell line was obtained from the American Type Culture Collection (ATCC, reference R CRL-1586) (LGC standards SARL, Illkirch, France) and cultured in Dulbecco's modified Eagle's medium (DMEM, Gibco™) supplemented with 10% of heat-inactivated foetal bovine serum (FBS, Gibco™) (Thermo Fisher Scientific, Waltham, MA, 209 USA). The A549 enriched with human ACE2 and TMPRSS-2 surface proteins was obtained from *In vivo*Gen© and cultured in the same medium than Vero E6 cell line, added with puromycin and hygromycin B as recommended. Both cell lines were incubated at 37°C in a humidified atmosphere with 5% of CO_2. The viral strains of human SARS-CoV-2 variant were obtained from a positive nasopharyngeal PCR sample. The viruses have been treated in biosafety level-3 laboratory (BSL-3). The SARS-CoV-2 primo-culture stocks used as B (n = 1 viral strain) (EPI_ISL_4537783), Alpha (n = 2) (EPI_ISL_4536454 and EPI_ISL_4536996), Beta (n = 2) (EPI_ISL_4537125 and EPI_ISL_4537284), Gamma (n = 1) (EPI_ISL_4536760), and A.27 (n = 1) (EPI_ISL_4537460) was produced in Vero E6 cells. The supernatant were quantified with viral RNA levels and titrated by lysis plaque assay (Gordon et al., 2020), aliquoted, and stored at −80°C.

Kinetic and Viral Infection Assays

Vero E6 and A549 cells were seeded onto 12-well plates at a density of 100,000 cells per well for Vero E6 cells or 200,000 cells per well for A549. For all virus strains, 18 h postseeding, cells were infected with multiplicity of infection (MOI) titres of 0.01. Briefly, cells were washed once with a serum-free medium and infected with 500 µl of a SARS-CoV-2 serum-free medium viral suspension. After virus adsorption for 1 h at 37°C, the viral inoculum was removed and the cells were washed with a FBS-free medium. A total of 1 ml of DMEM supplemented with 2% FBS was then added onto the infected cells. For each tested condition, three corresponding wells were used to collect cells and supernatants on a daily basis. After centrifugation, cells were washed three times with PBS. Cells and supernatants were immediately tested for viral SARS-CoV-2 RNA and albumin cell DNA PCR, allowing quantifying viral copy genome number per million cells. The remaining samples were stored at −80°C before testing by N antigen titration and infectious titre evaluation by lysis plaque assay as depicted below. Each assay was performed with three replicates conducted independently for each tested viral strain.

Nucleic Acid Extraction and Quantitative PCR

Both cells and supernatants were extracted from 100 µl of each supernatant or resuspended cells sample with the Total NA Isolation kit - Large Volume assay on a MagNA Pure LC 2.0

analyser (Roche, Basel, Switzerland). All nucleic acids were eluted in a 50-µl elution buffer. A quantitative PCR of the albumin gene with a standard human DNA (0.2 µg/µl) dilution, for quantifying cellular DNA, was performed as previously described (Desire et al., 2001). The SARS-CoV-2 RNA was quantified from 10 µl of extracted samples with the RealStar™ SARS-CoV-2 RT-PCR Kit 1.0 assay (Altona Diagnostics GmbH, Hamburg, Germany) (Visseaux et al., 2020). The viral quantification was performed using a standardised RNA transcript control obtained from the European Virus Archive Program and targeting E gene as previously described (Visseaux et al., 2020). Moreover, an internal control was used in all PCR assay to check the absence of PCR inhibitors.

Viral Titration

SARS-CoV-2 was titrated by a lysis-plaque assay as previously described (Gordon et al., 2020). Briefly, Vero E6 cells were seeded onto a 12-well plate at a density of 100,000 in DMEM with 10% FBS. The next day, cells were infected by 10 to 10 serial viral dilutions with the same infection protocol than for our viral infection assays. After the viral adsorption period of 1 h at 37°C, 500 µl of an agarose medium mix was added. After 3-day incubation at 37°C with 5% of CO_2, the supernatant was removed and cells were fixed with 1 ml to 6% of formalin solution for 30 min. The formalin solution was then removed, and cells were coloured with a 10% crystal violet solution for 15 min. All wells were then washed with distilled water and dried on bench-coat paper.

N-Antigen Level Assessment

N-antigenemia levels were determined with a being marketed CE-IVD ELISA microplate assay, COV-Quanto® (AAZ, Boulogne-Billancourt, France), according to manufacturer recommendations (Le Hingrat et al., 2020). Briefly, in each well of 96-well microplates, coated with anti-SARS-CoV-2 N-antibodies, 50 µl of a solution containing biotinylated anti-SARS-CoV-2 N antibodies and 50 µl of cells or supernatants were added. After incubation at 37°C for 60 min, 100 µl of a solution containing HRP-conjugated streptavidin were added, followed by a 30-min incubation at 37°C. After being washed, 50 µl of a solution containing the peroxide substrate and 50 µl of a second substrate (3,3′,5,5′-tetramethylbenzidine (TMB)) were then added. After 15 min at 37°C, the colorimetric reaction was stopped by adding 50 µl of H_2SO_4. Absorbance values were measured at 450 nm, with a reference set at 630 nm. Standards, made of recombinant N antigens, were added to each microplate, as recommended by the manufacturer, to allow N-antigenemia-level determination.

Statistical Analysis

For each time point, potential differences were tested across all lineage groups using the Kruskal-Wallis test. Differences between two lineages were then tested using a Mann-Whitney *U* test. All statistics were calculated using R 4.1.0.

Ethical Consideration

According to current French ethical laws and regulations, written informed consents are not required for viral strain characterisation.

RESULTS

The Alpha variant presented an earlier production of infectious viral particles than the other tested viral variants on both Vero E6 and A549 cell lines (cf. **Figure 1**). Indeed, as early as 15 h after infection, the infectious particle production was statistically different across strains ($p = 0.005$). All non-Alpha strains presented similar viral particles amounting up to 40 PFU/ml ($p = 0.19$), statistically lower than the Alpha variant presenting at 600 to 900 PFU/ml ($p = 0.005$). At 24 h, all non-Alpha strains produced similar detectable viral particle amount comprising between 2 and 220 PFU/ml ($p = 0.24$).

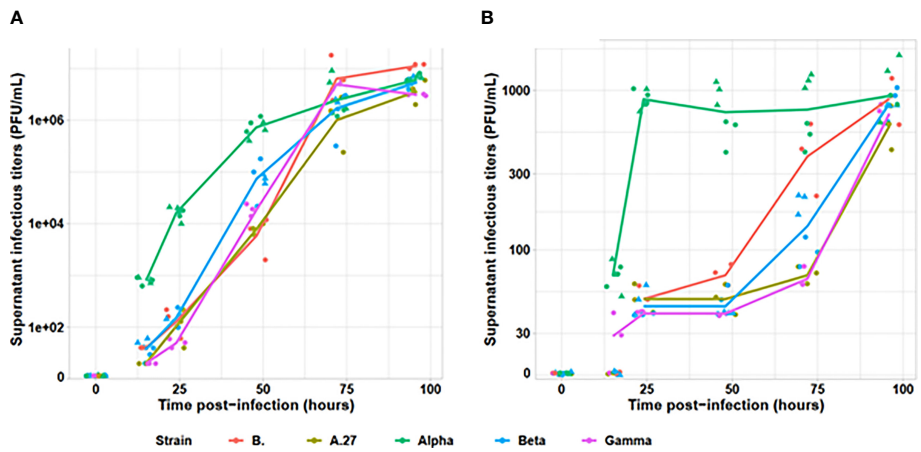

FIGURE 1 | Evaluation of infectious viral particle production kinetics for tested viral variants. The infectious titers, determined by plaque assay on **(A)** Vero E6 and **(B)** A549 cell lines, are indicated on a logarithmic scale. The Alpha variant is indicated in green, the Beta in blue, the Gamma in purple, the A.27 in khaki and the B strain in red. For Alpha and Beta, two strains were tested and are identified by the dot triangle or circle shapes. Each strain was tested by two independent replicates.

However, the two Alpha strains produced from 18,000 to 21,000 PFU/ml across replicates, statistically higher than non-Alpha variants ($p = 0.02$). Similar pattern was also observed at 24 and 48 h, with similar levels for all non-Alpha strains ($p = 0.24$ and $p = 0.19$, respectively) and statistically higher levels for Alpha strains ($p < 0.001$ and $p = 0.009$, respectively). We observed similar infectious titres for all strains at 72 h, plateauing around 10^7 PFU/ml. Those observations were confirmed on A549 human pulmonary cells, despite lower levels of infectious viral particle production, as Alpha strain was able to produce significant amount of infectious viral particles at 15 h, statistically higher than the very low amount of non-Alpha strains ($p = 0.001$). Similar levels of infectious viral particles were only observed for all strains at 96 h.

Assessment of SARS-CoV-2 viral production was also performed by RNA and antigen N intracellular and extracellular productions (cf. **Figure 2**). RNA in culture supernatant provided earlier kinetics than supernatant infectious titres or intracellular RNA. Moreover, the Alpha variant produced around 10 times higher RNA loads than the other strains, both in culture supernatant (Vero E6: $p < 0.001$; A549: $p < 0.001$) and intracellular fraction (Vero E6: $p < 0.001$; A549 $p < 0.001$). All non-Alpha viral strains produced similar amounts of viral RNA at 15 h in both supernatant (Vero E6: $p = 0.26$; A549: $p = 0.07$) and intracellular RNA (Vero E6: $p = 0.15$; A549: $p = 0.06$). Similar pattern was also observed at 24 and 48 h, with similar levels for all non-Alpha strains ($p = 0.08$ and $p = 0.07$, respectively), despite slightly lower levels for the A.27 strain, and statistically higher levels for Alpha strains ($p < 0.001$ and $p < 0.001$, respectively) on Vero E6 cells. The same profile has been confirmed on A549 cell line. Finally, all RNA levels reached similar plateaus for all tested variants after 72 h of infection. Production of N antigen in the culture supernatant provided similar kinetics to infectious viral particle titres with statistically earlier Alpha viral N-antigen production since 15 h after infection up to a final plateau at 48 h postinfection while the other strains reached similar plateaus but only at 72 h postinfection. Intracellular N-antigen levels detected at 15 h postinfection was also similar for all non-Alpha strains on both cell lines (Vero E6: $p = 0.11$; A549: $p = 0.57$), but statistically lower than for the two Alpha strains with levels between 5.12×10^2 and 9.85×10^3 pg/10^5 cells (Vero E6: $p < 0.001$; A549: $p < 0.001$). This pattern was also observed in supernatant N antigen at 24 and 48 h, as well as for intracellular N-antigen levels.

DISCUSSION

The emergence of new SARS-CoV-2 variants, with several data suggesting higher viral loads and/or better resistance to seroneutralisation, is forcing the scientific community to quickly react and provide new data for assessing and understanding the new threats. In the current work, we investigated the viral replication kinetics and production of viral particles of four variants, Alpha, Beta, Gamma, and A.27, in parallel to the historical strain B. We highlight here, a shorter replication cycle and quicker production of infectious viral particle with the Alpha (i.e., the UK variant) than with B strain (a historical variant), Beta (i.e., the South-African variant), Gamma (i.e., the Brazilian variant), or A.27 variant, a recent variant under investigation observed in France.

Many efforts are focusing on the response of variants to immunoglobulin and vaccines (Planas et al., 2021; Zhou et al., 2021), a cornerstone question for public health policies. However, the potential differences among variants on the global viral fitness have not been characterised to date. This is of importance, especially as the Alpha variant provides higher viral loads and higher death rates than the historical strains (Challen et al., 2021; Davies et al., 2021) and as we are lacking such data on the other newly emerged variants. For the Alpha variant, the higher viral loads seem associated with earlier consultation since patients are consulting one day earlier since symptoms onset than with historical variants (Challen et al., 2021; Davies et al., 2021). It is unclear how these two facts are related.

Our results confirm those epidemiological observations. The almost 10 times higher *in vitro* production of viral RNA observed with the Alpha strain between 15 and 48 h postinfection is in line with the higher viral loads observed in the UK (Davies et al., 2021; Challen et al., 2021). We also observed earlier production of infectious viral particles with the Alpha strain, 1 day before the other variants and even detectable since 15 h postinfection. This shorter *in vitro* replication cycle is in line with the earlier consultation observed in the UK (Challen et al., 2021; Davies et al., 2021).

Our results have been confirmed on two cellular models, the reference Vero E6 model and the A549 human pulmonary immortalised cell line, as well as with different markers including viral RNA or N-antigen production in the culture supernatant and within the cells. Interestingly, in the culture supernatant, the results observed with the N antigen were much closer to the infectious titres than the viral RNA detection. This could be explained by high levels of genomic and mRNA since the earliest stage of cell infection which can be released by the cells but do not reflect the presence of viable viral particles. When studying the cellular layers, the N-antigen titres were remarkably similar to intracellular RNA measurements, suggesting that they adequately reflect viral accumulation within the infected cells. Thus, N-antigen measurements appear to provide a quick, easy, and highly informative tool for SARS-CoV-2 cellular culture assessment. The detectable levels of intracellular N-antigen and RNA immediately after cellular infection should also reflect the viral entry during the infection steps. Thus, the higher levels observed with the A549 cells than Vero E6 are in line with the presence of the TMPRSS2 coreceptor expressed by those former cells.

To date, only little preliminary data are available on replicative advantage of the recent variants of concerns. A study in a mice model depicts a lower lung viral load for B.1 and Alpha than Beta and Gamma (Montagutelli et al., 2021). In another preprint study, conducted in hamster model, low Alpha lung infectious particle titres were also identified but, on the contrary, with higher Alpha nasal infectious titres than several B.1 strains (HK-15, GH 405, and HK-95) (Mok et al., 2021).

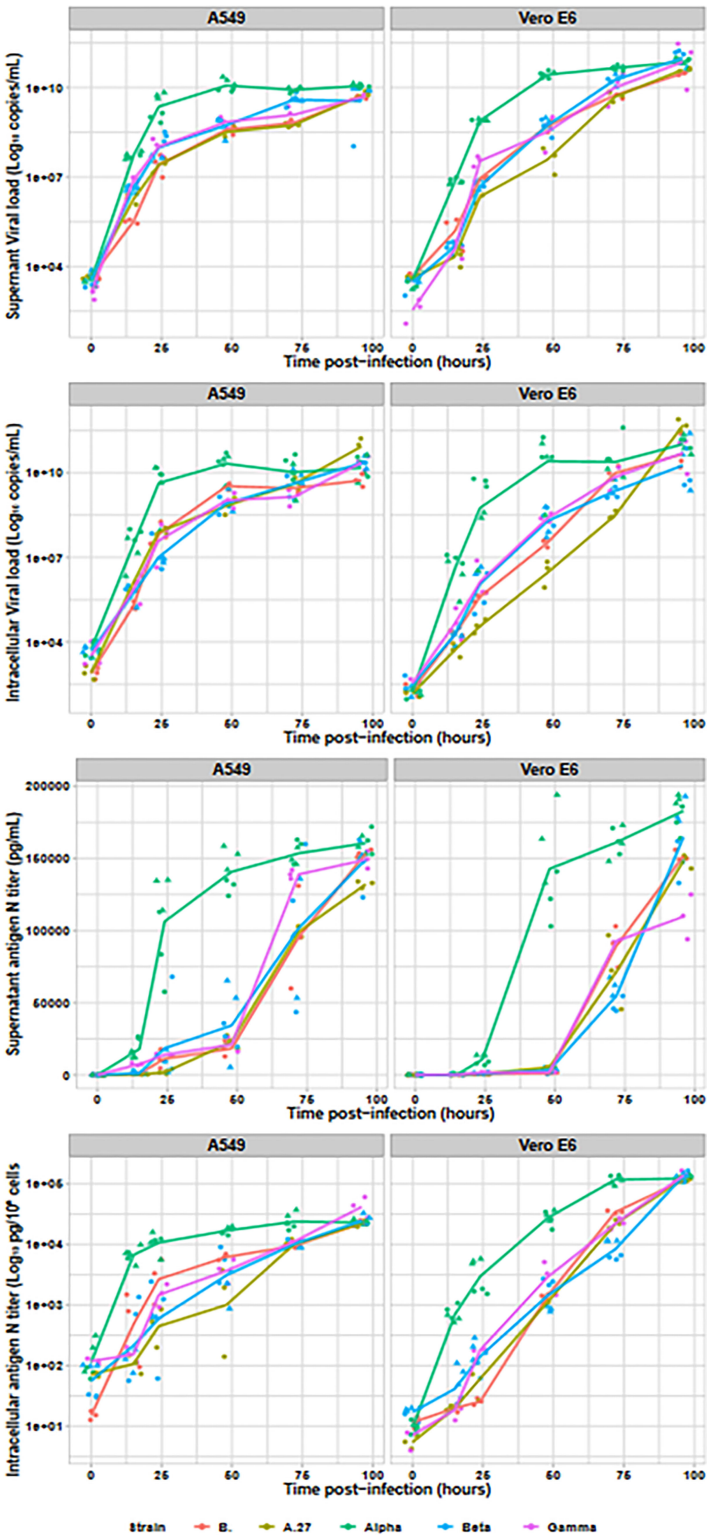

FIGURE 2 | Viral replication assessment in culture supernatant and intracellular fraction. The Alpha variant is indicated in green (n=6), the Beta in blue (n=6), the Gamma in purple (n=3), the A27 in khaki (n=3) and the B. strain in red (n=3). For Alpha and Beta, two strains were tested and are identified by the dot triangle or circle shapes. With the exception of the N antigen in culture supernatant, all data were plotted on logarithmic scales.

Using Vero and primary human airway epithelial cells, Brown et al. did not evidence a replicative advantage of Alpha cells over some other variants but did not tested historical B strains nor Beta or Gamma (Brown et al., 2021). All these results will need further confirmation. Our study provides complementary data on two reference cell lines, Vero E6 and human airway A549-ACE2-TMPRSS2 cell lines, using standardised viral inoculum and several complementary replication measurement methods. Our observation, of quicker high viral load and infectious titres for Alpha, are also in line with the higher viral loads also observed in France (Teyssou et al., 2021) and culture positivity rates from clinical nasopharyngeal samples evidenced in a recent larger German study (Jones et al., 2021). In our work, we also tested the three more widely spread variants of concerns that do not show quicker or stronger replication capabilities. This reassuring observation is in line with a first study including clinical viral load data for Beta, presenting lower viral loads than for the Alpha variant (Teyssou et al., 2021), but will need to be confirmed by other larger clinical studies.

The current study presents several limitations. Despite the use of two different cell lines, including one immortalised human respiratory cell line, those observations should be confirmed on primary respiratory cells. As the viral variants studied present numerous differential mutations over their whole genomes. If the international research effort is mainly focusing on S-glycoprotein mutations, for predicting viral adhesion to cellular receptors and viral escape to neutralising antibodies, the mutations found in all the other genes are expected to play major roles in viral fitness differences. Further studies will be needed to correlate the phenotypic differences observed with any mutation or combination of those mutations. In our work, highlighting the viral fitness of Alpha variant, we found only one additional mutation compared with the archetypal Alpha strains for the first tested strain: ORF1b P314L, which is not described in the literature to our knowledge (GISAID: EPI_ISL_4536454). The second tested Alpha strain depicts the same mutation, along with ORF1a E1363G, ORF1b S2027L, and ORF3a W131C (GISAID: EPI_ISL_4536996). Due to the absence of kinetic difference between our two strains, we do not believe that they play any role in the shorter Alpha replication rate. The individual role of all mutations observed between the tested variants, and their associations, still have to be described by further studies.

In conclusion, we highlight in this work a shorter replication cycle and a quicker production of infectious viral particle with the Alpha than with several other variants currently circulating or emerging in France and worldwide. This is expected to play a role and explain a part of the higher viral loads, higher mortality rates, and earlier consultations observed in the UK and Germany with the Alpha. The comparable replication cycles observed for all the other variants tested in this work is also reassuring regarding their fitness and virulence, but will need to be confirmed by large cohort studies as done in the UK.

DATA AVAILABILITY STATEMENT

The original contributions presented in the study are included in the article/supplementary material. Further inquiries can be directed to the corresponding author.

AUTHOR CONTRIBUTIONS

SL, HC, and BV contributed to conception and design of the study. RM and SL organized the database. SL performed the statistical analysis. SL and BV wrote the first draft of the manuscript. SL, BV, and HC wrote sections of the manuscript. All authors contributed to manuscript revision and read and approved the submitted version. All authors contributed to the article and approved the submitted version.

FUNDING

This study has been funded in part by AC43 of the French Agence Nationale de Recherche sur le SIDA et les hépatites virales (ANRS).

ACKNOWLEDGMENTS

We wish to thank the team of the National Reference Center (CNR) of Mycobacteria for their valuable help in this work.

REFERENCES

Brown, J. C., Goldhill, D. H., Zhou, J., Peacock, T. P., Frise, R., Goonawardane, N., et al. (2021). Increased Transmission of SARS-CoV-2 Lineage B.1.1.7 (VOC 2020212/01) Is not Accounted for by a Replicative Advantage in Primary Airway Cells or Antibody Escape. *bioRxiv*, 2021.02.24.432576. doi: 10.1101/2021.02.24.432576

Buss, L. F., Prete, C. A., Abrahim, C. M. M., Mendrone, A., Salomon, T., Almeida-Neto, C., et al. (2021). Three-Quarters Attack Rate of SARS-CoV-2 in the Brazilian Amazon During a Largely Unmitigated Epidemic. *Science* 371, 288 – 2292. doi: 10.1126/science.abe9728

Challen, R., Brooks-Pollock, E., Read, J. M., Dyson, L., Tsaneva-Atanasova, K., and Danon, L. (2021). Risk of Mortality in Patients Infected with SARS-CoV-2 Variant of Concern 202012/1: Matched Cohort Study. *BMJ* 372, n579. doi: 10.1136/bmj.n579

Chen, X., Li, R., Pan, Z., Qian, C., Yang, Y., You, R., et al. (2020). Human Monoclonal Antibodies Block the Binding of SARS-CoV-2 spike Protein to Angiotensin Converting Enzyme 2 Receptor. *Cell. Mol. Immunol.* 1, –3. doi: 10.1038/s41423-020-0426-7

Davies, N. G., Jarvis, C. I.CMMID COVID-19 Working Group, , Edmunds, W. J., Jewell, N. P., Diaz-Ordaz, K., et al. (2021). Increased Mortality in Community-Tested Cases of SARS-CoV-2 Lineage B.1.1.7. *Nature*. doi: 10.1038/s41586-021-03426-1

Desire, N., Dehee, A., Schneider, V., Jacomet, C., Goujon, C., Girard, P.-M., et al. (2001). Quantification of Human Immunodeficiency Virus Type 1 Proviral Load by a TaqMan Real-Time PCR Assay. *J. Clin. Microbiol.* 39, 1303 –11310. doi: 10.1128/JCM.39.4.1303-1310.2001

Duerr, R., Dimartino, D., Marier, C., Zappile, P., Wang, G., Lighter, J., et al. (2021). Dominance of Alpha and Lota Variants in SARS-CoV-2 Vaccine Breakthrough Infections in New York City. *J. Clin. Invest.* 131:152702. doi: 10.1172/JCI152702

Fourati, S., Decousser, J.-W., Khouider, S., N'Debi, M., Demontant, V., Trawinski, E., et al. Early Release - Novel SARS-CoV-2 Variant Derived from Clade 19B, France - Volume 27, Number 5 –May 2021 - Emerging Infectious Diseases journal - CDC. doi: 10.3201/eid2705.210324

Garcia-Beltran, W. F., Lam, E. C., St. Denis, K., Nitido, A. D., Garcia, Z. H., Hauser, B. M., et al. (2021). Multiple SARS-CoV-2 Variants Escape Neutralization by Vaccine-induced Humoral Immunity. *Cell* 184, 2372–2383.e9. doi: 10.1016/j.cell.2021.03.013

Gordon, D. E., Jang, G. M., Bouhaddou, M., Xu, J., Obernie2r, K., White, K. M., et al. (2020). A SARS-CoV-2 Protein Interaction Map Reveals Targets for Drug Repurposing. *Nature* 583, 459 –4468. doi: 10.1038/s41586-020-2286-9

Harrison, A. G., Lin, T., and Wang, P. (2020). Mechanisms of SARS-CoV-2 Transmission and Pathogenesis. *Trends Immunol.* 41, 1100 –11115. doi: 10.1016/j.it.2020.10.004

Hodcroft, E. B., Zuber, M., Nadeau, S., Vaughan, T. G., Crawford, K. H. D., Althaus, C. L., et al. (2021). Emergence and Spread of a SARS-CoV-2 Variant Through Europe in the Summer of 2020. *MedRxiv Prepr. Serv. Health Sci.*, 2020.10.25.20219063. doi: 10.1101/2020.10.25.20219063

Jones, T. C., Biele, G., Mühlemann, B., Veith, T., Schneider, J., Beheim-Schwarzbach, J., et al. (2021). Estimating Infectiousness Throughout SARS-CoV-2 Infection Course Science. doi: 10.1126/science.abi5273

Korber, B. , Fischer, W. M., Gnanakaran, S., Yoon, H., Theiler, J., Abfalterer, W., et al. (2020). Tracking Changes in SARS-CoV-2 Spike: Evidence that D614G Increases Infectivity of the COVID-19 Virus. *Cell* 182, 812–827.e19. doi: 10.1016/j.cell.2020.06.043

Le Hingrat, Q. L., Visseaux, B., Laouenan, C., Tubiana, S., Bouadma, L., Yazdanpanah, Y., et al. (2020). Detection of SARS-CoV-2 N-Antigen in Blood During Acute COVID-19 Provides a Sensitive New Marker and New Testing Alternatives. *Clin. Microbiol. Infect. Off. Publ. Eur. Soc Clin. Microbiol. Infect. Dis.* doi: 10.1016/j.cmi.2020.11.025

Mok, B. W.-Y., Liu, H., Lau, S.-Y., Deng, S., Liu, S., Tam, R. C.-Y., et al. (2021). Low Dose Inocula of SARS-CoV-2 B.1.1.7 Variant Initiate More Robust Infections in the Upper Respiratory Tract of Hamsters than Earlier D614G Variants. *bioRxiv*, 2021.04.19.440414. doi: 10.1101/2021.04.19.440414

Montagutelli, X., Prot, M., Levillayer, L., Salazar, E. B., Jouvion, G., Conquet, L., et al. (2021). The B1.351 and P.1 Variants Extend SARS-CoV-2 Host Range to Mice. *bioRxiv*, 2021.03.18.436013. doi: 10.1101/2021.03.18.436013

Planas, D., Bruel, T., Grzelak, L., Guivel-Benhassine, F., Staropoli, I., Porrot, F., et al. (2021). Sensitivity of Infectious SARS-CoV-2 B.1.1.7 and B.1.351 Variants to Neutralizing Antibodies. *Nat. Med.* doi: 10.1038/s41591-021-01318-5

Sun, S., Gu, H., Cao, L., Chen, Q., Ye, Q., Yang, G., et al. (2021). Characterization and Structural Basis of a Lethal Mouse-Adapted SARS-CoV-2. *Nat. Commun.* 12, 5654. doi: 10.1038/s41467-021-25903-x

Tegally, H., Wilkinson, E., Giovanetti, M., Iranzadeh, A., Fonseca, V., Giandhari, J., et al. (2020). Emergence and Rapid Spread of a New Severe Acute Respiratory Syndrome-Related Coronavirus 2 (SARS-CoV-2) Lineage With Multiple Spike Mutations in South Africa. doi: 10.1101/2020.12.21.20248640

Tegally, H., Wilkinson, E., Giovanetti, M., Iranzadeh, A., Fonseca, V., Giandhari, J., et al. (2021a). Detection of a SARS-CoV-2 Variant of Concern in South Africa. *Nature*. doi: 10.1038/s41586-021-03402-9

Tegally, H., Wilkinson, E., Lessells, R. J., Giandhari, J., Pillay, S., Msomi, N., et al. (2021b). Sixteen Novel Lineages of SARS-CoV-2 in South Africa. *Nat. Med.* 27, 440 –4446. doi: 10.1038/s41591-021-01255-3

Teyssou, E., Soulie, C., Visseaux, B., Lambert-Niclot, S., Ferre, V., Marot, S., et al. (2021). The 501Y.V2 SARS-CoV-2 Variant has an Intermediate Viral Load Between the 501Y.V1 and the Historical Variants in Nasopharyngeal Samples from Newly Diagnosed COVID-19 Patients. *J. Infect.* doi: 10.1016/j.jinf.2021.04.023

Visseaux, B., Le Hingrat, Q., Collin, G., Ferré, V., Storto, A., Ichou, H., et al. (2020). Evaluation of the RealStar® SARS-CoV-2 RT-PCR kit RUO Performances and Limit of Detection. *J. Clin. Virol. Off. Publ. Pan Am. Soc Clin. Virol.* 129:104520. doi: 10.1016/j.jcv.2020.104520

Weisblum, Y., Schmidt, F., Zhang, F., DaSilva, J., Poston, D., Lorenzi, J. C., et al. (2020). Escape from Neutralizing Antibodies by SARS-CoV-2 Spike Protein Variants. *eLife* 9. doi: 10.7554/eLife.61312

Zhou, D., Dejnirattisai, W., Supasa, P., Liu, C., Mentzer, A. J., Ginn, H. M., et al. (2021). Evidence of Escape of SARS-CoV-2 Variant B.1.351 From Natural and Vaccine-Induced Sera. *Cell*. doi: 10.1016/j.cell.2021.02.037

Zhu, N., Zhang, D., Wang, W., Li, X., Yang, B., Song, J., et al. (2020). A Novel Coronavirus From Patients With Pneumonia in Chin. *N. Engl. J. Med.* 382, 727–733. doi: 10.1056/NEJMoa2001017

Conflict of Interest: The authors declare that the research was conducted in the absence of any commercial or financial relationships that could be construed as a potential conflict of interest.

Publisher's Note: All claims expressed in this article are solely those of the authors and do not necessarily represent those of their affiliated organizations, or those of the publisher, the editors and the reviewers. Any product that may be evaluated in this article, or claim that may be made by its manufacturer, is not guaranteed or endorsed by the publisher.

frontiers in Cellular and Infection Microbiology

REVIEW
published: 18 January 2022
doi: 10.3389/fcimb.2021.781429

SARS-COV-2 Variants: Differences and Potential of Immune Evasion

Sandro M. Hirabara[1†], Tamires D. A. Serdan[2†], Renata Gorjao[1], Laureane N. Masi[1], Tania C. Pithon-Curi[1], Dimas T. Covas[3,4], Rui Curi[1,5] and Edison L. Durigon[6,7]*

[1] Interdisciplinary Program of Health Sciences, Cruzeiro do Sul University, São Paulo, Brazil, [2] Department of Molecular Pathobiology, New York University, New York, NY, United States, [3] Butantan Institute, São Paulo, Brazil, [4] Ribeirão Preto Medical School, University of São Paulo, Ribeirão Preto, Brazil, [5] Immunobiological Production Section, Bioindustrial Center, Butantan Institute, São Paulo, Brazil, [6] Laboratory of Clinical and Molecular Virology, Department of Microbiology, Institute of Biomedical Sciences, University of São Paulo, São Paulo, Brazil, [7] Scientific Platform Pasteur University of São Paulo, São Paulo, Brazil

The structural spike (S) glycoprotein of severe acute respiratory syndrome coronavirus-2 (SARS-CoV-2) plays an essential role in infection and is an important target for neutralizing antibody recognition. Mutations in the *S* gene can generate variants of concern (VOCs), which improve "viral fitness" through selective or survival advantages, such as increased ACE-2 receptor affinity, infectivity, viral replication, higher transmissibility, resistance to neutralizing antibodies and immune escape, increasing disease severity and reinfection risk. Five VOCs have been recognized and include B.1.1.7 (U.K.), B.1.351 (South Africa), P.1 (Brazil), B.1.617.2 (India), and B.1.1.529 (multiple countries). In this review, we addressed the following critical points concerning VOCs: a) characteristics of the SARS-CoV-2 VOCs with mutations in the *S* gene; b) possible evasion of variants from neutralizing antibodies generated through vaccination, previous infection, or immune therapies; c) potential risk of new pandemic waves induced by the variants worldwide; and d) perspectives for further studies and actions aimed at preventing or reducing the impact of new variants during the current COVID-19 pandemic.

Keywords: COVID-19, variant of concern, neutralizing antibody, vaccines, immune escape, delta variant, omicron variant

OPEN ACCESS

Edited by:
Guiqing Peng,
Huazhong Agricultural University, China

Reviewed by:
Sonia Zuñiga,
National Center for Biotechnology (CSIC), Spain
Bryce Warner,
Public Health Agency of Canada (PHAC), Canada

****Correspondence:***
Sandro M. Hirabara
sandro.hirabara@cruzeirodosul.edu.com.br

†These authors have contributed equally to this work

Specialty section:
This article was submitted to Virus and Host, a section of the journal Frontiers in Cellular and Infection Microbiology

Received: *22 September 2021*
Accepted: *20 December 2021*
Published: *18 January 2022*

Citation:
Hirabara SM, Serdan TDA, Gorjao R, Masi LN, Pithon-Curi TC, Covas DT, Curi R and Durigon EL (2022) SARS-COV-2 Variants: Differences and Potential of Immune Evasion. Front. Cell. Infect. Microbiol. 11:781429. doi: 10.3389/fcimb.2021.781429

INTRODUCTION

Severe acute respiratory syndrome coronavirus-2 (SARS-CoV-2) is a single-stranded positive-sense RNA virus containing a genome with 29,903 nucleotides and 29 proteins (Focosi and Maggi, 2021). The virus has six major open-reading frames (ORFs): ORF1a, ORF1b, S (spike), E (envelope), M (membrane), and N (nucleocapsid), and several accessory ORFs: ORF3a/b, ORF6, ORF7a, ORF7b, ORF8, ORF9b/c, and ORF10 (Kim et al., 2020; Zhu et al., 2020; Finkel et al., 2021).

ORF1a and ORF1b account for two-thirds of the SARS-CoV-2 genome. ORF1a encodes the polyprotein PP1a and the polyprotein PP1ab is a result of the overlapping translation of ORF1a and ORF1b. Both polyproteins (PP1a and PP1ab) are cleaved into 16 nonstructural proteins (NSPs 1 to 16): NSP1 (leader protein), NSP2 (unknown function), NSP3 (papain-like proteinase), NSP4 (transmembrane nsp containing four transmembrane domains and one luminal domain), NSP5 (3C-like proteinase), NSP6 (putative transmembrane nsp containing six transmembrane domains and two small luminal domains), NSP7 and NSP8 (the NSP7-NSP8 heterodimer interacts with the NSP12

forming the RNA polymerase complex), NSP9 (RNA-binding protein), NSP10 (cofactor for nsp14 and nsp16), NSP11 (unknown function), NSP12 (RNA-dependent RNA polymerase, RdRp), NSP13 (helicase), NSP14 (3′ to 5′ Endonuclease, N7-Methyltransferase), NSP15 (endoribonuclease, NendoU), and NSP16 (2′-O-Ribose-Methyltransferase) (Snijder et al., 2016; Finkel et al., 2021). ORFs S, E, M, and N encode four structural proteins, whereas accessory ORFs lead to the formation of several accessory proteins (Kim et al., 2020) (**Figure 1**).

The M protein is the most abundant transmembrane protein and is associated with virus assembly and morphology. The E protein also participates in virus assembly, release, and ion channel activity processing. In coronaviruses, ion channel activity has been implicated in viral infectivity. The N protein encapsulates the viral RNA and, along with NSPs, plays a crucial role in virus replication, transcriptional processes, and genome assembly (Nieto-Torres et al., 2014; Abdel-Moneim et al., 2021).

The S glycoprotein is a homotrimer, and each monomer contains two subunits, S1 and S2. S1 contains the N-terminal domain (NTD) and the receptor-binding domain (RBD), which recognize and bind to the angiotensin-converting enzyme-2 (ACE-2) receptor required for virus attachment and entry into host cells (Ou et al., 2020; Abdel-Moneim et al., 2021). The RBD, precisely the receptor-binding motif (RBM) region, also contains the main antigenic epitopes recognized by neutralizing antibodies (nAbs) (Abdel-Moneim et al., 2021). S2 has several domains and mediates membrane fusion between the viral envelope and the host cell (Abdel-Moneim et al., 2021). The S protein is highly

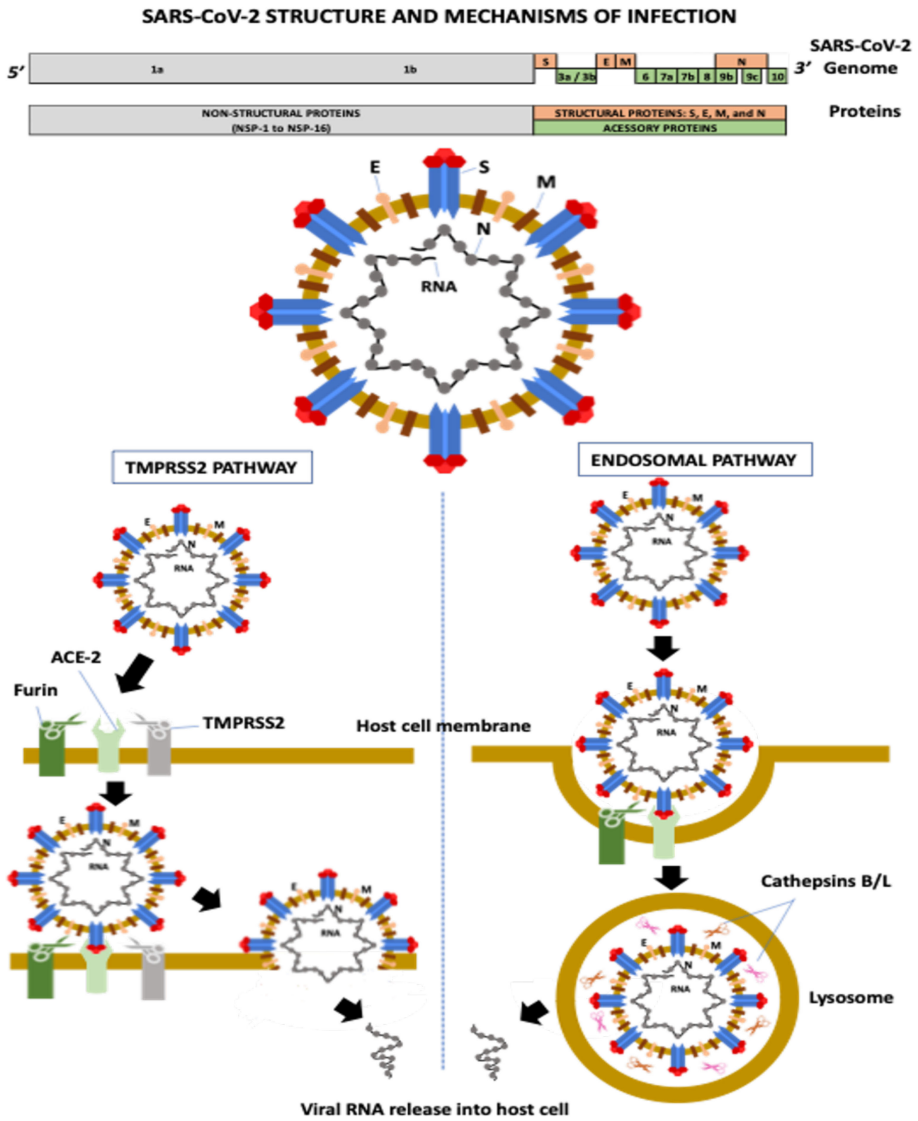

FIGURE 1 | SARS-CoV-2 structure and mechanisms of infection. ACE-2, angiotensin-converting enzyme-2; E, envelope; M, membrane; N, nucleocapsid; NSP, non-structural protein; S, spike; TMPRSS-2, transmembrane serine protease-2.

N-glycosylated at at least 22 sites: 13 in S1 and nine in S2 (Yao et al., 2020). Two main RBD conformations have been described, standing-up and lying-down states, with high and low affinity to ACE2, respectively (Yao et al., 2020). Although RBD of SARS-CoV-2 presents a higher affinity to ACE2 than the RBD of SARS-CoV, most RBD in the entire SARS-CoV-2 is in the lying-down state, resulting in a similar or even lower affinity to the receptor than SARS-CoV (Yao et al., 2020). The exposure of N-linked glycans is modified according to the RBD conformation (10 in the RBD-down and 7 in the RBD-up states), suggesting that these molecules can participate in the interaction between SARS-CoV-2 and the host cell (Yao et al., 2020).

The first step of viral infection is RBD binding to ACE2 on the host cell. Several proteases then help S glycoprotein cleavage, including transmembrane serine protease-2 and -4 (TMPRSS-2 and -4), furin-like enzymes, and endosomal cathepsins B/L (Shang et al., 2020) (**Figure 1**). Cleavage is required for S protein priming and activation, allowing the membrane fusion process and viral RNA entry into a host cell (Hoffmann et al., 2020; Zang et al., 2020). The activity of these proteases is associated with increased transmissibility, virulence, and cell and tissue tropism (Abdel-Moneim et al., 2021).

Furin is a serine protease involved in the preactivation of the S protein, which enhances virus entry mainly in host cells with low expression of other proteases, including TMPRSS2 and cathepsins (Shang et al., 2020). The protease recognizes the furin-like cleavage site, a multibasic site composed of three arginine molecules and one alanine (RRAR) located at the S1-S2 junction. After this cleavage preactivation of the S protein (S1-S2 junction), a second cleavage site located in the S2 subunit (S2′ site) is critical for membrane fusion during virus entry (Takeda, 2022). The cleavage of the S2' site occurs by two pathways: a) the TMPRSS2 pathway and b) the endosomal pathway (Hoffmann et al., 2020) (**Figure 1**). TMPRSS2 is a serine protease with trypsin-like endopeptidase activity located at the cell surface that promotes priming and activation of the S protein, allowing the interaction of the S2 fusion peptide (FP) domain with the host cell membrane, consequently leading to membrane fusion and viral RNA release into the host cytosol (Kielian, 2020).

The second SARS-CoV-2 infection mechanism occurs through the endosomal pathway, in a process that depends on phosphatidylinositol-3-phosphate-5-kinase activity, required for the synthesis of phosphatidylinositol-3,5-biphosphate (PI-3,5-P2), which is critical for endosome maturation, and on two-pore channel subtype 2 (TPC2), present in late endosomes and lysosomes, which is the main downstream effector of PI-3,5-P2, mediating cation transport, mainly Na^+ and Ca^{2+} (Ou et al., 2020). Inhibition of the TPC2 activity or PI-3,5-P2 production prevents SARS-CoV-2 endocytosis (Ou et al., 2020). In lysosomes, cysteine proteases (cathepsins B and L) promote S protein cleavage at the S2' site, allowing the interaction and fusion of the viral envelope and the lysosomal membrane and, consequently, the viral nucleocapsid is released into the host cytosol (Shang et al., 2020).

Any disturbance in the S protein structure can modulate one or more processes involved in the viral infection and eventually provide some selective advantage for the virus (Harvey et al., 2021). For instance, a specific mutation (or a combination of mutations) in the *S1* or *S2* subunits can modify: a) the affinity of S1 RBD to ACE2, increasing the virus binding to the host cells; b) the number and exposition of glycosylated sites, facilitating the interaction/accessibility between the viral envelope and host cell plasma membrane; c) the percentage of lying-down and standing-up states of the S1 RBD, elevating the general virus affinity to ACE2; d) the affinity of cleavage sites for proteases, improving the membrane fusion process; and e) recognition by nAbs, reducing the humoral immune response and inducing immune evasion.

The humoral response against SARS-CoV-2 involves specific nAbs against viral epitopes, mainly against the S glycoprotein (Ni et al., 2020). Epitopes of the N protein are highly conserved among different coronaviruses, inducing cross-reacting antibody generation. However, nAbs against the S protein protect against SARS-CoV-2 infections (Melenotte et al., 2020). Therefore, nAb activity against S glycoprotein allows for the evaluation of the responses induced by vaccines, convalescent plasma, and antibody therapies, as well as the potential immune evasion by different VOCs. The emergence of new variants at the end of 2020 raised new concerns about viral fitness and antibody-based therapies, including vaccines, convalescent sera, and monoclonal antibodies (mAbs) (Fontanet et al., 2021). In addition, new waves of the COVID-19 pandemic have been attributed to the new variants in several parts of the world (Fontanet et al., 2021).

In this review, we address the following critical points concerning SARS-CoV-2 variants: the characteristics of the variants with concerning mutations in the spike gene; the possible evasion of VOCs from nAbs generated through vaccination or previous infection; and perspectives for further studies and actions aimed at preventing or reducing the impact of new VOCs on the COVID-19 pandemic.

SARS-COV-2 SPIKE GENE MUTATIONS

Several genes of SARS-CoV-2, including *S*, *N*, and *NSP12* (RdRP), present a high mutational range (Focosi and Maggi, 2021). However, compared to other RNA viruses, coronaviruses present a low mutational frequency due to NSP14, which exhibits 3′ to 5′ Exonuclease (ExoN) activity that is critical for high viral replication fidelity (Smith et al., 2014). It has been suggested that other factors can increase the number of mutations in SARS-CoV-2.

For example, control measures have had a sizeable negative impact on the economy. Most countries adopted incomplete or insufficient preventive/restrictive measures, with partial participation/adherence, resulting in ineffective control of the COVID-19 pandemic. Consequently, virus transmission and spread increased the probability of new mutations, leading to the emergence of variants with selective advantages (Chen and Lu, 2021). Additionally, individuals with impaired immune competence suffer from prolonged SARS-CoV-2 infections, which increases the likelihood of new mutations (Choi et al., 2020).

There have also been many SARS-CoV-2 reinfections reported, raising immune pressure and selecting mutations that potentially can help escape immune defense (Abdel-Moneim et al., 2021). Lastly, viral adaptation in susceptible animals and subsequent human infection can produce additional mutations in SARS-CoV-2 (Abdel-Moneim et al., 2021).

Mutations can occur in any region of the SARS-CoV-2 genome. Most mutations are silent, meaning that they do not modify the primary amino acid sequence, the function of the translated proteins or viral infectivity. However, a single mutation, or a combination of mutations, can yield variants with selective and survival advantages and improved viral fitness. These mutational variants can present increased infectivity and/or transmissibility, human ACE-2 receptor binding affinity, viral replication, pathogenicity and reinfection risk. Moreover, depending on the location of the mutation, changes in antigenicity and host-, vaccine- or mAb-induced immune response evasion with alteration in crucial epitopes recognized by nAbs and/or decreased T cell immunity (Dearlove et al., 2020; Abdel-Moneim et al., 2021; Altmann et al., 2021; Callaway and Ledford, 2021; Focosi and Maggi, 2021).

While mutations in other genes could generate variants with enhanced viral infectivity, replication, and immune escape potential (Khateeb et al., 2021; Nguyen et al., 2021), this review will focus on *S* gene mutations because the spike protein is the most extensively studied viral infection protein and the main protein target for vaccine development. For instance, recent studies have reported that R203K/G204R modifications in the N protein are associated with high viral replication, infectivity, and transmissibility in cellular and animal models (Wu et al., 2021; Zhu et al., 2021b); it has been observed that these modifications appear at a high prevalence in the B.1.1.7 variant (Collier et al., 2021). NSP1 protein is important for suppressing interferon I signaling and increasing viral replication (Xia et al., 2020; Lin et al., 2021). Notably, Lin et al. (2021) observed that a deletion in NSP1 (Δ500-532) is related to low plasma IFN-β levels and viral load. The high prevalence of the P323L mutation in NSP12 (RdRp) has been implicated in viral replication (Koyama et al., 2020).

Mutations in ORF8 have been suggested to augment viral transmission and immune evasion potential because its gene products participate in the RNA polymerase complex and are involved in controlling the host cells' major histocompatibility complex class I (Young et al., 2020; Flower et al., 2021; Pereira, 2021). Pereira (2021) observed a high prevalence of a premature stop codon at position 27 in ORF8 (Q27stop) that occurs in the B.1.1.7 variant, potentially contributing to its high transmission rate and spread.

Emerging variants can be considered a variant under investigation (VUI), a variant of interest (VOI), or a variant of concern (VOC). The WHO has recognized several VOIs, including B.1.427 and B.1.429 from the USA (California, WHO alert since July 6, 2021), B.1.525 from the United Kingdom and Nigeria, B.1.526 from the USA (New York), B.1.617.1 and B.1.617.3 from India, P2 from Brazil, and C.37 from Peru. Furthermore, the WHO has classified five variants as VOCs: B.1.1.7 from the United Kingdom (501Y. V1, VOC 202012/01, alpha variant), B.1.351 from South Africa (501Y. V2, VOC 202012/02, beta variant), P.1 from Brazil (501Y. V3, VOC 202101/02, gamma variant); B.1.617.2 from India (VOC 202104/02, delta), and B.1.1.529 from multiple countries (omicron variant). Notably, the B.1.617.2 variant was linked to the fast spread of SARS-CoV-2 in several countries (Adam, 2021).

The D614G mutant in the *S* gene, first identified in Europe in January 2020, was one of the first SARS-CoV-2 mutations to spread worldwide (Conti et al., 2021; Dearlove et al., 2020). This mutation is positioned between the S1 and S2 subunits (Dearlove et al., 2020) and has been reported to increase *in vitro* viral infectivity (Dearlove et al., 2020; Korber et al., 2020; Groves et al., 2021), affinity binding to the ACE-2 receptor and transmissibility (Volz et al., 2020; Ozono et al., 2021), protease-induced S protein cleavage (Gobeil et al., 2021), replication, and viral loads (Abdel-Moneim et al., 2021). Despite the apparently enhanced "viral fitness" (Dearlove et al., 2020; Plante et al., 2020) and its ability to neutralize the activity of antibodies induced by previous infections or vaccines (Dearlove et al., 2020; Groves et al., 2021), the clinical outcomes or pathogenicity remain unchanged (Volz et al., 2020; Groves et al., 2021). It has been proposed that the D614G mutation causes the ACE-2 receptor to assume "open conformation", increasing the binding affinity (Yurkovetskiy et al., 2020) and the virus's susceptibility to nAbs (Garcia-Beltran et al., 2021a).

The B.1.1.298 variant (mink Cluster 5) was one of the first to contain the D614G mutation. This variant was associated with an outbreak on Denmark mink farms (Oude Munnink et al., 2021), resulting in 17 million Danish minks being culled as a preventive measure to stop virus evolution and spread (Garcia-Beltran et al., 2021b). It has been suggested that other modifications, including Y453F in the RBD of the S protein, P323L in NSP12 (a component of RdRp), and R203K and G204R in the N protein, also contributed to the improved viral fitness of the B.1.298 variant (Plante et al., 2021). Notably, the D614G mutation has become more predominant, appearing in all recently identified variants.

The first VOC described (VOC 202012/01) was the B.1.1.7 lineage (20I/501Y. V1), identified in the United Kingdom (Sep 2020). This variant is now present on all continents. In December 2020, B.1.1.7 was responsible for one-quarter of the total COVID-19 cases worldwide and two-thirds of the cases in the United Kingdom (Conti et al., 2021). Compared to the original virus, B.1.1.7 exhibits a 40–70% increase in transmissibility (Graham et al., 2021; Volz et al., 2021). The B.1.1.7 lineage has 23 mutations in the *S*, *N*, and *ORF-8* genes, but the impact of each mutation on viral fitness and survival or vaccine efficacy is not completely known (Conti et al., 2021; Focosi and Maggi, 2021).

The S protein of the B.1.1.7 lineage contains several amino acid mutations, including D614G and N501Y, and deletions ΔH69/ΔV70 (Focosi and Maggi, 2021). The S RBD N501Y mutation increases the binding affinity to the ACE-2 receptor and transmissibility (Starr et al., 2020; Graham et al., 2021;

Focosi and Maggi, 2021). Gu et al. (2020) developed a mouse-adapted strain model (MASCp6) to evaluate the SARS-CoV-2 infectivity and virulence after intranasal inoculation and observed that the N501Y mutation favors interaction with ACE2 and promotes virus entry, consequently leading to enhanced virulence. Recent studies have suggested that the N501Y mutation has a low impact on clinical outcomes and pathogenicity (Conti et al., 2021; Graham et al., 2021) and the immune response generated by mAbs, vaccines, or previous infection (Muik et al., 2021; Focosi and Maggi, 2021). However, Davies et al. (2021) evaluated more than 2.2 million people with SARS-CoV-2 positive tests and 17,452 related deaths in England and observed a 61% higher risk of death risk in those infected with the B.1.1.7 variant than other pre-existing variants. Thus, the B.1.1.7 variant presents increased transmissibility and disease severity.

The B.1.351 lineage (20H/501Y. V2, VOC 202012/02) emerged in South Africa (Oct 2020), probably favored by the high immune pressure, and spread to other African countries, Asia, Australia, and North and Central America (Focosi and Maggi, 2021). By the end of 2020, this variant was responsible for more than 90% of all COVID-19 cases in South Africa (Callaway and Mallapaty, 2021). This lineage has several structural and nonstructural mutations, including three critical mutations in the RBD of the S protein (K417N, E484K, and N501Y) that seem to play a crucial role in the improved "viral fitness" and survival adaptations compared to the other strains in some regions where it was prevalent (Focosi and Maggi, 2021). The K417N mutation exacerbated immune escape from nAbs and reduced vaccine effectivity against infection (Callaway and Mallapaty, 2021; Focosi and Maggi, 2021), and the E484K modification is associated with increased binding to the ACE-2 receptor (Focosi and Maggi, 2021) and a decreased or even abrogated response to Ab neutralization induced by previous infection, vaccination, or monoclonal Ab therapy (Liu Z. et al., 2021). Furthermore, five mutations in the NTD of the *S* gene were proposed to contribute to improved viral microenvironment adaptations (Li et al., 2021). This lineage is also associated with increased spreading (Garcia-Beltran et al., 2021a) and reinfection cases in subjects previously infected with the original SARS-CoV-2 (Staub et al., 2021).

In December 2020, the P.1 lineage (20J/501Y. V3, VOC 202101/02, also called P.1) accounted for 42% of the total cases in Manaus, Brazil (Chen and Lu, 2021), and in February 2021, it was discovered in Japan in samples from individuals traveling from Manaus. The three main mutations are the same as in B.1.351: K417T, E484K, and N501Y (Focosi and Maggi, 2021). This lineage has increased ACE-2 receptor binding affinity, transmissibility (Focosi and Maggi, 2021; Francisco et al., 2021), infectivity in mice (Chen and Lu, 2021), resistance to immune response (Focosi and Maggi, 2021; Francisco et al., 2021), and risk of reinfection (Chen and Lu, 2021; Taylor, 2021; Sabino et al., 2021). The main similarities and differences among B.1.1.7, B.1.351, and P.1 are summarized in **Figure 2**. Similar and differential mutations of the main SARS-CoV-2 variants are shown in **Figure 3**.

The B.1.617 lineage contains three sublineages: B.1.617.1, B.617.2 (delta variant), and B.1.617.3. B1.617.2 exhibits higher transmissibility than the ancestral strain, and studies suggest a high risk of hospitalization compared to the original strain or the B.1.1.7 variant (Liu and Rocklöv, 2021; Ong et al., 2021; Sheikh et al., 2021). In a short review, Liu and Rocklöv (2021) reported a

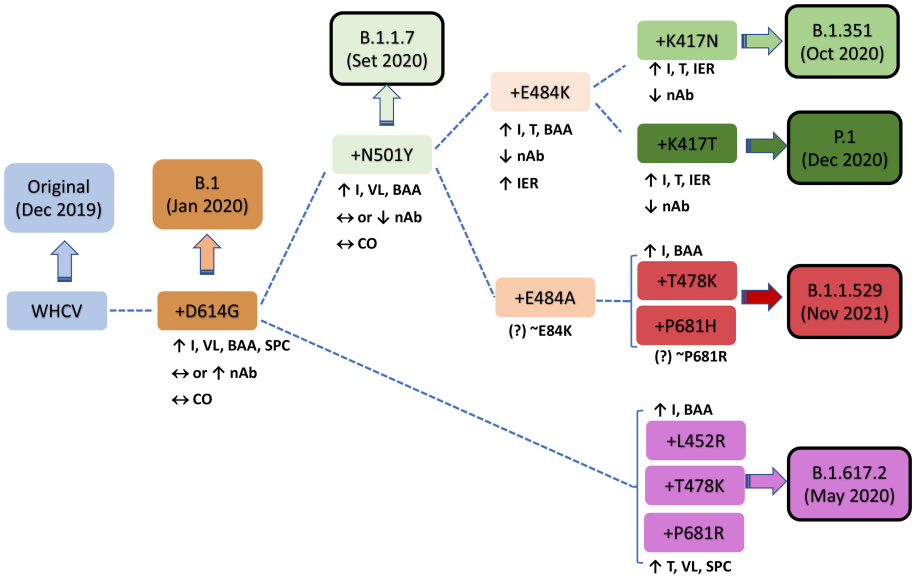

FIGURE 2 | Characteristics of key mutations in variants of concern (VOCs). A comparison was performed versus the original virus (WHCV) or the B.1 strain (+D614G). BAA, binding affinity to ACE2; CO, clinical outcome; I, infectivity; IER, immune evasion risk; nAb, neutralizing antibody; SPC, spike protein cleavage; T, transmissibility; VL, viral load; WHCV, WH-Human 1 coronavirus.

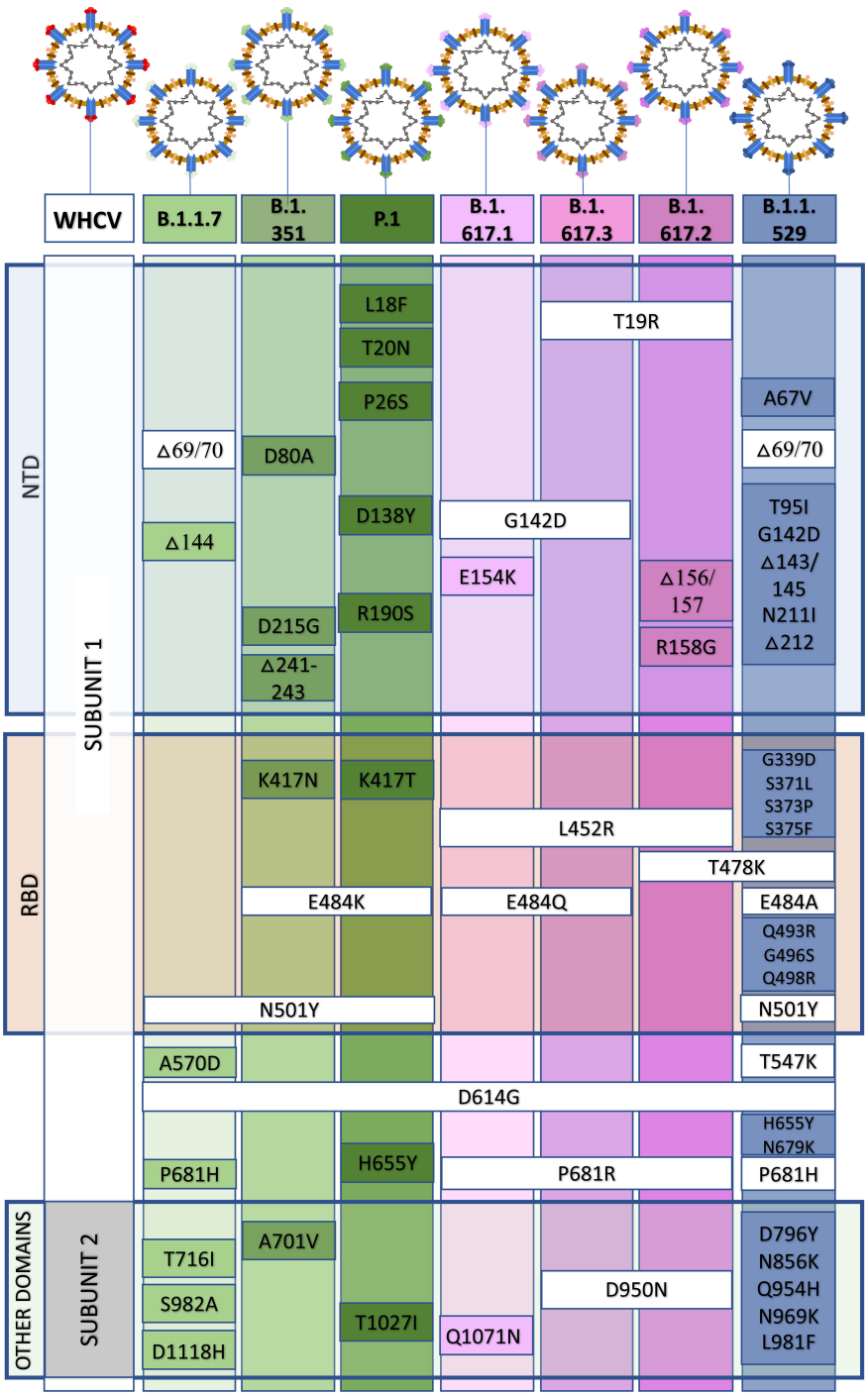

FIGURE 3 | Similar and differential mutations in the spike (S) protein from the B.1.1.7, B.1.351, P.1, B.1.617, and B.1.1.529 variants of concern. NTD, N terminal domain; RBD, receptor-binding domain.

basic reproductive number (R_0) of 5.08 for the delta variant versus 2.79 for the ancestral SARS-CoV-2 strain. Since no difference was observed in the median age and disease duration between patients infected with B.1.617.2 or non-B.1.617.2 strains (Mlcochova et al., 2021), the elevated risk of hospitalization is probably due to the high transmissibility of the B.1.627.2 variant compared to other strains. Most fully vaccinated people are protected against the B.1.617 variants (Lopez Bernal et al., 2021). However, even after full vaccination, people can be infected by B.1.617.2 or other

variants and transmit them to others, albeit with a lower risk of disease severity and shorter infection period than unvaccinated individuals (Ong et al., 2021; Sheikh et al., 2021). Notable mutations in the B.1.617.2 variant include L452R, T478K and E484Q in the S RBD and P681R in the cleavage site between S1 and S2.

The L452R mutation appears to increase the interaction between RBD and the ACE-2 and infectivity (Kirola, 2021). Moreover, the T478K mutation, together with L452R, helps stabilize the RBD–ACE-2 complex and elevate the virus infectivity rate (Cherian et al., 2021). The E484Q mutation enhances binding affinity to ACE-2 and potentially reduces antibody binding affinity, an observation similar to the E484K mutation (Kirola, 2021). In addition, the P681R mutation, located at the cleavage site between S1 and S2, has been associated with augmented transmissibility and viral load (Lopez Bernal et al., 2021). In a preprint work, Liu et al. (bioRxiv [Preprint]. 2021 Sep 5:2021.08.12.456173) observed that P681R modification leads to the increased furin cleavage site (S1-S2 junction), resulting in higher infectivity than the B.1.1.7 strain. The combination of mutations in the B.1.617.2 variant (delta variant) seems to impart the virus a selective advantage compared to the original virus and other variants, as evidenced by high transmissibility and infectivity, and potential immune evasion (Cherian et al., 2021; Kirola, 2021; Lopez Bernal et al., 2021).

Recently, an emerging SARS-CoV-2 variant was initially identified in South Africa, but it has been simultaneously detected in several other countries. On November 26, 2021, the WHO classified this variant as a VOC (B.1.1.529, omicron variant) because of the alarming epidemiological situation in South Africa (Callaway, 2021). The B.1.1.529 variant contains several mutations present in other variants, such as N501Y (alpha), E484A ~ E484K (beta and gamma), and T478K; P681H ~ P681R (delta). As discussed above, several of these changes observed in alpha, beta, and delta have been related to enhanced infectivity, transmissibility, and potential immune escape. However, it remains unclear whether or not the similarities with previous VOCs are related to the omicron variant's rapid spread. In total, the B.1.1.529 (omicron) variant has more than 50 mutations, with more than 30 in the *S* gene alone (Callaway, 2021; GISAID, 2021). In addition, Wang and Cheng (2021) have identified potential mutations that can affect ACE2 and/or antibody binding. Omicron variant accumulates numerous mutations, including Q498R and S477N, which have been previously associated with elevated binding to ACE2 receptor, potentially enhancing viral infectivity to the host cells. Recently, it was observed a close connection between Omicron and the Alpha variants, suggesting that the omicron variant was circulating for an long period before its discovery (Kandeel et al., 2021). Ongoing research is trying to elucidate the role and effect of each mutation in the omicron variant. Currently, it appears as though the omicron variant does not increase disease severity or fatality (hospitalization and number of deaths), and there is no evidence of immune escape from approved vaccines.

In South Africa, the emergence of the omicron variant rapidly and concomitantly increased the number of daily cases from 273 cases/day on November 16 to more than 1,200 cases/day on November 25. Additionally, as of December 9, 2021, the omicron variant was confirmed in 63 countries in Africa, Europe, Australia, Asia and North, Central and South America (GISAID, 2021; Torjesen, 2021).

EFFICACY AND ANTIBODY NEUTRALIZATION ACTIVITY OF VACCINES AGAINST SARS-COV-2 VARIANTS

Most COVID-19 vaccines use the S protein as the primary target, aiming to produce nAbs against the RBM regions, block the viral binding sites to the ACE-2 receptor in the host cells, and prevent infection (Chen R. E. et al., 2021). Since the first generation of vaccines was developed based on the original SARS-CoV-2 without S protein amino acid mutations (Chen R. E. et al., 2021; Dearlove et al., 2020), medical professionals now face the challenge of determining if the efficacy of these vaccines against the new variants is preserved or impaired (Chen R. E. et al., 2021; Dearlove et al., 2020). Presently, most approved COVID-19 vaccines protect against the described VOCs; however, constant surveillance and new studies about vaccine efficacies against the current VOCs and future SARS-CoV-2 variants globally are critical. It is also important to point out that most studies concerning nAbs activity were performed using SARS-CoV-2 pseudoviruses, which may not reflect the virus's behavior in the real world. Furthermore, a reduction in nAb activity does not necessarily result in poor vaccine efficacy or effectiveness, as demonstrated by several recent studies.

For example, the mRNA-based BNT 162b2 vaccine (Pfizer/BioNTech) reached 95% efficacy against the original SARS-CoV-2 infection (Polack et al., 2020). Notably, using immune sera from vaccinated subjects, no difference (Kuzmina et al., 2021) or mild to moderately decreased nAb activity (1.7 to 6.0-fold) against the B.1.1.7 pseudovirus has been described (Collier et al., 2021; Hoffmann et al., 2021; Lustig et al., 2021; Muik et al., 2021; Supasa et al., 2021). Thus, this variant probably does not increase immune escape or attenuate vaccine efficacy (Muik et al., 2021; Supasa et al., 2021). In contrast, the nAb activity provided by the BNT 162b2 vaccine was significantly reduced (6.5 to 10.4-fold) or abrogated against the B.1.351 pseudovirus (Chen R. E. et al., 2021; Dejnirattisai et al., 2021; Hoffmann et al., 2021; Kuzmina et al., 2021; Lustig et al., 2021; Zhou et al., 2021). Additionally, a reduction of 2.1 to 5.1-fold and 1.4 to 3.0-fold in nAb activity was reported for the P.1 and B.1.617.2 variants, using the serum from vaccinated individuals (Dejnirattisai et al., 2021; Hoffmann et al., 2021; Liu J. et al., 2021; Lustig et al., 2021; Planas et al., 2021).

BNT 162b2 vaccine effectiveness was also evaluated in the Qatar population, when the B.1.1.7 and B.1.351 variants accounted for 50% and 44.5% of the total COVID-19 cases from February to March 2021 (Abu-Raddad et al., 2021). A mass vaccination campaign was performed in the country, with

385,853 people receiving one dose and 265,410 receiving two doses of the vaccine by the end of March 2021 (Abu-Raddad et al., 2021). After 14 days or more after the second dose of the BNT 162b2 vaccine, the effectiveness against B.1.1.7 variant infection was 89.5%, and 75.0% against B.1.351. Moreover, the vaccine's effectiveness against severe COVID-19 cases or death was 97.4% against both variants (Abu-Raddad et al., 2021). In another real-world study performed in Qatar between December 2020 and September 2021, 950,232 people received at least one dose and 916,290 people two doses of the BNT162b2 vaccine (with an average of 21 days between doses) (Tang et al., 2021). The authors observed similar results against infection (74.3%) and severe/critical/fatal disease (92.7%) caused by B.1.351 variant and low effectiveness against B.1.617.2 infection (51.9%). Despite the reduced protection against infection, the vaccine was still highly effective against severe/critical/fatal disease (93.4%) caused by the B.1.617.2 variant.

Another mRNA-based vaccine, the mRNA-1273 vaccine (Moderna), also reached a high global efficacy of 94% and induced nAb production (Baden et al., 2021). Against the B.1.1.7 pseudovirus, no difference or a modest reduction in nAb activity was reported (Shen et al., 2021; Wu et al., 2021). On the other hand, a pronounced reduction in nAb activity (6.4-fold) against the B.1.351 variant was observed (Wu et al., 2021). Another study demonstrated that IgG antibody binding and neutralization activity are moderately impaired against the B.1.351 variant, but this vaccine is still efficient/effective against this variant (Edara et al., 2021b). Compared to B.1.351, the reduction in nAB activity was less pronounced in the P.1 and B.1.427/429 variants (Wu et al., 2021). The mRNA-1273 vaccine also exhibited reduced nAb activity (2.1 to 3.3-fold) against B.1.617.2 compared to the D614G strain (Choi et al., 2021). In the real-world study performed in Qatar described above (Tang et al., 2021), 564,468 people received at least one dose, and 509,322 received two doses of the mRNA-1273 vaccine (with an average of 28 days between doses). The authors reported 80.8% effectiveness against infection and 100% against severe, critical, or fatal disease caused by B.1.351 and 73.1% effectiveness against infection and 96.1% against severe, critical, or fatal disease caused by B.1.167.2 variant.

The recombinant spike protein-based NVX-CoV2373 vaccine (Novavax) presents an efficacy of 95.6% against the original SARS-CoV-2 strain (Callaway and Mallapaty, 2021; Moore and Offit, 2021). Against the B.1.1.7 pseudovirus, this vaccine has a low reduction in nAb activity (Shen et al., 2021), which is followed by a modest decrease in efficacy (85.6%) (Shen et al., 2021). In a South African phase 2a/b clinical trial, vaccine efficacy against mild to moderate disease was significantly reduced (49.4%) in a population of 4,387 participants when the B.1.351 variant was predominant (92.7%) (Shinde et al., 2021). In another study performed in South Africa, when more than 90% of the total COVID-19 cases were due to the B.1.351 variant (i.e., end of 2020 and the beginning of 2021), the vaccine reached an efficacy of 60% (https://www.novavax.com/sites/default/files/2021-02/20210202-NYAS-Novavax-Final.pdf). Currently, the B.1.617.2 variant is predominant in South Africa and worldwide, and data regarding effectiveness against this variant is crucial for understanding the real protection elicited by the Novavax vaccine.

The adenovirus vector-based ChAOx1-nCoV-19 vaccine (University of Oxford/AstraZeneca) was shown to have 66.7% efficacy against SARS-CoV-2 infection (Voysey et al., 2020). Against the B.1.1.7 pseudovirus vaccinee sera display reduced (9-fold and 2.5-fold) nAb activity without affecting vaccine efficacy (74.6%) in 499 infected people with the variant (Zhou et al., 2021; Supasa et al., 2021). Similar results were reported in another study comparing B.1.1.7 and non-B.1.1.7 lineages, with 70.4% and 81.5% efficacy against infection, respectively (Emary et al., 2021). For the B.1.351 lineage, the ChAOx-1nCoV-19 vaccine elicits less potent nAb production against the B.1.351 pseudovirus. B.1.351 is mainly characterized by the triple mutations in the RBD of the S protein and associated with reduced nAb titers (9-fold) and global efficacy against infection (10.4-20.4%) and impaired efficacy (21.9%) to prevent mild to moderate COVID-19 (Dejnirattisai et al., 2021; Madhi et al., 2021; Planas et al., 2021; Zhou et al., 2021). A small reduction in nAb activity was also reported for the P.1 (2.9-fold) and B.1.617.2 variants (5.0-fold) (Dejnirattisai et al., 2021; Planas et al., 2021). Notably, the real-world effectiveness against B.1.617.2 infection (67%) was similar to the wild-type (66.7%) and B.1.1.7 (74.6%) strains (Lopez Bernal et al., 2021).

The Ad26.COV2. S or JNJ-78436735 vaccine (Janssen), another adenovirus vector-based vaccine, has an efficacy of 72% against B.1.1.7 infection. The vaccine's efficacy is reduced to 57% against the B.1.351 variant but is 89% effective at protecting against severe COVID-19 (https://www.jnj.com/johnson-johnson-announces-single-shot-janssen-covid-19-vaccine-candidate-met-primary-endpoints-in-interim-analysis-of-its-phase-3-ensemble-trial).

The vector-based Sputnik V vaccine or Gam-COVID-Vac (Gamaleya Institute) (Moore and Offit, 2021) presents 91.6% efficacy against SARS-CoV-2 infection (Logunov et al., 2021). However, the efficacies against B.1.1.7, B.1.351, and P.1 were reduced to 81%, 59%, and 52%, respectively. The serum nAb activity was not significantly altered against B.1.1.7 but was decreased against the B.1.1.351 (3.1-fold), P.1 (2.8-fold), and B.1.617.2 (2.5-fold) variants (Gushchin et al., 2021).

The Sinopharm and CoronaVac vaccines use inactivated virus-based technology. The CoronaVac vaccine was shown to be 83.5% (Tanriover et al., 2021) and 65.9% effective in studies conducted in Turkey and Chile, respectively (Jara et al., 2021). It was also demonstrated that nAb activity was unaffected against B.1.429 but was decreased against the B.1.1.7, B.1.351, and P.1 variants by 2.0, 5.2, and 3.9-fold, respectively (Chen Y. et al., 2021; Wang et al., 2021). For the Sinopharm vaccine, nAb activity was reduced against the B.1.1.7 (~2.0-fold) and B.1.351 (2.5 to 3.0-fold) variants (Wang et al., 2021).

More results related to the B.1.617.2 variant are necessary for all these vaccines to verify the real-world effectiveness against infection and severe or critical COVID-19 disease. Furthermore, a thorough analysis of this variant's potential immune response evasion in vaccinated individuals must be conducted. In relation

to omicron variant, there are some preliminary results from few studies with limited sample size suggesting that the incidence of virus reinfection in South Africa can be associated with humoral (antibody-mediated) immune evasion and nAb activity in vaccinated or previously infected individuals (Zhang et al., 2021).

Besides vaccines, convalescent sera have been used to evaluate the impact of variants on the nAb activity induced by the previous infection with the original SARS-CoV-2. Several studies observed a mild reduction (~2.9 to 3.0-fold) in nAb activity against the B.1.1.7 variant (Dejnirattisai et al., 2021; Supasa et al., 2021; Zhou et al., 2021). Partial (11 to 33 X). Variants containing the E484K mutation (e.g., B.1.351 and B.1.1.248 variants) were found to escape the immune response completely (Chen R. E. et al., 2021; Kuzmina et al., 2021; Zhou et al., 2021;14). Additionally, convalescent sera of individuals infected with the original SARS-CoV-2 displayed impaired or nonexistent IgG antibody binding and neutralization activity against the B.1.351 variant (4 to 8-fold; 13.3-fold) (Dejnirattisai et al., 2021; Edara et al., 2021a), persisting eight months post-infection (2.1-fold) (Edara et al., 2021b). Indeed, it has been estimated that 41.1 to 48% of convalescent sera are incapable of neutralizing the B.1.351 pseudovirus (Zhou et al., 2021; Wibmer et al., 2021). Furthermore, a similar reduction in nAb activity was observed against the P.1 and B.1.1.7 variants (3.1 and 2.9-fold, respectively) (Dejnirattisai et al., 2021).

A summary of the efficacy and nAb activity of the main vaccines against SARS-CoV-2 variants is presented in **Table 1**. In **Table 2**, we have provided the details of the protocols used in the studies.

VARIANTS OF CONCERN AND POTENTIAL RISK OF NEW PANDEMIC WAVES

From December 2019 until December 16th 2021, there have been more than 271,376,000 COVID-19 cases and 5,325,969 COVID-19-related deaths (1.96% mortality rate) worldwide (World Health Organization, https://covid19.who.int). Moreover, approximately 3.4 million SARS-CoV-2 genome sequences have been submitted to the Global Initiative on Sharing All Influenza Data (GISAID; https://gisaid.org), which has detected more than 4,100 mutations in the *S* gene. About 1,200 of these mutations lead to amino acid substitutions, with 187 in the RBD of the S protein (Focosi and Maggi, 2021; Liu C. et al., 2021).

We performed a monthly analysis of the VOC emergence using the GISAID in several countries for one year (September 2020 to November 2021). The analysis of the epidemiological data of SARS-CoV-2 variants has several limitations, including a) a limited number of genome sequencing data from a particular country; b) samples from a particular group, city, or region that does not accurately represent the country; c) the virus' behavior in a specific group, city or region; and d) data release delay (data were extracted and analyzed on September 2, 2021, but new sequencing genomes are continuously submitted and updated, especially in the last few months). However, it provides a general overview of specific variants globally and highlights some important points.

For example, after the emergence of the B.1.1.7 variant in the United Kingdom (September 2020), it rapidly spread to several countries across all continents (169 countries on Sep 2, 2021). In 34 of the 67 countries analyzed, the B.1.1.7 variant became highly predominant, present at rates greater than 80%; thus, demonstrating a clear selective advantage of this variant versus the original B.1 strain, which was the most prevalent strain at that moment in time (**Figure 4**). Additionally, in 12 of the 67 countries, this VOC was detected in 50.1 to 80% of the new monthly cases. In some countries, where other VOCs emerged before or even simultaneously, as in the case of B.1.351 in South Africa and Reunion and P.1 in Brazil, Chile, and French Guiana, the B.1.1.7 variant did not become predominant. This observation suggests that B.1.1.7 has no selective advantage over the B.1.351 and P.1 VOCs.

The B.1.351 variant emerged in South Africa in August 2020 and rapidly disseminated worldwide, reaching 111 countries as

TABLE 1 | VOCs and vaccine-induced immune response resistance.

VOCs		WHCV (Wuhan/China)	B.1.1.7 UK	B.1.351 South Africa	P.1 Brazil	B.1.617.2 India
Pfizer	Efficacy	90.4-95.5%	89.5-93.7%*	75.0*%	N.D.	70-88%*
	NABs	–	↓ 0-3.3 X	↓ 3.3-16 X	↓ 2.2-6.7 X	↓ 2.1- 3.3 X
Moderna	Efficacy	94.1%	~	N.D.	N.D.	N.D.
	NABs	–	↓ 0-2.3 X	↓ 3-9 X	↓ 3.5-4.5 X	↓ 3 X
AstraZeneca	Efficacy	54-79%	70.4-74.5%*	10.4%	N.D.	67-77.3%*
	NABs	–	↓ 0-2.5 X	↓ 9 X	↓ 2.8-2.9 X	↓ 4.2-5 X
Novavax	Efficacy	89.3-95.6%	85.6%	49.4-60%	N.D.	N.D.
	NABs	–	↓ 2 X			
Janssen	Efficacy	66%	72%	57%	68.1%	N.D.
	NABs	–	↓ 2.8-3.3 X	↓ 5-10.6 X	↓ 3.3 X	
Sputnik V	Efficacy	91.6%	81%	59%	52%	N.D.
	NABs	–	↓ 0 X	↓ 3.1-3.5 X	↓ 2.8 X	↓ 2.5 X
Sinovac	Efficacy	65.9*-83.5%	N.D.	50%	N.D.	N.D.
	NABs	–	↓ 0 - 2.0 X	↓ 2.5 - 5.2 X	↓ 3.9 X	
Sinopharm	Efficacy	79.0-86%	N.D.	N.D.	N.D.	N.D.
	NABs	–	↓ 0-2.0 X	↓ 2.5 - 3.0 X		

*NABs, neutralizing antibodies; N.D., not determined or under investigation; VOC, variant of concern; *: effectiveness evaluation instead efficacy analysis.*

TABLE 2 | Studies about efficacy/effectiveness and neutralizing antibody activity of vaccines and convalescent plasma against SARS-CoV-2 variants.

Study	Vaccine or plasma	Sample size	Methodology	Main findings
Abu-Raddad et al., 2021	BNT 162b2	>383,000 individuals with at least 1 dose and >265,000 with 2 doses; analysis >14 d after the 2nd dose	Effectiveness in a mass immunization campaign and virus sequencing of positive cases in Qatar	89.5% against B.1.1.7; 75.0% against B.1.351; 97.4% against severe disease
Alter et al., 2021	Ad6.COV2.S	25 adults at different vaccination regimens (14 d after the last dose)	Luciferase-based pseudovirus neutralizing antibody (psVNA) assay against WA1/2020, D614G, B.1.1.7, B.1.351, and P.1	↓ 2.8, 5-10.6, and 3.3 X in neutralizing B.1.1.7, B.1.351, and P.1 variants, respectively
Lopez Bernal et al., 2021	BNT 162b2	171,834 individuals: 96,371 unvaccinated; 51,470 vaccinated with 1 dose (analysis at >21 d); and 23,993 with 2 doses (analysis at >14 d)	Effectiveness by a test negative casecontrol design study and whole-genome sequencing in England	1 dose: 47.5% for B.1.1.7 and 35.6% for B.1.617.2 2 doses: 93.7% for B.1.1.7 and 88% for B.1.617.2
	ChAdOx1-S			1 dose: 48.7% for B.1.1.7 and 30% for B.1.617.2 2 doses: 74.5% for B.1.1.7 and 67% for B.1.617.2
Chen R. E. et al., 2021	BNT 162b2	10 vaccinee serum (one week after the 2nd dose)	FRNT using D614G wild-type, B.1.1.7, B.1.351, and B1.1.28 strains	↓ 2, 10, and 2.2 X in neutralizing B.1.1.7, B.1.351, and P.1
	Convalescent plasma	10 convalesdent plasma (30 d after infection)		↓ 2.5 X in neutralizing P.1
Chen Y. et al., 2021	CoronaVac	93 vaccinee serum (14 d after the 2nd dose)	Pseudovirus neutralization against different strains (Wuhan-1 wild-type, D614G, B.1.1.7, B.1.351, and P.1)	↓ 0, 5.2, and 3.9 X in neutralizing B.1.1.7, B.1.351, and P.1
Choi et al., 2021	mRNA-1273	8 vaccinee serum (7 d after the 2nd dose)	Pseudovirus neutralization against different strains (D614G, B.1.1.7, B.1.351, P.1, and B.1.617.2)	↓ 1.2, 6.9-8.4, 3.2, and 2.1-3.3 X in neutralizing B.1.1.7, B.1.351, P.1, and B.1.617.2
Collier et al., 2021	BNT 162b2	25 vaccinee serum (3 wks after the 2nd dose)	Pseudovirus neutralization against D614G strain and B.1.1.7 variant	↓ 1.9 X in neutralizing B.1.1.7
	Convalescent plasma	27 convalesdent plasma		↓ 4.5 X in neutralizing B.1.1.7
Dejnirattisai et al., 2021	BNT 162b2	25 vaccinee serum (4-14 d after the 2nd dose)	FRNT using Victoria and B.1.351 strains	↓ 3.3, 7.6, and 2.6 X in neutralizing B.1.1.7, B.1.351, and P.1
	AZD1222	25 vaccinee serum (14-2		↓ 2.5, 9, and 2.9 X in neutralizing B.1.1.7, B.1.351, and P.1
	Convalescent plasma	34 convalesdent plasma (4- 9 mo after infection)		↓ 2.9, 13.3, and 3.1 X in neutralizing B.1.1.7, B.1.351, and P.1
	BNT162b2	10 participants (7-27 d ater the 2nd dose)		↓ 3.3 X in neutralizing B.1.617.2
Edara et al., 2021a	mRNA-1273	15 participants (35-51 d ater the 2nd dose)	FRNT using WA1/2020 and B.1.617.2	↓ 3 X in neutralizing B.1.617.2
	Convalescent plasma	24 convalescent plasma (31-91 d after the onset of symptons)		↓ 2.4 X in neutralizing B.1.617.2
Edara et al., 2021b	mRNA-1273	19 participants (14 d after the 2nd dose)	IgG Ab binding by electrochemiluminescence- based multiplex immune assay	↓ 3.7 and 3.8 X Ab binding and virus neutralization (B.1.351)
	Acutely infected people	19 acutely infected participants (5-19 d after the onset of symptons)	Live virus neutralization using B.1 and B.1.351	↓ 4.4 and 3.3 X Ab binding and virus neutralization (B.1.351)
	Convalescent plasma	30 participants (1-3 and 3-8 mo after the onset of symptons)		↓ 4.4 and 3.3 X Ab binding and 4.8 and 2.1 X virus neutralization (B.1.351)
Emary et al., 2021	AZD1222	8,534 participants (1:1 AZD1222 vaccine vs meningococcal vaccine)	Clinical trial, phase 2/3, in the U.K.	70.4% efficacy against B.1.1.7 variant vs 81.5% efficacy against non-B.1.1.7 lineages

(Continued)

TABLE 2 | Continued

Study	Vaccine or plasma	Sample size	Methodology	Main findings
Geers et al., 2021	BNT 162b2	25 health care workers (2- 3 wks after the 1st dose and 3-4 wks after the 2nd dose)	PRNT assay against D614G strain and VOCs (B.1.1.7 and B.1.351)	↑ 2.5 and 2.2 X after the 1st and 2nd dose in neutralizing B.1.1.7 ↓ 2.7 and 3.3 X after the 1st and 2nd dose in neutralizing B.1.351
	Convalescent plasma	13 health care workers (3 wks after the onset of symptons)		↑ 2.8 X in neutralizing B.1.1.7 and ↓ 3X in neutralizing B.1.351
Gushchin et al., 2021	Sputnik V	27 vaccinee serum (30 d after the 2nd dose)	Virus neutralization against different strains (D614G, B.1.1.7, B.1.351, P.1, and B.1.617.2)	↓ 0, 3.1, 2.8, and 2.5 X in neutralizing B.1.1.7, B.1.351, P.1, and B.1.617.2
Hoffmann et al., 2021	BNT 162b2	15 donors, 13-15 d after the 2 nd dose	Entry of pseudotyped particles with different S protein strains (W.T., B.1.1.7, B.1.31, or P1) into target Vero cells	B.1.1.7: slight effect B.1.351 and P1: ↓ nAb activity
	Convalescent plasma	Individuals previously infected with WT SARSCoV-2		B.1.1.7: slight effect B.1.351 and P1: ↓ nAb activity
Kuzmina et al., 2021	BNT 162b2	10 vaccinee serum (21 d after the 1st dose or 9-11 d after the 2nd dose)	Pseudovirus neutralization against wildtype strain or VOCs (B.1.1.7 and B.1.351)	No effect in neutralizing B.1.1.7 ↓ 6.8 X in neutralizing B.1.351
	Convalescent plasma	10 COVID19 recovered patients		↓ 1.5 X in neutralizing B.1.1.7 ↓ 6.8 X in neutralizing B.1.351
Liu C. et al., 2021	BNT 162b2	25 vaccinee serum (7-17 d after the 2nd dose)	Live virus neutralization assay by FRNT using Victoria strain and VOCs (B.1.1.7, B.1.351, P.1, and B.1.617.2 variants)	↓ 3.2, 7.5, 2.6, and 2.5 X in neutralizing B.1.1.7, B.1.351, P.1, and B.1.617.2
	AZD1222	25 vaccinee serum (14-28 d after the 2nd dose)		↓ 2.3, 9, 2.8, and 4.2 X in neutralizing B.1.1.7, B.1.351, P.1, and B.1.617.2
	Convalescent plasma	34 volunteers (4-9 wks after the infection)		↓ 2.9, 13.3, 3.1, and 2.6 X in neutralizing B.1.1.7, B.1.351, P.1, and B.1.617.2
Lustig et al., 2021	BNT 162b2	15-19 vaccinee serum (30 d after the 2nd dose)	Neutralizing original (B.1) and VOCs strains (B.1.1.7, B.1.351, P.1, and B.1.617.2) and virus entry in VERO-E6 cells	↓ 1.7, 10.4, 2.3, and 2.1-2.6 X in neutralizing B.1.1.7, B.1.351, P.1 and B.1.617.2
Madhi et al., 2021	AZD1222	2,026 participants (1:1 AZD1222 vaccine or placebo)	Clinical, multicenter, double-blind, randomized trial, in the South Africa	21.9% efficacy against mild to moderate COVID-19 10.4% efficacy against B.1.351
	ChAdOx1-S	10 vaccinee serum (after the 2nd dose)	Pseudovirus neutralization against D614G strain and B.1.1.7 and B.1.617.2 variants	↓ 3.4 and 9.0 X in neutralizing B.1.1.7 and B.1.617.2
Mlcochova et al., 2021	BNT 162b2	10 vaccinee serum (after the 2nd dose)	Pseudovirus neutralization against D614G strain and B.1.1.7 and B.1.617.2 variants	↓ 5.8 and 8.4 X in neutralizing B.1.1.7 and B.1.617.2
	Convalescent plasma	12 volunteers	Pseudovirus neutralization against D614G strain and B.1.1.7, B.1.351, and B.1.617.2 variants	↓ 2.3, 8.2, and 5.7 X in neutralizing B.1.1.7, B.1.351, and B.1.617.2
Muik et al., 2021	BNT 162b2	40 vaccinee serum (7 or 21 d after the 2nd dose)	Neutralizing VSV pseudovirus (Wuhan strain and B.1.1.7 S mutants) entry in HEK-hACE2 cells	↓ (light reduction) in neutralizaing B.1.1.7
Planas et al., 2021	BNT 162b2	16 vaccinee serum (5 wks after the 2nd dose)	S-Fuse neutralization assay against D614G strain and VOCs strains (B.1.1.7, B.1.351, and B.1.617.2)	↓ 0, 16, and 3 X in neutralizing B.1.1.7, B.1.351, and B.1.617.2

(Continued)

TABLE 2 | Continued

Study	Vaccine or plasma	Sample size	Methodology	Main findings
	AZD1222	20 vaccinee serum (4 wks after the 2nd dose)		↓ 0, 9, and 5 X in neutralizing B.1.1.7, B.1.351, and B.1.617.2
	Convalescent plasma	26 convalesdent plasma (12 mo after the onset of symptons)		↓ 0, 4, and 4 X in neutralizing B.1.1.7, B.1.351, and B.1.617.2
Shen et al., 2021	mRNA-1273	28 vaccinee serum (28 d after the 2nd dose)		↓ 2X in neutralizing B.1.1.7
	NVX-CoV2373	28 vaccinee serum (2 wks after the 2nd dose)	Pseudovirus neutralization assay using D614G strain and B.1.1.7 variant	↓ 2 X in neutralizing B.1.1.7
	Convalescent plasma	15 convalesdent plasma (4- 9 mo after infection)		↓ 1.5 X in neutralizing B.1.1.7
Shinde et al., 2021	NVX-CoV2373	4,387 participants (2,199 vaccinated and 2,188 with placebo)	Clinical trial, phase 2a/b, in the South Africa	↓ Efficacy against B.1.351 (49.4%)
Supasa et al., 2021	BNT 162b2	25 vaccinee serum (7-17 d after the 2nd dose)		↓ 3.3 X in neutralizing B.1.1.7
	AZD1222	10-15 vaccinee serum (14- 28 d after the 2nd dose)	FRNT using Victoria and B.1.1.7 strains	↓ 2.1-2.5 X in neutralizing B.1.1.7
	Convalescent plasma	34 convalesdent plasma (4- 9 mo after infection)		↓ 2.9 X in neutralizing B.1.1.7
Wall et al., 2021	BNT 162b2	250 Individuals who worked at UCLH in UK and had received the vaccine (3 weeks, 6 and 12 weeks pos-vaccination)	RT-qPCR to exclude active infection; Blood was collected for serological assays including anti-spike IgG, IgM and live-virus neutralization; High-throughput live virus microneutralization assays	Reduction neutralizing antibodies activity against B.1.617.2 and B.1.351.
Wang et al., 2021	CoronaVac	25 vaccinee serum (2-3 wks after the 2nd dose)		↓ 2 and 3.3 X in neutralizing B.1.1.7 and B.1.351
	BBIBP-CorV	25 vaccinee serum (2-3 wks after the 2nd dose)	Pseudovirus neutralization against different strains (Wuhan-1 wild-type, D614G, B.1.1.7, and B.1.351)	↓ 0 and 2.5 X in neutralizing B.1.1.7 and B.1.351
	Convalescent plasma	34 convalescent plasma (5 mo. After infection)		↓ 1.1 and 2 X in neutralizing B.1.1.7 and B.1.351
Wibmer et al., 2021	Convalescent plasma	44 participants (mild-tomoderate and severe COVID-19)	Pseudovirus neutralization assay using D614G strain and B.1.351 variant	48% of the samples: loss of the neutralizing activity against B.1.351
Wu et al., 2021	mRNA-1273	28 vaccinee serum (one week after the 2nd dose)	Pseudovirus neutralization assay using D614G strain and VOCs (B.1.1.7, B.1.351, and P.1 strains)	↓ 1.2, 6.4, 3.5 X in neutralizing B.1.1.7, B.1.351, and P.1
Zhou et al., 2021	BNT 162b2	25 vaccinee serum (4-17 d after the 2nd dose)		↓ 7.6 X in neutralizing B.1.1.7
	AZD1222	25 vaccinee serum (28 d after the 2nd dose)	FRNT using Victoria and B.1.351 strains	↓ 9 X in neutralizing B.1.1.7
	Convalescent plasma	34 convalesdent plasma (4- 9 mo after infection)		↓ 13.3 X in neutralizing B.1.351

FRNT, focus reduction neutralization test; PRNT, plaque reduction neutralization test; VSV, vesicular stomatitis virus.

of September 2, 2021. Except for South Africa, Reunion, Angola, Philippines, Hong Kong, Bangladesh, and Qatar, the B.1.351 variant did not increase by more than 10% in most countries analyzed (**Figure 4**). A similar result was observed with the P.1 variant, which emerged in Brazil in December 2020. This variant disseminated at low rates (<10%) in 78 countries (Sep 2, 2021) but had a high prevalence in Brazil, Chile, and French Guiana (**Figure 4**).

The emergent B.1.617.2 variant appeared in India in October 2020. It has been dispersed throughout 147 countries (Sep 2, 2021) and has a high predominance rate in most analyzed countries. For example, more than 80% of COVID-19 cases were B.1.617.2-induced in 52 of the 67 countries analyzed; 4 had between 50.1 to 80%, and 11 had less than 50%. Notably, there is an increasing trend in the countries with fewer B.1.617.2-related cases. Currently, this variant is the most prevalent VOC, displaying rapid transmission and spread and indicative of selective advantages against other VOCs such as B.1.1.7, B.1.351, and P.1. It will likely become predominant worldwide. Fortunately, B.1.617.2's high predominance has not increased the number of cases, hospitalizations or deaths, and the current vaccines effectively protect against all known VOCs.

PERSPECTIVES AND CONCLUDING REMARKS

Viral evolution is a constant process and can eventually improve "viral fitness" and selective adaptation. Emerging SARS-CoV-2 variants have posed challenges for authorities and scientists around the world. Although vaccines currently provide high protection against all VOCs, constant surveillance of vaccine efficacy is essential for combating the main SARS-CoV-2 strains and potentially new emerging variants.

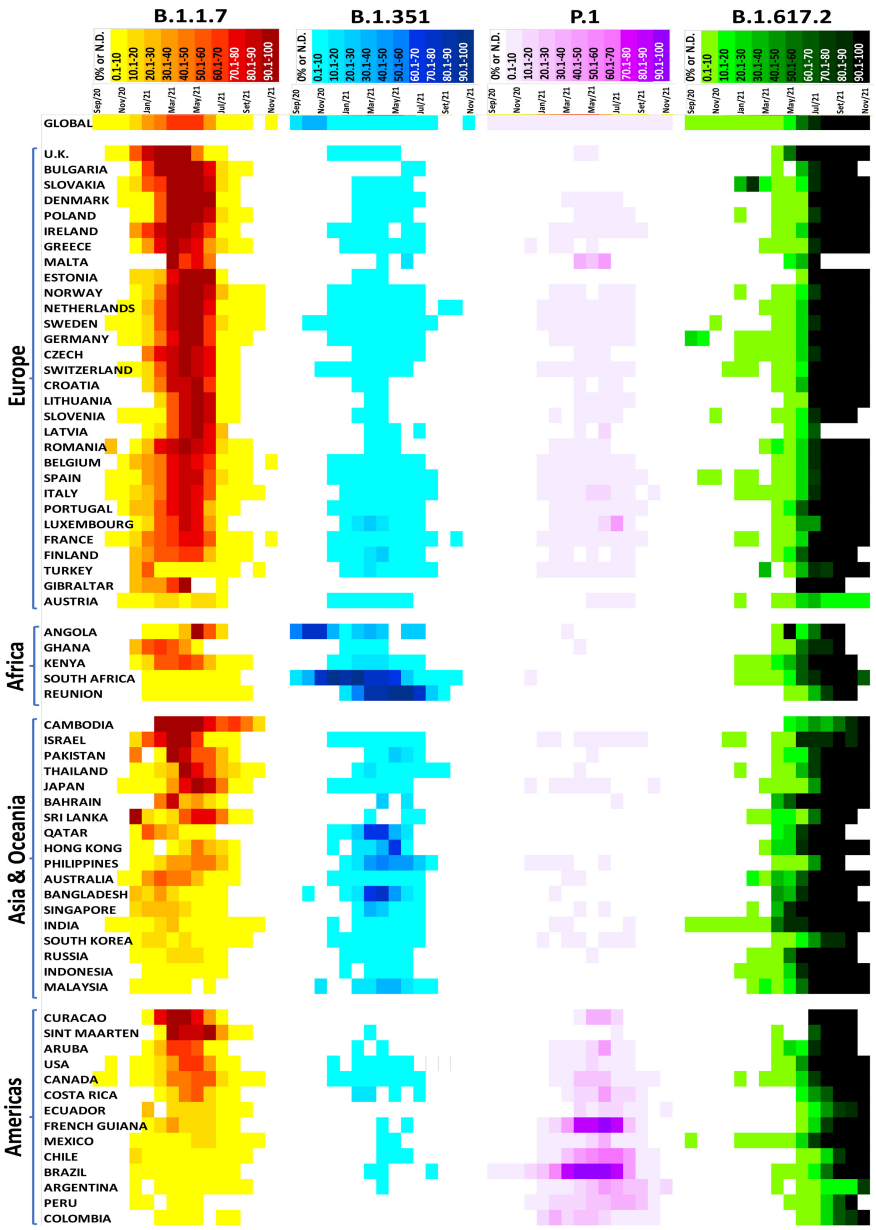

FIGURE 4 | Distribution of the SARS-CoV-2 variants of concern in several countries. Data were analyzed from GISAID from September 2020 to November 2021 (https://www.gisaid.org/hcov19-variants/).

The main concern is that a VOC can partially or completely evade the immune response, increasing reinfection of the individuals already infected by previous strains, limited protection induced by vaccination, and impaired efficacy of therapies based on monoclonal nAbs or convalescent plasma and consequently heightening the risk for future COVID-19 pandemic waves. Indeed, it has been proposed that the COVID-19 pandemic will persist for a long time with more mutations and emerging VOCs. Thus, actions must be undertaken to combat the COVID-19 pandemic and emerging VOCs. Below, we have highlighted seven key points that could prevent the rise of new SARS-CoV-2 variants:

1. *Rapid and massive worldwide vaccinations against COVID-19 to reduce new infections*. This point is based on the fact that slowing viral dissemination will reduce the probability of viral mutations and the emergence of new variants. However, vaccination campaigns are limited in some parts of the world. Thus, in these areas, strict public health measures and efficient strategies to stop or decrease virus transmission

(e.g., face masks, frequent hand sanitation, social distancing, and other precautions) are the best defense against this virus.
2. *Constant and active global surveillance and identification of circulating and emerging VOCs and subsequent characterization*. Efficient monitoring systems will allow rapid detection, isolation, and response against new VOCs, avoiding uncontrolled dissemination and future pandemic waves.
3. *Determining vaccine and neutralizing antibody efficacy against VOCs*. If the vaccines do not present broad protection against the virus variants, periodic vaccine updates or redevelopment will be required, as occurs with the H1N1 vaccine. Other possibilities include developing new vaccines that induce nAbs against different variants by targeting highly conserved antigenic epitopes of the S protein and/or combining different vaccines or monoclonal Abs to target specific variants.
4. *Establish plasma repositories from individuals previously infected with different variants and immunized with different COVID-19 vaccines*. This point aims to rapidly determine the nAb activity against new VOCs and the potential for immune evasion. Determining the nAb titers and the period of protection induced by previous infection or vaccination is essential to determine further actions.
5. *Surveillance of reinfections, especially in already immunized or previously infected individuals*. This action could be a good strategy for assessing the potential immune evasion of new VOCs.
6. *Studies with combinations of available vaccines to improve efficacy and protection*. Monitoring the nAb levels for the S protein in fully vaccinated people can provide insights into protection since high levels of these antibodies seem to confer defense against emerging VOCs.
7. *Application of an additional booster vaccine dose to increase/prolong the neutralizing antibody titers over time*. This proposal is based on three points: a) high-risk groups, including immunocompromised and the elderly, present a reduced immune response following immunization; b) antibody titers decrease months after the complete vaccination schedule (14-21 days after the single dose Janssen vaccine or two doses of the other vaccines); and c) the emergence of VOCs may require high nAb titers for protection. Vaccine booster administration is already occurring in some countries, including the USA, Israel, and Brazil, especially in high-risk groups/individuals.

AUTHOR CONTRIBUTIONS

All authors attended the criteria to justify the authorship. Specifically, SH, DC, RC, and ED conceived the study. SH, TS, RG, LM, and TP-C elaborated the figures and tables, made the literature review and wrote the manuscript. DC, RC, and ED assisted the writing and revision of the manuscript. All authors have read, revised, and approved the final version of the submitted manuscript.

FUNDING

The authors of this study are supported by grants from the São Paulo Research Foundation (FAPESP, Sao Paulo, SP, Brazil; 2018/09868-7 and 2021/00200-6), the Coordination for the Improvement of Higher Education Personnel (CAPES, Brasilia, Brazil), the National Council for Scientific and Technological Development (CNPq, Brasilia, Brazil), the John Simon Guggenheim Memorial Foundation (JSGMF, New York, NY, USA), and the Pro-Rectory of Post-Graduate and Research of the Cruzeiro do Sul University (PRPGP/Cruzeiro do Sul, São Paulo, SP, Brazil).

ACKNOWLEDGMENTS

The authors would like to thank Dr. Renato Padovese from the Cruzeiro do Sul University, São Paulo, SP, Brazil, for the continuous academic and financial support. The Authors also want to acknowledge the *Global Initiative on Sharing All Influenza Data* (GISAID) and the scientists who contributed and submitted genomic data to this public database.

REFERENCES

Abdel-Moneim, A. S., Abdelwhab, E. M., and Memish, Z. A. (2021). Insights Into SARS-CoV-2 Evolution, Potential Antivirals, and Vaccines. *Virology* 558, 1–12. doi: 10.1016/j.virol.2021.02.007

Abu-Raddad, L. J., Chemaitelly, H., and Butt, A. A., National Study Group for COVID-19 Vaccination. (2021). Effectiveness of the BNT162b2 Covid-19 Vaccine against the B.1.1.7 and B.1.351 Variants. *N. Engl. J. Med.* 385 (2), 187–189. doi: 10.1056/NEJMc2104974

Adam, D. (2021). What Scientists Know About New, Fast-Spreading Coronavirus Variants. *Nature* 594, 19–20. doi: 10.1038/d41586-021-01390-4

Alter, G., Yu, J., Liu, J., Chandrashekar, A., Borducchi, E. N., Tostanoski, L. H., et al. (2021). Immunogenicity of Ad26.COV2.S Vaccine Against SARS-CoV-2 Variants in Humans. *Nature* 596 (7871), 268–272. doi: 10.1038/s41586-021-03681-2

Altmann, D. M., Boyton, R. J., and Beale, R. (2021). Immunity to SARS-CoV-2 Variants of Concern. *Science* 371 (6534), 1103–1104. doi: 10.1126/science.abg7404

Baden, L. R., El Sahly, H. M., Essink, B., Kotloff, K., Frey, S., Novak, R., et al. (2021). Efficacy and Safety of the mRNA-1273 SARS-CoV-2 Vaccine. *N. Engl. J. Med.* 384, 403–416. doi: 10.1056/NEJMoa2035389

Callaway, E. (2021). Heavily Mutated Omicron Variant Puts Scientists on Alert. *Nature* 600 (7887), 21. doi: 10.1038/d41586-021-03552-w

Callaway, E., and Ledford, H. (2021). How to Redesign COVID Vaccines So They Protect Against Variants. *Nature* 590 (7844), 15–16. doi: 10.1038/d41586-021-00241-6

Callaway, E., and Mallapaty, S. (2021). Novavax Offers First Evidence That COVID Vaccines Protect People Against Variants. *Nature* 590 (7844), 17. doi: 10.1038/d41586-021-00268-9

Chen, J., and Lu, H. (2021). New Challenges to Fighting COVID-19: Virus Variants, Potential Vaccines, and Development of Antivirals. *Biosci. Trends.* 15 (2), 126–128. doi: 10.5582/bst.2021.01092

Chen, Y., Shen, H., Huang, R., Tong, X., and Wu, C. (2021). Serum Neutralising Activity Against SARS-CoV-2 Variants Elicited by CoronaVac. *Lancet Infect. Dis.* 21 (8), 1071–1072. doi: 10.1016/S1473-3099(21)00287-5

Chen, R. E., Zhang, X., Case, J. B., Winkler, E. S., Liu, Y., VanBlargan, L. A., et al. (2021). Resistance of SARS-CoV-2 Variants to Neutralization by Monoclonal and Serum-Derived Polyclonal Antibodies. *Nat. Med.* 27 (4), 717–726. doi: 10.1038/s41591-021-01294-w

Cherian, S., Potdar, V., Jadhav, S., Yadav, P., Gupta, N., Das, M., et al. (2021). SARS-CoV-2 Spike Mutations, L452R, T478K, E484Q and P681R, in the Second Wave of COVID-19 in Maharashtra, India. *Microorganisms* 9 (7), 1542. doi: 10.3390/microorganisms9071542

Choi, B., Choudhary, M. C., Regan, J., Sparks, J. A., Padera, R. F., Qiu, X., et al. (2020). Persistence and Evolution of SARS-CoV-2 in an Immunocompromised Host. *N. Engl. J. Med.* 383, 2291–2293. doi: 10.1056/NEJMc2031364

Choi, A., Koch, M., Wu, K., Dixon, G., Oestreicher, J., Legault, H., et al. (2021). Serum Neutralizing Activity of mRNA-1273 Against SARS-CoV-2 Variants. *J. Virol.* 95 (23), e0131321. doi: 10.1128/JVI.01313-21

Collier, D. A., De Marco, A., Ferreira, I. A. T. M., Meng, B., Datir, R. P., Walls, A. C., et al. (2021). Sensitivity of SARS-CoV-2 B.1.1.7 to mRNA Vaccine-Elicited Antibodies. *Nature* 593 (7857), 136–141. doi: 10.1038/s41586-021-03412-7

Conti, P., Caraffa, A., Gallenga, C. E., Kritas, S. K., Frydas, I., Younes, A., et al. (2021). The British Variant of the New Coronavirus-19 (Sars-Cov-2) Should Not Create a Vaccine Problem. *J. Biol. Regul. Homeost. Agents.* 35 (1), 1–4. doi: 10.23812/21-3-E

Davies, N. G., Jarvis, C. I.CMMID COVID-19 Working Group, , Edmunds, W. J., Jewell, N. P., Diaz-Ordaz, K., et al. (2021). Increased Mortality in Community-Tested Cases of SARS-CoV-2 Lineage B.1.1.7. *Nature* 593 (7858), 2707–274. doi: 10.1038/s41586-021-03426-1

Dearlove, B., Lewitus, E., Bai, H., Li, Y., Reeves, D. B., Joyce, M. G., et al. (2020). A SARS-CoV-2 Vaccine Candidate Would Likely Match All Currently Circulating Variants. *Proc. Natl. Acad. Sci. U. S. A.* 117 (38), 23652–23662. doi: 10.1073/pnas.2008281117

Dejnirattisai, W., Zhou, D., Supasa, P., Liu, C., Mentzer, A. J., Ginn, H. M., et al. (2021). Antibody Evasion by the P.1 Strain of SARS-CoV-2. *Cell* 184 (11), 2939–2954.e9. doi: 10.1016/j.cell.2021.03.055

Edara, V. V., Norwood, C., Floyd, K., Lai, L., Davis-Gardner, M. E., Hudson, W. H., et al. (2021b). Infection- and Vaccine-Induced Antibody Binding and Neutralization of the B.1.351 SARS-CoV-2 Variant. *Cell Host Microbe* 29 (4), 516–521. doi: 10.1016/j.chom.2021.03.009

Edara, V. V., Pinsky, B. A., Suthar, M. S., Lai, L., Davis-Gardner, M. E., Floyd, K., et al. (2021a). Infection and Vaccine-Induced Neutralizing-Antibody Responses to the SARS-CoV-2 B.1.617 Variants. *N. Engl. J. Med.* 385 (7), 664–666. doi: 10.1056/NEJMc2107799

Emary, K. R. W., Golubchik, T., Aley, P. K., Ariani, C. V., Angus, B., Bibi, S., et al. (2021). Efficacy of ChAdOx1 Ncov-19 (AZD1222) Vaccine Against SARS-CoV-2 Variant of Concern 202012/01 (B.1.1.7): An Exploratory Analysis of a Randomised Controlled Trial. *Lancet* 397 (10282), 1351–1362. doi: 10.1016/S0140-6736(21)00628-0

Finkel, Y., Mizrahi, O., Nachshon, A., Weingarten-Gabbay, S., Morgenstern, D., Yahalom-Ronen, Y., et al. (2021). The Coding Capacity of SARS-CoV-2. *Nature* 589 (7840), 125–130. doi: 10.1038/s41586-020-2739-1

Flower, T. G., Buffalo, C. Z., Hooy, R. M., Allaire, M., Ren, X., and Hurley, J. H. (2021). Structure of SARS-Cov-2 ORF8, a Rapidly Evolving Immune Evasion Protein. *Proc. Natl. Acad. Sci. U. S. A.* 118, 1–6. doi: 10.1073/pnas.2021785118

Focosi, D., and Maggi, F. (2021). Neutralising Antibody Escape of SARS-CoV-2 Spike Protein: Risk Assessment for Antibody-Based Covid-19 Therapeutics and Vaccines. *Rev. Med. Virol.* 31 (6), e2231. doi: 10.1002/rmv.2231

Fontanet, A., Autran, B., Lina, B., Kieny, M. P., Karim, S. S. A., and Sridhar, D. (2021). SARS-CoV-2 Variants and Ending the COVID-19 Pandemic. *Lancet* 397 (10278), 952–954. doi: 10.1016/S0140-6736(21)00370-6

Francisco, R. D. S. Jr, Benites, L. F., Lamarca, A. P., de Almeida, L. G. P., Hansen, A. W., Gularte, J. S., et al. (2021). Pervasive Transmission of E484K and Emergence of VUI-NP13L With Evidence of SARS-CoV-2 Co-Infection Events by Two Different Lineages in Rio Grande do Sul, Brazil. *Virus Res.* 296, 198345. doi: 10.1016/j.virusres.2021.198345

Garcia-Beltran, W. F., Lam, E. C., Astudillo, M. G., Yang, D., Miller, T. E., Feldman, J., et al. (2021b). COVID-19-Neutralizing Antibodies Predict Disease Severity and Survival. *Cell* 184, 476–488.e11. doi: 10.1016/j.cell.2020.12.015

Garcia-Beltran, W. F., Lam, E. C., St Denis, K., Nitido, A. D., Garcia, Z. H., Hauser, B. M., et al. (2021a). Multiple SARS-CoV-2 Variants Escape Neutralization by Vaccine-Induced Humoral Immunity. *Cell* 184 (9), 2372–2383.e9. doi: 10.1016/j.cell.2021.03.013

Geers, D., Shamier, M. C., Bogers, S., den Hartog, G., Gommers, L., Nieuwkoop, N. N., et al. (2021). SARS-CoV-2 Variants of Concern Partially Escape Humoral But Not T-Cell Responses in COVID-19 Convalescent Donors and Vaccinees. *Sci. Immunol.* 6 (59), eabj1750. doi: 10.1126/sciimmunol.abj1750

GISAID (Global Initiative on Sharing All Influenza Data). (2021). *Tracking of Variants*. Available at: https://www.gisaid.org/hcov19-variants/.

Gobeil, S. M., Janowska, K., McDowell, S., Mansouri, K., Parks, R., Manne, K., et al. (2021). D614G Mutation Alters SARS-CoV-2 Spike Conformation and Enhances Protease Cleavage at the S1/S2 Junction. *Cell Rep.* 34, 108630. doi: 10.1016/j.celrep.2020.108630

Graham, M. S., Sudre, C. H., May, A., Antonelli, M., Murray, B., Varsavsky, T., et al. (2021). Changes in Symptomatology, Reinfection, and Transmissibility Associated With the SARS-CoV-2 Variant B.1.1.7: An Ecological Study. *Lancet Public Health* 6 (5), e335–e345. doi: 10.1016/S2468-2667(21)00055-4

Groves, D. C., Rowland-Jones, S. L., and Angyal, A. (2021). The D614G Mutations in the SARS-CoV-2 Spike Protein: Implications for Viral Infectivity, Disease Severity and Vaccine Design. *Biochem. Biophys. Res. Commun.* 538, 104–107. doi: 10.1016/j.bbrc.2020.10.109

Gu, H., Chen, Q., Yang, G., He, L., Fan, H., Deng, Y. Q., et al. (2020). Adaptation of SARS-CoV-2 in BALB/c Mice for Testing Vaccine Efficacy. *Science* 369, 1603–1607. doi: 10.1126/science.abc4730

Gushchin, V. A., Dolzhikova, I. V., Shchetinin, A. M., Odintsova, A. S., Siniavin, A. E., Nikiforova, M. A., et al. (2021). Neutralizing Activity of Sera From Sputnik V-Vaccinated People Against Variants of Concern (VOC: B.1.1.7, B.1.351, P.1, B.1.617.2, B.1.617.3) and Moscow Endemic SARS-CoV-2 Variants. *Vaccines* 9, 779. doi: 10.3390/vaccines9070779

Harvey, W. T., Carabelli, A. M., Jackson, B., G upta, R. K., Thomson, E. C., Harrison, E. M., et al. (2021). SARS-CoV-2 Variants, Spike Mutations and Immune Escape. *Nat. Rev. Microbiol.* 19 (7), 409–424. doi: 10.1038/s41579-021-00573-0

Hoffmann, M., Kleine-Weber, H., Schroeder, S., Kruger, N., Herrler, T., Erichsen, S., et al. (2020). SARS-CoV-2 Cell Entry Depends on ACE2 and TMPRSS2 and Is Blocked by a Clinically Proven Protease Inhibitor. *Cell* 181, 271–280.e8. doi: 10.1016/j.cell.2020.02.052

Hoffmann, M., Arora, P., Groß, R., Seidel, A., Hörnich, B. F., Hahn, A. S., et al. (2021). SARS-CoV-2 Variants B.1.351 and P.1 Escape From Neutralizing Antibodies. *Cell* 184 (9), 2384–2393.e12. doi: 10.1016/j.cell.2021.03.036

Jara, A., Undurraga, E. A., González, C., Paredes, F., Fontecilla, T., Jara, G., et al. (2021). Effectiveness of an Inactivated SARS-CoV-2 Vaccine in Chile. *N. Engl. J. Med.* 385(10), 875–884. doi: 10.1056/NEJMoa2107715

Kandeel, M., Mohamed, M. E. M., Abd El-Lateef, H. M., Venugopala, K. N., and El-Beltagi, H. S. (2021). Omicron Variant Genome Evolution and Phylogenetics. *J. Med. Virol.* 1– 6. doi: 10.1002/jmv.27515

Khateeb, J., Li, Y., and Zhang, H. (2021). Emerging SARS-CoV-2 Variants of Concern and Potential Intervention Approaches. *Crit. Care* 25 (1), 244. doi: 10.1186/s13054-021-03662-x

Kielian, M. (2020). Enhancing Host Cell Infection by SARS-CoV-2. *Science* 370 (6518), 765–766. doi: 10.1126/science.abf0732

Kim, D., Lee, J. Y., Yang, J. S., Kim, J. W., Kim, V. N., and Chang, H. (2020). The Architecture of SARS-CoV-2 Transcriptome. *Cell* 181, 914–921.e10. doi: 10.1016/j.cell.2020.04.011

Kirola, L. (2021). Genetic Emergence of B.1.617.2 in COVID-19. *New Microbes New Infect.* 43, 100929. doi: 10.1016/j.nmni.2021.100929

Korber, B., Fischer, W. M., Gnanakaran, S., Yoon, H., Theiler, J., Abfalterer, W., et al. (2020). Tracking Changes in SARS-CoV-2 Spike: Evidence That D614G Increases Infectivity of the COVID-19 Virus. *Cell* 182, 812–827.e819. doi: 10.1016/j.cell.2020.06.043

Koyama, T., Platt, D., and Parida, L. (2020). Variant Analysis of SARS-CoV-2 Genomes. Bull. *World Health Organ* 98, 495–504. doi: 10.2471/BLT.20.253591

Kuzmina, A., Khalaila, Y., Voloshin, O., Keren-Naus, A., Boehm-Cohen, L., Raviv, Y., et al. (2021). SARS-CoV-2 Spike Variants Exhibit Differential Infectivity and Neutralization Resistance to Convalescent or Post-Vaccination Sera. *Cell Host Microbe* 29 (4), 522–528.e2. doi: 10.1016/j.chom.2021.03.008

Li, Q., Nie, J., Wu, J., Zhang, L., Ding, R., Wang, H., et al. (2021). SARS-CoV-2 501y.V2 Variants Lack Higher Infectivity But do Have Immune Escape. *Cell* 184 (9), 2362–2371.e9. doi: 10.1016/j.cell.2021.02.042

Lin, J., Tang, C., Wei, H., Du, B., Chen, C., Wang, M., et al. (2021). Genomic Monitoring of SARS-CoV-2 Uncovers an Nsp1 Deletion Variant That Modulates Type I Interferon Response. *Cell Host Microbe* 29 (3), 489–502.e8. doi: 10.1016/j.chom.2021.01.015

Liu, C., Ginn, H. M., Dejnirattisai, W., Supasa, P., Wang, B., Tuekprakhon, A., et al. (2021). Reduced Neutralization of SARS-CoV-2 B.1.617 by Vaccine and Convalescent Serum. *Cell* 184 (16), 4220–4236. doi: 10.1016/j.cell.2021.06.020

Liu, J., Liu, Y., Xia, H., Zou, J., Weaver, S. C., Swanson, K. A., et al. (2021). BNT162b2-Elicited Neutralization of B.1.617 and Other SARS-CoV-2 Variants. *Nature* 596 (7871), 273–275. doi: 10.1038/s41586-021-03693-y

Liu, Y., and Rocklöv, J. (2021). The Reproductive Number of the Delta Variant of SARS-CoV-2 Is Far Higher Compared to the Ancestral SARS-CoV-2 Virus. *J. Travel. Med.* 28 (7), taab124. doi: 10.1093/jtm/taab124

Liu, Z., VanBlargan, L. A., Bloyet, L. M., Rothlauf, P. W., Chen, R. E., Stumpf, S., et al. (2021). Identification of SARS-CoV-2 Spike Mutations That Attenuate Monoclonal and Serum Antibody Neutralization. *Cell Host Microbe* 29 (3), 477–488.e4. doi: 10.1016/j.chom.2021.01.014

Logunov, D. Y., Dolzhikova, I. V., Shcheblyakov, D. V., Tukhvatulin, A. I., Zubkova, O. V., Dzharullaeva, A. S., et al. (2021). Safety and Efficacy of an Rad26 and Rad5 Vector-Based Heterologous Prime-Boost COVID-19 Vaccine: An Interim Analysis of a Randomised Controlled Phase 3 Trial in Russia. *Lancet* 397 (10275), 671–681. doi: 10.1016/S0140-6736(21)00234-8

Lopez Bernal, J., Andrews, N., Gower, C., Gallagher, E., Simmons, R., Thelwall, S., et al. (2021). Effectiveness of Covid-19 Vaccines Against the B.1.617.2 (Delta) Variant. *N. Engl. J. Med.* 385 (7), 585–594. doi: 10.1056/NEJMoa2108891

Lustig, Y., Zuckerman, N., Nemet, I., Atari, N., Kliker, L., Regev-Yochay, G., et al. (2021). Neutralising Capacity Against Delta (B.1.617.2) and Other Variants of Concern Following Comirnaty (BNT162b2, BioNTech/Pfizer) Vaccination in Health Care Workers, Israel. *Euro. Surveill.* 26 (26), 2100557. doi: 10.2807/1560-7917.ES.2021.26.26.2100557

Madhi, S. A., Baillie, V., Cutland, C. L., Voysey, M., Koen, A. L., Fairlie, L., et al. (2021). Efficacy of the ChAdOx1 Ncov-19 Covid-19 Vaccine Against the B.1.351 Variant. *N. Engl. J. Med.* 384 (20), 1885–1898. doi: 10.1056/NEJMoa2102214

Melenotte, C., Silvin, A., Goubet, A. G., Lahmar, I., Dubuisson, A., Zumla, A., et al. (2020). Immune Responses During COVID-19 Infection. *Oncoimmunology* 9 (1), 1807836. doi: 10.1080/2162402X.2020.1807836

Mlcochova, P., Kemp, S. A., Dhar, M. S., Papa, G., Meng, B., Ferreira, I. A. T. M., et al. (2021). SARS-CoV-2 B.1.617.2 Delta Variant Replication and Immune Evasion. *Nature* 599 (7883), 114–119. doi: 10.1038/s41586-021-03944-y

Moore, J. P., and Offit, P. A. (2021). SARS-CoV-2 Vaccines and the Growing Threat of Viral Variants. *JAMA* 325 (9), 821–822. doi: 10.1001/jama.2021.1114

Muik, A., Wallisch, A. K., Sänger, B., Swanson, K. A., Mühl, J., Chen, W., et al. (2021). Neutralization of SARS-CoV-2 Lineage B.1.1.7 Pseudovirus by BNT162b2 Vaccine-Elicited Human Sera. *Science* 371 (6534), 1152–1153. doi: 10.1126/science.abg6105

Nguyen, T. T., Pathirana, P. N., Nguyen, T., Nguyen, Q. V. H., Bhatti, A., Nguyen, D. C., et al. (2021). Genomic Mutations and Changes in Protein Secondary Structure and Solvent Accessibility of SARS-CoV-2 (COVID-19 Virus). *Sci. Rep.* 11 (1), 3487. doi: 10.1038/s41598-021-83105-3

Nieto-Torres, J. L., DeDiego, M. L., Verdiá-Báguena, C., Jimenez-Guardeño, J. M., Regla-Nava, J. A., Fernandez-Delgado, R., et al. (2014). Severe Acute Respiratory Syndrome Coronavirus Envelope Protein Ion Channel Activity Promotes Virus Fitness and Pathogenesis. *PloS Pathog.* 10 (5), e1004077. doi: 10.1371/journal.ppat.1004077

Ni, L., Ye, F., Cheng, M. L., Feng, Y., Deng, Y. Q., Zhao, H., et al. (2020). Detection of SARS-CoV-2-Specific Humoral and Cellular Immunity in COVID-19 Convalescent Individuals. *Immunity* 52, 971–977.e973. doi: 10.1016/j.immuni.2020.04.023

Ong, S. W. X., Chiew, C. J., Ang, L. W., Mak, T. M., Cui, L., Toh, M. P. H. S., et al. (2021). Clinical and Virological Features of SARS-CoV-2 Variants of Concern: A Retrospective Cohort Study Comparing B.1.1.7 (Alpha), B.1.315 (Beta) and B.1.617.2 (Delta). *SSRN. J.* doi: 10.2139/ssrn.3861566

Oude Munnink, B. B., Sikkema, R. S., Nieuwenhuijse, D. F., Molenaar, R. J., Munger, E., Molenkamp, R., et al. (2021). Transmission of SARS-CoV-2 on Mink Farms be- Tween Humans and Mink and Back to Humans. *Science* 371, 172–177. doi: 10.1126/science.abe5901

Ou, X., Liu, Y., Lei, X., Li, P., Mi, D., Ren, L., et al. (2020). Characterization of Spike Glycoprotein of SARS-CoV-2 on Virus Entry and Its Immune Cross-Reactivity With SARS-CoV. *Nat. Commun.* 11, 1620. doi: 10.1038/s41467-020-15562-9

Ozono, S., Zhang, Y., Ode, H., Sano, K., Tan, T. S., Imai, K., et al. (2021). SARS-CoV-2 D614G Spike Mutation Increases Entry Efficiency With Enhanced ACE2-Binding Affinity. *Nat. Commun.* 12, 848. doi: 10.1038/s41467-021-21118-2

Pereira, F. (2021). SARS-CoV-2 Variants Combining Spike Mutations and the Absence of ORF8 may be More Transmissible and Require Close Monitoring. *Biochem. Biophys. Res. Commun.* 550, 8–14. doi: 10.1016/j.bbrc.2021.02.080

Planas, D., Veyer, D., Baidaliuk, A., Staropoli, I., Guivel-Benhassine, F., Rajah, M. M., et al. (2021). Reduced Sensitivity of SARS-CoV-2 Variant Delta to Antibody Neutralization. *Nature* 596 (7871), 276–280. doi: 10.1038/s41586-021-03777-9

Plante, J. A., Liu, Y., Liu, J., Xia, H., Johnson, B. A., Lokugamage, K. G., et al. (2020). Spike Mutation D614G Alters SARS-CoV-2 Fitness. *Nature* 592 (7852), 116–121. doi: 10.1038/s41586-020-2895-3

Plante, J. A., Mitchell, B. M., Plante, K. S., Debbink, K., Weaver, S. C., and Menachery, V. D. (2021). The Variant Gambit: COVID-19's Next Move. *Cell Host Microbe* 29 (4), 508–515. doi: 10.1016/j.chom.2021.02.020

Polack, F. P., Thomas, S. J., Kitchin, N., Absalon, J., Gurtman, A., Lockhart, S., et al. (2020). Safety and Efficacy of the BNT162b2 mRNA Covid-19 Vaccine. *N. Engl. J. Med.* 383, 2603–2615. doi: 10.1056/NEJMoa2034577

Sabino, E. C., Buss, L. F., Carvalho, M. P. S., Prete, C. A. Jr., Crispim, M. A. E., Fraiji, N. A., et al. (2021). Resurgence of COVID-19 in Manaus, Brazil, Despite High Seroprevalence. *Lancet* 397, 452–455. doi: 10.1016/S0140-6736(21)00183-5

Shang, J., Wan, Y., Luo, C., Ye, G., Geng, Q., Auerbach, A., et al. (2020). Cell Entry Mechanisms of SARS-CoV-2. *Proc. Natl. Acad. Sci. U. S. A.* 117 (21), 11727–11734. doi: 10.1073/pnas.2003138117

Sheikh, A., McMenamin, J., Taylor, B., and Robertson, C. (2021). SARS-CoV-2 Delta VOC in Scotland: Demographics, Risk of Hospital Admission, and Vaccine Effectiveness. *Lancet* 397 (10293), 2461–2462. doi: 10.1016/s0140-6736(21)01358-1

Shen, X., Tang, H., McDanal, C., Wagh, K., Fischer, W., Theiler, J., et al. (2021). SARS-CoV-2 Variant B.1.1.7 Is Susceptible to Neutralizing Antibodies Elicited by Ancestral Spike Vaccines. *Cell Host Microbe* 29 (4), 529–539.e3. doi: 10.1016/j.chom.2021.03.002

Shinde, V., Bhikha, S., Hoosain, Z., Archary, M., Bhorat, Q., Fairlie, L., et al. (2021). Efficacy of NVX-CoV2373 Covid-19 Vaccine Against the B.1.351 Variant. *N. Engl. J. Med.* 384 (20), 1899–1909. doi: 10.1056/NEJMoa2103055

Smith, E. C., Sexton, N. R., and Denison, M. R. (2014). Thinking Outside the Triangle: Replication Fidelity of the Largest RNA Viruses. *Annu. Rev. Virol.* 1 (1), 111–132. doi: 10.1146/annurev-virology-031413-085507

Snijder, E. J., Decroly, E., and Ziebuhr, J. (2016). The Nonstructural Proteins Directing Coronavirus RNA Synthesis and Processing. *Adv. Virus Res.* 96, 59–126. doi: 10.1016/bs.aivir.2016.08.008

Starr, T. N., et al. (2020). Deep Mutational Scanning of SARS-CoV-2 Receptor Binding Domain Reveals Constraints on Folding and ACE2 Binding. *Cell* 182, 1295–1310.e20. doi: 10.1016/j.cell.2020.08.012

Staub, T., Arendt, V., Lasso de la Vega, E. C., Braquet, P., Michaux, C., Kohnen, M., et al. (2021). Case Series of Four Re-Infections With a SARS-CoV-2 B.1.351 Variant, Luxembourg, February 2021. *Euro. Surveill.* 26 (18), 2100423. doi: 10.2807/1560-7917.ES.2021.26.18.2100423

Supasa, P., Zhou, D., Dejnirattisai, W., Liu, C., Mentzer, A. J., Ginn, H. M., et al. (2021). Reduced Neutralization of SARS-CoV-2 B.1.1.7 Variant by Convalescent and Vaccine Sera. *Cell* 184 (8), 2201–2211.e7. doi: 10.1016/j.cell.2021.02.033

Tan, M., Liu, Y., Zhou, R., Deng, X., Li, F., Liang, K., et al. (2020). Immunopathological Characteristics of Coronavirus Disease 2019 Cases in Guangzhou, China. *Immunology* 160 (3), 261–268. doi: 10.1111/imm.13223

Tang, P., Hasan, M. R., Chemaitelly, H., Yassine, H. M., Benslimane, F. M., Al Khatib, H. A., et al. (2021). BNT162b2 and mRNA-1273 COVID-19 Vaccine Effectiveness Against the SARS-CoV-2 Delta Variant in Qatar. *Nat. Med.* 27 (12), 2136–2143. doi: 10.1038/s41591-021-01583-4

Takeda, M. (2022). Proteolytic Activation of SARS-CoV-2 Spike Protein. *Microbiol. Immunol.* 66 (1), 15–23. doi: 10.1111/1348-0421.12945

Tanriover, M. D., Doğanay, H. L., Akova, M., Güner, H. R., Azap, A., Akhan, S., et al. (2021). Efficacy and Safety of an Inactivated Whole-Virion SARS-CoV-2 Vaccine (CoronaVac): Interim Results of a Double-Blind, Randomised, Placebo-Controlled, Phase 3 Trial in Turkey. *Lancet* 398 (10296), 213–222. doi: 10.1016/S0140-6736(21)01429-X

Taylor, L. (2021). Covid-19: Is Manaus the Final Nail in the Coffin for Natural Herd Immunity? *BMJ* 372, n394. doi: 10.1136/bmj.n394

Torjesen, I. (2021). Covid-19: Omicron May Be More Transmissible Than Other Variants and Partly Resistant to Existing Vaccines, Scientists Fear. *BMJ* 375, n2943. doi: 10.1136/bmj.n2943

Volz, E., Hill, V., McCrone, J. T., Price, A., Jorgensen, D., O'Toole, A., et al. (2020). Evaluating the Effects of SARS-CoV-2 Spike Mutation D614G on Transmissibility and Pathogenicity. *Cell* S0092–8674, 31537–31543. doi: 10.1101/2020.07.31.20166082

Volz, E., Mishra, S., Chand, M., Barrett, J. C., Johnson, R., Geidelberg, L., et al. (2021). Assessing Transmissibility of SARS-CoV-2 Lineage B.1.1.7 in England. *Nature* 593 (7858), 266–269. doi: 10.1038/s41586-021-03470-x

Voysey, M., Clemens, S. A. C., Madhi, S. A., Weckx, L. Y., Folegatti, P. M., Aley, P. K., et al. (2020). Safety and Efficacy of the ChAdOx1 Ncov-19 Vaccine (AZD1222) Against SARS-CoV-2: An Interim Analysis of Four Randomised Controlled Trials in Brazil, South Africa, and the UK. *Lancet*. 397, 99–111. doi: 10.1016/S0140-6736(20)32661-1

Wang, E. C., Wu, M., Harvey, R., Kelly, G., Warchal, S., and Sawyer, C.. (2021). Neutralising Antibody Activity Against SARS-CoV-2 VOCs B.1.617.2 and B.1.351 by BNT162b2 Vaccination. *Lancet* 397 (10292), 2331–2333. doi: 10.1016/S0140-6736(21)01290-3

Wang, L., and Cheng, G. (2011). Sequence Analysis of the Emerging SARS-CoV-2 Variant Omicron in South Africa. *J. Med. Virol.* doi: 10.1002/jmv.27516

Wang, G. L., Wang, Z. Y., Duan, L. J., Meng, Q. C., Jiang, M. D., Cao, J., et al. (2021). Susceptibility of Circulating SARS-CoV-2 Variants to Neutralization. *N. Engl. J. Med.* 384 (24), 2354–2356. doi: 10.1056/NEJMc2103022

Wibmer, C. K., Ayres, F., Hermanus, T., Madzivhandila, M., Kgagudi, P., Oosthuysen, B., et al. (2021). SARS-CoV-2 501y.V2 Escapes Neutralization by South African COVID-19 Donor Plasma. *Nat. Med.* 27 (4), 622–625. doi: 10.1038/s41591-021-01285-x

Wu, K., Werner, A. P., Koch, M., Choi, A., Narayanan, E., Stewart-Jones, G. B. E., et al. (2021). Serum Neutralizing Activity Elicited by mRNA-1273 Vaccine. *N. Engl. J. Med.* 384 (15), 1468–1470. doi: 10.1056/NEJMc2102179

Xia, H., Cao, Z., Xie, X., Zhang, X., Chen, J. Y. C., Wang, H., et al. (2020). Evasion of Type I Interferon by SARS-CoV-2. *Cell Rep.* 33, 108234. doi: 10.1016/j.celrep.2020.108234

Yao, H., Song, Y., Chen, Y., Wu, N., Xu, J., Sun, C., et al. (2020). Molecular Architecture of the SARS-CoV-2 Virus. *Cell* 183 (3), 730–738.e13. doi: 10.1016/j.cell.2020.09.018

Young, B. E., Fong, S. W., Chan, Y. H., Mak, T. M., Ang, L. W., Anderson, D. E., et al. (2020). Effects of a Major Deletion in the SARS-CoV-2 Genome on the Severity of Infection and the Inflammatory Response: An Observational Cohort Study. *Lancet* 396, 603–611. doi: 10.1016/S0140-6736(20)31757-8

Yurkovetskiy, L., Wang, X., Pascal, K. E., Tomkins-Tinch, C., Nyalile, T. P., Wang, Y., et al. (2020). Structural and Functional Analysis of the D614G SARS-CoV-2 Spike Protein Variant. *Cell* 183 (3), 739–751.e8. doi: 10.1016/j.cell.2020.09.032

Zang, R., Gomez Castro, M. F., McCune, B. T., Zeng, Q., Rothlauf, P. W., Sonnek, N. M., et al. (2020). TMPRSS2 and TMPRSS4 Promote SARS-CoV-2 Infection of Human Small Intestinal Enterocytes. *Sci. Immunol.* 5, eabc3582. doi: 10.1126/sciimmunol.abc3582

Zhang, L., Li, Q., Liang, Z., Li, T., Liu, S., Cui, Q., et al. (2021). The Significant Immune Escape of Pseudotyped SARS-CoV-2 Variant Omicron. *Emerg. Microbes Infect.* 10, 1–11. doi: 10.1080/22221751.2021.2017757

Zhou, D., Dejnirattisai, W., Supasa, P., Liu, C., Mentzer, A. J., Ginn, H. M., et al. (2021). Evidence of Escape of SARS-CoV-2 Variant B.1.351 From Natural and Vaccine-Induced Sera. *Cell* 184 (9), 2348–2361.e6. doi: 10.1016/j.cell.2021.02.037

Zhu, Z., Liu, G., Meng, K., Yang, L., Liu, D., and Meng, G. (2021). Rapid Spread of Mutant Alleles in Worldwide SARS-CoV-2 Strains Revealed by Genome-Wide Single Nucleotide Polymorphism and Variation Analysis. *Genome Biol. Evol.* 13 (2), evab015. doi: 10.1093/gbe/evab015

Zhu, N., Zhang, D., Wang, W., Li, X., Yang, B., Song, J., et al. (2020). A Novel Coronavirus From Patients With Pneumonia in Chin. *N. Engl. J. Med.* 382, 727–773. doi: 10.1056/NEJMoa2001017

Conflict of Interest: The authors declare that the research was conducted in the absence of any commercial or financial relationships that could be construed as a potential conflict of interest.

frontiers in Cellular and Infection Microbiology

ORIGINAL RESEARCH
published: 24 January 2022
doi: 10.3389/fcimb.2021.795026

A Model Predicting Mortality of Hospitalized Covid-19 Patients Four Days After Admission: Development, Internal and Temporal-External Validation

Stefan Heber[1], David Pereyra[2,3], Waltraud C. Schrottmaier[2], Kerstin Kammerer[2], Jonas Santol[2,3], Benedikt Rumpf[4], Erich Pawelka[4], Markus Hanna[2], Alexander Scholz[2], Markus Liu[2], Agnes Hell[2], Klara Heiplik[2], Benno Lickefett[2], Sebastian Havervall[5], Marianna T. Traugott[4], Matthias J. Neuböck[6], Christian Schörgenhofer[7], Tamara Seitz[4], Christa Firbas[7], Mario Karolyi[4], Günter Weiss[8], Bernd Jilma[7], Charlotte Thålin[5], Rosa Bellmann-Weiler[8], Helmut J. F. Salzer[6], Gero Szepannek[9], Michael J. M. Fischer[1], Alexander Zoufaly[4], Andreas Gleiss[10] and Alice Assinger[2]*

[1] Institute of Physiology, Centre of Physiology and Pharmacology, Medical University of Vienna, Vienna, Austria, [2] Department of Vascular Biology and Thrombosis Research, Centre of Physiology and Pharmacology, Medical University of Vienna, Vienna, Austria, [3] Department of General Surgery, Division of Visceral Surgery, Medical University of Vienna, General Hospital Vienna, Vienna, Austria, [4] Department of Medicine IV, Kaiser Franz Josef Hospital, Vienna, Austria, [5] Division of Internal Medicine, Department of Clinical Sciences, Karolinska Institutet, Danderyd Hospital, Stockholm, Sweden, [6] Department of Pulmonology, Kepler University Hospital and Johannes Kepler University, Linz, Austria, [7] Department of Clinical Pharmacology, Medical University of Vienna, General Hospital Vienna, Vienna, Austria, [8] Department of Internal Medicine II, Medical University of Innsbruck, Innsbruck, Austria, [9] Institute of Applied Computer Science, Stralsund University of Applied Sciences, Stralsund, Germany, [10] Section for Clinical Biometrics, Center for Medical Statistics, Informatics, and Intelligent Systems, Medical University of Vienna, Vienna, Austria

OPEN ACCESS

Edited by:
Yu Chen,
Wuhan University, China

Reviewed by:
Rameez Raja,
Cleveland Clinic, United States
Thomas Higgins,
Center for Case Management,
United States

***Correspondence:**
Stefan Heber
stefan.heber@meduniwien.ac.at

Specialty section:
This article was submitted to Virus and Host, a section of the journal Frontiers in Cellular and Infection Microbiology

Received: 14 October 2021
Accepted: 13 December 2021
Published: 24 January 2022

Citation:
Heber S, Pereyra D, Schrottmaier WC, Kammerer K, Santol J, Rumpf B, Pawelka E, Hanna M, Scholz A, Liu M, Hell A, Heiplik K, Lickefett B, Havervall S, Traugott MT, Neuböck MJ, Schörgenhofer C, Seitz T, Firbas C, Karolyi M, Weiss G, Jilma B, Thålin C, Bellmann-Weiler R, Salzer HJF, Szepannek G, Fischer MJM, Zoufaly A, Gleiss A and Assinger A (2022) A Model Predicting Mortality of Hospitalized Covid-19 Patients Four Days After Admission: Development, Internal and Temporal-External Validation. Front. Cell. Infect. Microbiol. 11:795026. doi: 10.3389/fcimb.2021.795026

Objective: To develop and validate a prognostic model for in-hospital mortality after four days based on age, fever at admission and five haematological parameters routinely measured in hospitalized Covid-19 patients during the first four days after admission.

Methods: Haematological parameters measured during the first 4 days after admission were subjected to a linear mixed model to obtain patient-specific intercepts and slopes for each parameter. A prediction model was built using logistic regression with variable selection and shrinkage factor estimation supported by bootstrapping. Model development was based on 481 survivors and 97 non-survivors, hospitalized before the occurrence of mutations. Internal validation was done by 10-fold cross-validation. The model was temporally-externally validated in 299 survivors and 42 non-survivors hospitalized when the Alpha variant (B.1.1.7) was prevalent.

Results: The final model included age, fever on admission as well as the slope or intercept of lactate dehydrogenase, platelet count, C-reactive protein, and creatinine. Tenfold cross validation resulted in a mean area under the receiver operating characteristic curve (AUROC) of 0.92, a mean calibration slope of 1.0023 and a Brier score of 0.076. At temporal-external validation, application of the previously developed model showed an

AUROC of 0.88, a calibration slope of 0.95 and a Brier score of 0.073. Regarding the relative importance of the variables, the (apparent) variation in mortality explained by the six variables deduced from the haematological parameters measured during the first four days is higher (explained variation 0.295) than that of age (0.210).

Conclusions: The presented model requires only variables routinely acquired in hospitals, which allows immediate and wide-spread use as a decision support for earlier discharge of low-risk patients to reduce the burden on the health care system.

Clinical Trial Registration: Austrian Coronavirus Adaptive Clinical Trial (ACOVACT); ClinicalTrials.gov, identifier NCT04351724.

Keywords: COVID-19, survival, prediction model, blood parameter, logistic regression, hospitalized patients

INTRODUCTION

Background

The Covid-19 pandemic evokes a complex global public health crisis with clinical, organizational, and system-wide challenges. Although vaccinations ease the situation, a substantial proportion of the world's population is still not immunized. Recurrent Covid-19 waves challenge health care systems. Although age is a relatively strong biomarker, additional information on disease progression and patient outcome would be beneficial given the intensive workload of health care providers worldwide.

Although a plethora of prognostic models for Covid-19 were quickly published at the beginning of the pandemic to support medical decision making at a time when they were urgently needed, a large consortium including clinical scientists, epidemiologists, biologists, and statisticians, concluded that 'almost all published prediction models are poorly reported, and at high risk of bias such that their reported predictive performance is probably optimistic' (Wynants et al., 2020). However, they identified one prognostic model (Knight et al., 2020) that should soon be validated. The authors further recommended building on previous literature and expert opinion to select predictors, rather than selecting predictors in a purely data driven way. Promising candidates include age, body temperature, sex, blood pressure, creatinine, basophils, neutrophils, lymphocytes, alanine transaminase, albumin, platelets, eosinophils, calcium, bilirubin, creatinine, CRP, and comorbidities, including hypertension, diabetes, cardiovascular disease, and respiratory disease.

Besides the critically ill patients who need to be treated in intensive care units, the multitude of patients being treated in general wards binds substantial resources. Nevertheless, many of these Covid-19 cases cannot be discharged since the critical phase of Covid-19 frequently starts around 7-10 days after onset of the initial symptoms. However, a large proportion of patients will ultimately not require hospital care. Accordingly, a tool predicting the likelihood of a severe or fatal disease could support the decision for an earlier discharge. While such a predictive tool should be available as early as possible for hospitalized patients, the sole use of data available at time of hospital admission might not suffice in order to allow for a robust predictive accuracy. Hence, the expense of a slightly later forecast date might be relevant to exploit changes in biomarkers that may contain prognostic information.

Objectives

The objective of this study was to develop a prognostic model with predictors selected based on pathophysiological considerations and literature. The model should also include the time course of the variables within the first four days after admission and only be applicable thereafter.

METHODS

Participants and Source of the Data

We conducted an observational cohort study to develop and validate a prognostic model to predict in-hospital mortality of patients with Covid-19. Only data collected in clinical routine were used and data of all consecutive patients were accessed. The model was developed and internally validated in a cohort of the Clinic Favoriten in Vienna, Austria, hospitalized between 7 January 2020 and 8 December 2020, well before the widespread dissemination of the new corona variants. The cohort consisted of 679 patients, of which 578 including 98 deaths were used as they had at least two blood samples and survived at least 4 days.

The model was temporarily and externally validated in a mixed cohort consisting of additional patients from the Clinic Favoriten (350 patients, 58 deaths) and in patients from the Department of Pulmonology, Kepler University Hospital, Linz, Austria (97 patients, 9 deaths). Of these 447 patients, 392 were included in the analysis due to the above-mentioned reasons. These patients were hospitalized between 24 December 2020 and 07 April 2021, when the B.1.1.7/Alpha variant was more prevalent. SARS-CoV-2 positivity was determined from nasopharyngeal or oropharyngeal swabs *via* real-time polymerase chain reaction (qPCR) according to the Charité protocol (Corman et al., 2020). All patients had available outcome data at time of analysis. Recovery of data at the Clinic Favoriten in Vienna is part of the ACOVACT study

(ClinicalTrials.gov NCT04351724) approved by the local ethics committee (EK1315/2020). This study was further approved by the ethics committee of the Kepler University Clinics (1085/2020).

Outcome

The predicted outcome is death from any cause during the hospital stay after day 4. There was no loss to follow up as patients were either discharged or died.

Predictors

The aim was to build a prognostic model that has widespread applicability. Thus, only the following routinely measured variables were considered: Age, Fever (>38°C) on admission, platelet count (PLT), C-reactive protein (CRP), lactate dehydrogenase (LDH), Creatinine (CREA), Lymphocyte count (LYM). Selection of possibly useful predictors considered pathophysiological processes, the published literature (Gansevoort and Hilbrands, 2020; Jiang et al., 2020; Manson et al., 2020; Wang, 2020; Fouladseresht et al., 2021), and had a special focus on the reported Covid-19-associated coagulopathy. The graphical exploration suggested that although some potential predictors are not out of range to a relevant extent at the time of admission, their development is considerably different between survivors and non-survivors during hospital stay. Therefore, the time course of PLT, CRP, LDH, CREA and LYM was included in the prognostic model. Since blood samples were often taken only every two days from admission, and as data from two days seemed too short potentially prognostic changes over time, the pragmatic decision was made to use the data from day 0 to 4 (i.e., 5 calendar days) after admission for prognosis. As summary measures, slopes and intercept at day 2 for each of the five blood-based parameters were estimated by linear mixed models.

Blinding

The individuals accessing the medical records to extract variables were not blinded to the outcome.

Sample Size

Sample size calculation was performed according to Riley et al. (2020). It was based on an anticipated proportion of deaths of 0.15, a desired margin of error in the overall outcome proportion estimate of 0.05, a mean absolute prediction error of 0.05, a shrinkage of 0.9, a Cox-Snell R squared statistic of 0.2 as anticipated model performance (maximum possible value of Cox-Snell R squared = 0.57), an expected optimism of 0.05 and 12 candidate predictors, i.e. age, fever on admission as well as intercept and slope for each of the blood based parameters. These assumptions resulted in a total sample size of 478 for model development.

Missing Data

There were no missing data regarding outcome. For 101 of 679 patients only a single measurement of a blood parameter within days 0 to 4 was available, and these had to be excluded as no slope could be calculated. The model is thus only applicable to patients with at least two measurements within days 0 to 4.

Statistical Analysis Methods

Estimation of Intercepts and Slopes by Linear Mixed Models

The predictors containing the information regarding the intra-individual level and change in the laboratory variables during the first 4 days after admission were calculated using a linear mixed model for each laboratory parameter as follows: First, time was re-scaled to zero at day 2 such that an estimated intercept represents a value in the middle (instead of the margin) of the interval between day 0 and day 4. Then each parameter was regressed on re-scaled time, using a fixed as well as a random intercept and slope with unstructured variance-covariance matrix. For these models, only patients with at least two observations up to day 4 were included. The mixed model approach deals with missing data due to varying measurement patterns (such that "missingness at random" is plausible) and shrinks slope estimates to the common mean obtained for the fixed effects. For each patient the intercept and slope were estimated as best linear unbiased predictors (BLUP) by the Empirical Bayes method (Fitzmaurice et al., 2011).

For future patients as well as for patients from a test set or validation cohort, intercept and slope were estimated using the empirical BLUP formula restricted to the available measurements after plugging in the parameter estimates obtained from the original data or training set (Fitzmaurice et al., 2011).

Building of Logistic Regression Based Prediction Model

The statistical approach is summarized in **Figure 1**. The first step of model development (**Figure 1** left) was to estimate intercepts and slopes for hematological parameters using linear mixed models as described below. Thereafter 1000 random bootstrap samples were generated. In each bootstrap sample, a logistic regression model was used to select predictors using backward elimination based on repeated likelihood ratio tests at a significance level of 0.1. For a predictor to be ultimately selected, it had to remain in at least 50% of all bootstrap samples. Hence, the final model was fit using the original dataset and the selected predictors only. A linear shrinkage factor for the regression coefficients was estimated as follows. Using the regression coefficients estimated in each of the 1000 bootstrap samples and the characteristics of each patient in the original sample, 1000 bootstrapped prognostic indices were calculated for each patient. Corresponding to each bootstrap sample we fit a logistic model to the original data with the bootstrapped prognostic indices as the only covariable. The mean regression coefficient of that covariable over the 1000 bootstrap repetitions was used as the linear shrinkage factor 's' (Steyerberg et al., 2001). The logistic regression coefficients of the final model were multiplied by s, and the intercept recalibrated.

Further, the apparent explained variation (EV) together with degrees of necessity (DN) and of sufficiency (DS) were computed (Gleiss and Schemper, 2019). These measures were derived on

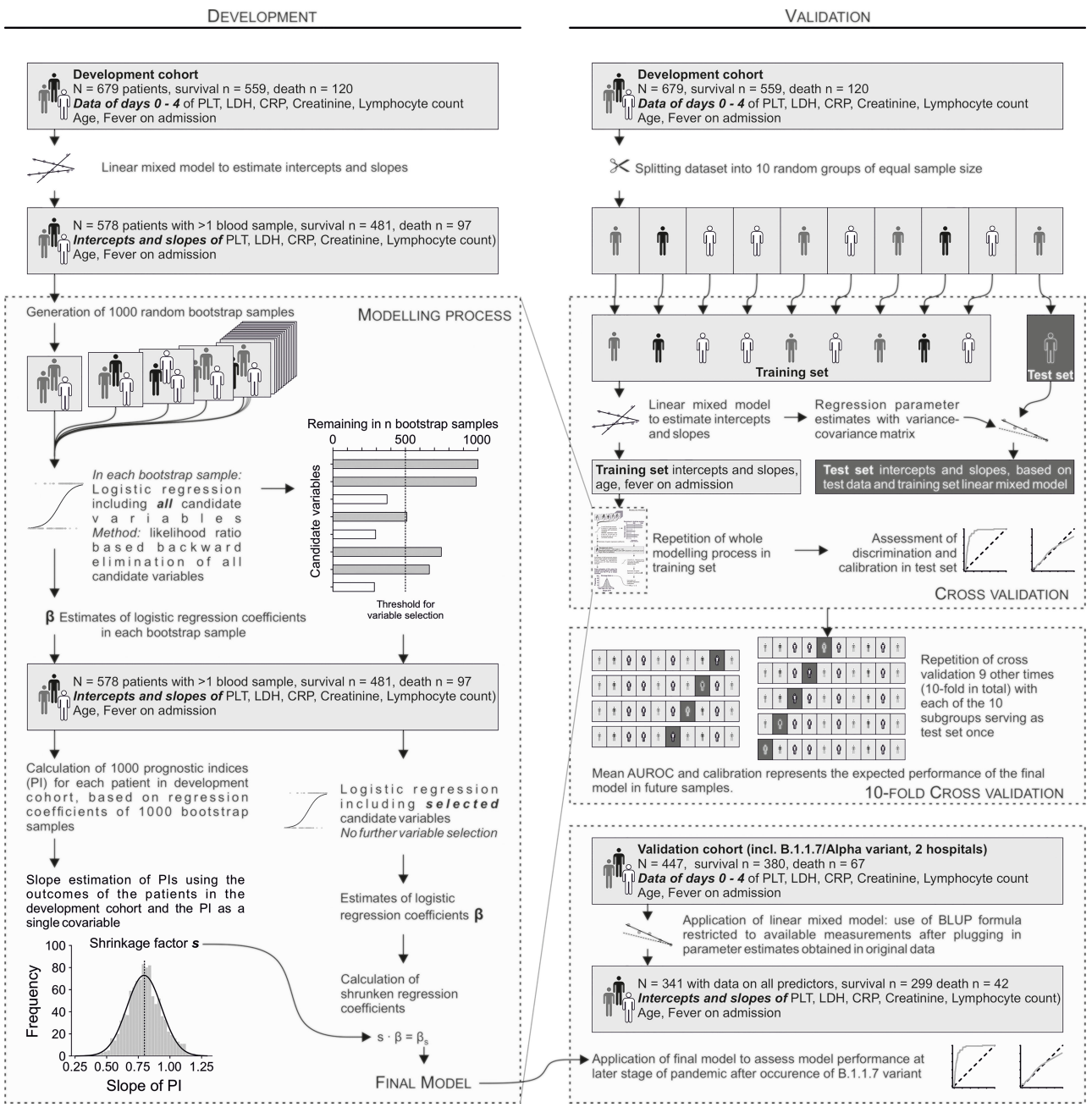

FIGURE 1 | Model development and validation strategy.

the original data leading to considerable over-optimism but are able to quantify the *relative* importance of predictors.

Validation (**Figure 1** right) was first performed internally as 10-fold cross validation. First, the dataset including the raw blood values was randomly split into 10 groups of equal size. Next, 9 of these were used as training set, and the remaining one as test set. Importantly, separate linear mixed models were fitted in each training set to avoid data leakage between these sets. Thereafter, the whole modelling process (i.e. including bootstrapping and shrinkage) was repeated in the training set as described above for the original data. The resulting model was then validated in the training set. This procedure was repeated with each of the 10 random groups serving as test set once. The mean of the 10 resulting AUROCs on the respective test sets estimates the expected AUROC in a new dataset from the same target population. In addition to 10-fold cross validation, the final model was tested in a new dataset from a later period. The Brier score was computed by calculating the mean of the squared

differences between predicted death probabilities and outcome (with death = 1 and survival = 0). Thus, it can take on a value between 0 and 1, whereby 0 indicates perfect prediction.

Handling of Predictors

For all continuous potential predictors, a linear functional form was assumed. Body temperature was only available as dichotomous variable fever on admission, 'Yes' was coded as 1, 'No' as 0.

Differences Between Development and Validation

The cohorts differ regarding the period in which patients were hospitalized and the virus variants.

Machine Learning

In order to benchmark the model, in addition random forests (Liaw and Wiener, 2002) were trained as they achieve good performance in many machine learning benchmark studies (Fernández-Delgado et al., 2014). As random forests are less sensitive to hyperparameter tuning compared to other machine learning algorithms (Szepannek, 2017; Probst et al., 2019), forests were trained using the default parameterization ($ntree = 500$ and $mtry = \sqrt{\#\ variables}$). Details on random forests can be found in the **Online Supplement**.

RESULTS

Participants

An overview of the cohorts including the number of survivors and non-survivors is shown in **Figure 1**. Patient characteristics are listed in **Table 1**.

Model Development

An exploratory analysis showed that platelet count increases over time in survivors compared to non-survivors, while survivors showed a decrease in CRP-levels and non-survivors an increase. This observation motivated us to investigate intercepts and slopes of variables as potential predictors of survival. Twelve subject matter-based predictors were pre-selected to be narrowed down by the described bootstrap approach. Sample size estimation showed that the number of events sufficed for this number of predictors. The predictors with a selection frequency higher than 50% were selected for the final model (**Figure 2**), the shrunk regression coefficients represent the final model.

The apparent variation in mortality explained by all variables selected for the final model amounts to 0.493. Age is the most important predictor with a marginal explained variation (EV) of 0.210 and a high degree of necessity (DN=0.734) and low sufficiency (DS=0.274). All six predictors derived from laboratory parameters together explain 0.295 of variation in mortality with moderately high necessity (DN=0.658) and moderate sufficiency (DS=0.395). Fever on admission is the least important predictor (EV=0.007).

TABLE 1 | Patient characteristics development cohort.

Parameter	Survivors (N=559)	Non-survivors (N=120)
	% / Median (IQR)	% / Median (IQR)
Sex		
Female	40	36
Male	60	64
Age (years)	58 (44-72)	81 (77-89)
BMI	27 (24-31)	26 (25-32)
Comorbidities		
Current smoker	8	10
Overweight (BMI > 25)	62	64
Diabetes type II	18	36
Hypertension	45	74
Coronary heart disease	12	30
Chronic heart failure	6	26
Atrial fibrillation	14	38
Peripheral arterial disease	5	14
Chronic obstructive pulmonary disease	11	14
Asthma	4	6
Hypo- / Hyperthyroidism	8	10
Chronic renal insufficiency	10	44
Chronic liver disease	4	6
Malignancy	9	18
Symptoms at admission		
Asymptomatic	12	2
Fatigue	57	67
Cough	61	51
Fever	52	60
Requirement of oxygen	35	70
Dyspnea	43	41
Diarrhea	16	6
Sore throat	14	0
Nausea or vomiting	7	0
Predictors upon admission		
Platelet count (10^3/ µl)	195 (154-264)	178 (138-220)
CRP (mg/l)	49 (25-88)	60 (33-169)
Creatinine (mg/dl)	0.9 (0.8 - 1.1)	1.4 (1.1-1.8)
LDH (U/l)	283 (231-379)	326 (237-370)

Validation

Tenfold cross validation resulted in a mean AUROC of 0.92, a mean calibration slope of 1.0023 and a mean Brier score of 0.076. In a subsequent cohort, partly from another hospital in Austria and from a period in which the B.1.1.7/Alpha variant of SARS CoV-2 was prevalent, application of the previously developed model showed an AUROC of 0.88, a calibration slope of 0.95 and a Brier score of 0.073 (**Figure 3** and **Table 2**).

Benchmarking Using Machine Learning

Using random forests instead of logistic regression did not result in an increased performance in samples used for 10-fold cross validation. In the cohort used for temporal-external validation, random forests showed a nearly identical performance with strongly overlapping (bootstrap-)confidence intervals for the AUROC (0.88, 95% CI 0.83 - 0.93) with the proposed regression model. Furthermore, accumulated local effects plots (Apley and Zhu, 2020) from the forest confirmed the predictors' effects of our model (**Online Supplement**).

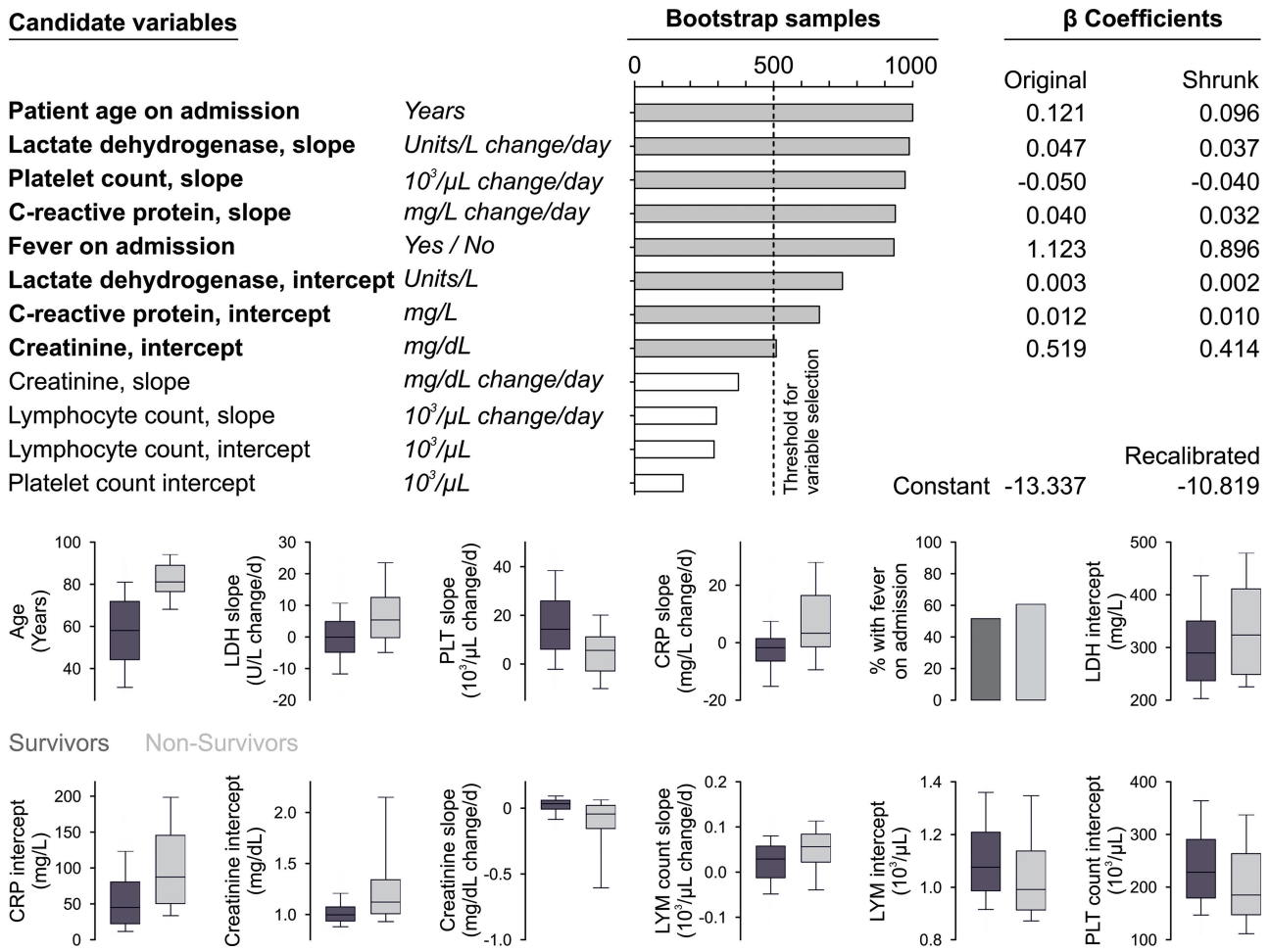

FIGURE 2 | Model development. Candidate variables in bold were selected as they remained in the model after backward elimination in more than 50% of all bootstrap samples. Coefficients were shrunk according to a linear shrinkage factor, which was 0.7974 (Steyerberg et al., 2001). The constant was recalibrated that the mean estimated mortality probability corresponded to the mortality in the training sample. The boxplots show median, interquartile range as well as 10th and 90th percentile of continuous candidate variables or percentages for fever on admission according to outcome.

DISCUSSION

Herein we present a calculator that predicts the risk of death of hospitalized patients with Covid-19 within the period of their stay. It uses the data of the day of admission and the four subsequent days and can therefore be used thereafter as additional decision support regarding discharge of clinically stable Covid-19 patients in case adequate therapy is also available at home. The formula is based on predictors routinely measured in hospitals or naturally available on admission, namely patient age on admission, lactate dehydrogenase, platelet count, C-reactive protein, presence of fever, and creatinine, which allows immediate and widespread use. This is also facilitated by a publicly available online calculator.

The selection of variables to be further narrowed down by bootstrapping was based on pathophysiological considerations. The underlying pathogenesis of Covid-19 seems complex, yet four main intertwined loops (the viral, the hyperinflammatory, the non-canonical renin-angiotensin system (RAS) axis and the hypercoagulatory loop) responsible for patient deterioration have been identified. Three out of the four loops are represented in the presented model. The pathology starts with the viral loop and is rapidly followed by the second loop, the hyperinflammatory loop, which is represented by CRP. Lymphocyte counts have been suggested previously as prognostic markers as well, constituting a major line of defense against viruses (Fouladseresht et al., 2021). Further, LDH is related to inflammation and cell damage and has been suggested as a risk factor for severe Covid-19 (Chen et al., 2020; Poggiali et al., 2020). In addition, the third loop, the non-canonical renin-angiotensin system (RAS) axis loop was described, which is in a broader sense represented by creatinine

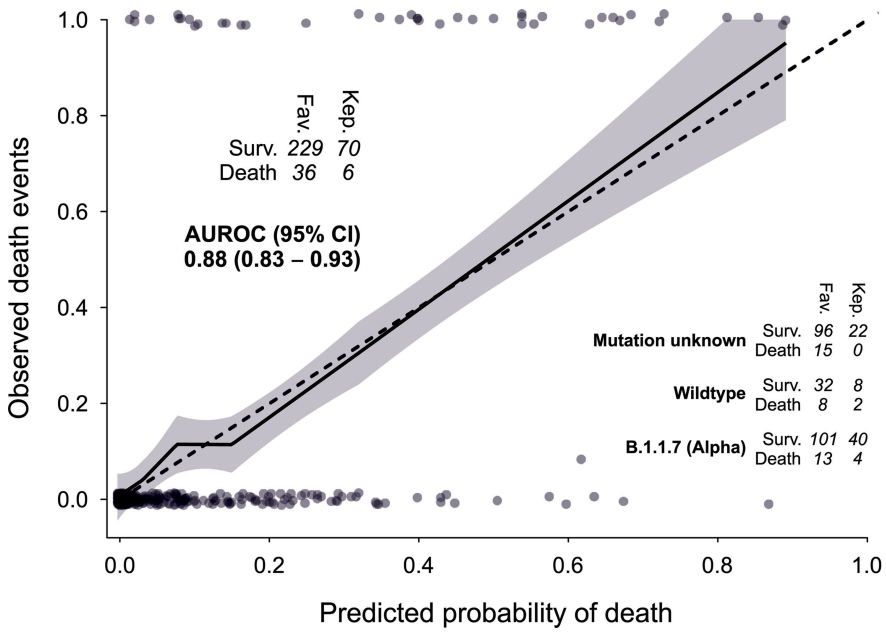

FIGURE 3 | Model performance. Discrimination and calibration in another cohort admitted to hospital while the B.1.1.7/Alpha variant of SARS CoV-2 was widespread. Fav., Clinic Favoriten; Kep., Kepler University Clinics.

TABLE 2 | Predictors in temporal-external validation.

Predictor	Unit	Survivors (N=299) % / Median (IQR)	Non-survivors (N=42) % / Median (IQR)
Patient age on admission	Years	59.00 (49.00 - 73.81)	80.44 (73.00 - 88.92)
Lactate dehydrogenase, slope	Units/L change/day	-1.27 (-9.69 - 4.04)	3.78 (-3.78 - 10.73)
Platelet count, slope	10^3/μL change/day	16.21 (6.95 - 25.66)	11.88 (5.39 - 25.21)
C-reactive protein, slope	mg/L change/day	-2.66 (-10.46 - 0.31)	-7.16 (-14.04-0.36)
Fever on admission		63.5	52.4
Lactate dehydrogenase, intercept	Units/L	31 1.52 (253.39 - 400.49)	439.72 (326.59 - 513.26)
C-reactive protein, intercept	mg/L	32.86 (13.92 - 61.43)	68.19 (53.97 - 94.61)
Creatinine, intercept	mg/dL	0.85 (0.72 - 1.00)	1.02 (0.85 - 1.50)

in our model. Kidney involvement in Covid-19 is common and associated with high mortality and was described to serve as an independent risk factor for all-cause in-hospital mortality in patients with Covid-19 (Ali et al., 2020). Renal viral tropism has been reported, which is also associated with age and comorbidities as well as decreased survival (Braun et al., 2020). Data of more than 17 million people in the UK suggest that patients with chronic kidney disease are at higher risk for adverse events in Covid-19 than those with other known risk factors, including chronic heart and lung disease (Gansevoort and Hilbrands, 2020). The fact that the slope of creatinine seemed to have less prognostic value than the intercept might reflect the importance of chronic kidney disease. The fourth loop is the hypercoagulatory loop, which is represented by platelet count in this model. A meta-analysis of 7,613 Covid-19 patients revealed that patients with severe disease had a lower platelet count than those with non-severe disease (Jiang et al., 2020), which is in line with our data. However, not all studies have found platelet counts to be a predictor of Covid-19 mortality (Amgalan and Othman, 2020). Undoubtedly the most important predictor of severe Covid-19 is age. A meta-analysis of 88 articles (69,762 patients) shows that age along with CRP were strong risk-factors for ICU admission and/or mortality (Katzenschlager et al., 2020). Concerning fever, a recent meta-analysis reported that fever is a predictor of adverse outcome in Covid-19 (Li et al., 2020). In line with studies on other viral infectious diseases, a study found that prolonged fever for 7 days from onset of illness is associated with adverse outcomes from Covid-19, while saddleback fever is not indicative of adverse outcome (Ng et al., 2020). In our model fever at admission was incorporated in the prediction model. The time course of body temperature would have been interesting to include, however, available records only allowed inclusion as a binary variable. As our data show, many differences between survivors and non-survivors only develop over the course of a

few days, and Mueller et al. (2020) showed that trends in inflammatory biomarkers precede respiratory failure. Thus, we sought to include the time courses of variables as predictors.

Regarding the relative importance of the variables included in our final model, the (apparent) variation in mortality explained by the six variables deduced from the laboratory parameters measured during the first four days is slightly higher than that of age. While our data confirm that high age is a principal risk factor for dying from Covid-19, these laboratory variables are able to add considerably to the sufficiency of age and, thus, to the predictive importance of the model.

Concerning machine learning, the results of the benchmark do not show a performance increase by using random forests instead of logistic regression and thus confirm the conclusions from Bücker et al. (2021) to carefully analyze the benefits of using more complex models and to prefer simple models such as the shrunk logistic regression model otherwise.

Limitations

Our prognostic model is far from being the first. Compared to other well developed and validated models, e.g., the 4C mortality Score (Knight et al., 2020), ours tends to distinguish patients who die from those who survive better than many others, indicated by an externally validated c index significantly above 0.8. However, this good performance may be geographically limited, for example due to differences in health care systems that lead to varying periods between infection and admission and consequently to different disease stages upon admission. As a result, we can only recommend the use of the model in Austria before the model has been validated in or updated for other regions. Of note, the calibration plot indicates slight underestimation of death probabilities in the upper range of death probabilities.

A major aspect that discriminates our model from others is the use of the time course of biological parameters as predictors. Many others included the values at admission exclusively, which is reasonable, as information regarding prognosis should generally be available as early as possible. Thus, it might be viewed as a drawback of our model that decision making takes until day 4 of hospitalization. However, we think that the time course of variables after admission generally contains information regarding future disease progression. Considering that based on over 10,000 patients from Germany (Karagiannidis et al., 2020), even the less critical non-ventilated patients have a median stay of 9 days, it seems reasonable to improve prognostic accuracy by delaying the prognosis time point by 4 days.

Further, it remains uncertain whether further mutations of SARS CoV-2 might render the model unsuitable. However, this is a general problem regarding prediction models for rapidly developing diseases, and it may require frequent recalibration of models. The currently dominating Delta-variant is not yet considered by the model.

Implications

For the time being, the model is applicable to patients hospitalized with verified Covid-19 and should support decision making on earlier discharge. Validation of the model in different regions is required to assess where it can be used in its original form and where it needs to be recalibrated. The model was developed for and its use should be restricted to this specific clinical application, if not validated for other purposes. In case the number of patients with Covid-19 in the general ward exceeds numbers that can easily be handled and thus binds resources that would be urgently needed elsewhere, the attending physicians could decide to discharge those patients with the lowest model-predicted death probabilities. It is vital that the estimated probability is not the sole criterion for decision-making and that the physician should always include a further assessment of the situation. Furthermore, it should be ascertained that discharge has no relevant impact on treatments, i.e., only those patients should be discharged where an adequate treatment can be implemented on an outpatient basis or in quarantine. It is necessary to emphasize that high estimated death probabilities should not be overinterpreted, as their reliability is not as well determined as low death probabilities, as visualized by the calibration plot. There is no general recommendation for a cut-off value, below which an earlier discharge would be justified. This cut-off depends on current strain on the healthcare system. In case patients need to be discharged, one could start with the ones with the lowest death probabilities.

AUTHOR'S NOTE

For commercial use of the prediction model, please contact the corresponding author and the Technology Transfer Office of the Medical University of Vienna at technologietransfer@muv.ac.at.

DATA AVAILABILITY STATEMENT

The raw data supporting the conclusions of this article will be made available by the authors, without undue reservation.

ETHICS STATEMENT

The studies involving human participants were reviewed and approved by Ethical commission of the Medical University of Vienna (EK1315/2020). The patients/participants provided their written informed consent to participate in this study.

AUTHOR CONTRIBUTIONS

SHe, AZ, and AA contributed to conception and design of the study. DP, WS, KK, JS, BR, EP, MH, AS, ML, AH, KH, BL, SHe, MT, MN, CS, TS, CF, MK, GW, BJ, CT, RB-W, and HS organized the database. SHe, GS, and AG performed the statistical analysis. SHe, MF, and AA wrote the first draft of the manuscript. GS wrote sections of the manuscript. All authors

contributed to manuscript revision, read, and approved the submitted version.

FUNDING

This work is part of the ACOVACT study of the Medical University of Vienna and is financially supported by the Austrian Federal Ministry of Education, Science and Research, the Medical-Scientific Fund of the Mayor of Vienna (COVID024) and the Austrian Science Fund (P32064; P34783; SFB-54) and by Region Stockholm, Knut and Alice Wallenberg foundation, Jonas & Christina af Jochnick foundation (CT). The funders had no role in the design of this study.

ACKNOWLEDGMENTS

We thank Prof. Zimmermann and Prof. Hahn from the AI Solution Group GmbH, Frankfurt for recomputing and discussions on data interpretation.

SUPPLEMENTARY MATERIAL

The Supplementary Material for this article can be found online at: https://www.frontiersin.org/articles/10.3389/fcimb.2021.795026/full#supplementary-material

REFERENCES

Ali, H., Daoud, A., Mohamed, M. M., Salim, S. A., Yessayan, L., Baharani, J., et al. (2020). Survival Rate in Acute Kidney Injury Superimposed COVID-19 Patients: A Systematic Review and Meta-Analysis. *Renal Failure* 42 (1), 393–397. doi: 10.1080/0886022X.2020.1756323

Amgalan, A., and Othman, M. (2020). Hemostatic Laboratory Derangements in COVID-19 With a Focus on Platelet Count. *Platelets* 31 (6), 740–745. doi: 10.1080/09537104.2020.1768523

Apley, D. W., and Zhu, J. (2020). Visualizing the Effects of Predictor Variables in Black Box Supervised Learning Models. *J. R. Stat. Soc.: Ser. B (Stat. Method)* 82 (4), 1059–1086. doi: 10.1111/rssb.12377

Braun, F., Lütgehetmann, M., Pfefferle, S., Wong, M. N., Carsten, A., Lindenmeyer, M. T., et al. (2020). SARS-CoV-2 Renal Tropism Associates With Acute Kidney Injury. *Lancet* 396 (10251), 597–598. doi: 10.1016/S0140-6736(20)31759-1

Bücker, M., Szepannek, G., Gosiewska, A., and Biecek, P. (2021). Transparency, Auditability, and Explainability of Machine Learning Models in Credit Scoring. *J. Oper. Res. Soc.* 1–21. doi: 10.1080/01605682.2021.1922098

Chen, X. Y., Huang, M. Y., Xiao, Z. W., Yang, S., and Chen, X. Q. (2020). Lactate Dehydrogenase Elevations Is Associated With Severity of COVID-19: A Meta-Analysis. *Crit. Care* 24 (1), 459. doi: 10.1186/s13054-020-03161-5

Corman, V. M., Landt, O., Kaiser, M., Molenkamp, R., Meijer, A., Chu, D. K., et al. (2020). Detection of 2019 Novel Coronavirus (2019-Ncov) by Real-Time RT-PCR. *Eur. Surveillance Bull. Eur. Sur Les Maladies Transmissibles = Eur. Commun Dis. Bull.* 25 (3), pii=2000045. doi: 10.2807/1560-7917.ES.2020.25.3.2000045

Fernández-Delgado, M., Cernadas, E., Barro, S., and Amorim, D. (2014). Do We Need Hundreds of Classifiers to Solve Real World Classification Problems? *J. Mach. Learn Res.* 15 (1), 3133–3181.

Fitzmaurice, G. M., Laird, N. M., and Ware, J. H. (2011). *Applied Longitudinal Analysis. 2nd*. Ed. N. J. Hoboken (Hoboken, New Jersey: Wiley-Interscience).

Fouladseresht, H., Doroudchi, M., Rokhtabnak, N., Abdolrahimzadehfard, H., Roudgari, A., Sabetian, G., et al. (2021). Predictive Monitoring and Therapeutic Immune Biomarkers in the Management of Clinical Complications of COVID-19. *Cytokine Growth Factor Rev.* 58, 32–48. doi: 10.1016/j.cytogfr.2020.10.002

Gansevoort, R. T., and Hilbrands, L. B. (2020). CKD Is a Key Risk Factor for COVID-19 Mortality. *Nat. Rev. Nephrol.* 16 (12), 705–706. doi: 10.1038/s41581-020-00349-4

Gleiss, A., and Schemper, M. (2019). Quantifying Degrees of Necessity and of Sufficiency in Cause-Effect Relationships With Dichotomous and Survival Outcomes. *Stat. Med.* 38 (23), 4733–4748. doi: 10.1002/sim.8331

Jiang, S. Q., Huang, Q. F., Xie, W. M., Lv, C., and Quan, X. Q. (2020). The Association Between Severe COVID-19 and Low Platelet Count: Evidence From 31 Observational Studies Involving 7613 Participants. *Br. J. Haematol.* 190 (1), e29–e33. doi: 10.1111/bjh.16817

Karagiannidis, C., Mostert, C., Hentschker, C., Voshaar, T., Malzahn, J., Schillinger, G., et al. (2020). Case Characteristics, Resource Use, and Outcomes of 10 021 Patients With COVID-19 Admitted to 920 German Hospitals: An Observational Study. *Lancet Respir. Med.* 8 (9), 853–862. doi: 10.1016/S2213-2600(20)30316-7

Katzenschlager, S., Zimmer, A. J., Gottschalk, C., Grafeneder, J., Seitel, A., Maier-Hein, L., et al. (2021). Can We Predict the Severe Course of COVID-19 - A Systematic Review and Meta-Analysis of Indicators of Clinical Outcome? *PLoS One* 16 (7), e0255154. doi: 10.1371/journal.pone.0255154

Knight, S. R., Ho, A., Pius, R., Buchan, I., Carson, G., Drake, T. M., et al. (2020). Risk Stratification of Patients Admitted to Hospital With Covid-19 Using the ISARIC WHO Clinical Characterisation Protocol: Development and Validation of the 4C Mortality Score. *BMJ* 370, m3339. doi: 10.1136/bmj.m3339

Liaw, A., and Wiener, M. (2002). Classification and Regression by Randomforest. *R News* 2, 18–22.

Li, J., He, X., Yuan, Y., Zhang, W., Li, X., Zhang, Y., et al. (2020). Meta-Analysis Investigating the Relationship Between Clinical Features, Outcomes, and Severity of Severe Acute Respiratory Syndrome Coronavirus 2 (SARS-CoV-2) Pneumonia. *Am. J. Infect. Cont.* 49 (1), 82–89. doi: 10.1016/j.ajic.2020.06.008

Manson, J. J., Crooks, C., Naja, M., Ledlie, A., Goulden, B., Liddle, T., et al. (2020). COVID-19-Associated Hyperinflammation and Escalation of Patient Care: A Retrospective Longitudinal Cohort Study. *Lancet Rheumatol.* 2 (10), e594–e602. doi: 10.1016/S2665-9913(20)30275-7

Mueller, A. A., Tamura, T., Crowley, C. P., DeGrado, J. R., Haider, H., Jezmir, J. L., et al. (2020). Inflammatory Biomarker Trends Predict Respiratory Decline in COVID-19 Patients. *Cell Rep. Med.* 1 (8), 100144. doi: 10.1016/j.xcrm.2020.100144

Ng, D. H. L., Choy, C. Y., Chan, Y. H., Young, B. E., Fong, S. W., Ng, L. F. P., et al. (2020). Fever Patterns, Cytokine Profiles, and Outcomes in COVID-19. *Open Forum Infect. Dis.* 7 (9), ofaa375. doi: 10.1093/ofid/ofaa375

Poggiali, E., Zaino, D., Immovilli, P., Rovero, L., Losi, G., Dacrema, A., et al. (2020). Lactate Dehydrogenase and C-Reactive Protein as Predictors of Respiratory Failure in CoVID-19 Patients. *Clin. Chim. Acta* 509, 135–138. doi: 10.1016/j.cca.2020.06.012

Probst, P., Boulesteix, A.-L., and Bischl, B. (2019). Tunability: Importance of Hyperparameters of Machine Learning Algorithms. *J. Mach. Learn. Res.* 20 (1), 1934–1965.

Riley, R. D., Ensor, J., Snell, K. I. E., Harrell, F. E. Jr., Martin, G. P., Reitsma, J. B., et al. (2020). Calculating the Sample Size Required for Developing a Clinical Prediction Model. *BMJ* 368, m441. doi: 10.1136/bmj.m441

Steyerberg, E. W., Eijkemans, M. J. C., and Habbema, J. D. F. (2001). Application of Shrinkage Techniques in Logistic Regression Analysis: A Case Study. *Stat. Neerlandica* 55 (1), 76–88. doi: 10.1111/1467-9574.00157

Szepannek, G. (2017). *On the Practical Relevance of Modern Machine Learning Algorithms for Credit Scoring Applications*. Ed. H.-J. Mucha, WIAS Report Series 29 (Berlin: WIAS). Available at: https://www.wias-berlin.de/publications/wias-publ/index.jsp?lang=1.

Wang, L. (2020). C-Reactive Protein Levels in the Early Stage of COVID-19. *Med. Maladies Infect.* 50 (4), 332–334. doi: 10.1016/j.medmal.2020.03.007

Wynants, L., Van Calster, B., Collins, G. S., Riley, R. D., Heinze, G., Schuit, E., et al. (2020). Prediction Models for Diagnosis and Prognosis of Covid-19: Systematic Review and Critical Appraisal. *BMJ* 369, m1328. doi: 10.1136/bmj.m1328

Conflict of Interest: The authors declare that the research was conducted in the absence of any commercial or financial relationships that could be construed as a potential conflict of interest.

Publisher's Note: All claims expressed in this article are solely those of the authors and do not necessarily represent those of their affiliated organizations, or those of the publisher, the editors and the reviewers. Any product that may be evaluated in this article, or claim that may be made by its manufacturer, is not guaranteed or endorsed by the publisher.

frontiers in Cellular and Infection Microbiology

BRIEF RESEARCH REPORT
published: 28 January 2022
doi: 10.3389/fcimb.2022.823306

The Impact of Accumulated Mutations in SARS-CoV-2 Variants on the qPCR Detection Efficiency

*Liu Cao†, Tiefeng Xu†, Xue Liu†, Yanxi Ji, Siyao Huang, Hong Peng, Chunmei Li and Deyin Guo**

Centre for Infection and Immunity Study (CIIS), School of Medicine, Sun Yat-sen University, Shenzhen, China

OPEN ACCESS

Edited by:
Guiqing Peng, Huazhong Agricultural University, China

Reviewed by:
Nannan Wu, Fudan University, China
J. Stephen Lodmell, University of Montana, United States

***Correspondence:**
Deyin Guo
guodeyin@mail.sysu.edu.cn

†These authors have contributed equally to this work

Specialty section:
This article was submitted to Virus and Host, a section of the journal Frontiers in Cellular and Infection Microbiology

Received: *27 November 2021*
Accepted: *05 January 2022*
Published: *28 January 2022*

Citation:
Cao L, Xu T, Liu X, Ji Y, Huang S, Peng H, Li C and Guo D (2022) The Impact of Accumulated Mutations in SARS-CoV-2 Variants on the qPCR Detection Efficiency. Front. Cell. Infect. Microbiol. 12:823306. doi: 10.3389/fcimb.2022.823306

SARS-CoV-2 is evolving with mutations throughout the genome all the time and a number of major variants emerged, including several variants of concern (VOC), such as Delta and Omicron variants. In this study, we demonstrated that mutations in the regions corresponding to the sequences of the probes and 3'-end of primers have a significant impact on qPCR detection efficiency. We also found that the G28916T mutation of the N gene accounts for 78.78% sequenced genomes of Delta variant. It was found that detection sensitivity of G28916T mutant was 2.35 and 1.74 times less than that of the wt sequence and detection limit was reduced from 1 copy/μl to 10 copies/μl for the commercially available CP3 and CP4 primer/probe sets. These results indicate that the detection probes and primers should be optimized to keep maximal detection efficiency in response to the emergence of new variants.

Keywords: SARS-CoV-2, SARS-COV-2 variants, delta variant, quantitative PCR, qPCR detection efficiency

INTRODUCTION

Coronavirus disease 2019 (COVID-19) caused by severe acute respiratory syndrome coronavirus 2 (SARS-CoV-2) has caused a severe global pandemic. Virus detection is the first step to fight against COVID-19 epidemic. SARS-CoV-2 tests can be grouped as nucleic acid, serological, antigen, and ancillary tests, all of which play distinct roles in hospital, point-of-care, or large-scale population testing (Ravi et al., 2020; Shi et al., 2020). Especially, the real-time quantitative PCR (qPCR) method is the most common and the most widely used. qPCR-based assays performed on respiratory specimens have emerged as the cornerstone of COVID-19 diagnostic and screening testing (Corman et al., 2020; Vogels et al., 2020). However, mutations and deletions on the SARS-CoV-2 genome may reduce the detection efficiency of qPCR (Penarrubia et al., 2020; Ziegler et al., 2020; Hasan et al., 2021). Although the coronavirus has a certain proofreading ability (Robson et al., 2020), it still has a high mutation rate, which leads to the emergence of new variants. At present, the WHO has classified many variants of the SARS-CoV-2 (WHO, 2021), including the variants of concern (VOC), such as the Alpha variant (B.1.1.7), Beta variant (B.1.351), Gamma variant (P.1), Delta variant (B.1.671.2) and Omicron variant (B.1.1.529). Delta and Omicron variants are highly

contagious, and have rapidly become the prevalent variants, accounting for more than 99% of SARS-CoV-2 variants from December 1 to December 27, 2021. Delta variant may lead to vaccine breakthrough infections associated with higher viral load and long duration of shedding (Reardon, 2021). Omicron variant has higher transmission capacity and exhibits stronger ability to evade the protection of previously existing antibodies and currently available vaccines (Cao et al., 2021; Cele et al., 2021; Chen et al., 2021; Liu et al., 2021; Planas et al., 2021). In this study, we systematically analysed the mutations of the SARS-CoV-2 genome and showed that some mutations that correspond to the target sequences of qPCR probe/primer may have significant impact on the detection efficiency.

METHODS

Sources and Analyze of Sequences

As of 1 January to 19 February, 2021, there were a total of 89791 high-quality SARS-CoV-2 genomes sequences available in Global Initiative on Sharing All Influenza Data (GISAID) (Shu and McCauley, 2017). These high-quality genomic sequences of SARS-CoV-2 were screened out under the following criteria: 1) the genome is full-length; 2) exclusion of the sequences with unsolved nucleotides (i.e continuous Ns). Meanwhile, we downloaded the high-quality genomic sequences for "Variants of concern" that accord with above conditions: Alpha (B.1.1.7) with 108791 sequences; Beta (B.1.351) with 13871 sequences and Gamma (P.1) with 18808 sequences from May 1 to June 15, 2021; Delta (B.1.617.2) with 302879 sequences as of August 11, 2021; Omicron with 20356 sequences from November to December 22, 2021. "Variants of interest" include Lambda (C.37) with 627 sequences and Mu (B.1.621) with 2771 sequences until September 11, 2021 (**Figure S1**).

Sequence Processing

To do unbiased genomic variation analysis, we further filtered and deleted those sequences with more than 50 consecutive N bases (50NNNs or 50nnns). Finally, 145,044 SARS-CoV-2 sequences were screened out. There were 92214, 6341, 13655, 211740, 2333, 345 and 2276 sequences selected for Alpha (B.1.1.7), Beta (B.1.351), Gamma (P.1), Delta (B.1.617.2), Omicron (B.1.1.529), Lambda (C.37) and Mu (B.1.621), respectively.

The SARS-CoV-2 genome of NC_045512.2 (Wu et al., 2020) was utilized as the reference sequence. Multiple sequences alignments were performed using the progressive method (FFT-NS-2) implemented in MAFFT (version 7.4) (Katoh et al., 2002). The whole genome mutation analysis was carried out used the pipeline provided by CoVa (version 0.2) software (Ali et al. 2020). For substitution analysis, we first deleted the gap generated in the multi-sequence alignments based on the ref NC_045512.2 and then used the CoVa pipeline for substitution calculation (**Figure S1**).

We summarize the mutation frequency of each mutant sequences. In order to avoid false positive results caused by errors in sequencing and multi-sequence alignments, we only analyzed the mutations with frequency greater than or equal to 10.

Plasmid Constructs

Standard plasmids were purchased from Sangon Biotech (Shanghai). Point mutations were introduced into standard plasmids by PCR-mediated mutagenesis, with appropriate primers (**Table S1**) containing the desired nucleotide changes and subsequently selected by DpnI digestin.

qPCR Analysis

The plasmids was amplified by a fast two-step amplification program using Taq Pro HS Universal Probe Master Mix (Vazyme Biotech Co., Ltd.).

RESULTS

Mutations of SARS-CoV-2 Lead to Decrease in Detection Efficiency of qPCR

To explore the impact of mutations on qPCR detection of the circulating strains of SARS-CoV-2, we downloaded and analyzed the overall mutations and deletions of 89,791 high-quality SARS-CoV-2 sequences from the GISAID database (detailed information in methods).

We first made an analysis of the overall mutations. We calculated the mutation frequency and quantity at each site along the SARS-CoV-2 genomes in comparison with the wildtype strain (**Figures 1A, B**). In general, the mutation frequency and quantity of the genomic regions encoding structural proteins and accessory proteins are higher than that of non-structural proteins. In the regions of ORF3a, ORF7a, ORF8 and N genes, mutations were observed at the positions of more than 30% of the bases, indicating a high propencity of mutations throughout the genes. For example, we found that there are mutations at 445 sites in N gene, which account for 35.3% of the total 1260 nucleotides. In the analyzed sequences, the average number of mutations per base of S, ORF8, N and ORF10 genes exceeds 100, indicating that, on average, at least 100 of the analyzed sequences contain a mutation at one nucleotide position of the genes. In the S gene, we found a total of 434360 mutations in the 89,791 SARS-CoV-2 sequences, with an average of 113.6 sequences having mutation at one site of the S gene (**Figures 1A, B**). S and N genes belong to the main targets for qPCR detections. These two genes have a high probability of mutation, which may have a potential impact on qPCR detection.

Next, we analyzed the preference of the base mutations and found that the ratio of transition to transversion mutation is about 2:1. And the results show that the most frequently mutated base is cytosine (C) followed by guanine (G), uracil (U) and adenine (A). C and G mutations accounted for 46.85% and 27.39% of the total number of mutations (**Figures 1C, D**). The mutation from C to U is most frequent and accounted for 39.77% of the total number of mutations. A→C and C→G are the two

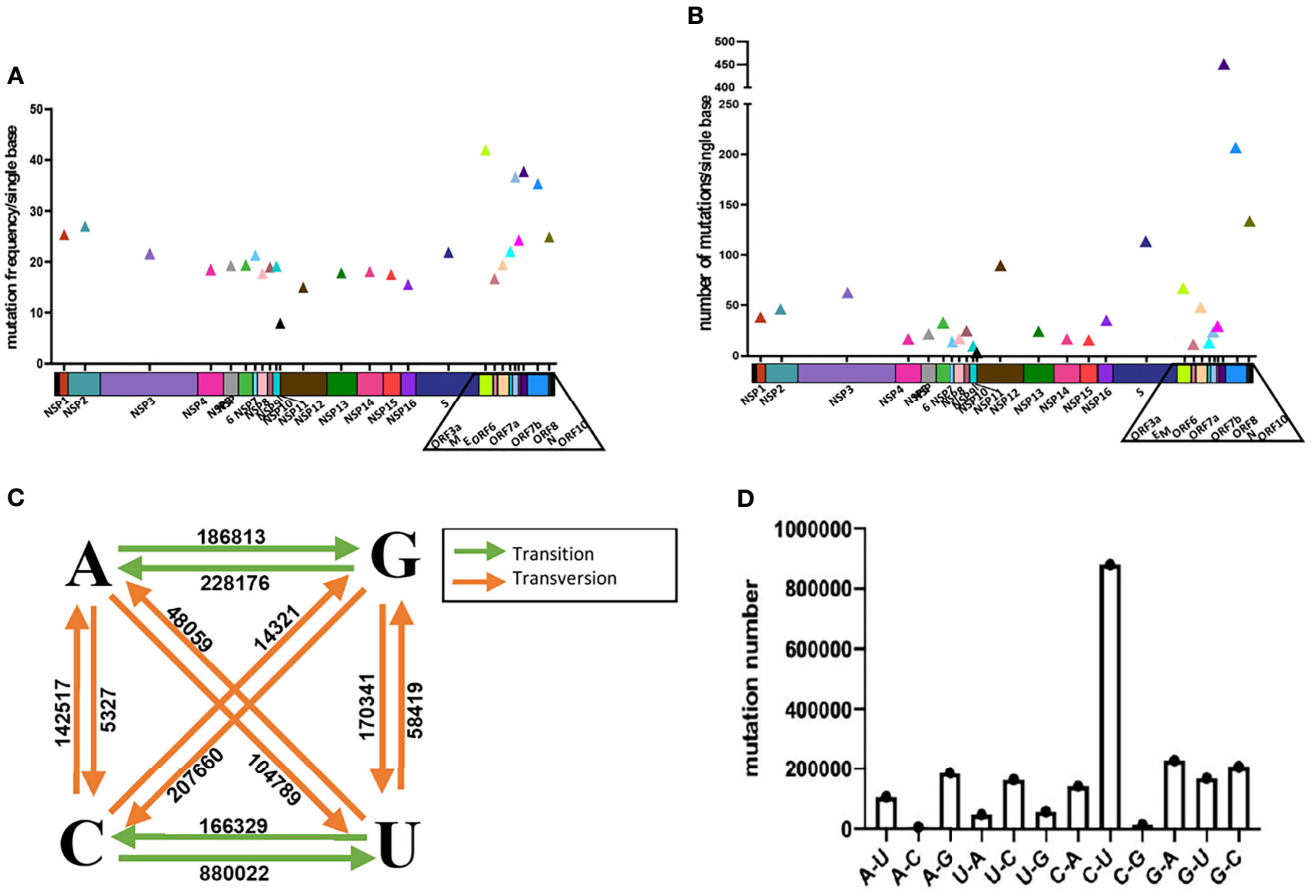

FIGURE 1 | Analysis of the mutations in SARS-CoV-2. Analyze the average mutation frequency **(A)** and number **(B)** of mutations per base of 89,791 SARS-CoV-2 sequences in 26 viral genes. Average mutation frequency = The total number of mutation sites of gene in 89,791 SARS-CoV-2 sequences/the total number bases of the gene. Average mutation number = The total number of mutations of gene in 89,791 SARS-CoV-2 sequences/the total number bases of the gene. **(C, D)** Analysis of base selection for mutations in 89,791 SARS-CoV-2 sequences.

least mutations, accounting for only 0.24% and 0.64% of the total number of mutations.

Then we compared mutations with the primer/probe sequences of qPCR most commonly used in the commercial providers or public institutions (13 pairs from China, and 15 pairs from other countries were selected) (**Figure S2** and **Tables S2**, **S3**). The positions and numbers of nucleotide substitutions in more than 25 sequences and all deletions in the regions corresponding to the primer/probe sequences in **Table S2** and **Table S3**. We found that all the primer/probe-targeting sequences have varying degrees of mutations.

To explore the impact of these mutations on detection efficiency, we divide the mutations on the targets of primers/probes into 3 types:the mutation on the probe, the last two base mutation at the 3'-end of the primer and the mutation at other positions of primer.

We took the two pairs of primer/probe sets of China CDC, targeting the 1ab and the N gene as an example, and generated sequence template with single mutations and multi-site mutations that exist in the primer/probe target sequences on standard plasmids. These mutants are listed in **Table S2**. We detected the difference of detection efficiency between the wildtype (wt) and the mutant sequences by qPCR. The results showed that the detection sensitivity of the mutations on the probe target was 3-32 times less than that of the wildtype sequence (**Figures 2A, B**). All mutations on the probe target would affect the detection efficiency of qPCR, and the detection sensitivity of the double-mutation template was 9900 times less than that of the wt sequence. Most individual mutations in the primer targets basically did not affect the detection efficiency of qPCR, except for some cases of multiple mutations (**Figures S3**, **S4**). In particular, the multiple mutations at the 3'-end of the primer affected the detection efficiency, and the closer the mutation is to 3'-end of primer, the greater the impact (**Figure S4**).

Then, we found that there are mutations in the 3'-end of primers in the three primer/probe sets (Japan-NIDS, USCDC, Institute of Microbiology and Virology (IMV)) with target sites

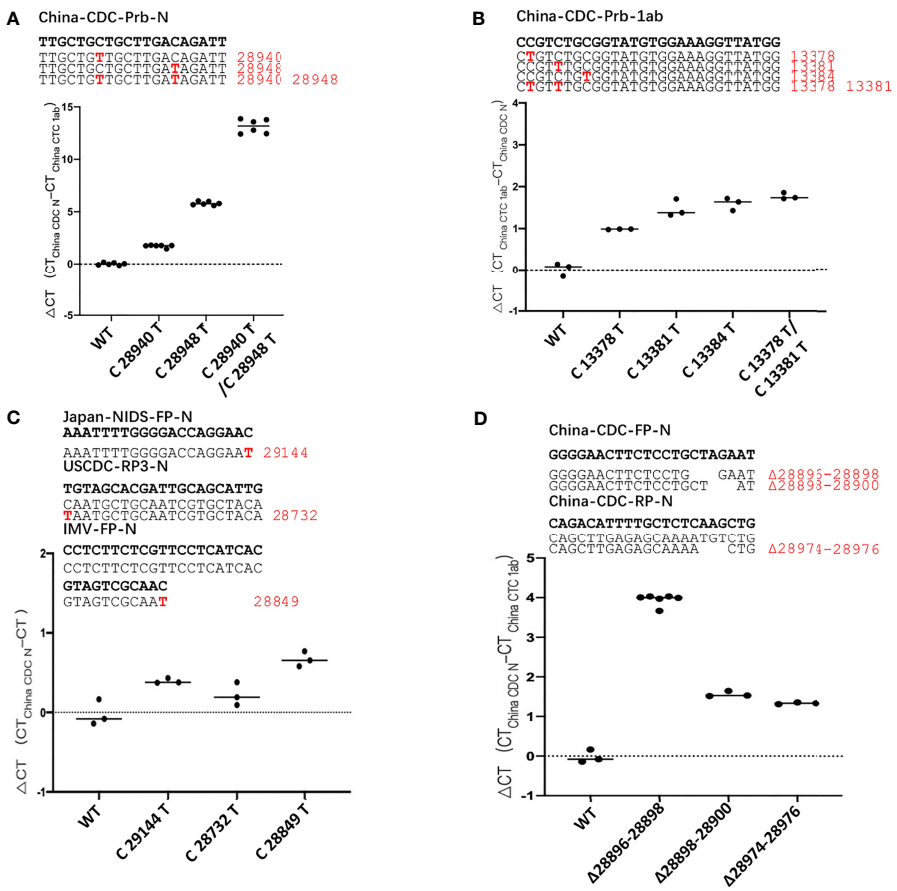

FIGURE 2 | The mutation of SARS-CoV-2 leads to poor detection of qPCR. ΔCt values for testing of the standard plasmid and the mutant plasmid **(A, B)** mutations in the probe, **(C)** mutations in the 3'-end of primer, **(D)** deletion mutant on primer using primer/probe sets by qPCR. The red letters represent the mutation bases, and the red numbers represent the mutation positions. All plasmid used in the figure are 8.5 x 10^2 copies.

on the N gene and constructed the corresponding site mutations on N gene sequence (**Table S2**). We used qPCR to detect the difference of detection efficiency between the wt and the mutant sequences (**Figure 2C**). It was found that a single mutation on 3'-end of primer had little effect on detection. According to previous reports, the degree of mismatch of 3'-end of primer that affects the detection efficiency, especially the mismatches of A: A, G: A and C:C cause the detection efficiency to be markedly reduced (Kwok et al., 1990; Ghedira et al., 2009; Stadhouders et al., 2010; Rejali et al., 2018). But, in the transition of C→U, mismatches of T:G has the least influence on the efficiency of qPCR detection, compared to other types of mismatches (Rejali et al., 2018). Therefore, we substituted the last 3'-base of primer target with any of the other 3 bases and compared the detection efficiency of qPCR with primer/probe sets of Japan-NIDS FP-N, USCDC RP-N3, IMV-FP-N etc. (**Figure S5**). It was found that the mismatch of A:G, G:G, A:A, T:C, C:C and T:T had apparent influence on the efficiency of qPCR. However, the mismatch of T:G and C:A had little effect on the efficiency of qPCR. Coincidentally, we found that the 3'-end of primer mutation sites (Japan-NIDS FP-N, USCDC RP-N3, IMV-FP-N) are T:G and C:A mismatches. However, A:G, G:G, A:A, T:C, C:C and T:T mismatches at the 3'-end of primer may affect the detection efficiency of qPCR.

We also tested the impact of deletion mutants on detection efficiency, and we took the primer/probe sets of China CDC targeting the N gene as an example. We found that a number of variant sequences contain a 3'-base deletion on the forward primer target (28896-28898, 28898-28900), and a 3'-base deletion on the reverse primer target (28974-28976). The deletion mutants were generated and detected by the qPCR (**Figure 2D**). It was found that the detection sensitivity of the deletion mutants was 3-16 times less than that of the wt sequence. Finally, we analyzed the detection limit of wt and deletion mutants template sequences. We diluted the templates to the concentration of 100, 10, 1 and 0.1 copies/μl (**Figure S6**). The results showed that wt template could be detected at 1 copy/μl, but only 10 copies/μl for mutant sequence.

In general, through the above experiments, we have determined that mutations on the probe and 3'-end of primer sequences have a significant impact on qPCR detection, while mutations at the remaining positions have relatively little impact.

TABLE 1 | The point mutation of primer/probe sets in SARS-CoV-2 Variants.

92,214 high quality SARS-CoV-2 Alpha variant			
CP1	FP-S5	**CAGGTATATGCGCTAGTTATCAGAC**	23565-23589
(sigma)	RP-S5	**CCAAGTGACATAGTGTAGGCAATG**	23638-23661
	Prb-S5	**AGACTAATTCTCCTCGGCGGGCACG**	23592-23616
		AGACTAATTCTC**A**TCGGCGGGCACG **(91682)**	
		Mutation rate:99.42%	
6,341 high-quality SARS-CoV-2 Beta variants			
CP3	FP-S	**CCTACTAAATTAAATGATCTCTGCTTTACT**	22712-22741
(State Key Laboratory of Emerging Infectious	RP-S	**CAAGCTATAACGCAGCCTGTA**	22849-22869
Diseases)	Prb-S	**CGCTCCAGGGCAAACTGGAAAG**	22792-22813
		CGCTCCAGGGCAAACTGGAAA**T (5877)**	
		Mutation rate:92.68%	
13,655 high-quality SARS-CoV-2 Gamma variants			
CP3	FP-S	**CCTACTAAATTAAATGATCTCTGCTTTACT**	22712-22741
(State Key Laboratory of Emerging Infectious	RP-S	**CAAGCTATAACGCAGCCTGTA**	22849-22869
Diseases)	Prb-S	**CGCTCCAGGGCAAACTGGAAAG**	22792-22813
		CGCTCCAGGGCAAACTGGAA**C**G **(13609)**	
		Mutation rate:99.66%	
211,740 high-quality SARS-CoV-2 Delta variants			
CP4	FP-N	**AAGAAATTCAACTCCAGGCAGC**	28855-28876
(Da An Gene of Sun Yat-sen University)	RP-N	**GCTGGTTCAATCTGTCAAGCAG**	28940-28961
	Prb-N	**TCACCGCCATTGCCAGCCA**	28902-28920
		TGGCTGGCAATGGCGGTGA	
		TGGCTGGCAATGGC**T**GTGA **(166809)**	
		Mutation rate:78.78%	
CP5 (Institute of Microbiology and Virology)	FP-N	**CCTCTTCTCGTTCCTCATCACGTAGTCGCAAC**	28818-28849
	RP-N	**AGTGACAGTTTGGCCTTGTTGTTGTTGGCCTT**	28983-29014
	Prb-N	**CCTGCTAGAATGGCTGGCAATGGCGGTGA**	28892-28920
		CCTGCTAGAATGGCTGGCAATGGC**T**GTGA **(166809)**	
		Mutation rate:78.78%	
CP1	FP-S5	**CAGGTATATGCGCTAGTTATCAGAC**	23565-23589
(sigma)	RP-S5	**CCAAGTGACATAGTGTAGGCAATG**	23638-23661
	Prb-S5	**AGACTAATTCTCCTCGGCGGGCACG**	23592-23616
		AGACTAATTCTC**G**TCGGCGGGCACG **(211272)**	
		Mutation rate:99.78%	
2,333 high-quality SARS-CoV-2 Omicron variants			
Institute	Name	Sequence	Position
CP6(USCDC)	FP-N1	**GACCCCAAAATCAGCGAAAT**	28287–28306
	RP-N1	**TCTGGTTACTGCCAGTTGAATCTG**	28335–28358
		CATATTCAACTGGCAGTAACCAGA	
	Prb-N1	**ACCCCGCATTACGTTTGGTGGACC**	28309–28332
		AC**T**CCGCATTACGTTTGGTGGACC **(2297)**	
		Mutation rate:98.45%	
CP2 (Northwell Health Laboratories)	FP-S	**TCAACTCAGGACTTGTTCTTAC**	21710-21731
	RP-S	**TGGTAGGACAGGGTTATCAAAC**	21796-21817
		GTTTGATAACCCTGTCCTACCA	
	Prb-S	**TGGTCCCAGAGACATGTATAGCAT**	21759-21782
		ATGCTATACATGTCTCTGGGACCA	
		ATG**T**TATACATGTCTCTGGGACCA **(2297)**	
		Mutation rate:98.45%	
CP1	FP-S5	**CAGGTATATGCGCTAGTTATCAGAC**	23565-23589
(Sigma)	RP-S5	**CATTGCCTACACTATGTCACTTGG**	23638-23661
		CCAAGTGACATAGTGTAGGCAATG	
	Prb-S5	**AGACTAATTCTCCTCGGCGGGCACG**	23592-23616
		AGACTAA**G**TCTCCTCGGCGGGCACG **(2315)**	
		Mutation rate:99.23%	
		AGACTAATTCTC**A**TCGGCGGGCACG **(2312)**	
		Mutation rate:99.10%	
345 high-quality SARS-CoV-2 Lambda variants			
CP4	FP-N	**AAGAAATTCAACTCCAGGCAGC**	28855-28876
(Da An Gene Co., Ltd. of Sun Yat-sen University)	RP-N	**GCTGGTTCAATCTGTCAAGCAG**	28940-28961
		CTGCTTGACAGATTGAACCAGC	
	Prb-N	**TCACCGCCATTGCCAGCCA**	28902-28920
		TGGCTGGCAATGGCGGTGA	

(Continued)

TABLE 1 | Continued

		TGGCTGGCAAT**T**GCGGTGA **(333)**	
		Mutation rate:96.52%	
CP5	FP-N	**CCTCTTCTCGTTCCTCATCACGTAGTCGCAAC**	28818-28849
(Institute of Microbiology and Virology)		CCTCTTCTCGTTCCTCATCACGTAGTCGCAA**T (91)**	
		Mutation rate:26.38%	
	RP-N	**AGTGACAGTTTGGCCTTGTTGTTGTTGGCCTT**	28983-29014
		AAGGCCAACAACAACAAGGCCAAACTGTCACT	
	Prb-N	**CCTGCTAGAATGGCTGGCAATGGCGGTGA**	28892-28920
		TCTGCTAGAATGGCTGGCAATGGCGGTGA	
		TCTGCTAGAATGGCTGGCAAT**T**GCGGTGA **(333)**	
		Mutation rate:96.52%	
2,276 high-quality SARS-CoV-2 Mu variants			
CP1	FP-S5	**CAGGTATATGCGCTAGTTATCAGAC**	23565-23589
(sigma)	RP-S5	**CCAAGTGACATAGTGTAGGCAATG**	23638-23661
		CATTGCCTACACTATGTCACTTGG	
	Prb-S5	**AGACTAATTCTCCTCGGCGGGCACG**	23592-23616
		CGACTAATTCTC**A**TCGGCGGGCACG **(2270)**	
		Mutation rate:99.74%	

The red letters represent the mutated bases. The red number represents the total number of mutation sequences.

The G28916T Mutation in the Delta Variant Severely Affected the Detection Efficiency and Detection Limit of the Primer/Probe Set of CP4 and CP5

The currently circulating SARS-CoV-2 variants include 5 VOCs (Alpha, Beta, Gamma, Delta and Omicron) and two VOIs (Lambda (C.37) and Mu (B.1.621)). We downloaded high-quality sequences of these SARS-CoV-2 variants from the GISAID database and compared mutations with the primer/probe sequences of 28 commonly used commercial qPCR kits (**Table S4**). We marked the mutation positions in the primer/probe targets with a mutation rate higher than 10% in **Table S4**.

The sequence corresponding to the primers/probes designed for the S gene had the largest number of mutations. Mutation

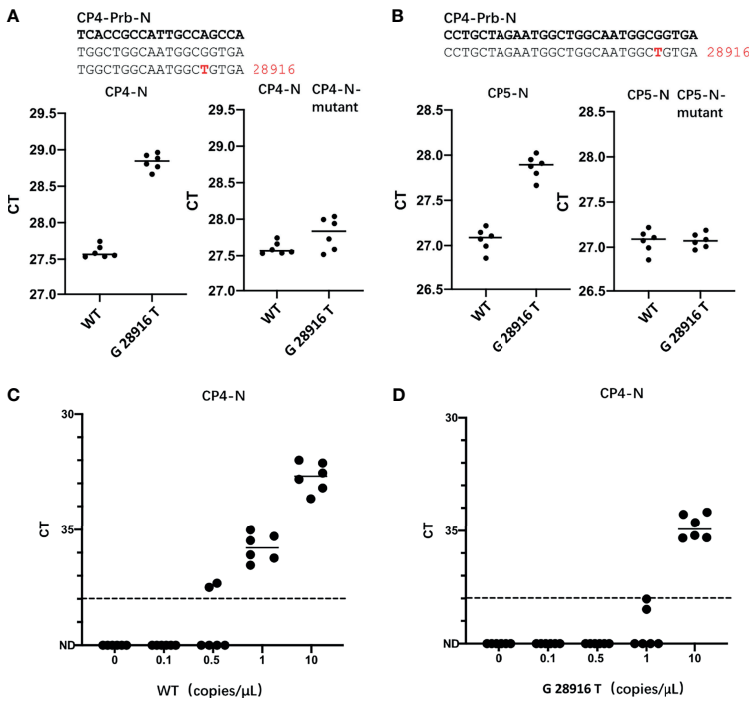

FIGURE 3 | The G28916T mutation in the Delta variant severely affected the detection efficiency and detection limit of the primer/probe set of CP4 and CP5. **(A, B)** Ct values for testing of the standard plasmid and the G28916T mutant plasmid using CP3 and CP4 by qPCR. The plasmid used in Figures 3A, B are 8.5 x 10^2 copies. **(C, D)** The lower detection limit of primer/probe, each primer-probe set uses 6 replicates, which contains standard and 28916 mutant plasmids, diluted according to 10, 1, 0.5 and 0.1 copies/ul. The red letters represent the mutated bases. The red number represents the position of the mutation.

C23604A was found in Alpha, Omicron and Mu variants, mutation C23604G was found in Delta variant, and mutation T23599G was found in Omicron variant, accounting for more than 99% of the total sequences. These mutations in the CP1 Prb-S target sequence may affect the detection efficiency of qPCR (**Table 1**). Among the 5 main epidemic strains, we also found that G22813T was in Beta and Omicron variant, A22812C was in Gamma variant, and C21762T was in Omicron variant, accounting for 92.6%, 99.6% and 98.5% respectively. All major mutations that may influence the qPCR detection are listed in **Table 1**.

In the currently most prevalent SARS-CoV-2 variant, the Delta variant, we found that there are 166809 sequences where the G at position 28916 was mutated to T, among the 211740 sequences in total, accounting for 78.78%. This mutation exists in the target sequence of CP4 and CP5 probes of the N gene (**Table 1**). Therefore, we generated the G28916T mutation on the N gene template. We used qPCR to detect the difference of detection efficiency between the wt and the mutant sequences. It was found that the detection sensitivity of the mutations on probe was 2.35 and 1.74 times less than that of the wt sequence (**Figures 3A, B**). Next, we changed the probe sequences of CP4 and CP5 to match with the mutant sequence. We found that if the G28916T was matched with primer sequence, the detection efficiency of qPCR was not affected (**Figures 3A, B**). Finally, we analyzed the detection limit of wt and mutant template sequences using the primer/probe CP4 for N gene. We diluted the templates to the concentration of 10, 1, 0.5 and 0.1 copies/μl (**Figures 3C, D**). The results showed that CP4 could detect the samples of 1 copies/μl for wt template, but only 10 copies/μl for mutant sequence. This showed that the mutation of G28916T in Delta variant increases the detection limit of the N gene primer/probe set of CP4 and CP5 by 10 times. Meanwhile, mutation G28913T and C28849T were found in Lambda variant, accounting for 96.52% and 26.38% respectively, which also affect the detection efficiency of CP4 and CP5 (**Table 1**).

DISCUSSION

In summary, we found that primers/probes targeting the S gene and N gene are commonly used for qPCR detection of SARS-CoV-2, and the detection efficiency of various SARS-CoV-2 variants may be significantly reduced if the original primer/probe sets are used. For efficient detection of the newly emerging SARS-CoV-2 variants, the mutations of the qPCR target sequence should be closely monitored, and the primers/probes sequence be correspondingly optimized in time to ensure the detection sensitivity and efficiency for various SARS-CoV-2 variants.

DATA AVAILABILITY STATEMENT

The original contributions presented in the study are included in the article/**Supplementary Material**. Further inquiries can be directed to the corresponding author.

AUTHOR CONTRIBUTIONS

DG and LC designed the research. LC, TX, YJ, and SH performed the experiments. LC, XL, HP, and CL analyzed the data. DG and LC wrote and revised the manuscript. All authors contributed to the article and approved the submitted version.

ACKNOWLEDGMENTS

The study was supported by the National Natural Science Foundation of China (#32041002), Shenzhen Science and Technology Program (JSGG20200225150431472 and KQTD20180411143323605), Guangdong Zhujiang Talents Program (#2016LJ06Y540).

SUPPLEMENTARY MATERIAL

The Supplementary Material for this article can be found online at: https://www.frontiersin.org/articles/10.3389/fcimb.2022.823306/full#supplementary-material

Supplementary Figure 1 | Flow chart of sequence collection and screening.

Supplementary Figure 2 | The primer/probe sequences of 28 commonly used commercial qPCR kits and their corresponding viral target genes. The 28 letters of A-AB correspond to 28 commonly used commercial qPCR kits, The position of the letter in SARS-CoV-2 genome corresponds to the target gene of the primer/probes.

Supplementary Figure 3 | The mutation of forward/reverse on the primer pair basically has no effect on the efficiency of qPCR detection. ΔCt values for testing of the standard plasmid and the multiple mutations plasmid **(A)** mutations in China-CDC-FP-N, **(B)** China-CDC-RP-N, **(C)** China-CDC-1ab using China CDC 1ab and N primer/probe sets by qPCR. The red letters represent the mutation bases, and the red numbers represent the mutation positions. The red letters represent the mutated bases. The red number represents the position of the mutation. All plasmid used in the figure are 8.5×10^2 copies.

Supplementary Figure 4 | The multiple mutations close to the 3'-end of primer have a great impact on the efficiency of qPCR detection. ΔCt values for testing of the standard plasmid and the mutant plasmid on China CDC ORF1a primer using China CDC ORF1a and N primer/probe sets by qPCR. The red letters represent the mutation bases, and the red numbers represent the mutation positions. The red letters represent the mutated bases. The red number represents the position of the mutation. All plasmid used in the figure are 8.5×10^2 copies.

Supplementary Figure 5 | 3'-end of primer mispairing influence detection efficiency of qPCR. We choose Japan-NIDS-FP-N **(A)**, USCDC-RP3-N **(B)**, IMV-FP-N **(C)**, USCDC-FP1-N **(D)**, USCDC-RP1-N **(E)**, China-CDC-FP-N **(F)**, USCDC-FP2-N **(G)**, China-CDC-RP-1ab **(H)** to construct four mutants (A, T, C, G) at 3'-end of primer, and detect the detection efficiency by qPCR on standard plasmid. The red letters represent the mutation bases. The red letters represent the mutated bases. All plasmid used in the figure are 8.5×10^2 copies.

Supplementary Figure 6 | The deletion mutation of SARS-CoV-2 affected the detection limit of the primer/probe set. **(A-D)** The lower detection limit of primer/probe, each primer-probe set uses 6 replicates, which contains standard and deletion mutant plasmids, diluted according to 100, 10, 1 and 0.1 copies/ul. The red letters represent the mutated bases. The red number represents the position of the mutation.

REFERENCES

Ali, F., Sharda, M., and Seshasayee, A. S. N. (2020). SARS-CoV-2 Sequence Typing, Evolution and Signatures of Selection Using CoVa, a Python-Based Command-Line Utility. *bioRxiv* 2020.2006.2009.082834. doi: 10.1101/2020.06.09.082834

Cao, Y., Wang, J., Jian, F., Xiao, T., Song, W., Yisimayi, A., et al. (2021). Omicron Escapes the Majority of Existing SARS-CoV-2 Neutralizing Antibodies. *Nature*. doi: 10.1038/d41586-021-03796-6

Cele, S., Jackson, L., Khoury, D. S., Khan, K., Moyo-Gwete, T., Tegally, H., et al. (2021). Omicron Extensively But Incompletely Escapes Pfizer BNT162b2 Neutralization. *Nature*. doi: 10.1038/d41586-021-03824-5

Chen, J., Wang, R., Gilby, N. B., and Wei, G. W. (2021). Omicron (B.1.1.529): Infectivity, Vaccine Breakthrough, and Antibody Resistance. *ArXiv* https://www.ncbi.nlm.nih.gov/pmc/articles/PMC8647651/.

Corman, V. M., Landt, O., Kaiser, M., Molenkamp, R., Meijer, A., Chu, D. K., et al. (2020). Detection of 2019 Novel Coronavirus, (2019-Ncov) by Real-Time RT-PCR. *Euro Surveill.* 25 (3), 2000045. doi: 10.2807/1560-7917.ES.2020.25.3.2000045

Ghedira, R., Papazova, N., Vuylsteke, M., Ruttink, T., Taverniers, I., and De Loose, M. (2009). Assessment of Primer/Template Mismatch Effects on Real-Time PCR Amplification of Target Taxa for GMO Quantification. *J. Agric. Food Chem.* 57 (20), 9370–9377. doi: 10.1021/jf901976a

Hasan, M. R., Sundararaju, S., Manickam, C., Mirza, F., Al-Hail, H., Lorenz, S., et al. (2021). A Novel Point Mutation in the N Gene of SARS-CoV-2 May Affect the Detection of the Virus by Reverse Transcription-Quantitative PCR. *J. Clin. Microbiol.* 59 (4), e03278–e03220. doi: 10.1128/jcm.03278-20

Katoh, K., Misawa, K., Kuma, K., and Miyata, T. (2002). MAFFT: A Novel Method for Rapid Multiple Sequence Alignment Based on Fast Fourier Transform. *Nucleic Acids Res.* 30 (14), 3059–3066. doi: 10.1093/nar/gkf436

Kwok, S., Kellogg, D. E., McKinney, N., Spasic, D., Goda, L., Levenson, C., et al. (1990). Effects of Primer-Template Mismatches on the Polymerase Chain Reaction: Human Immunodeficiency Virus Type 1 Model Studies. *Nucleic Acids Res.* 18 (4), 999–1005. doi: 10.1093/nar/18.4.999

Liu, L., Iketani, S., Guo, Y., Chan, J. F. W., Wang, M., Liu, L., et al. (2021). Striking Antibody Evasion Manifested by the Omicron Variant of SARS-CoV-2. *Nature*. doi: 10.1038/d41586-021-03826-3

Penarrubia, L., Ruiz, M., Porco, R., Rao, S. N., Juanola-Falgarona, M., Manissero, D., et al. (2020). Multiple Assays in a Real-Time RT-PCR SARS-CoV-2 Panel can Mitigate the Risk of Loss of Sensitivity by New Genomic Variants During the COVID-19 Outbreak. *Int. J. Infect. Dis.* 97, 225–229. doi: 10.1016/j.ijid.2020.06.027

Planas, D., Saunders, N., Maes, P., Guivel-Benhassine, F., Planchais, C., Buchrieser, J., et al. (2021). Considerable Escape of SARS-CoV-2 Omicron to Antibody Neutralization. *Nature*. doi: 10.1038/d41586-021-03827-2

Ravi, N., Cortade, D. L., Ng, E., and Wang, S. X. (2020). Diagnostics for SARS-CoV-2 Detection: A Comprehensive Review of the FDA-EUA COVID-19 Testing Landscape. *Biosens. Bioelectron.* 165, 112454. doi: 10.1016/j.bios.2020.112454

Reardon, S. (2021). How the Delta Variant Achieves its Ultrafast Spread. *Nature*. doi: 10.1038/d41586-021-01986-w

Rejali, N. A., Moric, E., and Wittwer, C. T. (2018). The Effect of Single Mismatches on Primer Extension. *Clin. Chem.* 64 (5), 801–809. doi: 10.1373/clinchem.2017.282285

Robson, F., Khan, K. S., Le, T. K., Paris, C., Demirbag, S., Barfuss, P., et al. (2020). Coronavirus RNA Proofreading: Molecular Basis and Therapeutic Targeting. *Mol. Cell* 79 (5), 710–727. doi: 10.1016/j.molcel.2020.07.027

Shi, J., Han, D., Zhang, R., Li, J., and Zhang, R. (2020). Molecular and Serological Assays for SARS-CoV-2: Insights From Genome and Clinical Characteristics. *Clin. Chem.* 66 (8), 1030–1046. doi: 10.1093/clinchem/hvaa122

Shu, Y., and McCauley, J. (2017). GISAID: Global Initiative on Sharing All Influenza Data - From Vision to Reality. *Euro Surveill.* 22 (13), 30494. doi: 10.2807/1560-7917.ES.2017.22.13.30494

Stadhouders, R., Pas, S. D., Anber, J., Voermans, J., Mes, T. H., and Schutten, M. (2010). The Effect of Primer-Template Mismatches on the Detection and Quantification of Nucleic Acids Using the 5' Nuclease Assay. *J. Mol. Diagn.* 12 (1), 109–117. doi: 10.2353/jmoldx.2010.090035

Vogels, C. B. F., Brito, A. F., Wyllie, A. L., Fauver, J. R., Ott, I. M., Kalinich, C. C., et al. (2020). Analytical Sensitivity and Efficiency Comparisons of SARS-CoV-2 RT-qPCR Primer-Probe Sets. *Nat. Microbiol.* 5 (10), 1299–1305. doi: 10.1038/s41564-020-0761-6

WHO (2021) *SARS-CoV-2 Variants, Working Definitions and Actions Taken*. Available at: https://www.who.int/en/activities/tracking-SARS-CoV-2-variants.

Wu, F., Zhao, S., Yu, B., Chen, Y. M., Wang, W., Song, Z. G., et al. (2020). A New Coronavirus Associated With Human Respiratory Disease in China. *Nature* 579 (7798), 265–269. doi: 10.1038/s41586-020-2008-3

Ziegler, K., Steininger, P., Ziegler, R., Steinmann, J., Korn, K., and Ensser, A. (2020). SARS-CoV-2 Samples may Escape Detection Because of a Single Point Mutation in the N Gene. *Euro Surveill.* 25 (39), 2001650. doi: 10.2807/1560-7917.ES.2020.25.39.2001650

Conflict of Interest: The authors declare that the research was conducted in the absence of any commercial or financial relationships that could be construed as a potential conflict of interest.

frontiers in Cellular and Infection Microbiology

ORIGINAL RESEARCH
published: 03 March 2022
doi: 10.3389/fcimb.2022.802147

Development of an Adeno-Associated Virus-Vectored SARS-CoV-2 Vaccine and Its Immunogenicity in Mice

Xi Qin[1†], Shanhu Li[2†], Xiang Li[1†], Dening Pei[1], Yu Liu[3], Youxue Ding[1], Lan Liu[1], Hua Bi[1], Xinchang Shi[1], Ying Guo[1], Enyue Fang[4], Fang Huang[2], Lei Yu[1], Liuqiang Zhu[1], Yifang An[1], C. Alexander Valencia[3], Yuhua Li[4], Biao Dong[3*] and Yong Zhou[1*]*

[1] Department of Recombinant Products, National Institutes for Food and Drug Control, Beijing, China, [2] Department of Cell Engineering, Beijing Institute of Biotechnology, Beijing, China, [3] Department of Geriatrics and National Clinical Research Center for Geriatrics, State Key Laboratory of Biotherapy, West China Hospital, Sichuan University, Chengdu, China, [4] Department of Arboviral Vaccine, National Institutes for Food and Drug Control, Beijing, China

Owing to the outbreak of the novel coronavirus (SARS-CoV-2) worldwide at the end of 2019, the development of a SARS-CoV-2 vaccine became an urgent need. In this study, we developed a type 9 adeno-associated virus vectored vaccine candidate expressing a dimeric receptor binding domain (RBD) of the SARS-CoV-2 spike protein (S protein) and evaluated its immunogenicity in a murine model. The vaccine candidate, named AAV9-RBD virus, was constructed by inserting a signal peptide to the N-terminus of two copies of RBD, spaced by a linker, into the genome of a type 9 adeno-associated virus. *In vitro* assays showed that HeLa cells infected by the recombinant AAV virus expressed high levels of the recombinant RBD protein, mostly found in the cell culture supernatant. The recombinant AAV9-RBD virus was cultured and purified. The genome titer of the purified recombinant AAV9-RBD virus was determined to be 2.4×10^{13} genome copies/mL (GC/mL) by Q-PCR. Balb/c mice were immunized with the virus by intramuscular injection or nasal drip administration. Eight weeks after immunization, neutralizing antibodies against the new coronavirus pseudovirus were detected in the sera of all mice; the mean neutralizing antibody EC_{50} values were 517.7 ± 292.1 (n=10) and 682.8 ± 454.0 (n=10) in the intramuscular injection group and nasal drip group, respectively. The results of this study showed that the recombinant AAV9-RBD virus may be used for the development of a SARS-CoV-2 vaccine.

Keywords: SARS-CoV-2, AAV9, vaccine, immune, long term protection

OPEN ACCESS

Edited by:
Ke Xu,
Wuhan University, China

Reviewed by:
Huanle Luo,
SYSU, China
Yu Zhou,
Institut Pasteur of Shanghai (CAS), China

****Correspondence:***
Yuhua Li
liyuhua@nifdc.org.cn
Biao Dong
biaodong@scu.edu.cn
Yong Zhou
zhouyong@nifdc.org.cn

[†]These authors have contributed equally to this work and share first authorship

Specialty section:
This article was submitted to Virus and Host, a section of the journal Frontiers in Cellular and Infection Microbiology

Received: *26 October 2021*
Accepted: *08 February 2022*
Published: *03 March 2022*

Citation:
Qin X, Li S, Li X, Pei D, Liu Y, Ding Y, Liu L, Bi H, Shi X, Guo Y, Fang E, Huang F, Yu L, Zhu L, An Y, Valencia CA, Li Y, Dong B and Zhou Y (2022) Development of an Adeno-Associated Virus-Vectored SARS-CoV-2 Vaccine and Its Immunogenicity in Mice. Front. Cell. Infect. Microbiol. 12:802147. doi: 10.3389/fcimb.2022.802147

INTRODUCTION

At the end of 2019, there was an outbreak of the novel coronavirus (SARS-CoV-2), leading to an ongoing pandemic that has caused five million deaths, since November of 2011, and two hundred million cases. The SARS-CoV-2 virus is a positive-strand RNA virus belonging to the coronavirus family that had never been reported in humans previously (Zhu et al., 2020). After infecting a

human body, SARS-CoV-2 can cause severe inflammation in the lungs and even death. Studies have shown that SARS-CoV-2 binds to human cell receptor angiotensin-converting enzyme 2 (ACE2) through the receptor-binding domain (RBD) of the spike glycoprotein, thus triggering a viral invasion of the host cells (Zhou et al., 2020). At present, RBD has become an important target for the development of therapeutic drugs and vaccines against SARS-CoV-2 (Wu et al., 2020). The RBD-based protein subunit vaccine (Min and Sun, 2021; Yang et al., 2021) and mRNA vaccine (Tai et al., 2020; Karpenko et al., 2021) have achieved good clinical results, exhibiting excellent immunogenicity in animal models and humans. At least one such vaccine is authorized for emergency use (Yang et al., 2021). Several mRNA vaccines or adenovirus vectored vaccines-based on the full length S protein are also licensed for use as this article is being written.

The duration of protection conferred by a vaccine is an important indicator of the vaccine's effectiveness. Studies have shown that neutralizing antibodies in SARS-CoV-2 patients declined rapidly after recovery (Long et al., 2020). The immunity generated by all currently licensed vaccines decreases within months and has raised the need for booster immunization in many countries. Therefore, the development of a vaccine that can continuously stimulate the body to produce high levels of neutralizing antibody over long period of time represents an improvement to the current vaccines.

The wild-type adeno-associated virus is a single stranded, linear, DNA deficient virus that has never been found to cause any human disease (Schultz and Chamberlain, 2008; Hüser et al., 2010). Recombinant adeno-associated virus (rAAV) is derived from non-pathogenic wild-type AAV, in which *rep*, which is related to replication, and *cap*, which encodes the shell protein, are replaced by foreign genes. After inoculation into a human body, recombinant adeno-associated viruses carrying the exogenous gene can continuously express the antigen in the human cells for more than 3 years (Pasi et al., 2020) and even up to 15 years (George et al., 2020). In 2012, the EMA (European Medicines Agency) approved Glybera (rAAV1 as the vector) for the treatment of lipoprotein lipase deficiency. In 2017, the FDA (Food and Drug Administration) unanimously approved Luxturna (rAAV2 as the vector) for the treatment of Leber congenital amaurosis. In 2019, the FDA approved Zolgensma (rAAV9 as the vector) for the treatment of spinal muscular atrophy in children. As of November 2018, a total of 145 clinical trials involving rAAV were registered in *ClinicalTrials.gov* (Wang et al., 2019). Because of its advantages, including low immunogenicity and cytotoxicity, wide host range, stable physical and chemical properties, and ability to express exogenous genes over the long-term (van der Laan et al., 2011; Dismuke et al., 2013; Wang et al., 2019), rAAV is considered as a safe and effective virus vector (Schultz et al., 2008; Donsante et al., 2007). It has been widely used in clinical trials for gene therapy (Rakoczy et al., 2015; Bennett et al., 2016; George et al., 2017; Mueller et al., 2017; Rangarajan et al., 2017) and the recombinant adeno-associated virus may be also effectively used for vaccine development (Demminger et al., 2020).

In this study, we selected the recombinant adeno-associated virus type 9 with a relatively wide tissue tropism (Zincarelli et al., 2008) as a vector to develop an RBD-based SARS-CoV-2 vaccine. Recombinant RBD protein is expressed and secreted by the infected cells over a long period of time. After mice were immunized with this virus, neutralizing antibodies against the SARS-CoV-2 pseudovirus persisted and may offer durable protection.

MATERIALS AND METHODS

Reagents and Materials

HEK293 cells and HeLa cells were purchased from ATCC, cultured in DMEM containing 10% fetal bovine serum and 1% Penicillin-Streptomycin. All culture reagents were purchased from GIBCO (USA). The inserted gene was synthesized by Synbio Technologies Co., Ltd. (China). pAAV-MCS, pAAV-RC9, and pAAV-Help were purchased from Biofeng (China). The transfection reagent Lipofectamine 3000 was purchased from Thermo Fisher (USA). Three plasmid transfection reagents, FectoVIR-AAV, were purchased from Polyplus (USA). The anti-RBD monoclonal antibody was obtained from Sino Biological (China). The plasmid extraction kit was purchased from QIAGEN (USA). The AAVpro Titration Kit (for Real Time PCR) Ver.2 was obtained from TaKaRa (Japan). The benzonase and iodixanol reagents were purchased from Sigma (USA). The luciferase detection reagent was obtained from PerkinElmer (USA). The novel corona pseudovirus and Huh-7 cells were donated by Professor Wang Youchun and Professor Huang Weijin, respectively, from the National Institutes for Food and Drug Control.

Construction of the Eukaryotic Expression Vector

After the synthetic target gene (**Figure 1**) and pAAV-MCS vector were digested with BamH I and Sal I, respectively, the target gene and the vector were ligated and used to transform *E. coli* DH5α competent cells. Transformed cells were plated on LB culture medium plates with kanamycin. Positive clones were screened, identified, and sequenced. The sequence of RBD used was at amino acids 319 to 541 of the Spike protein (WH-Human_1). The signal peptide tPA had the specific sequence of MDAMKRGLCCVLLLCGAVFVSA, while Glu had the sequence MGVKVLFALICIAVAEVTG, and the sequence of GC linker was GSGGSG.

Transfection

HEK293 cells were seeded onto a 24-well plate at a density of 40,000-50,000 cells/well, and the culture medium was replaced on the second day of inoculation. After 2 h, the recombinant expression plasmid was used to transfect cells using Lipofectamine 3000 at a ratio of 0.5 μg/well. Cells were incubated at 37°C with 5% CO2 for 6 h, and subsequently cultured in new media for 48 h. At the end, cell lysates and cell culture supernatants were collected after 24 h and 48 h

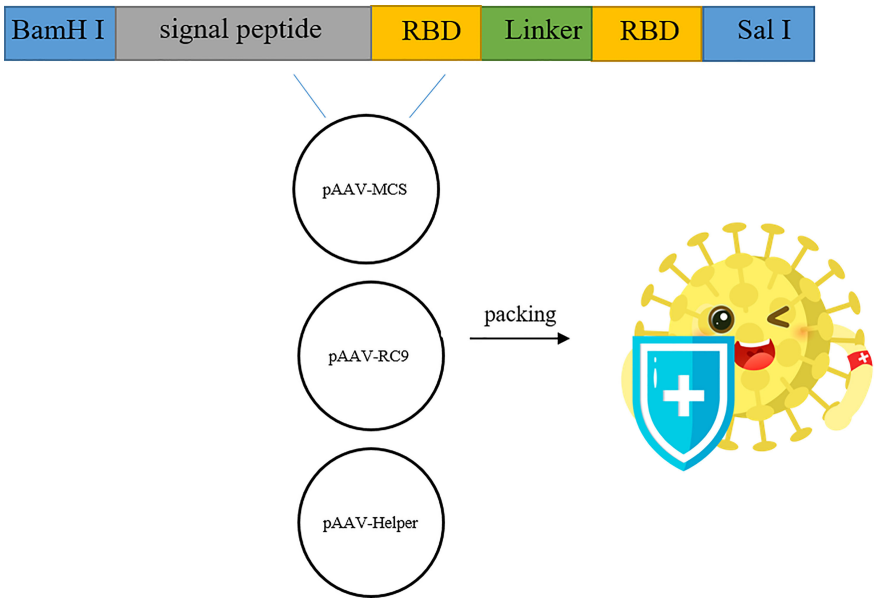

FIGURE 1 | Construction and genome composition of recombinant AAV9-RBD. Four pAAV-RBD plasmids were constructed. Clone 1 contains tPA signal peptide in self-complementary form. Clone 2: contains tPA signal peptide in single-stranded form. Clone 3 contains Glu signal peptide in self-complementary form. Clone 4 contains Glu signal peptide in single-stranded form.

transfection. RBD expression was detected using an anti-RBD monoclonal antibody *via* Western blotting (WB).

Western Blotting

After performing electrophoresis using 4-12% NuPAGE Bis-Tris Gel (NP0321BOX, Invitrogen, USA), proteins were transferred onto membranes and blocked with 5% BSA for 30 min. Membranes were incubated with the primary antibody for 1 h, washed three times with PBST (phosphate buffered saline with Tween 20), incubated with the secondary antibody for 1 h, washed 3 times with PBST, and then developed using an ECL luminescent solution. Images were generated using X-ray film.

Packaging of the Recombinant Adeno-Associated Virus

HEK293 cells were seeded onto a 10-cm culture dish at a density of 40,000 cells/cm^2, and the cells in one of the dishes were counted after 24 h of culture. The total amount of plasmids to be transfected was calculated based on 1 μg of plasmid having the ability to transfect one million cells, pAAV-RC9 dosage, recombinant eukaryotic expression of plasmid, and pAAV-Help. They were combined at a mass ratio of 1:1:1. The three plasmids were added into 0.5 mL of a high-sugar DMEM medium and vortexed for 3-4 s. A fixed amount of FectoVIR-AAV was added. The solution was vortexed for 3-4 s, and the amount of FectoVIR-AAV and transfected plasmids combined at a 1 μL:1 μg ratio. After incubation for 30 min at room temperature, the mixture was added onto the HEK293 cells, and incubated at 37°C with 5% CO_2 conditions for 72 h. At the end of incubation, the packaged cell culture supernatant and cells were collected.

Preliminary Purification of Recombinant Adeno-Associated Virus

The collected cells were resuspended in 1 mL of PBS, and frozen. If necessary, cells had a maximum of 3 thawing cycles between liquid nitrogen and room temperature. After each thawing step, the cells were hand-shaken vigorously for 2 min to break the cells and release the virus. The lysed cells were centrifuged at 10,000 g for 10 min at 4°C. The supernatant was collected and combined with the cell culture supernatant from the initial harvest containing recombinant AAV virus. Benzonase was added at a concentration of 50 U/mL to the above solution to remove the residual DNA. The solution was incubated at 37°C for 30 min, and inverted every 10 min to ensure that benzonase was evenly mixed. Then, the solution was centrifuged at 10000 g for 20 min at 4 °C. The supernatant was filtered with a 0.45 μm filter and the filtrate was transferred to a new tube. The supernatant was transferred to an ultracentrifuge tube and density gradient centrifugation (iodixanol) was performed for 100 min at 300,000 g and 12°C. The liquid containing the virus (transparent liquid) was collected, desalted, and concentrated.

Titer Determination of Recombinant Adeno-Associated Virus

Serial diluted RBD plasmid in the range of 10^9 to 10^4 genome copies was used as the standard to quantify the concentration of recombinant adeno-associated virus. Two μL of AAV vector

samples were incubated at 37°C in 99 μL of DNase digestion buffer (400 mM Tris-HCl, pH 8.0, 100 mM $MgSO_4$, 10 mM $CaCl_2$, and 10 units DNase I) for 30 min, and treated by adding 99 μL of stop solution (20 mM EDTA, pH 8.0) following an incubation at 65°C for 10 min. Then, 20 μL of protease K digestion buffer (100 mM Tris, pH 8.0, 2 mM EDTA, 1% SDS, and 2 mg/mL proteinase K) was added and incubated at 56 °C for 90 min followed by an incubation at 95°C for 15 min. After treatment, the AAV vector samples were diluted at1000-fold in ddH_2O. A qPCR reaction system (PowerUp SYBR Green Master Mix, Thermo fisher scientific) with a total volume of 20 μL was set up in duplicate for each sample in accordance with the manufacturer's instructions. Specifically, each reaction mixture contained 5 μL of the diluted AAV vector sample and 0.5 μL of each of the designed primer pairs, forward primer TGGGACTTTCCTACTTGGCA, and reverse primer CCACGCCCATTGATGTACTG. The qPCR program was 50°C for 2 min and 95 °C for 2 min, followed by 40 cycles at 95°C for 15 sec and 60°C for 30 sec. The AAV genome titers were calculated according to a standard curve using the $2^{\wedge-\Delta\Delta CT}$ method.

Purity Determination of Recombinant Adeno-Associated Virus

In a 200- μL Eppendorf tube, the standard rAAV9 vector was diluted to obtain solutions with 1×10^{10} and 2×10^{10} copies. For AAV vector samples, 1 μL, 2 μL, or 4 μL of each sample was added to one tube. ddH_2O was added to each tube and the final volume was 15 μL. Then, 3 μL of 6× loading buffer was added to each tube and the tubes were incubated at 95°C for 10 min. The capsid proteins were assessed by performing 10% SDS-PAGE at 120 V for 90 min. Silver staining was performed at room temperature according to the manufacturer's instructions (Pierce, OJ190653) The AAV titers were semi-quantified using the standards.

Verifying the Expression of Recombinant Adeno-Associated Virus

HeLa cells were seeded onto a 24-well plate at a density of 40,000-50,000 cells/well. After a 24 h of inoculation, the purified recombinant adeno-associated virus was diluted to 5×10^6 vg/μL (the titer was determined using the AAVpro Titration Kit Ver.2) and 10 μL per well added to cells (10 μL per well) in the 24-well plate. The cells were incubated at 37 °C for 48 h with 5% CO_2. At the end, cell lysates and cell culture supernatants were collected and used for the determination of the expression of RBD by Western blotting.

Immunization of Mice

Female Balb/c mice (6-8 weeks) were randomly divided into groups of 10 animals per group. Each animal was immunized with 10^{11} genome copies of recombinant adeno-associated virus in 50 μL of PBS. For intramuscular injection, the 50 μL samples were divided and injected into each rear leg at two sites. For nasal drip immunization, a total of 50 μL were applied to the both of their nostrils. A negative control was immunized with PBS by either intramuscular injection or nasal drops. The neutralizing antibody titer in the serum was detected before immunization and at 4 and 8 weeks after immunization.

Enzyme-Linked Immunosorbent Assay (ELISA)

The sera of immunized mice were collected by tail bleeding the day before immunization at different time points, and were analyzed for the presence of anti-RBD antibodies with ELISA. The sera of non-immune mice served as the negative control. 96-well plate were coated with RBD protein to serve as the antigen. Serial diluted serum samples were then added to each well and the plate was incubated at 4 °C overnight. After washing with PBS, secondary antibodies labeled with streptavidin–horseradish peroxidase (HRP) were added to each well. After washing and color development, the absorbance was read at 492 nm. The end-point titers of the antibodies were determined as the reciprocal of the highest dilution, giving an optical density twice that of the non-immune serum. The geometric mean value of end-point titers (GMT) of antibodies in each group was calculated.

The Detection of Neutralizing Antibody

The serum to be evaluated (Nie et al., 2020a; Nie et al., 2020b) was treated in a water bath at 56°C for 30 min to inactivate complement compoents, centrifuged at 6000 g for 3 min, and the supernatant was collected. The supernatant was serially diluted and added to 96-well plates. Then, 650 TCID 50/mL of novel corona pseudovirus was added to each well and the plate was incubated at 37 °C and 5% CO_2 for 1 h. Then, 2×10^4 Huh-7 cells were added to each well and cultured at 37°C and 5% CO_2 for 24 h. Next, 75 μL of liquid was removed from each well and dispensed to a new 96-well plate,75 μL of luciferase detection reagent was added to each well. The 96-well plate was placed on a chemiluminescence detector after a 3 min incubation at room temperature and the neutralization inhibition rate was calculated using the following equation: Inhibition rate = [1 - (mean luminous intensity of the sample group - mean value of blank control)/(mean luminous intensity of the negative group - mean value of blank control)] × 100%.

Based on the results of the neutralization inhibition rate, the neutralizing antibody EC_{50} was calculated using the Reed-Muench method. If the EC_{50} value was less than 30, it was determined to be 15.

Enzyme-Linked Immunospot Assay (ELISPOT)

Splenocytes from immunized mice were analyzed for cytokine production using an ELISPOT kit (DAKEWE, China) following the manufacturer's instructions. Specifically, the levels of interferon (IFN)-γ, interleukin (IL)-2, IL-4, and IL-10 were determined to evaluate the immune responses *in vivo*. In brief, splenocytes were placed on 96-well filtration plates pre-coated with capturing Abs at 10^5 cells/well and then stimulated with an overlapping spike glycoprotein peptide pool. Splenocytes stimulated with PMA+ Ionomycin served as a positive control, and RPMI 1640 medium alone served as a negative control. After incubation with biotinylated detection Abs followed by streptavidin-HRP, spots at the sites of cytokine secretion were developed by adding a 3-amino-

9-ethylcarbazole substrate and were counted automatically by an ELISPOT reader system (Mabtech, Switzerland).

RESULTS

Construction of Recombinant Eukaryotic Expression Plasmid

After the synthesized target genes (**Figure 1**) were ligated into the ssAAV-MCS (single chain AAV expression plasmid) vector or scAAV-MCS (self-complementary AAV expression plasmid) vector at the BamH I and Sal I digestion sites, the recombinant expression plasmid with the correct sequence was transfected into 293T cells. The cell lysate and culture medium supernatant were collected at 24 and 48 h after transfection, respectively, and the expression of RBD was detected *via* an RBD-specific antibody by WB. The four recombinant expression plasmids constructed in the experiment were as follows: clone no. 1: scAAV-RBD (tPA signal peptide), clone no. 2: ssAAV-RBD (tPA signal peptide); clone no. 3: scAAV-RBD (Glu signal peptide); and clone no. 4: ssAAV-RBD (Glu signal peptide). The results are shown in **Figure 2**. The expression of recombinant RBD was detected in the cell lysate and cell culture supernatant 24 h after the transfection of the recombinant expression plasmid (clone no. 2 and clone no. 4). Meanwhile, the expression of recombinant RBD was also detected in the cell culture supernatant 48 h after transfection, and a little higher expression levels of recombinant RBD were observed in the cell culture supernatant at that time. The molecular weight was approximately 50 Kda, which is larger than the expected 27 KDa due to glycosylation.

The Expression and Identification of Recombinant AAV9-RBD Virus

The 293T cells were co-transfected with four groups of three plasmids, namely, pAAV-RC9, pAAV-Help, and one of the four constructed recombinant plasmids. The packaged recombinant AAV9 virus was collected 72 h later. The sequence numbers of the four recombinant viruses corresponded to the sequence numbers of the four recombinant expression plasmids. The plasmids were used to infect HeLa cells that were assessed by Western Blot. After 48 h, the expression of recombinant RBD was detected in the cell lysate and cell culture supernatant of the recombinant AAV9-RBD virus infection group packaged with clone no. 2 (virus no. 2, single-chain AAV9-RBD; the signal peptide was tPA signal peptide). Moreover, the concentration of the target protein in the cell culture supernatant was much higher than that in the cell lysate (**Figure 3**). While other viruses were either not expressed (virus no. 1, self-complementary AAV9-RBD, the signal peptide was tPA signal peptide; virus no. 3, self-complementary AAV9-RBD, the signal peptide was Glu signal peptide) or low in expression in cell culture supernatant (virus no. 4, single-chain AAV9-RBD; the signal peptide was Glu signal peptide). Virus no. 2 was used in subsequent trials.

Packaging, Purification, and Titer Determination of Recombinant AAV9-RBD Virus

After the recombinant AAV9-RBD virus was purified, the level of purity was determined by silver nitrate staining (**Figure 4A**). Three major bands representing VP1, VP2, and VP3 were detected in both standard and AAV9-RBD viruses. No bands were observed for the recombinant AAV9-RBD virus, indicating that the purity level were sufficient for animal experiments. Approximately 10^{13} recombinant

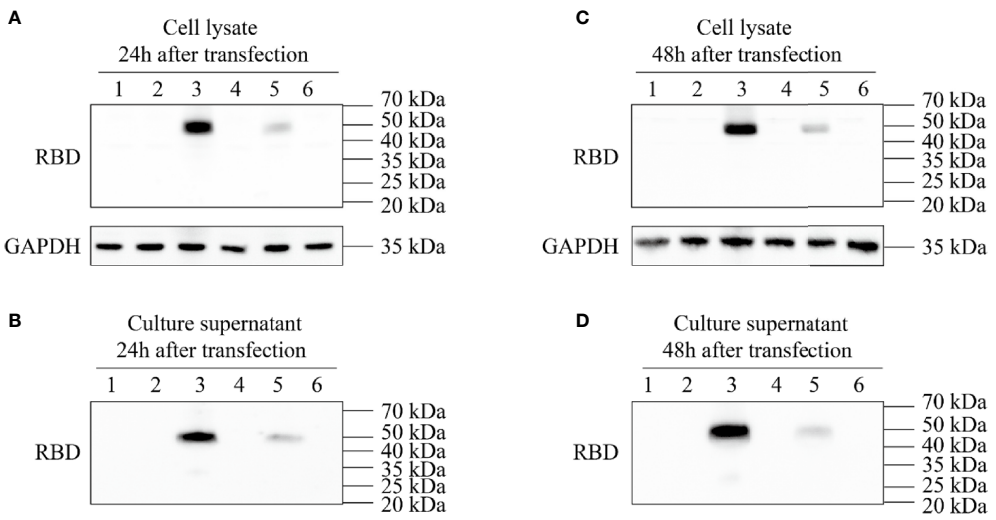

FIGURE 2 | Expression identification of recombinant plasmid pAAV-RBD. HEK293 cells were transfected with the four different plasmids and the RBD expressions were detected in the cell lysates or supernatants. 1: Negative control; 2: Clone 1; 3: Clone 2; 4: Clone 3; 5: Clone 4; 6: EGFP plasmid. **(A)** Expression of RBD in the cell lysate 24 hours post-transfection. **(B)** Expression of RBD in the culture supernatant 24 hours post-transfection. **(C)** Expression of RBD in the cell lysate 48 hours post-transfection. **(D)** Expression of RBD in the culture supernatant 48 hours post-transfection.

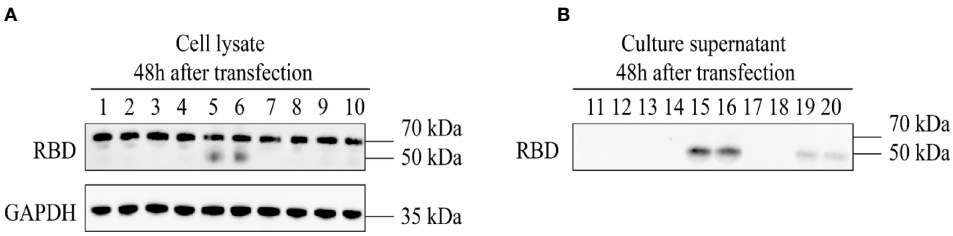

FIGURE 3 | Expression identification of recombinant AAV9-RBD. The four different AAV vectors were packaged in duplicate and used to infect HeLa cells. The expression of RBD in the cell lysates and supernatants were detected at 48 hours after infection. 1,2: AAV9-EGFP; 3,4: AAV vectors from clone 1; 5,6: AAV vectors from clone 2; 7,8: AAV vectors from clone 3; 9,10: AAV vectors from clone 4. **(A)** Expression of RBD in the cell lysate at 48 hours after AAV vector infection. **(B)** Expression of RBD in the culture supernatant at 48 hours after AAV vector infection.

AAV9-RBD viral particles/mL were detected. After Q-PCR, 2 mL of the recombinant AAV9-RBD virus solution with a genome titer of approximately 2.4×10^{13} GC/mL (the recombinant AAV9-RBD virus packaged by clone no. 2) was detected (**Figure 4B**).

Humoral Immune Responses in AAV9-RBD Virus Immunized Mice

After 8 weeks of administration, all mice survived and weighed (**Figure 5A**). The humoral immune response, including specific IgG and neutralizing antibodies were determined after two immunizations. The results were shown in **Figure 5**. The AAV9-RBD virus elicited the production of specific an IgG antibody against RBD with a GMT of 1:4873 (intramuscular injection) and 1:5385 (nasal drip), respectively, representing a significant difference ($p < 0.0003$). The EC_{50} values of the neutralizing antibody titers for each mouse group were mostly less than 30 before immunization. The neutralizing antibody was generated 4 and 8 weeks after mice were immunized. In the intramuscular injection group, the EC_{50} value of the neutralizing antibody was 24.0 ± 12.0 (n=10) before immunization, 61.6 ± 25.5 (n=10) at the 4^{th} week, and 517.7 ± 292.1 (n=10) at the 8^{th} week, representing a 2.6 and 21.6-fold increase, respectively. In the nasal drip group, the EC_{50} value of neutralizing antibody before immunization was 24.9 ± 13.3 (n=10), 113.2 ± 70.6 (n=10) at the 4^{th} week, and 682.8 ± 454.0 (n=10) at the 8^{th} week; thus, an 4.5-and 27.4-fold increase, respectively, was observed. In short, the results showed that vaccination with the AAV9-RBD virus expressing RBD antigens induced both humoral and RBD-specific strong antibody responses in mice.

Cytokine Production in AAV Vectored COVID-19 Vaccine Immunized Mice

To determine the cellular immune response, levels of splenocyte-derived cytokines were determined by ELISPOT at 8 weeks after immunization. Significant increases in the levels of IFN-γ, IL-2, IL-4, and IL-10 were detected in the nasal drip group and intramuscular injection group compared to those of the negative control ($p < 0.01$, **Figure 6**). These findings from intracellular cytokine staining and cytokine profiling suggested a AAV9-RBD-induced T-helper-2 and T-helper-1 cell dominant response after both intramuscular injection and nasal drip administration.

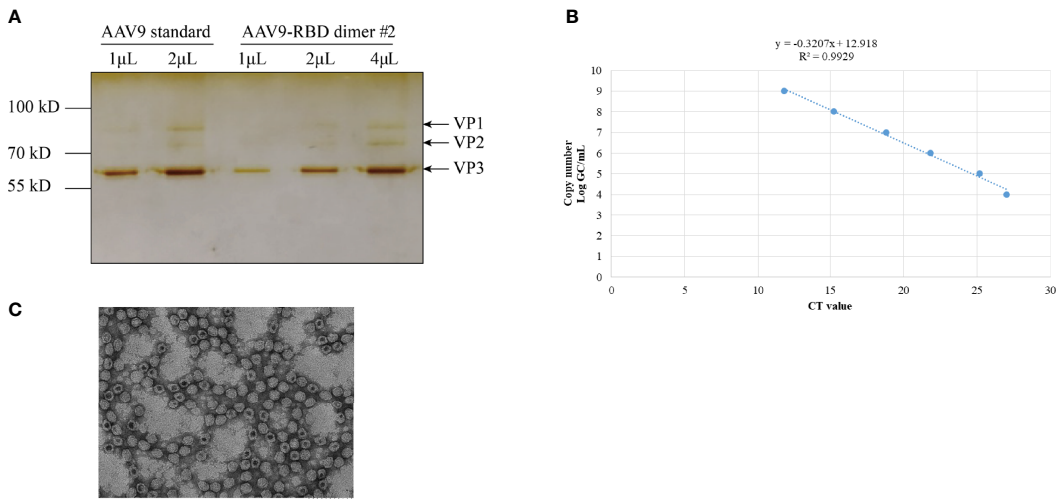

FIGURE 4 | AAV vector quantification by sliver staining and Q-PCR. The AAV vector was characterized by Silver staining **(A)**, Q-PCR **(B)** and electron microscopy **(C)**.

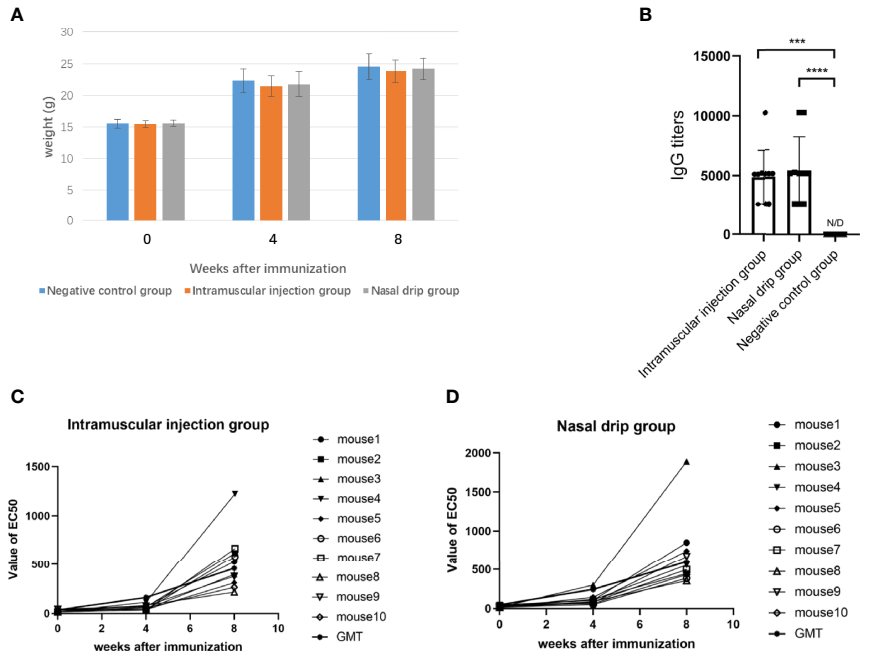

FIGURE 5 | The mice were immunized with recombinant AAV9-RBD *via* intramuscular injection and nasal drip administration. Weight changes of mice before and after immunization **(A)**. RBD-specific antibody responses in sera of immunized mice 8 weeks after immunization. Endpoint titers of IgG determined by ELISA. The reciprocals of titers were represented as the mean ± SD. n = 10. ****p< 0.0003; ****p<0.0001* **(B)**. The levels of the neutralizing antibody in each mouse group were determined before immunization, and 4 and 8 weeks after immunization *via* intramuscular injection **(C)** and intranasal administration **(D)**.

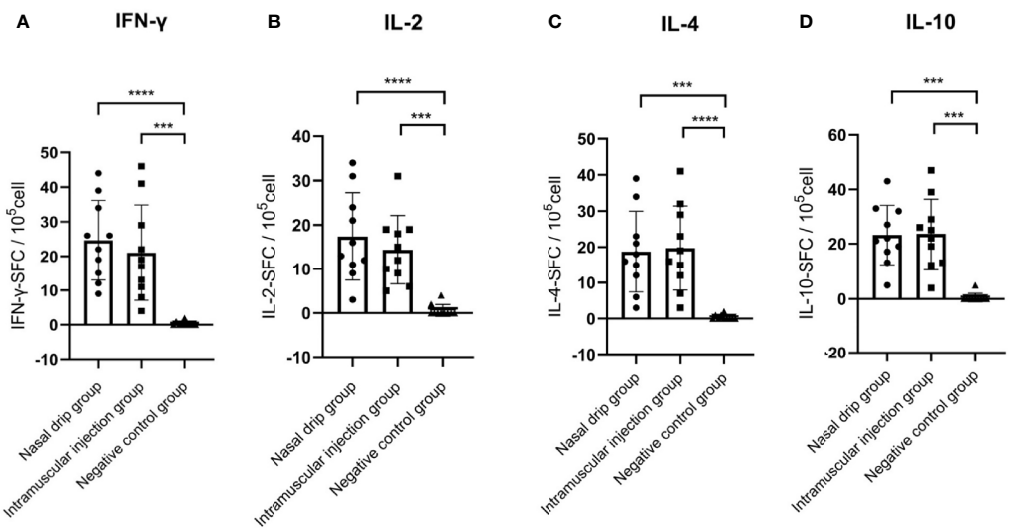

FIGURE 6 | Levels of splenocyte secreted cytokines in immunized BALB/c mice at 8 weeks after immunization detected by ELISPOT. **(A)** IFN-γ, **(B)** IL-2, **(C)** IL-4, and **(D)** IL-10 levels. The numbers of cytokinepositive cells were shown as the mean counts of spot-forming unit (SFU) ± SD per 1×10^5 splenocytes. n = 10. Results were analyzed by the t test. ****p< 0.0003; ****p<0.0001*.

DISCUSSION

Due to its high gene delivery efficiency, low immunogenicity, lack of pathogenicity, and excellent safety profile, the adeno-associated virus is a preferred vector for gene therapy (Kotterman and Schaffer, 2014; Naso et al., 2017). After the recombinant adeno-associated virus infects cells, it releases its viral DNA into the cell, synthesizes the complementary chain after entering the nucleus, and connects the

head and tail into a ring, to form a double-stranded chain, which can exist in the free form in mammalian cells for a long time without being degraded as exogenous DNA (Carter, 2004; Penaud-Budloo et al., 2008), thus achieving the long-term and stable expression of exogenous genes. At present, there are 12 AVV serotypes (AAV1 to AAV 12) and more than 130 mutants of AAV in existence (Daya and Berns, 2008). Different AAV serotypes have different spatial structures, capsid protein sequences and tissue specificities. Hence, the cell surface receptors that recognize and bind to the AAV are also different, which results in different cell types being transfected by different serotypes of AAV with varying infection efficiencies (Mohan et al., 2003; Burger et al., 2004; Evans et al., 2006).

We selected the AAV9 virus, which had a relatively wide tissue tropism, for constructing the SARS-CoV-2 vaccine, as it would enable us provide a low dose of viral inoculum to achieve a desirable immunity and safety. In 2019, the FDA approved the recombinant AAV9 drug Zolgensma, produced by Novartis, for the treatment of spinal muscular atrophy in children, which demonstrated the safety of this vector. The viral shell of recombinant AAV9 (rAAV9) can be used as an adjuvant to promote the induction of the neutralizing antibody against the recombinant RBD protein. In addition, rAAV9 may infect mammals *via* a nasal spray (Demminger et al., 2020). Nasal delivery of rAAV9 vaccine is not only convenient, but also provide protection to the nasal and lung mucosa.

To further improve antigen expression and reduce the dosage of the recombinant virus, we introduced two copies of RBD with a flexible linker region in the middle to ensure that the expressed RBD has the correct conformation. To achieve the secretory expression of the recombinant RBD protein, we included the signal peptide of the human tissue plasminogen activator (tPA) at the N-terminus of the recombinant RBD protein. The signal peptide was hydrolyzed after the recombinant protein was secreted outside the cells (Choo and Ranganathan, 2008). To find a suitable signal peptide, we also compared the effect of the glutamate (Glu) signal peptide on recombinant protein secretion (clone no. 4 and recombinant virus 4). As demonstrated in **Figures 2**, **4** that the tPA signal peptide was stronger than the Glu signal peptide in promoting secretion of the recombinant RBD during the expression of eukaryotic plasmids. Glu signal peptide's effect was much weaker than that observed with the tPA signal peptide during the recombinant viral infection. Therefore, we used the tPA signal peptide for the construction of rAAV-RBD.

At week 8 after immunization with a single dose of AAV-RBD, mice in the intramuscular injection and nasal drip groups had high levels of anti-pseudovirus neutralizing antibodies with EC_{50} values of 517.7 and 682.8, respectively. These antibody levels exceeded those shown to have protective effects against SARS-CoV-2 infection (Robbiani et al., 2020; Khoury et al., 2021). We speculate that the neutralizing antibody levels in these mice may continue to rise over time. The results of our experiment suggested that the AAV9-RBD virus vaccine when administered by intramuscular injection or a nasal spray is a promising candidate worthy of further development.

Cellular and humoral immune responses are considered to be equally important for the prevention against SARS-CoV-2 as a safe and efficient vaccine. In this study, IFN-γ, IL-2, IL-4, and IL-10 were all markedly increased in the nasal drip and intramuscular injection groups. The Th1 response is mediated by Th1 helper cells with the production of IFN-γ and IL-2, which are associated with the cellular immune response, while the Th2 response is closely related with the production of IL-4 and IL-10, which boosts the humoral response. These findings from the intracellular cytokine staining and cytokine profiling suggested that the AAV9-RBD virus induced balanced cellular and humoral responses after both intramuscular injection and nasal drip administration.

The blood samples were taken from the retro-orbital sinus in mice *via* capillary tubes at different time points. We did not measure the neutralization antibodies for AAV9 because the blood samples at different time points were used for the calculation of RBD antibody titers, the main purpose of this study, and there was not enough for quantification of AAV9 antibody titers. Injection of AAV9 vector either in muscle or intranasal can elicit neutralization antibodies in mice, which is well documented (Murrey et al., 2014).

There are also other AAV based vaccines for COVID-19, like AAVhu68-ACE2 (Sims et al., 2021) and AAVrh32.33-S (Zabaleta et al., 2021). Compared with them, the pros for AAV9-RBD are (1) two linked RBDs are more efficient antigens to elicit immune responses than single S protein or S1 protein, which has been showed by recombinant protein vaccine study. (2) AAV9 can infect both muscle and airway epithelia cells efficiently to overexpress RBD to elicit immune response. While, the cons for AAV9-RBD are (1) in the absence of AAV9 neutralizing antibody inhibitors, the vector may not be used for 20-40% patients that have the AAV9 neutralization antibodies while AAVrh32.33 may be used for more patient due to less neutralization antibody in population; (2) the overexpression of S or S1 protein may elicit more immune protection due to more antigens.

The recombinant AAV9-RBD virus vaccine induced sustained expression of RBD in infected host cells over a long period, and stimulated the immune system to produce long-lasting antibody and cellular immune responses. Therefore, the AAV9-RBD virus vaccine has the potential of offering long-term protection against SARS-CoV-2. The vaccine may be used to immunize naïve humans or as a booster vaccine for those who have previously been immunized but with a waning immunity.

DATA AVAILABILITY STATEMENT

The raw data supporting the conclusions of this article will be made available by the authors, without undue reservation.

ETHICS STATEMENT

The animal study was reviewed and approved by Institutional Animal Care and Use Committee of Beijing Institute of Biotechnology.

AUTHOR CONTRIBUTIONS

Conceived and designed the experiments: YZ and YHL. Performed the experiments: XQ and SL. Contributed reagents/

materials/analysis tools: BD and YL. Wrote the paper: XQ and XL. Participated in the experiments: YD, LL, HB, XS, EF, LZ, and YA. Guided the experiments: DP and YG. Data analysis: FH and LY. Guided the writing and revised the manuscript: SL and YZ. All authors contributed to the article and approved the submitted version.

REFERENCES

Bennett, J., Wellman, J., Marshall, K. A., McCague, S., Ashtari, M., DiStefano-Pappas, J., et al. (2016). Safety and Durability of Effect of Contralateral-Eye Administration of AAV2 Gene Therapy in Patients With Childhood-Onset Blindness Caused by RPE65 Mutations: A Follow-on Phase 1 Trial. *Lancet* 388, 661–672. doi: 10.1016/S0140-6736(16)30371-3

Burger, C., Gorbatyuk, O. S., Velardo, M. J., Peden, C. S., Williams, P., Zolotukhin, S., et al. (2004). Recombinant AAV Viral Vectors Pseudotyped With Viral Capsids From Serotypes 1, 2, and 5 Display Differential Efficiency and Cell Tropism After Delivery to Different Regions of the Central Nervous System. *Mol. Ther.* 10, 302–317. doi: 10.1016/j.ymthe.2004.05.024

Carter, B. J. (2004). Adeno-Associated Virus and the Development of Adeno-Associated Virus Vectors: A Historical Perspective. *Mol. Ther.* 10, 981–989. doi: 10.1016/j.ymthe.2004.09.011

Choo, K. H., and Ranganathan, S. (2008). Flanking Signal and Mature Peptide Residues Influence Signal Peptide Cleavage. *BMC Bioinf.* 9 (Suppl) 12, S15. doi: 10.1186/1471-2105-9-S12-S15

Daya, S., and Berns, K. I. (2008). Gene Therapy Using Adeno-Associated Virus Vectors. *Clin. Microbiol. Rev.* 21, 583–593. doi: 10.1128/CMR.00008-08

Demminger, D. E., Walz, L., Dietert, K., Hoffmann, H., Planz, O., Gruber, A. D., et al. (2020). Adeno-Associated Virus-Vectored Influenza Vaccine Elicits Neutralizing and Fcγ Receptor-Activating Antibodies. *EMBO Mol. Med.* 12, e10938. doi: 10.15252/emmm.201910938

Dismuke, D. J., Tenenbaum, L., and Samulski, R. J. (2013). Biosafety of Recombinant Adeno-Associated Virus Vectors. *Curr. Gene Ther.* 13, 434–452. doi: 10.2174/15665232113136660007

Donsante, A., Miller, D. G., Li, Y., Vogler, C., Brunt, E. M., Russell, D. W., et al. (2007). AAV Vector Integration Sites in Mouse Hepatocellular Carcinoma. *Science* 317, 477. doi: 10.1126/science.1142658

Evans, C. H., Gouze, E., Gouze, J. N., Robbins, P. D., and Ghivizzani, S. C. (2006). Gene Therapeutic Approaches-Transfer *In Vivo*. *Adv. Drug Delivery Rev.* 58, 243–258. doi: 10.1016/j.addr.2006.01.009

George, L. A., Ragni, M. V., Rasko, J., Raffini, L. J., Samelson-Jones, B. J., Ozelo, M., et al. (2020). Long-Term Follow-Up of the First in Human Intravascular Delivery of AAV for Gene Transfer: AAV2-Hfix16 for Severe Hemophilia B. *Mol. Ther.* 28, 2073–2082. doi: 10.1016/j.ymthe.2020.06.001

George, L. A., Sullivan, S. K., Giermasz, A., Rasko, J., Samelson-Jones, B. J., Ducore, J., et al. (2017). Hemophilia B Gene Therapy With a High-Specific-Activity Factor IX Variant. *N. Engl. J. Med.* 377, 2215–2227. doi: 10.1056/NEJMoa1708538

Hüser, D., Gogol-Döring, A., Lutter, T., Weger, S., Winter, K., Hammer, E. M., et al. (2010). Integration Preferences of Wildtype AAV-2 for Consensus Rep-Binding Sites at Numerous Loci in the Human Genome. *PloS Pathog.* 6, e1000985. doi: 10.1371/journal.ppat.1000985

Karpenko, L. I., Rudometov, A. P., Sharabrin, S. V., Shcherbako, D. N., Borgoyakova, M. B., Bazhan, S. I., et al. (2021). Delivery of mRNA Vaccine Against SARS-CoV-2 Using a Polyglucin: Spermidine Conjugate. *Vaccines* 9, 76. doi: 10.3390/vaccines9020076

Khoury, D. S., Cromer, D., Reynaldi, A., Schlub, T. E., Wheatley, A. K., Juno, J. A., et al. (2021). Neutralizing Antibody Levels are Highly Predictive of Immune Protection From Symptomatic SARS-CoV-2 Infection. *Nat. Med.* 27, 1205–1211. doi: 10.1038/s41591-021-01377-8

Kotterman, M. A., and Schaffer, D. V. (2014). Engineering Adeno-Associated Viruses for Clinical Gene Therapy. *Nat. Rev. Genet.* 15, 445–451. doi: 10.1038/nrg3742

Long, Q. X., Tang, X. J., Shi, Q. L., Li, Q., Deng, H. J., Yuan, J., et al. (2020). Clinical and Immunological Assessment of Asymptomatic SARS-CoV-2 Infections. *Nat. Med.* 26, 1200–1204. doi: 10.1038/s41591-020-0965-6

Min, L., and Sun, Q. (2021). Antibodies and Vaccines Target RBD of SARS-CoV-2. *Front. Mol. Biosci.* 8, 671633. doi: 10.3389/fmolb.2021.671633

Mohan, R. R., Schultz, G. S., Hong, J. W., Mohan, R. R., and Wilson, S. E. (2003). Gene Transfer Into Rabbit Keratocytes Using AAV and Lipid-Mediated Plasmid DNA Vectors With a Lamellar Flap for Stromal Access. *Exp. Eye Res.* 76, 373–383. doi: 10.1016/S0014-4835(02)00275-0

Mueller, C., Gernoux, G., Gruntman, A. M., Borel, F., Reeves, E. P., Calcedo, R., et al. (2017). 5 Year Expression and Neutrophil Defect Repair After Gene Therapy in Alpha-1 Antitrypsin Deficiency. *Mol. Ther.* 25, 1387–1394. doi: 10.1016/j.ymthe.2017.03.029

Murrey, D. A., Naughton, B. J., Duncan, F. J., Meadows, A. S., Ware, T. A., Campbell, K. J., et al. (2014). Feasibility and Safety of Systemic Raav9-hNAGLU Delivery for Treating Mucopolysaccharidosis IIIB: Toxicology, Biodistribution, and Immunological Assessments in Primates. *Hum. Gene Ther. Clin. Dev.* 25, 72–84. doi: 10.1089/humc.2013.208

Naso, M. F., Tomkowicz, B., Perry, W. L.3rd, and Strohl, W. R. (2017). Adeno-Associated Virus (AAV) as a Vector for Gene Therapy. *BioDrugs* 31, 317–334. doi: 10.1007/s40259-017-0234-5

Nie, J., Li, Q., Wu, J., Zhao, C., Hao, H., Liu, H., et al. (2020a). Quantification of SARS-CoV-2 Neutralizing Antibody by a Pseudotyped Virus-Based Assay. *Nat. Protoc.* 15, 3699–3715. doi: 10.1038/s41596-020-0394-5

Nie, J., Li, Q., Wu, J., Zhao, C., Hao, H., Liu, H., et al. (2020b). Establishment and Validation of a Pseudovirus Neutralization Assay for SARS-CoV-2. *Emerg. Microbes Infect.* 9, 680–686. doi: 10.1080/22221751.2020.1743767

Pasi, K. J., Rangarajan, S., Mitchell, N., Lester, W., Symington, E., Madan, B., et al. (2020). Multiyear Follow-Up of AAV5-hFVIII-SQ Gene Therapy for Hemophilia A. *N Engl. J. Med.* 382, 29–40. doi: 10.1056/NEJMoa1908490

Penaud-Budloo, M., Le Guiner, C., Nowrouzi, A., Toromanoff, A., Chérel, Y., Chenuaud, P., et al. (2008). Adeno-Associated Virus Vector Genomes Persist as Episomal Chromatin in Primate Muscle. *J. Virol.* 82, 7875–7885. doi: 10.1128/JVI.00649-08

Rakoczy, E. P., Lai, C. M., Magno, A. L., Wikstrom, M. E., French, M. A., Pierce, C. M., et al. (2015). Gene Therapy With Recombinant Adeno -Associated Vectors for Neovascular Age-Related Macular Degeneration: 1 Year Follow-Up of a Phase 1 Randomised Clinical Trial. *Lancet* 386, 2395–2403. doi: 10.1016/S0140-6736(15)00345-1

Rangarajan, S., Walsh, L., Lester, W., Perry, D., Madan, B., Laffan, M., et al. (2017). AAV5-Factor VIII Gene Transfer in Severe Hemophilia A. *N. Engl. J. Med.* 377, 2519–2530. doi: 10.1056/NEJMoa1708483

Robbiani, D. F., Gaebler, C., Muecksch, F., Lorenzi, J., Wang, Z., Cho, A., et al. (2020). Convergent Antibody Responses to SARS-CoV-2 in Convalescent Individuals. *Nature* 584, 437–442. doi: 10.1038/s41586-020-2456-9

Schultz, B. R., and Chamberlain, J. S. (2008). Recombinant Adeno-Associated Virus Transduction and Integration. *Mol. Ther.* 16, 1189–1199. doi: 10.1038/mt.2008.103

Sims, J. J., Greig, J. A., Michalson, K. T., Lian, S., Martino, R. A., Meggersee, R., et al. (2021). Intranasal Gene Therapy to Prevent Infection by SARS-CoV-2 Variants. *PloS Pathog.* 17, e1009544. doi: 10.1371/journal.ppat.1009544

Tai, W., Zhang, X., Drelich, A., Shi, J., Hsu, J. C., Luchsinger, L., et al. (2020). A Novel Receptor-Binding Domain (RBD)-Based mRNA Vaccine Against SARS-CoV-2. *Cell Res.* 30, 932–935. doi: 10.1038/s41422-020-0387-5

van der Laan, L. J. W., Wang, Y., Tilanus, H. W., Janssen, H. L. A., and Pan, Q. (2011). AAV-Mediated Gene Therapy for Liver Diseases: The Prime Candidate for Clinical Application? *Expert Opin. Biol. Ther.* 11, 315–327. doi: 10.1517/14712598.2011.548799

Wang, D., Tai, P., and Gao, G. (2019). Adeno-Associated Virus Vector as a Platform for Gene Therapy Delivery. *Nat. Rev. Drug Discov.* 18, 358–378. doi: 10.1038/s41573-019-0012-9

Wu, Y., Wang, F., Shen, C., Peng, W., Li, D., Zhao, C., et al. (2020). A Noncompeting Pair of Human Neutralizing Antibodies Block COVID-19 Virus Binding to its Receptor ACE2. *Science* 368, 1274–1278. doi: 10.1126/science.abc2241

Yang, S., Li, Y., Dai, L., Wang, J., He, P., Li, C., et al. (2021). Safety and Immunogenicity of a Recombinant Tandem-Repeat Dimeric RBD-Based

Protein Subunit Vaccine (ZF2001) Against COVID-19 in Adults: Two Randomised, Double-Blind, Placebo-Controlled, Phase 1 and 2 Trials. *Lancet Infect. Dis.* 21, 1107–1119. doi: 10.1016/S1473-3099(21)00127-4

Zabaleta, N., Dai, W., Bhatt, U., Hérate, C., Maisonnasse, P., Chichester, J. A., et al. (2021). An AAV-Based, Room-Temperature-Stable, Single-Dose COVID-19 Vaccine Provides Durable Immunogenicity and Protection in Non-Human Primates. *Cell Host Microbe* 29, 1437–1453. doi: 10.1016/j.chom.2021.08.002

Zhou, P., Yang, X. L., Wang, X. G., Hu, B., Zhang, L., Zhang, W., et al. (2020). A Pneumonia Outbreak Associated With a New Coronavirus of Probable Bat Origin. *Nature* 579, 270–273. doi: 10.1038/s41586-020-2012-7

Zhu, N., Zhang, D., Wang, W., Li, X., Yang, B., Song, J., et al. (2020). A Novel Coronavirus From Patients With Pneumonia in China 2019. *N. Engl. J. Med.* 382, 727–733. doi: 10.1056/NEJMoa2001017

Zincarelli, C., Soltys, S., Rengo, G., and Rabinowitz, J. E. (2008). Analysis of AAV Serotypes 1-9 Mediated Gene Expression and Tropism in Mice After Systemic Injection. *Mol. Ther.* 16, 1073–1080. doi: 10.1038/mt.2008.76

Conflict of Interest: The authors declare that the research was conducted in the absence of any commercial or financial relationships that could be construed as a potential conflict of interest.

Publisher's Note: All claims expressed in this article are solely those of the authors and do not necessarily represent those of their affiliated organizations, or those of the publisher, the editors and the reviewers. Any product that may be evaluated in this article, or claim that may be made by its manufacturer, is not guaranteed or endorsed by the publisher.

frontiers in Cellular and Infection Microbiology

ORIGINAL RESEARCH
published: 04 March 2022
doi: 10.3389/fcimb.2022.807332

Inflammation/Coagulopathy/ Immunology Responsive Index Predicts Poor COVID-19 Prognosis

Hui An[1,2†], Jitai Zhang[2†], Ting Li[1], Yuxin Hu[2], Qian Wang[2], Chengshui Chen[3], Binyu Ying[4], Shengwei Jin[1,2] and Ming Li[1,2*]*

[1] The Second Affiliated Hospital and Yuying Children's Hospital of Wenzhou Medical University, Zhejiang, China, [2] School of Basic Medical Science, Wenzhou Medical University, Wenzhou, China, [3] Department of Pulmonary and Critical Care Medicine, The First Affiliated Hospital of Wenzhou Medical University, Wenzhou, China, [4] Department of Critical Care Medicine, The Second Affiliated Hospital and Yuying Children's Hospital of Wenzhou Medical University, Wenzhou, China

In the early stage of coronavirus disease 2019 (COVID-19), most cases are identified as mild or moderate illnesses. Approximately 20% of hospitalised patients become severe or critical at the middle or late stage of the disease. The predictors and risk factors for prognosis in those with mild or moderate disease remain to be determined. Of 694 patients with COVID-19, 231 patients with mild or moderate disease, who were hospitalised at 10 hospitals in Wenzhou and nearby counties in China, were enrolled in this retrospective study from 17 January to 20 March 2020. The outcomes of these patients included progression from mild/moderate illness to severe or critical conditions. Among the 231 patients, 49 (21.2%) had a poor prognosis in the hospital. Multivariate logistic regression analysis showed that higher inflammation/coagulopathy/immunology responsive index (ICIRI=[c-reactive protein × fibrinogen × D-dimer]/CD8 T cell count) on admission (OR=345.151, 95% CI=23.014–5176.318) was associated with increased odds ratios for poor prognosis. The area under the receiver operating characteristic curve for ICIRI predicting severe and critical condition progression was 0.65 (95% CI=0.519–0.782) and 0.80 (95% CI=0.647–0.954), with cut-off values of 870.83 and 535.44, respectively. Conversely, age, sex, comorbidity, neutrophil/lymphocyte ratio, CD8 T cell count, and c-reactive protein, fibrinogen, and D-dimer levels alone at admission were not good predictors of poor prognosis in patients with mild or moderate COVID-19. At admission, a novel index, ICIRI, tends to be the most promising predictor of COVID-19 progression from mild or moderate illness to severe or critical conditions.

Keywords: COVID-19, inflammation/coagulopathy/Immunology responsive index, predict, moderate, severe, critical patient

OPEN ACCESS

Edited by:
Ke Xu,
Wuhan University, China

Reviewed by:
Carlo Contini,
University of Ferrara, Italy
Kuldeep Shah,
Beaumont Health, United States

****Correspondence:***
Ming Li
mingli@wmu.edu.cn
Shengwei Jin
jinshengwei69@163.com

†These authors share first authorship

Specialty section:
This article was submitted to Virus and Host, a section of the journal Frontiers in Cellular and Infection Microbiology

Received: *02 November 2021*
Accepted: *08 February 2022*
Published: *04 March 2022*

Citation:
An H, Zhang J, Li T, Hu Y, Wang Q, Chen C, Ying B, Jin S and Li M (2022) Inflammation/Coagulopathy/ Immunology Responsive Index Predicts Poor COVID-19 Prognosis. Front. Cell. Infect. Microbiol. 12:807332. doi: 10.3389/fcimb.2022.807332

1 INTRODUCTION

Severe acute respiratory syndrome coronavirus 2 (SARS-CoV-2) continues to spread globally. Coronavirus disease 2019 (COVID-19) is generally categorised as mild, moderate, severe, and critical (He et al., 2020; Wu and McGoogan, 2020; Jin et al., 2021a). The majority of patients (~81%) experience mild or moderate symptoms (Zhou et al., 2020), while the other patients experience severe (14%) and critical (5%) symptoms (Sun et al., 2020). This is consistent with the finding that

approximately 20% of hospitalised patients with COVID-19 require admission in the intensive care unit (ICU) (Rodriguez-Morales et al., 2020; Yang et al., 2020). Patients with critical COVID-19 usually experience worsening mild or moderate illness from the 7th–14th day of the disease course, developing severe pneumonia and acute respiratory distress syndrome.

Thus, identifying early biomarkers of disease severity on admission could expedite the early intensified therapy to reduce mortality. However, there are few reports of the prognostic capacity of early biomarkers of the disease, and the information in published studies are limited to age, sex (Jin et al., 2021a), neutrophil-to-lymphocyte ratio (NLR) (Yang et al., 2020), immunological cell defects (Du et al., 2020; Jin et al., 2021a), systemic inflammation response index; liver, heart, and kidney injuries, coagulation defects, and aggregate index of systemic inflammation in predicting mortality in COVID-19 patients (Bhargava et al., 2020; Fois et al., 2020; Huang et al., 2020; Bahardoust et al., 2021; Gallo Marin et al., 2021; Hariyanto et al., 2021). However, inflammatory responses and indicators to the microorganism-induced infection are not specific for COVID-19, leading to an uncertain diagnosis.

Previously, we found that C-reactive protein (CRP, a sensitive inflammatory marker), fibrinogen, D-dimer (a coagulopathy marker), and CD8 T cell count (CD8, an immunological marker) were associated with the progression of COVID-19 (An et al., 2021; Jin et al., 2021a; Jin et al., 2021b). In this study, we sought to apply the combination of these parameters [inflammation/coagulopathy/immunology responsive index (ICIRI)] to predict poor COVID-19 prognosis at the time of admission.

2 METHODS

2.1 Study Design and Participants

2.1.1 Ethics Statement

The present study was conducted in accordance with the ethical guidelines of the 1975 Declaration of Helsinki and was approved by the Ethics Committee of Wenzhou Medical University (Ref 2020002). Given the urgency of the COVID-19 pandemic and global health concerns, the requirement of informed consent was waived by the Ethics Committee of Wenzhou Medical University.

This multicentre observational study retrospectively studied 694 COVID-19 patients admitted to 10 hospitals in Wenzhou City and nearby counties in Zhejiang Province, China, from 17 January 2020 to 20 March 2020. COVID-19 was confirmed by reverse transcription polymerase chain reaction in all cases, as described previously (Huang et al., 2020). Patients with COVID-19 were stratified into mild (mild symptoms with no sign of pneumonia), moderate (fever, respiratory tract symptoms, and pneumonia on chest computed tomography scan), severe (respiratory distress syndrome, respiratory rates ≥30/min, finger oxygen saturation [measured after 5 minutes of rest] ≤93%, or oxygenation index [PaO2/FiO2] ≤300 mmHg), and critical (respiratory failure requiring intubation, shock, other organ failures, or admission to the ICU) illness groups (Jin et al., 2021a). Clinical and laboratory data were recorded in a dedicated electronic database. The exclusion criteria were as follows: lack of data on $CD8^+$ T cell count, CRP level, fibrinogen level, or oxygenation index ≤300 mmHg at admission.

2.2 Data Collection and Laboratory Procedures

We collected epidemiological, demographic, clinical, laboratory, treatment, and outcome data using a standardised data collection from electronic medical records. Three physicians (CC, BY, and TL) and a researcher (SJ) checked all data, and differences in interpretation were adjudicated between the three primary reviewers.

According to the onset of the first symptoms before admission, the day-by-day data during the course of COVID-19 were collected, as described previously (An et al., 2021). Routine clinical blood examinations, including complete blood count and serum biochemical tests, were performed on the day of admission. In particular, we assessed white blood cell count, lymphocyte count, neutrophil count, CRP level, FIB level, DD level, and CD8 count as we described previously (An et al., 2021; Jin et al., 2021a; Jin et al., 2021b). Subsequently, we extrapolated combined blood cell indexes of systemic inflammation (neutrophil/lymphocyte ratio, NLR) and formulated the inflammation/coagulopathy/immunology responsive index, which was calculated as follows: ICIRI= (CRP [mg/L] × FIB [g/L] ×DD [μg/L]/CD8 T cell count [n/μL]).

2.3 Statistical Analysis

Results are expressed as median (interquartile range, IQR) or number (percentage), according to the data distribution. The D'Agostino & Pearson omnibus normality, Shapiro–Wilk normality, and Kolmogorov–Smirnov tests were applied to determine data distribution. The Kruskal–Wallis test, χ^2 test, chi-square test with Yates' correction, or Fisher's exact test were used for nonparametric data.

To adjust for risk factors associated with 12-day illness progression from moderate infection to severe or critical infection during admission, univariable and multivariable logistic regression models were applied. Considering the total number of prognoses in our study (n=231) and avoiding overfitting of the model, 11 variables (sex, age, CRP, fibrinogen, D-dimer, ICIRI, leukocyte count, neutrophil count, lymphocyte count, NLR, and $CD8^+$ T cell count) were selected for multivariable logistic analysis, based on univariable logistic analysis results and clinical significance. Receiver operating characteristic (ROC) curves were applied to assess the potential predictive value of risk factors for in-hospital prognosis.

A P value < 0.05 was considered statistically significant. Statistical analysis was performed using SPSS (version 19.0) and GraphPad Prism (version 9.0, La Jolla, CA, USA) software.

3 RESULTS

3.1 Clinical Characteristics of Moderate Cases on Admission

After the exclusion of 463 cases using the exclusion criteria, 231 patients, grouped by their subsequent COVID-19 severities as

mild (9 patients), moderate (173 patients), severe (36 patients), and critical (13 patients), were finally enrolled. Of the 231 patients, 73 (31.60%) had one or more pre-existing diseases, such as cardiovascular disease (including hypertension), cardio-cerebrovascular disease, diabetes, respiratory disease, cancers, benign tumours, chronic liver and kidney diseases, and hypercholesterolemia. Because a previous study demonstrated that comorbidities in cases of moderate disease were not a risk factor for poor prognosis (Cheng et al., 2020), we included patients with comorbidities in our data analysis. All patients received antiviral, Chinese herbs and supportive therapies after the diagnosis was confirmed and were discharged alive.

Of 231 patients with COVID-19, 182 (77.78%) did not progress to severe disease, and 49 (21.21%) had poor in-hospital prognosis. Briefly, in 15.58% (36/231) of patients, the condition worsened and became severe, and in 5.63% (13/231) of patients, it became critical without death (**Table 1**). Previously, we provided detailed information about this COVID-19 cohort. This study reanalysed this cohort with different onset days, days 1 to 15 before admission, 12 days post-hospitalisation, and only selected parameters for the analysis, as shown in **Table 1**. The mean patient ages were 40.0 (25.0–48.0) years in the cohort of mild cases, 48.0 (37.5–56.0) years in that of moderate cases, 48.0 (40.3–56.5) years among those who subsequently had severe cases, and 63.0 (49.0–76.5) years among those who subsequently had critical cases. Compared to patients that did not experience disease progression, patients who became critically ill were significantly older (**Table 1**).

3.2 Laboratory Data of Patients With Moderate Infection on Admission

Inflammatory and immunological variables were significantly associated with outcome, and patients with poor prognoses generally had higher levels of CRP, NLR, fibrinogen, and D-dimer, and lower lymphocyte and CD8 T cell counts (**Table 1**). Although the oxygenation index was normal in patients with subsequently critical COVID-19, CRP (41.5 [12.853–69.7] mg/L, reference: <10.00 mg/L) and D-dimer (1170.0 [640.0–1525.0] μg/L, reference: <500.0 μg/L) levels, leukocyte and neutrophil counts, and NLR (6.3 [3.1–21.1], reference: <3.2) were significantly higher in these patients than in those with moderate COVID-19. Conversely, patients with subsequently critical disease had lower lymphocyte and $CD8^+$ T cell (137 [137–150] n/μL, reference >320/μL) counts than those with moderate disease at the time of admission. Plasma fibrinogen levels were significantly higher in patients with moderate (4.1 [3.2–4.9 g/L]), subsequently severe (3.7 [2.8–6.2] g/L), and critical (5.0 [3.8–6.3] g/L) COVID-19 than in those with mild (2.5 [2.4–3.4] g/L, reference <4.0 g/L) disease on admission. However, NLR >3.2 was predominant among those who subsequently had critical disease (NLR >3.2, 76.9%), but not among those who subsequently had severe disease (25.0%) when compared with those with moderate disease (28.3%) (**Table 1**). Compared to patients with moderate disease (ICIRI >800, 4.62%) at admission, higher proportions of patients with subsequently severe or critical COVID-19 had ICIRI >800 (47.22% and 75.00%, respectively, both $p < 0.0001$) at admission. Compared to patients with ICIRI <800 at admission, normal oxygenation index (>300 mmHg) curve, analysed *via* log-rank test, revealed that the hazard ratio of ICIRI >800 was 4.037 (95% CI=2.538–6.422, P<0.0001), after 27 days since the onset of COVID-19 symptoms (**Figure 1**). On admission, only an increase of plasma aspartate aminotransferase (AST), but not alanine aminotransferase (ALT) and bilirubin, was associated with subsequently critical patients (**Table 1**).

3.3 Risk Factors Associated With Poor Prognosis, Which Can Predict the Prognosis of Moderate COVID-19 Symptoms

Table 2 summarises the results of univariable and multivariable logistic analyses of risk factors associated with progression from moderate to severe or critical conditions. After adjusting for sex, age, neutrophil count, lymphocyte count, NLR, CD8 T cell count, CRP level, fibrinogen level, D-dimer level, and ICIRI, we found that a higher ICIRI (>800) was associated with increased odds ratios for poor prognosis in both univariable (OR=26.174, 95% CI=10.661-64.261, P <0.001) and multivariable regression analyses (OR=345.151, 95% CI=23.014-5176.318, P <0.001). However, older age (>65 years), higher CRP level (>10.0 mg/L), higher D-dimer level (>500.0 μg/L), neutrophil count, lymphocyte count, and lower CD8 T cell count (<320/μL) were associated with increased odds ratios of poor prognosis in univariable regression alone. Notably, a higher AST was associated with increased odds ratios for poor prognosis in both univariable (OR=5.027, 95% CI=2.165-11.674, P <0.001) and multivariable regression analyses (OR=4.138, 95% CI=1.132-15.129, P <0.05). Among those with mild or moderate COVID-19 at admission, sex (male), higher NLR ratio (>3.2), and higher fibrinogen (>4.0 g/L) were non-significantly associated with increased odds ratios for poor prognosis in both univariable and multivariable regression analyses (**Table 2**).

The AUC of ICIRI for predicting total poor prognosis, progression to severe disease, and progression to critical disease were 0.704 (95% CI=0.599–0.809, P<0.001), 0.650 (95% CI=0.519–0.782, P<0.01), and 0.800 (95% CI=0.647–0.954, P<0.001), respectively, with cut-off values of 870.8, 870.8, and 535.4, respectively (**Table 3**). Other results of the ROC curve analysis, including sensitivity, specificity, Youden Index, and cut-off values, are shown in **Table 3**.

4 DISCUSSION

In the present study, the major hepatic functional symptom of moderate COVID-19 on admission, oxygenation index, did not differ between the subsequent outcome groups. Therefore, predicting prognosis based on hepatic symptoms is challenging. Using comparative and multivariable analyses of

TABLE 1 | Laboratory findings of patients with mild, moderate, subsequently severe, and subsequently critical COVID-19 at admission and on post-medication days 6 and 12.

	Total (n=231)	Mild case (n = 9)	Moderate case (n = 173)	severe case (n = 36)	critical case (n = 13)	P
Age, years	48.0 (39.0, 56.0)	40.0 (25.0, 48.0)	48.0 (37.5, 56.0)	48.0 (40.3, 56.5)	63.0 (49.0, 76.5) $^{aa/b}$	0.007
Disease history						
Health (%)	158/231 (68.4)	8/9 (88.9)	122/173 (70.5)	23/36 (63.9)	5/13 (38.5)^{b}	
Comorbidities (%)	73/231 (31.6)	1/9 (11.1)	51/173 (29.5)	13/36 (36.1)	8/13 (61.5)^{b}	
HP (%)	42/231 (18.2)	1/9 (11.1)	25/173 (14.5)	11/36 (30.6)^{b}	5/13 (38.5)	
CCD (%)	7/231 (3.0)	0/9 (0)	4/173 (2.3)	2/36 (5.6)	1/13 (7.7)	
Diabetes (%)	24/231 (10.4)	0/9 (0)	14/173 (8.1)	6/36 (16.7)	4/13 (30.8)^{b}	
HP and Diabetes (%)	15/231 (6.5)	0/9 (0)	7/173 (4.0)	4/36 (11.1)	4/13 (30.8)^{bb}	
Kidney (%)	2/231 (0.9)	0/9 (0)	0/173 (0)	1/36 (2.8)	1/13 (7.7)	
Lung (%)	8/231 (3.5)	0/9 (0)	7/173 (4.0)	0/36 (0)	1/13 (7.7)	
Cancer (%)	7/231 (3.0)	0/9 (0)	4/173 (2.3)	1/36 (2.8)	2/13 (15.4)	
Laboratory parameters						
C-reactive protein, mg/L	9.8 (3.8, 29.3)	1.7 (0.5, 3.1)	9.7 (4.5, 24.5) ^{aa}	11.1 (1.5, 74.3) ^{a}	41.5 (12.8, 69.7) $^{aaaa/b}$	0.0001
> 10 mg/L	114/230 (49.6)	0/9 (0)	85/173 (49.1) ^{aa}	18/36 (50.0) ^{aa}	11/12 (91.7) $^{aaaa/bb/c}$	
Fibrinogen, g/L	4.1 (3.1, 5.1)	2.5 (2.4, 3.4)	4.1 (3.2, 4.9) ^{aa}	3.7 (2.8, 6.2) ^{a}	5.0 (3.8, 6.3) ^{aaa}	0.0009
> 4 g/L	115/230 (50.0)	0/9 (0)	89/173 (51.5) ^{aa}	17/35 (48.6) ^{aa}	9/13 (69.2) ^{aa}	
D-dimer, μg/L	290.0 (170.0, 500.0)	250.0 (150.0, 356.0)	280.0 (170.0, 410.0)	390.0 (130.0, 1320.0)	1170.0 (640.0, 1525.0) $^{a/bbb}$	0.001
> 500 μg/L	55/230 (23.9)	1/9 (11.1)	29/173 (16.8)	14/35 (40.0) ^{bb}	11/13 (84.6) $^{aa/bbbb/cc}$	
ICIRI	39.2 (7.0, 256.7)	4.4 (1.2, 10.3)	35.8 (7.6, 137.7) ^{a}	597.4 (5.7, 3870.0) $^{aaa/b}$	1588.0 (717.0, 2632.0) $^{aaaa/bbb}$	<0.0001
> 800	34/230 (14.8)	0/9 (0)	8/173 (4.6)	17/36 (47.2) $^{aa/bbbb}$	9/12 (75.0) $^{aa/bbbb}$	
Oxygen index, mmHg	453.4 (393.6, 500.0)	500.0 (472.1, 500.0)	444.0 (394.6, 495.1) ^{a}	489.0 (414.3, 500.0)	372.9 (365.5, 491.1) ^{a}	0.0027
< 300 mmHg	0/196 (0)	0/9 (0)	0/138 (0)	0/36 (0)	0/13 (0)	
Leukocyte count, ×10^{9}/L	5.0 (4.0, 6.3)	5.1 (4.5, 7.3)	4.9 (4.0, 6.1)	4.8 (3.9, 6.4)	9.9 (5.5, 12.1) $^{bbb/cc}$	0.0011
> 10 ×10^{9}/L	13/231 (5.6)	0/9 (0)	6/173 (3.5)	1/36 (2.8)	6/13 (46.2) $^{a/bbbb/cc}$	
Neutrophil count, ×10^{9}/L	3.1 (2.3, 4.2)	3.2 (2.4, 4.8)	3.0 (2.2, 3.9)	3.0 (2.1, 4.1)	7.0 (3.4, 10.4) $^{bb/c}$	0.0074
> 6.3 ×10^{9}/L	19/231 (8.2)	0/9 (0)	9/173 (5.2)	3/36 (8.3)	7/13 (53.9) $^{a/bbbb/cc}$	
Lymphocyte count, ×10^{9}/L	1.3 (0.9,1.6)	1.4 (1.3, 2.4)	1.3 (1.0, 1.6)	1.3 (0.9, 1.7)	0.9 (0.5, 1.1) $^{aa/b}$	0.0042
< 1.1 ×10^{9}/L	79/231 (34.2)	1/9 (11.1)	54/173 (31.2)	15/36 (41.7)	9/13 (69.2) $^{a/b}$	
NLR	2.4 (1.6, 3.4)	2.0 (1.7, 2.6)	2.4 (1.6, 3.3)	2.3 (1.5, 3.7)	6.3 (3.1, 21.1) $^{a/bbb/cc}$	0.0013
> 3.2	69/231 (29.9)	1/9 (11.1)	49/173 (28.3)	9/36 (25.0)	10/13 (76.9) $^{aa/bb/cc}$	
CD8^{+} T cells/μL	299.0 (186.0, 436.0)	327.0 (259.5, 470.2)	330.0 (224.5, 464.5)	237.5 (137.5, 335.3) ^{bb}	137.0 (137.0, 150.0) $^{aa/bbbb}$	<0.0001
< 320/μL	122/231 (52.8)	4/9 (44.4)	82/173 (47.4)	24/36 (66.67) ^{b}	12/13 (92.3) $^{a/bb}$	
ALT, IU/L	23.0 (15.0, 39.0)	22.0 (13.0,29.5)	22.0 (14.0, 35.0)	25.0 (16.0, 48.0)	23.0 (19.5, 68.0)	0.3002
Male >40 IU/L; Female >35 IU/L	52/227 (22.9)	1/9 (11.1)	35/171 (20.5)	12/34 (35.3)	4/13 (30.8)	
AST, IU/L	24.0 (18.0, 34.0)	20.0 (16.0,28.0)	23.0 (18.0, 31.0)	24.2 (20.0, 41.0)	44.0 (33.5, 67.5)$^{aa/bb}$	0.0009
>40 IU/L	35/209 (16.7)	1/9 (11.1)	18/156 (11.5)	8/31 (25.8)	8/13 (61.5)^{bbbb}	
Total bilirubin, μmol/L	10.9 (7.3, 15.5)	9.9 (6.1, 14.8)	10.7 (7.1, 15.6)	13.4 (9.2, 15.9)	10.0 (7.0, 15.0)	0.4189
Direct Bilirubin, μmol/L	4.1 (2.9, 5.9)	2.9 (2.6, 4.4)	4.2 (2.8, 6.0)	4.8 (3.2, 6.0)	4.0 (3.5, 6.5)	0.2444
Post-medication day 6						
Oxygen index, mmHg	369.2 (265.0, 479.0)	337.9 (320.5, 481.0)	407.0 (352.8, 499.5)	207.4 (124.1, 271) ^{bbbb}	301.3 (213.5, 500.0)	<0.0001
< 300 mmHg	26/84 (31.0)	0/5 (0)	2/48 (4.2)	21/25 (84.0) $^{aa/bbbb}$	3/6 (50.0) ^{bb}	
Post-medication day 12						
Oxygen index, mmHg	338.0 (233.2, 428.7)	371.0 (351.1, 377.3)	416.5 (337.3, 492.9)	201.5 (121.9, 282.5) ^{bbbb}	281.5 (226.8, 397.5)	<0.0001
< 300 mmHg	29/77 (37.7)	0/4 (0)	0/34 (0)	23/29 (79.3) $^{aa/bbbb}$	6/10 (60.0) ^{bbbb}	

*Data are median (IQR), or n/N (%). P values were calculated by Kruskal-Wallis test, χ^2 test, or Fisher's exact test, as appropriate. ICIRI: ([c-reactive protein, mg/L*Fibrinogen, g/L*D-dimer, μg/L]/CD8^{+} T cell number, n/μL); NLR, neutrophil to lymphocyte ratio; HP, hypertension; CCD, cardio-cerebrovascular disease; ALT, alanine aminotransferase; AST, aspartate aminotransferase.*

^{a}p values indicate a significant difference compared with mild group; $^{a}p < 0.05$, $^{aa}p < 0.01$, $^{aaa}p < 0.001$, $^{aaaa}p < 0.0001$.

^{b}p values indicate a significant difference compared with moderate group; $^{b}p < 0.05$, $^{bb}p < 0.01$, $^{bbb}p < 0.001$, $^{bbbb}p < 0.0001$.

^{c}p values indicate a significant difference compared with Subsequently severe case; $^{c}p < 0.05$, $^{c\ c}p < 0.01$.

the laboratory findings of patients with moderate COVID-19, we found that ICIRI was positively and significantly associated with poor prognosis in both patients with subsequently severe (>800: ~47%) and critical (~75%) disease when compared with those with moderately severe (~5%) disease. This suggests that among patients with moderate disease who have ICIRI >800 on admission, 5%, 47%, and 75% of cases may subsequently experience moderate, severe, and critical COVID-19, respectively. To initially differentiate mild or moderate cases from those that would subsequently become severe or critical

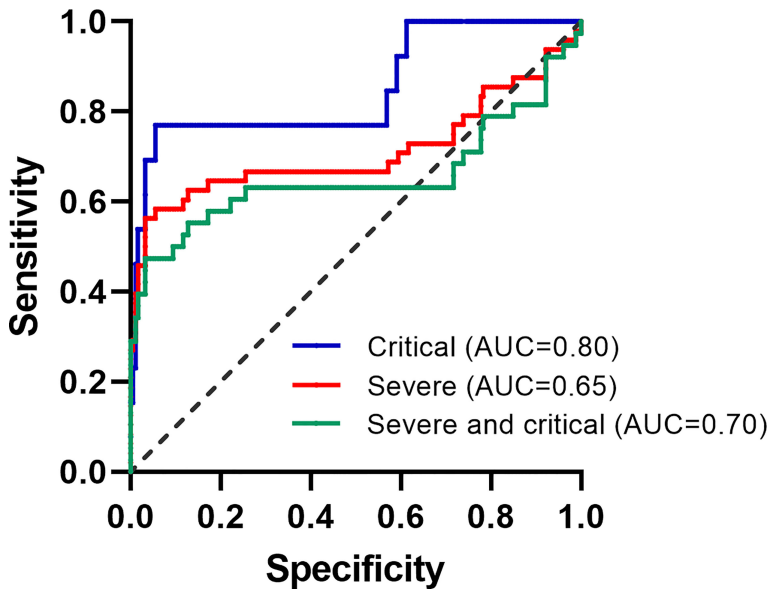

FIGURE 1 | ROC curves of ICIRI in patients with moderate COVID-19.

would be helpful because it would indicate those who require close monitoring, enabling earlier treatment for patients with ICIRI >800, preventing deteriorating outcomes. In this study, the AUC of ICIRI in predicting progression to a critical condition was more than 0.80, indicating that ICIRI may act as a predictor of poor progression of COVID-19.

We also observed that higher CRP (>10.0 mg/L), higher D-dimer level (>500 μg/L), and lower CD8 T cell count (<320/μL)

TABLE 2 | Risk factors associated with progression from mild or moderate to severe case.

	Univariable regression		Multivariable regression	
Demographics and clinical characteristics	**OR (95% CI)**	**P value**	**OR (95% CI)**	**P value**
Male (vs female)	0.789 (0.418-1.487)	0.46		
Age, years				
<65	Reference			
≥65	3.878 (1.741-8.641)	0.001	3.300 (0.631-17.246)	0.16
Comorbidity	2.086 (1.094-3.977)	0.03	2.313(0.699-7.658)	0.17
C-reactive protein, mg/L				
≤10	Reference			
>10	2.143 (1.124-4.083)	0.02	1.991 (0.465-8.522)	0.35
Fibrinogen, g/L				
≤4	Reference			
>4	1.348 (0.72-2.522)	0.35	0.281(0.056-1.398)	0.12
D-dimer, μg/L				
≤500	Reference			
>500	5.858 (2.972-11.544)	<0.001	0.916 (0.105-7.976)	0.94
$CD8^+$ T cells/μL				
<320	2.623 (1.343-5.124)	0.005	2.975(0.905-9.777)	0.07
≥320	Reference			
ICIRI				
≤800	Reference			
>800	26.174 (10.661-64.261)	<0.001	345.151 (23.014-5176.318)	<0.001
Neutrophil count, × 10^9/L	1.184 (1.037-1.351)	0.01	1.566 (1.055-2.325)	0.03
Lymphocyte count, ×10^9/L	0.512 (0.274-0.958)	0.04	0.825 (0.252-2.702)	0.75
NLR				
≤3.2	Reference			
>3.2	1.418 (0.733-2.745)	0.3	0.504 (0.068-3.723)	0.50
AST, IU/L				
<40	Reference			
≥40	5.027 (2.165-11.674)	<0.001	4.138 (1.132-15.129)	0.03

*OR, odds ratio; ICIRI, ([c-reactive protein, mg/L*Fibrinogen, g/L*D-dimer, μg/L]/$CD8^+$ T cell number, n/μL); NLR, neutrophil to lymphocyte ratio. AST, aspartate aminotransferase.*

TABLE 3 | The parameters results of ROC cure analysis. .

	AUC (95%CI)	P value	Sensitivity (%)	Specificity (%)	Youden Index	Cut-off value
Prediction for total prognoses						
ICIRI	0.704 (0.599-0.809)	<0.001	0.529	0.967	0.496	870.830
Prediction for severe progression						
ICIRI	0.650 (0.519-0.782)	0.004	0.486	0.967	0.453	870.830
Prediction for critical progression						
ICIRI	0.800 (0.647-0.954)	<0.001	0.733	0.906	0.639	535.441

*AUC, area under the curve; ICIRI: ([c-reactive protein, mg/L*Fibrinogen, g/L*D-dimer, μg/L]/CD8⁺ T cell number, n/μL).*

were accompanied by increased odds ratios of poor prognosis in univariable regression alone. Our study and others have shown that severe SARS-CoV-2 infection decreases $CD8^+$ T cells (Jin et al., 2021a and Jiang et al., 2020; Wang et al., 2020). In the present study, although decrease of CD8 T cell count was accompanied by significantly increased odds ratios of poor prognosis in univariable regression alone, the multivariable regression analysis indicates that predictive relationship between severity of COVID-19 and CD8 T cell count was not reached to the significance. This might result because SARS-CoV-2 virus-induced damage to CD8 T cell count remains limited and not altered at the early stage of COVID-19. This indicates that these inflammation, coagulation, and immunology parameters alone are not strong indicators of poor COVID-19 prognosis at an early stage of COVID-19. This information is consistent with the finding of our previous study in which the use of medication after patient hospitalisation decreased inflammatory response and plasma CRP and fibrinogen levels. Medication use gradually normalised CRP concentration on post-treatment day 12 and suppressed fibrinogen levels. However, although the use of medications hindered COVID-19 progression, coagulation/fibrinolysis remained significant (An et al., 2021). This suggests that although medication use reduces the occurrence of illness due to COVID-19 progression, the antecedent thrombus resulted in an elevation in fibrinolytic activities to dissolve the preceding thrombi and gain coagulation/fibrinolysis homeostasis.

SARS-CoV-2 virus-induced overt disseminated intravascular coagulation (DIC) has been observed in patients with critical COVID-19 (Tang et al., 2020). After a viral attack, CRP activates inflammatory response and blood coagulation, impairs endogenous fibrinolytic capacity, and stimulates or enhances platelet adhesiveness and responsiveness (Chen et al., 2009). Fibrinogen has overlapping roles in blood clotting, fibrinolysis, cellular and matrix interactions, inflammatory response, wound healing, and neoplasia (Mosesson, 2005). Thus, elevated plasma CRP and fibrinogen levels could significantly influence the development or progression of the pre-DIC stage. SARS-CoV-2 not only causes damage to the lungs (Sungnak et al., 2020), endothelial cells (Varga et al., 2020), smooth muscle cells, and other cells (Meftahi et al., 2020), it also markedly decreases lymphocyte count, especially CD8 T cell count (Jin et al., 2021a). Combining our findings with other previous findings suggests that ICIRI can be a good predictor of COVID-19 progression. Further, the risk stratification of ICIRI could facilitate patient management because it suggests that patients with mild or moderate COVID-19, who have ICIRI <800 on admission, are highly unlikely to develop severe or critical illness and can be treated in a community hospital or quarantined at home. Further, the risk stratification indicates that patients with ICIRI ≥800 have a high risk of developing severe or critical diseases. They need to be prepared for transfer to a special care centre or the ICU for invasive respiratory support. We believe that by examining this concept using large-scale studies with a larger number of cases, the resultant risk stratification and management system would ease the healthcare burden associated with COVID-19 and lessen COVID-19-induced mortality.

Dissimilar to previous findings that NLR predicts the development of critical illness in COVID-19 (Cheng et al., 2020; Liu et al., 2020), we found that neutrophil count, lymphocyte count, and lower CD8 T cell count were associated with increased odds ratios for poor prognosis in univariable regression alone. Furthermore, we did not find that a higher NLR ratio was significantly associated with increased odds ratios for poor prognosis in univariable and multivariable regression analyses. This is not a surprising finding. It is well known that inflammatory responses induced by COVID-19 are influenced by both the viral infection and subsequent bacterial infections; thus, inflammatory response is not specific to COVID-19. The disparity between our data and previous findings may have been caused by the inclusion of patients at different stages of the disease in the derivation and validation cohorts, leading to an imbalance in laboratory parameters, such as leukocyte, neutrophil, and lymphocyte counts.

Previous studies show that hepatic damage marker AST is significantly higher in severe or non-survival patients with COVID-19 (Li et al., 2020; Zhang et al., 2020). In the present study, we found that only AST, but not ALT and bilirubin levels, was significantly increased in subsequently critical patients at the early stage of COVID-19. Interestingly, AST≥40 was associated with increased odds ratios for poor prognosis in univariable and multivariable regression analyses. This data suggest that AST indicator alone at an early stage of COVID-19 could be a good predictor of disease progression to critical COVID-19.

This retrospective multicentre study found that a novel index, ICIRI, at admission tends to be the most promising predictor of COVID-19 progression from mild or moderate illness to severe or critical conditions. However, this study had two main limitations. First, the study included a relatively small sample size. Second, patients with moderate COVID-19 who were enrolled in this study for prediction purposes were receiving medication (such as Chinese herbs, which have been shown to perform anti-virus, anti-inflammation, and immunoregulation *via* acting on multiple pathways to mitigate damages induced by

the SARS-CoV-2 virus (Dai et al., 2020), and this may have altered their COVID-19 outcomes. Therefore, the rate of COVID-19 progression in this study may not reflect the true rate.

In summary, ICIRI seems to be the most promising predictor of progression to severe and critical COVID-19 at the time of hospital admission. AST indicator alone at the early stage of COVID-19 can be a good predictor of disease progression to critical COVID-19. Early application of these predictors and age-related prognostic data will be advantageous in patient management to prejudge cases that would become critical, requiring intensive medical care. Additionally, this would reduce the high medical care and medication burden of COVID-19. Age, sex, NLR, and CRP levels alone, measured at hospital admission, were not good predictors of a poor prognosis in patients with moderate COVID-19.

DATA AVAILABILITY STATEMENT

The original contributions presented in the study are included in the article/supplementary material. Further inquiries can be directed to the corresponding authors.

ETHICS STATEMENT

The studies involving human participants were reviewed and approved by Ethics Committee of Wenzhou Medical University (Ref 2020002). Given the urgency of the COVID-19 pandemic and global health concerns, the requirement of informed consent was waived by the Ethics Committee of Wenzhou Medical University. Written informed consent for participation was not required for this study in accordance with the national legislation and the institutional requirements.

AUTHOR CONTRIBUTIONS

ML and SJ contributed equally to this study and are the joint corresponding authors. HA and JZ are joint first authors. The corresponding author conceived and designed the study. ML, SJ, HA, and JZ drafted the manuscript. ML, SJ, HA, and JZ performed data analysis, and all authors critically revised the manuscript for important intellectual content and gave final approval for the version to be published. TL, CC, YH, QW, and BY collected the data. All authors agree to be accountable for all aspects of the work in ensuring that questions related to the accuracy or integrity of any part of the work are appropriately investigated and resolved. All authors contributed to the article and approved the submitted version.

FUNDING

This work was supported by the National Natural Science Foundation of China 82070855 and 81670336 (to ML), the Wenzhou Grant for Scientific Talents, Wenzhou Science and Technology Bureau RX2016003 (to ML), the Key Research and Development Program of Zhejiang Province 2019C03011 (to SJ and TL), the Special Project for Significant New Drug Research and Development in the Major National Science and Technology Projects of China 2020ZX09201002 (to TL), and the Wenzhou Science and Technology Key problem program ZY2020001 (to TL). The funders had no role in the study design, data collection, analysis, decision to publish, or preparation of the manuscript. The funder had no role in the study design, data collection, analysis, interpretation, or report writing. The corresponding authors (ML and SJ) had full access to all the data in the study and had the final responsibility for the decision to submit the manuscript for publication.

ACKNOWLEDGMENTS

We acknowledge all healthcare workers involved in diagnosing and treating patients in the 10 hospitals in Wenzhou, Zhejiang, China, involved in this study; we thank Mengzhen Xie, Saijing Chen, and Juan Bai for help with collating the material reported in this investigation.

REFERENCES

An H., Zhang J., Zhou T., Li T., Li S., Huang C., et al. (2021). Inflammation/coagulopathy/fibrinolysis: Dynamic Indicators of COVID-19 Progression in Patients With Moderate COVID-19 in Wenzhou, China. *Clin. Immunol.* 232, 108852. doi: 10.1016/j.clim.2021.108852

Bahardoust M., Heiat M., Khodabandeh M., Karbasi A., Bagheri-Hosseinabadi Z., Ataee M. H., et al. (2021). Predictors for the Severe Coronavirus Disease 2019 (COVID-19) Infection in Patients With Underlying Liver Disease: A Retrospective Analytical Study in Iran. *Sci. Rep.* 11, 3066. doi: 10.1038/s41598-021-82721-3

Bhargava A., Fukushima E. A., Levine M., Zhao W., Tanveer F., Szpunar S. M., et al. (2020). Predictors for Severe COVID-19 Infection. *Clin. Infect. Dis.* 71, 1962–1968. doi: 10.1093/cid/ciaa674

Cheng B., Hu J., Zuo X., Chen J., Li X., Chen Y., et al. (2020). Predictors of Progression From Moderate to Severe Coronavirus Disease 2019: A Retrospective Cohort. *Clin. Microbiol. Infect.* 26, 1400–1405. doi: 10.1016/j.cmi.2020.06.033

Chen Y., Wang J., Yao Y., Yuan W., Kong M., Lin Y., et al. (2009). CRP Regulates the Expression and Activity of Tissue Factor as Well as Tissue Factor Pathway Inhibitor *via* NF-kappaB and ERK 1/2 MAPK Pathway. *FEBS Lett.* 583, 2811–2818. doi: 10.1016/j.febslet.2009.07.037

Dai Y., Wan S., Gong S., Liu J., Fang L, Kou J. (2020). Recent Advances of Traditional Chinese Medicine on the Prevention and Treatment of COVID-19. *Chin. J. Natural Medicines* 18, 881–889. doi: 10.1016/S1875-5364(20)60031-0

Du R. H., Liang L. R., Yang C. Q., Wang W., Cao T. Z., Li M., et al. (2020). Predictors of Mortality for Patients With COVID-19 Pneumonia Caused by SARS-CoV-2: A Prospective Cohort Study. *Eur. Respir. J.* 55 (5), 2000524. doi: 10.1183/13993003.00524-2020

Fois A. G., Paliogiannis P., Scano V., Cau S., Babudieri S., Perra R., et al. (2020). The Systemic Inflammation Index on Admission Predicts in-Hospital Mortality in COVID-19 Patients. *Molecules* 25 (23), 5725. doi: 10.3390/molecules25235725

Gallo Marin B., Aghagoli G., Lavine K., Yang L., Siff E. J., Chiang S. S., et al. (2021). Predictors of COVID-19 Severity: A Literature Review. *Rev. Med. Virol.* 31, 1–10. doi: 10.1002/rmv.2146

Hariyanto T. I., Japar K. V., Kwenandar F., Damay V., Siregar J. I., Lugito N. P. H., et al. (2021). Inflammatory and Hematologic Markers as Predictors of Severe Outcomes in COVID-19 Infection: A Systematic Review and Meta-Analysis. *Am. J. Emerg. Med.* 41, 110–119. doi: 10.1016/j.ajem.2020.12.076

He F., Deng Y., Li W. (2020). Coronavirus Disease 2019: What We Know? *J. Med. Virol.* 92, 719–725. doi: 10.1002/jmv.25766

Huang C., Wang Y., Li X., Ren L., Zhao J., Hu Y., et al. (2020). Clinical Features of Patients Infected With 2019 Novel Coronavirus in Wuhan, China. *Lancet* 395, 497–506. doi: 10.1016/S0140-6736(20)30183-5

Huang M., Yang Y., Shang F., Zheng Y., Zhao W., Luo L., et al. (2020). Clinical Characteristics and Predictors of Disease Progression in Severe Patients With COVID-19 Infection in Jiangsu Province, China: A Descriptive Study. *Am. J. Med. Sci.* 360, 120–128. doi: 10.1016/j.amjms.2020.05.038

Jiang Y., Wei X., Guan J., Qin S., Wang Z., Lu H., et al. (2020). COVID-19 Pneumonia: CD8(+) T and NK Cells are Decreased in Number But Compensatory Increased in Cytotoxic Potential. *Clin. Immunol.* 218, 108516. doi: 10.1016/j.clim.2020.108516

Jin S., An H., Zhou T., Li T., Xie M., Chen S., et al. (2021a). Sex- and Age-Specific Clinical and Immunological Features of Coronavirus Disease 2019. *PloS Pathog.* 17, e1009420. doi: 10.1371/journal.ppat.1009420

Jin S., An H., Zhou T., Li T., Chen C., Ying B., et al. (2021b). Age Cohorts Stratified According to Age-Distributions of COVID-19 Morbidity Statistics Identify Uniquely Age-Dependent CD3CD8 T-Cell Lymphocytopenia in COVID-19 Patients Without Comorbidities on Admission. *Aging* 13, 7713–7722. doi: 10.18632/aging.202691

Liu J., Liu Y., Xiang P., Pu L., Xiong H., Li C., et al. (2020). Neutrophil-To-Lymphocyte Ratio Predicts Critical Illness Patients With 2019 Coronavirus Disease in the Early Stage. *J. Transl. Med.* 18, 206. doi: 10.1186/s12967-020-02374-0

Li X., Xu S., Yu M., Wang K., Tao Y., Zhou Y., et al. (2020). Risk Factors for Severity and Mortality in Adult COVID-19 Inpatients in Wuhan. *J. Allergy Clin. Immunol.* 146, 110–118. doi: 10.1016/j.jaci.2020.04.006

Meftahi G., Jangravi Z., Sahraei H., Bahari Z. (2020). The Possible Pathophysiology Mechanism of Cytokine Storm in Elderly Adults With COVID-19 Infection: The Contribution of "Inflame-Aging". *Inflammation Res.* 69, 825–839. doi: 10.1007/s00011-020-01372-8

Mosesson M. W. (2005). Fibrinogen and Fibrin Structure and Functions. *J. Thromb. Haemost.* 3, 1894–1904. doi: 10.1111/j.1538-7836.2005.01365.x

Rodriguez-Morales A. J., Cardona-Ospina J. A., Gutierrez-Ocampo E., Villamizar-Peña R., Holguin-Rivera Y., Escalera-Antezana J. P., et al. (2020). Clinical, Laboratory and Imaging Features of COVID-19: A Systematic Review and Meta-Analysis. *Travel Med. Infect. Dis.* 34, 101623. doi: 10.1016/j.tmaid.2020.101623

Sungnak W., Huang N., Becavin C., Berg M., Queen R., Litvinukova M., et al. (2020). SARS-CoV-2 Entry Factors are Highly Expressed in Nasal Epithelial Cells Together With Innate Immune Genes. *Nat. Med.* 26, 681–687. doi: 10.1038/s41591-020-0868-6

Sun P., Qie S., Liu Z., Ren J., Li K., Xi J. (2020). Clinical Characteristics of Hospitalized Patients With SARS-CoV-2 Infection: A Single Arm Meta-Analysis. *J. Med. Virol.* 92, 612–617. doi: 10.1002/jmv.25735

Tang N., Li D., Wang X., Sun Z. (2020). Abnormal Coagulation Parameters are Associated With Poor Prognosis in Patients With Novel Coronavirus Pneumonia. *J. Thromb. Haemost.* 18, 844–847. doi: 10.1111/jth.14768

Varga Z., Flammer A. J., Steiger P., Haberecker M., Andermatt R., Zinkernagel A. S., et al. (2020). Endothelial Cell Infection and Endotheliitis in COVID-19. *Lancet* 395, 1417–1418. doi: 10.1016/S0140-6736(20)30937-5

Wang F., Nie J., Wang H., Zhao Q., Xiong Y., Deng L., et al. (2020). Characteristics of Peripheral Lymphocyte Subset Alteration in COVID-19 Pneumonia. *J. Infect. Dis.* 221, 1762–1769. doi: 10.1093/infdis/jiaa150

Wu Z., McGoogan J. M. (2020). Characteristics of and Important Lessons From the Coronavirus Disease 2019 (COVID-19) Outbreak in China: Summary of a Report of 72314 Cases From the Chinese Center for Disease Control and Prevention. *JAMA* 323, 1239–1242. doi: 10.1001/jama.2020.2648

Yang A. P., Liu J. P., Tao W. Q., Li H. M., et al. (2020). The Diagnostic and Predictive Role of NLR, D-NLR and PLR in COVID-19 Patients. *Int. Immunopharmacol.* 84, 106504. doi: 10.1016/j.intimp.2020.106504

Yang X., Yu Y., Xu J., Shu H., Xia J., Liu H., et al. (2020). Clinical Course and Outcomes of Critically Ill Patients With SARS-CoV-2 Pneumonia in Wuhan, China: A Single-Centered, Retrospective, Observational Study. *Lancet Respir. Med.* 8, 475–481. doi: 10.1016/S2213-2600(20)30079-5

Zhang B., Zhou X., Qiu Y., Song Y., Feng F., Feng J., et al. (2020). Clinical Characteristics of 82 Cases of Death From COVID-19. *PLoS One* 15, e0235458. doi: 10.1371/journal.pone.0235458

Zhou F., Yu T., Du R., Fan G., Liu Y., Liu Z., et al. (2020). Clinical Course and Risk Factors for Mortality of Adult Inpatients With COVID-19 in Wuhan, China: A Retrospective Cohort Study. *Lancet* 395, 1054–1062. doi: 10.1016/S0140-6736(20)30566-3

Conflict of Interest: The authors declare that the research was conducted in the absence of any commercial or financial relationships that could be construed as a potential conflict of interest.

Publisher's Note: All claims expressed in this article are solely those of the authors and do not necessarily represent those of their affiliated organizations, or those of the publisher, the editors and the reviewers. Any product that may be evaluated in this article, or claim that may be made by its manufacturer, is not guaranteed or endorsed by the publisher.

frontiers in Cellular and Infection Microbiology

ORIGINAL RESEARCH
published: 16 March 2022
doi: 10.3389/fcimb.2022.863399

Whole Genome Profiling of Lung Microbiome in Solid Organ Transplant Recipients Reveals Virus Involved Microecology May Worsen Prognosis

Lingai Pan[1,2†], Fengsheng Wu[3†], Qingqing Cai[3], Zhuofei Xu[3], Huan Hu[2], Tian Tang[2], Ruiming Yue[2], Yifu Hou[4], Xiaoqin Zhang[2], Yuan Fang[3], Xiaobo Huang[2] and Yan Kang[1*]*

[1] Department of Critical Care Medicine, West China Hospital, West China Clinical Medical School, Sichuan University, Chengdu, China, [2] Department of Critical Care Medicine, Sichuan Provincial People's Hospital, University of Electronic Science and Technology of China, Chengdu, China, [3] Genoxor Medical Science and Technology Inc., Zhejiang, China, [4] Department of Organ Transplant Center, Sichuan Provincial People's Hospital, University of Electronic Science and Technology of China, Chengdu, China

Solid organ transplantation (SOT) is the final therapeutic option for recipients with end-stage organ failure, and its long-term success is limited by infections and chronic allograft dysfunction. Viral infection in SOT recipients is considered an important factor affecting prognosis. In this study, we retrospectively analyzed 43 cases of respiratory infections in SOT recipients using metagenomic next-generation sequencing (mNGS) for bronchoalveolar lavage fluid (BALF). At least one virus was detected in 26 (60.5%) recipients, while 17 (39.5%) were virus-negative. Among virus-positive recipients, cytomegalovirus (CMV) was detected in 14 (32.6%), Torque teno virus (TTV) was detected in 9 (20.9%), and other viruses were detected in 6 (14.0%). Prognostic analysis showed that the mortality of the virus-positive group was higher than that of the virus-negative group regardless whether it is the main cause of infection. Analysis of different types of viruses showed that the mortality of the CMV-positive group was significantly higher than that of the CMV-negative group, but no significant difference was observed in other type of virus groups. The diversity analysis of the lung microbiome showed that there was a significant difference between the virus-positive group and the negative group, in particular, the significant differences in microorganisms such as *Pneumocystis jirovecii* (PJP) and *Moraxella osloensis*were detected. Moreover, in the presence of CMV, *Pneumocystis jirovecii*, *Veillonella parvula*, and other species showed dramatic changes in the lung of SOT patients, implying that high degree of co-infection between CMV and *Pneumocystis jirovecii may occur*. Taken together, our study shows that the presence of virus is associated with worse prognosis and dramatically altered lung microbiota in SOT recipients.

Keywords: solid organ transplant, virus, mortality, lung microbiome, cytomegalovirus

OPEN ACCESS

Edited by:
Yu Chen,
Wuhan University, China

Reviewed by:
Fan Bai,
Peking University, China
Kun Qin,
National Institute for Viral Disease Control and Prevention (China CDC), China

***Correspondence:**
Yan Kang
kangyan@scu.edu.cn
Xiaobo Huang
drhuangxb@163.com

†These authors have contributed equally to this work and share first authorship

Specialty section:
This article was submitted to Clinical Microbiology, a section of the journal Frontiers in Cellular and Infection Microbiology

Received: *27 January 2022*
Accepted: *22 February 2022*
Published: *16 March 2022*

Citation:
Pan L, Wu F, Cai Q, Xu Z, Hu H, Tang T, Yue R, Hou Y, Zhang X, Fang Y, Huang X and Kang Y (2022) Whole Genome Profiling of Lung Microbiome in Solid Organ Transplant Recipients Reveals Virus Involved Microecology May Worsen Prognosis. Front. Cell. Infect. Microbiol. 12:863399. doi: 10.3389/fcimb.2022.863399

INTRODUCTION

Solid organ transplantation (SOT) is the final therapeutic option for recipients with end-stage organ failure, and its long-term success is limited by infections and chronic allograft dysfunction (Timsit et al., 2019). For lung transplantation, infections and allograft dysfunction problems account for 25% - 30% of mortality during the first year post-transplant (Trulock et al., 2007). Because of their immunocompromised state, SOT recipients are at high risk for viral infections, which are a major complication post-transplant and continue to be a potential contributor to graft failure or cause of severe mortality (Fishman, 2007). Recent research found the association of respiratory viruses such as respiratory syncytial virus (RSV), parainfluenza virus, and influenza viruses with increased morbidity following transplant (Bailey et al., 2019).

Cytomegalovirus (CMV), the most common viral pathogen, historically has been associated with worse mortality in SOT recipients (Razonable, 2010). Recent antiviral drugs have improved treatment and prophylaxis of CMV infection. However, other viruses have been recently recognized as having a potential role in affecting the outcome in the SOT recipients (Zanella et al., 2020). The use of immunosuppressive therapies may change the viral spectrum, and the immunopathological mechanisms of viral infection in SOT recipients remain incompletely understood. Sensitive and comprehensive methods to detect the viral pathogen are essential for diagnosis because of the varying immunocompromised status of the hosts, and sometimes the clinical syndromes are nonspecific. Metagenomic next-generation sequence (mNGS) with rapid turnaround times greatly improved the ability to detect the viral infections in a timely fashion.

In this study, we aimed to comprehensively examine the real-world clinical impact of virus on the outcome in SOT recipients. Bronchoalveolar lavage fluid (BALF) samples were collected from SOT recipients with lung infections for mNGS. According to the results of mNGS, we analyzed the prognostic difference between the virus-positive group and the negative group and studied the contribution of different viruses to the prognosis. In addition, we analyzed the impact of virus on the microbiome of the lungs. Our results indicate that the virus is associated with a worse prognosis, whether or not it is the main cause of infection. Our results may have important implications for the clinical management and follow-up research in SOT recipients.

MATERIALS AND METHODS

Recipient Enrollment and Specimen Collection

The solid organ transplant recipients included in this study were all from Sichuan Provincial People's Hospital. Our study passed the review of the Medical Ethics Committee of Sichuan Provincial People's Hospital, and each enrolled recipient or their family signed a written informed consent. From November 2018 to September 2020, recipients with suspected infection were enrolled in this study following kidney, lung, or liver transplantation, and the recipients' alveolar lavage fluid was collected from suspected lung infection recipients for mNGS analysis. The diagnosis of lung infection is based on the following: (1) There are related clinical symptoms, such as cough and sputum, difficulty breathing, fever, etc.; (2) There are related manifestations in imaging, such as pulmonary exudation; (3) Two or more SOT experts highly suspect lung infection with other content. Data collected on the enrolled recipients included body mass index (BMI), ICU length of stay, sequential organ failure assessment (SOFA) and Acute Physiology and Chronic Health Evaluation (APACHE II) scores, chronic disease history, and findings on other routine examinations.

Sample Processing and mNGS Detection

Samples were taken from recipients in two situations: BALF was collected when lung infection occurred during hospitalization, and β-lactam or carbapenem antibiotics were used for prophylactic treatment; when lung infection occurred after discharge, BALF was collected before anti-infective treatment. Samples of 1.5-3 mL BALF were collected according to standard procedures. A 1.5- mL microcentrifuge tube with 0.6-mL sample, enzyme, and 1 g of 0.5 mm glass beads was attached to a horizontal platform on a vortex mixer and agitated vigorously at 2800-3200 rpm for 30 min. Then the 0.3-mL sample was separated into new 1.5-mL microcentrifuge tubes and DNA was extracted using the TIANamp Micro DNA Kit (DP316, Tiangen Biotech) according to the manufacturer's instructions. Then, DNA libraries were constructed through DNA fragmentation, end repair, adapter ligation, and PCR amplification. Agilent 2100 was used for quality control of the DNA libraries. Quality-qualified libraries were sequenced on the BGISEQ-50/MGISEQ-2000 platform. High-quality sequencing data were generated by removing low-quality reads, followed by computational subtraction of human-host sequences mapped to the human reference genome (hg19) using Burrows-Wheeler Alignment. After removal of low-complexity reads, the remaining data were classified by simultaneous alignment with four microbial genome databases, consisting of bacteria, fungi, viruses, and parasites.

Data Analysis

Survival Proportions

The survival of recipients within 90 days after transplantation was recorded, and the survival curve was made using GraphPad Prism 9. Comparison of survival curves was performed by the log-rank (Mantel-Cox) test.

Alpha Diversity

The analysis of alpha diversity was used to estimate complexity of taxonomic diversity for individual samples based on the Shannon index. The data matrix consisting of relative abundance for individual taxa across the samples was used for the Shannon index boxplot using R packages ggplot2 v3.3.2 and ggpubr v0.4.0. The visualization was implemented in the R environment v4.03.

Beta Diversity (NMDS)

To assess the compositional similarity among the studied samples from different microbial communities, the Bray-Curtis measure of beta diversity was employed to compare all pairwise

taxonomic relative abundances using an R function vegdist in the package vegan v2.5-7. Based on the resulting Bray-Curtis similarity distance matrix, non-metric multidimensional scaling (NMDS) was adopted to display the dispersion of community structure using an R function metaMDS in the package vegan v2.5-7. The scatterplot was implemented by using ggplot2 v3.3.2 in the R environment v4.03.

Beta Diversity (PCoA)

To assess the compositional similarity among the studied samples from different microbial communities, the Bray-Curtis measure of beta diversity was employed to compare all pairwise taxonomic relative abundances using an R function vegdist in the package vegan v2.5-7. Based on the resulting Bray-Curtis similarity distance matrix, Principal Coordinate Analysis (PCoA) was adopted to display the dispersion of community structure using an R function cmdscale in the package vegan v2.5-7. The scatterplot was implemented by using ggplot2 v3.3.2 in the R environment v4.03.

Differential Analysis Between Groups of Microbial Communities

The statistical difference for the taxonomic profiles between study groups was evaluated using the function ANOSIM from the R package vegan v2.5-7. The similarity boxplot between groups was implemented using R package ggplot2 v3.3.2.

Heatmap of Microbial Community Structure

Based on the taxonomic relative abundance profile, the heatmap for visualizing relative abundances of the top 20 taxa was created using pheatmap v1.0.12 in the R environment v4.03.

Relative Abundance Boxplot of the Top 20 Taxa

Based on the taxonomic relative abundance profile, the boxplot of the top 20 taxa is created using ggplot2 v3.3.2 in the R environment v4.03.

RESULTS

Enrollment Information of Solid Organ Transplant Recipients

A total of 43 SOT recipients were enrolled in this study (**Figure 1**) , including 26 with kidney transplants, 13 with lung transplants, and 4 with liver transplants. The average age of all recipients was 52 years old, 31 were males, and the average BMI was 20.8 kg/m^2. Of which, 32 recipients have been admitted to the ICU, average ICU stay was 8.8 days. There were 32 recipients evaluated by SOFA and APACHE II with average scores of 6.7 and 10.9, respectively. The most frequent chronic disease among the recipients was hypertension (17 cases), followed by hepatitis B viral infection (8 cases), diabetes, chronic obstructive pulmonary disease, and coronary heart disease (**Table 1**). The information of all recipients is listed in **Supplementary Table 1**.

Virus Detected in Respiratory Sample of Transplant Recipients Is Associated With Increased Mortality

The mNGS in bronchoalveolar lavage fluid (BALF) samples was performed in all SOT recipients to study virus and other microbial communities. At least one virus was detected in 26 (60.5%) recipients, while 17 (39.5%) were virus-negative. Among virus-positive recipients, cytomegalovirus (CMV) was

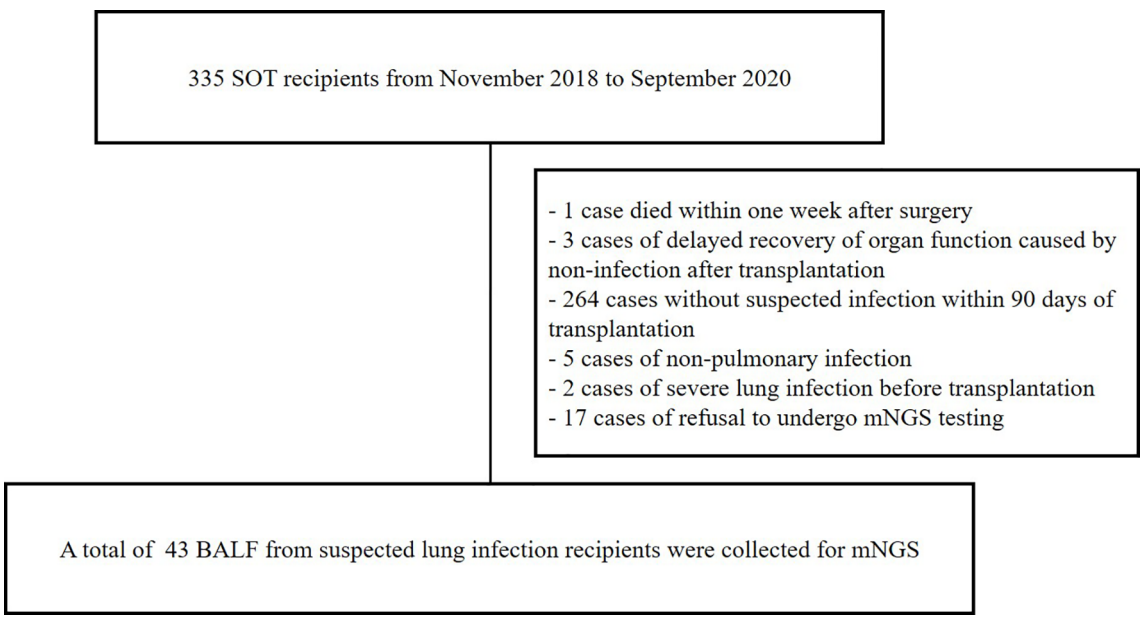

FIGURE 1 | Study design in solid organ transplantation.

TABLE 1 | Demographic and Clinical Characteristics of the 43 Recipients with solid organ transplantation.

Characteristic	Value
Mean age, y	52
Male	31
BMI, kg/m^2	20.8
Severity of illness	
Mean SOFA	6.7
Mean APACHE II	10.9
Previous history of chronic disease-no. (%)	
HBV	4 (9.3)
HBV and HTN	3 (7.0)
HBV, HTN and DM	1 (2.3)
HTN	12 (27.9)
HTN and COPD	1 (2.3)
TB	1 (2.3)
TB and CHD	1 (2.3)
Chronic bronchitis	1 (2.3)
DM	1 (2.3)
Uremia	1 (2.3)
Non	17 (39.5)
Type of solid organ transplantation	
Kidney*	26
Lung	13
Liver^	4
ICU outcomes	
Mean ICU length of stay, days	8.8

BMI, Body Mass Index; SOFA, Sequential Organ Failure Score; APACHE II, Acute Physiology and Chronic Health Score II; HBV, Hepatitis B Virus; HTN, Hypertension; DM, Diabetes mellitus; COPD, Chronic obstructive pulmonary disease; CHD, Coronary heart disease.

**1 recipient underwent a second renal transplant. ^1 recipient underwent a second liver transplant. BALF of the two recipients were collected after the first transplant with lung infection.*

detected in 14 (32.6%) recipients, and TTV was detected in 9 (20.9%) recipients, and other viruses were detected in 6 (14.0%) recipients, as shown in **Figure 2**. Moreover, we analyzed the viral profiles of the three transplant types individually. Interestingly, the results showed that CMV was more frequently detected in kidney transplantation, and the both two BKV-positive cases were detected in kidney transplantation, as shown in **Supplementary Table 3**.

To observe the impact of virus on prognosis in these recipients, we evaluated the severity of disease (SOFA and APACHE II scores) and mortality (whether the recipient survived 90 days after transplantation). The results showed that there was no significant difference in SOFA and APACHE II scores between the virus-positive group and the virus-negative group. In this study, a total of 8 cases died within 90 days after transplantation, all of which were related to infection. However, in some cases, the virus may not be considered as the main cause of infection (**Supplementary Table 1**). The 90-days mortality of the virus-positive group was higher than that of the virus-negative group (26.9% vs. 5.9%). In order to explore the impact and contribution of different viruses to the increasing mortality, we separately analyzed the mortality of the CMV-positive group, TTV-positive group, and other virus-positive groups along with mortality in the CMV- and TTV-negative groups). The results showed that the prognosis in the CMV-positive group was significantly worse than that in the CMV-negative group (mortality 35.7% vs. 10.3%, respectively). The mortality of the TTV-positive group (22.2% vs. 17.6%) and the other virus group (18.2% vs. 18.8%) was similar to that of the corresponding negative group (**Table 2**). The survival curves of the virus-positive group and the virus-negative group were significantly separated, but the difference between the two groups was not significant ($p = 0.0828$). In single-virus groups, the curves of CMV-positive and CMV-negative recipients were significantly separated, and the difference was statistically significant ($p = 0.0456$). There was no significant difference between TTV-positive and TTV-negative groups (**Figure 3**). At the same time, we analyzed the impact of virus on the mortality of different types of SOT recipients. The data showed that the results of kidney and lung transplantation were similar, and the mortality of liver transplantation was not statistically significant due to the small number of samples (**Supplementary Table 2**). Our results indicated that virus detected in respiratory sample was associated with increased mortality of SOT recipients, and CMV may be the main cause.

Virus Affects the Lung Microbiome of Solid Organ Transplant Recipients

The mNGS results of all recipients can reflect the status of their lung microbial communities. We analyzed the same amount of random data from all samples to explore whether there are differences in the lung microbiome among these recipients. The diversity analysis of the community structure showed that there was a significant difference between the virus-positive group and the virus-negative group, and analysis showed that the difference between the groups was greater than that within the group, as shown in **Supplementary Figure 1**. A further comparison of species of microorganisms in the virus-positive group and the virus-negative group showed significant differences in the top 20 lung species (such as *Pneumocystis jirovecii*, *Moraxella osloensis*, CMV) and other species beyond the top 20 (**Figure 4**). These results indicate that the virus affects the composition of lung microbial species in solid organ transplant recipients.

Considering that CMV is the main type of virus in our study (14/26) and its impact on mortality, we did a similar analysis of the microbiome between CMV-positive and CMV-negative groups. Diversity analysis and difference analysis showed that there was no significant difference between the CMV-positive group and the CMV-negative group, as shown in **Supplementary Figure 2**. Microbial analysis showed significant differences in top-20 species (such as *Pneumocystis jirovecii* and *Veillonella parvula*) and other species, as shown in **Figure 4**. Our results indicated that virus especially CMV may affect the microbial composition of the lungs of SOT recipients, especially the proportion of *Pneumocystis jirovecii*.

DISCUSSION

In this study, we explored virus detected in respiratory sample of 43 solid organ transplant recipients by mNGS. Viruses were detected in the bronchoalveolar lavage fluid

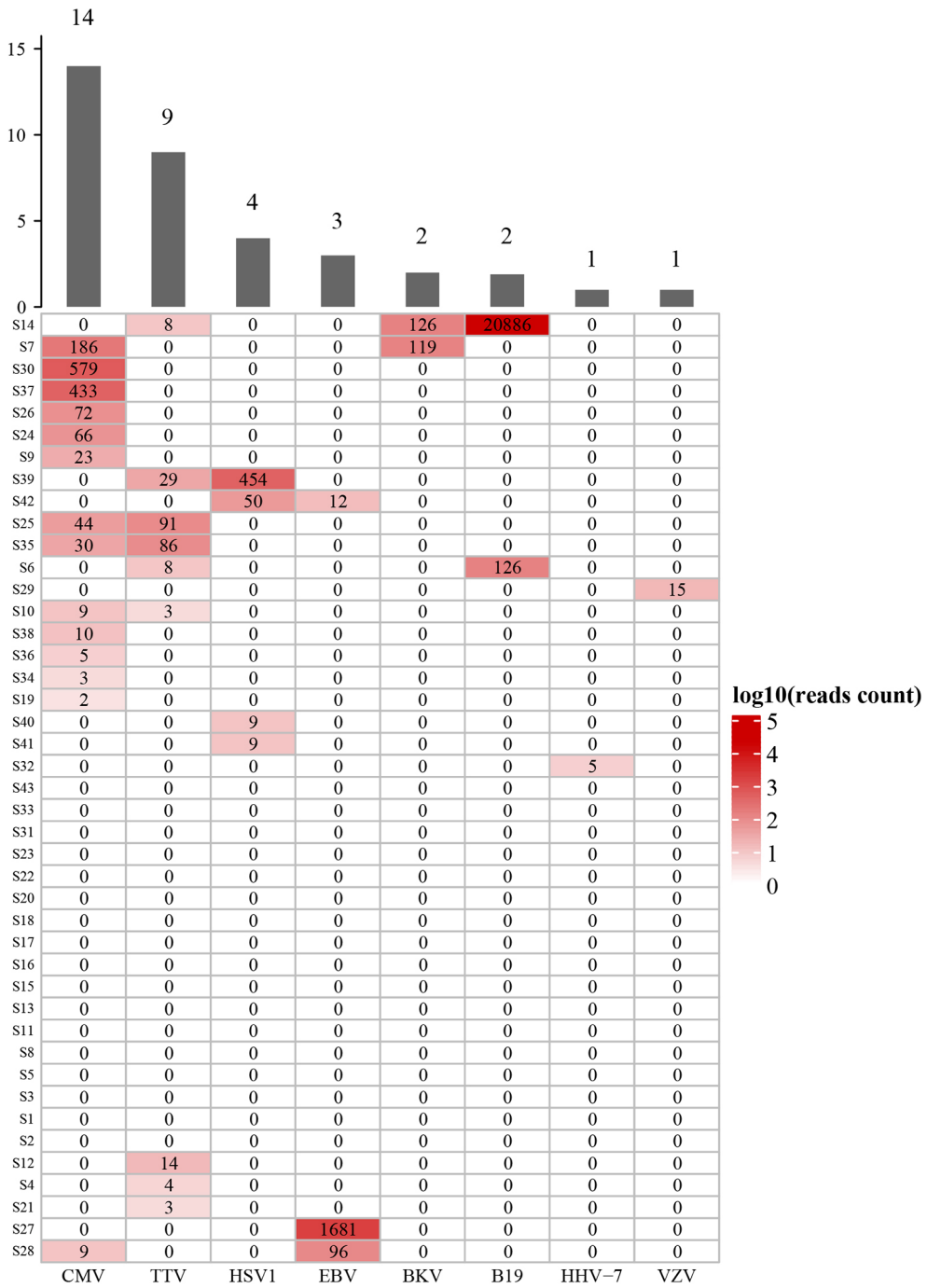

FIGURE 2 | Diversity and reads counts of viruses identified in this study. CMV, Human betaherpesvirus 5; TTV, Torque teno virus; HSV1, Human alphaherpesvirus 1; EBV, Human gammaherpesvirus 4; BKV, BK virus; B19, Human erythroparvovirus 19; HHV-7, Human betaherpesvirus 7; VZV, Varicella Zoster Virus. The numbers on the histogram represent the sample sizes of the corresponding virus. The numbers in the table represent the reads of mNGS results. S14 and S7 etc, sample number. The samples are sorted according to hierarchical clustering with Euclidean distance.

(BALF) of 26 recipients. The most common type was CMV. The results showed that virus was associated with increased mortality in SOT recipients, and CMV may be the main virus. In addition, our results indicated that the virus may affect the composition of lung microbial species in solid organ transplant recipients.

Unfortunately, although there are differences in mortality between the virus-positive group and the virus-negative group,

TABLE 2 | Demographic and Clinical Characteristics of study cohort.

Severity of illness	Virus	Non-virus	P-value
Mean SOFA	6.8	6.5	0.77
Mean APACHE II	10.7	11.1	0.53
The Prognosis of 90 days-no. (%)			
Good	19 (73.1%)	16 (94.1%)	0.083
Poor	7 (26.9%)	1 (5.9%)	
Severity of illness	**CMV**	**Non-CMV**	**P-value**
Mean SOFA	6.6	6.7	0.98
Mean APACHE II	11.6	10.6	0.52
The Prognosis of 90 days-no. (%)			
Good	9 (64.3%)	26 (89.7%)	0.046
Poor	5 (35.7%)	3 (10.3%)	

Good=survival; Poor=died.

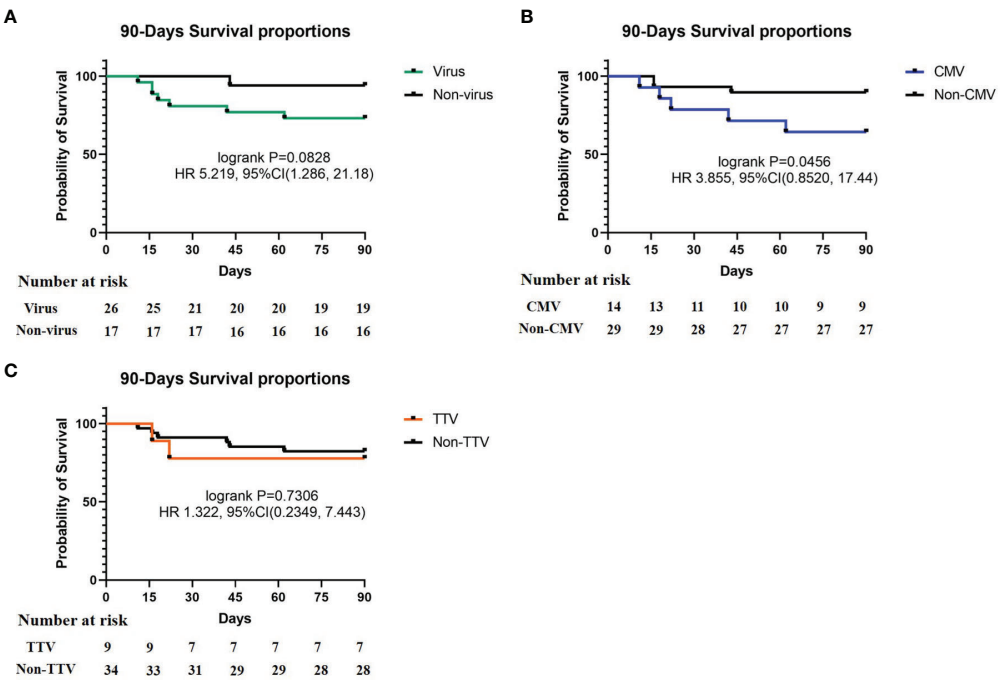

FIGURE 3 | 90-Days Survival proportions of different virus. **(A)** Survival proportions of virus and non-virus, p = 0.0828; **(B)** survival proportions of CMV and non-CMV, p = 0.0456; **(C)** survival proportions of TTV and non-TTV, p = 0.7306. Recipient number is displayed in the Number at risk.

the survival curve P value did not reach significance (p = 0.0828), which may be related to a small sample size. Previous studies have shown that CMV can increase mortality in SOT recipients (Beam et al., 2016; Teira et al., 2016; Haidar et al., 2020). In this study, our results are consistent with the results of previous studies. In addition, the mNGS detection used in this study can reveal the presence of other viruses in the samples other than CMV. Other viruses detected in this study include parvovirus (TTV), BK polyoma virus (BKV), Epstein-Barr virus (EBV), human parvovirus B19, human herpes virus 7 (HHV7), herpes simplex virus 1 (HSV1), and varicella-zoster virus. Bailey et al. (2019) retrospectively analyzed 39 studies on viral infections in lung transplantation. The most common ones related to mortality were RSV and adenovirus (AdV). Because of the high recipient mortality, it could not be determined whether other viruses were related to mortality (Bailey et al., 2019). Zanella et al. (2020) analyzed viruses other than CMV and EBV in the blood of SOT and hematopoietic stem cell transplant recipients. Hill et al. (2017) studied co-infection with double-stranded DNA viruses such as EBV, CMV, HHV-6, AdV, and BKV. Results showed that co-infection with the increased mortality, but the impact of a single virus was still unknown (Hill et al., 2017). Combining previous studies and our results, we believe that CMV infection is the most important factor in viral infection in SOT recipients, and it may be responsible for the increase in mortality. Whether other

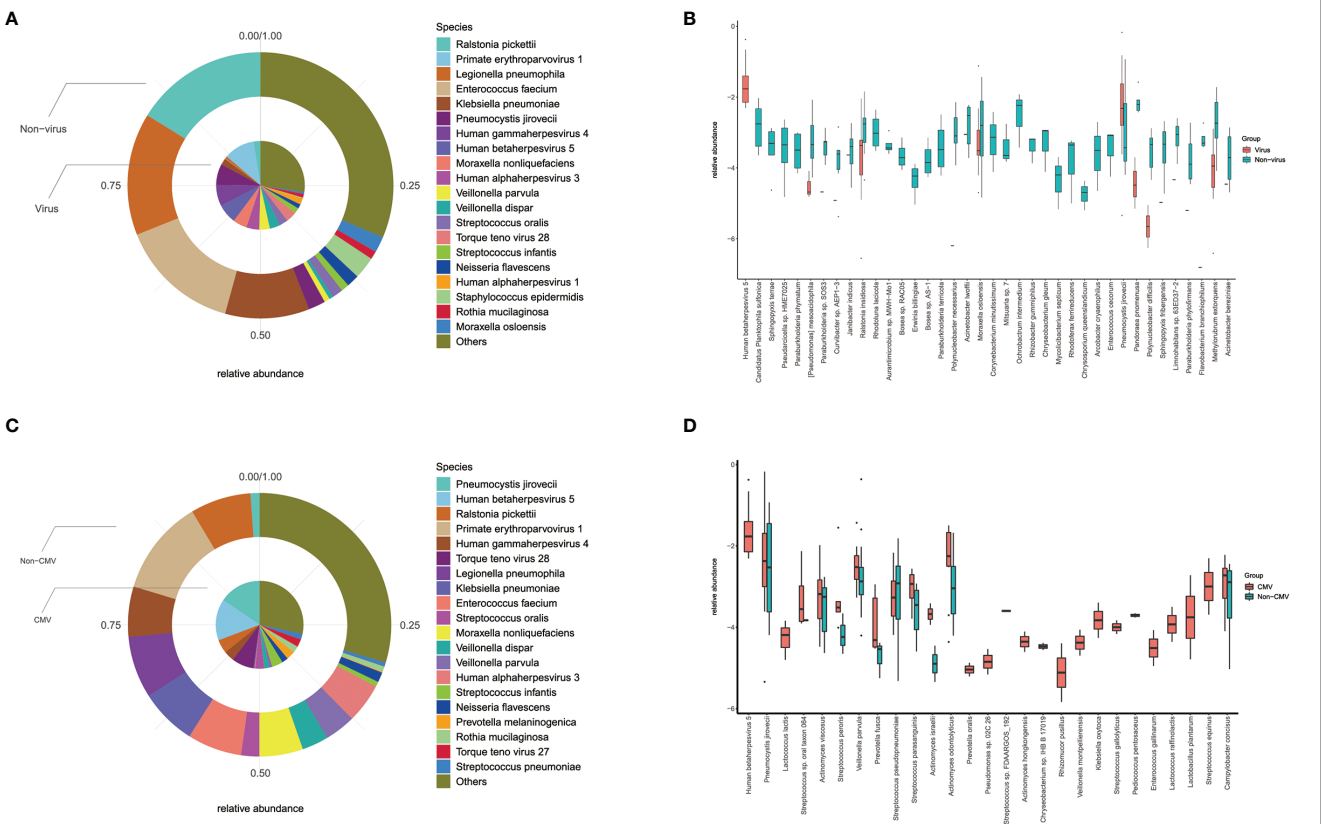

FIGURE 4 | Differences of lung microbiota in groups. **(A)** Top 20 most abundant species and their relative abundance in virus and non-virus recipients; **(B)** there were significant differences in top-20 species (such as *Pneumocystis jirovecii, Moraxella osloensis*, CMV) and other non-top species between virus and non-virus group; **(C)** top 20 most abundant species and their relative abundance in CMV and non-CMV infectious recipients; **(D)** there were significant differences in top-20 species (such as *Pneumocystis jirovecii, Veillonella parvula*) and other non-top species between CMV and non-CMV group.

single viruses increase mortality still needs further research for clarification.

Due to the immunosuppressive state, the infection of SOT recipients may be multi-pathogenic, and sometimes it is difficult to define a major pathogen. The 8 deaths in this study were all related to infection, of which at least one virus was detected in 6 cases, but in most cases the virus could not be considered as the main infectious agent. In order to check whether the death is related to other factors, we compared the age, BMI, and the proportions of chronic disease between the death group and the survival group, and the results showed no difference. Our results indicate that the virus is associated with a worse prognosis, whether or not it is the main source of infection. Previous related studies have judged the virus as the main pathogen and found that it leads to a worse prognosis. Our results indicate that the presence of the virus may be a marker of poor prognosis.

In this study, why viruses that are not considered as the main pathogens are also related to high mortality may be a topic of our concern. In many cases, the presence of the virus, such as TTV, is considered to be related to the patient's low immunity (Focosi et al., 2010; Görzer et al., 2014). One hypothesis is that the virus-positive recipients in this study may have a worse immune status than the virus-negative recipients. But whether a worse immune status is related to a worse prognosis also depends on the type of virus that appears, such as CMV or TTV. Although CMV is weakly pathogenic, infection occurs occasionally, while TTV is temporarily not considered to be the pathogen. This may be the reason that whether TTV is positive in this study is not related to the prognosis. This study also showed that the virus changed the lung microbiome, and the relationship between the immune status and the intestinal microbiome has been reported. Another hypothesis about virus is associated with worse prognosis is that the virus may affect the recipient's prognosis by affecting the lung microbiome. Unfortunately, there are no accurate quantitative indicators that directly reflect the immune status of the recipient.

mNGS is the main detection technique in this study. At present, there are fewer methods to detect viruses, and there are fewer types of viruses that can be detected. mNGS can cover almost all viruses except RNA viruses, which can be detected by mNGS in the RNA process. Therefore, mNGS is a very effective method for multi-virus detection. The virus was detected in 26 of the 43 recipients in this study, with as many as 8 types of viruses. Each recipient had undergone CMV and EBV serological testing on admission, now the data of antibody testing is added in

Supplementary Table 1. Given the accuracy of virus detection by mNGS has been proved in several previous studies (Miao et al., 2018; Han et al. 2019), that the difference of results between antibody testing and mNGS is due to the sensitivity and specificity of the methods. In addition to viruses, mNGS can simultaneously detect bacteria, fungi and other pathogens. mNGS is the best detection method for microorganisms that often coexist with viruses, such as PJP, which is difficult to cultivate and the positive rate of other detection methods is extremely low. mNGS is a revolutionary technology in pathogen detection. Our results also showed the advantages of mNGS in the detection of viruses and other microorganisms in SOT recipients.

There have been some studies on the microbiome in SOT recipients, but most of them focused on the intestinal flora (Sepulveda et al., 2019; Chong and Koh, 2020), and the research on the lung microbiome is mostly related to lung transplantation (Mitchell, 2019). Our study consisted of a comprehensive analysis of the lung microbiome in various types of SOT recipients, including cases of kidney, lung, and liver transplantation. Our results showed that compared with the corresponding negative group, PJP was significantly different in the virus-positive and CMV-positive groups. It is believed that CMV is often accompanied by PJP. The results of a study involving 52 PJP-infected kidney transplant recipients showed that the CMV co-infection group (14/52, 26.9%) had increased disease severity and risk of transplant failure. Co-infection with PJP and CMV also increased mortality, but the difference was not significant (21.4% vs. 10.5%, $p = 0.370$) (Lee et al., 2020). In another retrospective study including 70 recipients with non-HIV-infected PJP-positive pneumonia, pulmonary CMV infection rates were 54.3% (38/70), and there was no significant difference in mortality between those with and without co-infection (Yu et al., 2017). In our study, 71.4% (10/14) of CMV-positive cases were associated with PJP infection. The mortality of the PJP-free group appeared to be higher than that of the PJP group (2/4, 50% vs. 3/10, 30%). Among the enrolled recipients in our study, the proportion of PJP infection was relatively higher. A review about the medical history of all recipients revealed that it may be related to irregular prophylaxis. Most patients discontinue the drug by themselves due to digestive symptoms, such as nausea and vomiting or renal damage. Our results demonstrate the high degree of co-infection with CMV and PJP in SOT recipients, but co-infection with PJP may not increase the mortality of CMV-positive recipients.

In addition to PJP, our results also showed that virus affected the proportions of other microbes in the respiratory tract. For example, the proportion of *Moraxella osloensis*, one of the top 20 species in lung microbiology, decreased in the virus-positive group, and the proportion of *Veillonella parvula*, also one of the top 20 species in lung microbiology, decreased in the CMV-positive group. *Moraxella osloensis* is an aerobic gram-negative bacterium that is saprophytic on human skin and mucous membranes. It is also considered to be part of the normal flora of the human respiratory tract. The reported diseases caused by *Moraxella osloensis* infection include endocarditis, meningitis, osteomyelitis, septic arthritis, and bacteremia (Shah et al., 2000). *Veillonella parvula* is an anaerobic gram-negative bacterium and is considered to be a common bacterium in the oral cavity, gastrointestinal tract, and vagina. It has been reported as a pathogen related to meningitis, periodontitis, chronic maxillary sinusitis, sinusitis, osteomyelitis, bacteremia, pelvic abscess, and testicular epididymitis (Bhatti and Frank, 2000). Pathogenicity studies of the above two and other background bacteria are lacking, and the impact of their differences in SOT recipients with viral infections needs further research. The structure of the microbiome may be affected by many factors. In our study, the difference of PJP between CMV positive group and negative group is consistent with previous reports and clinical cognition. And there are only 2 or 3 species in the TOP 20 have significant differences, which indicates that there is no extreme fluctuation in the microbiome. These results imply the reliability of our microbiome analysis results.

Our study also has some limitations. Although the difference in survival curves between the virus-positive group and the negative group could be observed, it was not significant due to the small size of samples. For this same reason, only 6 cases were detected in other virus groups except CMV and TTV, which is meaningless in statistics. In this study, we only extracted DNA from BALF samples, so RNA viruses are outside the scope of our research. Three types of transplanted organs were enrolled in this study, but there were only 4 recipients of liver transplantation, no one died and one of them was virus-positive. So, the results of this study are more related to kidney and lung transplantation. Our research showed that virus had similar effects on mortality in kidney and lung transplantation. However, it is well known that the partial pulmonary microbiota of the recipient comes from the donor, which may undergo a complex reconstruction. Therefore, whether the impact of virus on the lung microbiome of lung transplant recipients is different from other SOT transplants needs more study and elucidation. Due to the BALF samples were collected by performing invasively endoscopy, the patients are unable to tolerate multiple collections during infections. Therefore, it is unlikely to monitor the change of microbiome at different time points in the patients. By realizing this difficulty, in this study, one time analysis of the microbiome in respiratory tract may not be able to demonstrate the dynamic changes.

In summary, we studied the impact of virus on mortality and the lung microbiome in SOT recipients. The results showed that virus increased mortality regardless whether it is the main reason of infection, and CMV may be responsible for this. The results indicate that the presence of the virus may be a marker of poor prognosis. The proportion of PJP in virus-positive recipients increased significantly; the co-infection rate with PJP reached 71.4% in CMV-infected recipients. The results suggest that we should attach great importance to the co-infection with PJP when dealing with CMV infection. The mNGS results revealed the viral spectrum of SOT recipient lung infection, which can provide clinical reference. At present, there is a lack of detection methods for viruses, and mNGS has been gradually applied in clinical pathogen diagnosis. Our study explored the advantages of mNGS for viral infection and simultaneous detection of other pathogens. In addition, virus can also change the respiratory microbiome, and the differences in some background bacteria may provide references for subsequent research and clinical management.

DATA AVAILABILITY STATEMENT

The raw data of mNGS in this study has been uploaded to the SRA database of NCBI, and the data is public. The project number is PRJNA806679.

ETHICS STATEMENT

The studies involving human participants were reviewed and approved by the Medical Ethics Committee of Sichuan Provincial People's Hospital. The patients/participants provided their written informed consent to participate in this study. Written informed consent was obtained from the parents. All the authors listed have approved the manuscript that is enclosed.

AUTHOR CONTRIBUTIONS

All authors contributed to the study conception and design. Research design and approval were completed by YK, XH, and YF. Recipient enrollment and management were completed by LP. Data analysis and the manuscript writing were completed by FW. Review and editing of manuscript were completed by LP, QC, ZX, and YF. Microbiome analysis were completed by ZX. Transplant and data collection were completed by HH, TT, RY, YH, and XZ. All authors contributed to the article and approved the submitted version.

SUPPLEMENTARY MATERIAL

The Supplementary Material for this article can be found online at: https://www.frontiersin.org/articles/10.3389/fcimb.2022.863399/full#supplementary-material

Supplementary Figure 1 | Lung microbiome of virus and non-virus infectious recipients with solid organ transplantation. **(A)** Lung microbiome in genus level; **(B)** lung microbiome in species level; **(C)** Estimated species richness was calculated as Shannon index, there were significant differences between virus and non-virus; **(D)** anosim analysis of lung microbiome; **(E)** nonmetric multidimensional scaling analysis revealed that the within-group variance is larger than the between-group variance.

Supplementary Figure 2 | Lung microbiome of CMV and non-CMV infectious recipients with solid organ transplantation. **(A)** Lung microbiome in genus level; **(B)** lung microbiome in species level; **(C)** Estimated species richness was calculated as Shannon index, there were no significant differences; **(D)** anosim analysis of lung microbiome; **(E)** nonmetric multidimensional scaling analysis revealed that the within-group variance is larger than the between-group variance.

REFERENCES

Bailey, E. S., Zemke, J. N., Choi, J. Y., and Gray, G. C. (2019). A Mini-Review of Adverse Lung Transplant Outcomes Associated With Respiratory Viruses. *Front. Immunol.* 10, 2861. doi: 10.3389/fimmu.2019.02861

Beam, E., Lesnick, T., Kremers, W., Kennedy, C. C., and Razonable, R. R. (2016). Cytomegalovirus Disease Is Associated With Higher All-Cause Mortality After Lung Transplantation Despite Extended Antiviral Prophylaxis. *Clin. Transplant* 30, 270–278. doi: 10.1111/ctr.12686

Bhatti, M. A., and Frank, M. O. (2000). *Veillonella Parvula* Meningitis: Case Report and Review of Veillonella Infections. *Clin. Infect. Dis.* 31, 839–840. doi: 10.1086/314046

Chong, P. P., and Koh, A. Y. (2020). The Gut Microbiota in Transplant Patients. *Blood Rev.* 39, 100614. doi: 10.1016/j.blre.2019.100614

Fishman, J. A. (2007). Infection in Solid-Organ Transplant Recipients. *N. Engl. J. Med.* 357, 2601–2614. doi: 10.1056/NEJMra064928

Focosi, D., Maggi, F., Albani, M., Macera, L., Ricci, V., Gragnani, S., et al. (2010). Torquetenovirus Viremia Kinetics After Autologous Stem Cell Transplantation Are Predictable and May Serve as a Surrogate Marker of Functional Immune Reconstitution. *J. Clin. Virol.* 47 (2), 189–192. doi: 10.1016/j.jcv.2009.11.027

Görzer, I., Haloschan, M., Jaksch, P., Klepetko, W., and Puchhammer-Stöckl, E. (2014). Plasma DNA Levels of Torque Teno Virus and Immunosuppression After Lung Transplantation. *J. Heart Lung Transplant* 33 (3), 320–323. doi: 10.1016/j.healun.2013.12.007

Haidar, G., Boeckh, M., and Singh, N. (2020). Cytomegalovirus Infection in Solid Organ and Hematopoietic Cell Transplantation: State of the Evidence. *J. Infect. Dis.* 221 (Suppl 1), S23–S31. doi: 10.1093/infdis/jiz454

Han, D., Li, Z., Li, R., Tan, P., Zhang, R., and Li, J. (2019). mNGS in Clinical Microbiology Laboratories: On the Road to Maturity. *Crit. Rev. Microbiol.* 45 (5-6), 668–685. doi: 10.1080/1040841X.2019.1681933

Hill, J. A., Mayer, B. T., Xie, H., Leisenring, W. M., Huang, M. L., Stevens-Ayers, B. T., et al. (2017). The Cumulative Burden of Double-Stranded DNA Virus Detection After Allogeneic HCT Is Associated With Increased Mortality. *Blood* 129, 2316–2325. doi: 10.1182/blood-2016-10-748426

Lee, S., Park, Y., Kim, S. G., Ko, E. J., Chung, B. H., and Yang, C. W. (2020). The Impact of Cytomegalovirus Infection on Clinical Severity and Outcomes in Kidney Transplant Recipients With *Pneumocystis Jirovecii* Pneumonia. *Microbiol. Immunol.* 64, 356–365. doi: 10.1111/1348-0421.12778

Miao, Q., Ma, Y., Wang, Q., Pan, J., Zhang, Y., Jin, W., et al. (2018). Microbiological Diagnostic Performance of Metagenomic Next-Generation Sequencing When Applied to Clinical Practice. *Clin. Infect. Dis.* 67 (suppl_2), S231–S240. doi: 10.1093/cid/ciy693

Mitchell, A. B. (2019). The Lung Microbiome and Transplantation. *Curr. Opin. Organ Transplant* 24, 305–310. doi: 10.1097/MOT.0000000000000631

Razonable, R. (2010). Direct and Indirect Effects of Cytomegalovirus: Can We Prevent Them? *Enferm. Infecc. Microbiol. Clin.* 28, 1–5. doi: 10.1016/j.eimc.2009.07.008

Sepulveda, M., Pirozzolo, I., and Alegre, M. L. (2019). Impact of the Microbiota on Solid Organ Transplant Rejection. *Curr. Opin. Organ Transplant* 24, 679–686. doi: 10.1097/MOT.0000000000000702

Shah, S. S., Ruth, A., and Coffin, S. E. (2000). Infection Due to *Moraxella Osloensis*: Case Report and Review of the Literature. *Clin. Infect. Dis.* 30, 179–181. doi: 10.1086/313595

Teira, P., Battiwalla, M., Ramanathan, M., Barrett, A. J., Ahn, K. W., Chen, M., et al. (2016). Early Cytomegalovirus Reactivation Remains Associated With Increased Transplant-Related Mortality in the Current Era: A CIBMTR Analysis. *Blood* 127, 2427–2438. doi: 10.1182/blood-2015-11-679639

Timsit, J. F., Sonneville, R., Kalil, A. C., Bassetti, M., Ferrer, R., Jaber, S., et al. (2019). Diagnostic and Therapeutic Approach to Infectious Diseases in Solid Organ Transplant Recipients. *Intensive Care Med.* 45, 573–591. doi: 10.1007/s00134-019-05597-y

Trulock, E. P., Christie, J. D., Edwards, L. B., Boucek, M., Aurora, P., Taylor, D. O., et al. (2007). Registry of the International Society for Heart and Lung Transplantation: Twenty-Fourth Official Adult Lung and Heart–Lung Transplantation Report—2007. *J. Heart Lung Transplant* 26, 782–795. doi: 10.1016/j.healun.2007.06.003

Yu, Q., Jia, P., Su, L., Zhao, H., and Que, C. (2017). Outcomes and Prognostic Factors of Non-HIV Patients With Pneumocystis Jirovecii Pneumonia and Pulmonary CMV Co-Infection: A Retrospective Cohort Study. *BMC Infect. Dis.* 17, 392. doi: 10.1186/s12879-017-2492-8

Zanella, M. C., Cordey, S., and Kaiser, L. (2020). Beyond Cytomegalovirus and Epstein-Barr Virus: A Review of Viruses Composing the Blood Virome of Solid Organ Transplant and Hematopoietic Stem Cell Transplant Recipients. *Clin. Microbiol. Rev.* 33 (4), e00027-20. doi: 10.1128/CMR.00027-20

Conflict of Interest: Authors FW, QC, ZX, and YF are employed by Genoxor Medical Science and Technology Inc.

The remaining authors declare that the research was conducted in the absence of any commercial or financial relationships that could be construed as a potential conflict of interest.

Publisher's Note: All claims expressed in this article are solely those of the authors and do not necessarily represent those of their affiliated organizations, or those of the publisher, the editors and the reviewers. Any product that may be evaluated in this article, or claim that may be made by its manufacturer, is not guaranteed or endorsed by the publisher.

frontiers | Frontiers in Cellular and Infection Microbiology

OPINION
published: 29 April 2022
doi: 10.3389/fcimb.2022.892323

Integrins as Therapeutic Targets for SARS-CoV-2

Timothy E. Gressett[1,2,3], Danielle Nader[4], Juan Pablo Robles[5], Tione Buranda[6], Steven W. Kerrigan[4]* and Gregory Bix[1,2,3]**

[1] Tulane University School of Medicine, Clinical Neuroscience Research Center (CNRC), New Orleans, LA, United States, [2] Department of Neurology, Tulane University School of Medicine, New Orleans, LA, United States, [3] Tulane Brain Institute, Tulane University, New Orleans, LA, United States, [4] RCSI University of Medicine and Health Sciences, School of Pharmacy and Biomolecular Sciences (PBS), Dublin, Ireland, [5] Instituto de Neurobiología, Universidad Nacional Autónoma de México (UNAM), Juriquilla, Mexico, [6] University of New Mexico Health Sciences Center (HSC), Department of Pathology, Albuquerque, NM, United States

Keywords: integrins, SARS-CoV-2, therapeutic, RGD, ATN-161, cilengitide

OPEN ACCESS

Edited by:
Guiqing Peng, Huazhong Agricultural University, China

Reviewed by:
Zhichao Fan, UCONN Health, United States

***Correspondence:**
Gregory Bix
gbix@tulane.edu
Tione Buranda
tburanda@salud.unm.edu
Steven W. Kerrigan
skerrigan@rcsi.ie

Specialty section:
This article was submitted to Virus and Host, a section of the journal Frontiers in Cellular and Infection Microbiology

Received: *08 March 2022*
Accepted: *11 April 2022*
Published: *29 April 2022*

Citation:
Gressett TE, Nader D, Robles JP, Buranda T, Kerrigan SW and Bix G (2022) Integrins as Therapeutic Targets for SARS-CoV-2. Front. Cell. Infect. Microbiol. 12:892323. doi: 10.3389/fcimb.2022.892323

INTRODUCTION

Severe acute respiratory syndrome coronavirus 2 (SARS-CoV-2) is an enveloped, positive-sense, single-stranded RNA virus of the genus Betacoronavirus. Its genome is composed of four structural proteins known as spike (S), envelope (E), membrane (M), and nucleocapsid (N), of which E, M, and N are integrated into the viral envelope. The S glycoprotein, which protrudes from the surface of mature virions as a spike, is essential for virus attachment, fusion, and entry into the host cell.

While the relationship between the spike protein of SARS-CoV-2 and the angiotensin-converting enzyme 2 (ACE2) receptor has been readily established, the S1 subunit also contains a solvent-exposed arginine-glycine-aspartic acid (RGD) binding motif that is predominantly recognized by integrins, specifically $\alpha_5\beta_1$ and $\alpha_V\beta_3$ (Sigrist et al., 2020; Tresoldi et al., 2020). These integrins, which are primarily expressed on vascular endothelial cells, are part of a large family of heterodimeric transmembrane receptors containing an α and a β subunit and are devoted to cell adhesion to the extracellular matrix and other signaling effects and functions to include the immune response (Hynes, 2002). Blockade of SARS-CoV-2 binding to $\alpha_5\beta_1$ and $\alpha_V\beta_3$ integrins using the small peptides ATN-161 and Cilengitide, respectfully, has been shown to reduce viral infectivity *in vivo* and attenuate vascular inflammation (Amruta et al., 2021; Nader et al., 2021; Robles et al., 2022). We therefore propose an urgent examination into the therapeutic potential of integrins as therapeutics targets for SARS-CoV-2 (**Figure 1**).

MECHANISM OF SPIKE PROTEIN-MEDIATED VIRAL ENTRY

The S glycoprotein—or "spike protein"—consists of two non-covalently associated subunits. The S1 subunit binds to receptors, while the S2 subunit anchors the spike protein to the virion membrane to mediate membrane fusion. SARS-CoV-2 fusion occurs mainly after the ACE2 receptor engages the S1 subunit of the spike protein, exposing a protease cleavage site on the S2 subunit (S2'). Cleavage at S2' by the transmembrane protease serine 2 (TMPRSS2) at the surface, or by cathepsins in endosomal compartments, triggers the fusion of the virus (Jackson et al., 2021).

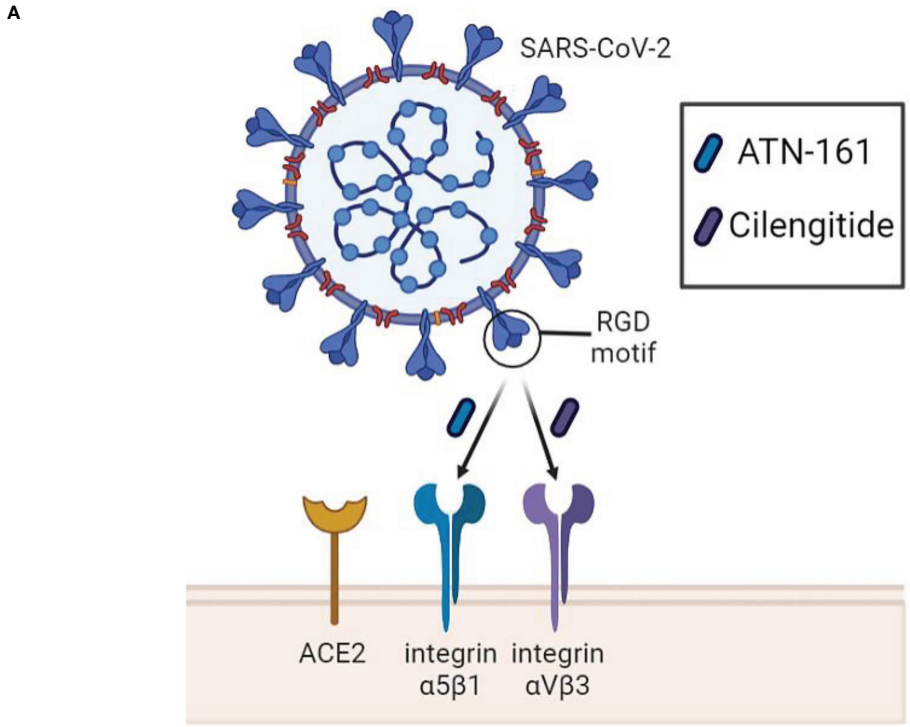

FIGURE 1 | **(A)** Schematic diagram of SARS-CoV-2 interaction with proposed receptors and therapeutics. Integrins α5β1 and αVβ3 have been reported to bind the RGD motif of the spike protein. Peptide compounds ATN-161 and Cilengitide target these integrins and have displayed efficacy in reducing SARS-CoV-2 infection and spike-mediated endothelial dysfunction. **(B)** Multiple sequence alignment using EMBL-EBI Clustal Omega tool between spike proteins of the SARS-CoV-2 Wuhan wild type, and variants of concern Alpha, Beta, Gamma, Delta, and Omicron. The symbols (*) and (.) indicate conserved and weakly similar amino acids, respectively. The RGD motif is highlighted in yellow, where it is preserved across all major variants.

Although canonically known to bind to ACE2, emerging evidence has shown that the S glycoprotein binds to integrins which influences SARS-CoV-2 infectivity (Makowski et al., 2021; Simons et al., 2021; Staufer et al., 2022). In addition, viruses such as SARS-CoV-2 have evolved to use integrins to facilitate cell entry, extending tissue tropism and infectivity (Hussein et al., 2015). Integrins, therefore, are potentially attractive targets for blocking viral infection.

INTEGRINS ARE RECEPTORS FOR SARS-COV-2

SARS-CoV-2 is unique among all other Betacoronaviruses in that it has a novel K403R substitution in the distal tip of the spike protein compared to SARS-CoV-1 (Sigrist et al., 2020). This sequence encodes an RGD motif which is recognized by RGD-binding integrins. Evidence of direct binding of spike protein to integrins has been reported and is successfully reduced upon adding RGD-blocking compounds or integrin-targeting monoclonal antibodies in several cell lines which express $\alpha_5\beta_1$ and $\alpha_V\beta_3$, such as human umbilical vascular endothelial cells, colonic cells, and primary derived aortic endothelial cells (Nader et al., 2021; Robles et al., 2022), important as RGD-motif integrins are differentially expressed on endothelial cells developmentally and assume this same phenotype during cytokine mediated-injury (Gonzalez and Medici, 2014; Wang et al., 2018). Interestingly, besides the RGD motif, additional potential integrin-binding motifs may have equal or better accessibility for integrin binding on not only $\alpha_5\beta_1$ and $\alpha_V\beta_3$ but on several other integrin subunits (Beaudoin et al., 2021), suggesting that potential non-RGD interactions on integrins may

also contribute to SARS-CoV-2 infectivity. Perhaps even more interesting is that emerging SARS-CoV-2 mutations of concern have conspicuously left the RGD motif untouched (Makowski et al., 2021), which supports the hypothesis that integrins may contribute to SARS-CoV-2 viral entry and infectivity beyond ACE2 binding alone.

Emerging data also suggests that the mutations within the Omicron variant facilitate a receptor-binding domain that allows more accessibility to the RGD motif, which may ultimately enhance integrin binding (Hossen et al., 2022) and be associated with higher transmission rates than other variants of concern. Mapping the tissue distribution of integrins also highlights its potential as an alternative receptor. While ACE2 has low expression in alveolar, bronchial, and pulmonary endothelial cells, high levels of integrins have been noted in both upper and lower epithelial and endothelial respiratory cells (Meng et al., 2022), a primary cellular target for SARS-CoV-2. In addition, integrins appear to be upregulated in COVID-19 affected patients (Wu et al., 2020; Calver et al., 2021). Taken together, integrins may be significant regulators of SARS-CoV-2 infection and potential determinants for tissue tropism and COVID-19 severity.

PRODUCTIVE INFECTION REQUIRES INTEGRINS

The putative integrin-dependent infection mechanism of SARS-CoV-2 is thus far unknown. However, ebolavirus (Schornberg et al., 2009) and reoviruses (Maginnis et al., 2008) rely on an integrin $\alpha_5\beta_1$-dependent and clathrin-mediated endocytosis that delivers their viral cargo to endo-lysosomes, where the S2' is cleaved by cathepsins to facilitate fusion between virus and host membranes (Maginnis et al., 2008; Schornberg et al., 2009). This process is mediated by the NPxY motif in the cytoplasmic tail of the β subunit of integrins, which recruits talin, an actin-binding focal adhesion protein essential for integrin activation, and clathrin-adaptor proteins required for delivery to endosomes and lysosomes (Caswell et al., 2009). Studies on reovirus infection in spinner-adapted fibroblast cells have demonstrated that mutations in the NPxY motif on β_1 integrins result in dysfunctional trafficking and non-productive infection (Maginnis et al., 2008). Likewise, steric inhibition of talin-binding to the NPxY motif on the ß cytoplasmic tail with the cell membrane permeable small-peptide mP13 blocks productive infection of Sars-CoV-2 (Simons et al., 2021). This highlights the critical role of integrins in SARS-CoV-2 productive infection.

INTEGRINS ARE INVOLVED IN VASCULAR DYSREGULATION

In endothelial cells, integrins regulate barrier integrity by mediating intracellular signaling cascades triggered upon ligand binding. Through its RGD motif, SARS-CoV-2 spike protein induces significant cellular permeability and vascular dysregulation through the downregulation or internalization of junction proteins, to include VE-Cadherin endothelial adherens junction protein, JAM-A tight junctional protein, Connexin-43 gap junctional protein, and Platelet endothelial cell adhesion molecule-1 (PECAM-1) in primary mouse brain microvascular endothelial cells (Biering et al., 2021; Raghavan et al., 2021). Strikingly, integrin $\alpha_5\beta_1$ activation by spike protein induces an endothelial inflammatory phenotype characterized by increased leukocyte attachment to the endothelium and the expression of inflammatory cytokines and coagulation factors (Robles et al., 2022). Blocking integrin receptors using antagonists which target $\alpha_V\beta_3$ or $\alpha_5\beta_1$ integrins successfully rescue barrier function as measured by VE-Cadherin and FITC-Dextran while additionally reducing immune leukocyte adhesion and permeability (Nader et al., 2021; Robles et al., 2022). The vasculopathy experienced in COVID-19 affected individuals, therefore, may very well be likely attributed to SARS-CoV-2 spike protein exploitation of integrins.

THERAPEUTICS FOR TARGETING INTEGRINS

Several integrin-targeting formulations have been safely administered to humans to treat various diseases, which could be repurposed to treat SARS-CoV-2 infection. These include the antibody natalizumab, which targets $\alpha_4\beta_1/\beta_7$ integrins for the treatment of Crohn's disease and multiple sclerosis (MS), the small molecule tirofiban, which targets $\alpha_{IIb}\beta_3$ integrins and is an anti-platelet therapy for the treatment of acute coronary syndrome, the experimental cancer therapy cyclic peptide Cilengitide which targets α_v integrins, and the experimental cancer and stroke therapy small peptide ATN-161, which primarily targets $\alpha_5\beta_1$ but also can inhibit $\alpha_V\beta_3$ integrin.

Natalizumab has shown favorable outcomes for COVID-19 patients while treating their multiple sclerosis, supporting the hypothesis that targeting integrins with prophylactic natalizumab might reduce SARS-CoV-2 host cell infection and subsequent replication in humans (Aguirre et al., 2020). Likewise, Tirofiban has improved hypoxemia in severe COVID-19 patients with hypercoagulability (Viecca et al., 2020). The cyclic RGD-based compound Cilengitide has demonstrated a high affinity for integrin $\alpha_V\beta_3$ (Kapp et al., 2017), and in cultured human endothelial cells, has also been shown to inhibit SARS-CoV-2 spike protein binding (Nader et al., 2021). Finally, our group has validated ATN-161 as an inhibitor of spike protein-mediated cell infection *in vitro* (Beddingfield et al., 2021). Then, for the first time, demonstrated the *in vivo* therapeutic potential of an integrin-based inhibition therapy for SARS-CoV-2 infection. Our results showed that ATN-161 administered post-SARS-CoV-2 infection limited viral load in the lungs, improved lung histology, and reduced the inflammatory potential in SARS-CoV-2 susceptible k18-hACE2 transgenic mice (Amruta et al., 2021).

Since integrins are critical receptors for multiple cellular functions, potential side effects of integrin-targeting drugs,

especially for antibody-based drugs, warrant further discussion. Natalizumab carries the risk of inducing progressive multifocal leukoencephalopathy (Babaesfahani et al., 2022), while Tirofiban carries a risk of hematuria and hemorrhage (Iqbal et al., 2022). Finally, antibody-based drugs may also have a cost concern, which, relative to a SARS-CoV-2 antibody-based therapy, might not be as cost effective or efficient.

ATN-161 is a five–amino-acid peptide derived from the synergy binding region of fibronectin to $\alpha_5\beta_1$ and has shown excellent safety profiles in intravenous infusion at multiple dose escalations, cycles, and timepoints during Phase I clinical trials in solid tumor glioblastoma with no significant toxicity reported at the maximum administered dose (Cianfrocca et al., 2006). Likewise, Cilengitide, which selectively blocks activation of $\alpha_v\beta_3$, shows a similar safety profile in patients with glioblastoma (Scaringi et al., 2012). Targeted integrin therapies towards SARS-CoV-2, specifically those involving $\alpha_5\beta_1$ and $\alpha_v\beta_3$, should therefore be seriously considered.

AN INTEGRIN-BASED TREATMENT FOR SARS-COV-2

Although comparative analysis of how integrins may participate in SARS-CoV-2 pathophysiology has yet to be conducted, we believe that integrin $\alpha_5\beta_1$ and $\alpha_V\beta_3$ may be promising targets to mediate productive infection in SARS-CoV-2. Besides robust experimental evidence, other considerations support this hypothesis. The cytoplasmic tail on $\alpha_5\beta_1$ has *in-cis* interactions between ACE2, which provide synergistic upregulation to cell adhesion signaling (Clarke et al., 2012), which may ultimately enhance SARS-CoV-2 infectivity and thus explain the reduction of pathophysiological outcomes after inhibiting this receptor *in vivo* (Amruta et al., 2021). In addition, several studies have shown that ACE2 and integrin β_1 are upregulated in tandem due to inflammatory cytokines released in severe COVID-19 and in several health comorbidities that reduce clinical outcomes, to include hypertension and hyperlipidemia, diabetes, chronic pulmonary diseases, old age, and smoking (Jackson et al., 2021).

Both ATN-161 and Cilengitide may be promising therapeutics as integrin inhibitors in treating SARS-CoV-2 infection. In addition to their excellent clinical safety profile, they are safe to administer systemically and may even be delivered as an intranasal spray for more targeted delivery to the respiratory tract as either a pre- or post-exposure prophylactic. Furthermore, a potential advantage for using ATN-161 for treating SARS-CoV-2 infection is its proclivity for binding to and inhibiting activated—that is, bound with viral spike protein or primed for binding—versus inactive forms of $\alpha_5\beta_1$ integrin (Beddingfield et al., 2021), thereby limiting its potential for off-target effects. Indeed, in addition to post-exposure prophylaxis with antivirals or monoclonal antibodies to prevent SARS-CoV-2 infection from progressing to severe COVID-19 in certain at-risk individuals, integrin inhibitors, such as ATN-161 or Cilengitide, may represent a novel pre-exposure prophylactic approach to preventing SARS-CoV-2 and are worthy of further study.

DISCUSSION

While vaccination combined with other mitigation strategies such as mask-wearing, avoiding large indoor crowds in poorly ventilated locations, and social distancing continue to be the most effective COVID-19 preventative approaches, new therapeutic strategies remain attractive. The evidence clarifies that the spike protein of SARS-CoV-2, through its integrin-binding RGD motif, allows integrins to mediate SARS-CoV-2 infection and spike-mediated endothelial dysfunction (Biering et al., 2021; Robles et al., 2022). What remains is to delineate how integrins participate in cell entry and trafficking of the virus, and ultimately, determine whether specific integrins, such as $\alpha_5\beta_1$, $\alpha V\beta 3$, or a group of integrins, play a crucial role in mediating infection. Clarifying these mechanisms may determine whether a specific integrin inhibitor, or perhaps an integrin inhibitor "cocktail" might be readily effective and repurposed to prevent and treat SARS-CoV-2 infection and related COVID-19 clinical sequelae.

AUTHOR CONTRIBUTIONS

All authors listed have made a substantial, direct, and intellectual contribution to the work and approved it for publication.

REFERENCES

Aguirre, C., Meca-Lallana, V., Barrios-Blandino, A., Del Río, B., and Vivancos, J. (2020). Covid-19 in a Patient With Multiple Sclerosis Treated With Natalizumab: May the Blockade of Integrins Have a Protective Role? *Mult Scler. Relat. Disord.* 44, 102250. doi: 10.1016/j.msard.2020.102250

Amruta, N., Engler-Chiurazzi, E. B., Murray-Brown, I. C., Gressett, T. E., Biose, I. J., Chastain, W. H., et al. (2021). *In Vivo* Protection From SARS-CoV-2 Infection by ATN-161 in K18-Hace2 Transgenic Mice. *Life Sci.* 284, 119881. doi: 10.1016/j.lfs.2021.119881

Babaesfahani, A., Khanna, N. R., and Kuns, B. (2022). "Natalizumab," in *StatPearls* (Treasure Island (FL: StatPearls Publishing).

Beaudoin, C. A., Hamaia, S. W., Huang, C. L.-H., Blundell, T. L., and Jackson, A. P. (2021). Can the SARS-CoV-2 Spike Protein Bind Integrins Independent of the RGD Sequence? *Front. Cell. Infect. Microbiol.* 11, 1116. doi: 10.3389/fcimb.2021.765300

Beddingfield, B. J., Iwanaga, N., Chapagain, P. P., Zheng, W., Roy, C. J., Hu, T. Y., et al. (2021). The Integrin Binding Peptide, ATN-161, As a Novel Therapy for SARS-CoV-2 Infection. *JACC Basic Transl. Sci.* 6 (1), 1–8. doi: 10.1016/j.jacbts.2020.10.003

Biering, S. B., de Sousa, F. T. G., Tjang, L. V., Pahmeier, F., Ruan, R., Blanc, S. F., et al. (2021). SARS-CoV-2 Spike Triggers Barrier Dysfunction and Vascular Leak *via* Integrins and TGF-β Signaling. *bioRxiv*. doi: 10.1101/2021.12.10.472112

Calver, J., Joseph, C., John, A., Organ, L., Fainberg, H., Porte, J., et al. (2021). S31 The Novel Coronavirus SARS-CoV-2 Binds RGD Integrins and Upregulates Avb3 Integrins in Covid-19 Infected Lungs. *Thorax* 76 (Suppl 1), A22–A23. doi: 10.1136/thorax-2020-BTSabstracts.37

Caswell, P. T., Vadrevu, S., and Norman, J. C. (2009). Integrins: Masters and Slaves of Endocytic Transport. *Nat. Rev. Mol. Cell Biol.* 10 (12), 843–853. doi: 10.1038/nrm2799

Cianfrocca, M. E., Kimmel, K. A., Gallo, J., Cardoso, T., Brown, M. M., Hudes, G., et al. (2006). Phase 1 Trial of the Antiangiogenic Peptide ATN-161 (Ac-PHSCN-NH2), A Beta Integrin Antagonist, In Patients With Solid Tumours. *Br. J. Cancer* 94 (11), 1621–1626. doi: 10.1038/sj.bjc.6603171

Clarke, N. E., Fisher, M. J., Porter, K. E., Lambert, D. W., and Turner, A. J. (2012). Angiotensin Converting Enzyme (ACE) and ACE2 Bind Integrins and ACE2 Regulates Integrin Signalling. *PloS One* 7 (4), e34747. doi: 10.1371/journal.pone.0034747

Gonzalez, D. M., and Medici, D. (2014). Signaling Mechanisms of the Epithelial-Mesenchymal Transition. *Sci. Signal* 7 (344), re8. doi: 10.1126/scisignal.2005189

Hossen, M. L., Baral, P., Sharma, T., Gerstman, B., and Chapagain, P. (2022). Significance of the RBD Mutations in the SARS-CoV-2 Omicron: From Spike Opening to Antibody Escape and Cell Attachment. *bioRxiv* 2022, 2001.2021.477244. doi: 10.1101/2022.01.21.477244

Hussein, H. A., Walker, L. R., Abdel-Raouf, U. M., Desouky, S. A., Montasser, A. K., and Akula, S. M. (2015). Beyond RGD: Virus Interactions With Integrins. *Arch. Virol.* 160 (11), 2669–2681. doi: 10.1007/s00705-015-2579-8

Hynes, R. O. (2002). Integrins: Bidirectional, Allosteric Signaling Machines. *Cell* 110 (6), 673–687. doi: 10.1016/s0092-8674(02)00971-6

Iqbal, A. M., Lopez, R. A., and Hai, O. (2022). "Antiplatelet Medications," in *StatPearls* (Treasure Island (FL: StatPearls Publishing).

Jackson, C. B., Farzan, M., Chen, B., and Choe, H. (2021). Mechanisms of SARS-CoV-2 Entry Into Cells. *Nat. Rev. Mol. Cell Biol.* 23, 3–20. doi: 10.1038/s41580-021-00418-x

Kapp, T. G., Rechenmacher, F., Neubauer, S., Maltsev, O. V., Cavalcanti-Adam, E. A., Zarka, R., et al. (2017). A Comprehensive Evaluation of the Activity and Selectivity Profile of Ligands for RGD-Binding Integrins. *Sci. Rep.* 7, 39805. doi: 10.1038/srep39805

Maginnis, M. S., Mainou, B. A., Derdowski, A., Johnson, E. M., Zent, R., and Dermody, T. S. (2008). NPXY Motifs in the Beta1 Integrin Cytoplasmic Tail Are Required for Functional Reovirus Entry. *J. Virol.* 82 (7), 3181–3191. doi: 10.1128/JVI.01612-07

Makowski, L., Olson-Sidford, W., and W-Weisel, J. (2021). Biological and Clinical Consequences of Integrin Binding *via* a Rogue RGD Motif in the SARS CoV-2 Spike Protein. *Viruses* 13 (2), 146. doi: 10.3390/v13020146

Meng, B., Abdullahi, A., Ferreira, I. A. T. M., Goonawardane, N., Saito, A., Kimura, I., et al. (2022). Altered TMPRSS2 Usage by SARS-CoV-2 Omicron Impacts Tropism and Fusogenicity. *Nature* 603, 706–714. doi: 10.1038/s41586-022-04474-x

Nader, D., Fletcher, N., Curley, G. F., and Kerrigan, S. W. (2021). SARS-CoV-2 Uses Major Endothelial Integrin αvβ3 to Cause Vascular Dysregulation *in-Vitro* During COVID-19. *PloS One* 16 (6), e0253347. doi: 10.1371/journal.pone.0253347

Raghavan, S., Kenchappa, D. B., and Leo, M. D. (2021). SARS-CoV-2 Spike Protein Induces Degradation of Junctional Proteins That Maintain Endothelial Barrier Integrity. *Front. Cardiovasc. Med.* 8. doi: 10.3389/fcvm.2021.687783

Robles, J. P., Zamora, M., Adan-Castro, E., Siqueiros-Marquez, L., Martinez de la Escalera, G., and Clapp, C. (2022). The Spike Protein of SARS-CoV-2 Induces Endothelial Inflammation Through Integrin α5β1 and NF-κb Signaling. *J. Biol. Chem.* 298 (3), 101695. doi: 10.1016/j.jbc.2022.101695

Scaringi, C., Minniti, G., Caporello, P., and Enrici, R. M. (2012). Integrin Inhibitor Cilengitide for the Treatment of Glioblastoma: A Brief Overview of Current Clinical Results. *Anticancer Res.* 32 (10), 4213–4223.

Schornberg, K. L., Shoemaker, C. J., Dube, D., Abshire, M. Y., Delos, S. E., Bouton, A. H., et al. (2009). Alpha5beta1-Integrin Controls Ebolavirus Entry by Regulating Endosomal Cathepsins. *Proc. Natl. Acad. Sci. U.S.A.* 106 (19), 8003–8008. doi: 10.1073/pnas.0807578106

Sigrist, C. J., Bridge, A., and Le Mercier, P. (2020). A Potential Role for Integrins in Host Cell Entry by SARS-CoV-2. *Antiviral Res.* 177, 104759. doi: 10.1016/j.antiviral.2020.104759

Simons, P., Rinaldi, D. A., Bondu, V., Kell, A. M., Bradfute, S., Lidke, D. S., et al. (2021). Integrin Activation Is an Essential Component of SARS-CoV-2 Infection. *Sci. Rep.* 11 (1), 20398. doi: 10.1038/s41598-021-99893-7

Staufer, O., Gupta, K., Hernandez Bücher, J. E., Kohler, F., Sigl, C., Singh, G., et al. (2022). Synthetic Virions Reveal Fatty Acid-Coupled Adaptive Immunogenicity of SARS-CoV-2 Spike Glycoprotein. *Nat. Commun.* 13 (1), 868. doi: 10.1038/s41467-022-28446-x

Tresoldi, I., Sangiuolo, C. F., Manzari, V., and Modesti, A. (2020). SARS-COV-2 and Infectivity: Possible Increase in Infectivity Associated to Integrin Motif Expression. *J. Med. Virol.* 92 (10), 1741–1742. doi: 10.1002/jmv.25831

Viecca, M., Radovanovic, D., Forleo, G. B., and Santus, P. (2020). Enhanced Platelet Inhibition Treatment Improves Hypoxemia in Patients With Severe Covid-19 and Hypercoagulability. A Case Control, Proof of Concept Study. *Pharmacol. Res.* 158, 104950. doi: 10.1016/j.phrs.2020.104950

Wang, W., Wang, Z., Tian, D., Zeng, X., Liu, Y., Fu, Q., et al. (2018). Integrin β3 Mediates the Endothelial-To-Mesenchymal Transition *via* the Notch Pathway. *Cell Physiol. Biochem.* 49 (3), 985. doi: 10.1159/000493229

Wu, M., Chen, Y., Xia, H., Wang, C., Tan, C. Y., Cai, X., et al. (2020). Transcriptional and Proteomic Insights Into the Host Response in Fatal COVID-19 Cases. *Proc. Natl. Acad. Sci. U.S.A.* 117 (45), 28336–28343. doi: 10.1073/pnas.2018030117

Conflict of Interest: The authors declare that the research was conducted in the absence of any commercial or financial relationships that could be construed as a potential conflict of interest.

Publisher's Note: All claims expressed in this article are solely those of the authors and do not necessarily represent those of their affiliated organizations, or those of the publisher, the editors and the reviewers. Any product that may be evaluated in this article, or claim that may be made by its manufacturer, is not guaranteed or endorsed by the publisher.

frontiers | Frontiers in Cellular and Infection Microbiology

ORIGINAL RESEARCH
published: 04 May 2022
doi: 10.3389/fcimb.2022.798767

Control of *CDH1*/E-Cadherin Gene Expression and Release of a Soluble Form of E-Cadherin in SARS-CoV-2 Infected Caco-2 Intestinal Cells: Physiopathological Consequences for the Intestinal Forms of COVID-19

Ikram Omar Osman[1,2], *Clémence Garrec*[1,2], *Gabriel Augusto Pires de Souza*[1], *Ana Zarubica*[3], *Djamal Brahim Belhaouari*[1,2], *Jean-Pierre Baudoin*[1], *Hubert Lepidi*[1,4], *Jean-Louis Mege*[1,2,4], *Bernard Malissen*[3], *Bernard La Scola*[1] *and Christian Albert Devaux*[1,2,5]*

[1] *Microbes Evolution Phylogeny and Infections (MEPHI), Institut de recherche pour le Développement (IRD), Assistance Publique Hôpitaux de Marseille (APHM), Institut Hospitalo-Universitaire (IHU)-Méditerranée Infection, Marseille, France,* [2] *Aix-Marseille Université, Marseille, France,* [3] *Centre d'Immunophénomique (CIPHE), Aix Marseille Université, Institut National de la Santé et de la Recherche Médicale (INSERM), Centre National de la Recherche Scientifique (CNRS), CELPHEDIA, PHENOMIN, Marseille, France,* [4] *Assitance Publique Hôpitaux de Marseille (APHM), Marseille, France,* [5] *Centre National de la Recherche Scientifique (CNRS), Marseille, France*

OPEN ACCESS

Edited by:
Yu Chen,
Wuhan University, China

Reviewed by:
Junki Maruyama,
University of Texas Medical Branch at Galveston, United States
Diane Bimczok,
Montana State University, United States

***Correspondence:**
Christian Albert Devaux
christian.devaux@mediterranee-infection.com

Specialty section:
This article was submitted to Virus and Host, a section of the journal Frontiers in Cellular and Infection Microbiology

Received: *05 November 2021*
Accepted: *22 March 2022*
Published: *04 May 2022*

Citation:
Osman IO, Garrec C, de Souza GAP, Zarubica A, Belhaouari DB, Baudoin J-P, Lepidi H, Mege J-L, Malissen B, Scola BL and Devaux CA (2022) Control of CDH1*/E-Cadherin Gene Expression and Release of a Soluble Form of E-Cadherin in SARS-CoV-2 Infected Caco-2 Intestinal Cells: Physiopathological Consequences for the Intestinal Forms of COVID-19. Front. Cell. Infect. Microbiol. 12:798767. doi: 10.3389/fcimb.2022.798767*

COVID-19 is the biggest pandemic the world has seen this century. Alongside the respiratory damage observed in patients with severe forms of the disease, gastrointestinal symptoms have been frequently reported. These symptoms (e.g., diarrhoea), sometimes precede the development of respiratory tract illnesses, as if the digestive tract was a major target during early SARS-CoV-2 dissemination. We hypothesize that in patients carrying intestinal SARS-CoV-2, the virus may trigger epithelial barrier damage through the disruption of E-cadherin (E-cad) adherens junctions, thereby contributing to the overall gastrointestinal symptoms of COVID-19. Here, we use an intestinal Caco-2 cell line of human origin which expresses the viral receptor/co-receptor as well as the membrane anchored cell surface adhesion protein E-cad to investigate the expression of E-cad after exposure to SARS-CoV-2. We found that the expression of *CDH1*/E-cad mRNA was significantly lower in cells infected with SARS-CoV-2 at 24 hours post-infection, compared to virus-free Caco-2 cells. The viral receptor ACE2 mRNA expression was specifically down-regulated in SARS-CoV-2-infected Caco-2 cells, while it remained stable in HCoV-OC43-infected Caco-2 cells, a virus which uses HLA class I instead of ACE2 to enter cells. It is worth noting that SARS-CoV-2 induces lower transcription of TMPRSS2 (involved in viral entry) and higher expression of B^0AT1 mRNA (that encodes a protein known to co-express with ACE2 on intestinal cells). At 48 hours post-exposure to the virus, we also detected a small but significant increase of

soluble E-cad protein (sE-cad) in the culture supernatant of SARS-CoV-2-infected Caco-2 cells. The increase of sE-cad release was also found in the intestinal HT29 cell line when infected by SARS-CoV-2. Beside the dysregulation of E-cad, SARS-CoV-2 infection of Caco-2 cells also leads to the dysregulation of other cell adhesion proteins (occludin, JAMA-A, zonulin, connexin-43 and PECAM-1). Taken together, these results shed light on the fact that infection of Caco-2 cells with SARS-CoV-2 affects tight-, adherens-, and gap-junctions. Moreover, intestinal tissues damage was associated to the intranasal SARS-CoV-2 infection in human ACE2 transgenic mice.

Keywords: SARS-CoV-2, E-cadherin, gastrointestinal tract, COVID-19, infection, intestinal barrier

INTRODUCTION

Since its first description in China in 2019, the coronavirus disease 2019 (COVID-19) has emerged as a world pandemic. Insomuch its aetiological agent, SARS-CoV-2, was considered to be an exclusive airborne pathogen with a preferential tropism for the angiotensin converting enzyme 2 (ACE2)-positive epithelial cells of the pulmonary alveoli (Devaux et al., 2020; Huang et al., 2020; Yan et al., 2020; Zhu et al, 2020), other routes of infection (e.g., oral route) and tropism for other tissues (e.g., intestinal epithelium) received less attention, despite growing importance in the pathophysiology of COVID-19 (Lamers et al., 2020; Xiao et al., 2020a; Devaux et al., 2021). Gastrointestinal tract (GIT) symptoms, including diarrhoea, nausea, abdominal pain, and vomiting, have been frequently reported in COVID-19 patients (D'Amico et al., 2020; Lin et al., 2020; Song et al., 2020; Wang et al., 2020; Zhang et al., 2020a). Moreover, GIT-symptoms sometimes precede the development of respiratory tract symptoms (Fang et al., 2020; Li et al., 2020; Pan et al., 2020; Redd et al., 2020), and people with GIT-symptoms were much more likely to have the SARS-CoV-2 detected in their stool samples (Han et al., 2020; Wölfel et al., 2020; Xu et al., 2020; Zheng et al., 2020). The process by which SARS-CoV-2 reaches the intestine is not yet clear and could occur either by the bloodstream (with or without a hepatic stage) or by the oral-intestinal route (from the trachea to the esophagus and intestine). The potential role of the oral-intestinal transmission of SARS-CoV-2 is currently considered as likely (Brogna et al., 2022; Heneghan et al., 2021; Meng and Liang, 2021; Wendling et al., 2021; Dergham et al., 2021). SARS-CoV-2 replication in the GIT is associated with modulation in the diversity of bacterial species (Dhar and Mohanty, 2020; Gu S. et al., 2020; Gu J. et al., 2020; Zuo et al., 2020). As in many invasive infection processes initiated within the GIT, the pathogen is expected to develop strategies aimed at destroying the adherens junctions insured by cell adhesion molecules (CAM), such as E-cadherin (E-Cad), to create epithelium micro-damage, to dysregulate the immune response, and/or to invade the host (Devaux et al., 2019). Several viruses with intestinal tropism such as Hepatitis B virus and Hepatitis C virus, and viruses with other organ tropism, modulate E-cad expression (Lee et al., 2005; D'Costa et al., 2012; Li et al., 2016). Using a mouse model expressing transgenic human ACE2 it was demonstrated that intragastric inoculation of SARS-CoV-2 causes productive infection, virus shedding was found in faeces, and the viral invasion *via* the GIT lead to secondary pulmonary pathological changes (Sun et al., 2021). Similar observations were reported using nonhuman primates as a model of SARS-CoV-2 intestinal infection (Jiao et al., 2021).

SARS-CoV-2 was reportedly able to infect human small intestinal organoids established from primary gut epithelial stem cells (Lamers et al., 2020). Intestinal biopsies of COVID-19 patients evidenced the presence of replicating SARS-CoV-2 in epithelial cells of the small and large intestine (Xiao et al., 2020b). The main SARS-CoV-2 receptor, ACE2, was found in the small intestine with the highest expression observed in the brush border of intestinal enterocytes (Hamming et al., 2004; Qi et al., 2020; Zuo et al., 2020). Although the most well-known physiological function of ACE2 is the regulation of the Renin Angiotensin System (Devaux et al., 2020), the main role of ACE2 in the GIT is to ensure nutrients absorption. In the GIT, ACE2 functions as a chaperone for the expression of the sodium-dependent neutral amino acid transporter B^0AT1 (B^0AT1 binds to the ferredoxin-like domain of ACE2) and amino acid (proline) SIT1 transporters (Camargo et al., 2009; Vuille-Dit-Bille et al., 2015). ACE2, B^0AT1, and aminopeptidase N form a complex in the brush border membrane of the intestine (Fairweather et al., 2012). It was recently shown that ACE2-B^0AT1 heterodimers are assembled through the collectrin-like domain of ACE2 (Yan et al., 2020). Although ACE2 is considered to be highly expressed on colonocytes, this viral receptor is poorly expressed on enteroendocrine cells and Paneth cells, and is almost undetectable in goblet cells and tuft cells (Wang et al., 2020). It was previously established that following ACE2 receptor binding, the SARS-CoV-2 spike (S) glycoprotein is processed by a type II transmembrane serine protease, TMPRSS2, prior to membrane fusion. Although both ACE2 and TMPRSS2 are highly expressed in the GIT, the co-expression of these molecules has not been shown on enterocyte, with TMPRSS2 being expressed on $ACE2^{neg}$ intestinal epithelial cells and not mature enterocytes. It should be emphasized that members of the same family, such as TMPRSS4, highly expressed in $ACE2^{+}$ mature enterocytes are probably involved in SARS-CoV-2 S glycoprotein processing (Zang et al., 2020). The enhanced spread of SARS-CoV-2 compared to SARS-CoV-1 has been correlated with the gain of a polybasic furin type cleavage site at the S1/S2 junction in the

SARS-CoV-2 S glycoprotein opening the possibility to this glycoprotein to interact with neuropilin1 (NRP-1), a protein known to bind furin-cleaved substrates (Daly et al., 2020; Cantuti-Castelvetri et al., 2020), through interaction with a C-end rule (CendR) terminal motif $RRAR_{OH}$ (Teesalu et al., 2009; Haspel et al., 2011). Both NRP-1 and NRP-2 are expressed in the GIT (Cohen, 2001; Hansel et al., 2004; Yu et al., 2011).

There is evidence indicating that Caco-2 cells, a cell line derived from a human colorectal adenocarcinoma, can serve as model for GIT cells SARS-CoV-2 replication. The replication of SARS-CoV-2 in Caco-2 cells was reported to be comparable to that found in Calu-3 (pulmonary) cells (Chu et al., 2020). It was also reported that Caco-2 cells exposed to vesicular stomatitis virus (VSV) particles pseudotyped with chimeric spike from SARS-CoV-2 that carry receptor binding domain (RBD) from different betacoronaviruses, become infected with VSV particles expressing the RBD from SARS-CoV-2 (Letko et al., 2020). In this study, most other RBDs were incompatible with infection, indicating a requirement for SARS-CoV-2 spike RBD-ACE2 receptor interaction. The requirement for SARS-CoV-2 spike glycoprotein priming by TMPRSS2 during Caco-2 cell infection has been demonstrated using drug-inactivation of TMPRSS2 that partially blocked viral entry (Hoffmann et al., 2020). Caco-2 cells infected with SARS-CoV-2 produce filopodia protrusions containing viral particles (Bouhaddou et al., 2020). However, previous experiments performed in our laboratory indicated that SARS-CoV-2 does not induce a cytopathic effect in Caco-2 cells at least over seven days of cell culture (Wurtz et al., 2021). In the present study we investigate the E-cad expression in Caco-2 cells after exposure to SARS-CoV-2, as well as the effect of infection on tight-, adherens-, and gap-junctions, and the intestinal tissues damages induced by SARS-CoV-2 infection of human ACE2 transgenic mice.

MATERIALS AND METHODS

Cells Culture

The Caco-2 cell line (ATCC® HTB-37 ™) isolated from a human colorectal adenocarcinoma was cultured in a Dulbecco's Modified Medium F-12 Nutrient Mixture (DMEM F-12) supplemented with 10% Fetal Bovine Serum (FBS; Invitrogen, USA). Caco-2 cells exhibit spontaneous epithelial differentiation *in vitro*. Another human colorectal adenocarcinoma, the HT29 cell line (ATCC® HTB-38 ™), cultured in DMEM F-12 supplemented with 10% FBS and 1% L-glutamine (L-Gln; Invitrogen) was used as control in some experiments.

The Simian Vero-E6 renal epithelial cell line (ATCC® CRL-1586 ™), isolated from *Chlorocebus sabaeus* (African green monkey) was cultured in minimum essential medium (MEM. Gibco; Invitrogen) containing 4% FBS and 1% L-glutamine (L-Gln; Invitrogen). The HCT-8 (ATCC® CCL-244™), a human tumor epithelial cell line isolated from an ileal colorectal adenocarcinoma, was cultured in Roswell Park Memorial Institute 1640 medium (RPMI) (Gibco, Thermo Fischer) supplemented with 10% FBS.

All cells were cultured in a 175-cm^2 flasks at 37°C in a 5% CO_2 atmosphere. Every two days the medium was replenished, and confluent cultures were sub-cultured after harvesting of adherent cells by trypsination (0,05% Trypsin-EDTA, Invitrogen, USA).

Virus Production

The SARS-CoV-2 (strain IHUMI-3, lineage B) was previously isolated from the liquid collected from a nasopharyngeal swab. The SARS-CoV-2 isolate was cultured in Vero-E6 cells grown in MEM supplemented with 4% FBS and 1% L-GLn.

The HCoV-OC43 (ATCC® VR-1558), another human coronavirus responsible for the common winter cold (Choi et al., 2021) and able to infect Caco-2 cells (Collins, 1990), was used as a control in this study. This virus was cultured in HCT-8 cells grown in RPMI1640 supplemented with 4% FBS, as described (Owczarek et al., 2018).

The cultures were incubated at 37°C in a 5% CO_2 atmosphere. After three passages with an almost complete cytopathic effect, the supernatant of each viral culture was collected, centrifuged at 3000 × g for 10 minutes at 4°C, then filtered through a 0.22 µm membrane. The filtrate was made up of 10% FBS and 1% of 2- [4-(2-96 hydroxyethyl) piperazin-1-yl] ethanesulfonic acid (HEPES), and stored at -80°C, to constitute the SARS-CoV-2 and HCoV-OC43 viral stocks.

For mouse infection, Vero E6 cells were cultured at 37°C in DMEM supplemented with 10% FBS, 10 mM HEPES (pH 7.3), 1 mM sodium pyruvate, 1% L-glutamine (L-Gln; Invitrogen). The strain BetaCoV/France/IDF0372/2020 was supplied by the National Reference Centre for Respiratory Viruses hosted by Institut Pasteur (Paris, France). The human sample from which strain BetaCoV/France/IDF0372/2020 was isolated, has been provided from the Bichat Hospital, Paris, France. Infectious stocks were grown by inoculating Vero E6 cells and collecting supernatant upon observation of cytopathic effect; debris were removed by centrifugation and passage through a 0.22-µm filter. Supernatants were stored at -80°C.

SARS-CoV-2 Replication Kinetics in Caco-2 Cells

The kinetics of viral replication in Caco-2 cells was performed over 72h of infection. For this purpose, cells were distributed in 24-well flat-bottomed plates (Thermo Fisher Scientific) at a concentration of 5×10^5 cells/mL in DMEM/F-12 supplemented with 10% FBS and 1% L-Glutamine and incubated overnight at 37°C under 5% CO_2 atmosphere. Infection occurred with an inoculum of 200 µL of SARS-CoV-2 or HCoV-OC43 viruses (MOI of 0.05). After one hour of adsorption at 37°C, the inoculum was removed, and the cells were washed twice with culture medium. Cells were resuspended in 500 µl of DMEM/F-12 medium. 200 µl aliquots were collected 4, 8, 16, 24, 48, and 72h after T0. qRT-PCR performed in triplicates on supernatants assessed the viral release rate. RNA was extracted from 100 µL of cell culture supernatants using the QIAamp 96 Virus QIAcube HT kit (Qiagen). To detect SARS-CoV-2 RNA, real-time RT-PCRs were carried out using N gene primers (Fwd: 5'-GACCCCAAAATCAGCGAAAT-3', Rev: 5'-TCTGGTTACTGCCAGTTGAATCTG-3'; probes 5' FAM-

ACCCCGCATTACGTTTGGTGGACC-QSY 3') and the Superscript III Platinium One-step Quantitative RT-qPCR systems with ROX kit (Invitrogen), with a final concentration of 400 nM of primers, 200 nM of probe, in a final volume of 25µl with 5 µl of RNA. The amplification cycles were carried out on a LightCycler 480 (Roche Diagnostics). The ΔCT calculations were performed considering the CT heats of T=0 subtracted from the other times (4, 8, 16, 24, 48, and 72h). The methods of RNA extraction from supernatants of cells inoculated with HCoV-OC43, as well as the qRT-PCR, were the same as described above, replacing the primers for the primers corresponding to this HCV-OC43 (Fwd: 5'-ATGTTAGGCCGATAATTGAGGACTAT-3'; Rev: 5'-AATGTAAAGATGGCCGCGTATT-3' and probe: 5' FAM-CATACTCTGACGGTCACAAT-TAMRA 3').

The viral release was also evaluated by tissue culture infectious dose 50 ($TCID_{50}$). For this purpose, 96-well plates containing 1×10^5 Vero E6 cell/well were prepared one day in advance and kept overnight in a 5% CO_2 atmosphere at 37°C. Culture supernatants from Caco-2 cells collected at 4h, 8h, 16h, 24h, 48h, and 72h times were thawed and serially diluted at base ten and inoculated in Vero E6 cells (8 replicates per dilution to a 10^{-10} dilution). The plate were kept at 37°C in a 5% CO_2 atmosphere for 7 days. Seven days post infection the presence of cytopathic effects was evaluated. The $TCID_{50}$ was calculated according to the Spearman and Kärber algorithm (Ramakrishnan, 2016).

RNA Extraction and Quantitative-Reverse Transcription Polymerase Chain Reaction (qRT-PCR)

The Caco-2 cell line (2 x 10^5 cells/well) was cultured in flat-bottom 24-well plates for 12 hours followed by infection with SARS-CoV-2 or HCoV-OC43 at a MOI of 0.5. Twenty-four hours post-infection, RNAs were extracted from cells using a RNeasy Mini Kit (QIAGEN SA) with a DNase I step to eliminate DNA contaminants, according to the manufacturer instructions. The quantity and quality of the RNA was evaluated using a Nanodrop 1000 spectrophotometer (Thermo Science). The first -strand cDNA was obtained using oligo(dT) primers and Moloney murine leukaemia virus-reverse transcriptase (MMLV-RT kit; Life Technologies), using 100 ng of purified RNA. The qPCR experiments were performed using specific oligonucleotide primers and hot-start polymerase (SYBR Green Fast Master Mix; Roche Diagnostics). The amplification cycles were performed using a C1000 Touch Thermal cycler (Biorad). Specific primers used in this study are listed in the **Table 1** and the results of qRT-PCR were normalized using the housekeeping gene β-Actin (ACTB) (Fwd: 5' CAT GCC ATC CTG CGT CTG GA 3'; Rev: 5' CCG TGG CCA TCT CTT GCT CG 3'), and expressed as relative expression ($2^{-\Delta CT}$), where ΔCt = Ct (Target gene) – Ct(Actin). A similar experimental procedure was chosen to analyze mRNA expression in HT29 cells.

Soluble E-Cadherin Quantification

Caco-2 cells (2 x 10^5 cells/well) were cultured in flat-bottom 12 well plates for 12 hours and were then infected with SARS-CoV-2 or HCoV-OC43 at a MOI (Multiplicity of Infection) of 0.5 for four hours, 24 hours, and 48 hours. For each kinetics, the culture supernatants were collected, centrifuged at 1000g for 10 minutes and stored at -20°C until use. The quantities of sE-cad in the supernatants were determined using a specific immunoassay (sE-cad kit Abcam, Cambridge, UK) according to the manufacturer's instruction. The minimal detectable concentration of human sE-cad is 156 pg/mL. The quantification of the soluble compounds in the cell culture supernatant was calculated by comparison to standard curves.

Detection of Protein Expression by Western Blot Analysis

For Western blot assays, cells were immediately washed with ice cold phosphate buffered saline (PBS), and lysed on the plate in a 1X RIPA buffer (100 mM Tris-HCl pH7.5; 750 mM NaCl; 5mM EDTA; 5% Igepal, 0.5% sodium dodecyl sulphate (SDS); 2.5% Na Deoxycholate) supplemented with protease inhibitor and phosphatase cocktail inhibitor (Roche, Germany). Fifty µg of protein was loaded onto a 10% SDS polyacrylamide gels. After the transfer, blockage with a saturation solution (5% Free Fat Milk -PBS-0.3% Tween 20) overnight at 4°C, the blots were incubated with a monoclonal antibody (mAb) directed against human E-cadherin (HECD-131700, Invitrogen, France) for two hours at room temperature. The expression of Glyceradehyde-3-Phosphate dehydrogenase (GADPH) was measured using a mouse anti-human GADPH mAb (1:5,000, Abnova, Taiwan), followed by incubation with a sheep anti-mouse horseradish peroxidase-conjugated antibody (1:10,000 dilution with a blocking solution) (Life Technologies, France) as the loading control. In some experiments the cells were labeled with anti-Occludin mouse mAb (Ref. 331500, Life Technologies SA), anti-connexin 43 mouse mAb (Ref 138300, Life Tech.), anti-JAM-A mouse mAb HU-CD321 (Ref. 14-3219-82, Life Tech.), and/or anti-zonulin mAb (Ref. UM500010, Life Tech.) The proteins were revealed using a ECL Western Blotting Substrate (Promega, USA) and images were digitized using a Fusion FX (Vilber Lourmat, France). The public domain program Image J was used to quantify the Western blot bands intensity.

Automated Western Immunoblotting for SARS-CoV-2 Nucleocapsid Protein Detection

The Jess™ Simple Western system (ProteinSimple, San Jose CA, USA) is an automated capillary-based size separation and nano-immunoassay system. The antibody-detection of SARS-CoV-2 nucleocapsid protein was performed according to the manufacturer's standard method for 12-230-kDa Jess separation module (SM-W004), as previously described (Edouard et al., 2021). Briefly, viral proteins were mixed with 0.1X Sample buffer and Fluorescent 5X Master mix (ProteinSimple) to achieve a final concentration of 0.25 µg/µL in the presence of fluorescent molecular weight markers and 400 mM dithiothreitol. After denaturation (95°C for 5 min), the viral proteins were separated in capillaries matrix at 375 volts. A ProteinSimple photoactivated capture chemistry was used to immobilize the proteins on the capillaries and then exposed to

TABLE 1 | Primers sequences used for the RT-qPCR.

Genes	Symbols	Primers sequence	
		Sense	Antisense
E-cadherin	CDH1	5'-GAAGGTGACAGAGCCTCTGGA T-3'	5'GATCGGTTACCGTGATCAAAA T-3'
Angiotensin Conversion Enzyme 2	ACE2	5'-CAGGGAACAGGTAGAGGACAT T-3'	5'CAGAGGGTGAACATACAGTTGG-3'
Transmembrane Protease Serine 2	TMPRSS2	5'-AAGTTCATGGGCAGCAAGTG-3'	5'-ACGCCATCACACCAGTTAGA-3'
Transmembrane Protease Serine 4	TMPRSS4	5'-CAAAGTAGAGGCAGGGGAAAA -3'	5'-CGGAAAAAGTTAGGACACAG GA-3'
Neuropilin 1	NRP-1	5'-GCTGGGAAGTGTGTTGATGAC-3'	5'ACAAAGGGGAGAGGAGAGAG AG-3'
Sodium-dependent neutral amino acid transporter	B^0AT1	5'-GGTGTGTGCCAGTATGATGTTC -3'	5'AAGAGCAGGAAAAGATGAGG TG-3'
α-Disintegrin and metalloproteinase domain-containing protein 10	ADAM-10	5'-AACCTACGAATGAAGAGGGAC A-3'	5'-TGACAGAGTGAAATGGCAGA GT-3'
α-Disintegrin and metalloproteinase domain-containing protein 17	ADAM-17	5'-GCAGGACTTCTTCACTGGACAC -3'	5'-TCTACTAACCCTTTTGGGAGC A-3'
Angiotensin II Receptors 1	AT1R	5'-TGTGGACTGAACCGACTTTTCT -3'	5'-GGAACTCTCATCTCCTGTTGC T-3'
Proto-oncogene Mas	MAS1	5'-GGAGAAAGAGACACCGCATAA C-3'	5'-GTGAAGAGACAGAGAACGA GCA-3'
Proto-oncogene Mas Like	MAS1L	5'-CTGCTCCTGACTGTGATGTTGT-3'	5'-GTTTGGGTTCTGTGCCTCCT-3'
Housekeeping gene β-Actin	ACTB	5'-CATGCCATCCTGCGTCTGGA-3'	5'-CCGTGGCCATCTCTTGCTCG-3'
Platelet endothelial cell adhesion molecule	PECAM-1/ CD31	5'-CAAAGACAACCCCACTGAAGAC-3'	5'-TCCAGACTCCACCACCTTACTT-3'
Junctional adhesion molecule A/Platelet adhesion molecule 1	F11R/JAM-A	5'-GGATTTCTCAGGTCATTTGGAG-3'	5'-TAGACTGGTGGATGGTGGTAGA-3'
Connexin-43	Cx43	5'-GGTTCAAGCCTACTCAACTGCT-3'	5'-GTTTCTCTTCCTTTCGCATCAC-3'
Occludin	OCLN	5'-CTTCCATCCTGTGTTGACTTTG-3'	5'-CACTTTTCTGCCCTGATTCTTC-3'
Zonulin	HP2	5'-ATGTGAAGCAGTATGTGGGAAG-3'	5'-AGAGATTTTTAGCCGTGGTCAG-3'
Glyceradehyde-3-Phosphate dehydrogenase	GAPDH	5'-ACACCCACTCCTCCACCTTT-3'	5'-CTCTTCCTCTTGTGCTCTTGCT-3'
Beta-2 microglobulin	B2M	5'-GGTTTCATCCATCCGACATT-3'	5'-GGCAGGCATACTCATCTTTTTC-3'

antibodies. The chemiluminescent revelation was established with peroxyde/luminol-S (ProteinSimple). Digital image of chemiluminescence of the capillary was captured with Compass Simple Western software (version 4.1.0, Protein Simple) that automatically calculated chemiluminescence intensity, area, and signal/noise ratio.

Confocal Microscopy Analysis

Caco-2 cells were cultured on sterile coverslips in 24-well plates at an initial concentration of 2×10^5 cells/well before being infected with SARS-CoV-2 or HCoV-OC43 at a MOI of 0.5 for 24 hours. After fixation with paraformaldehyde (3%), the cells were permeabilized with 0.1% Triton X-100 for three minutes and saturated with 3% BSA- 0,1% Tween 20-PBS for 30 minutes at room temperature. For the primary labelling, cells were incubated for one hour at room temperature with a mix (1:1000 dilution with 3% BSA- PBS-0.3% Tween 20) of mouse monoclonal anti-E-cadherin (4A2C7, Life Technologies, France) directed against the cytoplasmic domain of E-cad and a goat polyclonal anti-ACE2 (MAB933, R&D Systems, Minneapolis, USA). The 4',6'-diamino-2-fenil-indol (DAPI) (1:2500, Life Technologies) and the Phalloidin (Alexa-488) (1:500, OZYME) were used to stain the nucleus and the filamentous actin, respectively. After washing, cells were incubated for 30 minutes at room temperature with a mix (1:1000) of goat anti-rabbit IgG (H+L) secondary antibody (Alexa Fluor 647) (Life Technologies, France) and donkey anti-goat IgG (H+L) secondary antibody (Alexa Fluor 555) (Life Technologies, France). In some experiments the cells were labeled with anti-occludin mouse mAb (Ref. 331500, Life Technologies SA).

Electron Microscopy Analysis

Virus-free cells and SARS-CoV-2 infected Caco-2 cells at 48 hours post-infection were prepared as previously described (Le Bideau et al., 2021). Briefly, cells were fixed with glutaraldehyde (2.5%) in a 0.1 M sodium cacodylate buffer. Resin embedding was microwave-assisted with a PELCO BiowavePro+. Samples were washed with a mixture of 0.2 M saccharose/0.1 M sodium cacodylate and post-fixed with 1% OsO4 diluted in 0.2 M potassium hexa-cyanoferrate (III)/0.1 M sodium cacodylate buffer. After washes with distilled water, samples were gradually dehydrated by successive baths containing 30% to 100% ethanol. Substitution with Epon resin was achieved by incubations with 25% to 100% Epon resin, and samples were placed in a polymerization chamber. Resin microwave-curing was performed for a total of two hours. After curing, the resin blocks were manually trimmed with a razor blade and dish bottoms were detached from cell monolayers by cold shock *via* immersion in liquid nitrogen for 20 seconds. Resin blocks were placed in a UC7 ultramicrotome (Leica), trimmed to pyramids, and ultrathin 100 nm sections were cut and placed on HR25 300 Mesh Copper/Rhodium grids (TAAB). Sections were contrasted with uranyl acetate and lead citrate. Grids were attached with double-side tape to a glass slide and platinum-coated at 10 mA for 20 seconds with a MC1000 sputter coater (Hitachi High-Technologies, Japan). Electron micrographs were obtained on a

SU5000 SEM (Hitachi High-Technologies, Japan) operated in high-vacuum at 7 kV accelerating voltage and observation mode (spot size 30) with BSE detector.

Animals

Animal housing and experimental procedures have been conducted according to the French and European Regulations (Parlement Européen et du Conseil du 22 Septembre 2010. Décret n°2013-118 du 1er Février 2013 relatif à la protection des animaux utilisés à des fins scientifiques) and the National Research Council (U.S.), Institute for Laboratory Animal Research (U.S.), and National Academies Press (U.S.), Eds., Guide for the care of laboratory animals, 8th ed. Washington, D.C: National Academies Press, 2011. The CIPHE BSL3 facility operates under Agreement N° B 13 014 07 delivered by the French authorities. All animal procedures (including surgery, anesthesia and euthanasia as applicable) used in the current study have been submitted to the Institutional Animal Care and Use Committee of CIPHE approved by French authorities (CETEA DSV -APAFIS#26484-2020062213431976 v6). All the CIPHE BSL3 facility operations are oversee by a Biosecurity/ Biosafety Officer and accredited by Agence Nationale de Sécurité du Médicament (ANSM). K18-hACE C57BL/6J mice (strain: 2B6.Cg-Tg (K18-ACE2)2Prlmn/J) were obtained from The Jackson Laboratory. Animals were housed in groups and fed standard chow diets.

Infection of K18-hACE2 Transgenic Mice

8-12 weeks old K18-hACE2 transgenic mice (human ACE2+), kindly provided by The Jackson laboratory, were infected with $2.5x10^4$ PFU of Wuhan/D614 SARS-CoV-2 (BetaCoV/France/ IDF0372/2020) *via* intranasal administration. Mice were monitored daily for morbidity (body weight) and mortality (survival). During the mice monitoring period, mice were scored for clinical symptoms (weight loss, eye closure, appearance of fur, posture, and respiration). Mice showing clinical scoring defined as reaching experimental end-point were humanely euthanized.

Histological Analysis

Each mouse intestine removed was fixed with buffered formalin at 4% and embedded in paraffin. Serial sections (3 µm) of these specimens were obtained for hematoxylin-phloxin-saffron staining. Briefly, the presence of intestinal lesions was determined after a complete optical examination of at least three sections of intestine tissues from each K18-hACE2 transgenic mice (n=3) using the image analyzer NDP.view2 Viewing Software UT12 388-01 (Hamamatsu, Japan).

Statistical Analysis and Correlation Analysis

Analysis of variance (ANOVA) were performed using the GraphPad-Prism software (version 6.01). Data were analyzed using a one or a two-way ANOVA with the Holm-Sidak multiple *post-hoc* test for group comparison. A p-value <0.05 was considered statistically significant. The results are presented as the mean with standard error of the mean (SEM). The data were also submitted to multivariate principal component analysis (PCA) and hierarchical clustering heatmap analysis using the ClustVis software (https://biit.cs.ut.ee/clustvis/).

RESULTS

Caco-2 Cells, a Suitable Cellular Model for Studying the *CDH1*/E-Cadherin Gene and E-Cad Proteins Expression

Our main purpose was to compare the expression of both the *CDH1* gene (encoding E-cadherin mRNA) and E-cad proteins in virus-free Caco-2 cells and SARS-CoV-2 infected Caco-2 cells. This study was carried out in order to question the ability of the virus to modulate the expression of this cell adhesion molecule known to play a central role in the integrity of intestinal cell-to-cell adherens junctions. Caco-2 cells were previously reported to be a model of human intestinal cells susceptible to SARS-CoV-2 infection and able to support the *de novo* production of viral particles. However the expression of cellular genes coding for the viral receptor/co-receptor, had not thus far been quantified in these cells. It includes: i) ACE2 allowing the binding of the viral spike (S) and entry of the virus into the cell; ii) the cellular serine proteases TMPRSS2 and TMPRSS4 reported to be required for the S glycoprotein priming; and, iii) Neuropilin-1 (NRP-1), also described as able to potentiate SARS-CoV-2 entry. As a result, before investigating the transcriptomic response of Caco-2 cells to SARS-CoV-2 infection, the first part of this study thus consisted of estimating the expression of these genes in Caco-2 cells cultured in virus-free medium. Our objective was also to confirm the physiological relevance of the Caco-2 cells cellular model by analyzing the basal expression of the *CDH1*/E-cad gene to ensure that it was sufficiently expressed in those cells to be able to quantify a possible down modulation of this gene after infection. The basal expression of other genes that could possibly be involved in cell-surface receptor mediated modulation of *CDH1*/E-cad gene was also quantified.

As shown in **Figure 1A**, the qRT-PCR analysis indicated a very high expression of *CDH1*/E-cad mRNAs in virus-free Caco-2 cells. Regarding the genes coding for the ACE2 receptor and its intestinal ligand B^0AT1, the mRNAs encoding these proteins are detectable, although their expression is relatively low. As for the expression of mRNAs encoding the TMPRSS2 and TMPRSS4 proteases, we found that the gene encoding the TMPRSS2 protein is well expressed on Caco-2 cells. In contrast, we noted an absence of detectable expression of the TMPRSS4 mRNA. Finally, there is a high expression of the NRP-1 receptor which possibly acts as a co-receptor for SARS-CoV-2 at the intestinal level.

These results were then confirmed by using confocal imaging of Caco-2 cells labeled with anti-E-cad and anti-ACE2 antibodies and phalloidine to stain the nucleus and the filamentous actin as control (**Figure 1B**). Under these experimental conditions we also observed a high expression of E-cad protein in Caco-2 cells, and the intensity of fluorescence observed with the anti-E-cad labeling was above that of anti-ACE2 labeling.

ACE2 is a peptidase known to control the hydrolysis of angiotensin II (Ang II) into Ang-(1-7), and Ang-(1-7) inhibits

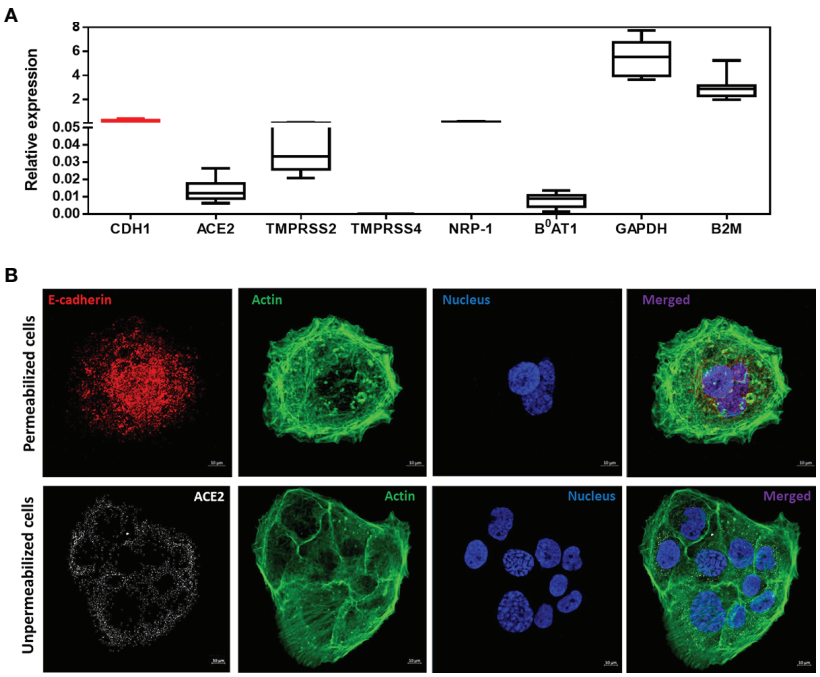

FIGURE 1 | **(A)** Expression of CDH1/E-Cad, ACE2, TMPRSS2, TMPRSS4, NRP-1, B^0AT1, GAPDH and B2M mRNA in virus-free Caco-2 cells. The results (n=8) are expressed as RE where RE = $2^{(-\Delta CT)}$. **(B)** Confocal microscope analysis of E-cad, ACE2 and actin expression on Caco-2 cells. The experiment was performed using cells permeabilized with 0.1% Triton X-100 (upper panel) and unpermeabilized cells (lower panel).

the PAK1/NF-KB/Snail 1 signaling pathway *via* activation of the MAS receptor leading to E-cad expression (Yu et al., 2016). In cell types regulated by Ang-(1-7), when the Ang-(1-7) concentration is insufficient the signaling pathway is activated and results in the inhibition of E-cad expression. To ensure that in Caco-2 cells such complex regulation does not interfere with E-Cad expression, we also investigated the expression of mRNAs coding for the Ang II and Ang-(1-7) receptors AT1R, MAS-1, and MA1-L, respectively and found that they are almost undetectable in Caco-2 cells, suggesting that they are unlikely to interfere with Caco-2 cell signaling (**Supplementary Figure 1**).

Taken as a whole, these data indicate that Caco-2 is a suitable cellular model for studying the *CDH1*/E-cadherin gene and E-cad proteins expression in intestinal epithelial cells

SARS-CoV-2 Replicates in Caco-2 Cells and Modulates ACE2 Transcription and Protein Expression

In order to confirm that the Caco-2 cells model is suitable to analyze the transcriptional response of genes of interest in intestinal epithelial cells infected with SARS-CoV-2, Caco-2 cell infection by SARS-CoV-2 has been precisely characterized. Cells were cultured either in the absence of virus (control) or in the presence of SARS-CoV-2 at a MOI of 0.5. To confirm the infection of Caco-2 cells with SARS-CoV-2, the kinetics of viral replication in Caco-2 cells exposed to SARS-CoV-2 was quantified using a qRT-PCR amplification of the SARS-CoV-2 N gene performed on cell culture supernatants of Caco-2 cells over 72h of infection (**Figure 2A**). The qRT-PCR data were considered positive when the cycle threshold (Ct) was below 30. At T=0 the Ct was 37. After 4h incubation the culture supernatants of Caco-2 cells remained negative (Ct=33.42; ΔCt=3.58) and started to be positive at 8h post-infection (Ct=28.98; ΔCt=8.02). The culture supernatants of Caco-2 cells became clearly positive at 16h post-infection with a Ct=21.02 (ΔCt=15.98) and then reached a plateau at 24h post-infection with ΔCt=17.76, ΔCt=18.86 and ΔCt=19.28 using 24h, 48h and 72h culture supernatants of SARS-CoV-2 exposed Caco-2 cells, respectively. The viral release was also estimated by the observation of the cytopathic effect (CPE) on Vero E6 cells after 7 days incubation with culture supernatants from Caco-2 cells collected at 4h, 8h, 16h, 24h, 36h, 48h and 72h after viral exposure (**Figure 2B**). The CPE was monitored under a photonic microscopy to determine the virus $TCID_{50}$. The culture supernatant from Caco-2 cells collected 4h after viral exposure gave a $TCID_{50}$ of 8.07 x 10^1/mL while the culture supernatants from Caco-2 cells collected 24h post infection gave a value of 1.39 x 10^6 $TCID_{50}$/mL. The plateau of CPE on Vero E6 cells was reached using Caco-2 cells culture supernatants collected after 24h of infection. These results were confirmed by the detection of the viral nucleocapsid using the high-speed capillary electrophoresis technologies that revealed the presence of the viral protein synthesis 24h post-infection (data not shown). Moreover, we also compared the viral receptor (ACE2) mRNA expression in virus-free Caco-2 cells and SARS-CoV-2-

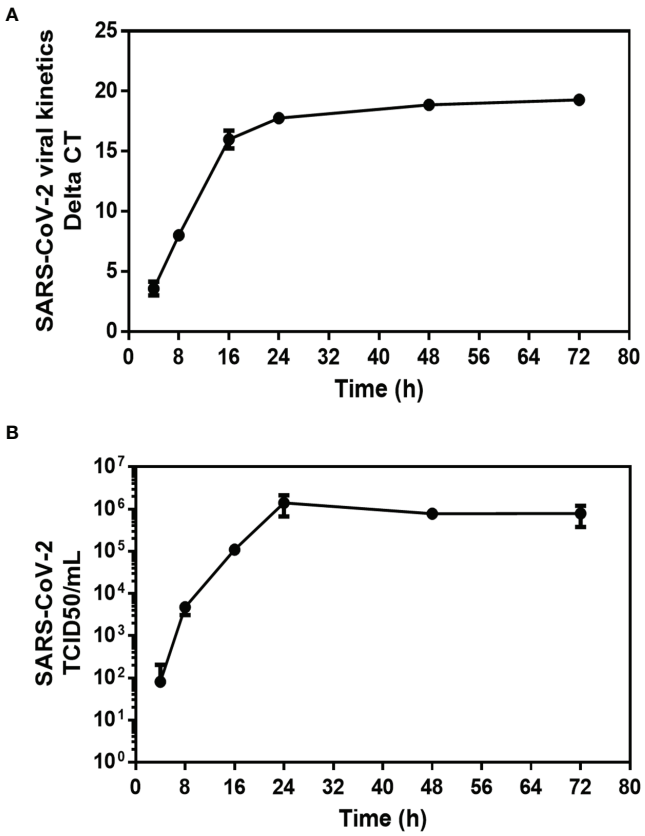

FIGURE 2 | Kinetics of SARS-CoV-2 infection in Caco-2 cells. After viral inoculation in Caco-2 cells, the viral release was monitored over 72 hours (T=0, 4h, 8h, 16h, 24h, 48h, and 72h) from the cell's supernatant. **(A)** Quantification of the viral release from Caco-2 cell by qRT-PCR: ΔCT represents the CT value obtained subtracted from the CT value at time T=0 (CT - CT_0), where T=0 is the moment immediately after removing the inoculum used in the adsorption step. Each value is the mean of triplicates **(B)** Quantification of SARS-CoV-2 infectious particles released in the supernatant of Caco-2. The $TCID_{50}$ was performed by inoculating supernatants collected from SARS-CoV-2 infected Caco-2 cells into a culture of Vero E6 cells. The cytopathic effect (CPE) was evaluated on Vero E6 cells at 7 days after exposure to Caco-2 culture supernatants. Each value is the mean of triplicates. The $TCID_{50}$/mL is calculated according to the Spearman and Kärber algorithm.

infected Caco-2 cells by qRT-PCR monitoring. We found a significantly ($p<0.001$) lower expression of the mRNA encoding ACE2 in cells infected with SARS-CoV-2 compared with SARS-CoV-2-free Caco-2 cells (**Figures 3A**). Regarding the expression of ACE2 protein it also undergoes a decrease in Caco-2 cells after exposure to SARS-CoV-2 (**Figures 3B**). This time course analysis demonstrated that the ACE2 production is markedly reduced 24 h after infection with SARS-CoV-2 and becomes almost undetectable at 48 h post-infection. This was further confirmed by a confocal microscopy analysis which highlights a significant (p-value <0.0001) down-regulation of ACE2 when Caco-2 cells were exposed to SAR-CoV-2 (**Figures 3C**). In contrast, no modulation of ACE2 expression was found when Caco-2 cells were exposed to the human betacoronavirus HCoV-OC43 that uses a different receptor (the ubiquitous HLA class I receptor, present on all human cells including intestinal cells) to enter cells. This is consistent with previous reports indicating that SARS-CoV-2 induces the modulation of its cell surface receptor ACE2 during the infection of cells.

To complete the transcriptional analysis of Caco-2 cells after SARS-CoV-2 infection, in addition to ACE2 we also performed a qRT-PCR monitoring of TMPRSS 2 and TMPRSS 4, NRP- 1 and B^0AT1. As shown in **Figure 4A**, we found that there is a significant lower expression of TMPRSS2 and NRP-1 mRNA in Caco-2 cells infected with SARS-CoV-2 compared to the basal levels of expression of these mRNAs in SARS-CoV-2-free Caco-2 cells. Finally, we also observed a lower expression of mRNAs encoding the protein B^0AT1. The comparison of pattern between SARS-CoV-2-, and HCoV-OC43-exposed Caco-2 cells indicated a difference of ACE2 and NRP-1 genes regulation by these two viruses, with a lack of ACE2 and NRP-1 mRNAs expression modulation during HCoV-OC43 infection of Caco-2 cells. Surprisingly, we observed an increased expression of mRNAs encoding the protein B^0AT1 in HCoV-OC43-exposed Caco-2 cells which is not accompanied by the modulation of ACE2 expression. According to the principal component analysis and hierarchical clustering heatmap (**Figures 4B, C**), it appears that the expression of cellular genes in virus-free conditions

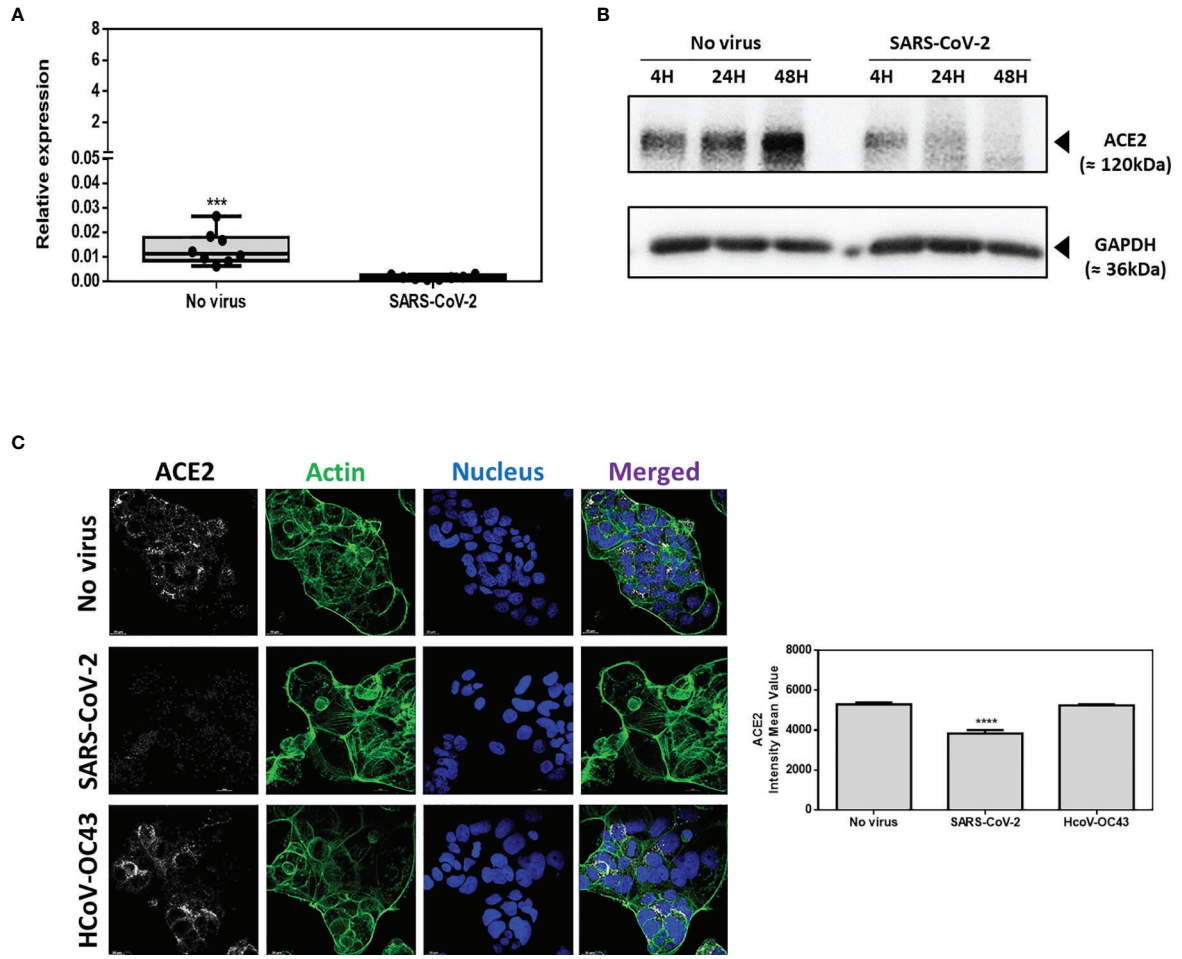

FIGURE 3 | ACE2 expression on Caco-2 cells. **(A)** ACE2 mRNA in virus-free Caco-2 cells or cells exposed for 24h to SARS-CoV-2 or HCoV-OC43 at MOI of 0.5. The results are expressed as RE where RE = $2^{(-\Delta CT)}$. **(B)** Time course (4h, 24h, 48h) Western blot analysis of ACE2 proteins expression in virus-free Caco-2 cells or cells exposed to SARS-CoV-2 at an MOI of 0.5. **(C)** Illustration of single plane confocal microscope analysis of ACE2 expression on Caco-2 virus-free cells or cells exposed for 24h to SARS-CoV-2 or HCoV-OC43 at MOI of 0.5. The analysis was performed on unpermeabilized cells. Actin expression was shown as control as well as the labeling of the nucleus (left panel). Quantitative representation (n=4) of mean fluorescence intensity corresponding to ACE2 protein expression on Caco-2 cells infected or not with SARS-CoV-2 or HCoV-OC43 (right panel). The symbol ****means a p-value < 0.0001; The symbol *** means a p-value <0.001.

segregated differently from the conditions with SARS-CoV-2-, and HCoV-OC43-exposed Caco-2 cells.

Modulation of CDH1/E-Cad Expression by SARS-CoV-2 in Caco-2 Cells

Then, we studied the effects of SARS-CoV-2 infection on CDH1/E-cad gene expression. We performed a qRT-PCR monitoring of the CDH1/E-cad mRNA expression in virus-free Caco-2 cells and SARS-CoV-2-infected Caco-2 cells. The qRT-PCR analysis (**Figure 5A**) revealed a significantly ($p<0.001$) lower expression of the mRNA encoding E-cad in cells infected with SARS-CoV-2 compared with SARS-CoV-2-free Caco-2 cells. To confirm this result, confocal immunofluorescence analysis was performed. As shown in **Figures 5B, C**, a significantly ($p<0.0001$) lower expression of E-cad was observed in SARS-CoV-2 infected cells when compared to virus-free Caco-2 cells. As an additional control, we performed similar experiments in the presence of HCoV-OC43, which does not depends on ACE2 interaction to infect cells. No decrease in E-cad protein expression was observed in Caco-2 cells exposed to HCoV-OC43.

Increased Release of Soluble E-Cad in the Culture Supernatant of SARS-CoV-2-Infected Caco-2 Cells

Due to the observed modulation of E-cad expression in cells infected with SARS-CoV-2, we wanted to study the possible over-release of sE-cad in the cell culture supernatant of Caco-2 infected with the virus. In several infection processes initiated in the GIT lumen, a soluble form of E-cad, sE-cad is released from the cell membrane after cleavage of the integral protein by sheddases, thereby disrupting the intercellular junctions required for epithelial cell barrier stability (e.g., this leads to

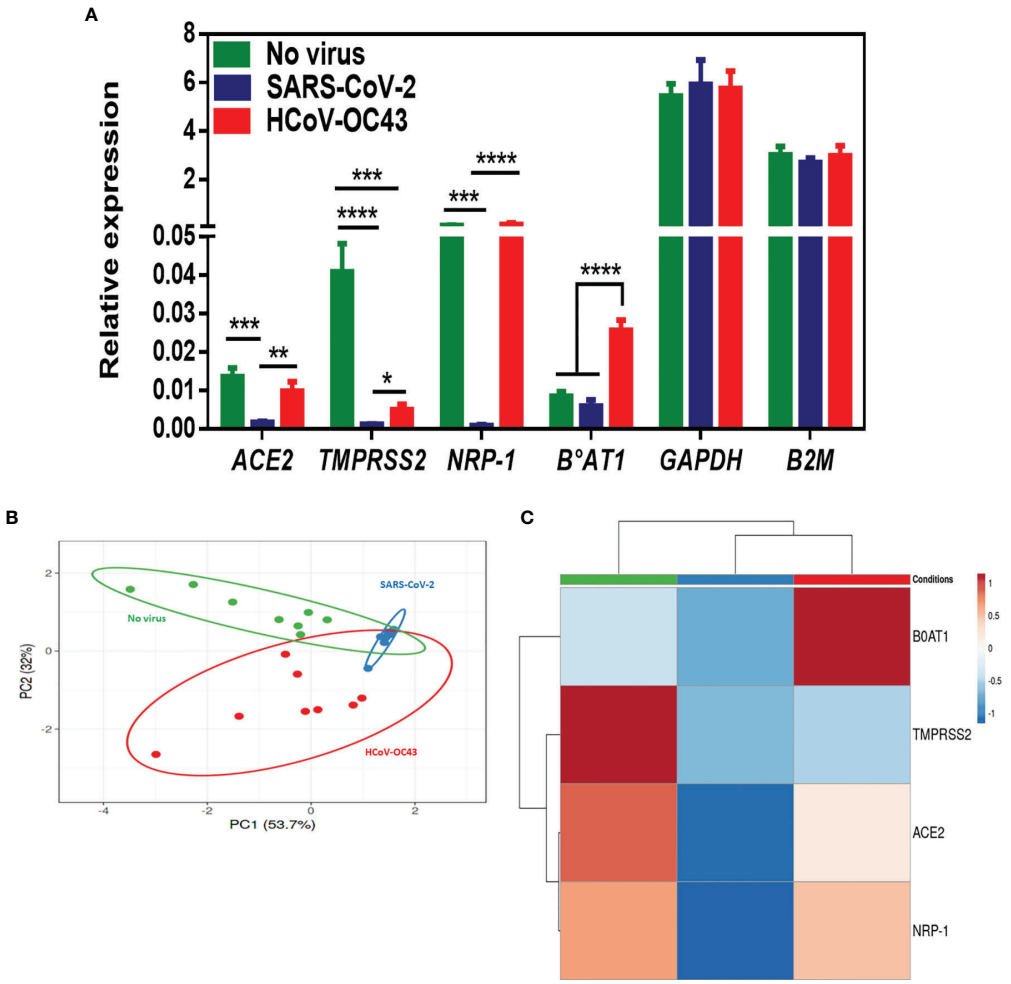

FIGURE 4 | **(A)** mRNA expression of ACE2, TMPRSS2, NRP-1, B^0AT1, GAPDH, and B2M in virus-free Caco-2 cells or cells exposed to coronaviruses SARS-CoV-2 or HCoV-OC43 at a MOI of 0.5 for 24 hours. The results (n=8) are expressed as RE where RE = $2^{(-\Delta CT)}$. **(B, C)** PCA and hierarchical clustering heatmap analysis of different molecules expressed on Caco-2 cells in virus-free cells, and cells exposed to coronaviruses SARS-CoV-2 or HCoV-43. The symbol *** means a p-value < 0.001; the symbol **** means a p-value < 0.0001.

pathogen transmigration). The concentration of sE-cad in cell culture supernatant (which naturally increase with time in cell culture) was measured using an ELISA (**Figure 6A**). We notice a significant ($p<0.01$) increase in sE-cad release in Caco-2 cells infected with SARS-CoV-2 at 48 h post-infection (mean value: 1274.65pg/mL), compared to the virus-free cell control (mean value: 961.42pg/mL). In contrast, we found no increase in sE-cad release in Caco-2 cells infected by HCoV-OC43 control (mean value: 944.92pg/mL). These results were confirmed by Western Blot on which we observed a significant ($p<0.05$) decrease in the amounts of the 120 kDa E-cad in the condition of infection with SARS-CoV-2 compared to virus-free cells and Caco-2 cells exposed to HCoV-OC43 (**Figures 6B, C**).

In order to verify whether this effect of SARS-CoV-2 on the expression of E-cad adherens junctions proteins is specific to the Caco-2 cell line or more generally affects the cells of the intestinal epithelium, the experiment was reproduced using the mucin-producing human colorectal adenocarcinoma HT29 cell line. Using qRT-PCR for phenotyping of genes expression in virus-free HT29 cells we found that expression of ACE2 and B^0AT1 were very low, while TMPRSS2, NRP-1 and *CDH1*/E-cad were highly expressed in these cells (**Figure 7A**). Although the basal level of expression of the *CDH1*/E-cad gene remained quite stable in HT29 cells exposed to SARS-CoV-2 (**Figure 7B**) and viral release was too low to be quantifiable in the culture supernatants of HT29 cells while SARS-CoV-2 proteins can be detected in these cells using high speed capillary electrophoresis (**Supplementary Figure 2**), a significantly ($p<0.05$) higher release of sE-cad in the supernatant of HT29 cells exposed to SARS-CoV-2 was also found when compared to the uninfected control. In those cells, HCoV-OC43 also induced sE-cad release (**Figure 7C**).

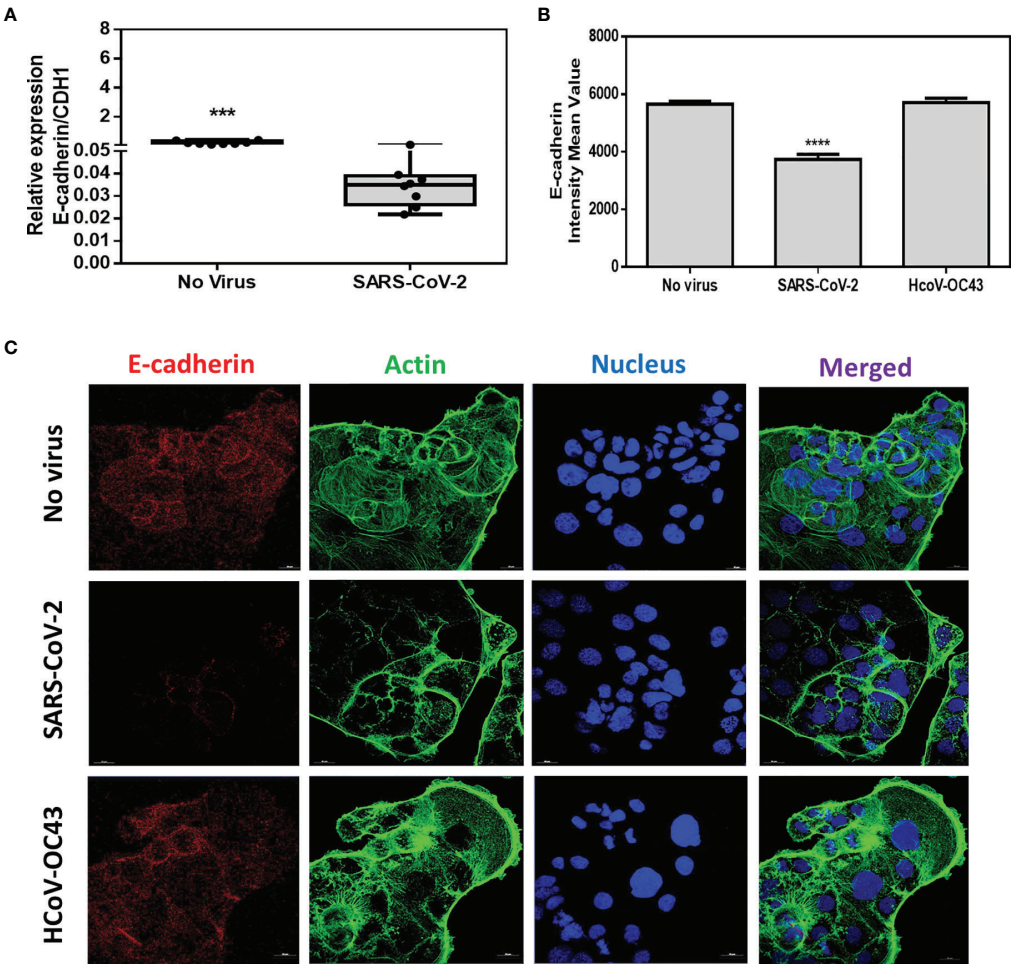

FIGURE 5 | Expression of CDH1/E-cad mRNA and E-cad protein. **(A)** Expression of CDH1/E-cad mRNA in virus-free Caco-2 cells or cells exposed to SARS-CoV-2 at an MOI of 0.5 for 24 hours. The results (n=8) are expressed as RE where RE = $2^{(-\Delta CT)}$.The symbol *** means a p-value < 0.001. **(B)** Quantitative representation of mean fluorescence intensity (n=4) corresponding to E-cad protein expression on Caco-2 cells infected or not with SARS-CoV-2 or HCoV-OC43. The symbol the symbol ****means a p-value < 0.0001. **(C)** Illustration of single plane confocal microscope analysis of E-cad expression on subconfluent virus-free Caco-2 cells or cells exposed to coronaviruses SARS-CoV-2 or HCoV-43 at an MOI of 0.5 for 24 hours. The analysis was performed on cells permeabilized with 0.1% Triton X-100. Actin expression was shown as control as well as the labeling of the nucleus.

Probable Involvement of Human Sheddases in SARS-CoV-2-Induced Release of Soluble E-Cad From Caco-2 Cells

Several sheddases have been reported able to lead to sE-cad release from cells during infectious processes resulting in intestinal tissues damages (Devaux et al., 2019). This is why we postulated that cellular sheddases could be induced to cleave E-cad in SARS-CoV-2 infected cells (the best known candidate to achieve cleavage of E-cad in the intestinal tract being ADAM-10, while ADAM-17, another member of the same family of proteases, is known to cleave ACE2), and compared the expression of ADAM-10 and ADAM-17 genes in Caco-2 cells following viral infection with their expression in virus-free cells. This experiment revealed a significantly ($p < 0.0001$) lower expression of ADAM-10 as well as ADAM-17 ($p<0.01$) sheddases in Caco-2 cells infected with SARS-CoV-2 (**Figure 8**). Expression of these sheddases was also reduced in HCoV-OC43 infected cells. Similar experiments were performed using other cellular sheddases, including ADAM-8, ADAM-15, MMP-3, MMP-9, MMP-12 and HtrA1. We found that the expression of most of these sheddases is lower in Caco-2 cells infected by SARS-CoV-2, although the expression of ADAM-15 expression was not modulated after SARS-CoV-2 infection (data not shown). The possible association between SARS-CoV-2 infection, sE-cad release, and the expression of sheddases remains to be further investigated in order to identify the sheddase(s) responsible for the cleavage of the membrane E-cad during SARS-CoV-2 infection of intestinal epithelial cells.

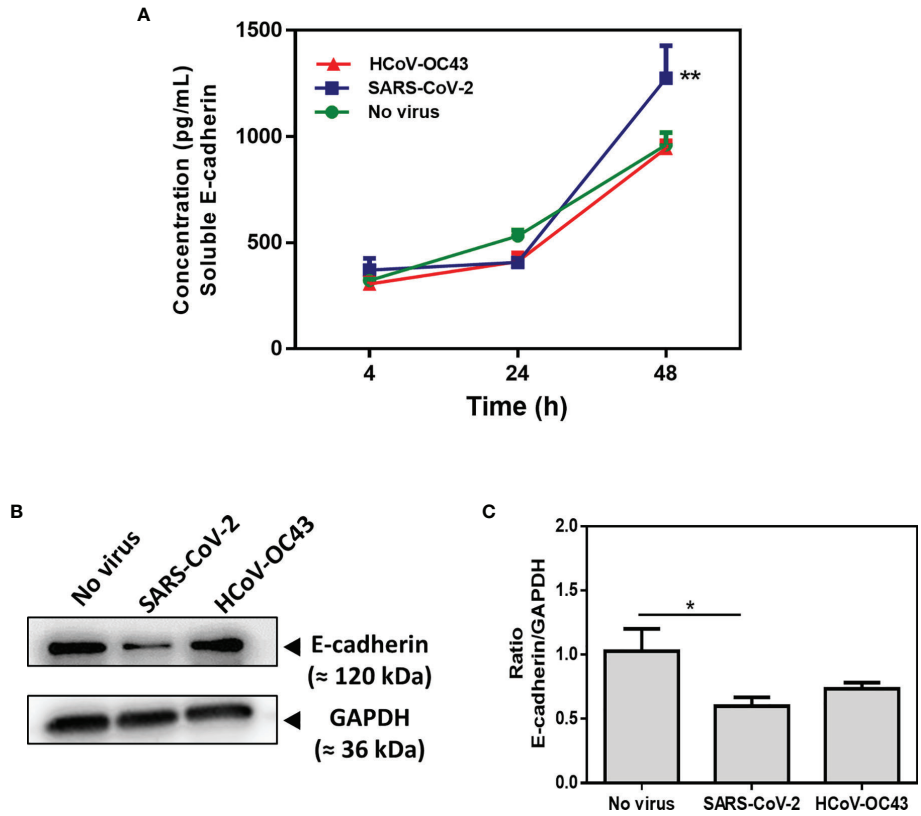

FIGURE 6 | Expression of E-cad and sE-cad. in Caco-2 cells. **(A)** Quantification of sE-cad (n=4) in the cell-culture supernatant of virus-free Caco-2 cells and cells exposed to coronaviruses SARS-CoV-2 or HCoV-OC43 at an MOI of 0.5 for 4 hours, 24 hours and 48 hours respectively, using antigen-specific ELISA. The results are the average of quadruplicates. **(B)** Western blot analysis of E-cad expression in virus-free Caco-2 cells and cells exposed for 48h to SARS-CoV-2 or HCoV-OC43 coronaviruses. GAPDH was used as loading control. **(C)** Quantitative representation of E-cad protein expression by Caco-2 cells infected or not with SARS-CoV-2 or HCoV-OC43 normalized with respect to GAPDH. The Image J program was used to quantify the Western blot bands intensity. The symbol ** means a p-value < 0.01. The symbol * means a p-value < 0.05.

Effect of SARS-CoV-2 Infection on Expression by Caco-2 Cells of Molecules Involved in Tight Junctions and Gap Junctions

E-cad is a major component of the so-called adherens junctions. In order to investigate whether SARS-CoV-2 triggers specific modulation of E-cad or more widely affects molecules required to maintain junctions between neighboring epithelial cells, we investigated the result of SARS-CoV-2 infection of Caco-2 cells on molecules (occludin, zonulin and connexin-43), involved in tight junctions or gap junctions. Intestinal epithelial cells express four types of junctional proteins that bind the cells together (Meenan et al., 1996; Chelakkot et al., 2018) and consist of: i) occluding junctions (zonula occludens or tight junctions), generated by the assembly of multiple integral transmembrane proteins (occludin, claudins, junctional adhesion molecule/JAM, and tricellulin) located near the apical part of the epithelium between neighboring cells (they maintain intestinal barrier function and control cell polarity and the permeability of the paracellular transport pathway) and peripheral membrane adaptor proteins (zonula occludens ZO-1, ZO-2, and ZO-3) acting as bridges to connect integral membrane proteins to the actin cytoskeleton; ii) adhering junctions (zonula adherens) which lies below the tight junction are composed of cadherins (E-cad) from adjacent cells that act to 'zipper' up together the gap between two adjacent cells playing a role in the morphogenesis of epithelial cells; iii) desmosomes (macula adherens) that lie on the basal membrane, to help stick the cells to the underlying basal lamina and involve keratin the function of which is to withstand abrasion; and, iv) gap junctions that are communicating junctions (also known as nexus) involving a group of proteins called connexins which form a continuous channel between adjacent cells. In addition, another cell adhesion protein, PECAM, is expressed in the basolateral epithelial membrane and is involved in the migration of leucocytes across the connective tissues.

We performed a qRT-PCR for monitoring the expression of *OCLN* gene encoding the occludin mRNA, *F11R* gene encoding the JAM-A mRNA, and the *Cx43* gene encoding the connexin-43 as well as *HP2* encoding zonulin and *PECAM1* encoding

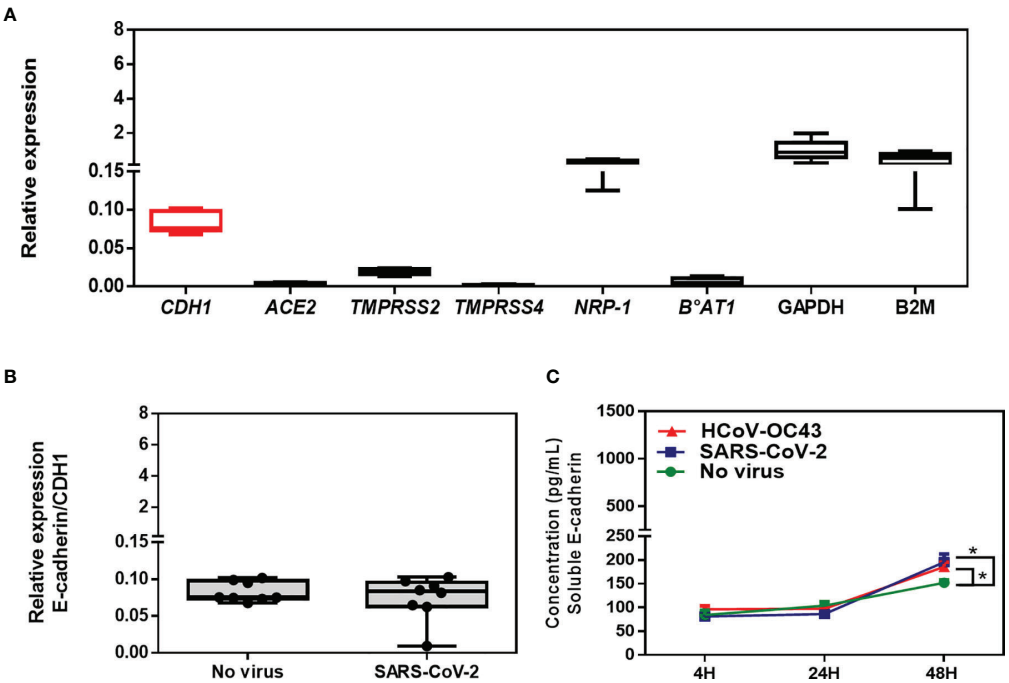

FIGURE 7 | **(A)** Expression of CDH1/E-Cad, ACE2, TMPRSS2, TMPRSS4, NRP-1, B^0AT1, GAPDH, and B2M mRNA in virus-free HT29 cells. The results (n=8) are expressed as RE where RE = $2^{(-\Delta CT)}$. **(B)** Expression of CDH1/E-cad mRNA in virus-free HT29 cells or cells exposed to SARS-CoV-2 at an MOI of 0.5 for 24 hours. **(C)** Quantification of sE-cad (n=4) in the cell-culture supernatant of virus-free HT29 cells and cells exposed to coronaviruses SARS-CoV-2 or HCoV-43 at an MOI of 0.5 for 4 hours, 24 hours and 48 hours respectively, using antigen-specific ELISA. The symbol * means a p-value < 0.05.

PECAM/CD31. We found that *OCLN*, and *F11R* genes encoding tight junctions molecules are highly expressed in Caco-2 cells while the *PECAM1*, *HP2*, and *Cx43* are poorly expressed in this cell line. Then, the mRNA expression of the different cell adhesion molecules was evaluated in the presence or absence of SARS-CoV-2 infection. As shown in **Figure 9A**, the expression of *OCLN* and *F11R* genes expression was found significantly lower in Caco-2 cells infected with SARS-CoV-2 compared to the basal levels of expression of these mRNAs in SARS-CoV-2-free Caco-2 cells. The expression of the Cx-43 gene was apparently also reduced (but it was not statistically significant) while the expression of the other genes tested remained stable. Moreover, we studied the expression of the corresponding proteins by western blot analysis. As shown in **Figures 9B**, the expression of JAM-A and occludin was apparently reduced in SARS-CoV-2 infected cells (but it was not statistically significant) when compared to virus-free Caco-2 cells, indicating that the SARS-CoV-2 infection dysregulates the expression of molecules required for the integrity of tight junctions. This result was further confirmed by confocal microscopy analysis of occludin expression in SARS-CoV-2 infected Caco-2 cells (**Figure 9C**). Under such experimental conditions we found a significant ($p<0.0001$) down-regulation of occludin. In Caco-2 cells, the expression of connexin-43 (gap junctions) was significantly ($p<0.05$) down-regulated by the SARS-CoV-2 infection. Interestingly, a significant ($p<0.05$) increase in zonulin was also observed in SARS-CoV-2 infected Caco-2 cells, suggesting increased GIT permeability during infection. Altogether, these data indicate that SARS-CoV-2 infection not only dysregulates the expression of E-cad required for adherens junctions but also affects several other molecules involved in intercellular adhesion. This is consistent with the observation that 48 hours post-infection with SARS-CoV-2, viral particles can be observed in the intercellular space of adjacent Caco-2 cells by scanning electron microscopy

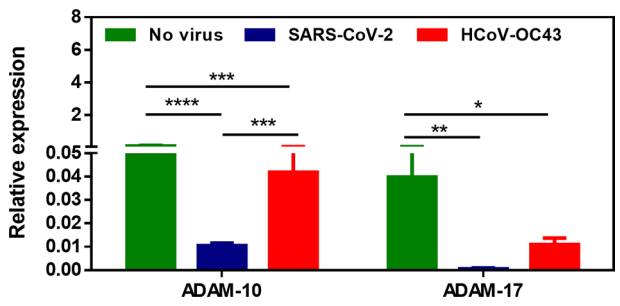

FIGURE 8 | Expression of ADAM-10 and ADAM-17 sheddases mRNA in virus-free Caco-2 cells or cells exposed to SARS-CoV-2 or HCoV-OC43 coronaviruses at an MOI of 0.5 for 24 hours. The results (n=8) are expressed as RE where RE = $2^{(-\Delta CT)}$. The symbol * means a p-value < 0.05; the symbol ** means a p-value < 0.01; the symbol *** means a p-value < 0.001; the symbol **** means a p-value < 0.0001.

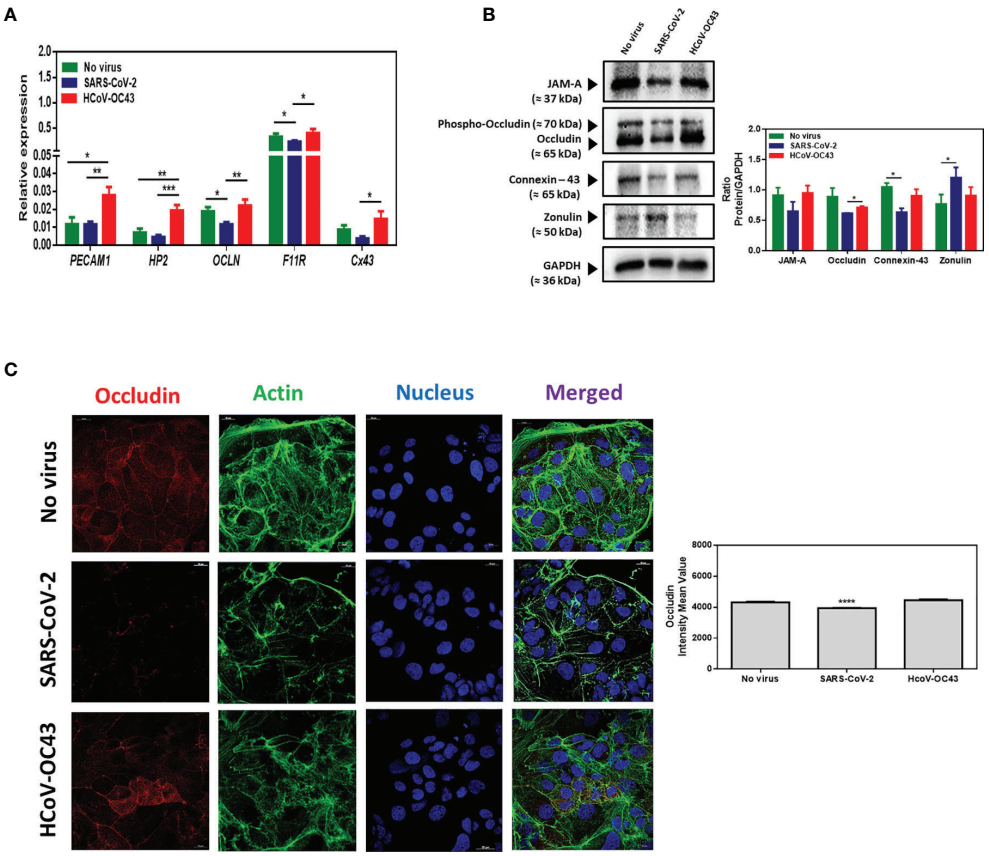

FIGURE 9 | **(A)** mRNA expression of PECAM1, HP2, OCLN, F11R and Cx43, in virus-free Caco-2 cells or cells exposed to coronaviruses SARS-CoV-2 or HCoV-OC43 at a MOI of 0.5 for 24 hours. The results (n=8) are expressed as RE where RE = $2^{(-\Delta CT)}$ **(B)** Western blot analysis (left panel) of JAM-A, occludin, connexin-43, and zonulin expression in virus-free Caco-2 cells and cells exposed for 48h to SARS-CoV-2 or HCoV-43 coronaviruses. GAPDH was used as loading control. The quantitative representation (Image J program) of these proteins expression is also illustrated (right panel). **(C)** Illustration of single plane confocal microscope analysis of occludin expression on subconfluent Caco-2 cells grown in RPMI1640 supplemented with 4% FCS only or exposed to coronaviruses SARS-CoV-2 or HCoV-43 at an MOI of 0.5 for 24 hours (left panel). The analysis was performed on unpermeabilized cells. Actin expression was shown as control as well as the labeling of the nucleus. A quantitative representation of mean fluorescence intensity corresponding to occludin protein expression on Caco-2 cells infected or not with SARS-CoV-2 or HCoV-OC43 is shown (right panel). The symbol * means a p-value < 0.05; ** means a p-value < 0.01; *** means a p-value < 0.001; **** means a p-value < 0.0001.

(**Figure 10**). Moreover, lysed cells containing SARS-CoV-2 particles are seen detached from the monolayer. Yet, membranous cell-cell contacts such as tight junctions are still found at contact zones between subsets of detaching cells and cells remaining intact within the monolayer, and desmosomes can be clearly depicted between intact cells in the monolayer.

SARS-CoV-2 Infection in Human ACE2 Transgenic Mice Leads to Intestinal Tissues Damage

Based on our *in vitro* data, we hypothesized that SARS-CoV-2-infected mice may exhibit virus-induced histological lesions. To this end, 8-12 weeks old K18-hACE2 transgenic mice were infected *via* intranasal administration of SARS-CoV-2 and maintained in solitary confinement in a BSL3 animal facilities. Mice with clinical symptoms (weight loss, eye closure, appearance of fur, prostrate posture, and difficulty of breathing) were humanely euthanized and intestine sample were collected. As shown in **Figure 11**, hematoxylin-phloxin-saffron staining to sections of intestine from the virus-free mice showed a normal tissue architecture while sections of intestine from K18-hACE2 transgenic mice infected *via* intranasal administration of SARS-CoV-2 showed a necrotizing enteritis, with sloughing and disruption of the normal architecture, necrosis of the lamina propria of intestinal villi with edema and leukocytic infiltration. These *in vivo* observations are consistent with the dysregulation of intercellular tight junctions, adherens junctions, and gap junctions leading to intestinal permeability.

DISCUSSION

In this study, we demonstrate that SARS-CoV-2 infection of non/low-mucus producing human colorectal adenocarcinoma

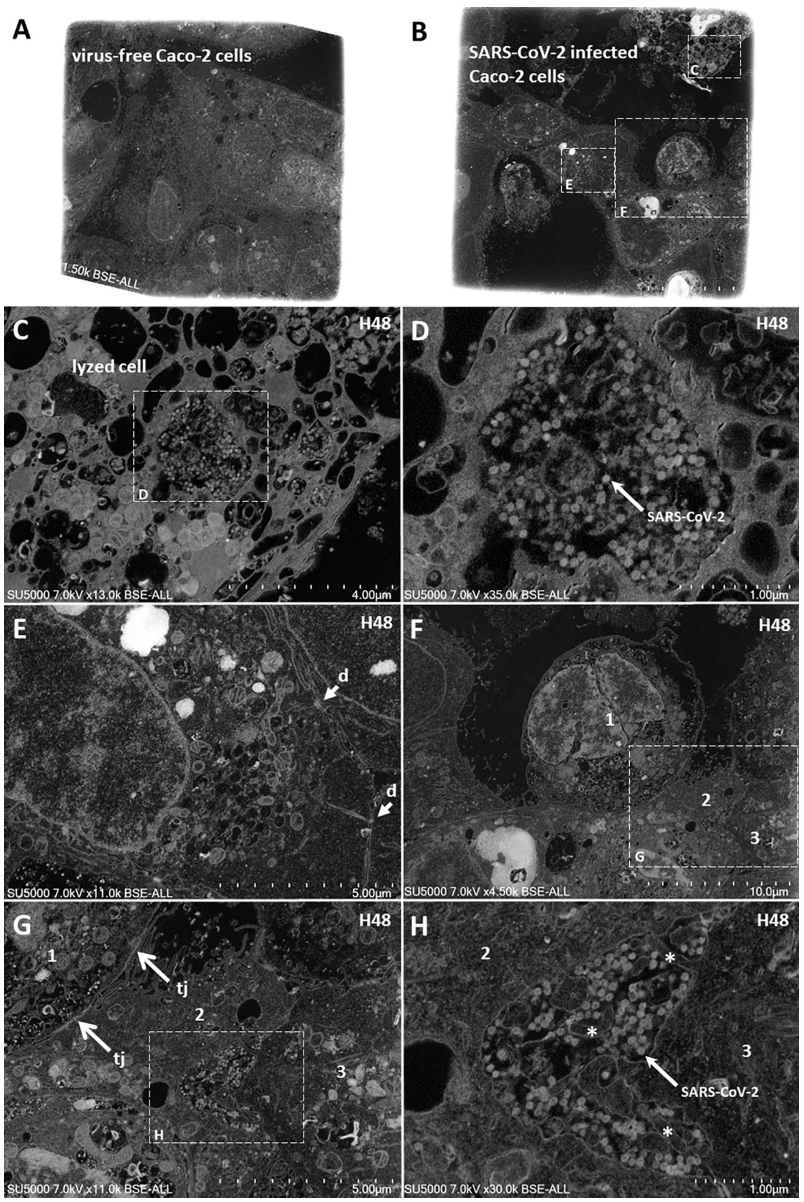

FIGURE 10 | Scanning electron microscopy of SARS-CoV-2 infected Caco-2 cells. **(A, B)** Low-magnification images of virus-free Caco-2 cells monolayer at 0 hours-post-infection (H0; **A**) and SARS-CoV-2 infected Caco-2 cells monolayer at 48 hours-post-infection (H48; **B**). **(C)** Zoom-in boxed region from **(B)** with a lysed cell detached from the cell monolayer. **(D)** Zoom-in boxed region in lysed cell **(C)** with Sars-CoV-2 particles. **(E)** Intact stitched cells from the monolayer with presence of desmosomes (d; arrows) at cell-cell membranous contacts. **(F)** a cell (1) at the center, partially detached from surrounding cells. **(G)** partially detached cell (1) contacting cell (2) *via* tight junctions (tj; arrows). **(H)** Sars-CoV-2 particles located in the monolayer between intact cells (2) and (3), with presence of microvilli (asterisks).

Caco-2 cells (Navabi et al., 2013) results in the modulation of the *CDH1* gene encoding the E-cad adhesion molecule as well as several other genes, including the gene encoding the virus receptor, ACE2. This modulation in the expression of *CDH1*/E-cad is accompanied by a lower surface expression of the E-cad protein and by a significant increase in the release of sE-cad into the culture medium. Our data corroborate the observations recently published by Guo and colleagues (Guo et al., 2021) who reported that SARS-CoV-2 infection of a microengineered gut-on-chip 3-D model mimicking the intestinal epithelium-vascular endothelium barrier by co-culture of Caco-2 cells, HT29 cells, and vascular endothelial cells under physiological fluid flow, showed permissiveness for viral infection, morphological changes with injury of intestinal villi, dispersed distribution of mucus-secreting cells, and reduced expression of E-cad, indicating the destruction of the intestinal barrier integrity. Using the mucin-secreting human colorectal adenocarcinoma HT29 cell line (Hanski et al., 1992; Niv et al., 1995), we also

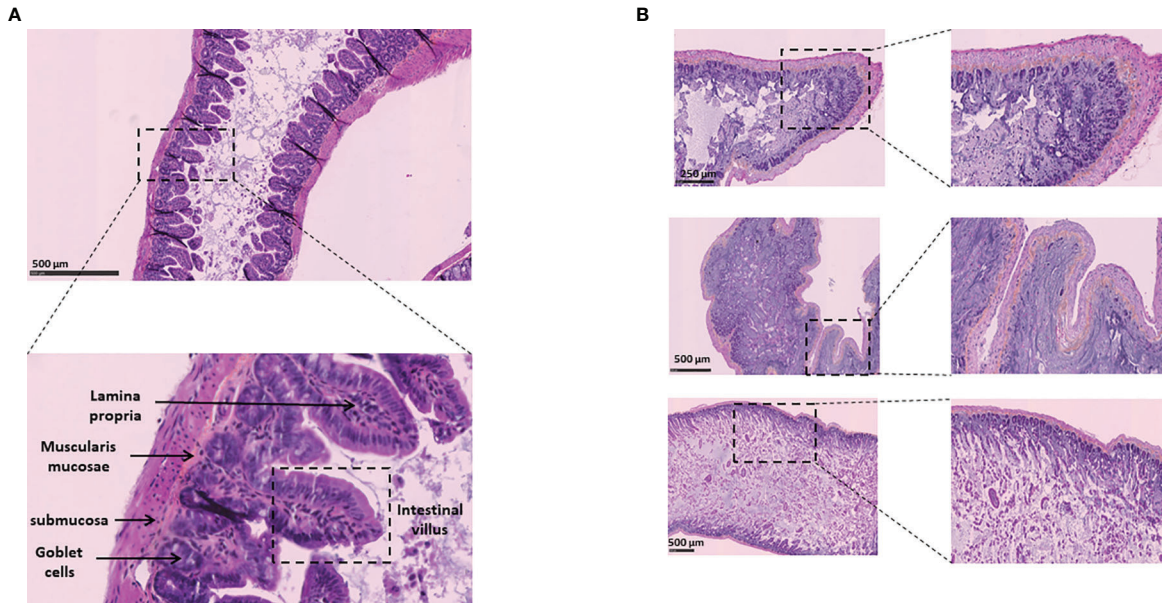

FIGURE 11 | Histological analysis of intestinal tissues from K18-hACE2 transgenic mice (virus free) and K18-hACE2 transgenic mice infected *via* intranasal administration of SARS-CoV-2. **(A)** Normal intestinal wall from control K18-hACE2 transgenic mouse (hematoxylin-phloxin-saffron staining). **(B)** Section of intestine from K18-hACE2 transgenic mouse infected with SARS-CoV-2. The upper, middle and lower panels correspond to samples from 3 different mice. Note the extensive necrosis and inflammation of the lamina propria of intestinal villi with degeneration of intestinal epithelial cells in the intestinal lumen.

confirmed a significantly increased release of sE-cad from these cells after exposure to SARS-CoV-2. However there was a lack of detectable viral production from HT29 cells exposed to SARS-CoV-2. This lack of viral production was unlikely to be due to the low expression of ACE2 at the surface of these cells and/or the expression of membrane-associated mucins reported to exhibit potent anti-SARS-CoV-2 activity (Rebendenne et al., 2021), since we find detectable viral proteins inside the cells by western blot analysis. It may be due to the existence of an unknown intracellular restriction factor (e.g. ATP8B1 flippase mutation) (Rebendenne et al., 2021), that remains to be identified. This corroborate previous observations reported by our laboratory indicating that HT29 cells, in contrast to Caco-2 cells, are poorly susceptible to SARS-CoV-2 replication and do not sustain viral production (Wurtz et al., 2021). The SARS-CoV-2-induced CDH1/E-cad gene down-modulation and E-cad protein expression was also recently reported in two human mammary epithelial cell lines (MCF10A and MCF12A) transduced with the human ACE2 (Lai et al., 2021).

In addition to the dysregulation of E-cad expression, we also found that SARS-CoV-2 infection of Caco-2 cells affects the expression of molecules involved in tight junctions (JAM-A and occludin) and gap junctions (connexin), suggesting a drastic effect on most or all molecules intended to maintain the integrity of the intercellular junctions between intestinal epithelial cells. We also found that SARS-CoV-2 infection of Caco-2 cells leads to an increased expression of zonulin. Zonulin is overexpressed in tissues and sera of subjects with intestinal permeability (Tripathi et al., 2009; Fasano, 2011). Our data also corroborate the observations recently published by Lai and colleagues (Lai et al., 2021) who reported that SARS-CoV-2 infection of ACE2-transduced human mammary epithelial cell lines is associated to loss of epithelial markers (E-cadherin and ZO-1) and gain of mesenchymal markers (N-cadherin, vimentin, and fibronectin). These results support the hypothesis that in COVID-19 patients shedding SARS-CoV-2 in stools, the virus is likely able to destroy the intercellular junctions insured by E-cad and other cell adhesion molecules thereby creating epithelium micro-damage allowing the transmigration of pathogens. The cleavage of E-cad will also result in the deregulation of the antiviral immune response. If later proven *in vivo*, this hypothesis that considers early intestinal infectious foci, could explain why some COVID-19 patients may show intestinal disorders that precede lung disorders. Interestingly, Raghavan and colleagues (Raghavan et al., 2021) very recently reported that a recombinant SARS-CoV-2 spike protein S1 induces the degradation of junctional proteins (VE-cadherin, JAM-A, Connexin-43 and PECAM-1) that maintain endothelial barrier integrity. This result corroborates and strengthen our present data. Moreover, in severe COVID-19 patients the plasma levels of adhesion molecules such as intercellular adhesion molecule 1 (I-CAM-1), vascular cell adhesion molecule-1 (VCAM-1), vascular adhesion protein-1 (VAP-1), were reported to be elevated (Tong et al., 2020; Escher et al., 2020). In addition, it was recently reported SARS-CoV-2 E protein can interfere with control of cell polarity and cell-cell junction integrity in human epithelial cells by binding to the PALS1 PDZ domain (Javorsky et al., 2021). In addition, the integrity of the GIT epithelium is controlled by the homotypic interaction of E-cad between adjacent cells. It was also recently

suggested that the SARS-CoV-2 ORF7b interfere with important cellular processes that involve leucine-zipper formation such as the transmembrane leucine zipper dependent dimerization of E-cad (Fogeron et al., 2021).

CDH1 gene modulation (e.g., by methylation of the *CDH1* gene), aberrant splicing of the E-cad transcript (e.g., premature termination codon mutation), and E-cad degradation (e.g., by enhancing ADAM-10 sheddase activity), counts among the mechanisms used by several pathogens to achieve tissue invasion and transmigration through epithelial cell barriers (reviewed in Devaux et al., 2019). Although our results were obtained using a model of a GIT epithelial cell line (a human colorectal adenocarcinoma) rather than a polarized monolayer of human intestinal epithelial cells, they suggest that in COVID-19 patients the dissemination of SARS-CoV-2 could trigger damage to the intestinal epithelium barrier thereby favouring the spread of the virus to other tissues (e.g., pulmonary tissues). Moreover, a lower expression of E-cad at the site of infection, could interfere with the homing of immune cells and could trigger their rerouting far from the infection site (Reyat et al., 2017). The release of sE-cad could also serve as a decoy for diverting immune cells expressing E-cad, CD103 or KLRG1 from their function (e.g., KLRG1+ CD8+ T-cells subpopulation) after engagement of such receptors with sE-cad (Streeck et al., 2011). The modulation of E-cad expression on the host epithelial cells and sE-cad release could therefore be considered as a very efficient stratagem to prevent the immune system being activated against SARS-CoV-2. It may also contribute to triggering modulation in the diversity of bacterial species present in the GIT (Dhar and Mohanty, 2020; Gu S. et al., 2020; Gu J. et al., 2020; Zuo et al., 2020), this SARS-CoV-2-associated dysbiosis being responsible for the GIT syndrome observed in COVID-19 patients.

Recently we quantified the replication of different SARS-CoV-2 isolates namely B, B.1.416, B.1.367, B.1.1.7 (Alpha), B.1.351 (Beta), B.1.617.2 (Delta), P.1 (Gama), A.27 and B.1.160 in three different cell lines including Caco-2. Although the genotypes B.1.1.7 and B.1.351 (which are considered to be variants of concern, VOC), presented lower replication capacities in Calu-3 cells compared to the virus from lineages B or B.1.160, we found that the different viral isolates replicate similarly in Caco-2 cells (Pires de Souza et al., 2022). To enter susceptible cells, SARS-CoV-2 binds to ACE2. ACE2 initially is known to allow the conversion of angiotensin II (Ang II) into angiotensin-(1-7) hereafter Ang-(1-7) (reviewed in Devaux et al., 2020). Ang II could induce store-operated calcium entry (SOCE) (Guo et al., 2021). Under physiological conditions when the Ang II peptide is hydrolyzed by ACE2 into Ang-(1-7), the Ang-(1-7) binds to the MAS receptor (a G-protein-coupled receptor well known to be expressed in the kidney, adrenals and vascular system cells among others), leading to the inhibition of the PAK1/NF-KB/Snail 1 signaling pathway that can otherwise be activated by SOCE. In the absence of Ang-(1-7), this signaling cascade is activated and results in the inhibition of E-cad expression (Yu et al., 2016). In light of these data, we postulated that SARS-CoV-2-mediated reduction of ACE2 peptidase activity (either by reduction of ACE2 mRNA expression, or by blocking the peptidase function of ACE2), is very likely to be accompanied by a down-regulation of E-cad surface expression. In our model of Caco-2 cells, we tested the expression of gene coding for AT1R (the Ang II receptor), MAS1 and MA1-L (the Ang-(1-7) receptor) (**Supplementary Figure 1**). We found a detectable but very low expression of AT1R and MA1-L mRNA in Caco-2 cells, while MAS1 was not detected. In addition, our experiments were performed in the absence of Ang II and Ang-(1-7) adjunction to the cell culture medium, therefore if the PAK1/NF-KB/Snail 1 signaling pathway does play a role in the down regulation of E-cad by SARS-CoV-2 in Caco-2 cells, the regulation could be downstream of AT1R and MAS1/MA1-L. Yet, cell-surface molecules such as AT1R and ACE2 are interconnected. Recently, we reported evidence that engagement of AT1R with angiotensin II receptor blockers triggers higher cell-surface expression of ACE2 and enhance SARS-CoV-2 replication (Pires de Souza et al., 2021). Moreover, although we recently reported that ACE2 gene expression and ACE2 peptidase activity is reduced in COVID-19 patients with the accumulation of Ang II, their plasma concentrations of Ang-(1-7) remain stable, likely *via* Ang-(1-7) production through the alternative NEP/TOP pathway (Osman et al., 2021). This suggests that in COVID-19 patients, the Ang-(1-7)/MASR is expected to keep the PAK1/NF-KB/Snail 1 signaling pathway under inhibition. However, it was recently reported *in vitro* that SARS-CoV-2 spike induces breast cancer metastasis (epithelial mesenchymal transition) through activation of NF-KB/Snail and that knockdown of Snail by lentiviral-based shRNA (shSnail-1) leads to E-cad expression rescue (Lai et al., 2021).

In parallel with the Ang-(1-7)/MASR axis, it remains possible that the E-cad inhibition observed in SARS-CoV-2-infected Caco-2 can be completed either by signal transduction leading to *CDH1* gene down-regulation through ACE2 after SARS-CoV-2-binding to its cellular receptor, or by activation of sheddases able to cleave the membrane E-cad. E-cad is a transmembrane protein containing five extracellular repeated domains (EC1 to EC5), a transmembrane region, and an intracytoplasmic C-terminal region (CTR). The extracellular portion of E-cad forms junction with cell adhesion molecules on proximal cell, whereas the CTR binds β-catenin and other signaling molecules (reviewed in Devaux et al., 2019). Extracellular E-cad cleavage can be achieved by endoproteases (which cleave internal peptide bonds) belonging to the large family of sheddases (Grabowska and Day, 2012). The human sheddases include zinc-dependent matrix metalloproteases (matrilysin/MMP-2, 3, 7, 9, and 14) (Lee et al., 2007; Symowicz et al., 2007; Klein and Bischoff, 2011), and members of the α-disintegrin metalloproteases family (adamalysin/ADAM-10 and -15) (Maretzky et al., 2008; Najy et al., 2008; Giebeler and Zigrino, 2016), among others (reviewed in Grabowska and Day, 2012; Devaux et al., 2019). For instance, the eukaryotic ADAM-10 sheddase, abundantly expressed throughout the gastrointestinal tract and during normal intestinal homeostasis (reviewed in Dempsey, 2017), catalyzes a cleavage of E-cad that results in the release of the N-terminal sE-cad fragment and a C-terminal fragment (Maretzky et al., 2005). Another member of the ADAM family, the tumour necrosis factor α-convertase ADAM-17, was previously

reported to be involved in soluble ACE2 shedding (Lambert et al., 2005; Zipeto et al., 2020). Unexpectedly, in our experiments we found a significantly lower expression of genes encoding the ADAM-10 and ADAM-17 sheddases in Caco-2 cells 24 hours after infected with SARS-CoV-2. It remains possible that these sheddases are activated during the early phase of infection to induce the release of sE-Cad and sACE2 following viral infection and then that a feedback regulation loop down-modulates the ADAM-10 and ADAM-17 genes expression. Interestingly, a few years ago Qian and colleagues (Qian et al., 2013) reported that over-expression of ACE2 attenuates the metastasis of cancer cells through inhibition of epithelial-mesenchymal transition, because it induces the up-regulation of cell surface E-cad. Accordingly, the down-regulation of *CDH1*/E-cad gene expression could be linked to the down-regulation of ACE2 induced by SARS-CoV-2 infection and be triggered through activation of the NF-KB/Snail pathway, as suggested by Lai and colleagues (Lai et al., 2021). The results obtained for the ADAM-10 gene expression should be considered preliminary observations and an exhaustive analysis of all the sheddases that may be involved in the release of sE-cad will have to be undertaken subsequently. Preliminary analyses indicate that SARS-CoV-2 infection induce the modulation of several other human sheddases (data not shown). In addition, in COVID-19 patients it is possible that the dysbiosis induced by SARS-CoV-2 infection results in the activation of prokaryotic sheddases (e.g., the HtrA bacterial serine protease), able to cleave E-cad. This hypothesis should be investigated, since it is likely to contribute to the induction of a pro-inflammatory process in the intestinal epithelium.

According to these data and in agreement with other publications (Lamers et al., 2020; Zhang et al., 2020b; Xiao et al., 2020a), we speculated that the gastrointestinal tract can be an alternative route for SARS-CoV-2 infection in humans. Zhang and colleagues suggested that although most virus would be dead in the acid environment in the stomach, it remains possible that the saliva and secretions could carry the virus into the digestive tract where viral replication may be sustained in epithelial cells. In K18-hACE2 transgenic mice expressing human ACE2 infected with SARS-CoV-2 *via* intranasal administration, extensive necrosis and inflammation of the lamina propria of intestinal villi associated to cell damages and increased intestinal permeability were observed. Recently, experiments performed in a nonhuman primate model support this hypothesis (Jiao et al., 2021). The intragastric inoculation of nonhuman primates with SARS-CoV-2 resulted in the productive infection of digestive tissues and inflammation in both the lung and digestive tissues. This route of inoculation induced Inflammatory cytokines production and immunohistochemistry and Alcian blue/periodic acid–Schiff staining showed decreased Ki67, increased cleaved caspase 3, and decreased numbers of mucin-containing goblet cells, suggesting that the inflammation process induced by intragastric SARS-CoV-2 impaired the gastrointestinal barrier. Moreover, ACE2 and TMPRSS molecules are highly expressed in the epithelial cells of the oral cavity and these cells are susceptible to SARS-CoV-2 infection and sustain viral replication (Huang et al., 2021). Altogether these observations support the hypothesis of a possible fecal-oral route of infection.

Taken as a whole, our results provide new insight into the complex molecular interactions between SARS-CoV-2 and intestinal cells and highlight the fact that the infection of Caco-2 cells is accompanied by down-modulation of the *CDH1*/E-cad gene, lower cell surface expression of E-cad and increased release of sE-cad. We speculate that similar changes in E-cad expression probably occur in the GIT of COVID-19 patients leading to micro-damage to the epithelium barrier, a deregulation of the immune response, pro-inflammation, and the invasion of distant host organs/tissues.

DATA AVAILABILITY STATEMENT

The original contributions presented in the study are included in the article/**Supplementary Material**. Further inquiries can be directed to the corresponding author.

ETHICS STATEMENT

The animal study have been submitted to the Institutional Animal Care and Use Committee of CIPHE approved by French authorities (CETEA DSV -APAFIS#26484-2020062213431976 v6).

AUTHOR CONTRIBUTIONS

IO and CD contributed to the design of the study and conceived the manuscript. IO, GP, and DB performed the viral infections. IO and CG performed the *in vitro* experiments. J-PB and DB performed the electron microscopy analysis. AZ performed the *in vivo* experiments. HL performed the pathological examination. BM, J-LM, BL and CD supervised the work. CD wrote the first draft of the manuscript. All authors participated in correction of the manuscript. All authors contributed to the article and approved the submitted version.

FUNDING

This work was supported by the French Government under the « Investissements d'avenir » (Investments for the Future) program managed by the Agence Nationale de la Recherche (French ANR, National Agency for Research, reference, Méditerranée Infection 10-IAHU-03 to Didier Raoult), annual funds from Aix-Marseille university and IRD to the MEPHI research unit, the COVIDHUMICE project (Fondation pour la Recherche Médicale-ANR Flash Covid-COVI-0066 to BM) and the PHENOMIN (French National Infrastructure for mouse Phenogenomics, ANR-10-INBS-07, to BM). Other funding sources were limited to the salaries of the authors (Centre National de la Recherche Scientifique for CD, Caisse Nationale de Sécurité Sociale de Djibouti for IO), with no other role or involvement.

ACKNOWLEDGMENTS

We thank J.-C. Lagier and D. Raoult for stimulating discussions and unwavering support. We thank H. Chaudet for helpful discussions about the statistical analyzes of the results. We thank C. Lutz and The Jackson Laboratory for providing K18-hACE2 mice and S. van der Werf, X. Lescure and Y. Yazdanpanah for strain BetaCoV/France/IDF0372/2020. We thank A. Sansoni, C. Pierrini, P. Hoest, Q. Bardin, M. Fabregue and S. Sharkaoui for their contribution to setting up the K18hACE2-Sars Cov 2 *in vivo* model.

SUPPLEMENTARY MATERIAL

The Supplementary Material for this article can be found online at: https://www.frontiersin.org/articles/10.3389/fcimb.2022.798767/full#supplementary-material

Supplementary Figure 1 | Relative expression of different cellular mRNA in virus-free Caco-2 cells, in particular the mRNA encoding SARS-CoV-2 receptor/coreceptors as well as AngII and Ang-(1-7) receptors, and mRNA encoding cell adhesion and tight junctions molecules. The results are expressed as RE where RE = $2^{(-\Delta CT)}$.

Supplementary Figure 2 | (A) Relative expression of different cellular mRNA in virus-free HT29 cells, in particular the mRNA encoding SARS-CoV-2 receptor/coreceptors as well as AngII and Ang-(1-7) receptors, and mRNA encoding cell adhesion molecules. The results are expressed as RE where RE = $2^{(-\Delta CT)}$. **(B)** Confocal microscope analysis of E-cad, ACE2, occludin and actin expression on virus-free HT29 cells. The experiment was performed using cells permeabilized with 0.1% Triton X-100 (upper panel) and unpermeabilized cells (lower panel). **(C)** Quantification of the viral release from HT29 cell by qRT-PCR: ΔCT represents the CT value obtained subtracted from the CT value at time T=0 (CT - CT_0), where T=0 is the moment immediately after removing the inoculum used in the adsorption step. Each value is the mean of triplicates. **(D)** Quantification of SARS-CoV-2 viral antigen in the HT29 cells exposed to the virus at an MOI of 0.5 for 4 hours, 24 hours and 48 hours, by antibody-detection of SARS-CoV-2 nucleocapsid protein using high-speed capillary electrophoresis JessTM automated immunoblotting system. Although the HT29 cells can be infected by SARS-CoV-2 (as shown in **D**), viral release was too low to be quantifiable in the culture supernatants of HT29 cells (as shown in **C**).

REFERENCES

Bouhaddou, M., Memon, D., Meyer, B., White, K. M., Rezelj, V. V., Correa Marrero, M., et al. (2020). The Global Phosphorylation Landscape of SARS-CoV-2 Infection. *Cell* 182 (3), 685–712. doi: 10.1016/j.cell.2020.06.034

Brogna, C., Cristoni, S., Petrillo, M., Bisaccia, D. R., Lauritano, F., Montan, L., et al. (2022). The First Report on Detecting SARS-CoV-2 Inside Human Fecal-Oral Bacteria: A Case Series on Asymptomatic Family Members and a Child With COVID-19. *F1000Research* 11, 135. doi: 10.12688/f1000research.77421.1

Camargo, S. M., Singer, D., Makrides, V., Huggel, K., Pos, K. M., Wagner, C. A., et al. (2009). Tissue-Specific Amino Acid Transporter Partners ACE2 and Collectrin Differentially Interact With Hartnup Mutations. *Gastroenterology* 136, 872–882. doi: 10.1053/j.gastro.2008.10.055

Cantuti-Castelvetri, L., Ojha, R., Pedro, L. D., Djannatian, M., Franz, J., Kuivanen, S., et al. (2020). Neuropilin-1 Facilitates SARS-CoV-2 Cell Entry and Infectivity. *Science* 370, 856–860. doi: 10.1126/science.abd2985

Chelakkot, C., Ghim, J., and Ryu, S. H. (2018). Mechanisms Regulating Intestinal Barrier Integrity and its Pathological Implications. *Exp. Mol. Med.* 50, 103. doi: 10.1038/s12276-018-0126-x

Choi, W. I., Kim, I. B., Park, S. J., Ha, E. H., and Lee, C. W. (2021). Comparison of the Clinical Characteristics and Mortality of Adults Infected With Human Coronaviruses 229E and OC43. *Sci. Rep.* 11 (1), 4499. doi: 10.1038/s41598-021-83987-3

Chu, H., Chan, J. F. W., Yuen, T. T. T., Shuai, H., Yuan, S., Wang, Y., et al. (2020). Comparative Tropism, Replication Kinetics, and Cell Damage Profiling of SARS-CoV-2 and SARS-CoV With Implications for Clinical Manifestations, Transmissibility, and Laboratory Studies of COVID-19: An Observational Study. *Lancet* 1, e14–e23. doi: 10.1016/S2666-5247(20)30004-5

Cohen, T. (2001). Neuroendocrine Cells Along the Digestive Tract Express Neuropilin-2. *Biochem. Biophys. Res. Commun.* 284, 395–403. doi: 10.1006/bbrc.2001.4958

Collins, A. R. (1990). Comparison of the Replication of Distinct Strains of Human Coronavirus OC43 in Organotypic Human Colon Cells (Caco-2) and Mouse Intestine. *Adv. Exp. Med. Biol.* 276, 497–503. doi: 10.1007/978-1-4684-5823-7_69

D'Costa, Z. J., Jolly, C., Androphy, E. J., Mercer, A., Matthews, C. M., and Hibma, M. H. (2012). Transcriptional Repression of E-Cadherin by Human Papillomavirus Type 16 E6. *PloS One* 7 (11), e48954. doi: 10.1371/journal.pone.0048954

Daly, J. L., Simonetti, B., Klein, K., Chen, K. E., Williamson, M. K., Anton-Plagaro, C., et al. (2020). Neuropilin-1 is a Host Factor for SARS-CoV-2 Infection. *Science* 370 (6518), 861–865. doi: 10.1126/science.abd3072

D'Amico, F., Baumgart, D. C., Danese, S., and Peyrin-Biroulet, L. (2020). Diarrhea During COVID-19 Infection: Pathogenesis, Epidemiology, Prevention and Management. *Clin. Gastroenterol. Hepatol.* 18, 1663–1672. doi: 10.1016/j.cgh.2020.04.001

Dempsey, P. J. (2017). Role of ADAM10 in Intestinal Crypt Homeostasis and Tumorigenesis. *Biochem. Biophys. Acta* 1864 (11), 2228–2239. doi: 10.1016/j.bbamcr.2017.07.011

Dergham, J., Delerce, J., Bedotto, M., La Scola, B., and Moal, V. (2021). Isolation of Viable SARS-CoV-2 Virus From Feces of an Immunocompromised Patient Suggesting a Possible Fecal Mode of Transmission. *J. Clin. Med.* 10, 2696. doi: 10.3390/jcm10122696

Devaux, C. A., Lagier, J.-C., and Raoult, D. (2021). New Insights Into the Physiopathology of COVID-19: SARS-CoV-2-Associated Gastrointestinal Illness. *Front. Med.* 8. doi: 10.3389/fmed.2021.640073

Devaux, C. A., Mezouar, S., and Mege, J.-L. (2019). The E-Cadherin Cleavage Associated to Pathogenic Bacteria Infections Can Favor Bacterial Invasion and Transmigration, Dysregulation of the Immune Response and Cancer Induction in Humans. *Front. Microbiol.* 10. doi: 10.3389/fmicb.2019.02598

Devaux, C. A., Rolain, J. M., and Raoult, D. (2020). ACE2 Receptor Polymorphism: Susceptibility to SARS-CoV-2, Hypertension, Multiorgan Failure, and COVID-19 Disease Outcome. *J. Microbiol. Immunol. Infect.* 53, 425–435. doi: 10.1016/j.micinf.2020.03.003

Dhar, D., and Mohanty, A. (2020). Gut Microbiota and COVID-19 Possible Link and Implications. *Virus Res.* 285, 198018. doi: 10.1016/j.virusres.2020.198018

Edouard, S., Jaafar, R., Orain, N., Parola, P., Colson, P., la Scola, B., et al. (2021). Automated Western Immunoblotting Detection of Anti-SARS-CoV-2 Serum Antibodies. *Eur. J. Clin. Microbiol. Infect. Dis.* 40 (6), 1309–1317. doi: 10.1007/s10096-021-04203-8

Escher, R., Breakey, N., and Lammle, B. (2020). Severe COVID-19 Infection Associated With Endothelial Activation. *Thromb. Res.* 190, 62. doi: 10.1016/j.thromres.2020.04.014

Fairweather, S. J., Broer, A., O'Mara, M. L., and Broer, S. (2012). Intestinal Peptidases From Functional Complexes With Neutral Amino Acid Transporter B0AT1. *Biochem. J.* 446, 135–148. doi: 10.1042/BJ20120307

Fang, D., Ma, J., and Guan, J. (2020). Manifestation of Digestive System in Hospitalized Patients With Novel Coronavirus Pneumonia in Wuhan, China: A Single-Center, Descriptive Study. *Chin. J. Dig.* 40, E005. doi: 10.3760/cma.j.i.ssn.0254-1432.2020.0005

Fasano, A. (2011). Zonulin and Its Regulation of Intestinal Barrier Function: The Biological Door to Inflammation, Autoimmunity, and Cancer. *Physiol. Rev.* 91, 151–175. doi: 10.1152/physrev.00003.2008

Fogeron, M. L., Montserret, R., Zehnder, J., Nguyen, M. H., Dujardin, M., Brigandat, L., et al. (2021). SARS-CoV-2 ORF7b: Is a Bat Virus Protein Homologue a Major Cause of COVID-19 Symptoms? *bioRxiv*. doi: 10.1101/2021.02.05.428650

Giebeler, N., and Zigrino, P. (2016). A Disintegrin and Metalloprotease (ADAM): Historical Overview of Their Functions. *Toxins* 8, 122. doi: 10.3390/toxins8040122

Grabowska, M. M., and Day, M. L. (2012). Soluble E-Cadherin: More Than a Symptom of Disease. *Front. Biosci.* 17, 1948–1964. doi: 10.2741/4031

Gu, S., Chen, Y., Wu, Z., Chen, Y., Gao, H., Lv, L., et al. (2020). Alterations of the Gut Microbiota in Patients With Coronavirus Disease 2019 or H1N1 Influenza. *Clin. Infect. Dis.* 71, 2669–2678. doi: 10.1093/cid/ciaa709

Gu, J., Han, B., and Wang, J. (2020). COVID-19: Gastrointestinal Manifestations and Potential Fecal-Oral Transmission. *Gastroenterology* 158, 1518–1519. doi: 10.1053/j.gastro.2020.02.054

Guo, Y., Luo, R., Wang, Y., Deng, P., Song, T., Zhang, M., et al. (2021). SARS-CoV-2 Induced Intestinal Responses With a Biomimetic Human Gut-on-Chip. *Sci. Bull.* 66, 783–793. doi: 10.1016/j.scib.2020.11.015

Guo, R. W., Yang, L. X., Li, M. Q., Pan, X. H., Liu, B., and Deng, Y. L. (2012). Stim1- and Orai1- Mediated Store-Operated Calcium Entry is Critical for Angiotensin II-Induced Vascular Smooth Muscle Cell Proliferation, Cardiovasc. *Res* 93, 360–370. doi: 10.1093/cvr/cvr307

Hamming, I., Timens, W., Bulthuis, M., Lely, T., Navis, G., and van Goor, H. (2004). Tissue Distribution of ACE2 Protein, the Functional Receptor for SARS Coronavirus. *J. Pathol.* 203, 631–637. doi: 10.1002/path.1570

Han, C., Duan, C., Zhang, S., Spiegel, B., Shi, H., Wang, W., et al. (2020). Digestive Symptoms in COVID-19 Patients With Mild Disease Severity: Clinical Presentation, Stool Viral RNA Testing, and Outcomes. *Am. J. Gastroenterol.* 115, 916–923. doi: 10.14309/ajg0000000000000664

Hansel, D. E., Wilentz, R. E., Yeo, C. J., Schulick, R. D., Montgomery, E., and Maitra, A. (2004). Expression of Neuropilin-1 in High-Grade Dysplasia, Invasive Cancer, and Metastases of the Human Gastrointestinal Tract. *Am. J. Surg. Pathol.* 28, 347–356. doi: 10.1097/00000478-200403000-00007

Hanski, C., Stolze, B., and Riecken, E. G. (1992). Tumorigenicity, Mucin Production and AM-3 Epitope Expression in Clones Selected From the HT-29 Colon Carcinoma Cell Line. *Int. J. Cancer* 50 (6), 924–929. doi: 10.1002/ijc.2910500618

Haspel, N., Zanuy, D., Nussinov, R., Teesalu, T., Ruoslahti, E., and Aleman, C. (2011). Binding of aPeptide to Neuropilin-1 Receptor: A Molecular Modeling Approach. *Biochemistry* 50 (10), 1755–1762. doi: 10.1021/bi101662j

Heneghan, C., Spencer, E., Brassey, J., Plüddemann, A., Onakpoya, I. J., Evans, D. H., et al. (2021). SARS-CoV-2 and the Role of Orofecal Transmission: Systematic Review. *F1000 Res*. 10, 232. doi: 10.12688/f1000research.51592.1

Hoffmann, N., Kleine-Weber, H., Schroeder, S., Krüger, N., Herrler, T., Erichsen, S., et al. (2020). SARS-CoV-2 Cell Entry Depends on ACE2 and TMPRSS2 and Is Blocked by a Clinically Proven Protease Inhibitor. *Cell*. 181, 1–10. doi: 10.1016/j.cell.2020.02.052

Huang, N., Pérez, P., Kato, T., Mikami, Y., Okuda, K., Gilmore, R. C., et al. (2021). SARS-CoV-2 Infection of the Oral Cavity and Saliva. *Nat. Med.* 27 (5), 892–903. doi: 10.1038/s41591-021-01296-8

Huang, C., Wang, Y., Li, X., Ren, L., Zhao, J., and Hu, Y. (2020). Clinical Features of Patients Infected With 2019 Novel Coronavirus in Wuhan, China. *Lancet* 395, 497–506. doi: 10.1016/S0140-6736(20)30183-5

Javorsky, A., Humbert, P. O., and Kvansakul, M. (2021). Structural Basis of Coronavirus E Protein Interactions With Human PALS1 PDZ Domain. *Commun. Biol.* 4, 724. doi: 10.1038/s42003-021-02250-7

Jiao, L., Li, H., Xu, J., Yang, M., Ma, C., Li, J., et al. (2021). The Gastrointestinal Tract is an Alternative Route for SARS-CoV-2 Infection in a Nonhuman Primate. *Gastroenterology* 160 (5), 1647–1661. doi: 10.1053/j.gastro.2020.12.001

Klein, T., and Bischoff, R. (2011). Physiology and Pathophysiology of Matrix Metalloproteases. *Amino Acids* 41, 271–290. doi: 10.1007/s00726-010-0689-x

Lai, Y. J., Chao, C. H., Liao, C. C., Lee, T. A., Hsu, J. M., Chaou, W. C., et al. (2021). Epithelial-Mesenchymal Transition Induced by SARS-CoV-2 Required Transcriptional Upregulation of Snail. *Am. J. Cancer Res.* 11 (5), 2278–2290.

Lambert, D. W., Yarski, M., Warner, F. J., Thornhill, P., Parkin, E. T., Smith, A. I., et al. (2005). Tumor Necrosis Factor-α Convertase (ADAM17) Mediates Regulated Ectodomain Shedding of the Severe-Acute Respiratory Syndrome-Coronavirus (SARS-CoV) Receptor, Angiotensin-Converting Enzyme-2 (Ace2). *J. Biol. Chem.* 280 (34), 30113–30119. doi: 10.1074/jbc.M505111200

Lamers, M. M., Beumer, J., van der Vaart, J., Knoops, K., Puschhof, J., Breugem, T. I., et al. (2020). SARS-CoV-2 Productively Infects Human Gut Enterocytes. *Science* 369, 50–54. doi: 10.1126/science.abc1669

Le Bideau, M., Wurtz, N., Baudoin, J. P., and La Scola, B. (2021). Innovative Approach to Fast Electron Microscopy Using the Example of a Culture of Virus-Infected Cells: An Application to SARS-CoV-2. *Microorganisms* 9 (6), 1194. doi: 10.3390/microorganisms9061194

Lee, K. H., Choi, E. Y., Hyun, M. S., Jang, B. I., Kim, T. N., Kim, S. W., et al. (2007). Association of Extracellular Cleavage of E-Cadherin Mediated by MMP-7 With HGF-Induced *In Vitro* Invasion in Human Stomach Cancer Cells. *Eur. Surg. Res.* 39, 208–215. doi: 10.1159/000101452

Lee, J. O., Kwun, H. J., Jung, J. K., Choi, K. H., Min, D. S., and Jang, K. L. (2005). Hepatitis B Virus X Protein Represses E-Cadherin Expression *via* Activation of DNA Methyltransferase 1. *Oncogene* 24, 6617–6625. doi: 10.1038/sj.onc.1208827

Letko, M., Marzi, A., and Munster, V. (2020). Functional Assessment of Cell Entry and Receptor Usage for SARS-CoV-2 and Other Lineage B Betacoronaviruses. *Nat. Microbiol.* 5, 562–569. doi: 10.1038/s41586-020-2012-7

Li, X. Y., Dai, W. J., Wu, S. N., Yang, X. Z., and Wang, H. G. (2020). The Occurrence of Diarrhea in COVID-19 Patients. *Clin. Res. Hepatol. Gastroenterol.* 44, 284–285. doi: 10.1016/j.clinre.2020.03.017

Lin, L., Jiang, X., Zhang, Z., Huang, S., Zhang, Z., Fang, Z., et al. (2020). Gastrointestinal Symptoms of 95 Cases With SARS-CoV-2 Infection. *Gut* 69, 997–1001. doi: 10.1136/gutjnl-2020-321013

Li, Q., Sodroski, C., Lowey, B., Schweitzer, C. J., Cha, H., Zhang, F., et al. (2016). Hepatitis C Virus Depends on E-Cadherin as an Entry Factor and Regulates its Expression in Epithelial-Tomesenchymal Transition. *Proc. Natl. Acad. Sci. U.S.A.* 113 (27), 7620–7625. doi: 10.1073/pnas.1602701113

Maretzky, T., Reiss, K., Ludwig, A., Buchholz, J., Scholz, F., Proksch, E., et al. (2005). ADAM10 Mediates E-Cadherin Shedding and Regulates Epithelial Cell-Cell Adhesion, Migration, and β-Catenin Translocation. *Proc. Natl. Acad. Sci. U.S.A.* 102 (26), 9182–9187. doi: 10.1073/pnas.0500918102

Maretzky, T., Scholz, F., Köten, B., Proksch, E., Saftig, P., and Reiss, K. (2008). ADAM10-Mediated E-Cadherin Release is Regulated by Proinflammatory Cytokines and Modulates Keratinocyte Cohesion in Eczematous Dermatitis. *J. Invest. Dermatol.* 128, 1737–1746. doi: 10.1038/sj.jid.5701242

Meenan, J., Mevissen, M., Monajemi, H., Radema, S. A., Soule, H. R., Moyle, M., et al. (1996). Mechanisms Underlying Neutrophil Adhesion to Apical Epithelial Membranes. *Gut* 38 (2), 201–205. doi: 10.1136/gut.38.2.201

Meng, X. J., and Liang, T. J. (2021). SARS-CoV-2 Infection in the Gastrointestinal Tract: Fecal–Oral Route of Transmission for COVID-19? *Gastroenterology* 160, 1467–1474. doi: 10.1053/j.gastro.2021.01.00

Najy, A. J., Day, K. C., and Day, M. L. (2008). The Ectodomain Shedding of E-Cadherin by ADAM15 Supports ErbB Receptor Activation. *J. Biol. Chem.* 283, 18393–18401. doi: 10.1074/jbc.M801329200

Navabi, N., McGuckin, M. A., and Lindén, S. K. (2013). Gastrointestinal Cell Lines Form Polarized Epithelia With an Adherent Mucus Layer When Cultured in Semi-Wet Interfaces With Mechanical Stimulation. *PloS One* 8 (7), e68761. doi: 10.1371/journal.pone.0068761

Niv, Y., Schwartz, B., Amsalem, Y., and Lamprecht, S. A. (1995). Human HT-29 Colon Carcinoma Cells: Mucin Production and Tumorigenicity in Relation to Growth Phases. *Anticancer Res.* 15 (5B), 2023–2027.

Osman, I. O., Melenotte, C., Brouqui, P., Million, M., Lagier, J.-C., Parola, P., et al. (2021). Expression of ACE2, Soluble ACE2, Angiotensin I, Angiotensin II and Angiotensin-(1-7) Is Modulated in COVID-19 Patients. *Front. Immunol.* 12. doi: 10.3389/fimmu.2021.625732

Owczarek, K., Szczepanski, A., Milewska, A., Baster, Z., Rajfur, Z., Sarna, M., et al. (2018). Early Events During Human Coronavirus OC43 Entry to the Cell. *Sci. Rep.* 8, 7124. doi: 10.1038/s41598-018-25640-0

Pan, L. M., Yang, M., Sun, P., Wang, Y., Yan, R., Li, J., et al. (2020). Clinical Characteristics of COVID-19 Patients With Digestive Symptoms in Hubei, China: A Descriptive, Cross-Sectional, Multicenter Study. *Am. J. Gastroenterol.* 115, 766–773. doi: 10.14309/ajg.0000000000000620

Pires de Souza, G. A., Le Bideau, M., Boschi, C., Ferreira, L., Wurtz, N., Devaux, C., et al. (2022). Emerging SARS-CoV-2 Genotypes Show Different Replication Patterns in Human Pulmonary and Intestinal Epithelial Cells. *Viruses* 14, 23. doi: 10.3390/v14010023

Pires de Souza, G. A., Osman, I. O., Le Bideau, M., Baudoin, J.-P., Jaafar, R., Devaux, C., et al. (2021). Angiotensin II Receptor Blockers (ARBs Antihypertensive Agents) Increase Replication of SARS-CoV-2 in Vero E6 Cells. *Front. Cell. Infect. Microbiol.* 11. doi: 10.3389/fcimb.2021.639177

Qi, F., Qian, S., Zhang, S., and Zhang, Z.. (2020). Single Cell RNA Sequencing of 13 Human Tissues Identify Cell Types and Receptors of Human Coronaviruses. *Biochem Biophys Res Commun* 526, 135–140. doi: 10.1016/j.bbrc.2020.03.044

Qian, Y. R., Guo, Y., Wan, H. Y., Fan, L., Feng, Y., Ni, L., et al. (2013). Angiotensin-Converting Enzyme 2 Attenuates the Metastasis of non-Small Cell Lung Cancer Through Inhibition of Epithelial-Mesenchymal Transition. *Oncol. Rep.* . 29, 2408–2414. doi: 10.3892/or.2013.2370

Raghavan, S., Kenchappa, D. B., and Leo, M. D. (2021). SARS-CoV-2 Spike Protein Induces Degradation of Junctional Proteins That Maintain Endothelial Barrier Integrity. *Front. Cardiovasc. Med.* 8. doi: 10.3389/fcvm.2021.687783

Ramakrishnan, M. A. (2016). Determination of 50% Endpoint Titer Using a Simple Formula. *World J. Virol.* 5 (2), 85–86. doi: 10.5501/wjv.v5.i2.85

Rebendenne, A., Priyanka, R., Bonaventure, B., Chaves Valadao, A. L., Desmarets, L., Rouillé, Y., et al. (2021). Bidirectional Genome-Wide CRISPR Screens Reveal Host Factors Regulating SARS-CoV-2, MERS-CoV and Seasonal Coronaviruses. *bioRxiv*. doi: 10.1101/2021.05.19.444823

Redd, W. D., Zhou, C., Hathorn, K. E., McCarthy, T. R., Bazarbashi, A. N., Thompson, C. C., et al. (2020). Prevalence and Characteristics of Gastrointestinal Symptoms in Patients With SARS-CoV-2 Infection in the United States: A Multicenter Cohort Study. *Gastroenterology* 159, 765–767. doi: 10.1053/j.gastro.2020.04.045

Reyat, J. S., Chimen, M., Noy, P. J., Szyroka, J., Rainger, G., and Tomlinson, M. G. (2017). ADAM10-Interacting Tetraspanins Tspan5 and Tspan17 Regulate VE-Cadherin Expression and Promote T Lymphocyte Transmigration. *J. Immunol.* 199, 666–676. doi: 10.4049/jimmunol.1600713

Song, Y., Liu, P., Shi, X. L., Chu, Y. L., Zhang, J., Xia, J., et al. (2020). SARS-CoV-2 Induced Diarrhoea as Onset Symptom in Patient With COVID-19. *Gut* 69, 1143–1144. doi: 10.1136/gutjnl-2020-320891

Streeck, H., Kwon, D. S., Pyo, A., Flanders, M., Chevalier, M. F., Law, K., et al. (2011). Epithelial Adhesion Molecules can Inhibit HIV-1-Specific CD8+ T-Cell Functions. *Blood* 117, 5112–5122. doi: 10.1182/blood-2010-12-321588

Sun, S. H., Chen, Q., Gu, H. J., Yang, G., Wang, Y. X., Huang, X. Y., et al. (2020). A Mouse Model of SARS-CoV-2 Infection and Pathogenesis. *Cell Host Microbe* 28, 124–133. doi: 10.1016/j.chom.2020.05.02

Symowicz, J., Adley, B. P., Gleason, K. J., Johnson, J. J., Ghosh, S., Fishman, D. A., et al. (2007). Engagement of Collagen-Binding Integrins Promotes Matrix Metalloproteinase-9–Dependent E-Lycadherin Ectodomain Shedding in Ovarian Carcinoma Cells. *Cancer Res.* 67, 2030–2039. doi: 10.1158/0008-5472.CAN-06-2808

Teesalu, T., Sugahara, K. N., Kotamraju, V. R., and Ruoslahti, E. (2009). C-End Rule Peptides Mediate Neuropilin-1-Dependent Cell, Vascular, and Tissue Penetration. *Proc. Natl. Acd. Sci. U.S.A.* 106 (38), 16157–16162. doi: 10.1073/pnas.0908201106

Tong, M., Jiang, Y., Xia, D., Xiong, Y., Zheng, Q., Chen, F., et al. (2020). Elevated Serum Endothelial Cell Adhesion Molecules Expression in COVID-19 Patients. *J. Infect. Dis.* 222 (6), 894–898. doi: 10.1093/infdis/jiaa349

Tripathi, A., Lammers, K. M., Goldblum, S., Shea-Donohue, T., Netzel-Arnett, S., Buzza, M. S., et al. (2009). Identification of Human Zonulin, a Physiological Modulator of Tight Junctions, as Prehaptoglobin-2. *Proc. Natl. Acad. Sci. U.S.A.* 106 (39), 16799–16804. doi: 10.1073/pnas.0906773106

Vuille-Dit-Bille, R. N., Camargo, S. M., Emmenegger, L., Sasse, T., Kummer, E., Jando, J., et al. (2015). Human Intestine Luminal ACE2 and Amino Acid Transporter Expression Increased by ACE-Inhibitors. *Amino Acids* 47, 693–705. doi: 10.1007/s00726-014-1889-6

Wang, D., Hu, B., Hu, C., Zhu, F., Liu, X., Zhang, J., et al. (2020). Clinical Characteristics of 138 Hospitalized Patients With 2019 Novel Coronavirus-Infected Pneumonia in Wuhan, China. *Jama* 323, 1061–1069. doi: 10.1001/jama.2020.1585

Wendling, J. M., Saulnier, A., and Sabatier, J. M. (2021). Share Food, Meals and Drinks: 10 Arguments Suggesting an Oral Transmission Route of COVID-19. *Infect. Disorders-Drug Targets*, 21. doi: 10.2174/1871526521666210716110603

Wölfel, R., Corman, V. M., Guggemos, W., Seilmaier, M., Zange, S., Müller, M. A., et al. (2020). Virological Assessment of Hospitalized Patients With COVID-19. *Nature* 581, 465–469. doi: 10.1038/s41586-020-2196-x

Wurtz, N., Penant, G., Jardot, P., Duclos, N., and La Scola, B. (2021). Culture of SARS-CoV-2 in a Panel of Laboratory Cell Lines, Permissivity, and Differences in Growth Profile. *Eur. J. Clin. Microbiol. Infect. Dis.* 40 (3), 477–484. doi: 10.1007/s10096-020-04106-0

Xiao, F., Sun, J., Xu, Y., Li, F., Huang, X., Li, H., et al. (2020b). Infectious SARS-CoV-2 in Feces of Patient With Severe COVID-19. *Emerg. Infect. Dis.* 26, 1920–1922. doi: 10.3201/eid2608.200681

Xiao, F., Tang, M., Zheng, X., Liu, Y., Li, X., and Shan, H. (2020a). Evidence for Gastrointestinal Infection of SARS-CoV-2. *Gastroenterology* 158, 1831–1833. doi: 10.1053/j.gastro.2020.02.055

Xu, Y., Li, X., Zhu, B., Liang, H., Fang, C., Gong, Y., et al. (2020). Characteristics of Pediatric SARS-CoV-2 Infection and Potential Evidence for Persistent Fecal Viral Shedding. *Nat. Med.* 26, 502–505. doi: 10.1038/s41591-020-0817-4

Yan, R., Zhang, Y., Li, Y., Xia, L., Guo, Y., and Zhou, Q. (2020). Structural Basis for the Recognition of the SARS-CoV-2 by Full-Length Human ACE2. *Science* 367, 1444–1448. doi: 10.1126/science.abb2762

Yu, D. C., Bury, J. P., Tiernan, J., Waby, J. S., Staton, C. A., and Corfe, B. M. (2011). Short-Chain Fatty Acid Level and Field Cancerization Show Opposing Associations With Enteroendocrine Cell Number and Neuropilin Expression in Patients With Colorectal Adenoma. *Mol. Cancer* 10, 27. doi: 10.1186/1476-4598-10-2

Yu, C., Tang, W., Wang, Y., Shen, Q., Wang, B., Cai, C., et al. (2016). Downregulation of ACE2/Ang-(1–7)/Mas Axis Promotes Breast Cancer Metastasis by Enhancing Store-Operated Calcium Entry. *Cancer Lett.* 376 (2), 268–277. doi: 10.1016/j.canlet.2016.04.006

Zang, R., Gomez Castro, M. F., McCune, B. T., Zeng, Q., Rothlauf, P. W., Sonnek, N. M., et al. (2020). TMPRSS2 and TMPRSS4 Promote SARS-CoV-2 Infection of Human Small Intestinal Enterocytes. *Sci. Immunol.* 5, eabc3582. doi: 10.1126/sciimmunol.abc3582

Zhang, H., Kang, Z., Gong, H., Xu, D., Wang, J., Li, Z., et al. (2020b). Digestive System is a Potential Route of COVID-19: An Analysis of Single-Cell Coexpression Pattern of Key Proteins in Viral Entry Process. *Gut* 69, 1010–1018. doi: 10.1136/gutjnl-2020-320953

Zhang, H., Li, H. B., Lyu, J. R., Lei, X. M., Li, W., Wu, G., et al. (2020a). Specific ACE2 Expression in Small Intestinal Enterocytes may Cause Gastrointestinal Symptoms and Injury After 2019-Ncov Infection. *Int. J. Infect. Dis.* 96, 19–24. doi: 10.1016/j.ijid.2020.04.027

Zheng, S., Fan, J., Yu, F., Feng, B., Lou, B., Zou, Q., et al. (2020). Viral Load Dynamics and Disease Severity in Patients Infected With SARS-CoV-2 in Zhejiang Province, China, January–March 2020: Retrospective Cohort Study. *BMJ* 369, m1443. doi: 10.1136/bmj.m1443

Zhu, N., Zhang, D., Wang, W., Li, X., Yang, B., and Song, J. (2020). A Novel Coronavirus From Patients With Pneumonia in China 2019. *N. Engl. J. Med.* 382, 727–733. doi: 10.1056/NEJMoa2001017

Zipeto, D., Palmeira, J., Argañaraz, G. A., and Argañaraz, E. R. (2020). ACE2/ADAM17/TMPRSS2 Interplay May Be the Main Risk Factor for COVID-19. *Front. Immunol.* 11. doi: 10.3389/fimmu.2020.576745

Zuo, T., Zhang, F., Lui, G. C. Y., Yeoh, Y. K., Li, A. Y. L., Zhan, H., et al. (2020). Alterations in Gut Microbiota of Patients With COVID-19 During Time of Hospitalization. *Gastroenterology* 159, 944–955. doi: 10.1053/j.gastro.2020.05.048

Conflict of Interest: The authors declare that the research was conducted in the absence of any commercial or financial relationships that could be construed as a potential conflict of interest.

Publisher's Note: All claims expressed in this article are solely those of the authors and do not necessarily represent those of their affiliated organizations, or those of the publisher, the editors and the reviewers. Any product that may be evaluated in this article, or claim that may be made by its manufacturer, is not guaranteed or endorsed by the publisher.

frontiers | Frontiers in Cellular and Infection Microbiology

REVIEW
published: 12 May 2022
doi: 10.3389/fcimb.2022.869832

SARS-CoV-2 and Emerging Variants: Unmasking Structure, Function, Infection, and Immune Escape Mechanisms

Jiaqi Li, Huimin Jia, Miaomiao Tian, Nijin Wu, Xia Yang, Jianni Qi, Wanhua Ren, Feifei Li and Hongjun Bian**

Shandong Provincial Hospital Affiliated to Shandong First Medical University, Jinan, China

OPEN ACCESS

Edited by:
You Zhou,
Cardiff University, United Kingdom

Reviewed by:
Parth Sarthi Sen Gupta,
Indian Institute of Science Education and Research Berhampur (IISER), India
Sai Ganesan,
University of California, San Francisco, United States

***Correspondence:**
Hongjun Bian
bhj0227@126.com
Feifei Li
slyylff@126.com.

Specialty section:
This article was submitted to Virus and Host, a section of the journal Frontiers in Cellular and Infection Microbiology

Received: *05 February 2022*
Accepted: *06 April 2022*
Published: *12 May 2022*

Citation:
Li J, Jia H, Tian M, Wu N, Yang X, Qi J, Ren W, Li F and Bian H (2022) SARS-CoV-2 and Emerging Variants: Unmasking Structure, Function, Infection, and Immune Escape Mechanisms. Front. Cell. Infect. Microbiol. 12:869832. doi: 10.3389/fcimb.2022.869832

As of April 1, 2022, over 468 million COVID-19 cases and over 6 million deaths have been confirmed globally. Unlike the common coronavirus, SARS-CoV-2 has highly contagious and attracted a high level of concern worldwide. Through the analysis of SARS-CoV-2 structural, non-structural, and accessory proteins, we can gain a deeper understanding of structure-function relationships, viral infection mechanisms, and viable strategies for antiviral therapy. Angiotensin-converting enzyme 2 (ACE2) is the first widely acknowledged SARS-CoV-2 receptor, but researches have shown that there are additional co-receptors that can facilitate the entry of SARS-CoV-2 to infect humans. We have performed an in-depth review of published papers, searching for co-receptors or other auxiliary membrane proteins that enhance viral infection, and analyzing pertinent pathogenic mechanisms. The genome, and especially the spike gene, undergoes mutations at an abnormally high frequency during virus replication and/or when it is transmitted from one individual to another. We summarized the main mutant strains currently circulating global, and elaborated the structural feature for increased infectivity and immune evasion of variants. Meanwhile, the principal purpose of the review is to update information on the COVID-19 outbreak. Many countries have novel findings on the early stage of the epidemic, and accruing evidence has rewritten the timeline of the outbreak, triggering new thinking about the origin and spread of COVID-19. It is anticipated that this can provide further insights for future research and global epidemic prevention and control.

Keywords: COVID-19, SARS-CoV-2, spike protein, receptor, variants

INTRODUCTION

Coronaviruses are genotypically divided into four genera (alpha, beta, gamma, and delta) (Woo et al., 2010), of which α- and β-coronavirus can be major human pathogens by crossing the animal-human barrier (Cui et al., 2019). Up to the present, there are seven known species of human coronaviruses: 229E (α-CoV), NL63 (α-CoV), OC43 (β-CoV), HKU1 (β-CoV), MERS-CoV (β-CoV), SARS-CoV (β-CoV), and SARS-CoV-2 (β-CoV) (Qiang et al., 2020). Specifically, SARS-

CoV-2 is a single-stranded, positive-sense RNA virus, belonging to the Sarbecovirus subgenus (Zhou et al., 2020). Like SARS-CoV and MERS-CoV, SARS-CoV-2 is classified as a zoonotic β-coronavirus that possibly originated from bats and was transmitted to humans through distinct intermediate hosts (Hu et al., 2021). As regards the origin of SARS-CoV-2, there is almost no theory. However, the most probable one is that it has a natural, zoonotic origin. Zoonotic viruses, including influenza viruses and coronaviruses, are most likely derived from wild animals and remain a continuous threat to humans. To date, no studies have completely elucidated any potential natural hosts or intermediate hosts for SARS-CoV-2. Based on phylogenetic analysis, SARS-CoV-2 is closely correlated with SARS-CoV and far from MERS-CoV and its nucleotide homology with SARS-CoV and MERS-CoV is 79 and 50%, respectively (Hu et al., 2021). Thus, comparative analysis of SARS-CoV-2 and SARS-CoV will contribute to further clarifying the pathogenesis of SARS-CoV-2.

The SARS-CoV-2 genome is between 26 kb and 32 kb in size and 60-140 nm in diameter (Khan et al., 2020). SARS-CoV-2 harbors 15 open reading frames (ORFs) encoding nonstructural proteins (NSP1-16), structural proteins (N, M, E, S proteins), and accessory proteins (ORF3a, 3b, 6, 7a, 7b, 8, 9a, 9b and 10) (Liu et al., 2014; Zinzula, 2021). The replicase genes located in the first two-thirds of the genome are first translated into two large polyproteins pp1a and pp1ab, which are then processed into 16 NSP *via* proteolytic cleavage by the viral main protease (M^{pro}, NSP5, or $3CL^{pro}$) and a papain-like protease (NSP3, PLpro). The remaining one-third of the genome contains ORFs for the structural proteins, namely the spike (S), envelope (E), membrane (M), and nucleocapsid (N) proteins (Liu et al., 2014; Majumdar and Niyogi, 2021).

During cellular infection by SARS-CoV-2, the trimeric spike (S) proteins located on the viral surface enter the host cell through the ACE2 receptor and TMPRSS2 (Lu et al., 2020) (Hoffmann et al., 2020; Hatmal et al., 2020). ACE2 is a type I membrane-bound protein that is widely expressed in the heart, lung (especially in type 2 pneumocytes), kidney, digestive organs, liver, testis, brain, and vascular endothelium (Hamming et al., 2004). This discrepancy remains hard to interpret the multi-organ tropism of SARS-CoV-2. Remarkably, both SARS-CoV-2 and SARS-CoV use ACE2 as a receptor in host cells (Hoffmann et al., 2020). However, they showed significant differences in epidemiological, target organs, pathogenetic and clinical characteristics. Previous work has indicated that SARS-CoV-2 may depend on co-receptor or other auxiliary membrane proteins to invade the human host and cause severe disease.

Mutations are integral parts of the virus life cycle and rarely significantly affect outbreaks. Nevertheless, as an RNA virus, SARS-CoV-2 has a high mutation rate and recombination events due to the low fidelity of RNA polymerase. The genetic evolution of SARS-CoV-2 occurred in a continuous adaptation to new human hosts, resulting in mutant variants that forced many countries have to endure the second or third wave of outbreaks. These variants not only seem to spread more effectively in susceptible hosts than the virus from the initial outbreak but also may be more resistant to naturally acquired or vaccine-induced immunity (Cai et al., 2021).

Overall, we summarized the latest research, demonstrated the epidemiological characteristics, basic virology including genome structural characteristics and potential receptors, and analyzed the effects of different variants on transmission and virulence. Subsequently, we elaborated on the clinical manifestations of COVID-19, including attacks and pathogenic mechanisms on various organs of the human body, along with classic and new therapeutic approaches.

EPIDEMIOLOGY OF ALL PERIOD

The Pandemic's Status

Three highly pathogenic coronaviruses, SARS-CoV, MERS-CoV, and SARS-CoV-2 frequently cause severe respiratory distress and multiple organ failure with high mortality. The third highly pathogenic strain of coronavirus, SARS-CoV-2, was reported for the first time in late December 2019 in the Hubei province in China and rapidly spread and broke out in the world (Zhu et al., 2020). The spread of SARS-CoV-2 is classified by the World Health Organization (WHO) as a public health emergency of international concern, and pneumonia caused by SARS-CoV-2 has been designated as coronavirus disease 2019 (COVID-19) ([[NoAuthor]]; Team EE, 2020). SARS-CoV-2 is highly contagious due to its direct and rapid human-to-human transmission, especially in comparison to the SARS-CoV and MERS-CoV coronaviruses, which were declared a pandemic by the World Health Organization on March 11, 2020 (Jee, 2020).

Countries that were hit hard by this outbreak in terms of the total number of individuals infected include (in descending order): the United States, India, Brazil, France, Germany and the United Kingdom (WHO, 2022a). The current ongoing pandemic wave has quickly spread to other parts of Asia and subsequently to Europe and other countries, and has caused countless morbidity and mortality worldwide. Among these, America had the largest number of SARS-CoV-2 confirmed cases and deaths and was recognized as the epicenter of the pandemic. This unexpected infection is threatening human health and, consequently, devastating the global economy.

Early Stage of Transmission in Different Regions

Wuhan, the hardest-hit area of China, the first recorded cases were reported in December 2019 and then reached an epidemic peak in February 2020. The emergency response and massive intervention measures were implemented by the Chinese governments at all levels to block the epidemic spread. Following a strict lockdown policy, the epidemic situation was generally under control in China, while the outbreak outside Mainland China is reported to begin on a large scale.

The first documented case in America was in Snohomish County, Washington, on January 20, 2020 (Holshue et al., 2020). The patient was a person who returned from a trip to Wuhan on January 15, 2020. Subsequently, the outbreak spread throughout all 50 states in America in early March, of which New York remains the region most severely affected to date. The genomic epidemiological

of SARS-CoV-2 demonstrates that the initial COVID-19 outbreak on the west coast of the United States was mainly derived from Chinese isolates, while the pandemic in New York and the east coast of the US came from European isolates (Zhang et al., 2020).

In Europe, the first confirmed case had contact with parents from Wuhan (Böhmer et al., 2020). The patient was reported to be infected with SARS-CoV-2 on Jan 26 which resulted in 16 subsequent cases of infection (Böhmer et al., 2020). Despite the implementation of multiple control measures, the epidemic continued to spread across Europe and North America and reached Africa (Egypt) on February 13, 2020. As for sub-Saharan Africa, the first confirmed case appeared in Nigeria (Giandhari et al., 2020). As the last continent where the pandemic spread, South America confirmed its first case on February 25, 2020. By then, no continent in the world was spared (Elizondo et al., 2021).

Novel Evidence of Epidemiological Origin

As the research continues to deepen, although the exact origin remains debatable, there is some small but increasing evidence regarding the source of this outbreak. Recently, many countries have made some discoveries about the early COVID-19 epidemic, and the continuous emergence of earlier cases has triggered deeper reflections on the origin and spread of the virus, which may rewrite the global timeline of the COVID-19 epidemic.

Outside of China, Italy was the first European country to be very strongly impacted by COVID-19 with the first autochthonous case identified in Lombardy on February, 21st, 2020 (Onder et al., 2020). Based on the complete genomic characteristics and phylogenetic analysis, SARS-CoV-2 emerged in Northern Italy a few weeks before the first case was reported. In a previous study, as early as mid-December 2019, environmental surveillance has unambiguously demonstrated that SARS-CoV-2 is present in untreated wastewater of the Milan area, and its concentration is the same as that of samples collected in the later stages of the pandemic (La Rosa et al., 2021). In addition, an oropharyngeal swab sample collected on December 5, 2019, suggested that a 4-year-old boy with no travel history in the Milan area tested positive for SARS-CoV-2, which was 3 months earlier than Italy's first reported case (Amendola et al., 2021). After that, an international research team led by the University of Milan in Italy reported that they found the new coronavirus gene sequence in a biopsy sample from a young female dermatologic patient on November 10, 2019 (Gianotti et al., 2021). This result advanced the appearance of the Italian "Patient Zero" from January 30, 2020 to November 2019. This finding is of considerable epidemiological significance as it substantially enhances our understanding of time and the map of the SARS-CoV-2 transmission routes.

Accumulating evidence has proved that in December 2019 the virus has spread throughout Europe and was misdiagnosed as cases of influenza (Deslandes et al., 2020). According to research, in many areas where wastewater has been sampled, including France (Paris), Spain (Murcia), and three cities and regions in northern Italy (Milan/Lombardy, Turin/Piedmont, and Bologna/Emilia Romagna), SARS-CoV-2 RNA has been detected in the effluent before the local government announced the first case of COVID-19, reflecting that the possible presence of large numbers of asymptomatic carriers and symptomatic patients who were shedding viral RNA prior to the first reported case (Randazzo et al., 2020; La Rosa et al., 2021). A French study has proved the fact through retrospective analysis, and a French with no aetiological diagnosis for hemoptysis tested positive for SARS-CoV-2 (Deslandes et al., 2020). The patient was hospitalized on 27 December 2019 and presented clinical features and radiological patterns frequently observed in Chinese and Italian cohorts previously, indicating that the virus was already spreading throughout the French population in late December 2019 owning to the lack of recent foreign travel (Deslandes et al., 2020).

In accordance with the recent SARS-CoV-2 genome diversity analysis results, all sequences as of the end of 2019 shared a common ancestor and the virus has existed in the human host for a considerable time before it was identified (van Dorp et al., 2020).

Transmission Routes of SARS-CoV-2

As we all know, respiratory droplets and direct contact are the main pathways of SARS-CoV-2 transmission. In common with other CoVs and influenza, SARS-CoV-2 can cause infection by invading mucosa of the eyes, nose, or mouth when infected persons cough or sneeze. Previous work has demonstrated that aerosol and fecal-oral routes also transmit SARS-CoV-2 (Wang et al., 2020). Based on evidence that the SARS-CoV-2 virus could remain viable in an aerosol for at least 3 hours in a closed environment (van Doremalen et al., 2020).

Although the precise mechanism of SARS-CoV-2 transmission is still unclear, with the deepening of research, other transmission routes have been hypothesized. There is growing evidence that, though extremely rare, vertical transmission *in utero* is possible and its underlying mechanism is possibly correlated to the transmission of the well-known SARS-CoV-2-related inflammatory status to the fetus (Fenizia et al., 2020). A recently published study has also shown that SARS-CoV-2 may not be transmitted during childbirth, as it was not detected in vaginal secretion, breastmilk, neonatal throat swab, umbilical cord blood, and amniotic fluid of pregnant women (Mohseni et al., 2020). However, due to the up-regulation of the ACE2 receptor expression, the fetal liver can be a target organ for SARS-CoV-2 infection during pregnancy (Mohseni et al., 2020). Therefore, the effect on the placenta and the intrauterine vertical transmission potential of SARS-CoV-2 need to be further carefully explored, and its adverse consequence for maternal and infant should not be underestimated. In addition, body fluids are risk factors for viruses to invade the body (Mohseni et al., 2020).

THE GENOME STRUCTURE GENERAL CHARACTERISTICS OF SARS-COV-2

The full-length genome of SARS-CoV-2 is 30 kb, including the 5′-region encoding for non-structural proteins and the 3′-region encoding for structural proteins. It has 14 open reading frames

(ORFs) coding for 27 proteins: structural proteins, nonstructural proteins, and accessory proteins (Hatmal et al., 2020).

Non-Structural Proteins

Transformation of the virus begins with the expression of ORF1a and ORF1b gene segments. ORF1a and ORF1b are encoded by the replicase gene and further translated into two large polyproteins (pp1a and pp1ab) (Plant and Dinman, 2008). The ORF1a gene encodes for pp1a protein, while ORF1b forms a fusion protein pp1a/b with pp1a through ribosomal frameshifting (Plant and Dinman, 2008). The processing products of pp1a are termed NSP1-NSP11, while NSP1-NSP10 and NSP12-NSP16 are processed products of pp1ab (**Figure 1**).

The translation frameshift site is a prominent feature of coronaviruses. It has been proposed that programmed ribosomal frameshifting, a crucial mechanism for regulation of ORF1b expression in coronaviruses, may depend on ribosome pausing (Lopinski et al., 2000). The slippery sequence (UUUAAAC) and a downstream hairpin-type pseudoknot help express proteins by causing a deformation of the reading frames (Bakhshandeh et al., 2021). Recently, it has been shown that the -PRRA- insertion sequence thought to be a translational pause site may be involved in the occurrence of stop codons (Postnikova et al., 2021). It has also been demonstrated that codon usage bias, which plays an important role in efficient RNA translation, determines programmed ribosomal frameshifting and ribosome pausing (Postnikova et al., 2021). Insertion of the furin site may be associated with the enhanced infectivity of SARS-CoV-2. This overlapping translation pausing is also strong evidence for the punctuated mode of evolution (Gould, 1994; Heasley et al., 2021). Furthermore, there are two variants (-HRRA- and -LRRA-), whose functional mechanism is not yet clear, that have recently been identified (Postnikova et al., 2021). Some believe that the -HRRA- probably impact infection and pathogenesis of the virus (Plante et al., 2021). Nevertheless, even furin's overall impact on infectivity has recently been questioned, so this remains somewhat controversial (Papa et al., 2021; Johnson et al., 2021). Besides, since the frequency of the variant codon usage was not significantly altered, they may not drastically diminish the translation of the inserted sequence (Postnikova et al., 2021). Of course, it cannot be ruled out that other differences in the variants may affect the pathogenicity of the virus.

Structural proteins provide the structural elements of viral particles, while nonstructural proteins have a multi-faceted role in viral replication, transcription, morphogenesis, and evasion of host antiviral immune responses (Majumdar and Niyogi, 2021). Assembly of the replication-transcription complex (RTC) for cytoplasmic and membrane protection is pivotal to the formation of the new virus in host cells. Nsp3, one of the components of RTC, can be cleaved by PL protease to promote cytokine expression and suppress the host's innate immune response (Bakhshandeh et al., 2021).

SARS-CoV-2 relies on RdRp, the central component of the replication/transcription mechanism, to replicate its genome, rather than host polymerase (Subissi et al., 2014; Gao et al., 2020). The NSP12 catalytic subunit, along with its auxiliary factors NSP7 and NSP8, constitutes the SARS-CoV-2 RdRp complex (Subissi et al., 2014). NSP12 can recognize templates, catalyze and extend nucleotide chains. The heterodimer composed of NSP7 and NSP8 acts as a cofactor not only to stabilize the complex but also to stimulate the enzymatic activity of NSP12 and enhance its binding to RNA. The second subunit of NSP8 is thought to play a role in extending the RNA template binding surface (Subissi et al., 2014; Zeng et al., 2021). Nucleotide incorporation errors caused by RdRp can be corrected by NSP14 (ExoN), a proofreading exonuclease, to improve the fidelity of RNA synthesis (Subissi et al., 2014).

Strains with RdRp mutations have been reported to have a 3-fold higher mutation rate than strains without RdRp mutations (Zeng et al., 2021). The mutation changes the hydrophobicity of the RdRp binding pocket, which may also be one of the reasons for the poor efficacy of remdesivir (Zeng et al., 2021).

Structural Proteins

Spike Protein

As with all coronavirus, SARS-CoV-2 encodes four structural proteins which are the spike, envelope, matrix, and nucleocapsid (**Figure 1**). Despite the high structural similarity, the S protein of

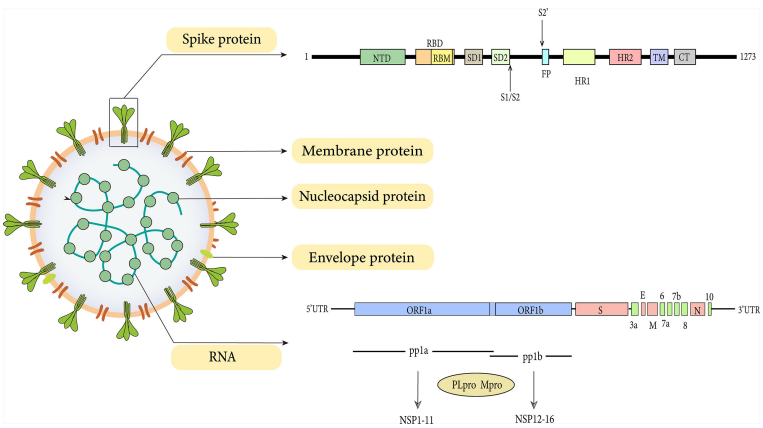

FIGURE 1 | Genome and structure of SARS-CoV-2.

SARS-CoV-2 has a 10-20 folds stronger affinity for ACE2 than SARS-CoV, indicating that SARS-CoV-2 possesses more invasive ability (Wrapp et al., 2020). The structure of SARS-CoV-2 by cryo-EM has demonstrated that, like SARS-CoV, the spike protein of SARS-CoV-2 is also extensively glycosylated (Watanabe et al., 2020).

Spike protein (150 kDa) is a class I fusion protein. It is a large inactive precursor composed of 1273 amino acids and exists as a trimer on the surface of virion and has a characteristic crown-like appearance. The S protein is further processed into receptor-binding subunit S1 and membrane-fusion subunit S2, which have different functions respectively (Heald-Sargent and Gallagher, 2012). The S1 subunit consists of the signal sequence, N-terminal domain (NTD), and receptor binding domain (RBD) (**Figure 1**), where the receptor binding motif (RBM) binds to the ACE2 receptor to enter into the host cell (Shang et al., 2020). Furthermore, the binding can also lead to a conformational change in S2 subunit from a pre-fusion to a post-fusion state (Sainz et al., 2005). These changes favor the exposure and activation of the S2 domain "fusion peptide" which further promotes the fusion of viral and host cell membrane, thus initiating the process of endocytosis (Belouzard et al., 2009; Madu et al., 2009).

Envelop Protein

As stated earlier, the S-protein contributes to the entry of the virus inside the host cell while E-protein (8–12 kDa) is an integral transmembrane protein involved in virus assembly, budding, morphogenesis, and trafficking (Schoeman and Fielding, 2019). It is composed of three domains: a 7–12 amino acid short hydrophilic NTD, a 25 amino acid long hydrophobic transmembrane domain, and a lengthy hydrophilic C terminal region (Sarkar and Saha, 2020). Due to the ion channel activity of the hydrophobic domain, E protein also acts as a viroporin to facilitate viral release, in turn, pathogenicity (Nieto-Torres et al., 2014). By changing the ion homeostasis of cellular organelles, viroporins complete production, maturation, and release processes of the virus (Nieva et al., 2012). Noteworthy, according to the E protein sequence alignment, unlike SARS-CoV, the amino acid residue of SARS-CoV-2 at position 69 replaces the negatively charged glutamic acid with the positively charged arginine (Yoshimoto, 2020). We speculate that the substitution of positively charged basic amino acids for negatively charged acidic amino acids here may be associated with mutations that increase fitness and decrease virulence (Sun et al., 2020).The effect of this amino acid substitution on host range and immune evasion remains unknown.Besides, more research is required to further clarify whether this substitution affects the structure, function, and stability of E protein.

Membrane Protein

M protein (25–30 kDa) is the most abundant structural protein in the CoVs family, with three transmembrane domains that play critical roles in virion formation and complex stabilization during virion assembly by binding of a short glycosylated N-terminal portion of M protein to Nucleocapsid protein (Arndt et al., 2010). M protein gives the virus its spherical virion structure. In addition, research on a variety of CoVs revealed that the viral size is determined by the interaction of M protein with S, N proteins, and viral genomic RNA (Neuman et al., 2011). The M-protein is more abundant in coronaviruses than the E and S proteins, and it is conserved among β-coronaviruses (Ye and Hogue, 2007). Because of its interactions with all other structural proteins, the M protein is thought to be the fundamental organizer of viral assembly (Nieto-Torres et al., 2014). Interestingly, on the one hand, the interaction between M protein and S protein is needed for S protein retention in the ER-Golgi intermediate compartment and incorporation into new virions (Opstelten et al., 1995). M protein, on the other hand, is required for the intracellular production of viral particles that lack S protein. Coronavirus produces noninfectious virion with M protein but no S protein when Tunicamycin is present (Mousavizadeh and Ghasemi, 2021). Additionally, M-protein also appears to alter immune responses by blocking nuclear factor kappa B (NF-κB), resulting in viral multiplication (Fang et al., 2007). However, this theory is controversial. A recent study has demonstrated that the M protein of SARS-CoV-2, along with ORF3a, ORF7a, and N proteins, are considered NF-κB activators and do not directly inhibit or stimulate the IFN response (Su et al., 2021).

Nuleocaspid Protein

Nucleocapsid protein (N protein) is essential for the integration and packaging of viral genomic RNA into virions. It has multiple functions including RNA synthesis control, RNA packaging in helical nucleocapsids, and cooperating with the M protein to assemble virions (McBride et al., 2014). The gene of N protein is conserved and stable with little change over time, with 91 percent and 50 percent sequence identities to SARS-CoV and MERS-CoV, respectively (Hodge et al., 2021). The S, M, E proteins are responsible for the viral coat's production, while the N protein is responsible for binding to the viral genome RNA and then condensing into a higher-order RNA-protein complex to initiate the assembly of virions, which is an essential step in the replication process of coronavirus.

In infected cells, N protein is produced in large amounts from sgRNA and is dynamically localized to the RTCs in the early stages of infection, where it promotes RNA template swapping and recruits host components to aid in the discontinuous transcription and translation of sgRNA (Verheije et al., 2010). The completion of the above functions depends on the characteristic modular structure evolved by the N protein. Similar to SARS-CoV, the N protein of SARS-CoV-2 is a 46 kDa protein that contains two conserved folding domains (the N-terminal RNA binding domain and the C-terminal dimerization domain), flanked by three intrinsically disordered regions (IDRs) (Peng et al., 2020). NTD mediates specific interactions with viral genome packaging signals, and CTD forms a compact dimer to facilitate vRNP assembly (Peng et al., 2020). A conserved core IDR with a serine/arginine-rich region separates two domains (SR). The degree of phosphorylation in SR can realize different functions by affecting the physical properties of N + RNA condensates (Lu et al., 2021).

RNA can trigger liquid-liquid phase separation (LLPS) of the N protein, which is a crucial step in viral assembly (Zhao et al., 2021). Acidic environments have been proven to facilitate the triggering process, so adjusting pH may also be a feasible antiviral treatment direction (Zhao et al., 2021). G3BP1 forms stress granules, which are an essential component of the host cell's antiviral response, and LLPS mediates their formation (Sanders et al., 2020). The N protein interacts directly with co-localized G3BP1, possibly leading to sequestration of G3BP1, depletion of the cytoplasmic pool, and hindering the formation of stress granules to attenuate the stress response and evade the host innate immune response (Cubuk et al., 2021). Alternatively, the N protein might boost viral replication by hijacking this protein or stress granules (Hou et al., 2017). Additionally, the M protein can interact with N protein's C-terminal region to independently mediate phase separation of N protein and promote the assembly of condensates without RNA (Neuman et al., 2011; Lu et al., 2021). RNA-mediated and M-mediated phase separation is achieved by forming condensates with distinct domains of the N protein (Lu et al., 2021). Individual vRNPs are assembled along the genomic RNA to form the packaging (Lu et al., 2021). Then the M protein interacts with these condensed RNPs and acts as an organizational hub for virion through a soluble CTD extending into the viral particle.

Taken together, proteins E, M, and N work together to assemble virions, whereas the S protein facilitates viral attachment, membrane fusion, and entrance (Mittal et al., 2020).

CO-RECEPTOR

ACE2

Early research has demonstrated that both SARS-CoV-2 and SARS-CoV employ ACE2 as a cell entrance receptor (Hoffmann et al., 2020). ACE2 is an integral membrane glycoprotein of type I that has a length of 805 amino acid residues (Jiang et al., 2014). It contains an N-terminal peptidase domain and a C-terminal collectrin-like domain (**Figure 2A**), ending with a 40 amino acid long single transmembrane intracellular segment (Yan et al., 2020). The C-terminal includes a transmembrane alpha-helix, while the N-terminal has one active site. There is also a signal peptide at the end of the N-terminal, in which the protein cleavage site is located next to it. As part of the renin-angiotensin system (RAS), ACE2 cleaves Ang I into Ang 1–9, which is then processed into Ang 1–7 (Yan et al., 2020). Angiotensin-(1–7), as a ligand, binds to the G-protein-coupled receptor MAS, which elicits responses that can counteract those of the ACE/angiotensin II/AT1 axis and exerts actions of vasodilation, vascular protection, anti-fibrosis, anti-proliferation, and anti-inflammation in multiple organs/systems (Patel et al., 2017; Santos et al., 2018). Moreover, ACE2 was found to have the functions of zinc metalloenzyme and carboxypeptidase on chromosome X (Beura et al., 2021). As a result, because men have only one X chromosome, they have a higher fatality rate from SARS-CoV-2 infection than women (Li et al., 2020).

After transcription, the N-terminal signal peptide is responsible for migration to the cell surface, while the C-terminal transmembrane domain is responsible for successful anchoring (Tipnis et al., 2000). The tip of one of the two lobes of the N-terminal peptidase domain binds to the spike RBD to initiate infection (Zhang et al., 2021).

Neuropilin-1

Based on published findings, Neuropilin-1 is an important co-receptor for viral entry which allows SARS-CoV-2 and ACE2 to communicate more easily (Cantuti-Castelvetri et al., 2020). Neuropilin-1 (NRP-1) and Neuropilin-2 (NRP-2) are two members of the Neuropilin family that have a profound impact on lymphangiogenesis, angiogenesis, and axon guidance (Schellenburg et al., 2017). Both NRP-1 and NRP-2 are composed of five extracellular domains (a1/a2, b1/b2, and c domains), a single transmembrane (TM) stretch, and an intracellular PDZ domain-binding motif at C-terminal (Gu et al., 2002) (**Figure 2B**). Daly et al. showed that NRP-1 binds more strongly to the host cell surface than the S1 subunit, possibly destabilizing the S protein complex and activating the escape of S2 from the S1 subunit (Daly et al., 2020). Notably, there is proof that NRP-1 promotes SARS-CoV-2 penetration into the central nervous system (Daly et al., 2020). It has been suggested that this process may be through the olfactory epithelium of the nasal cavity, which perhaps explains the phenomenon of olfactory dysfunction seen in SARS-CoV-2 infected patients (Hopkins et al., 2021). In addition, our research group has studied the contribution of NRP-1 in the occurrence and development of liver fibrosis, which may provide new insights into the mechanism of SARS-CoV-2 in liver injury (Wang et al., 2019).

AXL

AXL is a novel host receptor that not only enhances SARS-CoV-2 to enter human cells but also facilitates viral reproduction (Wang et al., 2021). It also known as Ark, UFO, or Tyro7, was originally a transforming gene isolated from human leukemia cells (O' et al., 1991). As one of three receptor tyrosine kinases in the TAM family, it plays a key role in regulating cell growth, proliferation, apoptosis, and migration (Axelrod and Pienta, 2014). AXL consists of two immunoglobulin (Ig)-like repeats and two fibronectin type III (FN III)-like repeats, a transmembrane domain, and an intracellular kinase domain (Linger et al., 2008) (**Figure 2C**). One of the unique features of the interaction between AXL and the SARS-CoV-2 S protein is that AXL interacts with the S protein NTD rather than RBD (Wang et al., 2021). Also, AXL is considered an ACE2-independent receptor, given that it is not co-expressed with ACE2 in the human lung or trachea (Wang et al., 2021).

Vimentin

Vimentin is a type III intermediate filament protein that is widely expressed on the outer surface of mesenchymal cells, including

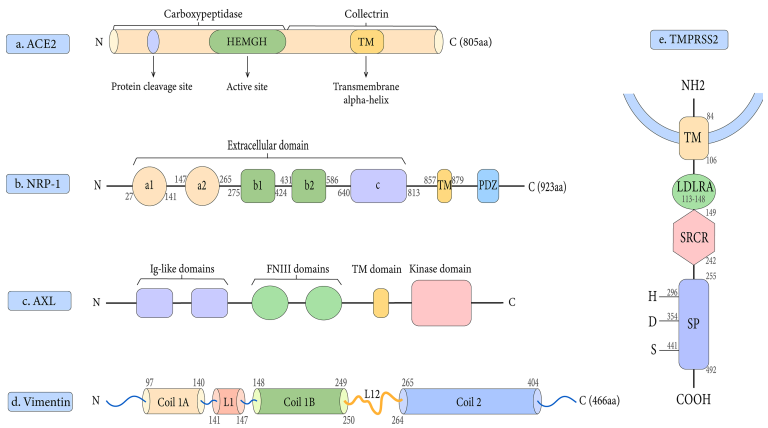

FIGURE 2 | Schematic representation of the structures of the receptor and host proteases. **(A)** The structure of ACE2. **(B)** The structure of NRP-1. **(C)** The structure of AXL.**(D)** The structure of Vimentin. **(E)** The structure of TMPRSS2.

endothelial cells, fibroblasts, macrophages, melanocytes, and lymphocytes (Lowery et al., 2015). In human lung tissue, vimentin expression is high in lung endothelial cells, macrophages, T cells, and granulocytes, but low in type I and II alveolar cells and fibroblasts (Amraei et al., 2022). Vimentin is a 53 kDa polypeptide of 466 amino acids consisting of a central α-helical rod domain flanked by non-α-helical N and C-terminal domains (head and tail) (Danielsson et al., 2018). Its highly conserved α-helical rod domain has a Coil 1 motif near the N-terminus and a Coil 2 motif near the C-terminus (**Figure 2D**). Together, these molecules bind in parallel and align to form a coiled coil, which constitutes the basic structural building block of the entire filament protein family.

Endothelial cells have been recently identified as a direct target of SARS-CoV-2, and their damage can cause a transition from an anticoagulant to a procoagulant phenotype, resulting in microvascular thrombosis and severe coagulation disorders (Varga et al., 2020; Tang et al., 2020). In addition, it is expressed in type II alveolar cells and nasal goblet secretory cells, which also express the known receptors ACE2 and TMPRSS2 (Ziegler et al., 2020; Li et al., 2020). Interestingly, a novel mechanism has recently been proposed by which cells that do not express vimentin can acquire vimentin from the extracellular environment through neutrophil NETosis, a program of neutrophil death that accompanies the formation of neutrophil extracellular traps (NETs) (Khandpur et al., 2013; Thiam et al., 2020; Suprewicz et al., 2022). They also believe that vimentin may enable the SARS-CoV-2 virus to adhere to the cell surface, stimulate the cell membrane to wrap the virus, and thus initiate viral endocytosis (Suprewicz et al., 2022). Previous work has shown that vimentin can act as an attachment factor or coreceptor for SARS-CoV-1, Japanese encephalitis virus, cowpea mosaic virus, human papilloma virus, and dengue virus (Koudelka et al., 2009; Das et al., 2011; Yu et al., 2016; Yang et al., 2016; Schäfer et al., 2017). And it can directly interact with the S protein to enhance the entry of SARS-CoV during the binding process of the S protein to ACE2 (Yu et al., 2016). Amraei et al. showed that vimentin can bind to the RBD of SARS-CoV-2 as an attachment factor to facilitate viral entry and infection of endothelial cells (Amraei et al., 2022). Notably, different motifs on the RBD bind vimentin and ACE2 to improve ACE2-dependent viral entry, respectively (Amraei et al., 2022). Vimentin filaments can be found in the cytoplasm and extracellular compartments, and they co-localize with ACE2 in the cell-cell contact area, acting as a link for spike-ACE2 binding (Amraei et al., 2022).

In summary of earlier studies, vimentin plays important roles in viral infection and lung injury in the following ways: a. interacting with spike proteins to facilitate viral entry; b. influencing virus production during replication or assembly; c. participating in inflammatory and immune responses d. promoting endothelial mesenchymal transition and fibrosis (Li et al., 2020). But its specific role in SARS-CoV-2 virus infection needs more research to confirm. However, anti-vimentin antibodies will certainly be an effective therapeutic strategy for SARS-CoV-2 by blocking the infection of variants or reducing clinical symptoms. Meanwhile, vimentin-coated viruses may bind and aggregate with anti-vimentin antibodies, thereby inhibiting viral infection and promoting viral clearance.

Other Co-Receptors

Besides all those mentioned above, there may be other receptors that mediate viral entry as research progresses. Several proteins that interact with SARS-CoV-2 S have been identified, including cellular heparan sulfate, sialic acids, CD147, and several C-type lectin receptors (DCL-SIGN, L-SIGN, MR, and MGL) (Clausen et al., 2020; Zhang et al., 2020; Gao et al., 2020; Wang et al., 2020; Thépaut et al., 2021; Sun, 2021). Because heparin significantly affects the open conformation of RBD making it more susceptible to ACE2 binding, cellular heparan sulfate plays an important role as a potential receptor in ACE2-dependent SARS-CoV-2 infection (Clausen et al., 2020). Sulfate and ACE2 binding sites on the RBD are next to each other, which provides the structural basis for this function (Clausen et al., 2020).

Furthermore, a receptor-overexpression and ligand-labeling system identified two additional potential candidate receptors, ASGR1 and KREMEN1, by screening more than 5000 human membrane proteins (Wang et al., 2021). They both interact with NTD and RBD, and KREMEN1 also interacts with the S2 domain. This diversity of receptor usage may explain why SARS-CoV-2 is more contagious than other coronaviruses.

SARS-CoV-2 Interaction With Host Proteases

The coronavirus spike protein is always subjected to proteolysis happens with the assistance of numerous protease activators when binding to host cell receptors and initiating subsequent plasma membrane fusion or endocytosis (Li, 2016). In particular, viral fusion and entrance begin with exposure of the internal fusion peptide following proteolysis of the S protein (Zhang et al., 2021). The fusion and entry process requires three categories of proteases that function at different stages of infection: (a) phase of viral attachment: proprotein convertases (e.g., furin), (b) phase of S1 cleavage and detachment from the S2 domain: cell surface proteases [e.g., type II transmembrane serine protease (TMPRSS2)] and (c) phase of intraviral endocytosis: lysosomal proteases (e.g., cathepsin B/L) (Zhang et al., 2021). However, it should be pointed out that many extracellular proteases and many other host proteases may be involved in the cleavage of SARS-CoV-2 S protein based on the *in vivo* complexity and ubiquitous infection (Zhang et al., 2021).

Furin

Furin is a calcium-dependent type I membrane-bound serine endoprotease enzyme that belongs to the seven-member family of subtilisin-like proprotein convertases (Thomas, 2002). Its main job is to complete the activation process by cutting off biologically inactive portions of the protein (Ganesan et al., 2020). SARS-CoV-2 inserts a polybasic residue (RRAR) at the junction of S1 and S2 cleavage sites, whereas SARS-CoV has only one basic amino acid (Amanat et al., 2021). Thus, the spike of SARS-CoV isn't separated by proprotein convertases during virus particle formation and stays untouched on mature virions (Li, 2016). SARS-CoV-related coronaviruses (SARSr-CoV) lack this particular multibasic cleavage site, but it is present in human coronaviruses HKU1, OC43, and MERS-CoV (Hoffmann et al., 2020). Furin cuts S1/S2 site, granting the virus to infect host cells (Shiryaev et al., 2013). Unlike the restricted expression of other endoserine proteases, furin is extensively distributed and is expressed to different extents in distinct tissues and organs throughout the body (Ganesan et al., 2020). As a result, the almost ubiquitous expression of furin-like proteases may explain the high pathogenicity and severity, broad cell and tissue tropism, multiple organ damage as well as increasing its transmissibility of COVID-19 (Ganesan et al., 2020). Moreover, the spike cleavability is thought to determine the zoonotic potential under coronavirus infection (Hoffmann et al., 2020).

Recent studies have demonstrated that the addition of basic residues at the furin cleavage site in viral variants increases cell-cell fusion but not virus-cell fusion (Hoffmann et al., 2020). However, it should be mentioned that although the loss of furin significantly reduces infection by reducing the infectivity of virus particles rather than reducing virus production, it does not eliminate it (Papa et al., 2021). As a result, there is no doubt that furin is an extremely critical cofactor, but it is not required for infection, and replication will proceed even without it (Papa et al., 2021). This is also one of the reasons why existing antiviral treatments for SARS-CoV-2 based on furin-targeted medicines may not completely prevent viral infection (Papa et al., 2021). In addition, considering that furin is essential for normal development, short-term inhibitor treatment might be well-tolerated, but blocking this enzyme for a prolonged time might lead to unwanted toxic effects (Hoffmann et al., 2020).

TMPRSS2

TMPRSS2 is a 492 amino acid residue long located on human chromosome 21q 22.3 (Antalis et al., 2011). It contains four different domains: a type II transmembrane domain, an LDL receptor class A (LDLRA) domain, a scavenger receptor cysteine-rich (SRCR) domain, and a serine protease domain (Thunders and Delahunt, 2020) (**Figure 2E**). To date, the physiological roles of TMPRSS2 are still not completely understood, but it is involved in a variety of biological processes (Thunders and Delahunt, 2020).

Another important function of TMPRSS2 is to cleave and trim the spike proteins to produce a better conformational state, and further activate the S protein to expose its fusion region to achieve the aim of ACE2 binding activity and virus-cell fusion (Hoffmann et al., 2020). It has been shown that TMPRSS2 expressing cells can isolate more SARS-CoV-2 virus particles than non-expressing cells (Matsuyama et al., 2020). It is characterized by a highly conserved catalytic serine protease domain stabilized by three intradomain disulphide bonds (Brooke and Prischi, 2020). The S1 domain contains the catalytic triad required for enzymatic activity, in analogy with the furin subtilisin-like domain (Brooke and Prischi, 2020). The catalytic triad binding site forms a negatively charged pocket, which is conducive to electrostatic interactions with the positively charged peptides of the Spike to catalyze the cleavage, leading to the viral entry (Brooke and Prischi, 2020; Abbasi et al., 2021). Unexpectedly, after the interaction of S protein with ACE2, TMPRSS2 cleaves at the arginine and lysine residues of ACE2, resulting inACE2 shedding and promoting viral particles uptake (Thunders and Delahunt, 2020). In addition to fusion mediated by virions, spike protein present at the plasma membrane can trigger the formation of receptor-dependent syncytia, and TMPRSS2 accelerates this process (Buchrieser et al., 2020). Furthermore, as an androgen-regulated gene, it may be one of the reasons for these gender disparities in the severity of disease course which persists across nations (Chakravarty et al., 2020). It is worth noting that loss of smell (anosmia), as one of the most prevalent and significant characteristics of COVID-19, may also be related to TMPRSS2 (Abbasi et al., 2021).

Indeed, it has been demonstrated that variants with loss of the TMPRSS2 cleavage site allow SARS-CoV-2 entry entirely *via* the endosome pathway and thus exhibit a more limited range of cell tropism (Lau et al., 2020; Sasaki et al., 2021). Under powerful selective pressure, these variants may exist at very low levels in some infected individuals, and it is necessary to screen more clinical samples of patients with mild or asymptomatic infections (Lau et al., 2020).

Cathepsin B/L

Two ways can be used by coronaviruses to enter host cells: In the early stage of entry, the direct fusion of the virus on the plasma membrane is mediated by TMPRSS2; while in the late entry pathway, the coronavirus can be internalized *via* cathepsin-mediated endocytosis (Tang et al., 2020). Cathepsins are classified into three main categories: serine proteases cathepsins, aspartic proteases cathepsins, and lysosomal cysteine cathepsins (Tabrez et al., 2020). Endo- and exopeptidase cathepsin B and endopeptidase cathepsin L that play a critical role in endocytosis are lysosomal cysteine proteases (Hoffmann et al., 2020). The endoplasmic reticulum produces them, and the Golgi apparatus transports them to the lysosome and endosome (Zhang et al., 2021). Low pH is required for their optimal enzymatic activity due to their subcellular location (Zhang et al., 2021). Cathepsin B and Cathepsin L are known fusion activators that become active in early and late endosomes, respectively (Tang et al., 2020). Low endosome pH can activate cathepsin L to release the genome by triggering the fusion of virion membrane with endosome membrane (Tang et al., 2020). Evidence suggests that it is also cathepsin L, not cathepsin B, that plays a key role in the initiation of the S protein (Ou et al., 2020). We believe that elevating endosomal pH to inhibit the activity of cathepsin B/L or simultaneously targeting TMPRSS2 and cathepsin B/L are both feasible therapeutic directions.

THE MECHANISM OF SARS-CoV-2 Infection

The lifecycle of SARS-CoV-2 commences by binding the S1 RBD to the peptidase domain of ACE2 (**Figure 3**). Upon binding, furin cleaves S protein into the S1 and S2 subunits at the multibasic site, resulting in structural change in the S2 subunit (Walls et al., 2020). TMPRSS2 cleavage at the S2 site further exposes the fusion peptide (Walls et al., 2020). In the meantime, the S2 subunit's heptad repeat 1 and heptad repeat 2 domains combine to produce a six-helix bundle fusion core, which brings the virus particles close to the host cell membrane (Xia et al., 2020). Cathepsins can work independently on cells lacking TMPRSS2 and form endocytosis and low pH endosomes, hence mediating virus-cell membrane fusion at the cell surface and endosomal compartments, respectively (Sasaki et al., 2021). Through either entry mechanism, the RNA genome is released into the cytosol, where it is translated into replicase protein and digested by chymotrypsin-like protease (3C-like protease or $3CL^{pro}$) and papain-like protease through a complicated multistep process to produce 16 non-structural proteins (Báez-Santos et al., 2015) (**Figure 3**). RdRp catalyzes viral genome replication and subgenomic transcription to assemble new viral particles.

The formation of double-membrane vesicles (DMVs) in the host cell induced by SARS-CoV-2 infection, is the first step in replication. NSP3 and NSP4 drive the rearrangement of the endoplasmic reticulum (ER) into DMV and promote genomic RNA (gRNA) and subgenomic RNAs (sgRNAs) replication (Tabata et al., 2021). The viral RNAs are stored in DMVs and transported to the cytosol for translation or through double-membrane-spanning pores for viral assembly (Zhang and Zhang, 2021). Structural proteins package gRNA to build progeny virus particles, while the shorter sgRNAs encode conserved structural and accessory proteins. The cytoplasm is the site of RNA and N protein synthesis, while S, M, and E proteins are synthesized in the endoplasmic reticulum and removed to the Golgi apparatus (**Figure 3**). From there, the viral RNA-N complex and S, M, and E proteins follow the secretory pathway to reach the endoplasmic reticulum-Golgi intermediate compartment (ERGIC) to assemble mature virions. After that, the virus particles are released through the budding process of the Golgi apparatus and exocytosis of the cell membrane to start a new round of infection. S protein monomer is also extensively modified *via* N-glycosylation and trimerizes in the ERGIC. The glycosylation of viral proteins has a wide range of roles, including mediating protein folding, affecting viral stability, infectivity, and immune evasion.

THE EMERGING SARS-CoV-2 Variants

Variants that are currently spreading rapidly around the world can be divided into variants of concern, variants of interest, and variants under monitoring (WHO, 2022b). All variants share one specific mutation called D614G which was the dominant variant early in the global epidemic. The D614G mutation occurs when aspartic acid is replaced with glycine at position 614 of the S protein (Jackson et al., 2021). It was first detected in late January 2020, and began to emerge in March 2020, and continuously derived different clades (Jackson et al., 2021). The D614G mutation promotes allosteric of the RBD domain to the "up" conformation bound to the receptor ACE2 by eliminating the hydrogen-bonding interaction with T859 of the adjacent protomer from the spike trimer, thereby enhancing virion infectivity and further enhancing the replication of SARS-CoV-2 in the upper respiratory tract (Plante et al., 2021). In addition, due to the presence of D614G in the SD2 domain, it also enhances furin cleavage at the S1/S2 domain junction (Mohammad et al., 2021). However, the D614G proved to potentially reduce the binding affinity to ACE2 and possibly alter the predicted MHC binding, the biological significance of which warrants further investigation (Mohammad et al., 2021).

Variants of Concern

Variants of concern (VOC) refer to VOI-defined variants with enhanced transmissibility, virulence, and poor response to

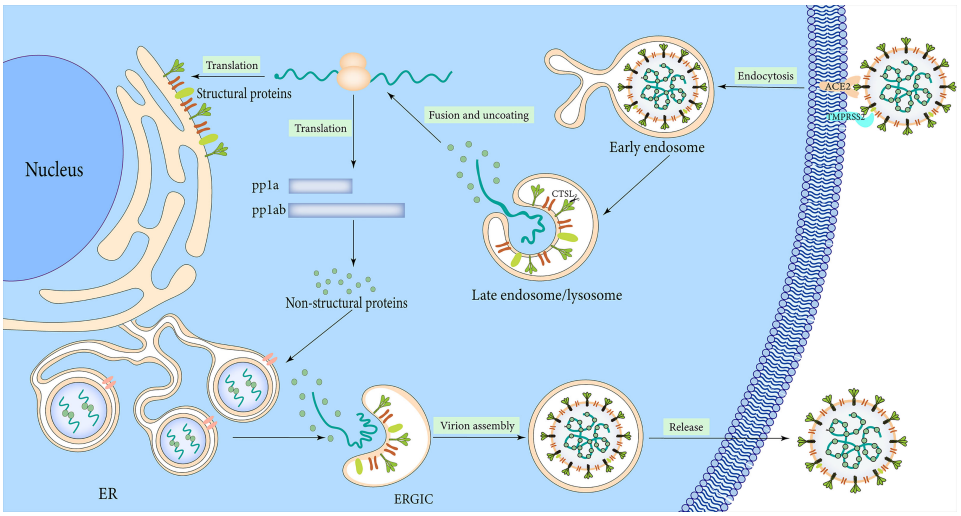

FIGURE 3 | Infection mechanism of SARS-CoV-2.

current diagnostics, vaccines, and treatments (WHO, 2022b). The five variants of concern are alpha, beta, gamma, delta, and omicron.

Alpha (B.1.1.7 Lineage)

B.1.1.7 lineage was circulating in Britain as early as September 2020 and was identified in America at the end of December 2020 (Cascella et al., 2021). Seventeen mutations were identified in the Alpha variant genome. Among them, eight mutations (Δ69-70 deletion, Δ144 deletion, N501Y, A570D, P681H, T716I, S982A, D1118H) are in the spike protein. Amino acid changes in the B.1.1.7 protein improve both the accessibility of RBD and the affinity for ACE2, which might be one of the causes for the increased transmission (Cai et al., 2021). This N501Y single mutation increases the affinity between RBD and ACE2 by ~10-fold (Liu et al., 2021). Studies have shown that the N501Y mutation disrupts the stability of the SARS-CoV-2 S protein in addition to increase transmission rates (Mohammad et al., 2021). More seriously, however, individuals infected with the B.1.1.7 lineage variant have a significantly higher severity of disease and risk of death relative to those who infected with other variants (Challen et al., 2021).

Beta (B.1.351 Lineage or 20H)

The beta variant was reported in South Africa during mid-December 2020 and triggered a second wave of infections in Nelson Mandela Bay (Tegally et al., 2021). Beta variant has nine mutations (L18F, D80A, D215G, R246I, K417N, E484K, N501Y, D614G, and A701V) in the spike protein, of which three mutations (K417N, E484K, and N501Y) are found in RBD and enhance the affinity for the receptors (Cascella et al., 2021). The E484K mutation was shown to significantly alter the electrostatic complementarity of antibody binding to RBD (Mohammad et al., 2021). In comparison with the previous three largest lineages (B.1.1.54, B.1.1.56, and C.1) circulating in South Africa, B.1.351 shows remarkable hypermutation including nonsynonymous mutations that result in amino acid changes (Tegally et al., 2021). The N501Y substitution has also been identified in rapidly spreading lineages (B.1.1.7 and B.1.351), and was the only shared mutation of RBD among the three variants, indicating that exert significant functions in transmission and epidemic (Cascella et al., 2021; Tegally et al., 2021). Previous studies have shown that both N501Y substitution and E484K substitution may increase the affinity with human ACE2, and the combination of N501Y and E484K further enhances the affinity (Tegally et al., 2021).

Notably, the P71L amino acid substitution was discovered in beta variant's E protein. And so far, no mutation of the E protein has been reported in all SARS-COV-2 variants except the Beta variant (Mohammad et al., 2021). The mutation is known to be associated with disease severity and mortality, but its specific mechanism needs further study. Although the full import of the mutations remains unclear, the genomic and epidemiological data demonstrate that this variant has a selective advantage as a result of greater transmissibility, immune escape, or both (Tegally et al., 2021).

Gamma (P.1 Lineage)

The gamma variant was reported in December 2020 in Brazil and was first identified in America in January 2021 (Cascella et al., 2021). The gamma variant includes ten mutations in the spike protein (L18F, T20N, P26S, D138Y, R190S, H655Y, T1027I V1176, K417T, E484K, and N501Y). Three mutations (L18F, K417N, E484K) are found in RBD, identical to the beta variant (Cascella et al., 2021).

Delta (B.1.617.2 Lineage)

The fourth variant of concern, delta variant is also known as the B.1.617.2 was initially identified in December 2020 in India and was responsible for the deadly second wave of COVID-19

infections in April 2021 in India (Cascella et al., 2021). In America, this variant was first reported in March 2021 and was reported to be more transmissible, surpassing preexisting variants of SARS-CoV-2 to emerge as the dominant SARS-CoV-2 variant in most countries (Cascella et al., 2021). The delta variant harbors ten mutations (T19R, (G142D*), 156del, 157del, R158G, L452R, T478K, D614G, P681R, D950N) in the spike protein (Cascella et al., 2021).

Omicron (B.1.1.529 Lineage)

The omicron variant, which has attracted the most global attention, was first reported in South Africa on November 23, 2021 and has been identified in over 100 countries and regions worldwide (Vaughan, 2021). The next day, WHO listed it as Variants under monitoring (VUM). On November 26, according to the evaluation results of the Virus Evolution Working Group, WHO named it omicron and listed it in VOC (Ferré et al., 2021). Preliminary data and analysis obtained locally show an exponential increase in the outbreak in South Africa, and in contrast to the prevalence of beta and delta variants, omicron reduces the risk of initial infection in the population but increases the risk of repeat infection (CDC, 2021).

Omicron has more than 50 mutations, 30 of which are on the S protein on the surface of the virus. Among them, there are more than 20 new mutations in the S1 domain, 8 mutations are located in NTD and 15 mutations are located in RBD, which may directly enhance the interaction between RBD and ACE2 and avoid binding to antibodies induced by previous infection or vaccination (Ferré et al., 2021). Mutations at the Flynn cleavage site may be linked to increased transmission (CoVariants, 2021). In addition, the insertion sequence (ins214EPE), which appeared for the first time in SARS-CoV-2, was shown to be expressed in the common cold coronavirus (HCoV-229E). This may explain the cold-like symptoms and short incubation period of around 3 days caused by omicron (CDC, 2021). Remarkably, however, other symptoms caused by omicron, such as loss of smell and taste, are not present in common influenza. Moreover, the long-term stay of the virus in the body can penetrate various organs. Even after recovery, it can still reignite and attack the CNS, causing many infected people to die of sequelae. Therefore, omicron will still have a serious impact in the long run.

Interestingly, traces of the omicron virus were found in wastewater in New York City on November 21, according to the latest traceability study published by the CDC (2022). This was the day before South African scientists announced the confirmation of the omicron variant and ten days before the first omicron variant infection was reported in the United States. Also in California and Texas, researchers found evidence of omicron in wastewater samples in late November (CDC, 2022). Besides, omicron variants have also been detected in wastewater treatment plants in France since mid-November (Ferré et al., 2021). Although the existing evidence cannot lead to the conclusive conclusion that omicron existed in these places at the time, it still has implications for the discovery and transmission of the virus.

Variants of Interest

Variants of interest (VOI) are defined as variants with specific genetic markers that affect infectivity, disease severity, immune escape, diagnostic or therapeutic escape, and spread across multiple countries and regions causing serious damage. In the early stages, VOI consisted of eight variants, including Epsilon (B.1.427 and B.1.429); Zeta (P.2); Eta (B.1.525); Theta (P.3); Iota (B.1.526); Kappa (B.1.617.1); Lambda (C.37) and Mu (B.1.621) (Cascella et al., 2021). The first six variants have been reclassified as they have finally proven to no longer pose a significant risk to global public health. Therefore, the current VOI only includes Lambda and Mu variants (WHO, 2022b).

Variants Under Monitoring

Variants under monitoring (VUM) are defined as a variant with genetic changes that may pose a risk in the future, requiring enhanced surveillance and repeated assessment (WHO, 2022b). The currently designated VUM mainly includes B.1.1.318, C.1.2, and B.1.640.

ANTI-VIRAL TREATMENTS OF COVID-19

Under the severe situation of repeated outbreaks and the prevalence of new variants, there is still a lack of effective vaccines and antiviral treatments to control the spread of the epidemic, which is a huge challenge for us humans. A growing number of research based on the structure, function, infection mechanism and immunology of virus are pointing the way to the development of effective vaccines and specific drugs against variants in the future. Generally, antiviral therapy that inhibits the entry and replication of SARS-CoV-2 virus plays a significant role in the early stage of the disease; while in the later stage of the disease, when the immune/inflammatory response is enhanced, immunomodulatory and anti-inflammatory therapy may be more beneficial to patient's recovery.

Inhibit SARS-CoV-2 Entry

The first step in the infection process is the attachment and entry of SARS-COV-2 into host cells, and blocking this process has critical implications for disease prevention and early treatment (**Figure 4A**). Blocking the S protein that binds to the receptor is essential for suppressing infection. At present, S protein inhibitors mainly include monoclonal antibodies, convalescent plasma, nanobodies, miniproteins, human soluble ACE2 and ACE2 receptor trap molecules (Rojas et al., 2020; Esparza et al., 2020; Cao et al., 2020; Monteil et al., 2020; Linsky et al., 2020; Corti et al., 2021). For receptors, lactoferrin blocks the attachment of virus to the host cell by binding heparan sulfate, and can synergize with remdesivir to exert an anti-viral effect (Hu et al., 2021). As research progresses, more co-receptors are identified and are expected to become drug targets for COVID-19 therapy. Inhibitors of co-receptors and their generic particles, while in principle suppressing SARS-CoV-2 infection, still need to be validated in more clinical trials.

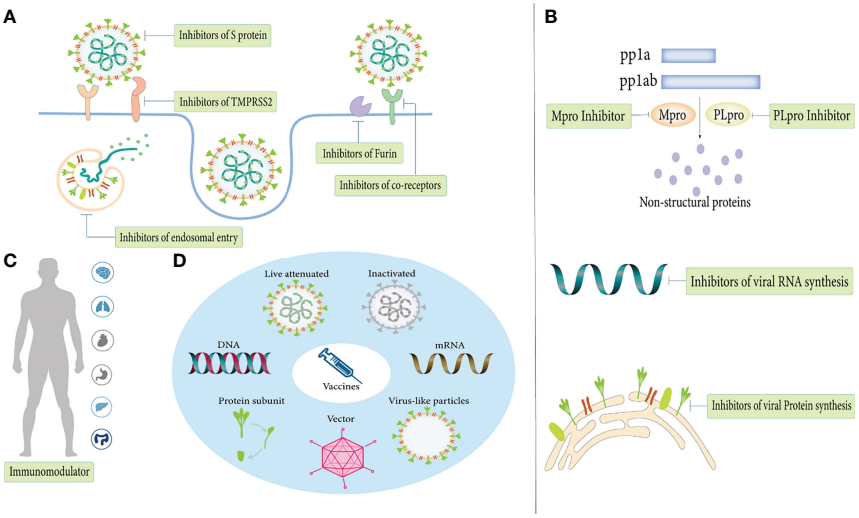

FIGURE 4 | Anti-viral treatments of COVID-19. **(A)** Inhibit SARS-CoV-2 entry. **(B)** Inhibit SARS-CoV-2 replication. **(C)** Immunomodulator. **(D)** Vaccines.

SARS-CoV-2 enters host cells *via* receptor-mediated membrane fusion or the endosomal pathway. Host proteases (eg, furin, TMMPRS2) can promote S protein attachment and virus-cell membrane fusion, so their inhibitors are essential to block fusion entry of SARS-COV-2. Furin inhibitors (decanoyl-RVKR-chloromethylketone) and TMPRSS2 inhibitors (camostat mesylate, neformastat, antiandrogens, bromhexine) have been shown to have varying degrees of effect in reducing SARS-COV-2 infection (Zhou et al., 2015; Hoffmann et al., 2020; Mollica et al., 2020; Ansarin et al., 2020; Cheng et al., 2020). In addition, Catepsin L inhibitors (SSAA09E1, teicoplanin, K1777), hydroxychloroquine, umifenovir, nitazoxanide and niclosamide all exert antiviral effects through the endosomal entry pathway (Axfors et al., 2021; Şimşek-Yavuz and Komsuoğlu Çelikyurt, 2021; Huang et al., 2021; Lokhande and Devarajan, 2021; Backer et al., 2021).

Inhibit SARS-CoV-2 Replication

After viral entry, inhibition of viral replication by inhibiting viral RNA and protein synthesis is another mechanism in antiviral therapy (**Figure 4B**). M^{pro} and PL^{pro} are attractive targets for drug development as proteases essential for viral replication. As M^{pro} is highly conserved and has no human homologues, its inhibitors (lopinavir/ritonavir, PF-07321332, PF-07304814, GC376) are currently in various stages of preclinical and clinical development (Şimşek-Yavuz and Komsuoğlu Çelikyurt, 2021). Inhibitors that inhibit RNA synthesis mainly include RdRp inhibitors (remdesivir, favipiravir, molnupiravir, AT-527), RNA synthesis-related host protein inhibitors (merimepodib and PTC299) and a gene-editing enzyme, Cas13a, that shreds RNA into pieces (Luban et al., 2020; Şimşek-Yavuz and Komsuoğlu Çelikyurt, 2021; Adegbola et al., 2021; Blanchard et al., 2021). In contrast to targeting viral proteins, targeting host proteins has multiple advantages. Precisely, because of such a high rate of mutation of the virus, anti-viral drugs will quickly lose their effectiveness, but due to the relatively host low mutation rate, targeting the host protein is a more feasible therapeutic strategy (Azouz et al., 2020). Host protein inhibitors that support viral protein synthesis including the eEF1A inhibitor (plitidepsin) and the ER chaperon protein inhibitor (fluvoxamine) exhibit potent antiviral activity (Şimşek-Yavuz and Komsuoğlu Çelikyurt, 2021). Of note, targeting human proteins is the potential risk of changing the physiological pathway. In conclusion, more study is required to definitively comprehend the specific effects of host proteins on the human body to guide the feasible direction of future antiviral therapy.

Immunomodulator

Immune responses play a key role in disease process, and the immune escape mechanisms of SARS-COV-2 and variants are not fully understood. Immunomodulators such as ivermectin and interferon have demonstrated antiviral activity in a variety of viruses, but their therapeutic effects on COVID-19 are still controversial (**Figure 4C**) (Caly et al., 2020; Alavi Darazam et al., 2021). Additionally, traditional Chinese medicine also has immunomodulatory effects, and can fight viruses independently or in synergy with Western medicine (An et al., 2021). Due to the lack of relevant studies, whether there are other antiviral mechanisms besides immune regulation remains to be further elucidated. Furthermore, in December 2021, China developed the first COVID-19 specific antibody drug, the combination therapy of BRII-196/BRII-198, and approved for marketing. Clinical data show that the antibody can remain in the human body for 9 to 12 months. It is active against the main popular variants and plays a certain role in preventing infection. On March 14, 2022, the drug was included in the ninth edition of China's COVID-19 diagnosis and treatment plan.

Vaccines

In the near future, newly developed vaccines are also expected to protect against existing and emerging variants of SARS-CoV-2 (**Figure 4D**). According to statistics, as of March 2022, there are

340 candidate vaccines in the world, with 122 in the clinical trial stage and 30 vaccines in routine use (LSHTM, 2021). The types of SARS-CoV-2 vaccines mainly include inactivated vaccines, live attenuated vaccines, vector vaccines (replicating and non-replicating vectors), protein subunit vaccines, virus-like particle vaccines, DNA vaccines, RNA vaccines and other unknown types. Among the three mainstream vaccines currently used in worldwide, RNA vaccines are the most effective, followed by viral vector vaccines and inactivated virus vaccines (Ling et al., 2021). However, inactivated vaccines have the lowest incidence of adverse events, and the safety of mRNA vaccines and viral vector vaccines remains controversial.

CONCLUSION AND PERSPECTIVES

Viral genomes have evolved due to mutations that allow them to adapt well to their hosts and reproduce continuously. They make the virus more infectious, transmissible and help evade the host's immune response by modifying the epitope of the gene. As the COVID-19 pandemic develops, a deeper study of those evolving SARS-CoV-2 variants is critical to understanding mutational adaptability and identifying control measures for the COVID-19 pandemic. A global survey of SARS-CoV-2 genes revealed that mutations in structural, nonstructural, accessory proteins, and untranslated regions were the most common (Majumdar and Niyogi, 2021). Furthermore, mutations in ORF1a, ORF1b, N, and S proteins were present in almost all countries, with the least number of variants in M and E, indicating that they are conserved proteins (Majumdar and Niyogi, 2021). Single nucleotide substitutions are the most common of the numerous forms of mutations. Additionally, insertions, deletions, and frameshift mutations have also been reported, albeit at lower frequencies.

Mutations can alter the antigenic properties of glycoproteins through a variety of different mechanisms, including increasing receptor binding affinity, deleting or inserting residues, altering epitope amino acid substitutions, glycosylation motifs, and protein conformation. Emerging SARS-CoV-2 variants share common features: increased virus transmissibility, infectivity, virulence, and antibody resistance from convalescent sera or vaccines, while also evolving the ability to immune escape. However, the emergence of attenuating mutations suggests an evolutionary trend toward reduced pathogenicity to achieve long-term coexistence with the host. Many scholars believe that the omicron variant is expected to end the COVID-19 pandemic, or at least reduce the impact on life in the future. A group of studies in South Africa argues that the omicron variant is highly contagious and can quickly replace the more pathogenic delta as the dominant variant in various countries (Khan et al., 2021). And, because it causes mild symptoms, the body produces enough neutralizing antibodies that when we encounter the more lethal variants, there will be no secondary infections. Reducing the pathogenicity of SARS-CoV-2 as well as improving immunity in the population may lead to a reduction in critical cases, resulting in a significantly weakened pandemic. Nonetheless, there is still very limited information on the current status of omicron, such as genomics, transmissibility, vaccine efficacy, treatment, and management. Some researchers hold different attitudes towards its future development because from the current evidence, the infectivity, pathogenicity, and immune escape of omicron have been comprehensively strengthened than previous variants, which may bring more serious consequences.

Another worrying fact is that on January 7, 2022, virologists from the University of Cyprus discovered a new variant with both delta and omicron mutations, and named it deltacron. At present, the variant has been found in countries such as France, the Netherlands and Denmark, and the WHO has also confirmed that deltacron is real and not the result of contamination of laboratory samples (Philippe et al., 2022; Kreier, 2022). Due to the small number of cases and unknown characteristics of the new variant, it is not classified as a VOC by the WHO for the time being. However, whether deltacron can be both highly pathogenic as the delta variant and highly transmissible as the omicron variant is a matter of global concern. Judging from the current situation, SARS-CoV-2 is still spreading rapidly around the world, the pandemic is far from over, and the future direction of the epidemic is still confusing. Therefore, better knowledge of how mutations affect people in the SARS-CoV-2 genome and its adaptation to the host will help to elucidate the drivers of transmission and evolutionary success. It is worth noting that an article published by Nature on January 12, 2022 elaborates a new perspective on evolution. Existing theories hold that mutations are completely random, and that natural selection determines which mutations survive. However, they found that mutations in plants are somewhat non-random and that essential genes with important biological functions have a much lower mutation frequency (Monroe et al., 2022). This adaptive mutational bias is a product of evolution and may vary between organisms, a finding that adds a surprising twist to Darwin's theory of evolution by natural selection. Although this theory has not been tested in other species, it may offer another explanation for many of the observations in viral mutations. Since this mutational bias in plants is to protect key genes to ensure survival, we wondered whether high-frequency mutations in key structures and key sites in viruses are also adaptive mutational biases that are forced by survival. As research continues to deepen and the knowledge base expands, we believe that mysteries about viruses and their variants will be revealed one by one.

AUTHOR CONTRIBUTIONS

Conception and design: HB and FL. Collection and assembly of data: JL, HJ, MT, NW, JQ, XY. Data analysis and interpretation: JL, NW, XY. Manuscript writing: JL, HB and FL, JQ. Administrative support: WR and JQ. All authors contributed to the article and approved the submitted version.

FUNDING

This work was supported in part by grants from the Clinical Medical Science and Technology Innovation Program (202019094), the Natural Science Foundation of Shandong Province (ZR2021MH139) and WBE Liver Fibrosis Foundation (CFHPC2021011).

REFERENCES

Abbasi, A. Z., Kiyani, D. A., Hamid, S. M., Saalim, M., Fahim, A., and Jalal, N. (2021). Spiking Dependence of SARS-CoV-2 Pathogenicity on TMPRSS2. *J. Med. Virol.* 93 (7), 4205–4218.

Adegbola, P. I., Fadahunsi, O. S., Adegbola, A. E., and Semire, B. (2021). In Silico Studies of Potency and Safety Assessment of Selected Trial Drugs for the Treatment of COVID-19. *In. Silico. Pharmacol.* 9 (1), 45.

Alavi Darazam, I., Shokouhi, S., Pourhoseingholi, M. A., Naghibi Irvani, S.S., Mokhtari, M., Shabani, M., et al. (2021). Role of Interferon Therapy in Severe COVID-19: The COVIFERON Randomized Controlled Trial. *Sci. Rep.* 11 (1), 8059.

Amanat, F., Strohmeier, S., Rathnasinghe, R., Schotsaert, M., Coughlan, L., García-Sastre, A., et al. (2021). Introduction of Two Prolines and Removal of the Polybasic Cleavage Site Lead to Higher Efficacy of a Recombinant Spike-Based SARS-CoV-2 Vaccine in the Mouse Model. *mBio* 12 (2).

Amendola, A., Bianchi, S., Gori, M., Colzani, D., Canuti, M., Borghi, E., et al. (2021). Evidence of SARS-CoV-2 RNA in an Oropharyngeal Swab Specimen, Milan, Italy, Early December 2019. *Emerg. Infect. Dis.* 27 (2), 648–650.

Amraei, R., Xia, C., Olejnik, J., White, M. R., Napoleon, M. A., Lotfollahzadeh, S., et al. (2022). Extracellular Vimentin is an Attachment Factor That Facilitates SARS-CoV-2 Entry Into Human Endothelial Cells. *Proc. Natl. Acad. Sci. U. S. A.* 119 (6), e2113874119

Ansarin, K., Tolouian, R., Ardalan, M., Taghizadieh, A., Varshochi, M., Teimouri, S., et al. (2020). Effect of Bromhexine on Clinical Outcomes and Mortality in COVID-19 Patients: A Randomized Clinical Trial. *Bioimpacts* 10 (4), 209–215.

Antalis, T. M., Bugge, T. H., and Wu, Q. (2011). Membrane-Anchored Serine Proteases in Health and Disease. *Prog. Mol. Biol. Transl. Sci.* 99, 1–50.

An, X., Zhang, Y., Duan, L., Jin, D., Zhao, S., Zhou, R., et al. (2021). The Direct Evidence and Mechanism of Traditional Chinese Medicine Treatment of COVID-19. *BioMed. Pharmacother.* 137, 111267.

Arndt, A. L., Larson, B. J., and Hogue, B. G. (2010). A Conserved Domain in the Coronavirus Membrane Protein Tail is Important for Virus Assembly. *J. Virol.* 84 (21), 11418–11428.

Coronaviridae Study Group of the International Committee on Taxonomy of Viruses. (2020). The Species Severe Acute Respiratory Syndrome-Related Coronavirus: Classifying 2019-Ncov and Naming it SARS-CoV-2. *Nat. Microbiol.* 5 (4), 536–544.

Axelrod, H., and Pienta, K. J. (2014). Axl as a Mediator of Cellular Growth and Survival. *Oncotarget* 5 (19), 8818–8852.

Axfors, C., Schmitt, A. M., Janiaud, P., Van't Hooft, J., Abd-Elsalam, S., Abdo, E. F., et al. (2021). Mortality Outcomes With Hydroxychloroquine and Chloroquine in COVID-19 From an International Collaborative Meta-Analysis of Randomized Trials. *Nat. Commun.* 12 (1), 2349.

Azouz, N. P., Klingler, A. M., Callahan, V., Akhrymuk, I. V., Elez, K., Raich, L., et al. (2021). Alpha 1 Antitrypsin is an Inhibitor of the SARS-CoV-2-Priming Protease TMPRSS2. *bioRxiv* 6 (1) 55–74.

Backer, V., Sjöbring, U., Sonne, J., Weiss, A., Hostrup, M., Johansen, H. K., et al. (2021). A Randomized, Double-Blind, Placebo-Controlled Phase 1 Trial of Inhaled and Intranasal Niclosamide: A Broad Spectrum Antiviral Candidate for Treatment of COVID-19. *Lancet Reg. Health Eur.* 4, 100084.

Báez-Santos, Y. M., St John, S. E., and Mesecar, A. D. (2015). The SARS-Coronavirus Papain-Like Protease: Structure, Function and Inhibition by Designed Antiviral Compounds. *Antiviral Res.* 115, 21–38.

Bakhshandeh, B., Jahanafrooz, Z., Abbasi, A., Goli, M. B., Sadeghi, M., Mottaqi, M.S., et al. (2021). Mutations in SARS-CoV-2; Consequences in Structure, Function, and Pathogenicity of the Virus. *Microb. Pathog.* 154, 104831.

Belouzard, S., Chu, V. C., and Whittaker, G. R. (2009). Activation of the SARS Coronavirus Spike Protein *via* Sequential Proteolytic Cleavage at Two Distinct Sites. *Proc. Natl. Acad. Sci. U. S. A.* 106 (14), 5871–5876.

Beura, S. K., Panigrahi, A. R., Yadav, P., and Singh, S. K. (2021). Phytochemicals as Potential Therapeutics for SARS-CoV-2-Induced Cardiovascular Complications: Thrombosis and Platelet Perspective. *Front. Pharmacol.* 12, 658273.

Blanchard, E. L., Vanover, D., Bawage, S. S., Tiwari, P. M., Rotolo, L., Beyersdorf, J., et al. (2021). Treatment of Influenza and SARS-CoV-2 Infections *via* mRNA-Encoded Cas13a in Rodents. *Nat. Biotechnol.* 39 (6), 717–726.

Böhmer, M. M., Buchholz, U., Corman, V. M., Hoch, M., Katz, K., Marosevic, D.V., et al. (2020). Investigation of a COVID-19 Outbreak in Germany Resulting From a Single Travel-Associated Primary Case: A Case Series. *Lancet Infect. Dis.* 20 (8), 920–928.

Brooke, G. N., and Prischi, F. (2020). Structural and Functional Modelling of SARS-CoV-2 Entry in Animal Models. *Sci. Rep.* 10 (1), 15917.

Buchrieser, J., Dufloo, J., Hubert, M., Monel, B., Planas, D., Rajah, M.M., et al. (2020). Syncytia Formation by SARS-CoV-2-Infected Cells. *EMBO J.* 39 (23), e106267.

Cai, Y., Zhang, J., Xiao, T., Lavine, C. L., Rawson, S., Peng, H., et al. (2021). Structural Basis for Enhanced Infectivity and Immune Evasion of SARS-CoV-2 Variants. *Science* 373 (6555), 642–648.

Caly, L., Druce, J. D., Catton, M. G., Jans, D. A., and Wagstaff, K. M. (2020). The FDA-Approved Drug Ivermectin Inhibits the Replication of SARS-CoV-2 In Vitro. *Antiviral Res.* 178, 104787.

Cantuti-Castelvetri, L., Ojha, R., Pedro, L. D., Djannatian, M., Franz, J., Kuivanen, S., et al. (2020). Neuropilin-1 Facilitates SARS-CoV-2 Cell Entry and Infectivity. *Science* 370 (6518), 856–860.

Cao, L., Goreshnik, I., Coventry, B., Case, J. B., Miller, L., Kozodoy, L., et al. (2020). *De Novo* Design of Picomolar SARS-CoV-2 Miniprotein Inhibitors. *Science* 370 (6515), 426–431.

Cascella, M., Rajnik, M., Aleem, A., Dulebohn, S. C., and Di Napoli, R. (2021). *Features, Evaluation, and Treatment of Coronavirus (COVID-19)* (Treasure Island, FL: StatPearls Publishing LLC.

CDC. (2021). *SARS-CoV-2 B.1.1.529 (Omicron) Variant—United States, December 1—8, 2021*. Available at: https://www.cdc.gov/mmwr/volumes/70/wr/mm7050e1.htm#T1_down.

CDC. (2022). *Notes From the Field: Early Evidence of the SARS-CoV-2 B.1.1.529 (Omicron) Variant in Comminity Wastewater —United States, November—December 2021*. Available at: https://www.cdc.gov/mmwr/volumes/71/wr/mm7103a5.htm.

Chakravarty, D., Nair, S. S., Hammouda, N., Ratnani, P., Gharib, Y., Wagaskar, V., et al. (2020). Sex Differences in SARS-CoV-2 Infection Rates and the Potential Link to Prostate Cancer. *Commun. Biol.* 3 (1), 374.

Challen, R., Brooks-Pollock, E., Read, J. M., Dyson, L., Tsaneva-Atanasova, K., and Danon, L. (2021). Risk of Mortality in Patients Infected With SARS-CoV-2 Variant of Concern 202012/1: Matched Cohort Study. *BMJ* 372, n579.

Cheng, Y. W., Chao, T. L., Li, C. L., Chiu, M. F., Kao, H. C., Wang, S. H., et al. (2020). Furin Inhibitors Block SARS-CoV-2 Spike Protein Cleavage to Suppress Virus Production and Cytopathic Effects. *Cell Rep.* 33 (2), 108254.

Clausen, T. M., Sandoval, D. R., Spliid, C. B., Pihl, J., Perrett, H. R., Painter, C. D., et al. (2020). SARS-CoV-2 Infection Depends on Cellular Heparan Sulfate and ACE2. *Cell* 183 (4), 1043–1057.e15.

Corti, D., Purcell, L. A., Snell, G., and Veesler, D. (2021). Tackling COVID-19 With Neutralizing Monoclonal Antibodies. *Cell* 184 (12), 3086–3108.

CoVariants. (2021). *Variant:21K (Omicron)*. Available at: https://covariants.org/variants/21K.Omicron.

Cubuk, J., Alston, J. J., Incicco, J. J., Singh, S., Stuchell-Brereton, M. D., Ward, M. D., et al. (2021). The SARS-CoV-2 Nucleocapsid Protein is Dynamic, Disordered, and Phase Separates With RNA. *Nat. Commun.* 12 (1), 1936.

Cui, J., Li, F., and Shi, Z. L. (2019). Origin and Evolution of Pathogenic Coronaviruses. *Nat. Rev. Microbiol.* 17 (3), 181–192.

Daly, J. L., Simonetti, B., Klein, K., Chen, K. E., Williamson, M. K., Antón-Plágaro, C., et al. (2020). Neuropilin-1 is a Host Factor for SARS-CoV-2 Infection. *Science* 370 (6518), 861–865.

Danielsson, F., Peterson, M. K., Caldeira Araújo, H., Lautenschläger, F., and Gad, A. (2018). Vimentin Diversity in Health and Disease. *Cells* 7 (10), 147.

Das, S., Ravi, V., and Desai, A. (2011). Japanese Encephalitis Virus Interacts With Vimentin to Facilitate its Entry Into Porcine Kidney Cell Line. *Virus Res.* 160 (1-2), 404–408.

Deslandes, A., Berti, V., Tandjaoui-Lambotte, Y., Alloui, C., Carbonnelle, E., Zahar, J.R., et al. (2020). SARS-CoV-2 was Already Spreading in France in Late December 2019. *Int. J. Antimicrob. Agents.* 55 (6), 106006.

Elizondo, V., Harkins, G. W., Mabvakure, B., Smidt, S., Zappile, P., Marier, C., et al. (2021). SARS-CoV-2 Genomic Characterization and Clinical Manifestation of the COVID-19 Outbreak in Uruguay. *Emerg. Microbes Infect.* 10 (1), 51–65.

Esparza, T. J., Martin, N. P., Anderson, G. P., Goldman, E. R., and Brody, D. L. (2020). High Affinity Nanobodies Block SARS-CoV-2 Spike Receptor Binding Domain Interaction With Human Angiotensin Converting Enzyme. *Sci. Rep.* 10 (1), 22370.

Fang, X., Gao, J., Zheng, H., Li, B., Kong, L., Zhang, Y., et al. (2007). The Membrane Protein of SARS-CoV Suppresses NF-kappaB Activation. *J. Med. Virol.* 79 (10), 1431–1439.

Fenizia, C., Biasin, M., Cetin, I., Vergani, P., Mileto, D., Spinillo, A., et al. (2020). Analysis of SARS-CoV-2 Vertical Transmission During Pregnancy. *Nat. Commun.* 11 (1), 5128.

Ferré, V. M., Peiffer-Smadja, N., Visseaux, B., Descamps, D., Ghosn, J., and Charpentier, C. (2021). Omicron SARS-CoV-2 Variant: What We Know and What We Don't. *Anaesth. Crit. Care Pain Med.* 41 (1), 100998.

Ganesan, S. K., Venkatratnam, P., Mahendra, J., and Devarajan, N. (2020). Increased Mortality of COVID-19 Infected Diabetes Patients: Role of Furin Proteases. *Int. J. Obes. (Lond).* 44 (12), 2486–2488.

Gao, Y., Yan, L., Huang, Y., Liu, F., Zhao, Y., Cao, L., et al. (2020). Structure of the RNA-Dependent RNA Polymerase From COVID-19 Virus. *Science* 368 (6492), 779–782.

Gao, C., Zeng, J., Jia, N., Stavenhagen, K., Matsumoto, Y., Zhang, H., et al. (2020). SARS-CoV-2 Spike Protein Interacts With Multiple Innate Immune Receptors. *bioRxiv*.

Giandhari, J., Pillay, S., Wilkinson, E., Tegally, H., Sinayskiy, I., Schuld, M., et al. (2020). Early Transmission of SARS-CoV-2 in South Africa: An Epidemiological and Phylogenetic Report. *medRxiv* 103, 234–241.

Gianotti, R., Barberis, M., Fellegara, G., Galván-Casas, C., and Gianotti, E. (2021). COVID-19-Related Dermatosis in November 2019: Could This Case be Italy's Patient Zero. *Br. J. Dermatol* 184 (5), 970–971.

Gould, S. J. (1994). Tempo and Mode in the Macroevolutionary Reconstruction of Darwinism. *Proc. Natl. Acad. Sci. U. S. A.* 91 (15), 6764–6771.

Gu, C., Limberg, B. J., Whitaker, G. B., Perman, B., Leahy, D. J., Rosenbaum, J. S., et al. (2002). Characterization of Neuropilin-1 Structural Features That Confer Binding to Semaphorin 3A and Vascular Endothelial Growth Factor 165. *J. Biol. Chem.* 277 (20), 18069–18076.

Hamming, I., Timens, W., Bulthuis, M. L., Lely, A. T., Navis, G., and van Goor, (2004). Tissue Distribution of ACE2 Protein, the Functional Receptor for SARS Coronavirus. A First Step in Understanding SARS Pathogenesis. *J. Pathol.* 203 (2), 631–637.

Hatmal, M. M., Alshaer, W., Al–Hatamleh, M. A. I., Hatmal, M., Smadi, O., Taha, M. O., et al. (2020). Comprehensive Structural and Molecular Comparison of Spike Proteins of SARS-CoV-2, SARS-CoV and MERS-CoV, and Their Interactions With ACE2. *Cells* 9 (12), 2638.

Heald-Sargent, T., and Gallagher, T. (2012). Ready, Set, Fuse! The Coronavirus Spike Protein and Acquisition of Fusion Competence. *Viruses* 4 (4), 557–580.

Heasley, L. R., Sampaio, N., and Argueso, J. L. (2021). Systemic and Rapid Restructuring of the Genome: A New Perspective on Punctuated Equilibrium. *Curr. Genet.* 67 (1), 57–63.

Hodge, C. D., Rosenberg, D. J., Wilamowski, M., Joachimiak, A., Hura, G. L., Hammel, M., et al. (2021). Rigid Monoclonal Antibodies Improve Detection of SARS-CoV-2 Nucleocapsid Protein. *MAbs* 13 (1), 1905978.

Hoffmann, M., Kleine-Weber, H., and Schroeder, S. (2020). A Multibasic Cleavage Site in the Spike Protein of SARS-CoV-2 Is Essential for Infection of Human Lung Cells. *Mol. Cell.* 78 (4), 779–784.e5.

Hoffmann, M., Kleine-Weber, H., Schroeder, S., Krüger, N., Herrler, T., Erichsen, S., et al. (2020). SARS-CoV-2 Cell Entry Depends on ACE2 and TMPRSS2 and Is Blocked by a Clinically Proven Protease Inhibitor. *Cell* 181 (2), 271–280.e8.

Holshue, M. L., DeBolt, C., Lindquist, S., Lofy, K. H., Wiesman, J., Bruce, H., et al. (2020). First Case of 2019 Novel Coronavirus in the United States. *N. Engl. J. Med.* 382 (10), 929–936.

Hopkins, C., Lechien, J. R., and Saussez, S. (2021). More That ACE2? NRP1 may Play a Central Role in the Underlying Pathophysiological Mechanism of Olfactory Dysfunction in COVID-19 and its Association With Enhanced Survival. *Med. Hypotheses.* 146, 110406.

Hou, S., Kumar, A., Xu, Z., Airo, A.M., Stryapunina, I., Wong, C.P., et al. (2017). Zika Virus Hijacks Stress Granule Proteins and Modulates the Host Stress Response. *J. Virol.* 91 (16) e00474–17.

Huang, D., Yu, H., Wang, T., Yang, H., Yao, R., and Liang, Z. (2021). Efficacy and Safety of Umifenovir for Coronavirus Disease 2019 (COVID-19): A Systematic Review and Meta-Analysis. *J. Med. Virol.* 93 (1), 481–490.

Hu, B., Guo, H., Zhou, P., and Shi, Z. L. (2021). Characteristics of SARS-CoV-2 and COVID-19. *Nat. Rev. Microbiol.* 19 (3), 141–154.

Hu, Y., Meng, X., Zhang, F., Xiang, Y., and Wang, J. (2021). The *In Vitro* Antiviral Activity of Lactoferrin Against Common Human Coronaviruses and SARS-CoV-2 is Mediated by Targeting the Heparan Sulfate Co-Receptor. *Emerg. Microbes Infect.* 10 (1), 317–330.

Jackson, C. B., Zhang, L., Farzan, M., and Choe, H. (2021). Functional Importance of the D614G Mutation in the SARS-CoV-2 Spike Protein. *Biochem. Biophys. Res. Commun.* 538, 108–115.

Jee, Y. (2020). WHO International Health Regulations Emergency Committee for the COVID-19 Outbreak. *Epidemiol. Health* 42, e2020013.

Jiang, F., Yang, J., Zhang, Y., Dong, M., Wang, S., Zhang, Q., et al. (2014). Angiotensin-Converting Enzyme 2 and Angiotensin 1-7: Novel Therapeutic Targets. *Nat. Rev. Cardiol.* 11 (7), 413–426.

Johnson, B. A., Xie, X., Bailey, A. L., Kalveram, B., Lokugamage, K. G., Muruato, A., et al. (2021). Loss of Furin Cleavage Site Attenuates SARS-CoV-2 Pathogenesis. *Nature* 591 (7849), 293–299.

Khandpur, R., Carmona-Rivera, C., Vivekanandan-Giri, A., Gizinski, A., Yalavarthi, S., Knight, J. S., et al. (2013). NETs are a Source of Citrullinated Autoantigens and Stimulate Inflammatory Responses in Rheumatoid Arthritis. *Sci. Transl. Med.* 5 (178), 178ra40.

Khan, K., Karim, F., Cele, S., San, J. E., Lustig, G., Tegally, H., et al. (2021). Omicron Infection Enhances Neutralizing Immunity Against the Delta Variant. *medRxiv*.

Khan, M. I., Khan, Z. A., Baig, M. H., Ahmad, I., Farouk, A. E., Song, Y. G., et al. (2020). Comparative Genome Analysis of Novel Coronavirus (SARS-CoV-2) From Different Geographical Locations and the Effect of Mutations on Major Target Proteins: An in Silico Insight. *PloS One* 15 (9), e0238344.

Koudelka, K. J., Destito, G., Plummer, E. M., Trauger, S. A., Siuzdak, G., and Manchester, M. (2009). Endothelial Targeting of Cowpea Mosaic Virus (CPMV) *via* Surface Vimentin. *PloS Pathog.* 5 (5), e1000417.

Kreier, F. (2022). Deltacron: The Story of the Variant That Wasn't. *Nature* 602 (7895), 19.

La Rosa, G., Mancini, P., Bonanno Ferraro, G., Veneri, C., Iaconelli, M., Bonadonna, L., et al. (2021). SARS-CoV-2 has Been Circulating in Northern Italy Since December 2019: Evidence From Environmental Monitoring. *Sci. Total. Environ.* 750, 141711.

Lau, S. Y., Wang, P., Mok, B. W., Zhang, A. J., Chu, H., Lee, A. C., et al. (2020). Attenuated SARS-CoV-2 Variants With Deletions at the S1/S2 Junction. *Emerg. Microbes Infect.* 9 (1), 837–842.

Li, F. (2016). Structure, Function, and Evolution of Coronavirus Spike Proteins. *Annu. Rev. Virol.* 3 (1), 237–261.

Li, Y., Jerkic, M., Slutsky, A. S., and Zhang, H. (2020). Molecular Mechanisms of Sex Bias Differences in COVID-19 Mortality. *Crit. Care* 24 (1), 405.

Linger, R. M., Keating, A. K., Earp, H. S., and Graham, D. K. (2008). TAM Receptor Tyrosine Kinases: Biologic Functions, Signaling, and Potential Therapeutic Targeting in Human Cancer. *Adv. Cancer Res.* 100, 35–83.

Ling, Y., Zhong, J., and Luo, J. (2021). Safety and Effectiveness of SARS-CoV-2 Vaccines: A Systematic Review and Meta-Analysis. *J. Med. Virol.* 93 (12), 6486–6495.

Linsky, T. W., Vergara, R., Codina, N., Nelson, J. W., Walker, M. J., Su, W., et al. (2020). *De Novo* Design of Potent and Resilient Hace2 Decoys to Neutralize SARS-CoV-2. *Science* 370 (6521), 1208–1214.

Li, Z., Paulin, D., Lacolley, P., Coletti, D., and Agbulut, O. (2020). Vimentin as a Target for the Treatment of COVID-19. *BMJ Open Respir. Res.* 7 (1), e000623.

Liu, D. X., Fung, T. S., Chong, K. K., Shukla, A., and Hilgenfeld, R. (2014). Accessory Proteins of SARS-CoV and Other Coronaviruses. *Antiviral Res.* 109, 97–109.

Liu, H., Zhang, Q., Wei, P., Chen, Z., Aviszus, K., Yang, J., et al. (2021). The Basis of a More Contagious 501Y.V1 Variant of SARS-COV-2. *bioRxiv* 31 (6), 720–722.

Lokhande, A. S., and Devarajan, P. V. (2021). A Review on Possible Mechanistic Insights of Nitazoxanide for Repurposing in COVID-19. *Eur. J. Pharmacol.* 891, 173748.

Lopinski, J. D., Dinman, J. D., and Bruenn, J. A. (2000). Kinetics of Ribosomal Pausing During Programmed -1 Translational Frameshifting. *Mol. Cell Biol.* 20 (4), 1095–1103.

Lowery, J., Kuczmarski, E. R., Herrmann, H., and Goldman, R. D. (2015). Intermediate Filaments Play a Pivotal Role in Regulating Cell Architecture and Function. *J. Biol. Chem.* 290 (28), 17145–17153.

LSHTM (London School of Hygiene & Tropical Medicine). (2021). COVID-19 vaccine tracker. Available at :https://vac-lshtm.shinyapps.io/ncov_vaccine_landscape/.

Luban, J., Sattler, R. A., Mühlberger, E., Graci, J. D., Cao, L., Weetall, M., et al. (2021). The DHODH Inhibitor PTC299 Arrests SARS-CoV-2 Replication and Suppresses Induction of Inflammatory Cytokines. *bioRxiv* 292, 198246.

Lu, S., Ye, Q., Singh, D., Cao, Y., Diedrich, J. K., Yates, J. R. 3rd., et al. (2021). The SARS-CoV-2 Nucleocapsid Phosphoprotein Forms Mutually Exclusive Condensates With RNA and the Membrane-Associated M Protein. *Nat. Commun.* 12 (1), 502.

Lu, R., Zhao, X., Li, J., Niu, P., Yang, B., Wu, H., et al. (2020). Genomic Characterisation and Epidemiology of 2019 Novel Coronavirus: Implications for Virus Origins and Receptor Binding. *Lancet* 395 (10224), 565–574.

Madu, I. G., Roth, S. L., Belouzard, S., and Whittaker, G. R. (2009). Characterization of a Highly Conserved Domain Within the Severe Acute Respiratory Syndrome Coronavirus Spike Protein S2 Domain With Characteristics of a Viral Fusion Peptide. *J. Virol.* 83 (15), 7411–7421.

Majumdar, P., and Niyogi, S. (2021). SARS-CoV-2 Mutations: The Biological Trackway Towards Viral Fitness. *Epidemiol. Infect.* 149, e110.

Matsuyama, S., Nao, N., Shirato, K., Kawase, M., Saito, S., Takayama, I., et al. (2020). Enhanced Isolation of SARS-CoV-2 by TMPRSS2-Expressing Cells. *Proc. Natl. Acad. Sci. U. S. A.* 117 (13), 7001–7003.

McBride, R., van Zyl, M., and Fielding, B. C. (2014). The Coronavirus Nucleocapsid is a Multifunctional Protein. *Viruses* 6 (8), 2991–3018.

Mittal, A., Manjunath, K., Ranjan, R. K., Kaushik, S., Kumar, S., and Verma, V. (2020). COVID-19 Pandemic: Insights Into Structure, Function, and Hace2 Receptor Recognition by SARS-CoV-2. *PloS Pathog.* 16 (8), e1008762.

Mohammad, T., Choudhury, A., Habib, I., Asrani, P., Mathur, Y., Umair, M., et al. (2021). Genomic Variations in the Structural Proteins of SARS-CoV-2 and Their Deleterious Impact on Pathogenesis: A Comparative Genomics Approach. *Front. Cell Infect. Microbiol.* 11, 765039.

Mohseni, A. H., Taghinezhad-S, S., Xu, Z., and Fu, X. (2020). Body Fluids may Contribute to Human-to-Human Transmission of Severe Acute Respiratory Syndrome Coronavirus 2: Evidence and Practical Experience. *Chin. Med.* 15, 58.

Mollica, V., Rizzo, A., and Massari, F. (2020). The Pivotal Role of TMPRSS2 in Coronavirus Disease 2019 and Prostate Cancer. *Future Oncol.* 16 (27), 2029–2033.

Monroe, J. G., Srikant, T., Carbonell-Bejerano, P., Becker, C., Lensink, M., Exposito-Alonso, M., et al. (2022). Mutation Bias Reflects Natural Selection in Arabidopsis Thaliana. *Nature* 602 (7895), 101–105.

Monteil, V., Kwon, H., Prado, P., Hagelkrüys, A., Wimmer, R. A., Stahl, M., et al. (2020). Inhibition of SARS-CoV-2 Infections in Engineered Human Tissues Using Clinical-Grade Soluble Human Ace2. *Cell* 181 (4), 905–913.e7.

Mousavizadeh, L., and Ghasemi, S. (2021). Genotype and Phenotype of COVID-19: Their Roles in Pathogenesis. *J. Microbiol. Immunol. Infect.* 54 (2), 159–163.

Neuman, B. W., Kiss, G., Kunding, A. H., Bhella, D., Baksh, M. F., Connelly, S., et al. (2011). A Structural Analysis of M Protein in Coronavirus Assembly and Morphology. *J. Struct. Biol.* 174 (1), 11–22.

Nieto-Torres, J. L., DeDiego, M. L., Verdiá-Báguena, C., Jimenez-Guardeño, J. M., Regla–Nava, J.A., Fernandez–Delgado, R., et al. (2014). Severe Acute Respiratory Syndrome Coronavirus Envelope Protein Ion Channel Activity Promotes Virus Fitness and Pathogenesis. *PloS Pathog.* 10 (5), e1004077.

Nieva, J. L., Madan, V., and Carrasco, L. (2012). Viroporins: Structure and Biological Functions. *Nat. Rev. Microbiol.* 10 (8), 563–574.

O'Bryan, J. P., Frye, R. A., Cogswell, P. C., Neubauer, A., Kitch, B., Prokop, C., et al. (1991). Axl, a Transforming Gene Isolated From Primary Human Myeloid Leukemia Cells, Encodes a Novel Receptor Tyrosine Kinase. *Mol. Cell Biol.* 11 (10), 5016–5031.

Onder, G., Rezza, G., and Brusaferro, S. (2020). Case-Fatality Rate and Characteristics of Patients Dying in Relation to COVID-19 in Italy. *JAMA* 323 (18), 1775–1776.

Opstelten, D. J., Raamsman, M. J., Wolfs, K., Horzinek, M. C., and Rottier, P. J. (1995). Envelope Glycoprotein Interactions in Coronavirus Assembly. *J. Cell Biol.* 131 (2), 339–349.

Ou, X., Liu, Y., Lei, X., Li, P., Mi, D., Ren, L., et al. (2020). Characterization of Spike Glycoprotein of SARS-CoV-2 on Virus Entry and its Immune Cross-Reactivity With SARS-CoV. *Nat. Commun.* 11 (1), 1620.

Papa, G., Mallery, D. L., Albecka, A., Welch, L. G., Cattin-Ortolá, J., Luptak, J., et al. (2021). Furin Cleavage of SARS-CoV-2 Spike Promotes But is Not Essential for Infection and Cell-Cell Fusion. *PloS Pathog.* 17 (1), e1009246.

Patel, S., Rauf, A., Khan, H., and Abu-Izneid, T. (2017). Renin-Angiotensin-Aldosterone (RAAS): The Ubiquitous System for Homeostasis and Pathologies. *BioMed. Pharmacother.* 94, 317–325.

Peng, Y., Du, N., Lei Dorje, Y. S., Qi, J., Luo, T., et al. (2020). Structures of the SARS-CoV-2 Nucleocapsid and Their Perspectives for Drug Design. *EMBO J.* 39 (20), e105938.

Philippe, C., Pierre-Edouard, F., Jeremy, D., and Matthieu, M. (2022). Culture and Identification of a "Deltamicron" SARS-CoV-2 in a Three Cases Cluster in Southern France. *medRxiv* (medRxiv). doi: 10.1101/2022.03.03.22271812

Plant, E. P., and Dinman, J. D. (2008). The Role of Programmed-1 Ribosomal Frameshifting in Coronavirus Propagation. *Front. Biosci.* 13, 4873–4881.

Plante, J. A., Liu, Y., Liu, J., Xia, H., Johnson, B. A., Lokugamage, K. G., et al . (2021). Spike Mutation D614G Alters SARS-CoV-2 Fitness. *Nature* 592 (7852), 116–121.

Plante, J. A., Mitchell, B. M., Plante, K. S., Debbink, K., Weaver, S. C., and Menachery, V. D. (2021). The Variant Gambit: COVID-19's Next Move. *Cell Host Microbe* 29 (4), 508–515.

Postnikova, O. A., Uppal, S., Huang, W., Kane, M. A., Villasmil, R., Rogozin, I. B., et al. (2021). The Functional Consequences of the Novel Ribosomal Pausing Site in SARS-CoV-2 Spike Glycoprotein RNA. *Int. J. Mol. Sci.* 22 (12), 6490.

Qiang, X. L., Xu, P., Fang, G., Liu, W. B., and Kou, Z. (2020). Using the Spike Protein Feature to Predict Infection Risk and Monitor the Evolutionary Dynamic of Coronavirus. *Infect. Dis. Poverty.* 9 (1), 33.

Randazzo, W., Truchado, P., Cuevas-Ferrando, E., Simón, P., Allende, A., and Sánchez, G. (2020). SARS-CoV-2 RNA in Wastewater Anticipated COVID-19 Occurrence in a Low Prevalence Area. *Water Res.* 181, 115942.

Rojas, M., Rodríguez, Y., Monsalve, D. M., Acosta-Ampudia, Y., Camacho, B., Gallo, J.E., et al. (2020). Convalescent Plasma in Covid-19: Possible Mechanisms of Action. *Autoimmun. Rev.* 19 (7), 102554.

Şimşek-Yavuz, S., and Komsuoğlu Çelikyurt, F. I. (2021). An Update of Anti-Viral Treatment of COVID-19. *Turk. J. Med. Sci.* 51 (SI-1), 3372–3390.

Sainz, B. Jr., Rausch, J. M., Gallaher, W. R., Garry, R. F., and Wimley, W. C. (2005). Identification and Characterization of the Putative Fusion Peptide of the Severe Acute Respiratory Syndrome-Associated Coronavirus Spike Protein. *J. Virol.* 79 (11), 7195–7206.

Sanders, D. W., Kedersha, N., Lee, D. S. W., Strom, A. R., Drake, V., Riback, J. A., et al. (2020). Competing Protein-RNA Interaction Networks Control Multiphase Intracellular Organization. *Cell* 181 (2), 306–324.e28.

Santos, R. A. S., Sampaio, W. O., Alzamora, A. C., Motta-Santos, D., Alenina, N., Bader, M., et al. (2018). The ACE2/Angiotensin-(1-7)/MAS Axis of the Renin-Angiotensin System: Focus on Angiotensin-(1-7). *Physiol. Rev.* 98 (1), 505–553.

Sarkar, M., and Saha, S. (2020). Structural Insight Into the Role of Novel SARS-CoV-2 E Protein: A Potential Target for Vaccine Development and Other Therapeutic Strategies. *PloS One* 15 (8), e0237300.

Sasaki, M., Uemura, K., Sato, A., Toba, S., Sanaki, T., Maenaka, K., et al. (2021). SARS-CoV-2 Variants With Mutations at the S1/S2 Cleavage Site are Generated *In Vitro* During Propagation in TMPRSS2-Deficient Cells. *PloS Pathog.* 17 (1), e1009233.

Schäfer, G., Graham, L. M., Lang, D. M., Blumenthal, M. J., Bergant Marušič, M., and Katz, A. A. (2017). Vimentin Modulates Infectious Internalization of Human Papillomavirus 16 Pseudovirions. *J. Virol.* 91 (16), e00307–17.

Schellenburg, S., Schulz, A., Poitz, D. M., and Muders, M. H. (2017). Role of Neuropilin-2 in the Immune System. *Mol. Immunol.* 90, 239–244.

Schoeman, D., and Fielding, B. C. (2019). Coronavirus Envelope Protein: Current Knowledge. *Virol. J.* 16 (1), 69.

Shang, J., Ye, G., Shi, K., Wan, Y., Luo, C., Aihara, H., et al. (2020). Structural Basis of Receptor Recognition by SARS-CoV-2. *Nature* 581 (7807), 221–224.

Shiryaev, S. A., Chernov, A. V., Golubkov, V. S., Thomsen, E. R., Chudin, E., Chee, M. S., et al. (2013). High-Resolution Analysis and Functional Mapping of

Cleavage Sites and Substrate Proteins of Furin in the Human Proteome. *PloS One* 8 (1), e54290.

Subissi, L., Posthuma, C. C., Collet, A., Zevenhoven-Dobbe, J. C., Gorbalenya, A.E., Decroly, E., et al. (2014). One Severe Acute Respiratory Syndrome Coronavirus Protein Complex Integrates Processive RNA Polymerase and Exonuclease Activities. *Proc. Natl. Acad. Sci. U. S. A.* 111 (37), E3900–E3909.

Sun, X. L. (2021). The Role of Cell Surface Sialic Acids for SARS-CoV-2 Infection. *Glycobiology* 31 (10), 1245–1253.

Sun, M., Zhang, L., Cao, Y., Wang, J., Yu, Z., Sun, X., et al. (2020). Basic Amino Acid Substitution at Residue 367 of the Envelope Protein of Tembusu Virus Plays a Critical Role in Pathogenesis. *J. Virol.* 94 (8), e02011–19.

Suprewicz, Ł., Swoger, M., Gupta, S., Piktel, E., Byfield, F. J., Iwamoto, D.V., et al. (2022). Extracellular Vimentin as a Target Against SARS-CoV-2 Host Cell Invasion. *Small* 18 (6), e2105640.

Su, C. M., Wang, L., and Yoo, D. (2021). Activation of NF-κb and Induction of Proinflammatory Cytokine Expressions Mediated by ORF7a Protein of SARS-CoV-2. *Sci. Rep.* 11 (1), 13464.

Tabata, K., Prasad, V., Paul, D., Lee, J. Y., Pham, M. T., Twu, W. I., et al. (2021). Convergent Use of Phosphatidic Acid for Hepatitis C Virus and SARS-CoV-2 Replication Organelle Formation. *Nat. Commun.* 12 (1), 7276.

Tabrez, S., Jabir, N. R., Khan, M. I., Khan, M. S., Shakil, S., Siddiqui, A. N., et al. (2020). Association of Autoimmunity and Cancer: An Emphasis on Proteolytic Enzymes. *Semin. Cancer Biol.* 64, 19–28.

Tang, T., Bidon, M., Jaimes, J. A., Whittaker, G. R., and Daniel, S. (2020). Coronavirus Membrane Fusion Mechanism Offers a Potential Target for Antiviral Development. *Antiviral Res.* 178, 104792.

Tang, N., Li, D., Wang, X., and Sun, Z. (2020). Abnormal Coagulation Parameters are Associated With Poor Prognosis in Patients With Novel Coronavirus Pneumonia. *J. Thromb. Haemost.* 18 (4), 844–847.

Team EE. (2020). Note From the Editors: World Health Organization Declares Novel Coronavirus (2019-Ncov) Sixth Public Health Emergency of International Concern. *Euro. Surveill.* 25 (5), 200131e.

Tegally, H., Wilkinson, E., Giovanett, M., Iranzadeh, A., Fonseca, V., Giandhari, J., et al. (2021). Detection of a SARS-CoV-2 Variant of Concern in South Africa. *Nature* 592 (7854), 438–443.

Thépaut, M., Luczkowiak, J., Vivés, C., Labiod, N., Bally, I., Lasala, F., et al. (2021). Dc/L-SIGN Recognition of Spike Glycoprotein Promotes SARS-CoV-2 Trans-Infection and can be Inhibited by a Glycomimetic Antagonist. *PloS Pathog.* 17 (5), e1009576.

Thiam, H. R., Wong, S. L., Qiu, R., Kittisopikul, M., Vahabikashi, A., Goldman, A.E., et al. (2020). NETosis Proceeds by Cytoskeleton and Endomembrane Disassembly and PAD4-Mediated Chromatin Decondensation and Nuclear Envelope Rupture. *Proc. Natl. Acad. Sci. U. S. A.* 117 (13), 7326–7337.

Thomas, G. (2002). Furin at the Cutting Edge: From Protein Traffic to Embryogenesis and Disease. *Nat. Rev. Mol. Cell Biol.* 3 (10), 753–766.

Thunders, M., and Delahunt, B. (2020). Gene of the Month: TMPRSS2 (Transmembrane Serine Protease 2). *J. Clin. Pathol.* 73 (12), 773–776.

Tipnis, S. R., Hooper, N. M., Hyde, R., Karran, E., Christie, G., and Turner, A. J. (2000). A Human Homolog of Angiotensin-Converting Enzyme. Cloning and Functional Expression as a Captopril-Insensitive Carboxypeptidase. *J. Biol. Chem.* 275 (43), 33238–33243.

van Doremalen, N., Bushmaker, T., Morris, D. H., Holbrook, M. G., Gamble, A., Williamson, B. N., et al. (2020). Aerosol and Surface Stability of SARS-CoV-2 as Compared With SARS-CoV-1. *N. Engl. J. Med.* 382 (16), 1564–1567.

van Dorp, L., Acman, M., Richard, D., Shaw, L. P., Ford, C. E., Ormond, L., et al. (2020). Emergence of Genomic Diversity and Recurrent Mutations in SARS-CoV-2. *Infect. Genet. Evol.* 83, 104351.

Varga, Z., Flammer, A. J., Steiger, P., Haberecker, M., Andermatt, R., Zinkernagel, A.S., et al. (2020). Endothelial Cell Infection and Endotheliitis in COVID-19. *Lancet* 395 (10234), 1417–1418.

Vaughan, A. (2021). Omicron Emerges. *New Sci.* 252 (3363), 7.

Verheije, M. H., Hagemeijer, M. C., Ulasli, M., Reggiori, F., Rottier, P. J., Masters, P.S., et al. (2010). The Coronavirus Nucleocapsid Protein is Dynamically Associated With the Replication-Transcription Complexes. *J. Virol.* 84 (21), 11575–11579.

Walls, A. C., Park, Y. J., Tortorici, M. A., Wall, A., McGuire, A. T., and Veesler, D. (2020). Structure, Function, and Antigenicity of the SARS-CoV-2 Spike Glycoprotein. *Cell* 181 (2), 281–292.e6.

Wang, K., Chen, W., Zhang, Z., Deng, Y., Lian, J. Q., Du, P., et al. (2020). CD147-Spike Protein is a Novel Route for SARS-CoV-2 Infection to Host Cells. *Signal Transduct. Target. Ther.* 5 (1), 283.

Wang, L., Feng, Y., Xie, X., Wu, H., Su, X. N., Qi, J., et al. (2019). Neuropilin-1 Aggravates Liver Cirrhosis by Promoting Angiogenesis *via* VEGFR2-Dependent PI3K/Akt Pathway in Hepatic Sinusoidal Endothelial Cells. *EBioMedicine* 43, 525–536.

Wang, S., Qiu, Z., Hou, Y., Deng, X., Xu, W., Zheng, T., et al. (2021). AXL is a Candidate Receptor for SARS-CoV-2 That Promotes Infection of Pulmonary and Bronchial Epithelial Cells. *Cell Res.* 31 (2), 126–140.

Wang, M. Y., Zhao, R., Gao, L. J., Gao, X. F., Wang, D. P., and Cao, J. M. (2020). SARS-CoV-2: Structure, Biology, and Structure-Based Therapeutics Development. *Front. Cell Infect. Microbiol.* 10, 587269.

Watanabe, Y., Allen, J. D., Wrapp, D., McLellan, J. S., and Crispin, M. (2020). Site-Specific Glycan Analysis of the SARS-CoV-2 Spike. *Science* 369 (6501), 330–333.

WHO. (2022a). *WHO Coronavirus (COVID-19) Dashboard*. Available at: https://covid19.who.int/.

WHO. (2022b). *Tracking SARS-CoV-2 Variants*. Available at: https://www.who.int/en/activities/tracking-SARS-CoV-2-variants/.

Woo, P. C., Huang, Y., Lau, S. K., and Yuen, K. Y. (2010). Coronavirus Genomics and Bioinformatics Analysis. *Viruses* 2 (8), 1804–1820.

Wrapp, D., Wang, N., Corbett, K. S., Goldsmith, J. A., Hsieh, C. L., Abiona, O., et al. (2020). Cryo-EM Structure of the 2019-Ncov Spike in the Prefusion Conformation. *Science* 367 (6483), 1260–1263.

Xia, S., Liu, M., Wang, C., Xu, W., Lan, Q., Feng, S., et al. (2020). Inhibition of SARS-CoV-2 (Previously 2019-Ncov) Infection by a Highly Potent Pan-Coronavirus Fusion Inhibitor Targeting its Spike Protein That Harbors a High Capacity to Mediate Membrane Fusion. *Cell Res.* 30 (4), 343–355.

Yang, J., Zou, L., Yang, Y., Yuan, J., Hu, Z., Liu, H., et al. (2016). Superficial Vimentin Mediates DENV-2 Infection of Vascular Endothelial Cells. *Sci. Rep.* 6, 38372.

Yan, R., Zhang, Y., Li, Y., Xia, L., Guo, Y., and Zhou, Q. (2020). Structural Basis for the Recognition of SARS-CoV-2 by Full-Length Human ACE2. *Science* 367 (6485), 1444–1448.

Ye, Y., and Hogue, B. G. (2007). Role of the Coronavirus E Viroporin Protein Transmembrane Domain in Virus Assembly. *J. Virol.* 81 (7), 3597–3607.

Yoshimoto, F. K. (2020). The Proteins of Severe Acute Respiratory Syndrome Coronavirus-2 (SARS CoV-2 or N-COV19), the Cause of COVID-19. *Protein J.* 39 (3), 198–216.

Yu, Y. T., Chien, S. C., Chen, I. Y., Lai, C. T., Tsay, Y. G., Chang, S. C., et al. (2016). Surface Vimentin is Critical for the Cell Entry of SARS-CoV. *J. BioMed. Sci.* 23, 14.

Zeng, L., Li, D., Tong, W., Shi, T., and Ning, B. (2021). Biochemical Features and Mutations of Key Proteins in SARS-CoV-2 and Their Impacts on RNA Therapeutics. *Biochem. Pharmacol.* 189, 114424.

Zhang, Q., Chen, C. Z., Swaroop, M., Xu, M., Wang, L., Lee, J., et al. (2020). Heparan Sulfate Assists SARS-CoV-2 in Cell Entry and can be Targeted by Approved Drugs *In Vitro*. *bioRxiv* 6(1) 80.

Zhang, W., Govindavari, J. P., Davis, B. D., Chen, S. S., Kim, J. T., Song, J., et al. (2020). Analysis of Genomic Characteristics and Transmission Routes of Patients With Confirmed SARS-CoV-2 in Southern California During the Early Stage of the US COVID-19 Pandemic. *JAMA Netw. Open* 3 (10), e2024191.

Zhang, Q., Xiang, R., Huo, S., Zhou, Y., Jiang, S., Wang, Q., et al. (2021). Molecular Mechanism of Interaction Between SARS-CoV-2 and Host Cells and Interventional Therapy. *Signal Transduct. Target. Ther.* 6 (1), 233.

Zhang, H., and Zhang, H. (2021). Entry, Egress and Vertical Transmission of SARS-CoV-2. *J. Mol. Cell Biol.* 13 (3), 168–174.

Zhao, M., Yu, Y., Sun, L.M., Xing, J. Q., Li, T., Zhu, Y., et al. (2021). GCG Inhibits SARS-CoV-2 Replication by Disrupting the Liquid Phase Condensation of its Nucleocapsid Protein. *Nat. Commun.* 12 (1), 2114.

Zhou, Y., Vedantham, P., Lu, K., Agudelo, J., Carrion, R. Jr., Nunneley, J. W., et al. (2015). Protease Inhibitors Targeting Coronavirus and Filovirus Entry. *Antiviral Res.* 116, 76–84.

Zhou, P., Yang, X. L., Wang, X. G., Hu, B., Zhang, L., Zhang, W., et al. (2020). A Pneumonia Outbreak Associated With a New Coronavirus of Probable Bat Origin. *Nature* 579 (7798), 270–273.

Zhu, N., Zhang, D., Wang, W., Li, X., Yang, B., Song, J., et al. (2020). A Novel Coronavirus From Patients With Pneumonia in China, 2019. *N. Engl. J. Med.* 382 (8), 727–733.

Ziegler, C. G. K., Allon, S. J., Nyquist, S. K., Mbano, I. M., Miao, V. N., Tzouanas, C. N., et al. (2020). SARS-CoV-2 Receptor ACE2 Is an Interferon-Stimulated Gene in Human Airway Epithelial Cells and Is Detected in Specific Cell Subsets Across Tissues. *Cell* 181 (5), 1016–1035.e19.

Zinzula, L. (2021). Lost in Deletion: The Enigmatic ORF8 Protein of SARS-CoV-2. *Biochem. Biophys. Res. Commun.* 538, 116–124.

Conflict of Interest: The authors declare that the research was conducted in the absence of any commercial or financial relationships that could be construed as a potential conflict of interest.

Publisher's Note: All claims expressed in this article are solely those of the authors and do not necessarily represent those of their affiliated organizations, or those of the publisher, the editors and the reviewers. Any product that may be evaluated in this article, or claim that may be made by its manufacturer, is not guaranteed or endorsed by the publisher.

frontiers | Frontiers in Cellular and Infection Microbiology

ORIGINAL RESEARCH
published: 10 June 2022
doi: 10.3389/fcimb.2022.911313

Evidence of Infection of Human Embryonic Stem Cells by SARS-CoV-2

Weijie Zeng†, Fan Xing†, Yanxi Ji, Sidi Yang, Tiefeng Xu, Siyao Huang, Chunmei Li, Junyu Wu, Liu Cao* and Deyin Guo**

Center for Infection and Immunity Study, School of Medicine, Sun Yat-sen University, Shenzhen, China

OPEN ACCESS

Edited by:
Guiqing Peng, Huazhong Agricultural University, China

Reviewed by:
Jian Chen, Fudan University, China
Yongquan He, Sichuan Academy of Medical Sciences and Sichuan Provincial People's Hospital, China
Shunbin Ning, East Tennessee State University, United States

***Correspondence:**
Deyin Guo
guodeyin@mail.sysu.edu.cn
Liu Cao
caoliu@mail.sysu.edu.cn
Junyu Wu
wujy68@mail.sysu.edu.cn

†These authors have contributed equally to this work

Specialty section:
This article was submitted to Virus and Host, a section of the journal Frontiers in Cellular and Infection Microbiology

Received: *02 April 2022*
Accepted: *13 May 2022*
Published: *10 June 2022*

Citation:
Zeng W, Xing F, Ji Y, Yang S, Xu T, Huang S, Li C, Wu J, Cao L and Guo D (2022) Evidence of Infection of Human Embryonic Stem Cells by SARS-CoV-2. Front. Cell. Infect. Microbiol. 12:911313. doi: 10.3389/fcimb.2022.911313

The severe acute respiratory syndrome coronavirus 2 (SARS-CoV-2) was initially described to target the respiratory system and now has been reported to infect a variety of cell types, including cardiomyocytes, neurons, hepatocytes, and gut enterocytes. However, it remains unclear whether the virus can directly infect human embryonic stem cells (hESCs) or early embryos. Herein, we sought to investigate this question in a cell-culture system of hESCs. Both the RNA and S protein of SARS-CoV-2 were detected in the infected hESCs and the formation of syncytium was observed. The increased level of subgenomic viral RNA and the presence of dsRNA indicate active replication of SARS-CoV-2 in hESCs. The increase of viral titers in the supernatants revealed virion release, further indicating the successful life cycle of SARS-CoV-2 in hESCs. Remarkably, immunofluorescence microscopy showed that only a small portion of hESCs were infected, which may reflect low expression of SARS-CoV-2 receptors. By setting |log2 (fold change)| > 0.5 as the threshold, a total of 1,566 genes were differentially expressed in SARS-CoV-2-infected hESCs, among which 17 interferon-stimulated genes (ISGs) were significantly upregulated. Altogether, our results provide novel evidence to support the ability of SARS-CoV-2 to infect and replicate in hESCs.

Keywords: SARS-CoV-2, infection, replication, mechanism, hESC

INTRODUCTION

In January 2020, a novel, severe, acute, respiratory coronavirus 2 (SARS-CoV-2) syndrome pandemic hit the world (Zhou et al., 2020). By May 6, 2022 there were over 513 million people infected with SARS-CoV-2, causing over 6.24 million deaths worldwide (World Health Organization, https://covid19.who.int).

At the beginning of the epidemic, cells with high expression of ACE2 and TMPRSS2 were found to be susceptible to SARS-CoV-2 infection, such as alveolar epithelial type II cells in the lungs and absorptive epithelial cells in the intestine (Ziegler et al., 2020). Later, it was found that other types of cells such as cardiomyocytes, neurons, and hepatocytes could also be infected by SARS-CoV-2 (Wang et al., 2020b; Zhao et al., 2020; Li et al., 2021b; Song et al., 2021). In May 2020, a study reported that SARS-CoV-2 was found in patients' semen samples (Li et al., 2020a), bringing attentions to the possibility of sexual transmission of SARS-CoV-2 (Sharun et al., 2020; Tatu et al., 2020). To date, there are no documents about SARS-CoV-2 infection in early embryo.

Embryonic stem cell (ESC) determines the embryonic development during early pregnancy and they can differentiate into any cell type of the body. Several types of viruses were found to infect pluripotent stem cells (Bilz et al., 2019; Zahedi-Amiri et al., 2019; Böhnke et al., 2021), which leads to decrease of the pluripotency, triggering autophagy and altering differentiation of stem cells. As the SARS-CoV-2 pandemic continues, the growth and development of the fetus would be severely affected if ESCs can be infected by SARS-CoV-2. However, whether embryos or embryonic stem cells could directly be infected with SARS-CoV-2 remained unclear. Since the establishment of cultured human embryonic stem cell lines such as H1 and H9 (Thomson et al., 1998), the research of human ESCs has been greatly boosted. These cultured human ESC lines can self-renew and differentiate into multiple lineage cell types. This makes it possible to obtain large numbers of hESC in a short period of time instead of preparing a small number of primary hESCs from preimplantation embryos. Thus, it provides convenience for the research of hESC and virus infection.

In this study, we explored the ability of SARS-CoV-2 virus to directly infect human ESCs. We found that H1 and H9 hESCs expressed SARS-CoV-2 viral receptors ACE2 and TMPRSS2 and SARS-CoV-2 could infect these hESCs. We demonstrated the increase of the level of viral RNA and viral protein in hESCs after SARS-CoV-2 infection. The formation of syncytium was observed after 72 hours post-infection (hpi). Moreover, subgenomic viral RNA and dsRNA were detected, and viral titers were increased in the cell culture medium. These results indicated the successful viral replication and viral particle release of SARS-CoV-2 in hESCs. Furthermore, RNA sequencing (RNA-seq) revealed that 17 interferon-stimulated genes (ISGs) were significantly upregulated, including type III interferon gene IFNL1. Taken together, our results provide novel evidence to support the ability of SARS-CoV-2 to infect and replicate in hESCs.

MATERIALS AND METHODS

Cell Culture

Human embryonic stem cell (hESC) H1 and H9 were obtained from Professor Andy Peng Xiang (Center for Stem Cell Biology and Tissue Engineering, Sun Yat-sen University). hESCs were cultured on Matrigel (Corning, 354277) coated plate with daily changed mTeSR Plus media (STEMCELL Technology). hESCs were passed every 4 days with ReleSR (STEMCELL Technology). Caco-2, Calu-3, HUVEC, and BEAS-2B cell lines were obtained from Chinese Academy of Sciences, Shanghai Cell Bank (https://www.cellbank.org.cn). Caco-2 and HUVEC cells were cultured in high glucose Dulbecco's Modified Eagle's Medium (DMEM, Gibco), Calu-3 cell was cultured in Minimum Essential Medium (MEM, Gibco), and BEAS-2B cell was cultured in Dulbecco's Modified Eagle Medium/Nutrient Mixture F-12 (DMEM/F-12, Gibco). Culture media contained 10% fetal bovine serum (FBS, Gibco) and 1% penicillin/streptomycin (Gibco). All cells were cultured in a humidified CO_2 incubator at 37°C.

SARS-CoV-2 Virus

SARS-CoV-2 (hCoV-19/CHN/SYSU-IHV/2020 strain, Accession ID on GISAID: EPI_ISL_444969) was isolated from a sputum sample from a woman admitted to the Eighth People's Hospital of Guangzhou (Ma et al., 2020). The SARS-CoV-2 infection experiments were performed in the BSL-3 laboratory of Sun Yat-sen University.

Infection of hESCs With SARS-CoV-2

hESCs were seeded in 12-well plates two days before SARS-CoV-2 infection and 2×10^5 cells (about 40% confluence) were infected at MOI of 0.1 or 0.01 with SARS-CoV-2 for 2 hours at 37°C. Then viral inoculum was removed and the media were replaced by fresh mTeSR Plus for post virus challenge 48 to 72 hours until harvest. At 48 and 72 hpi, supernatants or cells were harvested for Western blot or RT-qPCR analysis.

Western Blot Analysis

Cells were lysed for 30 min on ice with RIPA buffer and then centrifuged at 16,000g RCF for 15 min at 4°C. Cell lysate was collected and heated with a loading buffer for 10 min at 95°C. Proteins were resolved by SDS-PAGE on a 10% polyacrylamide gel and transferred to 0.45 μm PVDF membrane (Bio-Rad). The membrane was blocked with 5% milk (Solarbio) in TBST (0.05% Tween20) and then probed with a rabbit polyclonal anti-ACE2 antibody (Abcam, ab15348) at 1:1000 dilution or a rabbit monoclonal anti-TMPRSS2 antibody (Abcam, ab109131) or a mouse monoclonal anti-β-actin antibody (Santa Cruz, sc-47778) at 1:1000 dilution or a mouse monoclonal anti-SARS-CoV-2 spike antibody (GeneTex, GTX 632604) overnight at 4°C. The membrane was then incubated with goat-anti-mouse or goat-anti-rabbit secondary antibody conjugated to horseradish peroxidase (Life Technologies, 1:5000) at room temperature for 1 hour. Specific protein bands on the membrane were detected by the ECL detection reagent (Bio-Rad, 1705060) and visualized on a Tanon-5200 Chemiluminescent Imaging System (Tanon Science and Technology, Shanghai, China).

RNA Extraction and RT-qPCR

For detecting the viral load in the supernatant, SARS-CoV-2 RNA was isolated by Magbead Viral DNA/RNA Kit (CWBIO), and SARS-CoV-2 nucleic acid detection kit (Da an Gene Co., Ltd.) was used to quantify viral RNA. For detecting viral RNA or other gene expression in cells, the total RNA was extracted with TRIzol reagent (Thermo Fisher, USA) and reverse-transcribed into cDNA using PrimeScript RT Master Mix (Takara, RR036A) according to the manufacturer's instructions. RT-qPCR was performed with PowerUp SYBR Green Master Mix (Thermo Fisher, A25742) on the ABI QuantStudio5 (Applied Biosystems, USA). The relative abundance of target RNA was normalized to the human housekeeping gene actin beta *ACTB*. The primer sequences for detecting SARS-CoV-2 genome or other genes were shown in **Supplementary Material Table S1**.

RNA Sequencing

After 48 hours post SARS-CoV-2 infection, all cells were harvested for the cDNA library construction in the infection

samples. The generation and sequencing of cDNA libraries were done on Illumina Hiseq-2500 platform to generate 150bp PE reads. Raw RNA-seq reads were trimmed using cutadapt (v1.13) of adaptor sequences AGATCGGAAGAGCACACGTCTGA CTCCAG, AGATCGGAAGAGCGTCGTGTAGGGAAAGAG, and mapped to human genome (hg38) using STAR (v2.5.3a) with GENCODE (vM18) gene annotations. The number of reads mapping to each gene were calculated using HTSeq (v0.11.2). Differential gene transcriptions were analyzed using DESeq2 (v1.18.1) with $|\log2 \text{ (fold change)}| > 0.5$.

Immunofluorescent Staining and TUNEL Fluorescence Assay

hESCs were seeded onto the Matrigel coated coverslips two days before infected with SARS-CoV-2 for 48 hours. Cells were fixed with 4% paraformaldehyde (PFA) in BSL-3 laboratory at room temperature for 3 days and permeabilized by 0.2% Triton X-100 for 20 min. After blocking with 5% bovine serum albumin (BSA) (Abcone, B24726) for 30 min, cells were incubated overnight at 4°C with primary antibodies: mouse monoclonal anti-SARS-CoV-2 Spike antibody (GeneTex, GTX632604), rabbit polyclonal anti-SARS-CoV-2 Spike antibody (GeneTex, GTX135356), rabbit monoclonal anti-Nanog antibody (Cell Signaling Technology, 4903), rabbit monoclonal anti-Oct-4A antibody (Cell Signaling Technology, 2840), mouse monoclonal anti-double-stranded RNA (J2) antibody (SCICONS, 10010500). After the incubation, cells were washed three times with PBS and incubated with Alexa Fluor 488- or 555- or 647- conjugated secondary antibodies for 1 hour at room temperature. For multi-color TUNEL fluorescence assay, positive cells were first detected with CL488 TUNEL fluorescence assay kit (Proteintech, USA PF00006) according to the manufacturer's instructions and followed with immunofluorescent staining. The nuclei were stained with DAPI (1:10000 diluted in PBS). Cells were washed three times with PBS and mounted on a clean glass slide with Fluoromount-G mounting media (SouthernBiotech, USA). The slides were imaged under fluorescence microscope (Observer Z1, Zeiss) with ZEN microscope software (Zeiss) or confocal microscope (C2, Nikon) with NIS-elements software (Nikon).

Statistical Analysis

All images were processed and analyzed with ImageJ software (v1.52p). Data were displayed as the means ± standard deviation (± SD), and histograms were generated by GraphPad Prism 8.2.1. Unpaired *t*-test analysis was performed using GraphPad Prism 8.2.1 to evaluate significant differences between two groups being compared and $p < 0.05$ was considered statistically significant.

RESULTS

SARS-CoV-2 Virus Successfully Infects hESCs

To identify whether SARS-CoV-2 could infect hESCs, we challenged hESCs with SARS-CoV-2 virus at MOI of 0.1. We found that SARS-CoV-2 could directly infect both H1 and H9 hESCs (**Figure 1A**). The SARS-CoV-2 viral spike protein was detected in the cell lysates of both H1 and H9 hESCs at 72 hours post-infection (hpi). Moreover, the increase of viral RNA was also detected in H1 and H9 hESCs at 48 and 72 hpi (**Figures 1B, C**). The expression of ACE2 and TMPRSS2 is regarded as an important factor for SARS-CoV-2 infection (Chen et al., 2021). Thus, previous studies usually used ACE2 and TMPRSS2-expressing cell lines such as Caco-2 or Calu-3 for SARS-CoV-2 research (Yamamoto et al., 2020; Zecha et al., 2020). We have routinely used Caco-2 and Calu-3 cells to study SARS-CoV-2 infection and anti-SARS-CoV-2 drug development (Li et al., 2022). In this work, we evaluated the expression level of ACE2 and TMPRSS2 in hESCs to explore the pathway for SARS-CoV-2 infection. We found that H1 and H9 hESCs expressed a low level of ACE2 and TMPRSS2 compared to SARS-CoV-2-sensitive human differentiated cell lines (**Figure 1D**). The mRNAs of *ACE2* and *TMPRSS2* were also detected in H1 and H9 hESCs (**Figures 1E, F**). Thus, our results revealed that hESC could be infected with the SARS-CoV-2 virus through the ACE2/TMPRSS2 pathway. However, we found that the ACE2 and TMPRSS2 protein content was not correlated with their gene expression. This phenomenon had also been reported in previous studies and was related to the difference of cell types and cell ages (Bilinska et al., 2020; Qiao et al., 2020). Together, our findings showed that SARS-CoV-2 virus was able to infect human embryonic stem cells.

The Infection of SARS-CoV-2 Leads to the Formation of Syncytium in hESCs

It has been reported that cells infected with SARS-CoV-2 can form cell syncytia (Buchrieser et al., 2020; Cheng et al., 2020). Herein, syncytium was observed in the SARS-CoV-2-infected H1 and H9 hESCs (**Figures 2A, B**). We performed immunofluorescence microscopy and observed large, fused cells under a bright field which were co-located with the SARS-CoV-2 spike protein. H1 and H9 hESCs could form colonies in a normal culture condition (**Figures S1A, B**) and the colonies joined together to form large colonies at 72 hpi (**Figure 2** displayed). These colonies were not impaired by SARS-CoV-2 infection and did not display morphological abnormalities.

In addition, multiple Nanog staining for stem cell marker and DAPI for nucleus were observed in the fused cells. It provided evidence that syncytia were formed in both H1 and H9 hESCs (**Figures 2A, B**). This observation further revealed that the human embryonic stem cell could be infected by SARS-CoV-2. However, immunofluorescence microscopy showed that only a small portion of hESCs were infected and the infection rate of SARS-CoV-2 in H1 and H9 hESCs was 7.68‰ and 8.24‰, respectively (**Table S2**), consistent with the relatively low expression levels of ACE2 and TMPRSS2 in hESCs (**Figure 1D**).

The Successful Viral Replication and Viral Particle Release in SARS-CoV-2-Infected hESCs

Whether SARS-CoV-2 can replicate after an infection and produce progeny virus is an important part of the virus life cycle. It has been reported that the stem cells were highly resistant to viral infections (Wu et al., 2018) and this demonstrated that SARS-CoV-2 virus was able to infect hESCs (**Figures 1**, **2**). Therefore, we further studied

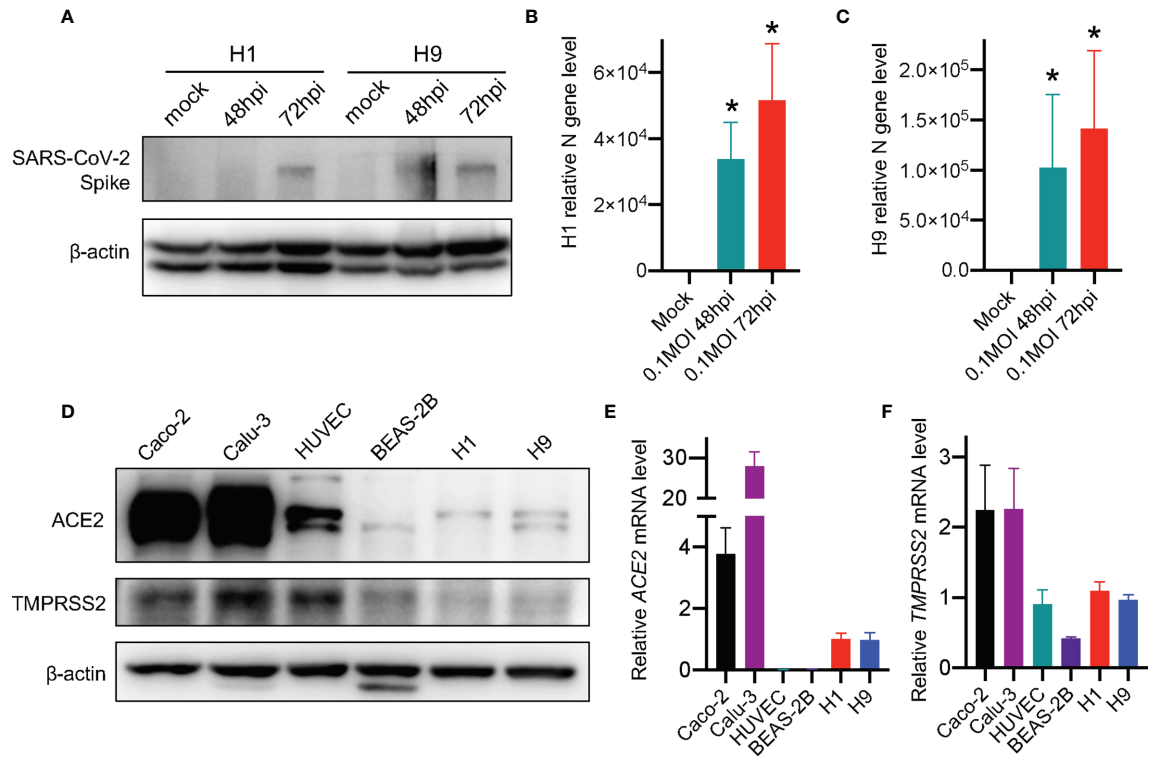

FIGURE 1 | SARS-CoV-2 virus infects hESCs. **(A)** Western blot detection of SARS-CoV-2 spike protein in hESCs after infection. **(B, C)** RT-qPCR detection of SARS-CoV-2 viral RNA in hESCs. Error bars indicate standard deviations of each group. **(D)** Western blot detection of the expression of ACE2 and TMPRSS2 in different cell lines. **(E)** RT-qPCR detection of *ACE2* mRNAs in different human cell lines. **(F)** RT-qPCR detection of *TMPRSS2* mRNAs in different human cell lines. The graphs represent means ± SD from three independent replicates. *$p < 0.05$.

whether SARS-CoV-2 virus could replicate and produce progeny virus in the hESCs. As SARS-CoV-2 is an RNA virus, formation of viral double-stranded RNA (dsRNA) represents an indicator of the viral replication (Klein et al., 2020; Li et al., 2021b). We performed immunofluorescence staining of dsRNA with dsRNA-specific antibody and the dsRNA signal was readily detected in the H1 and H9 hESCs infected by SARS-CoV-2 (**Figures 3A, B**). The subgenomic viral RNA, a unique indicator of coronavirus replication, was also detected (**Figures 3C, D**), suggesting that a successful viral replication took place in the infected hESC. More importantly, the virus titer in the supernatant was increased, indicating the successful viral particle release (**Figures 3E, F**). We used Calu-3 and Caco-2 cells as positive infection controls to evaluate SARS-CoV-2 infectivity and a high virus level was detected in the supernatant of Calu-3 and Caco-2 cells (**Figures S2A, B**), further proving that our SARS-CoV-2 infection system was well operated. These results further demonstrated that the SARS-CoV-2 virus could not only enter but also replicate in human embryonic stem cells.

SARS-CoV-2 Infection Alters the hESC Transcriptomics

We next performed RNA sequencing (RNAseq) to explore the change of hESC transcriptomes after SARS-CoV-2 infection. SARS-CoV-2 RNA reads were detected in RNAseq data (**Figures 4A**), indicating the successful infection of SARS-CoV-2 virus in H1 hESCs. These reads did not show uniform distribution but were enriched at the 3'-end of SARS-CoV-2 genome (**Figure 4A**). RNAseq transcriptome analyses detected expression changes in 1,566 of the 39,219 genes in SARS-CoV-2-infected H1 hESC at 48 hpi (**Figures 4B, C**), with 844 genes downregulated and 722 genes upregulated (log_2FC >0.5 was considered an upregulated gene and log_2FC <-0.5 was considered a downregulated gene, see **Supplementary DEG.xlsx File**). We found a set of interferon stimulated genes (ISGs) that were expressed in H1 hESCs (**Figure 4C**, and **Supplementary DEG.xlsx File**), which was consistent with previous research that shows hESCs expressed a subset of intrinsic ISGs (Wu et al., 2018). Among these differentially expressed genes, 17 ISGs were upregulated and 7 were downregulated significantly (**Figure 4D**). The Kyoto Encyclopedia of Genes and Genomes (KEGG) pathways enriched in SARS-CoV-2 48 hpi H1 hESCs were assessed. In KEGG, innate immune response and cell proliferation, differentiation, apoptosis, and migration regulatory function were observed (**Figure 4E**). We chose three of these 17 upregulated ISGs to confirm the RNAseq result by RT-qPCR (**Figures 4F–H**). The expression level of MT1F, C10orf10, and OAS2 gene was significantly upregulated (**Figures 4F–H**).

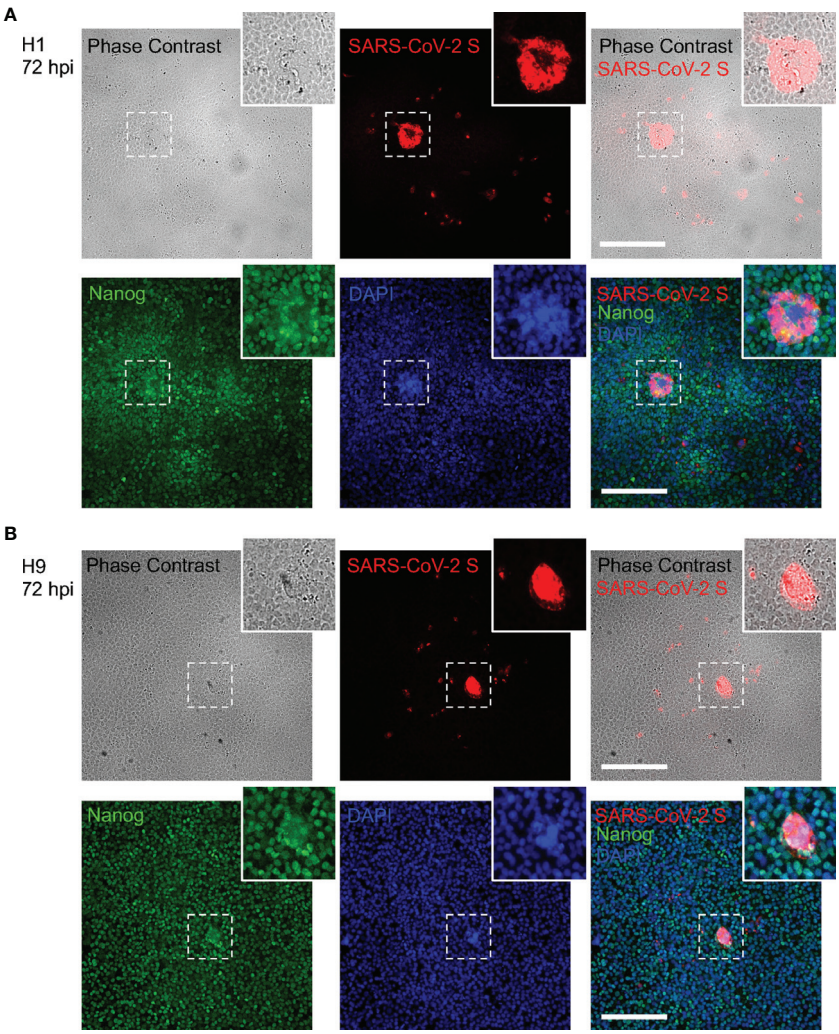

FIGURE 2 | Syncytium formation in hESCs after SARS-CoV-2 infection. **(A)** Combined bright field phase contrast and fluorescence images of H1 hESC after SARS-CoV-2 at 72 hpi. **(B)** Combined bright field phase contrast and fluorescence images of H9 hESC after SARS-CoV-2 at 72 hpi. The inset at the higher-right corner of each image is the enlarged image of the area bordered by the dashed line. Scale bars are 200 μm.

Pluripotent stem cells were widely considered as IFN pathway-defective during viral infection and responded weakly to IFN treatment (Hong and Carmichael, 2013). However, in a previous study, type III interferon IFNL1 was found to be upregulated after RNA virus infection in pluripotent stem cells (Bilz et al., 2019). Interestingly, we found a few reads of IFNL1 in RNAseq (about 1.6 RPKM) but there were no significant changes and the number of the reads was higher compared with type I interferon IFNB and IFNA reads (0 RPKM) in H1 hESC (**Figure 4C** and **Table S2**). Nevertheless, although the read levels in the RNAseq was low, we found that the type III interferon gene IFNL1 was upregulated after SARS-CoV-2 infection in H9 hESC by RT-qPCR (**Figure 4I**) and the downstream ISGs of IFNL1 were upregulated (**Figures 4J–M**). However, there were no significant changes of type I interferon genes in hESCs during SARS-CoV-2 infection (**Figure S3**). It was consistent with the previous report that the type I interferon pathway in hESC did not respond during RNA virus infection (Burke et al., 1978; Földes et al., 2010; Guo et al., 2015; Guo, 2017; Bilz et al., 2019). Our results show that the SARS-CoV-2 infection alters the hESC transcriptomes and the type III interferon pathway may be involved.

SARS-CoV-2 Infection Alters the hESC Viability and Pluripotency

In human embryonic stem cells, transcription factors such as Nanog and Oct-4 are connected with other factors to maintain hESC pluripotency (Heurtier et al., 2019). In a previous study, the human-induced pluripotent stem cell (hiPSC) was reported to have decreased viability and pluripotency after an influenza A virus infection (Zahedi-Amiri et al., 2019). In this study, we found the H1 and H9 hESCs pluripotency marker Nanog was

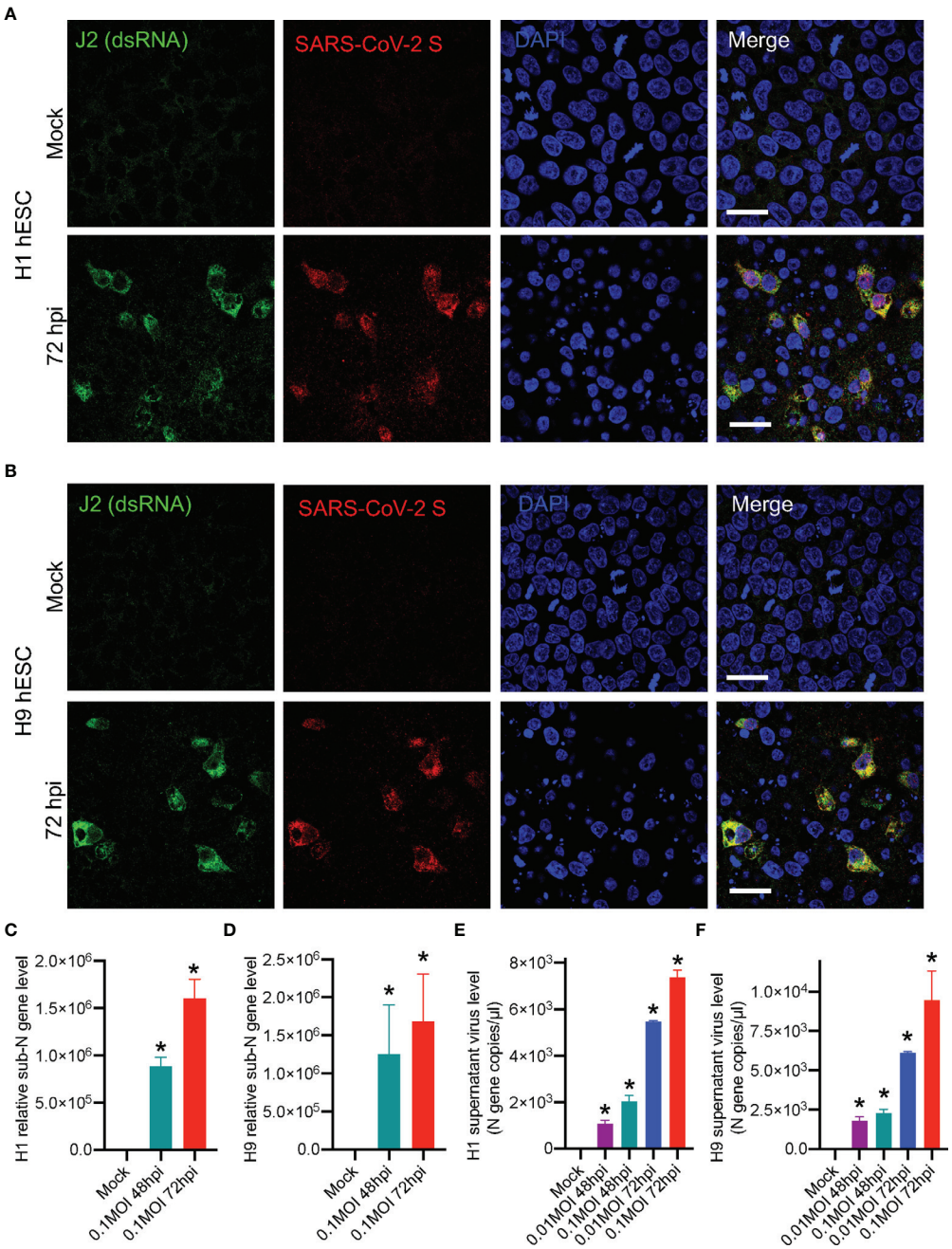

FIGURE 3 | Identifying SARS-CoV-2 replication and viral particle release in hESCs. **(A)** Fluorescence images of H1 hESC after SARS-CoV-2 72 hpi. **(B)** Fluorescence images of H9 hESC after SARS-CoV-2 72 hpi. **(C, D)** RT-qPCR detection of SARS-CoV-2 subgenomic RNA in hESCs. **(E, F)** Detection of SARS-CoV-2 viral RNA in the supernatant by using SARS-CoV-2 nucleic acid detection kit. Error bars indicate standard deviations of each group. *p < 0.05 in specific groups vs. Mock group with *t*-test. All scale bars are 25 μm.

decreased after SARS-CoV-2 infection (**Figures 5A, B**, indicated with white arrowhead). Recently, it has been demonstrated that the SARS-CoV-2 viral spike protein can induce apoptosis (Li et al., 2021a). Accordingly, we speculated that the viability may be affected in the pluripotency-decreasing hESCs. To evaluate possible apoptosis of the infected hESCs, we performed multi-color terminal deoxynucleotidyl transferase dUTP nick end labeling (TUNEL) in the SARS-CoV-2-infected H1 and H9 hESCs. We found that TUNEL-positive cells were significantly increased after SARS-CoV-2 infection (**Figures 5E, F**). In the SARS-CoV-2-infected cells, we confirmed that TUNEL-positive cells were accompanied by a

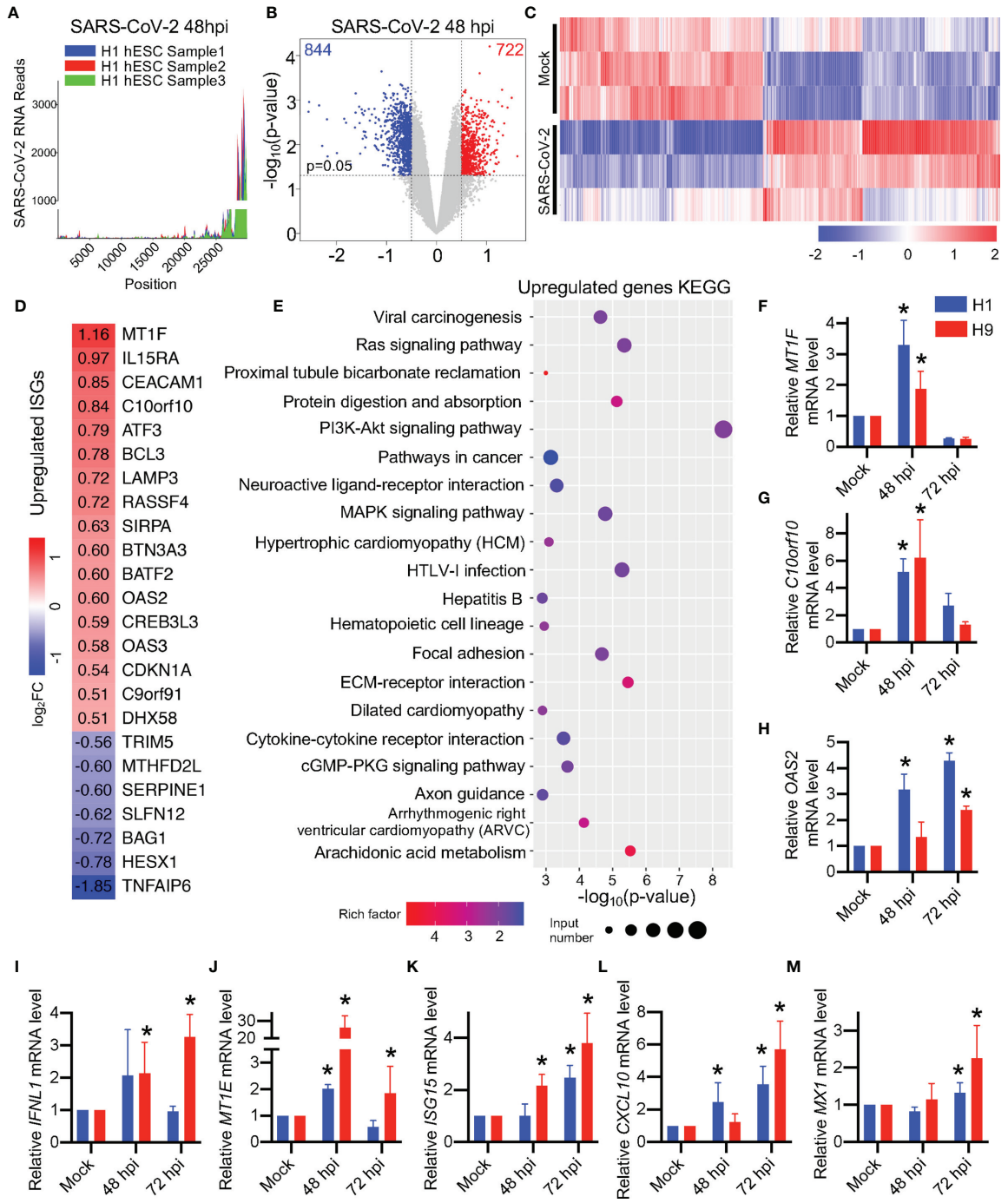

FIGURE 4 | Differentiated expression of transcriptomes in SARS-CoV-2-infected hESCs. **(A)** SARS-CoV-2 RNA reads in RNA-seq analysis. **(B)** Volcano plots showing the expression fold changes and the significance of differentially expressed genes in H1 hESC at 48 hpi ($Log_2FC > 0.5$, p-value < 0.05). **(C)** The heatmap of the whole transcriptomes of differentially expressed genes. **(D)** The heatmap of differentially expressed ISGs. **(E)** KEGG analysis of the whole transcriptome of differentially expressed genes. **(F-M)** RT-qPCR detection of ISGs in SARS-CoV-2 infected hESCs. Error bars indicate standard deviations of each group. *p < 0.05 in specific groups vs. Mock group with *t*-test.

decrease in Oct-4 (**Figures 5E, F**, indicated with white arrowhead). In addition, H1 hESC RNA-seq results showed that there were several genes with altered expression levels associated with the apoptosis (see **Supplementary DEG.xlsx File**). These genes include AATK (Apoptosis Associated Tyrosine Kinase), HRK (Harakiri, BCL2 Interacting Protein), PPP1R13B (Protein Phosphatase 1 Regulatory Subunit 13B), TMBIM1 (Transmembrane BAX Inhibitor Motif

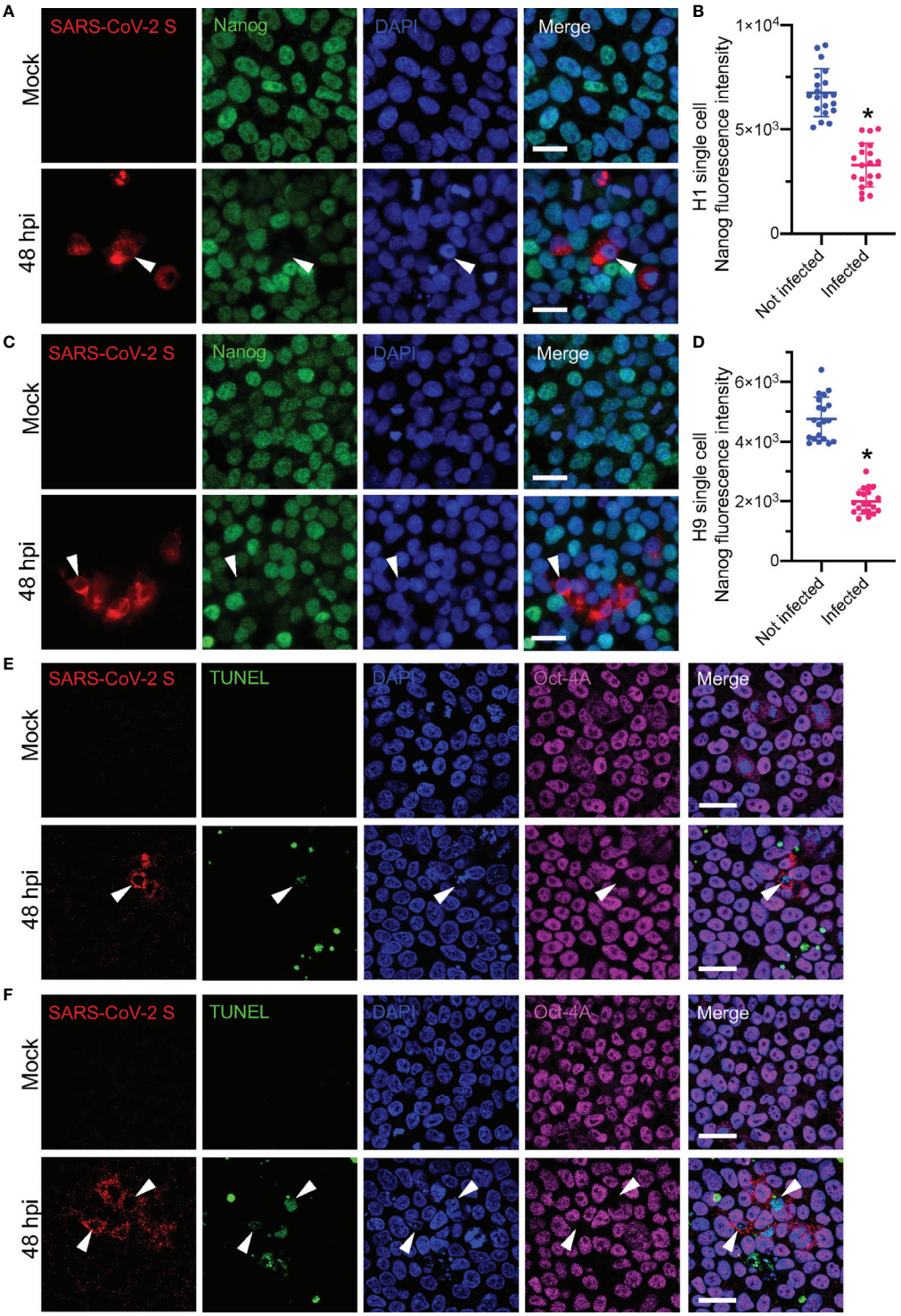

FIGURE 5 | Detecting apoptosis and stem cell pluripotency markers in SARS-CoV-2-infected hESCs. **(A)** Fluorescence images of H1 hESC after SARS-CoV-2 48 hpi. **(B)** Plots of Nanog fluorescence intensities of single cells of H1 hESC, related to **(A)**. **(C)** Fluorescence images of H9 hESC after SARS-CoV-2 48 hpi. **(D)** Plots of Nanog fluorescence intensities of H9 hESC single cells, related to **(C)**. **(E)** Multi-color TUNEL fluorescence assay of H1 hESC after SARS-CoV-2 48 hpi. **(F)** Multi-color TUNEL fluorescence assay of H9 hESC after SARS-CoV-2 48 hpi. White arrowhead indicated the pluripotency decreased SARS-CoV-2 infected hESC. Error bars indicate standard deviations of each group. *$p < 0.05$ in infected group vs. not infected group with *t*-test. All scale bars are 25 μm.

Containing 1), FAIM (Fas Apoptotic Inhibitory Molecule), TIA1 (TIA1 Cytotoxic Granule Associated RNA Binding Protein), CYCS (Cytochrome C, Somatic) and CASP3 (Caspase 3). In conclusion, SARS-CoV-2 infection triggered the apoptosis of hESC, the decrease in cell viability, and pluripotency.

DISCUSSION

Previously, human induced pluripotent stem cells overexpressing the SARS-CoV-2 viral receptor ACE2 (ACE2-iPSCs) or differentiated lineage cells derived from iPSCs were used in a SARS-CoV-2 study (Zhang et al., 2020; Sano et al., 2021). We are interested in whether hESC itself can be infected by SARS-CoV-2. In this study, we revealed that SARS-CoV-2 virus could directly infect hESC. Sano et al. reported that SARS-CoV-2 does not infect undifferentiated human iPSCs (Sano et al., 2021), the discrepancy between iPSC and hESCs needs to be further investigated. We found that hESCs expressed a low level of viral receptors ACE2 and TMPRSS2 but they still can contribute to the SARS-CoV-2 infection. Consequently, a small portion of hESCs were infected and the SARS-CoV-2 virus was reproduced in the infected hESC. However, the low infection rate of SARS-CoV-2 in hESC (**Figure 2**) suggested that only a small part of hESC could be infected, which was consistent with low ACE2 and TMPRSS2 expression in hESC (**Figure 1A**). These results suggest that ACE2-iPS cells or iPSC-derived cells or organoids might be more suitable for SARS-CoV-2 screening than hESC. Recently, CD147, ASGR1, KREMEN1, and AXL have been reported to function as potential receptors (Wang et al., 2020a; Wang et al., 2021; Gu et al., 2022). A few years ago, low expression level of CD147 was found in KhES-1 hESC cell line (Higashi et al., 2015). Therefore, our current study did not define which SARS-CoV-2 receptors mediated the viral infection in hESCs. Whether ACE2 was the main receptor that mediated SARS-CoV-2 infection in hESC needs to be further studied in the future.

SARS-CoV-2 was found to be mainly transmitted by air droplets (Li et al., 2020b) while other routes of transmission were reported. Pregnant women infected with SARS-CoV-2 could transmit the virus to their fetuses (Alzamora et al., 2020; Dong et al., 2020; Fenizia et al., 2020). However, vertical transmission was not reported in SARS-CoV and Middle East respiratory syndrome coronavirus (MERS-CoV) infection. The potential for the vertical transmission of SARS-CoV-2 needs to be carefully investigated. Our results show the SARS-CoV-2 virus could replicate and trigger apoptosis in the infected hESC (**Figures 3**, **5**) which could be fatal to the pregnant fetus.

It has been reported that embryonic stem cells were highly resistant to virus infection (Wu et al., 2019). Several antiviral mechanisms gave stem cells protection against viral infection (Wolf and Goff, 2009; Wu et al., 2018; Poirier et al., 2021; Wu et al., 2021). However, the antiviral resistance of stem cells is not effective against all viral infections. Unlike differentiated somatic cells, stem cells do not rely on the interferon pathway to exert antiviral effects and do not produce type I interferon during viral infection (Guo et al., 2015; Guo, 2017; Wu et al., 2019). In our study, we found that the type I interferon pathway was not activated in hESC with SARS-CoV-2 infection, and IFN-β, IL-1β, and IL-6 were not significantly increased (**Figure S2**). Other researchers also found that human iPSCs infected with the rubella virus exhibited an attenuated type I interferon response (Bilz et al., 2019).

However, a few of ISGs of hESCs were up-regulated (**Figures 4F–M**), indicating that hESCs may exhibit immune response in the SARS-CoV-2 infection. Previous studies have found that some RNA virus infections triggered the type III interferon pathway response in iPSCs (Bilz et al., 2019; Zahedi-Amiri et al., 2019). In this study, we also observed an upregulation of the type III interferon pathway IFNL1 (**Figure 4I**). However, only a few ISGs were altered in hESCs throughout the SARS-CoV-2 infection and we thought that it was unlikely that hESCs relied on the type III interferon pathway response to defend against SARS-CoV-2 infection. Some researchers have found that overexpression of some ISGs in hESCs can alter the differentiation of stem cells (He et al., 2020). It is reasonable to speculate that the type III interferon response of hESCs may relate to the regulation of stem cell differentiation rather than antiviral effects, which needs to be further studied.

Stem cells are found to be weakly responsive to interferon and usually have little change in ISG levels (Wu et al., 2018; Wu et al., 2019). Our RNA-seq results showed that a total of 17 ISGs were up-regulated in H1 hESC during SARS-CoV-2 infection. Among them, the highest $\log_2$FC value was MT1F, which reached 1.16 (about 2.23 times upregulation), and the $\log_2$FC values of the remainder of the up-regulated ISGs were between 0.5 and 1.0, indicating little change in the ISG levels of H1 hESC. When other stem cells such as hiPSCs were infected with the rubella virus, a small number of ISGs such as MX1, IFIT1, IFITM1, IFITM3, ISG15, IRF9, and STAT1 were also up-regulated but IFIT1 with the highest $\log_{10}$FC value was only 0.6 (about 3.98 times upregulation) (Bilz et al., 2019). These results indicate that the change in ISGs caused by the SARS-CoV-2 or other RNA virus infection of hESC were not dramatic. This is different from the differentiated somatic cells which may produce robust interferon responses during virus infection.

Studies have shown that SARS-CoV-2 could infect macrophages, monocytes, and T cells but only progressed to an abortive infection (Abdelmoaty et al., 2021; Swadling et al., 2022). Although we found only a small portion of hESCs were infected, the formation of viral subgenomic viral RNA and dsRNA, as well as the increase in SARS-CoV-2 titer in culture medium, demonstrated that the SARS-CoV-2 infection in hESC should be a productive infection.

DATA AVAILABILITY STATEMENT

The datasets presented in this study can be found in online repositories. The RNAseq raw reads after SARS-CoV-2 infection in H1 hESC can be found on SRA database (PRJNA817715, https://www.ncbi.nlm.nih.gov/sra/PRJNA817715). The names of

the repository/repositories and accession number(s) can be found in the article/**Supplementary Material**.

AUTHOR CONTRIBUTIONS

DG conceived and supervised the study; WZ, JW, and DG designed the experiments, analyzed the data and wrote the manuscript. WZ, FX, and LC conducted all the major experiments. YJ, SY, TX, SH, and CL participated in some of the experiments or helped with reagents and discussions. All authors contributed to the article and approved the submitted version.

FUNDING

The work is supported by the National Natural Science Foundation of China (#81620108020 and #32041002 to DG; #31800151 to JW; #81803568 to FX), Shenzhen Science and Technology Program (#KQTD20180411143323605 and #JSGG20200225150431472 to DG; #JCYJ20170818162249554 to FX; #GXWD20201231165807008, 20200825183117001 to JW). DG is also supported by National Ten-thousand Talents Program and Guangdong Zhujiang Talents Program (2016LJ06Y540).

SUPPLEMENTARY MATERIAL

The Supplementary Material for this article can be found online at: https://www.frontiersin.org/articles/10.3389/fcimb.2022.911313/full#supplementary-material

Supplementary Figure 1 | Morphology of hESC colony. **(A)** Bright field phase contrast image of H1 hESC in normal culture condition before SARS-CoV-2 infection. **(B)** Bright field phase contrast image of H9 hESC in normal culture condition before SARS-CoV-2 infection. Scale bars are 200 μm.

Supplementary Figure 2 | Detection of SARS-CoV-2 viral RNA in supernatant by using SARS-CoV-2 nucleic acid detection kit. **(A)** Calu-3 cell virus level in the supernatant after 48 hpi of SARS-CoV-2. **(B)** Caco-2 cell virus level in the supernatant after 48 hpi of SARS-CoV-2. Error bars indicate standard deviations of each group. *$p < 0.05$ in 0.05MOI 48hpi group vs. Mock group with *t*-test.

Supplementary Figure 3 | Not significantly changed ISGs in hESCs after SARS-CoV-2 infection. (**A-C**) RT-qPCR detection of ISGs in SARS-CoV-2 infected hESCs. Error bars indicate standard deviations of each group.

REFERENCES

Abdelmoaty, M. M., Yeapuri, P., Machhi, J., Olson, K. E., Shahjin, F., Kumar, V., et al. (2021). Defining the Innate Immune Responses for SARS-CoV-2-Human Macrophage Interactions. *Front. Immunol.* 12. doi: 10.3389/fimmu.2021.741502

Alzamora, M. C., Paredes, T., Caceres, D., Webb, C. M., Valdez, L. M., and La Rosa, M. (2020). Severe COVID-19 During Pregnancy and Possible Vertical Transmission. *Am. J. Perinatol.* 37 (8), 861–865. doi: 10.1055/s-0040-1710050

Bilinska, K., Jakubowska, P., Von Bartheld, C. S., and Butowt, R. (2020). Expression of the SARS-CoV-2 Entry Proteins, ACE2 and TMPRSS2, in Cells of the Olfactory Epithelium: Identification of Cell Types and Trends With Age. *ACS Chem. Neurosci.* 11 (11), 1555–1562. doi: 10.1021/acschemneuro.0c00210

Bilz, N. C., Willscher, E., Binder, H., Böhnke, J., Stanifer, M. L., Hübner, D., et al. (2019). Teratogenic Rubella Virus Alters the Endodermal Differentiation Capacity of Human Induced Pluripotent Stem Cells. *Cells* 8 (8), 870. doi: 10.3390/cells8080870

Böhnke, J., Pinkert, S., Schmidt, M., Binder, H., Bilz, N. C., Jung, M., et al. (2021). Coxsackievirus B3 Infection of Human iPSC Lines and Derived Primary Germ-Layer Cells Regarding Receptor Expression. *Int. J. Mol. Sci.* 22 (3), 1220. doi: 10.3390/ijms22031220

Buchrieser, J., Dufloo, J., Hubert, M., Monel, B., Planas, D., Rajah, M. M., et al. (2020). Syncytia Formation by SARS-CoV-2-Infected Cells. *EMBO J.* 39 (23), e106267. doi: 10.15252/embj.2020106267

Burke, D. C., Graham, C. F., and Lehman, J. M. (1978). Appearance of Interferon Inducibility and Sensitivity During Differentiation of Murine Teratocarcinoma Cells *In Vitro*. *Cell* 13 (2), 243–248. doi: 10.1016/0092-8674(78)90193-9

Cheng, Y. W., Chao, T. L., Li, C. L., Chiu, M. F., Kao, H. C., Wang, S. H., et al. (2020). Furin Inhibitors Block SARS-CoV-2 Spike Protein Cleavage to Suppress Virus Production and Cytopathic Effects. *Cell Rep.* 33 (2), 108254. doi: 10.1016/j.celrep.2020.108254

Chen, F., Zhang, Y., Li, X., Li, W., Liu, X., and Xue, X. (2021). The Impact of ACE2 Polymorphisms on COVID-19 Disease: Susceptibility, Severity, and Therapy. *Front. Cell. Infect. Microbiol.* 11 (1002). doi: 10.3389/fcimb.2021.753721

Dong, L., Tian, J., He, S., Zhu, C., Wang, J., Liu, C., et al. (2020). Possible Vertical Transmission of SARS-CoV-2 From an Infected Mother to Her Newborn. *JAMA* 323 (18), 1846–1848. doi: 10.1001/jama.2020.4621

Fenizia, C., Biasin, M., Cetin, I., Vergani, P., Mileto, D., Spinillo, A., et al. (2020). Analysis of SARS-CoV-2 Vertical Transmission During Pregnancy. *Nat. Commun.* 11 (1), 5128. doi: 10.1038/s41467-020-18933-4

Földes, G., Liu, A., Badiger, R., Paul-Clark, M., Moreno, L., Lendvai, Z., et al. (2010). Innate Immunity in Human Embryonic Stem Cells: Comparison With Adult Human Endothelial Cells. *PLoS One* 5 (5), e10501. doi: 10.1371/journal.pone.0010501

Gu, Y., Cao, J., Zhang, X., Gao, H., Wang, Y., Wang, J., et al. (2022). Receptome Profiling Identifies KREMEN1 and ASGR1 as Alternative Functional Receptors of SARS-CoV-2. *Cell Res.* 32 (1), 24–37. doi: 10.1038/s41422-021-00595-6

Guo, Y. L. (2017). Utilization of Different Anti-Viral Mechanisms by Mammalian Embryonic Stem Cells and Differentiated Cells. *Immunol. Cell Biol.* 95 (1), 17–23. doi: 10.1038/icb.2016.70

Guo, Y. L., Carmichael, G. G., Wang, R., Hong, X., Acharya, D., Huang, F., et al. (2015). Attenuated Innate Immunity in Embryonic Stem Cells and Its Implications in Developmental Biology and Regenerative Medicine. *Stem Cells* 33 (11), 3165–3173. doi: 10.1002/stem.2079

Heurtier, V., Owens, N., Gonzalez, I., Mueller, F., Proux, C., Mornico, D., et al. (2019). The Molecular Logic of Nanog-Induced Self-Renewal in Mouse Embryonic Stem Cells. *Nat. Commun.* 10 (1), 1109. doi: 10.1038/s41467-019-09041-z

He, Q., Wu, Z., Yang, W., Jiang, D., Hu, C., Yang, X., et al. (2020). IFI16 Promotes Human Embryonic Stem Cell Trilineage Specification Through Interaction With P53. *NPJ Regener. Med.* 5 (1), 18. doi: 10.1038/s41536-020-00104-0

Higashi, K., Yagi, M., Arakawa, T., Asano, K., Kobayashi, K., Tachibana, T., et al. (2015). A Novel Marker for Undifferentiated Human Embryonic Stem Cells. *Monoclon. Antibodies Immunodiagn. Immunother.* 34 (1), 7–11. doi: 10.1089/mab.2014.0075

Hong, X. X., and Carmichael, G. G. (2013). Innate Immunity in Pluripotent Human Cells: Attenuated Response to Interferon-β. *J. Biol. Chem.* 288 (22), 16196–16205. doi: 10.1074/jbc.M112.435461

Klein, S., Cortese, M., Winter, S. L., Wachsmuth-Melm, M., Neufeldt, C. J., Cerikan, B., et al. (2020). SARS-CoV-2 Structure and Replication Characterized by *In Situ* Cryo-Electron Tomography. *Nat. Commun.* 11 (1), 5885. doi: 10.1038/s41467-020-19619-7

Li, Y., Cao, L., Li, G., Cong, F., Li, Y., Sun, J., et al. (2022). Remdesivir Metabolite GS-441524 Effectively Inhibits SARS-CoV-2 Infection in Mouse Models. *J. Med. Chem.* 65 (4), 2785–2793. doi: 10.1021/acs.jmedchem.0c01929

Li, Q., Guan, X., Wu, P., Wang, X., Zhou, L., Tong, Y., et al. (2020b). Early Transmission Dynamics in Wuhan, China, of Novel Coronavirus-Infected Pneumonia. *N. Engl. J. Med.* 382 (13), 1199–1207. doi: 10.1056/NEJMoa2001316

Li, D., Jin, M., Bao, P., Zhao, W., and Zhang, S. (2020a). Clinical Characteristics and Results of Semen Tests Among Men With Coronavirus Disease 2019. *JAMA Netw. Open* 3 (5), e208292. doi: 10.1001/jamanetworkopen.2020.8292

Li, F., Li, J., Wang, P.-H., Yang, N., Huang, J., Ou, J., et al. (2021a). SARS-CoV-2 Spike Promotes Inflammation and Apoptosis Through Autophagy by ROS-Suppressed PI3K/AKT/mTOR Signaling. *Biochim. Biophys. Acta (BBA) Mol. Basis Dis.* 1867 (12), 166260. doi: 10.1016/j.bbadis.2021.166260

Li, Y., Renner, D. M., Comar, C. E., Whelan, J. N., Reyes, H. M., Cardenas-Diaz, F. L., et al. (2021b). SARS-CoV-2 Induces Double-Stranded RNA-Mediated Innate Immune Responses in Respiratory Epithelial-Derived Cells and Cardiomyocytes. *Proc. Natl. Acad. Sci. U. S. A.* 118 (16), e2022643118. doi: 10.1073/pnas.2022643118

Ma, X., Zou, F., Yu, F., Li, R., Yuan, Y., Zhang, Y., et al. (2020). Nanoparticle Vaccines Based on the Receptor Binding Domain (RBD) and Heptad Repeat (HR) of SARS-CoV-2 Elicit Robust Protective Immune Responses. *Immunity* 53 (6), 1315–1330.e1319. doi: 10.1016/j.immuni.2020.11.015

Poirier, E. Z., Buck, M. D., Chakravarty, P., Carvalho, J., Frederico, B., Cardoso, A., et al. (2021). An Isoform of Dicer Protects Mammalian Stem Cells Against Multiple RNA Viruses. *Science* 373 (6551), 231–236. doi: 10.1126/science.abg2264

Qiao, J., Li, W., Bao, J., Peng, Q., Wen, D., Wang, J., et al. (2020). The Expression of SARS-CoV-2 Receptor ACE2 and CD147, and Protease TMPRSS2 in Human and Mouse Brain Cells and Mouse Brain Tissues. *Biochem. Biophys. Res. Commun.* 533 (4), 867–871. doi: 10.1016/j.bbrc.2020.09.042

Sano, E., Deguchi, S., Sakamoto, A., Mimura, N., Hirabayashi, A., Muramoto, Y., et al. (2021). Modeling SARS-CoV-2 Infection and its Individual Differences With ACE2-Expressing Human iPS Cells. *iScience* 24 (5), 102428. doi: 10.1016/j.isci.2021.102428

Sharun, K., Tiwari, R., and Dhama, K. (2020). SARS-CoV-2 in Semen: Potential for Sexual Transmission in COVID-19. *Int. J. Surg.* 84, 156–158. doi: 10.1016/j.ijsu.2020.11.011

Song, E., Zhang, C., Israelow, B., Lu-Culligan, A., Prado, A. V., Skriabine, S., et al. (2021). Neuroinvasion of SARS-CoV-2 in Human and Mouse Brain. *J. Exp. Med.* 218 (3), e20202135. doi: 10.1084/jem.20202135

Swadling, L., Diniz, M. O., Schmidt, N. M., Amin, O. E., Chandran, A., Shaw, E., et al. (2022). Pre-Existing Polymerase-Specific T Cells Expand in Abortive Seronegative SARS-CoV-2. *Nature* 601 (7891), 110–117. doi: 10.1038/s41586-021-04186-8

Tatu, A. L., Nadasdy, T., and Nwabudike, L. C. (2020). Observations About Sexual and Other Routes of SARS-CoV-2 (COVID-19) Transmission and its Prevention. *Clin. Exp. Dermatol.* 45 (6), 761–762. doi: 10.1111/ced.14274

Thomson, J. A., Itskovitz-Eldor, J., Shapiro, S. S., Waknitz, M. A., Swiergiel, J. J., Marshall, V. S., et al. (1998). Embryonic Stem Cell Lines Derived From Human Blastocysts. *Science* 282 (5391), 1145–1147. doi: 10.1126/science.282.5391.1145

Wang, K., Chen, W., Zhang, Z., Deng, Y., Lian, J. Q., Du, P., et al. (2020a). CD147-Spike Protein is a Novel Route for SARS-CoV-2 Infection to Host Cells. *Signal Transd. Target. Ther.* 5 (1), 283. doi: 10.1038/s41392-020-00426-x

Wang, Y., Liu, S., Liu, H., Li, W., Lin, F., Jiang, L., et al. (2020b). SARS-CoV-2 Infection of the Liver Directly Contributes to Hepatic Impairment in Patients With COVID-19. *J. Hepatol.* 73 (4), 807–816. doi: 10.1016/j.jhep.2020.05.002

Wang, S., Qiu, Z., Hou, Y., Deng, X., Xu, W., Zheng, T., et al. (2021). AXL is a Candidate Receptor for SARS-CoV-2 That Promotes Infection of Pulmonary and Bronchial Epithelial Cells. *Cell Res.* 31 (2), 126–140. doi: 10.1038/s41422-020-00460-y

Wolf, D., and Goff, S. P. (2009). Embryonic Stem Cells Use ZFP809 to Silence Retroviral DNAs. *Nature* 458 (7242), 1201–1204. doi: 10.1038/nature07844

Wu, X., Dao Thi, V. L., Huang, Y., Billerbeck, E., Saha, D., Hoffmann, H. H., et al. (2018). Intrinsic Immunity Shapes Viral Resistance of Stem Cells. *Cell* 172 (3), 423–438.e425. doi: 10.1016/j.cell.2017.11.018

Wu, X., Kwong, A. C., and Rice, C. M. (2019). Antiviral Resistance of Stem Cells. *Curr. Opin. Immunol.* 56, 50–59. doi: 10.1016/j.coi.2018.10.004

Wu, J., Wu, C., Xing, F., Cao, L., Zeng, W., Guo, L., et al. (2021). Endogenous Reverse Transcriptase and RNase H-Mediated Antiviral Mechanism in Embryonic Stem Cells. *Cell Res.* 31 (9), 998–1010. doi: 10.1038/s41422-021-00524-7

Yamamoto, M., Kiso, M., Sakai-Tagawa, Y., Iwatsuki-Horimoto, K., Imai, M., Takeda, M., et al. (2020). The Anticoagulant Nafamostat Potently Inhibits SARS-CoV-2 S Protein-Mediated Fusion in a Cell Fusion Assay System and Viral Infection *In Vitro* in a Cell-Type-Dependent Manner. *Viruses* 12 (6), 629. doi: 10.3390/v12060629

Zahedi-Amiri, A., Sequiera, G. L., Dhingra, S., and Coombs, K. M. (2019). Influenza a Virus-Triggered Autophagy Decreases the Pluripotency of Human-Induced Pluripotent Stem Cells. *Cell Death Dis.* 10 (5), 337. doi: 10.1038/s41419-019-1567-4

Zecha, J., Lee, C. Y., Bayer, F. P., Meng, C., Grass, V., Zerweck, J., et al. (2020). Data, Reagents, Assays and Merits of Proteomics for SARS-CoV-2 Research and Testing. *Mol. Cell Proteomics* 19 (9), 1503–1522. doi: 10.1074/mcp.RA120.002164

Zhang, B. Z., Chu, H., Han, S., Shuai, H., Deng, J., Hu, Y. F., et al. (2020). SARS-CoV-2 Infects Human Neural Progenitor Cells and Brain Organoids. *Cell Res.* 30 (10), 928–931. doi: 10.1038/s41422-020-0390-x

Zhao, B., Ni, C., Gao, R., Wang, Y., Yang, L., Wei, J., et al. (2020). Recapitulation of SARS-CoV-2 Infection and Cholangiocyte Damage With Human Liver Ductal Organoids. *Protein Cell* 11 (10), 771–775. doi: 10.1007/s13238-020-00718-6

Zhou, P., Yang, X. L., Wang, X. G., Hu, B., Zhang, L., Zhang, W., et al. (2020). A Pneumonia Outbreak Associated With a New Coronavirus of Probable Bat Origin. *Nature* 579 (7798), 270–273. doi: 10.1038/s41586-020-2012-7

Ziegler, C. G. K., Allon, S. J., Nyquist, S. K., Mbano, I. M., Miao, V. N., Tzouanas, C. N., et al. (2020). SARS-CoV-2 Receptor ACE2 Is an Interferon-Stimulated Gene in Human Airway Epithelial Cells and Is Detected in Specific Cell Subsets Across Tissues. *Cell* 181 (5), 1016–1035.e1019. doi: 10.1016/j.cell.2020.04.035

Conflict of Interest: The authors declare that the research was conducted in the absence of any commercial or financial relationships that could be construed as a potential conflict of interest.

frontiers | Frontiers in Cellular and Infection Microbiology

ORIGINAL RESEARCH
published: 22 July 2022
doi: 10.3389/fcimb.2022.933190

Multiethnic Investigation of Risk and Immune Determinants of COVID-19 Outcomes

*Tomi Jun[1], Divij Mathew[2,3], Navya Sharma[4], Sharon Nirenberg[5], Hsin-Hui Huang[6], Patricia Kovatch[5], Edward John Wherry[2,3] and Kuan-lin Huang[7]**

[1] Division of Hematology and Medical Oncology, Tisch Cancer Institute, Icahn School of Medicine at Mount Sinai, New York, NY, United States, [2] Institute for Immunology, University of Pennsylvania Perelman School of Medicine, Philadelphia, PA, United States, [3] Department of Systems Pharmacology and Translational Therapeutics, University of Pennsylvania Perelman School of Medicine, Philadelphia, PA, United States, [4] University of California, Santa Barbara, Santa Barbara, CA, United States, [5] Scientific Computing, Icahn School of Medicine at Mount Sinai, New York, NY, United States, [6] Department of Population Health Science and Policy, Icahn School of Medicine at Mount Sinai, New York, NY, United States, [7] Department of Genetics and Genomic Sciences, Center for Transformative Disease Modeling, Tisch Cancer Institute, Icahn Institute for Data Science and Genomic Technology, Icahn School of Medicine at Mount Sinai, New York, NY, United States*

OPEN ACCESS

Edited by:
You Zhou, Cardiff University, United Kingdom

Reviewed by:
Yongfen Xu, Institut Pasteur of Shanghai (CAS), China
Sreedhar Chinnaswamy, National Institute of Biomedical Genomics (NIBMG), India

***Correspondence:**
Kuan-lin Huang
kuan-lin.huang@mssm.edu

Specialty section:
This article was submitted to Virus and Host, a section of the journal Frontiers in Cellular and Infection Microbiology

Received: *30 April 2022*
Accepted: *20 June 2022*
Published: *22 July 2022*

Citation:
Jun T, Mathew D, Sharma N, Nirenberg S, Huang H-H, Kovatch P, Wherry EJ and Huang K-l (2022) Multiethnic Investigation of Risk and Immune Determinants of COVID-19 Outcomes. Front. Cell. Infect. Microbiol. 12:933190. doi: 10.3389/fcimb.2022.933190

Background: Disparate COVID-19 outcomes have been observed between Hispanic, non-Hispanic Black, and White patients. The underlying causes for these disparities are not fully understood.

Methods: This was a retrospective study utilizing electronic medical record data from five hospitals within a single academic health system based in New York City. Multivariable logistic regression models were used to identify demographic, clinical, and lab values associated with in-hospital mortality.

Results: A total of 3,086 adult patients with self-reported race/ethnicity information presenting to the emergency department and hospitalized with COVID-19 up to April 13, 2020, were included in this study. While older age (multivariable odds ratio (OR) 1.06, 95% CI 1.05–1.07) and baseline hypoxia (multivariable OR 2.71, 95% CI 2.17–3.36) were associated with increased mortality overall and across all races/ethnicities, non-Hispanic Black (median age 67, interquartile range (IQR) 58–76) and Hispanic (median age 63, IQR 50–74) patients were younger and had different comorbidity profiles as compared to non-Hispanic White patients (median age 73, IQR 62–84; $p < 0.05$ for both comparisons). Among inflammatory markers associated with COVID-19 mortality, there was a significant interaction between the non-Hispanic Black population and interleukin-1-beta (interaction p-value 0.04).

Conclusions: This analysis of a multiethnic cohort highlights the need for inclusion and consideration of diverse populations in ongoing COVID-19 trials targeting inflammatory cytokines.

Keywords: COVID-19, interleukin-1beta, African American, electronic medical record, risk factors

BACKGROUND

Reports from the United States, the United Kingdom, and Brazil have highlighted racial disparities in the COVID-19 pandemic (Baqui et al., 2020; Price-Haywood et al., 2020; Oppel et al., 2020; Williamson et al., 2020). National studies from the United Kingdom and Brazil have found race to be an independent predictor of death (Baqui et al., 2020; Williamson et al., 2020). In the United States, Black and Hispanic individuals have disproportionately high rates of infection, hospitalization, and mortality (Hsu et al., 2020; Holtgrave et al., 2020; Price-Haywood et al., 2020; Oppel et al., 2020). These disparities have been attributed to greater representation of Black and Hispanic persons in essential services and a higher burden of comorbidities in minority communities, among others.

While Black and Hispanic individuals in the United States have been disproportionately affected by the pandemic, the majority of published studies investigating COVID-19 mortality risk factors have been in cohorts of individuals with predominantly European or Asian ancestry (Docherty et al., 2020; Gupta et al., 2020; Grasselli et al., 2020; Petrilli et al., 2020; Zhou et al., 2020). Few US studies have directly examined mortality risk factors and their effect sizes in Black or Hispanic as compared to White individuals (Gu et al., 2020; Price-Haywood et al., 2020). Rigorous analysis to establish risk factors and molecular predictors for each population is urgently needed.

We sought to identify race/ethnic-specific clinical and immune factors of mortality using a diverse cohort of White, Black, and Hispanic COVID-19 patients admitted to a single health system in New York. In addition to baseline characterization, we conducted stratified and interaction term analyses to identify risk and immune factors that may affect the outcomes of each patient population. The systematic analyses revealed population-specific effects of multiple risk factors that were previously unknown, highlighting the importance of including diverse patient populations and tailored consideration in precision medicine for COVID-19.

METHODS

Study Setting

The study was conducted within the Mount Sinai Health System, which is an academic healthcare system comprising 8 hospitals and more than 410 ambulatory practice locations in the New York metropolitan area. This analysis involves patients who presented to five hospitals: The Mount Sinai Hospital (MSH) (1,134 beds), Mount Sinai West (514 beds), and Mount Sinai Morningside (495 beds) in Manhattan; Mount Sinai Brooklyn (212 beds); and Mount Sinai Queens (235 beds).

Data Sources

Data were captured by the Epic electronic health record (Epic Systems, Verona, WI, USA) and directly extracted from Epic's Clarity and Caboodle servers. This de-identified dataset was developed and released by the Mount Sinai Data Warehouse (MSDW) team, with the goal of encompassing all COVID-19-related patient encounters within the Mount Sinai system, accompanied by selected demographics, comorbidities, vital signs, medications, and lab values. As part of de-identification, all patients over the age of 89 had their age set to 90.

This study utilized de-identified data extracted from the electronic health record and as such was considered non-human subject research. Therefore, this study was granted an exemption from the Mount Sinai institutional review board (IRB) review and approval process.

Patient Population and Definitions

The MSDW dataset captured any patient encounters at a Mount Sinai facility with any of the following: a COVID-19-related encounter diagnosis, a COVID-19-related visit type, a SARS-CoV-2 lab order, a SARS-CoV-2 lab result, or a SARS-CoV-2 lab test result from the New York State Department of Health's Wadsworth laboratory. For this study, patients with COVID-19-related visits to the emergency department (ED) on or before April 13, 2020, were identified, and patients who were admitted were selected. Their hospitalization outcomes through June 2, 2020, were observed.

Our analysis was limited to adults over 18 years old who were hospitalized for COVID-19 through a Mount Sinai ED. Self-reported race and ethnicity were classified into 3 mutually exclusive categories: non-Hispanic (NH) White (White), NH Black (Black), and Hispanic (**Supplementary Table 1**). COVID-19 positivity was determined by a positive or presumptive positive result from a nucleic acid-based test for SARS-CoV-2 in nasopharyngeal or oropharyngeal swab specimens. Baseline vital signs were the first documented vital signs for the encounter. Hypoxia was defined as oxygen saturation of less than 92%. Baseline labs were defined as the first lab value within 24 h of the start of the encounter.

University of Pennsylvania Cohort

Patients in the University of Pennsylvania cohort were identified based on a positive SARS-CoV-2 PCR test. Patients were screened and gave informed consent within 72 h of hospitalization. Clinical data were collected from electronic medical records into standardized case reports. Healthy donors (HDs) had no prior diagnosis or symptoms consistent with COVID-19. Recovered donors (RDs) were adults with a self-reported positive COVID-19 PCR test who recovered as defined by the Centers for Disease Control and Prevention. Cytokine levels were measured from peripheral blood plasma using a custom human cytokine 31-plex panel (EMD Millipore Corporation, Burlington, MA, USA; SPRCUS707), as described in Divij et al. (Mathew et al., 2020)

Logistic Regression

The primary outcome was in-hospital mortality. Univariable and multivariable logistic regression analyses were used to identify factors associated with death. Race/ethnicity-specific risk factors were identified by 1) constructing stratified models for each racial category and 2) constructing models including interaction terms between race/ethnicity and other covariates. Separate

interaction models were created to test the interactions of either Hispanic ethnicity or Black race with other covariates. Interactions were compared against the White race as the reference group.

Demographic factors, comorbidities, initial vital signs, baseline lab values, and treatment facility site (Manhattan vs. Brooklyn/Queens) were analyzed as covariates. There was minimal clustering of outcomes by treatment site (ICC(ρ) = 0.026), and this was modeled as a fixed effect. Covariates were chosen *a priori* based on prior reports. The odds ratios (ORs) derived from the coefficients of each model were reported, along with the Wald-type confidence interval and p-values.

Laboratory Value Analysis

Markers of inflammation, such as C-reactive protein (CRP), ferritin, and D-dimer, have been proposed as being correlated with COVID-19 severity. However, the missingness of these lab values varied across sites. Given the possibility of confounding by indication (if providers ordered these labs in more acutely ill patients), the analyses involving lab tests were limited to those obtained at the largest site (MSH) and those that had less than 15% missing values at that site. The cytokines interleukin-1-beta (IL-1β), interleukin-6 (IL-6), interleukin-8 (IL-8), and tumor necrosis factor-alpha (TNF-α) were exempted from this threshold because they were obtained on a subset of COVID-19 patients in the context of a study with broad inclusion criteria (Charney et al., 2020; Del Valle et al., 2020).

To test the associations of these lab values with mortality, each lab test was performed in race/ethnicity-stratified multivariable logistic regression models adjusting for age, sex, and hypoxia. The number of covariates in the model was limited due to the reduced sample size. Labs were standardized to a mean of 0 and an SD of 1 prior to regression analysis.

Statistical Analysis

Patient characteristics and baseline vitals and labs were described using medians and ranges for continuous variables and proportions for categorical variables. Continuous variables were compared using the Wilcoxon rank-sum test, and categorical variables were compared using Fisher's exact test. All statistical analyses and data visualizations were carried out using R 4.0.0 (The R Foundation, Vienna, Austria), along with the *tidyverse*, *ggpubr*, *forestplot*, and *Hmisc* packages (Wickham, 2017; Kassambara, 2020; Gordon and Lumley, 2021; Harrell et al., 2022). Statistical significance was defined as $p < 0.05$.

RESULTS

Study Population

There were 4,997 adult patients with COVID-19-related ED visits on or before April 13, 2020, of whom 3,086 (61.8%) were hospitalized. Hospitalization rates were significantly lower for NH Black patients compared to the other groups (NH Black 56.5%; NH White 63.4%; Hispanic 64.3%, Asian 62.6%; Other 63.6%; $p < 0.001$). Hospitalized patients were significantly older (median age 66 vs. 50, $p < 0.001$) and were more likely to have comorbidities such as hypertension (35.5% vs. 13.5%, $p < 0.001$), diabetes (24% vs. 7.8%, $p < 0.001$), and chronic kidney disease (11.9% vs. 3.1%, $p < 0.001$) (**Supplementary Table 1**). The clinical characteristics of non-hospitalized patients are summarized by race/ethnicity in **Supplementary Table 2**.

The hospitalized cohort included 3,086 adult patients. We excluded 78 patients with missing race or ethnicity data, 144 Asian patients, and 458 patients with other or unspecified race/ethnicity from the comparative/stratified analyses based on power considerations (**Figure 1**). The remaining 2,406 patients were 37.1% Hispanic, 34.3% NH Black, and 28.6% NH White.

Compared to NH White patients, NH Black and Hispanic patients were younger (median age 67 and 63 vs. 73, $p < 0.001$ for both) (**Table 1**). NH Black patients were more likely to have hypertension (40.6% vs. 31.8%, $p < 0.001$), diabetes (26.8% vs. 17.4%, $p < 0.001$), and chronic kidney disease (16.1% vs. 8%, $p < 0.001$) than NH White patients. Hispanic patients were more likely to have diabetes (27.4% vs. 17.4%, $p < 0.001$), chronic kidney disease (13% vs. 8%, $p = 0.001$), and chronic liver disease (4.3% vs. 1.6%, $p = 0.003$), compared to NH White patients. NH White patients were more likely to have coronary artery disease (17.1% vs. 12.2% and 11.3%, $p = 0.008$ vs. Black, $p = 0.001$ vs. Hispanic) and atrial fibrillation (12.3% vs. 5% and 4.5%, $p < 0.001$ for both) than NH Black or Hispanic patients.

These results demonstrate differences in the distributions of demographic and clinical COVID-19 mortality risk factors by race/ethnicity.

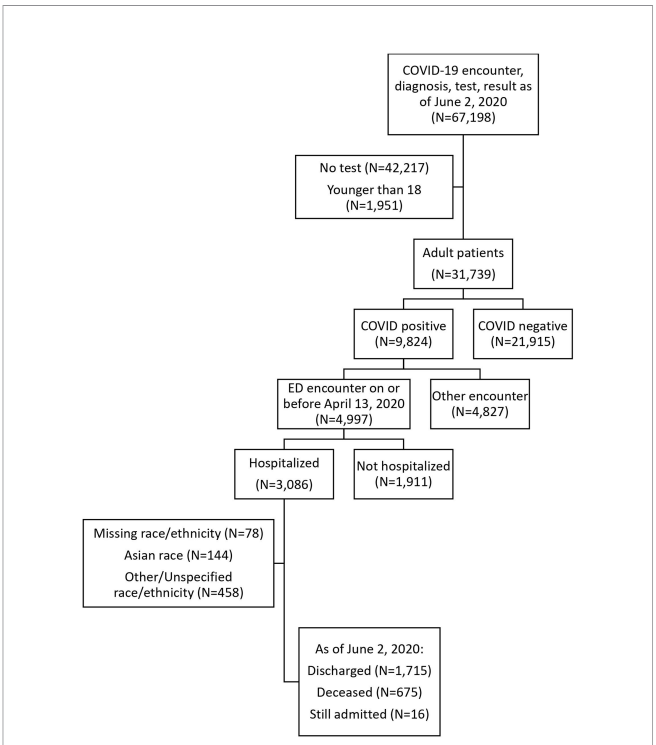

FIGURE 1 | Flow diagram of included patients.

TABLE 1 | Baseline demographic and clinical characteristics, by race/ethnicity.

	NH White (N = 689)	NH Black (N = 825)	Hispanic (N = 892)
Age (years)	73 (62–84)	67 (58–76)†	63 (50–74)†
Mount Sinai Brooklyn (MSB)	156 (22.6%)	258 (31.3%)†	17 (1.9%)†
Mount Sinai Queens (MSQ)	138 (20%)	61 (7.4%)†	271 (30.4%)†
Mount Sinai Morningside (MSSL)	51 (7.4%)	199 (24.1%)†	216 (24.2%)†
Mount Sinai West (MSW)	120 (17.4%)	65 (7.9%)†	100 (11.2%)†
The Mount Sinai Hospital (MSH)	224 (32.5%)	242 (29.3%)	288 (32.3%)
Current smoker*	22 (3.2%)	43 (5.2%)	25 (2.8%)
Former smoker*	147 (21.3%)	187 (22.7%)	190 (21.3%)
Never smoker*	375 (54.4%)	437 (53%)	478 (53.6%)
Hypertension	219 (31.8%)	335 (40.6%)†	318 (35.7%)
Diabetes	120 (17.4%)	221 (26.8%)†	244 (27.4%)†
Coronary artery disease	118 (17.1%)	101 (12.2%)†	101 (11.3%)†
Heart failure	59 (8.6%)	71 (8.6%)	60 (6.7%)
Atrial fibrillation	85 (12.3%)	41 (5%)†	40 (4.5%)†
Chronic kidney disease	55 (8%)	133 (16.1%)†	116 (13%)†
COPD/asthma	60 (8.7%)	75 (9.1%)	84 (9.4%)
Obesity	50 (7.3%)	75 (9.1%)	80 (9%)
Cancer	52 (7.5%)	63 (7.6%)	57 (6.4%)
Chronic liver disease	11 (1.6%)	24 (2.9%)	38 (4.3%)†
Obstructive sleep apnea	15 (2.2%)	18 (2.2%)	21 (2.4%)
HIV	12 (1.7%)	23 (2.8%)	13 (1.5%)
Temperature (°F)	98.7 (98–99.9)	98.9 (98.1–100.1)†	99 (98.3–100.4)†
Heart rate (bpm)	91 (79–106)	97 (85–110)†	99 (86–113)†
Systolic blood pressure (mmHg)	129 (114–146)	131 (116–148)	128 (115–144)
Respiratory rate (bpm)	20 (18–22)	20 (18–22)	20 (18–22)
Oxygen sat. <92%	184 (26.7%)	149 (18.1%)†	257 (28.8%)

Note. Values represent count (%) or median (IQR) for categorical and continuous variables, respectively.
NH, non-Hispanic; COPD, chronic obstructive pulmonary disease; IQR, interquartile range.
†p < 0.05 compared to White.
**22% missing values.*

Population-Specific Clinical Factors Associated with Death

Unadjusted mortality rates were lower among NH Black (27.5% vs. 34.1%, p = 0.006) and Hispanic (23.9% vs. 34.1%, p < 0.001) patients compared to NH White patients. The rates of intensive care were not significantly different between NH Black and NH White (19.8% vs. 21.5%, p = 0.44) or Hispanic and NH White (23.4% vs. 21.5%, p = 0.36) patients.

We first evaluated the association of demographic, clinical, and laboratory variables with in-hospital mortality (**Table 2**, **Supplementary Tables 4, 5**). In a univariate analysis, NH Black (OR 0.73, 95% CI 0.59–0.91) and Hispanic (OR 0.61, 95% CI 0.49–0.76) populations were associated with lower mortality as compared to NH White. However, race/ethnicity was not an independent predictor of mortality after adjusting for age, sex, comorbidities, and baseline hypoxia (oxygen saturation <92% at the first measurement

TABLE 2 | Multivariable model predicting in-hospital mortality, stratified by race/ethnicity.

Variable	NH White OR (95% CI)	NH Black OR (95% CI)	Hispanic OR (95% CI)	All patients OR (95% CI)
Male	1.51 (1.03–2.22)	1.55 (1.09–2.19)	1.04 (0.73–1.49)	1.29 (1.05–1.58)
Age (years)	1.07 (1.05–1.09)	1.06 (1.04–1.07)	1.05 (1.04–1.07)	1.06 (1.05–1.07)
Race: NH White	Reference	Reference	Reference	Reference
Race: NH Black	NA	NA	NA	1.03 (0.80–1.32)
Race: Hispanic	NA	NA	NA	0.94 (0.73–1.21)
Manhattan facility	0.45 (0.31–0.64)	0.53 (0.37–0.75)	0.62 (0.43–0.89)	0.53 (0.43–0.65)
Hypertension	0.86 (0.56–1.33)	0.69 (0.45–1.06)	0.78 (0.51–1.2)	0.77 (0.61–0.98)
Diabetes	0.99 (0.61–1.63)	1.67 (1.09–2.58)	1.21 (0.79–1.83)	1.26 (0.98–1.63)
Coronary artery disease	0.98 (0.58–1.65)	1.14 (0.67–1.93)	0.10 (0.57–1.73)	1.03 (0.76–1.39)
Heart failure	0.94 (0.48–1.85)	1.11 (0.6–2.06)	1.14 (0.55–2.36)	1.05 (0.72–1.54)
Atrial fibrillation	1.15 (0.66–2.02)	1.27 (0.62–2.59)	1.99 (0.97–4.11)	1.38 (0.95–2.00)
Chronic kidney disease	2.25 (1.18–4.28)	1.71 (1.06–2.77)	1.38 (0.80–2.38)	1.70 (1.25–2.31)
COPD/asthma	0.9 (0.48–1.68)	0.80 (0.42–1.54)	0.58 (0.32–1.06)	0.75 (0.52–1.07)
Obesity	0.72 (0.33–1.60)	1.33 (0.69–2.58)	1.59 (0.86–2.91)	1.25 (0.86–1.83)
Cancer	0.95 (0.49–1.85)	1.15 (0.61–2.16)	1.65 (0.88–3.07)	1.25 (0.86–1.8)
Oxygen sat. <92%	2.377 (1.6–3.54)	2.51 (1.69–3.75)	3.22 (2.24–4.61)	2.71 (2.17–3.36)

Note. OR, odds ratio; COPD, chronic obstructive pulmonary disease.

of the clinical encounter) in this cohort (Black HR 1.03, 95% CI 0.80–1.32; Hispanic HR 0.94, 95% CI 0.73–1.21) (**Figure 2A**). Our finding is consistent with several cohort studies in the United States (Gold et al., 2020; Price-Haywood et al., 2020; Suleyman et al., 2020), although UK and Brazil studies have reported race as an independent predictor of mortality (Baqui et al., 2020; Williamson et al., 2020), possibly due to population differences.

Previous patient cohort analyses rarely considered race/ethnic-specific risk factors, which require stratified modeling within each population cohort. We conducted stratified analyses within ethnic groups to determine the population-specific effect sizes of clinical factors and comorbidity. Diabetes was associated with an OR of 1.67 (95% CI 1.09–2.58) in the stratified NH Black population and an OR of 0.99 (95% CI 0.61–1.63) in the NH White population (**Figure 2B**). Obesity was associated with an OR of 1.33 (95% CI 0.69–2.58) in NH Black, compared to an OR of 0.72 (95% CI 0.33–1.60) in NH White (**Figure 2B**). Increased age and baseline hypoxia were consistently associated with increased mortality across all three populations (**Supplementary Table 6**). Altogether, these results highlight the shared and specific clinical risk factors of COVID-19 mortality across populations.

Baseline Laboratory Values

We analyzed baseline lab values among patients admitted to the largest site in our dataset, MSH. This site had the most complete records for routine and inflammatory lab values. We defined baseline labs as the first lab value within 24 h of the start of the encounter.

Among common lab values, Hispanic patients had higher baseline alanine aminotransferase values (median alanine transaminase (ALT), 33 vs. 28 U/L, $p = 0.03$) than NH White patients (**Table 3**), consistent with the increased prevalence of chronic liver disease among Hispanic patients.

Among inflammatory lab markers, NH Black patients had higher initial levels of procalcitonin (0.29 vs. 0.13 ng/ml, $p < 0.001$) and more abnormal ferritin levels (3.16 vs. 2.24 times the upper limit of normal, $p = 0.03$) as compared to NH White patients (**Table 3**). There were no significant differences in baseline D-dimer, lactate dehydrogenase (LDH), CRP, IL-1β, IL-6, IL-8, or TNF-α levels. Thus, population-specific associations identified for these immune factors would indicate contributions from their relative differences between patients of different outcomes within a population rather than baseline differences across populations.

Population-Specific Immune Factors Associated with Clinical Outcomes

We next conducted a multiethnic analysis to identify immune markers associated with patient outcomes in MSH cohort. Using multivariate models adjusting for age, sex, and hypoxia, we identified CRP (OR 1.39, 95% CI 1.16–1.68), albumin (OR 0.75, 95% CI 0.61–0.91), IL-6 (OR 1.43, 95% CI 1.12–1.82), white blood cell (WBC) (OR 1.35, 95% CI 1.08–1.65), and LDH (OR 1.34, 95% CI 1.07–1.68) as independent predictors of mortality (**Supplementary Table 7**).

To identify immune markers showing population specificity in predicting COVID-19 outcomes, we applied the multivariate regression model in each population-stratified cohort. Elevated levels of IL-1β were associated with a higher risk of mortality in Black (OR 2.35, 95% CI 1.13–4.86) compared to White patients (OR 0.78, 95% CI 0.41–1.51) (**Figure 3**, **Supplementary Table 7**). Increased procalcitonin levels were associated with an OR of 2.65 (95% CI 0.88–7.96) in Hispanic patients, compared to an OR of 0.98 (95% CI 0.58–1.66) among NH White patients. Increased IL-8 levels were associated with an OR of 1.51 (95% CI 0.59–3.86) among Hispanic patients and an OR of 8.76 (95% CI 0.95–80.7) among White patients (**Supplementary Table 7**). To validate the population specificity of these COVID-19 mortality-associated immune markers, we further utilized a multivariate model including interaction terms, finding a significant interaction between NH Black and IL-1β ($p = 0.04$), and suggestive but non-significant interactions between Hispanic and procalcitonin ($p = 0.07$) and IL-8 ($p = 0.09$) as compared to NH White (**Supplementary Table 6**).

Next, we sought to validate the immune marker findings of MSH cohort in an independent dataset. We utilized immunoprofiling data from the University of Pennsylvania cohort (Mathew et al., 2020) to compare levels of serum cytokines and immunologic markers between diverse patient populations vs. HDs and RDs. Among the COVID-19 patients with available race/ethnicity data, eight were NH Black, three were NH White, and four were Asian. Additionally, there were ten HDs and twelve RDs with no available race/ethnicity data.

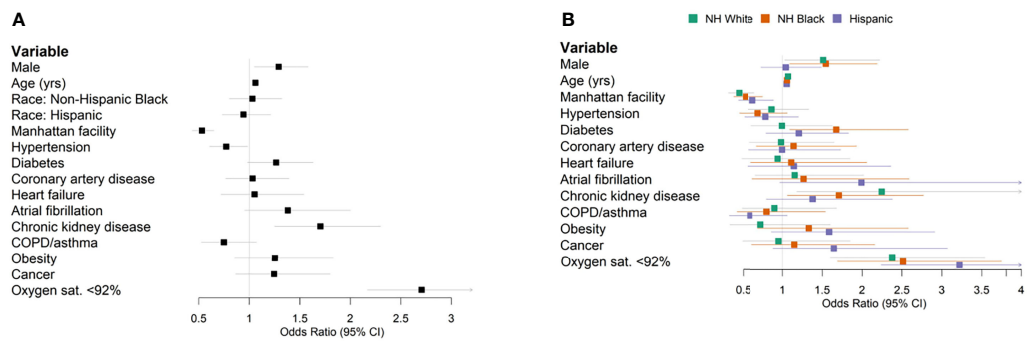

FIGURE 2 | Forest plots of multivariable logistic regression results predicting in-hospital mortality. **(A)** All patients. **(B)** Stratified by race/ethnicity.

TABLE 3 | Baseline laboratory values among patients admitted to The Mount Sinai Hospital, by race/ethnicity.

Laboratory test	Evaluablepatients	NH White	NH Black	Hispanic
White blood cells, $10^3/\mu l$	984	6.5 (5–9.825)	6.3 (4.9–9.2)	6.4 (5–9.1)
Hemoglobin, g/dl	985	13.15 (12–14.125)	12.6 (10.9–13.8)†	13.2 (11.4–14.5)
Platelets, $10^3/\mu l$	980	205 (159.5–256)	203 (157–264.25)	212.5 (165.25–279.5)
Sodium, mmol/L	984	136 (134–139)	137 (135–140)†	137 (134–139.25)
Potassium, mmol/L	941	4 (3.7–4.55)	4.3 (3.8–4.8)†	4.2 (3.8–4.6)
Chloride, mmol/L	984	101 (98–104)	102 (97.25–105)	102 (98–105)
Blood urea nitrogen, mg/dl	984	17 (12–28)	22 (14–46)†	15 (10–27)†
Creatinine, mg/dl	985	0.88 (0.7–1.22)	1.25 (0.9–2.705)†	0.87 (0.67–1.2325)
Aspartate aminotransferase, U/L	915	38 (29–63)	40 (28–59)	43 (30–68.25)
Alanine aminotransferase, U/L	958	28 (18–49)	26 (16.5–41.5)	33 (20–63)†
Total bilirubin, mg/dl	966	0.6 (0.5–0.8)	0.6 (0.4–0.9)	0.6 (0.4–0.8)
Albumin, g/dl	969	3.1 (2.7–3.5)	3.2 (2.8–3.55)	3.3 (2.9–3.6)†
D-dimer, µg/ml FEU	755	1.25 (0.78–2.0475)	1.59 (0.78–2.795)	1.15 (0.6575–2.2125)
Ferritin, ng/ml	904	679.5 (354.75–1423)	717 (328–2124)	665 (275.5–1649.75)
Ferritin, times upper limit of normal	904	2.24 (1.190625–4.76625)	3.16 (1.18–6.37)†	2.66 (1.15–5.15)
Procalcitonin, ng/ml	914	0.13 (0.06–0.375)	0.29 (0.09–0.855)†	0.17 (0.08–0.5075)
Lactate dehydrogenase, U/L	854	405 (326–488)	396.5 (312.5–574.75)	388 (296–525)
C-reactive protein, mg/L	903	119.35 (68.625–203.475)	100.25 (49.45–173.45)	100.4 (54.125–193.575)
Interleukin-1 beta, pg/ml	418	0.5 (0.375–0.7)	0.6 (0.4–0.9)	0.5 (0.4–0.8)
Interleukin-6, pg/ml	583	84.3 (44.8–149)	69.05 (39.9–120.75)	68.2 (40–135)
Interleukin-8, pg/ml	521	41.25 (29.725–58.7)	43.95 (24.725–70.15)	43.85 (28.025–64)
Tumor necrosis factor-alpha, pg/ml	522	24 (18.425–33)	26.35 (17.6–45.4)	22.3 (16.925–32.125)

Note. Values represent median (IQR).
NH, non-Hispanic; IQR, interquartile range.
†p < 0.05 compared to White.

We used the non-parametric Mood's median test to detect potential population differences in the median values of 13 measured immune markers against the combined cohort of HDs and RDs (HDs/RDs, **Supplementary Table 8**). NH Black patients had significantly higher median IL-6 (37.1 vs. 2.59, p = 0.003) and IP10 (227 vs. 55.6, p = 0.006) and lower median IL12p70 (1.98 vs. 3.41, p = 0.004) levels than HDs/RDs. IP10 was also found to be significant when comparing NH White or Asian patients with HDs/RDs ($p < 0.05$). Median IL-1β was 4.13 in NH Black patients compared to 2.66 in HDs/RDs (p = 0.115), providing a suggestive yet non-significant association to the finding in MSH cohort.

DISCUSSION

Racial disparities in COVID-19 infections and outcomes have become apparent in both the United States and elsewhere (Baqui

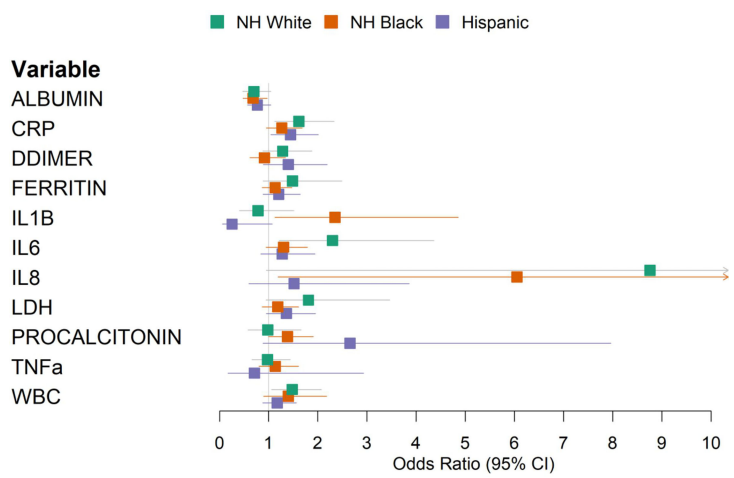

FIGURE 3 | Forest plot of multivariable logistic regression results predicting in-hospital mortality using laboratory values, stratified by race/ethnicity. Models were adjusted for age, sex, and baseline hypoxia.

et al., 2020; Price-Haywood et al., 2020; Oppel et al., 2020; Williamson et al., 2020). The causes of these disparities are complex and multifactorial and must be considered in the context of the social determinants of health (Williamson et al., 2020; Nguyen et al., 2020).

In this study, set in New York City during the height of the initial COVID-19 surge, we describe the characteristics and outcomes of a diverse cohort including substantial numbers of NH White, NH Black, and Hispanic patients. The three groups differed significantly in demographic and clinical factors. White patients were older and showed higher rates of cardiovascular disease such as coronary artery disease and atrial fibrillation. NH Black and Hispanic patients were younger and had different comorbidity profiles, e.g., hypertension, diabetes, chronic kidney disease, and chronic liver disease.

Unadjusted in-hospital mortality was the highest in NH White patients, but multivariable analysis showed that race/ethnicity was not an independent predictor of mortality in this cohort. It remains unclear whether race and ethnicity are independent risk factors for COVID-19 mortality after adjusting for confounding factors. Large national-level studies in the United Kingdom and Brazil have reported race as an independent predictor of mortality (Baqui et al., 2020; Williamson et al., 2020), whereas smaller studies in the United States have not (Gold et al., 2020; Price-Haywood et al., 2020; Suleyman et al., 2020), possibly due to statistical power or population differences. Changes in clinical management and outcomes of COVID-19 over the course of the pandemic may also complicate comparisons of results from different time periods (Horwitz et al., 2020). In this New York City patient population, race/ethnicity was not an independent predictor for mortality.

In addition to describing this cohort, we aimed to test established COVID-19 risk factors for race/ethnicity-specific effects. Despite recapitulating several known risk factors, such as age, male sex, and hypoxia, we found only suggestive but non-significant interactions between Black race, diabetes, and obesity, and both diabetes and obesity tended to increase the mortality risk of Black patients to a greater degree than White patients. Notably, when analyzing inflammatory markers for their association with mortality, we found a significant interaction between the NH Black population and the inflammatory cytokine IL-1β.

Excessive inflammation has emerged as an important aspect of COVID-19 pathophysiology, and the anti-inflammatory steroid dexamethasone has been shown to improve outcomes among those with severe disease (The RECOVERY Collaborative Group, 2020). The interaction between the NH Black population and IL-1β raises the possibility that differences in immunity may contribute to worse outcomes in some patients. Black Americans are at higher risk of autoimmune conditions such as systemic lupus erythematosus and lupus nephritis as compared to White Americans, with differences that can be linked in some cases to specific polymorphisms, which are more common in African Americans (Ness et al., 2004; Clatworthy et al., 2007; Richman et al., 2012; Freedman et al., 2014).

IL-1β is a pro-inflammatory cytokine that plays a role in both physiologic and pathologic inflammation. IL-1 inhibitors such as anakinra and canakinumab have been developed to target IL-1 in autoimmune diseases such as rheumatoid arthritis and Still's disease. These agents are also being actively investigated as COVID-19 treatments. Thus far, two randomized studies have found no clinical benefit from IL-1 inhibitors in COVID-19 [Novartis Provides Update on CAN-COVID Trial in Hospitalized Patients With COVID-19 Pneumonia and Cytokine Release Syndrome (CRS) (Novartis); Tharaux et al., 2021]. However, these studies have not reported analyses taking race/ethnicity into account.

The strengths of our database include its size and the inclusion of 37.1% Hispanic patients, a vulnerable population in this pandemic, which has been underrepresented in the literature to date. Additionally, our near-complete follow-up of the cohort's hospital outcomes (99.3%) strengthens the validity of our findings.

Our study has limitations that warrant specific mention. The cytokine analysis was limited to only a subset of the population and should be considered exploratory. We were not able to control for other comorbidities, which may have influenced cytokine levels (e.g., diabetes and IL-1β) (Dinarello et al., 2010). The dataset was derived from the electronic health record database without manual review, which may limit the completeness of comorbidity labels. Race and ethnicity were self-reported and were missing or unspecified in 17.4% of the initial cohort. The subset of patients with cytokine data was limited in number and had limited models testing interactions. Causal mechanisms underlying the correlations identified in this retrospective analysis remain to be elucidated.

In conclusion, our analysis of a diverse cohort drawn from the New York metropolitan area highlights both similarities and important differences across racial/ethnic groups in risk factors for death among hospitalized COVID-19 patients. The findings identified across populations call for conscious inclusion in future cohort studies and clinical trials to ensure the efficacy of potential diagnostics and treatments across diverse individuals.

DATA AVAILABILITY STATEMENT

The raw data supporting the conclusions of this article will be made available by the authors, without undue reservation.

ETHICS STATEMENT

Ethical review and approval was not required for the study on human participants in accordance with the local legislation and institutional requirements. Written informed consent for participation was not required for this study in accordance with the national legislation and the institutional requirements.

AUTHOR CONTRIBUTIONS

KH, EW, and TJ conceived and designed the study. DM collected and generated the data from the University of Pennsylvania

cohort. SN and PK collected and organized the clinical data from Mount Sinai. TJ, NS, and H-HH analyzed the data. TJ and K-lH drafted the manuscript. All authors read and approved the final manuscript.

FUNDING

This work was supported by NIGMS R35GM138113 to K-lH.

ACKNOWLEDGMENTS

We dedicate this work to the frontline health workers and staff of the Mount Sinai Healthcare System.

SUPPLEMENTARY MATERIAL

The Supplementary Material for this article can be found online at: https://www.frontiersin.org/articles/10.3389/fcimb.2022.933190/full#supplementary-material

REFERENCES

Baqui, P., Bica, I., Marra, V., Ercole, A., and van der Schaar, M. (2020). Ethnic and Regional Variations in Hospital Mortality From COVID-19 in Brazil: A Cross-Sectional Observational Study. *Lancet Glob Health* 8, e1018–e1026. doi: 10.1016/S2214-109X(20)30285-0

Charney, A. W., Simons, N. W., Mouskas, K., Lepow, L., Cheng, E., Le Berichel, J., et al. (2020). Sampling the Host Response to SARS-CoV-2 in Hospitals Under Siege. *Nat. Med.* 26, 1–2. doi: 10.1038/s41591-020-1004-3

Clatworthy, M. R., Willcocks, L., Urban, B., Langhorne, J., Williams, T. N., Peshu, N., et al. (2007). Systemic Lupus Erythematosus-Associated Defects in the Inhibitory Receptor Fcγriib Reduce Susceptibility to Malaria. *Proc. Natl. Acad. Sci. U.S.A.* 104, 7169–7174. doi: 10.1073/pnas.0608889104

Del Valle, D. M. D., Kim-schulze, S., Huang, H.-H., Beckmann, N. D., Nirenberg, S., Wang, B., et al. (2020). An Inflammatory Cytokine Signature Predicts COVID-19 Severity and Survival. *Nat. Med.* 26, 1636–1643. doi: 10.1038/s41591-020-1051-9

Dinarello, C. A., Donath, M. Y., and Mandrup-Poulsen, T. (2010). Role of IL-1beta in Type 2 Diabetes. *Curr. Opin. Endocrinol. Diabetes Obes.* 17, 314–321. doi: 10.1097/MED.0b013e32833bf6dc

Docherty, A. B., Harrison, E. M., Green, C. A., Hardwick, H. E., Pius, R., Norman, L., et al. (2020). Features of 20 133 UK Patients in Hospital With Covid-19 Using the ISARIC WHO Clinical Characterisation Protocol: Prospective Observational Cohort Study. *BMJ* 369, m1985. doi: 10.1136/bmj.m1985

Freedman, B. I., Langefeld, C. D., Andringa, K. K., Croker, J. A., Williams, A. H., Garner, N. E., et al. (2014). End-Stage Renal Disease in African Americans With Lupus Nephritis is Associated With APOL1. *Arthritis Rheumatol. (Hoboken NJ)* 66, 390–396. doi: 10.1002/art.38220

Gold, J. A. W., Wong, K. K., Szablewski, C. M., Patel, P. R., Rossow, J., da Silva, J., et al. (2020). Characteristics and Clinical Outcomes of Adult Patients Hospitalized With COVID-19 - Georgia, March 2020. *MMWR Morb Mortal Wkly Rep.* 69, 545–550. doi: 10.15585/mmwr.mm6918e1

Gordon, M., and Lumley, T. (2021) *Forestplot: Advanced Forest Plot Using 'Grid' Graphics*. Available at: https://CRAN.R-project.org/package=forestplot (Accessed June 13, 2022).

Grasselli, G., Greco, M., Zanella, A., Albano, G., Antonelli, M., Bellani, G., et al. (2020). Risk Factors Associated With Mortality Among Patients With COVID-19 in Intensive Care Units in Lombardy, Italy. *JAMA Intern. Med* 180, 1345–1355. doi: 10.1001/jamainternmed.2020.3539

Gu, T., Mack, J. A., Salvatore, M., Prabhu Sankar, S., Valley, T. S., Singh, K., et al. (2020). Characteristics Associated With Racial/Ethnic Disparities in COVID-19 Outcomes in an Academic Health Care System. *JAMA Netw. Open* 3, e2025197. doi: 10.1001/jamanetworkopen.2020.25197

Gupta, S., Hayek, S. S., Wang, W., Chan, L., Mathews, K. S., Melamed, M. L., et al. (2020). Factors Associated With Death in Critically Ill Patients With Coronavirus Disease 2019 in the US. *JAMA Intern. Med* 180, 1436–1447. doi: 10.1001/jamainternmed.2020.3596

Harrell, F. A.Jr., Dupont, C.contributed several functions and maintains latex functions (2022) *Hmisc: Harrell Miscellaneous*. Available at: https://CRAN.R-project.org/package=Hmisc (Accessed June 13, 2022).

Holtgrave, D. R., Barranco, M. A., Tesoriero, J. M., Blog, D. S., and Rosenberg, E. S. (2020). Assessing Racial and Ethnic Disparities Using a COVID-19 Outcomes Continuum for New York State. *Ann. Epidemiol.* 48, 9–14. doi: 10.1016/j.annepidem.2020.06.010

Horwitz, L. I., Jones, S. A., Cerfolio, R. J., Francois, F., Greco, J., Rudy, B., et al. (2020). Trends in Covid-19 Risk-Adjusted Mortality Rates in a Single Health System. *medRxiv* 16, 90–92. doi: 10.1101/2020.08.11.20172775

Hsu, H. E., Ashe, E. M., Silverstein, M., Hofman, M., Lange, S. J., Razzaghi, H., et al. (2020). Race/Ethnicity, Underlying Medical Conditions, Homelessness, and Hospitalization Status of Adult Patients With COVID-19 at an Urban Safety-Net Medical Center - Boston, Massachusetts, 2020. *MMWR Morb Mortal Wkly Rep.* 69, 864–869. doi: 10.15585/mmwr.mm6927a3

Kassambara, A. (2020) *Ggpubr: 'Ggplot2' Based Publication Ready Plots*. Available at: https://CRAN.R-project.org/package=ggpubr (Accessed June 13, 2022).

Mathew, D., Giles, J. R., Baxter, A. E., Oldridge, D. A., Greenplate, A. R., Wu, J. E., et al. (2020). Deep Immune Profiling of COVID-19 Patients Reveals Distinct Immunotypes With Therapeutic Implications. *Science* 369, eabc8511. doi: 10.1126/science.abc8511

Ness, R. B., Haggerty, C. L., Harger, G., and Ferrell, R. (2004). Differential Distribution of Allelic Variants in Cytokine Genes Among African Americans and White Americans. *Am. J. Epidemiol.* 160, 1033–1038. doi: 10.1093/aje/kwh325

Nguyen, A., David, J. K., Maden, S. K., Wood, M. A., Weeder, B. R., Nellore, A., et al. (2020). Human Leukocyte Antigen Susceptibility Map for Severe Acute Respiratory Syndrome Coronavirus 2. *J. Virol.* 94, e00510-20. doi: 10.1128/JVI.00510-20

Oppel, R. A.Jr., Gebeloff, R., Lai, K. K. R., Wright, W., and Smith, M. (2020) *The Fullest Look Yet at the Racial Inequity of Coronavirus. The New York Times*. Available at: https://www.nytimes.com/interactive/2020/07/05/us/coronavirus-latinos-african-americans-cdc-data.html (Accessed Aug 1, 2020).

Novartis Provides Update on CAN-COVID Trial in Hospitalized Patients With COVID-19 Pneumonia and Cytokine Release Syndrome (CRS) (Novartis). Available at: https://www.novartis.com/news/media-releases/novartis-provides-update-can-covid-trial-hospitalized-patients-covid-19-pneumonia-and-cytokine-release-syndrome-crs (Accessed March 29, 2021).

Petrilli, C. M., Jones, S. A., Yang, J., Rajagopalan, H., O'Donnell, L., Chernyak, Y., et al. (2020). Factors Associated With Hospital Admission and Critical Illness Among 5279 People With Coronavirus Disease 2019 in New York City: Prospective Cohort Study. *BMJ* 369, m1966. doi: 10.1136/bmj.m1966

Price-Haywood, E. G., Burton, J., Fort, D., and Seoane, L. (2020). Hospitalization and Mortality Among Black Patients and White Patients With Covid-19. *New Engl. J. Med.* 382, 2534–2543. doi: 10.1056/NEJMsa2011686

Richman, I. B., Taylor, K. E., Chung, S. A., Trupin, L., Petri, M., Yelin, E., et al. (2012). European Genetic Ancestry is Associated With a Decreased Risk of Lupus Nephritis. *Arthritis Rheum* 64, 3374–3382. doi: 10.1002/art.34567

Suleyman, G., Fadel, R. A., Malette, K. M., Hammond, C., Abdulla, H., Entz, A, et al. (2020). Clinical Characteristics and Morbidity Associated With Coronavirus Disease 2019 in a Series of Patients in Metropolitan Detroit. *JAMA Netw. Open* 3, e2012270. doi: 10.1001/jamanetworkopen.2020.12270

Tharaux, P.-L., Pialoux, G., Pavot, A., Mariette, X., Hermine, O., Resche-Rigon, M., et al. (2021). Effect of Anakinra Versus Usual Care in Adults in Hospital With COVID-19 and Mild-to-Moderate Pneumonia (CORIMUNO-ANA-1):

A Randomised Controlled Trial. *Lancet Respir. Med.* 9, 295–304. doi: 10.1016/S2213-2600(20)30556-7

The RECOVERY Collaborative Group (2020). Dexamethasone in Hospitalized Patients With Covid-19 — Preliminary Report. *New Engl. J. Med* 384, 693–704. doi: 10.1056/NEJMoa2021436

Wickham, H. (2017) *RStudio. Tidyverse: Easily Install and Load the 'Tidyverse'*. Available at: https://CRAN.R-project.org/package=tidyverse (Accessed Oct 9, 2019).

Williamson, E. J., Walker, A. J., Bhaskaran, K., Bacon, S., Bates, C., Morton, C. E., et al. (2020). OpenSAFELY: Factors Associated With COVID-19 Death in 17 Million Patients. *Nature* 584, 1–11. doi: 10.1038/s41586-020-2521-4

Zhou, F., Yu, T., Du, R., Fan, G., Liu, Y., Liu, Z, et al. (2020). Clinical Course and Risk Factors for Mortality of Adult Inpatients With COVID-19 in Wuhan, China: A Retrospective Cohort Study. *Lancet* 395, 1054–1062. doi: 10.1016/S0140-6736(20)30566-3

Conflict of Interest: EW has consulting agreements with and/or is on the scientific advisory board for Merck, Elstar, Janssen, Jounce, Related Sciences, Synthekine, and Surface Oncology. EW is a founder of Surface Oncology and Arsenal Biosciences. EW has a patent licensing agreement on the PD-1 pathway with Roche/Genentech. TJ is employed by and owns stock in Sema4.

The remaining authors declare that the research was conducted in the absence of any commercial or financial relationships that could be construed as a potential conflict of interest.

frontiers | Frontiers in Cellular and Infection Microbiology

TYPE Original Research
PUBLISHED 02 September 2022
DOI 10.3389/fcimb.2022.978440

OPEN ACCESS

EDITED BY
You Zhou,
Cardiff University, United Kingdom

REVIEWED BY
Christian Albert Devaux,
Centre National de la Recherche Scientifique (CNRS), France
Kun Qin,
National Institute for Viral Disease Control and Prevention (China CDC), China

*CORRESPONDENCE
Dan Li
lidan@chinaaids.cn
Yiming Shao
yishao16@zju.edu.cn

SPECIALTY SECTION
This article was submitted to Clinical Microbiology, a section of the journal Frontiers in Cellular and Infection Microbiology

RECEIVED 26 June 2022
ACCEPTED 08 August 2022
PUBLISHED 02 September 2022

CITATION
Hu C, Wang Z, Ren L, Hao Y, Zhu M, Jiang H, Wang S, Li D and Shao Y (2022) Pre-existing anti-HCoV-OC43 immunity influences the durability and cross-reactivity of humoral response to SARS-CoV-2 vaccination. *Front. Cell. Infect. Microbiol.* 12:978440. doi: 10.3389/fcimb.2022.978440

Pre-existing anti-HCoV-OC43 immunity influences the durability and cross-reactivity of humoral response to SARS-CoV-2 vaccination

Caiqin Hu[1], Zheng Wang[2], Li Ren[2], Yanling Hao[2], Meiling Zhu[2], He Jiang[3], Shuo Wang[2], Dan Li[2]* and Yiming Shao[1,2]*

[1]State Key Laboratory for Diagnosis and Treatment of Infectious Diseases, National Clinical Research Center for Infectious Diseases, National Medical Center for Infectious Diseases, Collaborative Innovation Center for Diagnosis and Treatment of Infectious Diseases, The First Affiliated Hospital, Zhejiang University School of Medicine, Zhejiang, China, [2]State Key Laboratory for Infectious Disease Prevention and Control, National Center for AIDS/STD Control and Prevention, Chinese Center for Disease Control and Prevention, Beijing, China, [3]Guangxi Key Laboratory of AIDS Prevention and Control and Achievement Transformation, Guangxi Center for Disease Prevention and Control, Nanning, China

Purpose: This study was conducted in order to properly understand whether prior seasonal human coronavirus (HCoV) immunity could impact the potential cross-reactivity of humoral responses induced by SARS-CoV-2 vaccine, thereby devising universal coronavirus vaccines for future outbreaks.

Methods: We performed enzyme-linked immunosorbent assay (ELISA) to quantify the immunoglobulin G (IgG) antibody levels to spike (S) protein and S1 subunit of HCoVs (HCoV-OC43, HCoV-HKU1, HCoV-NL63, and HCoV-229E), and ELISA [anti-RBD and anti-nucleoprotein (N)], chemiluminescence immunoassay assays (anti-RBD), pseudovirus neutralization test, and authentic viral neutralization test to detect the binding and neutralizing antibodies to SARS-CoV-2 in the vaccinees.

Results: We found that the antibody of seasonal HCoVs did exist before vaccination and could be boosted by SARS-CoV-2 vaccine. A further analysis demonstrated that the prior S and S1 IgG antibodies of HCoV-OC43 were positively correlated with anti-RBD and neutralization antibodies to SARS-CoV-2 at 12 and 24 weeks after the second vaccination, and the correlation is more statistically significant at 24 weeks. The persistent antibody levels of SARS-CoV-2 were observed in vaccinees with higher pre-existing HCoV-OC43 antibodies.

Conclusion: Our data indicate that inactivated SARS-CoV-2 vaccination may confer cross-protection against seasonal coronaviruses in most individuals, and more importantly, the pre-existing HCoV-OC43 antibody was associated

with protective immunity to SARS-CoV-2, supporting the development of a pan-coronavirus vaccine.

KEYWORDS

SARS-CoV-2, seasonal human coronavirus, antibody, cross-reactivity, protective immunity

Introduction

Since the COVID-19 pandemic status was declared by WHO on March 11, 2020, the prevalence of SARS-CoV-2 has been a major concern for clinicians and researchers. In addition to SARS-CoV-2, six other coronaviruses (SARS-CoV, MERS, HCoV-OC43, HCoV-HKU1, HCoV-NL63, and HCoV-229E) could also infect humans (Su et al., 2016; Corman et al., 2018). Patients of SARS-CoV, MERS, and SARS-CoV-2 have a variety of clinical manifestations, ranging from mild to severe and even death. While the endemic and seasonal HCoVs, including HCoV-OC43, HCoV-HKU1, HCoV-NL63, and HCoV-229E, typically cause upper respiratory symptoms and are usually self-limited in human. Unlike SARS-CoV and MERS, the seroprevalence could reach more than 90% for at least three of the seasonal HCoVs and account for at least 30% of seasonal colds (Severance et al., 2008; Gorse et al., 2010; Su et al., 2016; Chen et al., 2020; Jin et al., 2020).

SARS-CoV-2 vaccines could limit symptom burden, cutting down the number of hospitalizations and deaths (Al Kaabi et al., 2021; Bergwerk et al., 2021; Khoury et al., 2021), but reducing the efficacy against newly emerging variants and increasing cases of breakthrough infection had continuously been reported (Edara et al., 2021; Zhou et al., 2021; Muik et al., 2022). Knowledge of SARS-CoV-2 immunity, especially the cross-reactivity of antibodies against different coronaviruses, is critical for understanding the potential future immunity of vaccinees to other HCoVs and providing guidance for pan-coronavirus vaccine development.

In this study, we focused on the serologic antibodies of seasonal HCoVs and SARS-CoV-2 within 6 months post-vaccination and characterized the relationship among these coronaviruses. We performed enzyme-linked immunosorbent assay (ELISA) to test the immunoglobulin G (IgG) antibody levels to spike (S) protein and S1 subunit of HCoVs and ELISA [anti-RBD and anti-nucleoprotein (N)], chemiluminescence immunoassay assays (CLIA, anti-RBD), pseudovirus neutralization test (PVNT), and authentic viral neutralization test to detect the binding and neutralizing antibodies to SARS-CoV-2 in the vaccinees.

Materials and methods

Study participants

A total of 23 healthy people who have completed two doses of BBIBP-CorV vaccination were enrolled, and their informed consent was obtained. The study was conducted in accordance with the Declaration of Helsinki, and the protocol was approved by the Ethics Committee of the First Affiliated Hospital, Zhejiang University School of Medicine (reference number 2021376).

WANTAI SARS-CoV-2 Ab enzyme-linked immunosorbent assay

The anti-RBD and anti-N antibodies of SARS-CoV-2 were measured using SARS-CoV-2 RBD/N ELISA kits, respectively, in accordance with the instructions (Wantai Biological Pharmacy, China). Briefly, 96-well plates were pre-coated with 2019-nCoV-RBD antigen (recombinant protein expressed in HEK 293 T cells) or 2019-nCoV-N antigen (recombinant protein expressed in *E. coli*). Furthermore, 100 μl of plasma samples was added, incubated for 0.5 h at 37°C, and washed. Then, 100 μl of horseradish peroxidase (HRP)-labeled 2019-nCoV-Ag was incubated for 0.5 h at 37°C and washed. After that, 100 μl of substrate was added in each well for 15 min at 37°C. The reaction was stopped by adding 50 μl of 1 nm H_2SO4 to each well, and the reading was taken at 450 nm. The amino acid sequences of 2019-nCoV-RBD and 2019-nCoV-N are presented in Supplementary Table S3.

Enzyme-linked immunosorbent assay of seasonal human coronavirus

The spike protein and S1 subunits of seasonal hCoVs (HCoV-OC43, HCoV-HKU1, HCoV-NL63, and HCoV-229E) were purchased from Sino Biological (catalog numbers 40607-V08B, 40607-V08H, 40606-V08B, 40602-V08H, 40604-V08B, 40600-V08H, 40605-V08B, and 40601-V08H, respectively).

Furthermore, 100 µl of antigens at a concentration of 0.5 ug/ml was coated in 96-well ELISA plates overnight at 4°C. The plate was washed with PBS-T (0.05% Tween 20) five times and blocked with 250 ul of blocking buffer (PBS, ph 7.4, + 2% BSA + 5%milk) for 2 h at 37°C. The blocking solution was removed, and diluted serum samples from a starting concentration of 1:100 were incubated at 37°C for 1 h. The plates were washed five times with PBS-T and 100 µl HRP-goat anti-human IgG (1:5,000 dilution) in diluted blocking buffer for 1 h at 37°C. The plates were washed with PBST five times. Then, 100 ul of substrate was added in each well for 15 min at room temperature. The reaction was stopped by adding 50 µl of 1 nm H_2SO4 to each well, and the reading was taken at 450 nm.

Chemiluminescent microparticle immunoassay

The COVID-19 nAbs detection kits (Hotgen, Beijing, China, batch number: 21010115) were based on chemiluminescent microparticle immunoassay and used a competitive ELISA method to detect SARS-CoV-2 nAbs. In short, the test was performed by reacting the sample with alkaline phosphatase-labeled S-RBD antigen complex. Biotin-labeled receptor protein ACE2 and magnetic microspheres encapsulated with streptavidin were added to promote the attachment of the ACE2-S-RBD antigen complex to the magnetic microspheres by the specific binding of biotin and streptavidin. A matched automatic chemiluminescence immunoassay analyzer was used to analyze the nAb levels which were presented as the chemiluminescence signal values divided by the cutoff (absorbance/cutoff, S/CO). All operations were carried out in strict accordance with the instructions of the reagent manufacturer. Furthermore, 100 µl plasma sample was added, and the whole process took about 30 min. S/CO <1 was considered positive, while S/CO ≥1 was considered negative.

Pseudovirus neutralization test

The pseudovirus was generated by co-transfection of HEK 293 T cells with pcDNA3.1-S-COVID19 and pNL4-3Luc, which carries the optimized spike (S) gene and a human immunodeficiency virus type 1 backbone, respectively. Then, 150-ul serial dilutions of human sera (four serial threefold dilutions in Dulbecco's minimum essential medium with an initial dilution of 1:20) were added into 96-well plates. After that, 50 ul pseudoviruses of SARS-CoV-2 with a concentration of 1,300 TCID50/ml was added into the plates, followed by incubation at 37°C for 1 h. Afterward, Hu-h7 cells were added into the plates (1.5×10^4 cells/100 ul cells per well), followed by incubation at 37°C in a humidified atmosphere with 5% CO_2. Chemiluminescence detection was performed after 48 h of incubation. The Reed–Muench method was used to calculate the virus neutralization titers. The result was reported as half-maximal inhibitory concentration of PVNT (PVNT50).

Live viral neutralization test

The live viral neutralization test of SARS-CoV-2 was performed as previously described (Li et al., 2022). In brief, the neutralizing antibody titers against the wild-type strain and the variants (Beta B.1.1.7, Gamma P.1, and Delta B.1.617) in serum were determined by using a cytopathic effect-based microneutralization assay in Vero cells (National Collection of Authenticated Cell Cultures, National Academy of Science, China). The serum was then mixed with the same volume of viral solution to achieve a final concentration of 100 TCID50 per well. The reported titer was the reciprocal of the highest sample dilution that protected at least 50% of the cells from cytopathic effects. Serum dilution for the neutralization assay started from 1:4, and seropositivity was defined as titer ≥1:4.

Multiple sequence alignment

Multiple sequence alignment (MSA) that used to determine the spike protein and nucleoprotein sequence's identity and similarity among SARS-CoV-2 (MN908947.3), the seasonal human coronaviruses HKU1 (DQ415914.1), OC43 (MF374985), 229E (NC002645.1), and NL63 (AY567487.2) were aligned and analyzed by the BLOSUM50 method of MatGAT (version 2.0). The conservation and antigenic epitopes of SARS-CoV-2 RBD protein were conducted by the JaIview (version 2.11) and EMBOSS explorer (https://www.bioinformatics.nl/cgi-bin/emboss/antigenic), respectively.

Statistical analysis

All IgG antibody titers to seasonal HCoVs were log10-transformed to improve the linearity. The geometric mean titers (GMT) and 95% confidence intervals (95% CI) were computed as log10-transformed titers. Two-tailed, nonparametric Mann–Whitney *U*-test and Kruskal–Wallis test were performed on numerical data. Pearson and linear correlation were used on antibody response against seasonal HCoVs and SARS-CoV-2. The graphs and statistical analyses were conducted using GraphPad Prism (version 8.0.2), Origin2021b (version 9.8.5), and SPSS software (version 23.0). *P*-values less than 0.05 were considered statistically significant.

Results

Sequence homology between SARS-CoV-2 and seasonal human coronaviruses

To better evaluate the potential cross-reactivity, we compared the amino acid sequence of spike protein and nucleoprotein among SARS-CoV-2, HCoV-OC43, HCoV-HKU1, HCoV-NL63, and HCoV-229E. We also estimated the relative conservation scores and antigenic epitopes of the RBD region of SARS-CoV-2. The conservation and antigenic epitopes were conducted by the JaIview and EMBOSS explorer, respectively (Figure 1A). MSA was analyzed by the BLOSUM50 method of MatGAT (version 2.0) (James and Campanella*, 2003). The greatest homology of spike was between SARS-CoV-2 and HCoV-OC43 (29.8% identity and 49% similarity), followed by HCoV-HKU1(28.5% identity and 48.6% similarity), HCoV-229E (27.3% identity and 45.2% similarity), and HCoV-NL63 (25.9% identity and 45% similarity). The greatest homology of nucleoprotein was between SARS-CoV-2 and HCoV-OC43 (33.7% identity and 53.8% similarity), followed by HCoV-HKU1(31.9% identity and 51.9% similarity), HCoV-NL63 (27.6% identity and 44.9% similarity), and HCoV-229E (24.7% identity and 40.8% similarity) (Figure 1B). Both S and N proteins of HCoV-OC43 and HCoV-HKU1 were closer to SARS-CoV-2 than those of HCoV-NL63 and HCoV-229E.

Cross-reactivity of antibodies boosted by SARS-CoV-2 vaccine

To explore the antibody response induced by SARS-CoV-2 vaccine, 23 healthy people [17 female and six male, with a median age of 27 (interquartile range: 26–39) years old] who completed two doses of BBIBP-CorV vaccination were included in this study. The baseline characteristics of the healthy donors are presented in Supplementary Table S1. The interval between two doses of vaccine is 21 days. Plasma samples before the first dose of vaccination and at 4, 12, and 24 weeks after the second dose of inactivated BBIBP-CorV vaccine were collected to measure the antibody activity against seasonal HCoVs and the SARS-CoV-2. No neutralization and binding ability of SARS-CoV-2 were shown before vaccination (Hu et al., 2022). The IgG levels to spikes and S1 subunits of seasonal HCoVs were quantified as area under the curve (AUC) by plotting normalized optical density values against the serum sample dilutions for ELISAs (Supplementary Figure S1). The GMT (95% CI) at each time point for AUC ELISA against the seasonal HCoVs are shown in Supplementary Table S2. The serum IgG antibodies to the seasonal HCoVs pre-existed before the SARS-CoV-2 vaccine and were boosted after vaccination. Significant differences between groups are displayed (Figure 2).

Correlation of antibody levels between SARS-CoV-2 with seasonal HCoVs

We analyzed the correlations of prior IgG levels against seasonal HCoVs and the RBD, N, and neutralizing antibodies of SARS-CoV-2 at 4, 12, and 24 weeks after vaccination. Pearson correlation matrices according to seasonal HCoV subtype are shown in Figure 3. At 12 weeks after vaccination, the prior S-IgG antibodies of HCoV-OC43 were positively correlated with S-RBD antibodies by ELISA and nAb and negatively correlated with S-RBD antibodies by CLIA to SARS-CoV-2, while the S1 IgG antibody of HCoV-OC43 was not correlated with SARS-CoV-2. At 24 weeks after vaccination, the prior S and S1 IgG antibodies to HCoV-OC43 were all shown to be related with the

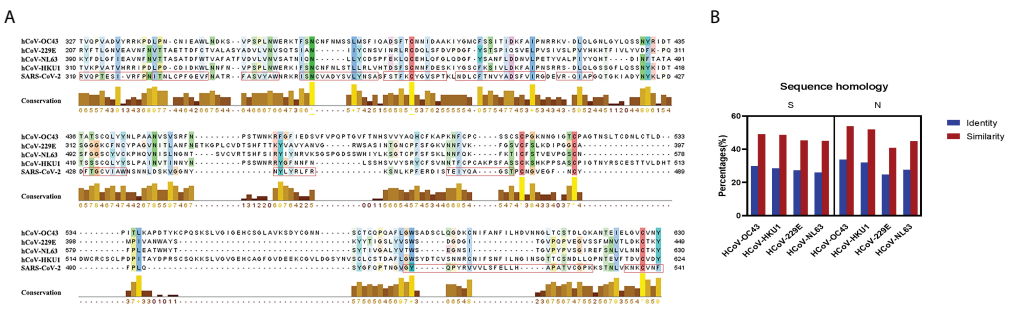

FIGURE 1
Sequence homology and conservation between SARS-CoV-2 and seasonal HCoVs. **(A)** The conservation and the antigenic epitopes of RBD are shown as a yellow bar chart and a red rectangle. The amino acid conservation scores were classified into 10 levels (1, most variable; +, most conserved). **(B)** Sequence homology and conservation of spike protein and nucleoprotein between SARS-CoV-2 and seasonal HCoVs. The identity and the similarity (%) of these two proteins were aligned and analyzed by the BLOSUM50 method of MatGAT (version 2.0) (James and Campanella*, 2003).

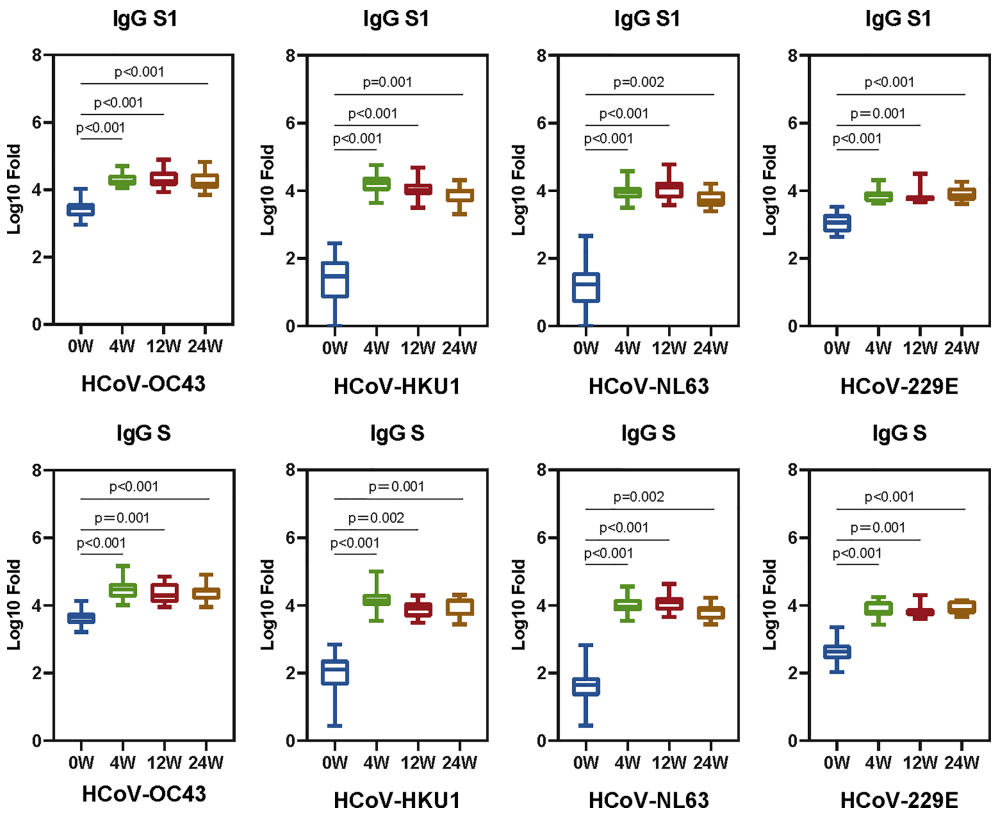

FIGURE 2
The SARS-CoV-2 vaccine boosts antibodies that are reactive to seasonal HCoVs. We quantified the serum IgG antibodies to the S and S1 proteins against HCoVs (HCoV-OC43, HCoV-HKU1, HCoV-NL63, and HCoV-229E). The IgG geometric mean titers (GMT) against seasonal HCoVs spike and S1 are shown in the boxplot. Two-tailed, nonparametric Dunn's Kruskal–Wallis test was used for multiple comparisons. The middle bars indicate the GMT values, the box indicates interquartile range, and the lines indicate minimum and maximum. Statistically significant values are marked in the figure.

S-RBD antibodies to SARS-CoV-2. The S-RBD antibody by CLIA was detected with a competitive method; the lower values of CLIA mean a higher antibody activity. Similarly, it is also evidenced that the pre-existing antibodies' response to other seasonal HCoVs (including HCoV-HKU1, HCoV-NL63, and HCoV-229E) were not related well with the humoral immunity to SARS-CoV-2. To show the relationship between the pre-existing antibody response to seasonal HCoVs and the S-RBD/N antibody and nAb to SARS-CoV-2 more clearly, the R^2 and P-values of the linear regressions are shown in Figure 4. The same results are shown in Figure 3; the correlations between prior S-IgG antibodies of HCoV-OC43 and S-RBD antibodies to SARS-CoV-2 at 24 weeks were stronger than at 12 weeks after the SARS-CoV-2 vaccine. In short, the higher the pre-existing antibody levels of HCoV-OC43, the higher the S-RBD binding antibodies against SARS-CoV-2, and the correlations tend to become stronger over time after vaccination.

Higher prior IgG antibody levels to HCoV-OC43 predict durable antibody responses to SARS-CoV-2

As mentioned above, the correlations between prior S-IgG antibodies of HCoV-OC43 and S-RBD antibodies to SARS-CoV-2 were highest at 24 weeks post-vaccination. Moreover, the antibody responses to SARS-CoV-2 at 24 weeks after vaccination can be regarded as a long-term immune response. We then divided the vaccinees into the two groups, with or without antibody responses to SARS-CoV-2 at 24 weeks after vaccination. PVNT50 above 20 was considered to be with a neutralizing activity and that less than 20 as without a neutralizing activity to SARS-CoV-2. S/CO less than 1 was regarded with anti-RBD antibody and that above 1 as without anti-RBD antibody to SARS-CoV-2. The pre-existing IgG antibody to spike and S1 of HCoV-HKU1, HCoV-NL63, and

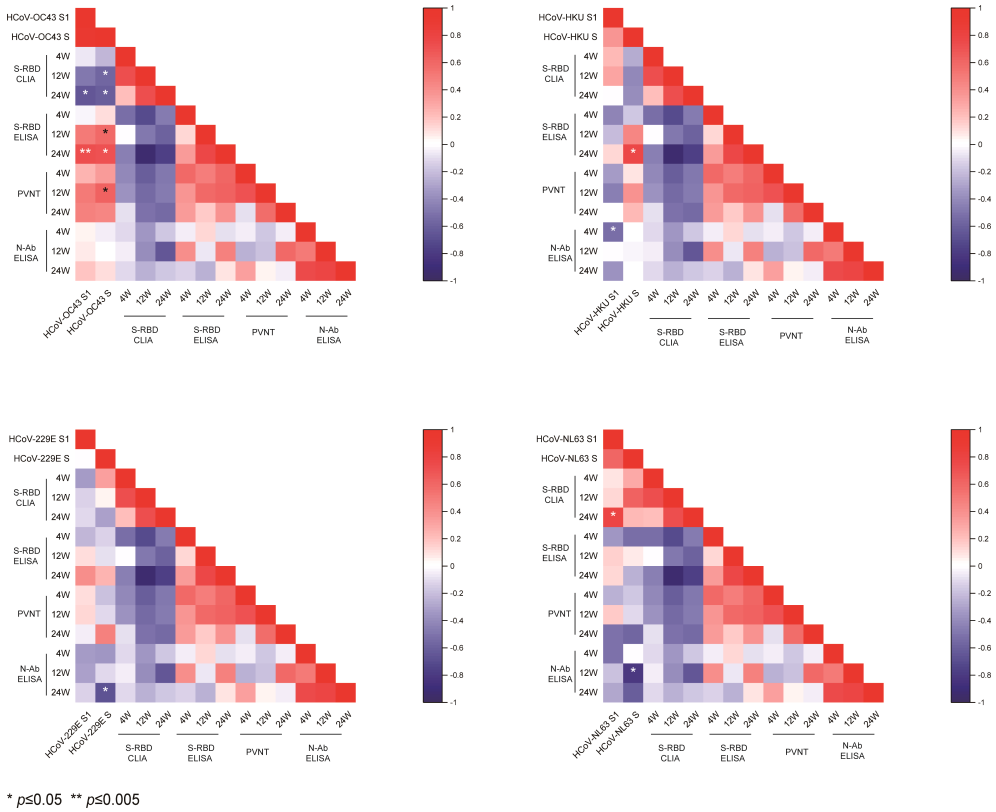

FIGURE 3
Pearson correlation matrices of antibody levels to SARS-CoV-2 and seasonal HCoVs. Heat map of the Pearson correlation matrices of pre-existing spike and S1 subunits' IgG antibody levels to seasonal HCoVs (HCoV-OC43, HCoV-HKU1, HCoV-NL63, and HCoV-229E) and S-RBD/N antibody and nAbs to SARS-CoV-2 at 4, 12, and 24 weeks after vaccination. Statistically significant correlations are indicated with an asterisk (*) in the first two columns of every heat map. *$P < 0.05$, **$P < 0.005$.

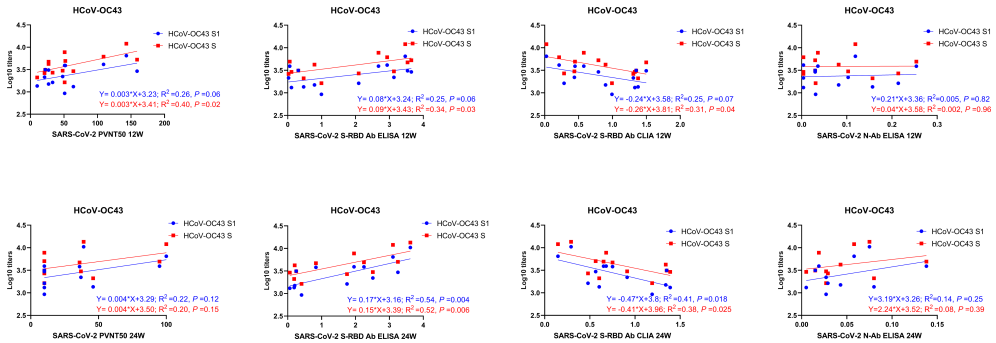

FIGURE 4
Linear correlation of antibody levels between SARS-CoV-2 and HCoV-OC43. The linear correlation between prior S/S1-IgG antibody levels to HCoV-OC43 and S-RBD/N/neutralizing antibodies to SARS-CoV-2 at 12 and 24 weeks after vaccination is shown in the figure. A scatter point represents a record. R^2 represents the degree of linear deviation obtained by fitting the experimental data. The p-value tests whether the regression equation is significant. The larger the R^2 value, the smaller the p-value. When the p-value is less than 0.05, this linear model can be considered valuable.

HCoV-229E all showed no difference in neutralizing and anti-RBD antibodies to SARS-CoV-2 in the two groups. However, a higher prior level of S/S1-IgG antibodies was to HCoV-OC43 exhibited in the group with neutralizing or anti-RBD antibodies to SARS-CoV-2 than another group (Figure 5). It has been speculated that the pre-existing antibody to HCoV-OC43 was associated with protective immunity to SARS-CoV-2.

Prior IgG antibody levels to seasonal HCoVs cannot influence the antibody activity to SARS-CoV-2 variants

Finally, in order to test whether prior HCoVs influence antibody responses against SARS-CoV-2 variants at 24 weeks after vaccination, we measured the levels of neutralizing antibodies against authentic SARS-CoV-2 variants, including Beta (B.1.1.7), Gamma (P.1), and Delta (B.1.617). Then, we divided the cohort into two groups: one group was able to neutralize at least one of the variants, and another was unable to neutralize the variants. Plasma dilution above 4 was considered to be with a neutralizing antibody and that less than 4 as without a neutralizing activity to SARS-CoV-2 variants. The pre-existing IgG antibody of seasonal HCoVs all showed no difference in the two groups (Figure 5C).

Discussion

Two doses of BBIBP-CorV vaccines showed 100% seroconversion rate and 78.1% efficacy against symptomatic illness separately (Al Kaabi et al., 2021; Jeewandara et al., 2021). Even though China has achieved 88% coverage with SARS-CoV-2 full vaccination, there are still breakthrough infection cases reported in populations. In our previous study, we found that the binding and neutralizing antibody to SARS-CoV-2 reached peaks at 4 weeks after the second dose vaccination and then gradually declined over time (Hu et al., 2022).

Cross-reactivity immunity is necessary to properly interpret results from serologic studies. In our study, the levels of prior IgG antibody to HCoV-229E and HCoV-OC43 were higher than the levels of IgG antibody to HCoV-NL63 and HCoV-HKU1, which were similar to the data reported previously by Gorse GJ et al. (Gorse et al., 2010). Most individuals possessed pre-existing serum antibodies reactive to HCoV-OC43, HCoV-HKU1, HCoV-NL63, and HCoV-229E, and the SARS-CoV-2 vaccine can boost the the level of antibodies of seasonal HCoVs. These results were consistent with previous studies (Severance et al., 2008; Aguilar-Bretones et al., 2021; Anderson et al., 2021; Camerini et al., 2021; Hicks et al., 2021; Majdoubi et al., 2021). Guo L et al. also tested the antigenic cross-reactivities of S protein between SARS-CoV-2 and seasonal HCoVs, and a two-way cross-reactivity was identified between SARS-CoV-2 and HCoVs (Guo et al., 2021). Regions within S antigens with high antigenic similarity between HCoVs are potential targets of cross-reactive antibodies (XiaoYan Che et al., 2005; Tso et al., 2021). The cross-reactive anti-spike IgG antibodies target not only the S2 domain but also the S1 domain, as suggested by Shrwani K et al. (Shrwani et al., 2021).

We found that the higher levels of pre-existing S and S1 IgG antibodies to HCoV-OC43 before vaccination were correlated with anti-RBD binding and neutralizing antibodies to SARS-CoV-2 at 12 and 24 weeks post-vaccination, and the correlation is more statistically significant at 24 weeks. It might give a signal to a more durable humoral response to SARS-CoV-2 infection in the population with a higher level of pre-existing antibodies to HCoV-OC43. Antibodies with a neutralizing activity are considered quite important in SARS-CoV-2 protection (Hall et al., 2021; Khoury et al., 2021). We speculate that the pre-existing antibody to HCoV-OC43 was also associated with the protective immunity to SARS-CoV-2. This conclusion is controversial—a study showed that pre-existing HCoV cross-reactive antibodies were not associated with protection from

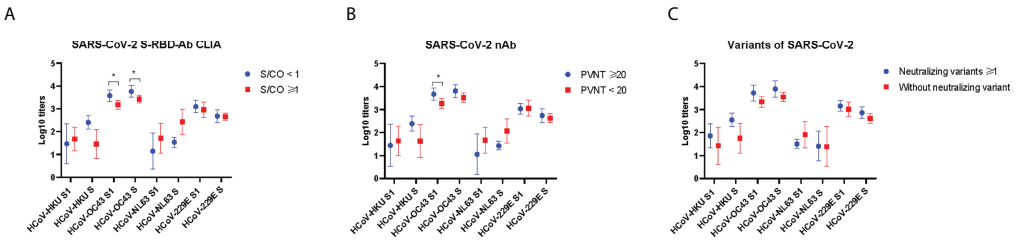

FIGURE 5
Prior antibody to seasonal HCoVs in the groups with and without antibodies to SARS-CoV-2 at 24 weeks after vaccination. The anti-RBD antibody levels were detected by chemiluminescent microparticle immunoassay **(A)**. The nAb levels were detected by pseudovirus neutralization test **(B)**, and neutralizing antibodies against authentic SARS-CoV-2 variants **(C)**. Two-tailed, nonparametric Mann–Whitney test was used for comparisons. The bars display the mean and SD. Part of the results between groups is shown in the figure. *$p < 0.05$.

SARS-CoV-2 infections (Anderson et al., 2021).The IgG of HCoVs was shown to have a higher significance in asymptomatic than symptomatic seropositive individuals. The authors have considered that the pre-existing cross-reactive HCoV antibodies may have a protective effect against SARS-CoV-2 infection and the severity of COVID-19 disease (Ortega et al., 2021). The inhibitor of HCoV-OC43 also exhibited broad fusion inhibitory activity against multiple HCoVs, including SARS-CoV-2 (Xia et al., 2019).

The humoral immunity discussed in this article is also complementary to previous literatures on cellular immunity. Some cell immunity studies have been carried out on SARS-CoV-2 and HCoVs. Aguilar-Bretones M et al. had elucidated the frequency of HCoV-OC43-S1-specific B cells that showed a positive correlation with PRNT50 titers (Aguilar-Bretones et al., 2021). Loyal L et al. had shown that the pre-existing cross-reactive $CD4^+$ T cells enhance the immune responses in SARS-CoV-2 infection and BNT162b2 vaccination (Loyal et al., 2021). Kundu R et al. put the conclusion straightly that high levels of pre-existing T cells of seasonal HCoVs can protect against SARS-CoV-2 infection (Kundu et al., 2022). These conclusions of cellular immunity further support our results. The pre-existing antibody to HCoV-OC43 may provide protective immunity to SARS-CoV-2.

Our study has several limitations. First, although we conducted a 24-week follow-up on vaccinees, the number of cases were relatively small. Second, low-pathogenic seasonal HCoVs typically cause self-limited colds with mild upper respiratory symptoms, so pathogenic detection is not routinely performed. Therefore, retrospective information on coronavirus infection cannot be effectively obtained. Third, the article was focused on humoral immunity in the vaccinated populations. The mechanism of the diversity in antibody responses after vaccination should be further explored in our study.

In conclusion, our study implied that the humoral immunity of seasonal HCoVs can be considered an important factor in assessing the antibody response to SARS-CoV-2. The results also suggest that the significant cross-reactive immune recognition between seasonal HCoVs and SARS-CoV-2 and the pre-existing HCoV-OC43 antibodies can prevent from SARS-CoV-2 infection. These findings may altogether shed new light on future vaccine strategies targeting newly emerging variants.

Data availability statement

The original contributions presented in the study are included in the article/Supplementary Material. Further inquiries can be directed to the corresponding authors.

Ethics statement

This study was granted by the Ethics Committee of First Affiliated Hospital, Zhejiang University School of Medicine (no. 2021376). The patients/participants provided their written informed consent to participate in this study.

Author contributions

Conceptualization: CH, DL, and YS. Funding acquisition: ZW and YS. Methodology: CH, ZW, LR, YH, MZ, SW, and HJ. Resources: DL and YS. Software: CH, HJ, and DL. Writing—original draft: CH. Writing—review and editing: DL and YS. All authors contributed to the article and approved the submitted version.

Funding

This research was funded by the National Natural Science Foundation of China under grant no. 20A20362 and Beijing Municipal Natural Science Foundation (M21015), the State Key Laboratory of Infections Disease Prevention and Control under grant no. 2021SKLID304 and no. 2020SKLID102, and the Science and Technology Project of Beijing under grant no. Z211100002521024.

Acknowledgments

The authors thank all study participants.

Conflict of interest

The authors declare that the research was conducted in the absence of any commercial or financial relationships that could be construed as a potential conflict of interest.

Publisher's note

Supplementary material

The Supplementary Material for this article can be found online at: https://www.frontiersin.org/articles/10.3389/fcimb.2022.978440/full#supplementary-material

References

Aguilar-Bretones, M., Westerhuis, B. M., Raadsen, M. P., de Bruin, E., Chandler, F. D., Okba, N. M., et al. (2021). Seasonal coronavirus-specific b cells with limited SARS-CoV-2 cross-reactivity dominate the IgG response in severe COVID-19. *J. Clin. Invest.* 131 (21), e150613. doi: 10.1172/JCI150613

Al Kaabi, N., Zhang, Y., Xia, S., Yang, Y., Al Qahtani, M. M., Abdulrazzaq, N., et al. (2021). Effect of 2 inactivated SARS-CoV-2 vaccines on symptomatic COVID-19 infection in adults: A randomized clinical trial. *JAMA* 326 (1), 35–45. doi: 10.1001/jama.2021.8565

Anderson, E. M., Goodwin, E. C., Verma, A., Arevalo, C. P., Bolton, M. J., Weirick, M. E., et al. (2021). Seasonal human coronavirus antibodies are boosted upon SARS-CoV-2 infection but not associated with protection. *Cell* 184 (7), 1858–1864, e1810. doi: 10.1016/j.cell.2021.02.010

Bergwerk, M., Gonen, T., Lustig, Y., Amit, S., Lipsitch, M., Cohen, C., et al. (2021). Covid-19 breakthrough infections in vaccinated health care workers. *New Engl. J. Med.* 385 (16), 1474–1484. doi: 10.1056/NEJMoa2109072

Camerini, D., Randall, A. Z., Trappl-Kimmons, K., Oberai, A., Hung, C., Edgar, J., et al. (2021). Mapping SARS-CoV-2 antibody epitopes in COVID-19 patients with a multi-coronavirus protein microarray. *Microbiol. Spectr.* 9 (2), e0141621. doi: 10.1128/Spectrum.01416-21

Chen, B., Tian, E. K., He, B., Tian, L., Han, R., Wang, S., et al. (2020). Overview of lethal human coronaviruses. *Signal Transduct target Ther.* 5 (1), 89. doi: 10.1038/s41392-020-0190-2

Corman, V. M., Muth, D., Niemeyer, D., and Drosten, C. (2018). Hosts and sources of endemic human coronaviruses. *Adv. Virus Res.* 100, 163–188. doi: 10.1016/bs.aivir.2018.01.001

Edara, V. V., Norwood, C., Floyd, K., Lai, L., Davis-Gardner, M. E., Hudson, W. H., et al. (2021). Infection- and vaccine-induced antibody binding and neutralization of the B.1.351 SARS-CoV-2 variant. *Cell Host Microbe* 29 (4), 516–521, e513. doi: 10.1016/j.chom.2021.03.009

Gorse, G. J., Patel, G. B., Vitale, J. N., and O'Connor, T. Z. (2010). Prevalence of antibodies to four human coronaviruses is lower in nasal secretions than in serum. *Clin. Vaccine immunol. CVI* 17 (12), 1875–1880. doi: 10.1128/CVI.00278-10

Guo, L., Wang, Y., Kang, L., Hu, Y., Wang, L., Zhong, J., et al. (2021). Cross-reactive antibody against human coronavirus OC43 spike protein correlates with disease severity in COVID-19 patients: a retrospective study. *Emerg Microbes Infect* 10 (1), 664–676. doi: 10.1080/22221751.2021.1905488

Hall, V. J., Foulkes, S., Charlett, A., Atti, A., Monk, E. J. M., Simmons, R., et al. (2021). SARS-CoV-2 infection rates of antibody-positive compared with antibody-negative health-care workers in England: A large, multicentre, prospective cohort study (SIREN). *Lancet* 397 (10283), 1459–1469. doi: 10.1016/S0140-6736(21)00675-9

Hicks, J., Klumpp-Thomas, C., Kalish, H., Shunmugavel, A., Mehalko, J., Denson, J. P., et al. (2021). Serologic cross-reactivity of SARS-CoV-2 with endemic and seasonal betacoronaviruses. *J. Clin. Immunol.* 41 (5), 906–913. doi: 10.1007/s10875-021-00997-6

Hu, C., Li, D., Liu, Z., Ren, L., Su, J., Zhu, M., et al. (2022). Exploring rapid and effective screening methods for anti-SARS-CoV-2 neutralizing antibodies in COVID-19 convalescent patients and longitudinal vaccinated populations. *Pathogens* 11 (2), 171. doi: 10.3390/pathogens11020171

James, J., and Campanella*, (2003). LBaJS MatGAT: An application that generates similarity/identity matrices using protein or DNA sequences. *BMC Bioinf.* 4, 29. doi: 10.1186/1471-2105-4-29.

Jeewandara, C., Aberathna, I. S., Pushpakumara, P. D., Kamaladasa, A., Guruge, D., Jayathilaka, D., et al. (2021). Antibody and T cell responses to Sinopharm/BBIBP-CorV in naïve and previously infected individuals in Sri Lanka. *medRxiv*. doi: 10.1101/2021.07.15.21260621

Jin, X., Lian, J. S., Hu, J. H., Gao, J. B., Zheng, L., Zhang, Y. M., et al. (2020). Epidemiological, clinical and virological characteristics of 74 cases of coronavirus-infected disease 2019 (COVID-19) with gastrointestinal symptoms. *Gut* 69 (6), 1002–1009. doi: 10.1136/gutjnl-2020-320926

Khoury, D. S., Cromer, D., Reynaldi, A., Schlub, T. E., Wheatley, A. K., Juno, J. A., et al. (2021). Neutralizing antibody levels are highly predictive of immune protection from symptomatic SARS-CoV-2 infection. *Nat. Med.* 27 (7), 1205–1211. doi: 10.1038/s41591-021-01377-8

Kundu, R., Narean, J. S., Wang, L., Fenn, J., Pillay, T., Fernandez, N. D., et al. (2022). Cross-reactive memory T cells associate with protection against SARS-CoV-2 infection in COVID-19 contacts. *Nat. Commun.* 13 (1), 80. doi: 10.1038/s41467-021-27674-x

Li, J., Hou, L., Guo, X., Jin, P., Wu, S., Zhu, J., et al. (2022). Heterologous AD5-nCOV plus CoronaVac versus homologous CoronaVac vaccination: A randomized phase 4 trial. *Nat. Med.* 28 (2), 401–409. doi: 10.1038/s41591-021-01677-z

Loyal, L., Braun, J., Henze, L., Kruse, B., Dingeldey, M., Reimer, U., et al. (2021). Cross-reactive CD4(+) T cells enhance SARS-CoV-2 immune responses upon infection and vaccination. *Science* 374 (6564), eabh1823. doi: 10.1126/science.abh1823

Majdoubi, A., Michalski, C., O'Connell, S. E., Dada, S., Narpala, S., Gelinas, J., et al. (2021). A majority of uninfected adults show preexisting antibody reactivity against SARS-CoV-2. *JCI Insight* 6 (8), e146316. doi: 10.1172/jci.insight.146316

Muik, A., Lui, B. G., Wallisch, A. K., Bacher, M., Muhl, J., Reinholz, J., et al. (2022). Neutralization of SARS-CoV-2 omicron by BNT162b2 mRNA vaccine-elicited human sera. *Science* 375 (6581), 678–680.doi: 10.1126/science.abn7591

Ortega, N., Ribes, M., Vidal, M., Rubio, R., Aguilar, R., Williams, S., et al. (2021). Seven-month kinetics of SARS-CoV-2 antibodies and role of pre-existing antibodies to human coronaviruses. *Nat. Commun.* 12 (1), 4740. doi: 10.1038/s41467-021-24979-9

Severance, E. G., Bossis, I., Dickerson, F. B., Stallings, C. R., Origoni, A. E., Sullens, A., et al. (2008). Development of a nucleocapsid-based human coronavirus immunoassay and estimates of individuals exposed to coronavirus in a U.S. metropolitan population. *Clin. Vaccine Immunol. CVI* 15 (12), 1805–1810. doi: 10.1128/CVI.00124-08

Shrwani, K., Sharma, R., Krishnan, M., Jones, T., Mayora-Neto, M., Cantoni, D., et al. (2021). Detection of serum cross-reactive antibodies and memory response to SARS-CoV-2 in prepandemic and post-COVID-19 convalescent samples. *J. Infect. Dis.* 224 (8), 1305–1315. doi: 10.1093/infdis/jiab333

Su, S., Wong, G., Shi, W., Liu, J., Lai, A. C. K., Zhou, J., et al. (2016). Epidemiology, genetic recombination, and pathogenesis of coronaviruses. *Trends Microbiol.* 24 (6), 490–502. doi: 10.1016/j.tim.2016.03.003

Tso, F. Y., Lidenge, S. J., Pena, P. B., Clegg, A. A., Ngowi, J. R., Mwaiselage, J., et al. (2021). High prevalence of pre-existing serological cross-reactivity against severe acute respiratory syndrome coronavirus-2 (SARS-CoV-2) in sub-Saharan Africa. *Int. J. Infect. dis: IJID* 102, 577–583. doi: 10.1016/j.ijid.2020.10.104

XiaoYan Che, L. Q., Liao, Z., Wang, Y., Wen, K., Pan, Y., Hao, W., et al. (2005). Antigenic cross-reactivity between severe acute respiratory syndrome-associated coronavirus and human coronaviruses 229E and OC43. *J. Infect. Dis* 191 (12), 2033–2037. doi: 10.1086/430355

Xia, S., Yan, L., Xu, W., Agrawal, A. S., Algaissi, A., Tseng, C. K., et al. (2019). A pan-coronavirus fusion inhibitor targeting the HR1 domain of human coronavirus spike. *Sci. Adv.* 5 (4), eaav4580.doi: 10.1126/sciadv.aav4580

Zhou, D., Dejnirattisai, W., Supasa, P., Liu, C., Mentzer, A. J., Ginn, H. M., et al. (2021). Evidence of escape of SARS-CoV-2 variant B.1.351 from natural and vaccine-induced sera. *Cell* 184 (9), 2348-2361. e6 doi: 10.1016/j.cell.2021.02.037

frontiers | Frontiers in Cellular and Infection Microbiology

TYPE Review
PUBLISHED 20 September 2022
DOI 10.3389/fcimb.2022.963239

OPEN ACCESS

EDITED BY
Yu Chen,
Wuhan University, China

REVIEWED BY
Salvatore Caradonna,
Rowan University School of Osteopathic Medicine, United States
Ye Qiu,
Hunan University, China

*CORRESPONDENCE
Wen-Hao Zhou
zhouwenhao@fudan.edu.cn

SPECIALTY SECTION
This article was submitted to Virus and Host, a section of the journal Frontiers in Cellular and Infection Microbiology

RECEIVED 07 June 2022
ACCEPTED 30 August 2022
PUBLISHED 20 September 2022

CITATION
Ji X-S, Chen B, Ze B and Zhou W-H (2022) Human genetic basis of severe or critical illness in COVID-19. *Front. Cell. Infect. Microbiol.* 12:963239. doi: 10.3389/fcimb.2022.963239

Human genetic basis of severe or critical illness in COVID-19

Xiao-Shan Ji[1,2], Bin Chen[1,2], Bi Ze[1,2] and Wen-Hao Zhou[1,2]*

[1]Department of Neonatology, Children's Hospital of Fudan University, National Children's Medical Center, Shanghai, China, [2]Key Laboratory of Birth Defects, Children's Hospital of Fudan University, National Children's Medical Center, Shanghai, China

Coronavirus Disease 2019 (COVID-19) caused by the novel severe acute respiratory syndrome coronavirus 2 (SARS-CoV-2) has led to considerable morbidity and mortality worldwide. The clinical manifestation of COVID-19 ranges from asymptomatic or mild infection to severe or critical illness, such as respiratory failure, multi-organ dysfunction or even death. Large-scale genetic association studies have indicated that genetic variations affecting SARS-CoV-2 receptors (angiotensin-converting enzymes, transmembrane serine protease-2) and immune components (Interferons, Interleukins, Toll-like receptors and Human leukocyte antigen) are critical host determinants related to the severity of COVID-19. Genetic background, such as 3p21.31 and 9q34.2 loci were also identified to influence outcomes of COVID-19. In this review, we aimed to summarize the current literature focusing on human genetic factors that may contribute to the observed diversified severity of COVID-19. Enhanced understanding of host genetic factors and viral interactions of SARS-CoV-2 could provide scientific bases for personalized preventive measures and precision medicine strategies.

KEYWORDS

COVID-19, disease severity, critical illness, genetic, SARS-CoV-2

1 Introduction

Coronavirus Disease 2019 (COVID-19) was caused by the novel severe acute respiratory syndrome coronavirus 2 (SARS-CoV-2). Since the first case reported in December 2019, it has been spreading worldwide and was announced a global pandemic in March 2020 (Taylor, 2022). COVID-19 presents a wide spectrum of manifestations, ranging from asymptomatic infection to critical clinical course (Figure 1). Though most cases are now known to be asymptomatic or mild, approximately 15% of infected patients developed severe disease and 5% progressed to critical status, leading to deleterious acute respiratory distress syndrome (ARDS), multi-organ dysfunction and death (Baj et al., 2020; Zhou et al., 2020).

Several risk factors that could predict the severity of disease have been identified, including age, male gender, smoking, underlying comorbidities such as hypertension,

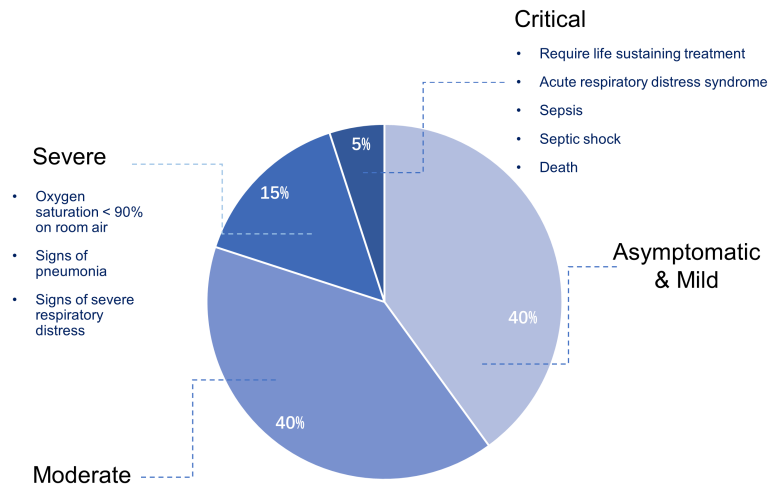

FIGURE 1
Overview of clinical characteristics of COVID-19.

diabetes mellitus, cardiac disease, chronic lung disease and cancer, clinically apparent immunodeficiencies, local immunodeficiencies and pregnancy (Williamson et al., 2020; Grasselli et al., 2021). Nevertheless, these conditions do not fully explain the variability in COVID-19 disease severity between individuals, and severe cases were observed in young individuals without pre-existing medical conditions, sometimes clustering in families, suggesting genetic background might be a risk factor (Yousefzadegan and Rezaei, 2020).

Several gene variants of infected patients were reported to explain the different levels of severity among individuals and their outcomes, which may provide a better understanding of host protein-SARS-CoV-2 interactions. Also, it sheds light on stratifying individuals according to risk, thus allowing for the prior protection of those at greater risk, and ideally, for innovative personalized treatments. To this end, we conduct a review on current studies focusing on associations between human genetic factors and the level of severity of COVID-19.

2 SARS-CoV-2 recognition and immune responses

There are two distinct biological steps relevant to the severe presentation of COVID-19: viral recognition and immune responses (Figure 2). First, the spike protein (S) on SARS-CoV-2 binds to the host ACE2 (Angiotensin-2 Conversion Enzyme) receptor (Dong et al., 2020). Following the receptor binding, Transmembrane and Serine Protease 2 (TMPRSS2) will trigger a proteolytic cleavage of the S domains to mediate membrane fusion (Hoffmann et al., 2020). Paired basic amino acid-cleaving enzyme (Furin) can also catalyze S protein proteolytic cleavage.

After the virus entering a target cell, the innate immune response is initiated with the recognition of SARS-CoV-2 by pattern recognition receptors such as Toll-like receptors (TLRs) 3, 7, 8 and 9. The TLR3 response triggers the activation of NOD-Like Receptor family and Pyrin domain-containing 3 protein (NLRP3) inflammasome pathway, which induces caspase-1-dependent cleavage and secretion of key proinflammatory cytokines interleukin-1β (IL-1β) and IL-18 (Brodin, 2021), inducing inflammation and coagulopathy (Hosseini et al., 2020). In adaptive immunity, T cells recognize a bimolecular complex of an epitope bound to the Major Histocompatibility Complex (MHC) class I and II. CD4+ T cells play a critical antiviral role through promoting the secretion of pathogen-specific antibodies, whereas CD8+ T cells reduce the viral burden by killing the infected cells. It has been reported that T cells in critical patients seemed to be more active (Maamari et al., 2022). SARS-CoV-2 also triggers a robust B cell response, as IgM, IgG, IgA and neutralizing IgG antibodies can be detected in a few days after infection (Grifoni et al., 2021).

Commonly, the proinflammatory cytokines activate immune cells, notably monocytes and T lymphocytes, which clean the lung infection and help the patient recover. However, in serious cases, uncontrolled systemic hyper-inflammation, called “cytokine storm”, may occur (Kim et al., 2021). Though the pathogenesis of cytokine storm is not yet elucidated, two stages of the cytokine storm has been considered: the first stage is a temporary immune-deficient condition in which early responses of type I Interferon (IFN) are impaired; the secondary stage is an overactive immune state to compensate

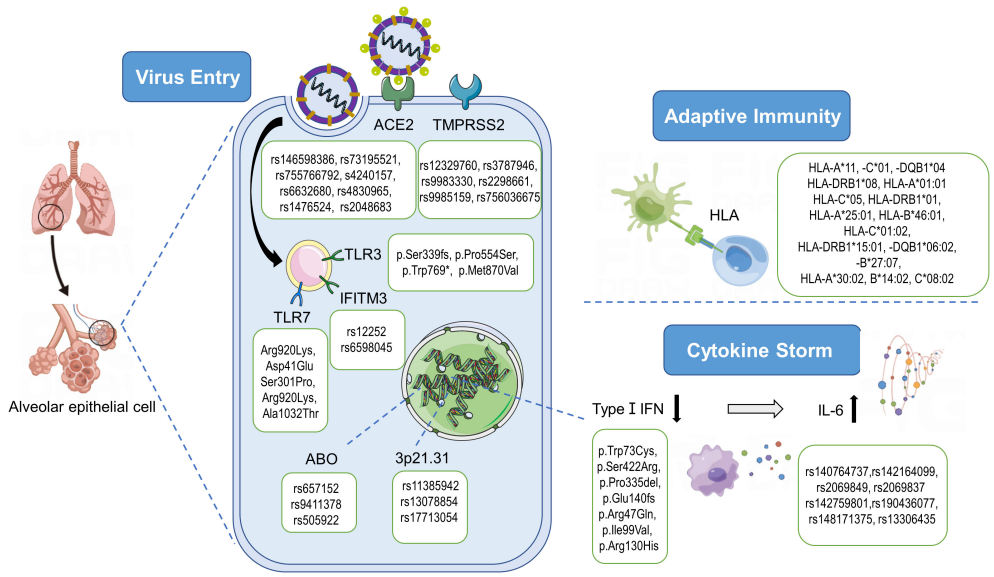

FIGURE 2
Pathogenesis of SARS-CoV-2 and genetic variants associated with severe COVID-19. After the recognition of ACE2 and the priming by TMPRSS2, SARS-CoV-2 enters the cell and starts the replication process. The innate immune response signaling cascade starts with the recognition of pathogen-associated molecular patterns (PAMPs) by endosomal toll-like receptors (TLRs). SARS-CoV-2 is able to inhibit the type I IFN responses in infected cells, leading to the cytokine storm characterized by an increase of inflammatory cytokines/chemokines such as IL-6. As an antiviral mechanism, antigen-presenting cells present antigenic peptides through the Major Histocompatibility Complex (MHC) class I and class II molecules to T cells. And 3p21.31 and ABO loci are significantly associated with Covid-19 severity. ACE2, angiotensin-converting enzyme-2; TMPRSS2, transmembrane serine protease-2; HLA, human leukocyte antigen; IFN, interferon; TLR, Toll-like receptor 7; IFITM3, interferon induced transmembrane protein 3; IL, Interleukin. By Figdraw (www.figdraw.com).

for the failure of target clearance (Blanco-Melo et al., 2020; McGonagle et al., 2020). A key feature of SARS-CoV-2 is its capability to shut down hosts' IFN production, leading to a delayed or even overall suppressed type I IFN response (Zhang et al., 2021). An immune analysis performed in critical COVID-19 patients showed a low level of IFN activity and downregulation of IFN stimulated genes. On the contrary, cytokine and chemokine-related genes such as IL-6 and TNF-α were found to be increasingly expressed (Hadjadj et al., 2020). Taken together, hyper-inflammatory responses followed by impaired IFN signaling pathway are likely to determine the severity of COVID-19.

3 Genetic variations associated with severity of COVID-19

Considering the pathogenesis of COVID-19, the gene variants described for disease severity were classified whether they were related to host entry mechanism, immune system or other genes associated with severity of COVID-19. Gene variants that show protective or risk factors on the severity of COVID-19 are summarized in Table 1.

3.1 Genetic variations of human receptors

3.1.1 ACE2

ACE2 is widely expressed in human tissues, especially in upper and lower respiratory tracts, heart, kidney, testis and gastrointestinal system (Bourgonje et al., 2020). Apart from the main receptor for SARS-CoV-2, ACE2 is also well-known for its downregulating the renin-angiotensin system (RAS), which is important for modulating the cardiovascular system (Bakhshandeh et al., 2021). However, the function of ACE2 is lost following the binding of virus, which may cause inflammation, thrombosis and death.

The expression level of ACE2 receptor, which differs among individuals across different ages, genders and ethnicities, potentially affects the severity of COVID-19. Based on the latest genome-wide association summary statistics for severe COVID-19, a recent study indicated an increased risk of severe COVID-19 for individuals who had genetically raised levels of circulating ACE2 protein (Yang et al., 2022). They also found that the variant rs4830984 was nominally significantly associated with severe COVID-19. A retrospective examination of nasal epithelium among people of different ages showed that

TABLE 1 Summary of genetic variations associated with COVID-19 severity.

Location	Gene(s)	Polymorphism(s)		Population	Ref.
		Risk	Protective		
Xp22.2	ACE2	rs146598386, rs73195521, rs755766792		Russian	(Shikov et al., 2020)
		s4240157, rs6632680, rs4830965, rs1476524, rs2048683		Caucasian	(Wooster et al., 2020)
		rs4830984		Worldwide	(Yang et al., 2022)
		rs2285666		Iranian	(Khalilzadeh et al., 2022)
			rs190509934	American	(Horowitz et al., 2022)
21p22.3	TMPRSS2	rs12329760 (p.Val160Met)		Italian	(Asselta et al., 2020)
		rs3787946, rs9983330, rs2298661, rs9985159	rs12329760 (p.V197M)	European	(Andolfo et al., 2021)
		rs756036675		Spanish	(Villapalos-Garcia et al., 2022)
			rs12329760 (p.V197M), rs2298659 (p.G296G)	Italian	(Monticelli et al., 2021)
		rs17854725, rs12329760, and rs4303795		Iranian	(Rokni et al., 2022)
21q22.1	IFNAR1	p.Trp73Cys, p.Ser422Arg, p.Pro335del		Chinese, Italian	(Zhang et al., 2020a)
	IFNAR2	p.Glu140fs		Belgian	(Zhang et al., 2020a)
		rs2236757		European	(Pairo-Castineira et al., 2021)
		Tyr322Ter		Asian	(Smieszek et al., 2021a)
		p.Ser53Pro		Canadian	(Duncan et al., 2022)
11p5.5	IFITM3	rs12252		Chinese, Saudi Arabian	(Zhang et al., 2020c)
		rs6598045		worldwide	(Kim and Jeong, 2021)
		rs12252 and rs34481144		British	(Nikoloudis et al., 2020)
12q24.13	OAS1	p.Arg47Gln, p.Ile99Val and p.Arg130His		Serbian	(Klaassen et al., 2020)
			rs10774671	Peruvian, Esan	(Wickenhagen et al., 2021)
		rs10735079		European	(Pairo-Castineira et al., 2021)
		rs1131454, rs4766676		British	(Magusali et al., 2021)
7p15.3	IL6		rs140764737, rs142164099, rs2069849, rs142759801, rs190436077, rs148171375, rs13306435	Italian	(Strafella et al., 2020)
			rs2069837	Chinese	(Gong et al., 2022)
			rs1800796, rs1524107, rs2066992	Chinese	(Chen et al., 2021)
1q21.3	IL6R		rs2228144, rs2229237, rs2228145, rs28730735, rs143810642	Italian	(Strafella et al., 2020)
		rs2228145		American	(Smieszek et al., 2021b)
20q13.13	TMEM189-UBE2V1	rs6020298		Chinese	(Wang et al., 2020)

(Continued)

TABLE 1 Continued

Location	Gene(s)	Polymorphism(s)		Population	Ref.
		Risk	Protective		
Xp22.2	TLR7	Arg920Lys, Asp41Glu		Italian	(Mantovani et al., 2022)
		c.2129_2132del; p.Gln710Argfs*18; c.2383G>T; p.Val795Phe		Dutch	(van der Made et al., 2020)
		Ser301Pro, Arg920Lys, Ala1032Thr		Italian	(Fallerini et al., 2021)
4q35.1	TLR3	p.Ser339fs, p.Pro554Ser, p.Trp769*, p.Met870Val		Italian, Spanish	(Zhang et al., 2020a)
6p21.3	HLA	HLA-A*11, -C*01, and -DQB1*04	HLA-A*32	Spanish	(Lorente et al., 2021)
		HLA-DRB1*08		Italian	(Amoroso et al., 2021)
		HLA-C*05		74 countries	(Sakuraba et al., 2020)
		HLA-A*01:01g, HLA-B*08:01g and HLA-DRB1*03:01g	HLA-B*18:01, HLA-C*07:01 and HLA-DRB1*11:04	Italian	(Pisanti et al., 2020)
		HLA-A*25:01, HLA-B*46:01, and HLA-C*01:02	HLA-B*15:03	American	(Nguyen et al., 2020)
		HLA-A*11:01, -B*51:01, and -C*14:02		Chinese	(Wang et al., 2020)
		HLA-DRB1*15:01, -DQB1*06:02, and -B*27:07		Italian	(Novelli et al., 2020)
		HLA-A*30:02, B*14:02 and C*08:02	HLA-A*02:05-B*58:01-DRB1*08:01 and HLA-A*02:05-B*58:01-C*07:01	Sardinian	(Littera et al., 2020)
		HLA-A*01:01	HLA-A*02:01 and HLA-A*03:01	Russian	(Shkurnikov et al., 2021)
3p21.31	SLC6A20, LZTFL1, CCR9, FYCO1, CXCR6 and XCR1	rs11385942		Italian, Spanish	(Ellinghaus et al., 2020)
		rs13078854		American, British	(Shelton et al., 2021)
		rs17713054		British	(Downes et al., 2021)
9q34.2	ABO	rs657152		Italian, Spanish	(Ellinghaus et al., 2020)
		rs9411378		American, British	(Shelton et al., 2021)
12q24.33	GOLGA3	rs143359233		Chinese	(Wang et al., 2020)
19p13.3	DPP9	rs2109069		European	(Pairo-Castineira et al., 2021)
19p13.2	TYK2	rs11085727		European	(Pairo-Castineira et al., 2021)
2q24.2	IFIH1	rs1990760		Spanish	(Amado-Rodriguez et al., 2022)

*The separator used to separate gene names from alleles groups in the naming of HLA allele.

expression level of *ACE2* gene was low in younger children but increased with age (Bunyavanich et al., 2020), which may explain why children have fewer and less severe symptoms compared with adults (Patel and Verma, 2020). In addition, compared with women, men are 65% more likely to develop severe complications or even die from COVID-19. This gender difference could be explained by the well-established role of androgen receptor signaling in modulating *ACE2* transcription, as well as its location on X chromosome (Samuel et al., 2020). Also, the *ACE2* gene expression varies among ethnic populations. A recent study based on expression quantitative trait locus (eQTL) found that people from an Arab background had lower levels of ACE2 compared with Europeans, possibly led to lower mortality in this population (Al-Mulla et al., 2020).

Genetic variations in *ACE2* may affect its binding with SARS-CoV-2 and the subsequent infection severity. Several missense changes, such as p.(Asn720Asp), p.(Lys26Arg), and p.(Gly211Arg), can affect the protein structure and stabilization, and therefore influence the internalization process of the virus (Benetti et al., 2020). Some other variants, such as rs961360700, are known to cause an increase in affinity for S protein (MacGowan et al., 2022; Ren et al., 2022). Accumulating evidence suggests that polymorphisms in *ACE2* gene may modulate inflammatory responses and thus may aggravate pulmonary and systemic injuries (Li et al., 2020). In a cohort of Russian COVID-19 patients, several rare *ACE2* variants (including rs146598386, rs73195521, and rs755766792) tended to cause an active inflammatory response to infection, which partially explained the variation of disease severity (Shikov et al., 2020). In another study, six variants (re4240157, rs6632680, rs1548474, rs4820965, rs1476524 and rs2048683) out of 61 evaluated ones were identified to be markedly associated with hospitalization (Wooster et al., 2020). A recent genome-wide association study (GWAS) identified a rare variant, rs190509934, that downregulated *ACE2* expression and reduced disease severity among COVID-19 patients (Horowitz et al., 2022).

Nevertheless, the relationship between *ACE2* polymorphism and COVID-19 severity remain controversial. A negative correlation between ACE2 expression and COVID-19 fatality at both population and molecular levels was reported (Chen et al., 2020; El Baba and Herbein, 2020). In addition, *ACE2* genetic variants were analyzed by whole-exome sequencing (WES) in 137 DNA samples of COVID-19 patients, compared with the 536 age-matched controls. They found that *ACE2* polymorphism was not associated with an increased risk of critical illness (Gomez et al., 2020). However, they indicated that the balance between ACE1 and ACE2 played a role in the severity of COVID-19. Another study also revealed a strong correlation between *ACE1* insertion/deletion (I/D) genotype with COVID-19 mortalities (Yamamoto et al., 2020). Larger cohort of severe/critical patients and further functional studies are required to reveal the role of *ACE2* genotypes in COVID-19.

3.1.2 TMPRSS2

The *TMPRSS2* gene, located on the human chromosome 21q22.3, encodes a serine protease enzyme that primes the S protein of SARS-CoV-2, allowing fusion of viral and cellular membrane (Baughn et al., 2020). *TMPRSS2* is a key gene in prostate cancer and its transcription is regulated by androgen. Thus, TMPRSS2 expression and enzymatic activity was detected significantly higher in males than in females, which may explain the male predominance of higher severity and mortality (Alshahawey et al., 2020; Okwan-Duodu et al., 2021). Also, TMPRSS2 expression increases with aging in mice and humans, and this may relatively protect children from severe illness (Rossi et al., 2021; Schuler et al., 2021). The localization of the gene on 21q22.3 place Down syndrome individuals at high risk for critical illness (De Toma and Dierssen, 2021), and its oncogenic role may be related to poor outcomes of cancer patients with COVID-19 as well (Stopsack et al., 2020).

Seven variants (rs3787946, rs9983330, rs12329760, rs2298659, rs2298661, rs9985159 and rs756036675) within *TMPRSS2* were identified to be associated with severe COVID-19 (Andolfo et al., 2021; Monticelli et al., 2021; Villapalos-Garcia et al., 2022). Among them, rs12329760 (p.Val197Met) emerged as a common variant that weakened TMPRSS2 protein stability and inhibited the binding of S protein and ACE2 (Wang et al., 2020). It played a protective role and appeared less in critical patients than in mild and general cases (Wang et al., 2020; Monticelli et al., 2021; David et al., 2022). However, rs12329760 (p.Val160Met) and 2 distinct haplotypes trigger higher TMPRSS2 expression may explain the significantly higher severity and mortality rates in Italy than those in East Asia (Asselta et al., 2020). It was suggested that more genotyping studies of COVID-19 was needed to explore the contribution of *TMPRSS2* variants to clinical outcomes (Stopsack et al., 2020).

3.2 Genetic variations of immunity components

3.2.1 Interferons

Interferons (IFNs) are a family of specialized cytokines central to antiviral immunity. Viral recognition induces IFN production, which in turn triggers the transcription of IFN-stimulated genes (ISGs), mediating antiviral responses (Yang et al., 2021). Specifically, type I IFNs are the first line of defense against viral infections, and IFN-I signaling is required for the recruitment of pro-inflammatory cells in the lung (Ramasamy and Subbian, 2021). It was reported that inborn errors of type I IFNs were the genetic and immunological basis of at least 15% of cases of critical COVID-19 pneumonia (Hadjadj et al., 2020).

IFN-I signaling is initiated by the binding of IFN-I to the interferon receptor (IFNAR) complex, composed of IFNAR1 and IFNAR2 at the same proximal location (Schreiber, 2020). *IFNAR1* (p.Trp73Cys, p.Ser422Arg, p.Pro335del) and *IFNAR2* (p.Glu140fs) variants were identified in patients with life-threatening COVID-19, highlighting the importance of type I IFN production in severe disease (Zhang et al., 2020a). A GWAS also reported that an intron variant rs2236757 in the *IFNAR2* gene increased the odds of severe COVID-19 (Pairo-Castineira et al., 2021). Loss-of-function mutations in *IFNAR2* including Tyr322Ter may increase susceptibility to critical COVID-19 infection, especially Asian descent populations, where this variant is more prevalent (Smieszek et al., 2021a).

The interferon-induced transmembrane proteins (IFITM) are a group of proteins localized in the plasma and endolysosomal membranes, preventing viruses from traversing the cellular lipid bilayer (Shaath et al., 2020). Homozygosity for

the C allele of rs12252 within the *IFITM3* gene was associated with the severity of COVID-19 (Zhang et al., 2020c). Rs34481144, another polymorphism of *IFITM3*, was reported to be associated with increased severity in influenza. It has been reported that the combined haplotypes of rs12252 and rs34481144 implicated in more severe outcomes of COVID-19 (Nikoloudis et al., 2020). However, a meta-analysis indicated that rs34481144 was not correlated to COVID-19 severity (Li et al., 2022).

2′-5′-Oligoadenylate synthase (OAS) family genes are induced by IFNs at the early phase of viral infection. Once in the right place, OAS1 binds to dsRNA structures of the SARS-CoV-2, leading to the viral RNA degradation and inhibition of viral replication (Wickenhagen et al., 2021). A common polymorphism in *OAS1* (rs10774671), where the protective allele resulted in a more active *OAS1* enzyme, probably led to less severe COVID-19 (Wickenhagen et al., 2021). On the contrary, decreased expression levels of *OAS1* was implicated in COVID-19 disease severity (D'Antonio et al., 2021). Three variants (p.Arg47Gln, p.Ile99Val and p.Arg130His) were detected to impair OAS1 activity and weaken its bond with RNA (Klaassen et al., 2020). Also, a recent GWAS suggested that the variant rs10735079 was associated with critical illnesses in COVID-19 (Pairo-Castineira et al., 2021). In addition, *OAS1* was identified as a putative new risk gene for Alzheimer's disease, and 4 alleles within *OAS1* gene were identified to contribute to both the high incidence of Alzheimer's disease and critical illness of COVID-19 (Magusali et al., 2021).

3.2.2 Interleukin

As mentioned above, cytokine storm plays a critical role in severe COVID-19 cases, in which increased levels of cytokines are observed in plasma blood. Interleukin 6 (IL-6) is a soluble mediator in response to infections and tissue injuries (Tanaka et al., 2014). In COVID-19, critically ill patients showed significantly higher levels of IL-6, indicating that IL-6 was a strong predictor for disease severity and survival possibility (Zhang et al., 2020b). The association of *IL-6* polymorphisms with cytokine expression and disease severity have been reported. Seven variants in *IL-6* (rs140764737, rs142164099, rs2069849, rs142759801, rs190436077, rs148171375, rs13306435) and five variants in *IL-6R* (rs2228144, rs2229237, rs2228145, rs28730735, rs143810642) appeared to alter the binding of IL-6 and IL-6R, which can be implicated in the pathogenetic mechanisms associated with COVID-19 severity and its complications (Strafella et al., 2020). A recent GWAS found that the genetic variant rs2069837 in *IL-6* decreased the expression of IL-6 in the serum and was protective against critical COVID-19 (Gong et al., 2022). An Asian-common *IL-6* haplotype defined by promoter SNP rs1800796 and intronic SNPs rs1524107 and rs2066992 was detected to be associated with a lower risk of severe symptoms. Mechanistically, the protective allele disrupted the CTCF-binding locus at the *IL-6* intron and resulted in attenuated IL-6 induction in response to viral infection (Chen et al., 2021). On the contrary, the minor allele rs2228145 was associated with higher plasma IL-6 levels in severe COVID-19 patients (Smieszek et al., 2021b).

Beyond IL-6, IL-1 is also a highly active proinflammatory cytokine. A Chinese cohort investigated 22.2 million genetic variants among 332 COVID-19 patients, rs6020298 within *TMEM189-UBE2V1*, a component of IL-1 signaling pathway, was found to be the most significant SNP associated with severity (Wang et al., 2020).

3.2.3 Toll-like receptors

TLRs are a family comprised of 11 transmembrane proteins, which are crucial components in the initiation of innate immune responses (Szeto et al., 2021). TLRs recognize pathogen-associated molecular patterns and trigger the production of pro-inflammatory cytokines as well as type I and II interferons system. TLR3 is the most widely expressed TLR that binds to double-stranded RNA viruses, while TLR7 and TLR8 recognize single-stranded RNA viruses (Mantovani et al., 2022). Inborn errors of TLR3-dependent type I IFN immunity have been found in life-threatening COVID-19 patients, and eight genetic loci have been identified (Zhang et al., 2020a). The polymorphism L412 in *TLR3* inhibited autophagy and made males at risk of severe COVID-19 (Croci et al., 2021). X-linked TLR7 deficiency has been identified as a novel immunodeficiency with an increased susceptibility to severe or critical COVID-19 infection and TLR7 has been established as a critical mediator of IFN-I immunity against the virus (Solanich et al., 2021). The burden of rare variants in *TLR7* was found to be significantly higher in patients with severe COVID-19 in pan-ancestry WES data from the UK biobank (Kosmicki et al., 2021). A recent study identified loss-of-function variants of *TLR7* (c.2129_2132del; p.Gln710Argfs*18; c.2383G>T; p.Val795Phe) in four severely affected young men from two unrelated families and among them found a lower production of IFNα and IFNγ proteins following stimulation (van der Made et al., 2020). Moreover, a nested case–control study identified *TLR7* loss-of-function variants in 2.1% of severely affected males but in none of the asymptomatic participants (Fallerini et al., 2021).

Since the production of IFN is mediated *via* the TLR7 signaling pathway, therapies that directly stimulate endogenous TLR7 could have potential therapeutic benefit for the prevention and treatment of severe COVID-19 infection (Szeto et al., 2021). In addition, genetic variations in *TLR7* that located on the X chromosome, may be a possible explanation of the sex biases in COVID-19 severity. Among women, *TLR7* may escape X-inactivation, leading to higher basal expression levels and elevated downstream IFN responses (van der Made et al., 2020).

3.2.4 Human leukocyte antigen

The Human Leukocyte Antigen (HLA) system, containing nearly 27,000 alleles in three distinct classes of genes (Class I, II and III), is the most highly polymorphic region in the human genome. HLA Classes I and II present antigenic peptides to T lymphocytes and enable the immune system to discriminate between self and foreign proteins (Lorente et al., 2021). In patients of COVID-19, different adaptive immune responses have been observed according to disease severity, including distinct IgM levels and S protein IgG titers (Ovsyannikova et al., 2020). As HLA plays a critical role in antigen presentation, different polymorphisms may potentially alter the severity of the disease.

Specific risk and protective *HLA* alleles for COVID-19 severity and mortality have been detected in several studies. A study evaluated the HLA binding affinity of all possible 8-mers to 12-mers from the SARS-CoV-2 proteome and noted three peptide-presenters (*HLA-A*25:01*, *B*46:01*, and *C*01:02*) that were most likely associated with severe infection (Nguyen et al., 2020). Another peptide binding prediction analyses showed that *HLA-DRB1*08* alleles were unable to bind any of the viral peptides with high affinity, thus individuals with those alleles were at high risk of severe COVID-19 (Amoroso et al., 2021). Several studies concluded that *HLA-A*11:01, HLA-B*51:01, HLA-C*14:02, HLA-DQB1*06:02* and *HLA-B*27:0* were correlated with a higher COVID-19 mortality (Novelli et al., 2020; Wang et al., 2020; Shkurnikov et al., 2021). In contrast, *HLA-A*02:01, HLA-A*03:01, HLA-B*18:01, HLA-C*07:01* and *HLA-DRB1*11:04* showed an inverse relationship to the number of deaths (Novelli et al., 2020; Wang et al., 2020; Shkurnikov et al., 2021). *HLA-A*11* was detected to predispose worse outcome of COVID-19 patients (Lorente et al., 2021), while another study suggested that *HLA-A*11:01* could generate efficient antiviral responses (Tomita et al., 2020).

Considering the high gene density of *HLA* locus, it was suggested that complete HLA genotypes for each individual, rather than most frequent alleles, should be analyzed (Deng et al., 2021). Based on the allele frequency data of *HLA* in 74 countries, *HLA-C*05* was identified as the most influential allele in increasing the mortality of COVID-19. Its receptor KIR2DS4fl is expressed on natural killer (NK) cells and recognizes viral peptides bound to HLA-C*05. It was hypothesized that this HLA-KIR pair induced immune hyperactivation and caused poor outcome (Sakuraba et al., 2020). An Italian study found that haplotype *HLAA*01:01, HLA-B*08:01* and *HLA-DRB1*03:01* contributed to the higher COVID-19 mortality in northern Italy. In contrast, *HLA-B*18:01, HLA-C*07:01* and *HLA-DRB1*11:04* directly correlated with the lower mortality in southern Italy (Pisanti et al., 2020).

Nevertheless, a study based on data from 6,919 infected individuals found that HLA genotypes as well as viral T-cell epitopes were not correlated with COVID-19 severity (Schetelig et al., 2021). More uniformly designed studies with the inclusion of global data are needed to clarify the role of single *HLA* alleles in COVID-19 severity. Furthermore, as COVID-19 may have variable potential epitopes with HLA complex, predicting good binds across *HLA* alleles may contribute to the design of an efficacious vaccine against COVID-19 (Prachar et al., 2020).

3.3 Other genetic variations

Apart from genes relevant to immune and SARS-CoV-2 receptors, other genetic variations have also been identified related to the severity of COVID-19. The association of loci 3p21.31 and 9q34.2 with COVID-19 severity were identified in two independent GWAS. The first study conducted in Italy and Spain revealed that rs11385942 at locus 3p21.31 and rs657152 at locus 9q34.2 were significantly associated with severe COVID-19 with respiratory failure (Ellinghaus et al., 2020). And the second study found that rs13078854 at locus 3p21.31 and rs9411378 at locus 9q34.2 were risk alleles for severe COVID-19 phenotypes (Shelton et al., 2021). At locus 3p21.31, the association signal compromised 6 genes (*SLC6A20, LZTFL1, CCR9, FYCO1, CXCR6* and *XCR1*). Among them, *SLC6A20* encodes a transporter that functionally interacts with ACE2 receptor. *CXCR6* and *CCR9* encode chemokine receptors that are implicated in T cell differentiation and recruitment. *LZTFL1* encodes a cytosolic leucine-zipper protein widely expressed in pulmonary epithelial cells and regulates epithelial-mesenchymal transition (EMT), a viral response pathway (Downes et al., 2021). Recent studies found that rs35081325 and rs1024611 in *LZTFL1*, appeared to strongly associated with increased infection severity (Roberts et al., 2022; Ruter et al., 2022). And a study integrating expression quantitative trait locus (eQTL) mapping identified *SLC6A20* and *CXCR6* as causal genes that modulate COVID-19 risk (Kasela et al., 2021). However, another study identified *CCR9* and *SLC6A20* as potential target genes (Yao et al., 2021). As they all have a potentially relevant role in the pathophysiology of COVID-19, further studies will be needed to delineate effector genes at the 3p21.31 locus.

The association signal at locus 9q34.2 coincided with *ABO* locus, suggesting the role of ABO blood type in COVID-19 severity. It has been reported that A-group was a significant risk factor for developing a severe form of COVID-19, while O-group was protective against severe COVID19 illness or death (Gomez et al., 2021; Khasayesi et al., 2021). A recent replication analysis of reported COVID-19 genetic associations with eight phenotypes found that the lead *ABO* SNP, rs505922, replicated in all four susceptibility phenotypes and one severity phenotype (Roberts et al., 2022). It is still unclear how ABO blood types affect outcomes of COVID-19. A proteomic profiling analysis showed that the ABO locus mediated the risk by modulating CD209/DC-SIGN, a binding site for SARS-CoV-2 (Katz et al., 2020). Another study hypothesized that ABO blood group

influenced the risk of venous thromboembolism, which is frequent in severe cases, by modifying glycosyltransferase activity (Ibrahim-Kosta et al., 2020).

ApoE is one of the highly co-expressed genes in type II alveolar cells in the lungs, and the *ApoE* e4e4 homozygous genotype was reported to increase the risk of severe COVID-19 (Kuo et al., 2020; Kurki et al., 2021). This may be explained by a regulatory mechanism underlying SARS-CoV-2 infection through ApoE interactions with ACE2 (Zhang et al., 2022).

Pedigree analysis in a Chinese family suggested that loss-of-function variants in *GOLGA3* and *DPP7* implicated in critically ill and asymptomatic COVID-19 patients as a monogenic factor (Wang et al., 2020). A GWAS performed in 2,244 critically ill patients with COVID-19 found significant associations in *DPP9, CCR2* and *TYK2*, all of which could cause inflammatory lung injury (Pairo-Castineira et al., 2021). A recent study found that patients with the TT variant in the *IFIH1* had an attenuated inflammatory response to severe SARS-CoV-2 infection, leading to better outcomes (Amado-Rodriguez et al., 2022).

4 Conclusions and perspectives

In this review, we provided an overview of genetic variants associated with COVID-19 severity. The variants influence at least two distinct biological progress: viral entrance to host cells and development of harmful inflammation. The world is still suffering from the COVID-19 outbreak, with high fatality rate in severe and critical patients. Therefore, identifying genetic markers associated with clinical outcomes of COVID-19 is helpful for classifying and safeguarding individuals at high risk, as well as finding potential therapeutic targets.

Future genetic studies need further sharing of individual-level data, yet ethical considerations such as perfecting genetic information-related legislation should also be considered. Furthermore, large-scale systematic investigations of the functional polymorphisms of these genes combining data among different populations would pave the way for personalized preventive measures and precision medicine strategies.

Author contributions

All the authors listed, have made substantial, direct and intellectual contribution to the work, and approved it for publication. All authors contributed to the article and approved the submitted version.

Funding

This study was funded by the National Key Research and Development Program of China (Nos. 2021YFC2701800).

Conflict of interest

The authors declare that the research was conducted in the absence of any commercial or financial relationships that could be construed as a potential conflict of interest.

Publisher's note

References

Al-Mulla, F., Mohammad, A., Al Madhoun, A., Haddad, D., Ali, H., Eaaswarkhanth, M., et al. (2020). A comprehensive germline variant and expression analyses of ACE2, TMPRSS2 and SARSCoV-2 activator FURIN genes from the middle East: Combating SARS-CoV-2 with precision medicine. *Heliyon* doi: 10.1101/2020.05.16.099176

Alshahawey, M., Raslan, M., and Sabri, N. (2020). Sex-mediated effects of ACE2 and TMPRSS2 on the incidence and severity of COVID-19; the need for genetic implementation. *Curr. Res. Transl. Med.* 68 (4), 149–150. doi: 10.1016/j.retram.2020.08.002

Amado-Rodriguez, L., Salgado Del Riego, E., Gomez de Ona, J., Lopez Alonso, I., Gil-Pena, H., Lopez-Martinez, C., et al. (2022). Effects of IFIH1 rs1990760 variants on systemic inflammation and outcome in critically ill COVID-19 patients in an observational translational study. *Elife* 11, e73012. doi: 10.7554/eLife.73012

Amoroso, A., Magistroni, P., Vespasiano, F., Bella, A., Bellino, S., Puoti, F., et al. (2021). HLA and AB0 polymorphisms may influence SARS-CoV-2 infection and COVID-19 severity. *Transplantation* 105 (1), 193–200. doi: 10.1097/Tp.0000000000003507

Andolfo, I., Russo, R., Lasorsa, V. A., Cantalupo, S., Rosato, B. E., Bonfiglio, F., et al. (2021). Common variants at 21q22.3 locus influence MX1 and TMPRSS2 gene expression and susceptibility to severe COVID-19. *Iscience* 24 (4), 102322. doi: 10.1016/j.isci.2021.102322

Asselta, R., Paraboschi, E. M., Mantovani, A., and Duga, S. (2020). ACE2 and TMPRSS2 variants and expression as candidates to sex and country differences in COVID-19 severity in Italy. *Aging-Us* 12 (11), 10087–10098. doi: 10.18632/aging.103415

Baj, J., Karakula-Juchnowicz, H., Teresinski, G., Buszewicz, G., Ciesielka, M., Sitarz, R., et al. (2020). COVID-19: Specific and non-specific clinical manifestations and symptoms: The current state of knowledge. *J. Clin. Med.* 9 (6), 1753. doi: 10.3390/jcm9061753

Bakhshandeh, B., Sorboni, S. G., Javanmard, A. R., Mottaghi, S. S., Mehrabi, M. R., Sorouri, F., et al. (2021). Variants in ACE2; potential influences on virus infection and COVID-19 severity. *Infect. Genet. Evol.* 90, 104773. doi: 10.1016/j.meegid.2021.104773

Baughn, L. B., Sharma, N., Elhaik, E., Sekulic, A., Bryce, A. H., and Fonseca, R. (2020). Targeting TMPRSS2 in SARS-CoV-2 infection. *Mayo Clin. Proc.* 95 (9), 1989–1999. doi: 10.1016/j.mayocp.2020.06.018

Benetti, E., Tita, R., Spiga, O., Ciolfi, A. A.-O., Birolo, G., Bruselles, A., et al. (2020). ACE2 gene variants may underlie interindividual variability and susceptibility to COVID-19 in the Italian population. *Eur. J. Hum. Genet.* 28 (11), 1602–1614. doi: 10.1038 s41431-020-0691-z

Blanco-Melo, D., Nilsson-Payant, B. E., Liu, W. C., Uhl, S., Hoagland, D., Moller, R., et al. (2020). Imbalanced host response to SARS-CoV-2 drives development of COVID-19. *Cell* 181 (5), 1036–1045.e1039. doi: 10.1016/j.cell.2020.04.026

Bourgonje, A. R., Abdulle, A. E., Timens, W., Hillebrands, J. L., Navis, G. J., Gordijn, S. J., et al. (2020). Angiotensin-converting enzyme 2 (ACE2),SARS-CoV-2 and the pathophysiology of coronavirus disease 2019 (COVID-19). *J. Pathol.* 251 (3), 228–248. doi: 10.1002/path.5471

Brodin, P. (2021). Immune determinants of COVID-19 disease presentation and severity. *Nat. Med.* 27 (1), 28–33. doi: 10.1038/s41591-020-01202-8

Bunyavanich, S., Do, A., and Vicencio, A. (2020). Nasal gene expression of angiotensin-converting enzyme 2 in children and adults. *JAMA* 323 (23), 2427–2429. doi: 10.1001/jama.2020.8707

Chen, J., Jiang, Q., Xia, X., Liu, K., Yu, Z., Tao, W., et al. (2020). Individual variation of the SARS-CoV-2 receptor ACE2 gene expression and regulation. *Aging Cell* 19 (7), e13168. doi: 10.1111/acel.13168

Chen, T., Lin, Y. X., Zha, Y., Sun, Y., Tian, J., Yang, Z., et al. (2021). A low-producing haplotype of interleukin-6 disrupting CTCF binding is protective against severe COVID-19. *mBio* 12 (5), 2150–7511. doi: 10.1128/mBio.01372-21

Croci, S., Venneri, M. A., Mantovani, S., Fallerini, C., Benetti, E., Picchiotti, N., et al. (2021). The polymorphism L412F in TLR3 inhibits autophagy and is a marker of severe COVID-19 in males. *Autophagy* 18 (7), 1662–1672. doi: 10.1080/15548627.2021.1995152

D'Antonio, M., Nguyen, J. P., Arthur, T. D., Matsui, H., Initiative, C.-H. G., D'Antonio-Chronowska, A., et al. (2021). SARS-CoV-2 susceptibility and COVID-19 disease severity are associated with genetic variants affecting gene expression in a variety of tissues. *Cell Rep.* 37 (7), 110020. doi: 10.1016/j.celrep.2021.110020

David, A., Parkinson, N., Peacock, T. P., Pairo-Castineira, E., Khanna, T., Cobat, A., et al. (2022). A common TMPRSS2 variant has a protective effect against severe COVID-19. *Curr. Res. Trans. Med.* 70 (2), 103333. doi: 10.1016/j.retram.2022.103333

Deng, H., Yan, X., and Yuan, L. (2021). Human genetic basis of coronavirus disease 2019. *Signal Transduct Target Ther.* 6 (1), 344. doi: 10.1038/s41392-021-00736-8

De Toma, I., and Dierssen, M. (2021). Network analysis of down syndrome and SARS-CoV-2 identifies risk and protective factors for COVID-19. *Sci. Rep.* 11 (1), 1930. doi: 10.1038/s41598-021-81451-w

Dong, M., Zhang, J., Ma, X., Tan, J., Chen, L., Liu, S., et al. (2020). ACE2, TMPRSS2 distribution and extrapulmonary organ injury in patients with COVID-19. *BioMed. Pharmacother.* 131, 110678. doi: 10.1016/j.biopha.2020.110678

Downes, D. J., Cross, A. R., Hua, P., Roberts, N., Schwessinger, R., Cutler, A. J., et al. (2021). Identification of LZTFL1 as a candidate effector gene at a COVID-19 risk locus. *Nat. Genet.* 53 (11), 1606–160+. doi: 10.1038/s41588-021-00955-3

Duncan, C. J. A., Skouboe, M. K., Howarth, S., Hollensen, A. K., Chen, R., Borresen, M. L., et al. (2022). Life-threatening viral disease in a novel form of autosomal recessive IFNAR2 deficiency in the Arctic. *J. Exp. Med.* 219 (6), e20212427. doi: 10.1084/jem.20212427

El Baba, R., and Herbein, G. (2020). Management of epigenomic networks entailed in coronavirus infections and COVID-19. *Clin. Epigenet.* 12 (1), 118. doi: 10.1186/s13148-020-00912-7

Ellinghaus, D., Degenhardt, F., Bujanda, L., Buti, M., Albillos, A., Invernizzi, P., et al. (2020). Genomewide association study of severe covid-19 with respiratory failure. *N Engl. J. Med.* 383 (16), 1522–1534. doi: 10.1056/NEJMoa2020283

Fallerini, C., Daga, S., Mantovani, S., Benetti, E., Picchiotti, N., Francisci, D., et al. (2021). Association of toll-like receptor 7 variants with life-threatening COVID-19 disease in males: findings from a nested case-control study. *Elife* 10, e67569. doi: 10.7554/eLife.67569

Gomez, J., Albaiceta, G. M., Garcia-Clemente, M., Garcia-Gala, J. M., and Coto, E. (2021). DNA Genotyping of the ABO gene showed a significant association of the a-group (A1/A2 variants) with severe COVID-19. *Eur. J. Internal Med.* 88, 129–132. doi: 10.1016/j.ejim.2021.02.016

Gomez, J., Albaiceta, G. M., Garcia-Clemente, M., Lopez-Larrea, C., Amado-Rodriguez, L., Lopez-Alonso, I., et al. (2020). Angiotensin-converting enzymes (ACE, ACE2) gene variants and COVID-19 outcome. *Gene* 762, 145102. doi: 10.1016/j.gene.2020.145102

Gong, B., Huang, L. L., He, Y. Q., Xie, W., Yin, Y., Shi, Y., et al. (2022). A genetic variant in IL-6 lowering its expression is protective for critical patients with COVID-19. *Signal Transduction Targeted Ther.* 7 (1), 112. doi: 10.1038/s41392-022-00923-1

Grasselli, G., Greco, M., and Zanella, A. (2021). Risk factors associated with mortality among patients with COVID-19 in intensive care units in Lombardy, Italy (vol 1802020). *JAMA Internal Med.* 181 (7), 1021–1021, pg 1345. doi: 10.1001/jamainternmed.2021.1229

Grifoni, A., Sidney, J., Vita, R., Peters, B., Crotty, S., Weiskopf, D., et al. (2021). SARS-CoV-2 human T cell epitopes: Adaptive immune response against COVID-19. *Cell Host Microbe* 29 (7), 1076–1092. doi: 10.1016/j.chom.2021.05.010

Hadjadj, J., Yatim, N., Barnabei, L., Corneau, A., Boussier, J., Smith, N., et al. (2020). Impaired type I interferon activity and inflammatory responses in severe COVID-19 patients. *Science* 369 (6504), 718–724. doi: 10.1126/science.abc6027

Hoffmann, M., Kleine-Weber, H., Schroeder, S., Kruger, N., Herrler, T., Erichsen, S., et al. (2020). SARS-CoV-2 cell entry depends on ACE2 and TMPRSS2 and is blocked by a clinically proven protease inhibitor. *Cell* 181 (2), 271–27+. doi: 10.1016/j.cell.2020.02.052

Horowitz, J. E., Kosmicki, J. A., Damask, A., Sharma, D., Roberts, G. H. L., Justice, A. E., et al. (2022). Genome-wide analysis provides genetic evidence that ACE2 influences COVID-19 risk and yields risk scores associated with severe disease. *Nat. Genet.* 54 (4), 382–38+. doi: 10.1038/s41588-021-01006-7

Hosseini, A., Hashemi, V., Shomali, N., Asghari, F., Gharibi, T., Akbari, M., et al. (2020). Innate and adaptive immune responses against coronavirus. *BioMed. Pharmacother.* 132, 110859. doi: 10.1016/j.biopha.2020.110859

Ibrahim-Kosta, M., Bailly, P., Silvy, M., Saut, N., Suchon, P., Morange, P. E., et al. (2020). ABO blood group, glycosyltransferase activity and risk of venous thromboembolism. *Thromb. Res.* 193, 31–35. doi: 10.1016/j.thromres.2020.05.051

Kasela, S., Daniloski, Z., Bollepalli, S., Jordan, T. X., tenOever, B. R., Sanjana, N. E., et al. (2021). Integrative approach identifies SLC6A20 and CXCR6 as putative causal genes for the COVID-19 GWAS signal in the 3p21.31 locus. *Genome Biol.* 22 (1), 242. doi: 10.1186/s13059-021-02454-4

Katz, Dh, Tahir, U. A., Tahir Ua Fau - Ngo, D., Ngo D Fau - Benson, M. D., Benson Md Fau - Bick, A. G., Bick Ag Fau - Pampana, A., et al. (2020). Proteomic profiling in biracial cohorts implicates DC-SIGN as a mediator of genetic risk in COVID-19. doi: 10.1101/2020.06.09.20125690

Khalilzadeh, F., Sakhaee, F., Sotoodehnejadnematalahi, F., Zamani, M. S., Ahmadi, I., Anvari, E., et al. (2022). Angiotensin-converting enzyme 2 rs2285666 polymorphism and clinical parameters as the determinants of COVID-19 severity in Iranian population. *Int. J. Immunogenet.* 49 (5), 325–332. doi: 10.1111/iji.12598

Khasayesi, M., Hosseini-Khah, Z., Mirzaei, N., Ghasemian, R., Eslami, M., and Kashi, Z. (2021). Association of ABO and rhesus blood groups with the severity of SARS-CoV-2 infection: A cross-sectional analytical study. *J. Clin. Diagn. Res.* 15 (12), Oc01–Oc05. doi: 10.7860/Jcdr/2021/51103.15716

Kim, Y. C., and Jeong, B. H. (2021). Strong correlation between the case fatality rate of COVID-19 and the rs6598045 single nucleotide polymorphism (SNP) of the interferon-induced transmembrane protein 3 (IFITM3) gene at the population-level. *Genes* 12 (1), 24. doi: 10.3390/genes12010042

Kim, J. S., Lee, J. Y., Yang, J. W., Lee, K. H., Effenberger, M., Szpirt, W., et al. (2021). Immunopathogenesis and treatment of cytokine storm in COVID-19. *Theranostics* 11 (1), 316–329. doi: 10.7150/thno.49713

Klaassen, K., Stankovic, B., Zukic, B., Kotur, N., Gasic, V., Pavlovic, S., et al. (2020). Functional prediction and comparative population analysis of variants in genes for proteases and innate immunity related to SARS-CoV-2 infection. *Infect. Genet. Evol.* 84, 104498. doi: 10.1016/j.meegid.2020.104498

Kosmicki, J. A., Horowitz, J. E., Banerjee, N., Lanche, R., Marcketta, A., Maxwell, E., et al. (2021). Pan-ancestry exome-wide association analyses of COVID-19 outcomes in 586,157 individuals. *Am. J. Hum. Genet.* 108 (7), 1350–1355. doi: 10.1016/j.ajhg.2021.05.017

Kuo, C. L., Pilling, L. C., Atkins, J. L., Masoli, J. A. H., Delgado, J., Kuchel, G. A., et al. (2020). APOE e4 genotype predicts severe COVID-19 in the UK biobank community cohort. *J. Gerontol A Biol. Sci. Med. Sci.* 75 (11), 2231–2232. doi: 10.1093/gerona/glaa131

Kurki, S. N., Kantonen, J., Kaivola, K., Hokkanen, L., Mayranpaa, M. I., Puttonen, H., et al. (2021). APOE epsilon4 associates with increased risk of severe COVID-19, cerebral microhaemorrhages and post-COVID mental fatigue: a Finnish biobank, autopsy and clinical study. *Acta Neuropathol. Commun.* 9 (1), 199. doi: 10.1186/s40478-021-01302-7

Li, G., He, X., Zhang, L., Ran, Q., Wang, J., Xiong, A., et al. (2020). Assessing ACE2 expression patterns in lung tissues in the pathogenesis of COVID-19. *J. Autoimmun* 112, 102463. doi: 10.1016/j.jaut.2020.102463

Littera, R., Campagna, M., Deidda, S., Angioni, G., Cipri, S., Melis, M., et al. (2020). Human leukocyte antigen complex and other immunogenetic and clinical factors influence susceptibility or protection to SARS-CoV-2 infection and severity of the disease course. the sardinian experience. *Front. Immunol.* 11. doi: 10.3389/fimmu.2020.605688

Li, Y., Wei, L., He, L., Sun, J., and Liu, N. (2022). Interferon-induced transmembrane protein 3 gene polymorphisms are associated with COVID-19 susceptibility and severity: A meta-analysis. *J. Infect.* 84 (6), 825–833. doi: 10.1016/j.jinf.2022.04.029

Lorente, L., Martin, M. M., Franco, A., Barrios, Y., Caceres, J. J., Sole-Violan, J., et al. (2021). HLA genetic polymorphisms and prognosis of patients with COVID-19. *Med. Intensiva (Engl Ed)* 45 (2), 96–103. doi: 10.1016/j.medin.2020.08.004

Maamari, K. A., Busaidi, I. A., Kindi, M. A., Zadjali, F., BaAlawi, F., Anesta, W., et al. (2022). Short and long-term immune changes in different severity groups of COVID-19 disease. *Int. J. Infect. Dis.* 122, 776–784. doi: 10.1016/j.ijid.2022.07.026

MacGowan, S. A., Barton, M. I., Kutuzov, M., Dushek, O., van der Merwe, P. A., and Barton, G. J. (2022). Missense variants in human ACE2 strongly affect binding to SARS-CoV-2 spike providing a mechanism for ACE2 mediated genetic risk in covid-19: A case study in affinity predictions of interface variants. *PloS Comput. Biol.* 18 (3), e1009922. doi: 10.1371/journal.pcbi.1009922

Magusali, N., Graham, A. C., Piers, T. M., Panichnantakul, P., Yaman, U., Shoai, M., et al. (2021). A genetic link between risk for alzheimer's disease and severe COVID-19 outcomes *via* the OAS1 gene. *Brain* 144, 3727–3741. doi: 10.1093/brain/awab337

Mantovani, S., Daga, S., Fallerini, C., Baldassarri, M., Benetti, E., Picchiotti, N., et al. (2022). Rare variants in toll-like receptor 7 results in functional impairment and downregulation of cytokine-mediated signaling in COVID-19 patients. *Genes Immun.* 23 (1), 51–56. doi: 10.1038/s41435-021-00157-1

McGonagle, D., Sharif, K., O'Regan, A., and Bridgewood, C. (2020). The role of cytokines including interleukin-6 in COVID-19 induced pneumonia and macrophage activation syndrome-like disease. *Autoimmun Rev.* 19 (6), 102537. doi: 10.1016/j.autrev.2020.102537

Monticelli, M., Mele, B. H., Benetti, E., Fallerini, C., Baldassarri, M., Furini, S., et al. (2021). Protective role of a TMPRSS2 variant on severe COVID-19 outcome in young males and elderly women. *Genes* 12 (4), 596. doi: 10.3390/genes12040596

Nguyen, A., David, J. K., Maden, S. K., Wood, M. A., Weeder, B. R., Nellore, A., et al. (2020). Human leukocyte antigen susceptibility map for severe acute respiratory syndrome coronavirus 2. *J. Virol.* 94 (13), e00510-20. doi: 10.1128/JVI.00510-20

Nikoloudis, D., Kountouras, D., and Hiona, A. (2020). The frequency of combined IFITM3 haplotype involving the reference alleles of both rs12252 and rs34481144 is in line with COVID-19 standardized mortality ratio of ethnic groups in England. *Peerj* 8, e10402. doi: 10.7717/peerj.10402

Novelli, A., Andreani, M., Biancolella, M., Liberatoscioli, L., Passarelli, C., Colona, V. L., et al. (2020). HLA allele frequencies and susceptibility to COVID-19 in a group of 99 Italian patients. *Hla* 96 (5), 610–614. doi: 10.1111/tan.14047

Okwan-Duodu, D., Lim, E. C., You, S., and Engman, D. M. (2021). TMPRSS2 activity may mediate sex differences in COVID-19 severity. *Signal Transduction Targeted Ther.* 6 (1), 100. doi: 10.1038/s41392-021-00513-7

Ovsyannikova, I. G., Haralambieva, I. H., Crooke, S. N., Poland, G. A., and Kennedy, R. B. (2020). The role of host genetics in the immune response to SARS-CoV-2 and COVID-19 susceptibility and severity. *Immunol. Rev.* 296 (1), 205–219. doi: 10.1111/imr.12897

Pairo-Castineira, E., Clohisey, S., Klaric, L., Bretherick, A. D., Rawlik, K., Pasko, D., et al. (2021). Genetic mechanisms of critical illness in COVID-19. *Nature* 591 (7848), 92–98. doi: 10.1038/s41586-020-03065-y

Patel, A. B., and Verma, A. (2020). Nasal ACE2 levels and COVID-19 in children. *JAMA* 323 (23), 2386–2387. doi: 10.1001/jama.2020.8946

Pisanti, S., Deelen, J., Gallina, A. M., Caputo, M., Citro, M., Abate, M., et al. (2020). Correlation of the two most frequent HLA haplotypes in the Italian population to the differential regional incidence of covid-19. *J. Trans. Med.* 18 (1), 352. doi: 10.1186/s12967-020-02515-5

Prachar, M., Justesen, S., Steen-Jensen, D. B., Thorgrimsen, S., Jurgons, E., Winther, O., et al. (2020). Identification and validation of 174 COVID-19 vaccine candidate epitopes reveals low performance of common epitope prediction tools. *Sci. Rep.* 10 (1), 20465. doi: 10.1038/s41598-020-77466-4

Ramasamy, S., and Subbian, S. (2021). Critical determinants of cytokine storm and type I interferon response in COVID-19 pathogenesis. *Clin. Microbiol. Rev.* 34 (3), e00299-20. doi: 10.1128/CMR.00299-20

Ren, W., Zhu, Y., Lan, J., Chen, H., Wang, Y., Shi, H., et al. (2022). Susceptibilities of human ACE2 genetic variants in coronavirus infection. *J. Virol.* 96 (1), e0149221. doi: 10.1128/JVI.01492-21

Roberts, G. H. L., Partha, R., Rhead, B., Knight, S. C., Park, D. S., Coignet, M. V., et al. (2022). Expanded COVID-19 phenotype definitions reveal distinct patterns of genetic association and protective effects. *Nat. Genet.* 54 (4), 374–381. doi: 10.1038/s41588-022-01042-x

Rokni, M., Heidari Nia, M., Sarhadi, M., Mirinejad, S., Sargazi, S., Moudi, M., et al. (2022). Association of TMPRSS2 gene polymorphisms with COVID-19 severity and mortality: a case-control study with computational analyses. *Appl. Biochem. Biotechnol.* 194 (8), 3507–3526. doi: 10.1007/s12010-022-03885-w

Rossi, A. D., de Araujo, J. L. F., de Almeida, T. B., Ribeiro-Alves, M., Velozo, C. D., de Almeida, J. M., et al. (2021). Association between ACE2 and TMPRSS2 nasopharyngeal expression and COVID-19 respiratory distress. *Sci. Rep.* 11 (1), 9658. doi: 10.1038/s41598-021-88944-8

Ruter, J., Pallerla, S. R., Meyer, C. G., Casadei, N., Sonnabend, M., Peter, S., et al. (2022). Host genetic loci LZTFL1 and CCL2 associated with SARS-CoV-2 infection and severity of COVID-19. *Int. J. Infect. Dis.* 122, 427–436. doi: 10.1016/j.ijid.2022.06.030

Sakuraba, A., Haider, H., and Sato, T. (2020). Population difference in allele frequency of HLA-C*05 and its correlation with COVID-19 mortality. *Viruses* 12 (11), 133. doi: 10.3390/v12111333

Samuel, R. M., Majd, H., Richter, M. N., Ghazizadeh, Z., Zekavat, S. M., Navickas, A., et al. (2020). Androgen signaling regulates SARS-CoV-2 receptor levels and is associated with severe COVID-19 symptoms in men. *Cell Stem Cell* 27 (6), 876–87+. doi: 10.1016/j.stem.2020.11.009

Schetelig, J., Heidenreich, F., Baldauf, H., Trost, S., Falk, B., Hossbach, C., et al. (2021). Individual HLA-a, -b, -c, and -DRB1 genotypes are no major factors which determine COVID-19 severity. *Front. Immunol.* 12. doi: 10.3389/fimmu.2021.698193

Schreiber, G. (2020). The role of type I interferons in the pathogenesis and treatment of COVID-19. *Front. Immunol.* 11. doi: 10.3389/fimmu.2020.595739

Schuler, B. A., Habermann, A. C., Plosa, E. J., Taylor, C. J., Jetter, C., Negretti, N. M., et al. (2021). Age-determined expression of priming protease TMPRSS2 and localization of SARS-CoV-2 in lung epithelium. *J. Clin. Invest.* 131 (1), e140766. doi: 10.1172/JCI140766

Shaath, H., Vishnubalaji, R., Elkord, E., and Alajez, N. M. (2020). Single-cell transcriptome analysis highlights a role for neutrophils and inflammatory macrophages in the pathogenesis of severe COVID-19. *Cells* 9 (11), 2374. doi: 10.3390/cells9112374

Shelton, J. F., Shastri, A. J., Ye, C., Weldon, C. H., Filshtein-Sonmez, T., Coker, D., et al. (2021). Trans-ancestry analysis reveals genetic and nongenetic associations with COVID-19 susceptibility and severity. *Nat. Genet.* 53 (6), 801–808. doi: 10.1038/s41588-021-00854-7

Shikov, A. E., Barbitoff, Y. A., Glotov, A. S., Danilova, M. M., Tonyan, Z. N., Nasykhova, Y. A., et al. (2020). Analysis of the spectrum of ACE2 variation suggests a possible influence of rare and common variants on susceptibility to COVID-19 and severity of outcome. *Front. Genet.* 11. doi: 10.3389/fgene.2020.551220

Shkurnikov, M., Nersisyan, S., Jankevic, T., Galatenko, A., Gordeev, I., Vechorko, V., et al. (2021). Association of HLA class I genotypes with severity of coronavirus disease-19. *Front. Immunol.* 12. doi: 10.3389/fimmu.2021.641900

Smieszek, S. P., Polymeropoulos, V. M., Xiao, C., Polymeropoulos, C. M., and Polymeropoulos, M. H. (2021a). Loss-of-function mutations in IFNAR2 in COVID-19 severe infection susceptibility. *J. Glob Antimicrob. Resist.* 26, 239–240. doi: 10.1016/j.jgar.2021.06.005

Smieszek, S. P., Przychodzen, B. P., Polymeropoulos, V. M., Polymeropoulos, C. M., and Polymeropoulos, M. H. (2021b). Assessing the potential correlation of polymorphisms in the IL6R with relative IL6 elevation in severely ill COVID-19 patients'. *Cytokine* 148, 155662. doi: 10.1016/j.cyto.2021.155662

Solanich, X., Vargas-Parra, G., van der Made, C. I., Simons, A., Schuurs-Hoeijmakers, J., Antoli, A., et al. (2021). Genetic screening for TLR7 variants in young and previously healthy men with severe COVID-19. *Front. Immunol.* 12. doi: 10.3389/fimmu.2021.719115

Stopsack, K. H., Mucci, L. A., Antonarakis, E. S., Nelson, P. S., and Kantoff, P. W. (2020). TMPRSS2 and COVID-19: Serendipity or opportunity for intervention? *Cancer Discovery* 10 (6), 779–782. doi: 10.1158/2159-8290.CD-20-0451

Strafella, C. A.-O., Caputo, V. A.-O., Termine, A. A.-O., Barati, S., Caltagirone, C., Giardina, E., et al. (2020). Investigation of genetic variations of IL6 and IL6R as potential prognostic and pharmacogenetics biomarkers: Implications for COVID-19 and neuroinflammatory disorders. *Life (Basel)* 10 (12), 351. doi: 10.3390/life10120351

Szeto, M. D., Maghfour, J., Sivesind, T. E., Anderson, J., Olayinka, J. T., Mamo, A., et al. (2021). Interferon and toll-like receptor 7 response in COVID-19: Implications of topical imiquimod for prophylaxis and treatment. *Dermatology* 237 (6), 847–856. doi: 10.1159/000518471

Tanaka, T., Narazaki, M., and Kishimoto, T. (2014). IL-6 in inflammation, immunity, and disease. *Cold Spring Harb. Perspect. Biol.* 6 (10), a016295. doi: 10.1101/cshperspect.a016295

Taylor, L. (2022). Covid-19: True global death toll from pandemic is almost 15 million, says WHO. *BMJ* 377, o1144. doi: 10.1136/bmj.o1144

Tomita, Y., Ikeda, T., Sato, R., and Sakagami, T. (2020). Association between HLA gene polymorphisms and mortality of COVID-19: An in silico analysis. *Immun. Inflammation Dis.* 8 (4), 684–694. doi: 10.1002/iid3.358

van der Made, C. I., Simons, A., Schuurs-Hoeijmakers, J., van den Heuvel, G., Mantere, T., Kersten, S., et al. (2020). Presence of genetic variants among young

men with severe COVID-19. *Jama-Journal Am. Med. Assoc.* 324 (7), 663–673. doi: 10.1001/jama.2020.13719

Villapalos-Garcia, G., Zubiaur, P., Rivas-Duran, R., Campos-Norte, P., Arevalo-Roman, C., Fernandez-Rico, M., et al. (2022). Transmembrane protease serine 2 (TMPRSS2) rs75603675, comorbidity, and sex are the primary predictors of COVID-19 severity. *Life Sci. Alliance* 5 (10), e202201396. doi: 10.26508/lsa.202201396

Wang, F., Huang, S., Gao, R., Zhou, Y., Lai, C., Li, Z., et al. (2020). Initial whole-genome sequencing and analysis of the host genetic contribution to COVID-19 severity and susceptibility. *Cell Discovery* 6 (1), 83. doi: 10.1038/s41421-020-00231-4

Wickenhagen, A., Sugrue, E., Lytras, S., Kuchi, S., Noerenberg, M., Turnbull, M. L., et al. (2021). A prenylated dsRNA sensor protects against severe COVID-19. *Science* 374 (6567), eabj3624. doi: 10.1126/science.abj3624

Williamson, E. J., Walker, A. J., Bhaskaran, K., Bacon, S., Bates, C., Morton, C. E., et al. (2020). Factors associated with COVID-19-related death using OpenSAFELY. *Nature* 584 (7821), 430–43+. doi: 10.1038/s41586-020-2521-4

Wooster, L., Nicholson, C. J., Sigurslid, H. H., Lino Cardenas, C. L., and Malhotra, R. (2020). Polymorphisms in the ACE2 locus associate with severity of COVID-19 infection. *medRxiv*. doi: 10.1101/2020.06.18.20135152

Yamamoto, N., Ariumi, Y., Nishida, N., Yamamoto, R., Bauer, G., Gojobori, T., et al. (2020). SARS-CoV-2 infections and COVID-19 mortalities strongly correlate with ACE1 I/D genotype. *Gene* 758, 144944. doi: 10.1016/j.gene.2020.144944

Yang, Z., Macdonald-Dunlop, E., Chen, J., Zhai, R., Li, T., Richmond, A., et al. (2022). Genetic landscape of the ACE2 coronavirus receptor. *Circulation* 145 (18), 1398–1411. doi: 10.1161/CIRCULATIONAHA.121.057888

Yang, L., Wang, J., Hui, P., Yarovinsky, T. O., Badeti, S., Pham, K., et al. (2021). Potential role of IFN-alpha in COVID-19 patients and its underlying treatment options. *Appl. Microbiol. Biotechnol.* 105 (10), 4005–4015. doi: 10.1007/s00253-021-11319-6

Yao, Y., Ye, F., Li, K. L., Xu, P., Tan, W. J., Feng, Q. S., et al. (2021). Genome and epigenome editing identify CCR9 and SLC6A20 as target genes at the 3p21.31 locus associated with severe COVID-19. *Signal Transduction Targeted Ther.* 6 (1), 85. doi: 10.1038/s41392-021-00519-1

Yousefzadegan, S., and Rezaei, N. (2020). Case report: Death due to COVID-19 in three brothers. *Am. J. Trop. Med. Hyg* 102 (6), 1203–1204. doi: 10.4269/ajtmh.20-0240

Zhang, Q., Bastard, P., Liu, Z., Le Pen, J., Moncada-Velez, M., Chen, J., et al. (2020a). Inborn errors of type I IFN immunity in patients with life-threatening COVID-19. *Science* 370 (6515), eabd4570. doi: 10.1126/science.abd4570

Zhang, Y., Qin, L., Zhao, Y., Zhang, P., Xu, B., Li, K., et al. (2020c). Interferon-induced transmembrane protein 3 genetic variant rs12252-c associated with disease severity in coronavirus disease 2019. *J. Infect. Dis.* 222 (1), 34–37. doi: 10.1093/infdis/jiaa224

Zhang, H., Shao, L., Lin, Z., Long, Q. X., Yuan, H., Cai, L., et al. (2022). APOE interacts with ACE2 inhibiting SARS-CoV-2 cellular entry and inflammation in COVID-19 patients. *Signal Transduct Target Ther.* 7 (1), 261. doi: 10.1038/s41392-022-01118-4

Zhang, X., Tan, Y., Ling, Y., Lu, G., Liu, F., Yi, Z., et al. (2020b). Viral and host factors related to the clinical outcome of COVID-19. *Nature* 583 (7816), 437–440. doi: 10.1038/s41586-020-2355-0

Zhang, J., Zhao, C., and Zhao, W. (2021). Virus caused imbalance of type I IFN responses and inflammation in COVID-19. *Front. Immunol.* 12. doi: 10.3389/fimmu.2021.633769

Zhou, F., Yu, T., Du, R., Fan, G., Liu, Y., Liu, Z., et al. (2020). Clinical course and risk factors for mortality of adult inpatients with COVID-19 in wuhan, China: a retrospective cohort study. *Lancet* 395 (10229), 1054–1062. doi: 10.1016/S0140-6736(20)30566-3

frontiers | Frontiers in Cellular and Infection Microbiology

TYPE Brief Research Report
PUBLISHED 29 September 2022
DOI 10.3389/fcimb.2022.905757

OPEN ACCESS

EDITED BY
Guiqing Peng,
Huazhong Agricultural University, China

REVIEWED BY
Yongfen Xu,
Institut Pasteur of Shanghai, Chinese Academy of Sciences (CAS), China
Julien Brechbühl,
Université de Lausanne, Switzerland

*CORRESPONDENCE
Renan Pedra de Souza
renanrps@ufmg.br
Diana Bahia
dianabahia@hotmail.com

†These authors have contributed equally to this work and share first authorship

‡These authors have contributed equally to this work and share senior authorship

SPECIALTY SECTION
This article was submitted to Virus and Host, a section of the journal Frontiers in Cellular and Infection Microbiology

RECEIVED 27 March 2022
ACCEPTED 17 August 2022
PUBLISHED 29 September 2022

CITATION
Braga-Paz I, Ferreira de Araújo JL, Alves HJ, de Ávila RE, Resende GG, Teixeira MM, de Aguiar RS, de Souza RP and Bahia D (2022) Negative correlation between ACE2 gene expression levels and loss of taste in a cohort of COVID-19 hospitalized patients: New clues to long-term cognitive disorders.
Front. Cell. Infect. Microbiol. 12:905757.
doi: 10.3389/fcimb.2022.905757

Negative correlation between ACE2 gene expression levels and loss of taste in a cohort of COVID-19 hospitalized patients: New clues to long-term cognitive disorders

Isabela Braga-Paz[1†], João Locke Ferreira de Araújo[1†], Hugo José Alves[1], Renata Eliane de Ávila[2], Gustavo Gomes Resende[3], Mauro Martins Teixeira[4], Renato Santana de Aguiar[1,5], Renan Pedra de Souza[1*‡] and Diana Bahia[1*‡]

[1]Departamento de Genética, Ecologia e Evolução, Instituto de Ciências Biológicas, Universidade Federal de Minas Gerais, Universidade Federal de Minas Gerais (UFMG), Belo Horizonte, Brazil, [2]Hospital Eduardo de Menezes, Belo Horizonte, Brazil, [3]Hospital das Clínicas, Universidade Federal de Minas Gerais (HC-UFMG/EBSERH), Belo Horizonte, Brazil, [4]Departamento de Bioquimica e imunologia, Instituto de Ciências Biológicas, Universidade Federal de Minas Gerais, Universidade Federal de Minas Gerais (UFMG), Belo Horizonte, Brazil, [5]Instituto D'Or de Pesquisa e Ensino, Instituto D'OR (IDOR), Rio de Janeiro, Brazil

In early 2020, one of the most prevalent symptoms of SARS-CoV-2 infection was the loss of smell (anosmia), found in 60-70% of all cases. Anosmia used to occur early, concomitantly with other symptoms, and often persisted after recovery for an extended period, sometimes for months. In addition to smell disturbance, COVID-19 has also been associated with loss of taste (ageusia). The latest research suggests that SARS-CoV-2 could spread from the respiratory system to the brain through receptors in sustentacular cells localized to the olfactory epithelium. The virus invades human cells *via* the obligatory receptor, angiotensin-converting enzyme II (ACE2), and a priming protease, TMPRSS2, facilitating viral penetration. There is an abundant expression of both *ACE2* and *TMPRSS2* in sustentacular cells. In this study, we evaluated 102 COVID-19 hospitalized patients, of which 17.60% presented anosmia and 9.80% ageusia. *ACE1*, *ACE2*, and *TMPRSS2* gene expression levels in nasopharyngeal tissue were obtained by RT-qPCR and measured using ΔCT analysis. ACE1 *Alu*287bp association was also evaluated. Logistic regression models were generated to estimate the effects of variables on ageusia and anosmia Association of *ACE2* expression levels with ageusia. was observed (OR: 1.35; 95% CI: 1.098-1.775); however, no association was observed between *TMPRSS2* and *ACE1* expression levels and ageusia. No association was observed among the three genes and anosmia, and the *Alu*287bp polymorphism was not associated with any of the outcomes. Lastly, we discuss whetherthere is a bridge linking these initial symptoms, including

molecular factors, to long-term COVID-19 health consequences such as cognitive dysfunctions.

KEYWORDS

COVID-19, severe COVID-19, anosmia, ageusia, genetic association, quantitative trait, long-COVID syndrome, cognitive dysfunction

1 Introduction

Severe Acute Respiratory Syndrome Coronavirus 2 (SARS-CoV-2) is the virus responsible for causing coronavirus disease 2019 (COVID-19). Among the most common COVID-19 symptoms are fever, cough, fatigue, and anosmia (loss of smell) with or without ageusia (loss of taste) in mild to moderate cases (Huang et al., 2020; Aghagoli et al., 2021).

The SARS-CoV-2 virus can lead to neurologic dysfunction by both direct and indirect mechanisms, including damage to olfactory sensory neurons, impairing the brain's olfactory perception center, and post-viral anosmia. The infection can also lead to a cytokine storm that can damage the blood-brain barrier and disrupt the normal functioning of the Central Nervous System (CNS). Reports of prothrombotic status were also associated with COVID-19, leading to the obstruction of cerebral vessels and causing ischemic CNS lesions (Yazdanpanah et al., 2020; Aghagoli et al., 2021).

Complete or partial loss of smell – leading to a decreased sense of taste- may be related to olfactory disorders, head trauma, or viral infections. Although the mechanism of how viral infection causes anosmia is unclear, it is believed to involve the destruction of the olfactory neuroepithelium or transmission of pathogens directly through the olfactory nerve (Whitcroft and Hummel, 2020; Meng and Pan, 2021).

In patients affected by SARS-CoV-2 in 2020, reports of anosmia were observed in the acute phase of the disease even in the absence of other symptoms, thus becoming a hallmark symptom of COVID-19 (Hopkins et al., 2020; Lechien et al., 2020; Whitcroft and Hummel, 2020; Glezer et al., 2021; Meng and Pan, 2021). In most cases, the sense of smell recovered in about two weeks or after other symptoms improved. However, in some patients, the recovery of smell and taste took longer, a phenomenon that may be associated with the effect of the virus on the CNS and warranted further investigation (Hopkins et al., 2020; Lechien et al., 2020; Glezer et al., 2021). Many patients are now experiencing long-term health consequences called long-COVID syndrome. As the pandemic progressed, SARS-CoV-2 variants of concern (VOCs) emerged (Mistry et al., 2021; Zawilska et al., 2021). These variants have been linked to higher mortality rates, clinical complications, and increased viral transmission rates (Choi and Smith, 2021; Raman et al., 2021). In addition, variability in COVID-19 symptomatology was observed with different variants (Pedro et al., 2021).

The Spike protein (S) of SARS-CoV-2 is a viral envelope glycoprotein responsible for binding to angiotensin-converter enzyme 2 (ACE2) after its cleavage at sites S1/S2 by type II transmembrane serine protease (TMPRSS2) (Johnson et al., 2021; Meinhardt et al., 2021). The SARS-CoV-2 virus invades human cells *via* the obligatory ACE2 receptor, and TMPRSS2 further facilitates viral uptake. Co-expression of *ACE2* and *TMPRSS2* was observed in ciliated epithelial cells, nasopharyngeal tissue, and on the surface of oligodendrocytes (Sardu et al., 2020; Martínez-Gómez et al., 2022). The ratio between *ACE1* and *ACE2* has been implicated in the pathogenesis of respiratory diseases, and the functional polymorphisms of these genes have been associated with an increased risk of lung and cardiovascular diseases. Therefore, these genes may contribute to COVID-19 outcomes (Choudhary et al., 2020; Galisa et al., 2021; Martínez-Gómez et al., 2022).

The *ACE1* gene modulates *ACE2* expression with increased levels of angiotensin II. Both are part of the renin-angiotensin-aldosterone system (RAAS) (D'ardes et al., 2020; Saad et al., 2021). A 287 bps *Alu* sequence rs4646994, repeated insertion/deletion (I/D) (indel) in intron 16, has been described in the *ACE1* gene, which leads to an expression modulation of this gene (Castellon and Hamdi, 2007; de Araújo et al., 2022). A recent study has shown that an *Alu* homozygous deletion (D/D) is associated with the progression of severe COVID-19 (de Araújo et al., 2022). However, studies are still required to evaluate the role of the genetic polymorphism in COVID-19 outcomes.

This study investigates the gene expression of potential viral targets in the olfactory epithelium in nasal swab samples obtained from 102 hospitalized patients with COVID-19 between April and September 2020. We explore *ACE1*, *ACE2*, and *TMPRSS2* expression in these patients and the relationship of these genes with the onset of symptoms such as anosmia and ageusia. Information on anosmia and ageusia was collected through the hospitalized patient's report. Moreover, we discuss whether the prevalence of these symptoms months after infection could lead to neurological problems or cognitive dysfunction such as short-term memory loss, difficulty concentrating, mental confusion, and imbalance.

2 Methods

2.1 Patients

Samples were collected from 102 COVID-19 positive patients confirmed by qPCR and were admitted to the Eduardo de Menezes hospital in Belo Horizonte, Minas Gerais, Brazil, between April and September 2020, before the appearance of SARS-CoV-2 variants of concern. Exclusion criteria were cancer, autoimmune diseases, and pregnancy. Smoking status was also reported. All participants gave informed consent (CAAE 32224420.3.0000.0008 and CAAE 31462820.3.0000.5149). When patients could not consent due to hospitalization, informed consent was obtained by a legal guardian. RT-qPCR confirmed COVID-19 diagnosis. The clinical data of the patients used in the study was obtained from hospital records. Patients self-reported anosmia and ageusia. Information about comorbidities is based on the medical history of each hospitalized patient. Nasopharyngeal swab samples were collected in a viral transport medium (DMEM or PBS) and stored at -80°C until extraction. The collection of biological material was performed on the first day of hospitalization of the patients.

2.2 Expression analysis

RNA extraction was performed using a Quick-RNA Viral kit (Zymo Research, CA, USA). Samples were treated with TURBO DNA-free kit (Thermo Fisher Scientific, MA, USA) when GoTaq SYBR green qPCR assay was employed. cDNA was generated using the High-Capacity cDNA Reverse Transcription Kit (Thermo Fisher Scientific, MA, USA). All above reactions were conducted following the manufacturer's instructions. *ACE1*, *ACE2*, *TMPRSS2*, and *B2M* (reference gene) gene expression levels were evaluated using the GoTaq Probe qPCR System (Promega, WI, USA). The specific probes (Integrated DNA Technologies, NJ, USA) used and designed for exon-exon junctions were: Hs.PT.58.19167084, Hs.PT.58.27645939, HS.PT.58.39738666, and Hs.PT.39a.22214847, respectively. ΔCt was calculated by subtracting the cycle threshold (Ct) of the gene of interest from the reference gene (B2M) Ct.

2.3 *Alu*287bp polymorphism (rs4646994) genotyping

For the genotyping of the rs4646994 polymorphism, the FastStart Universal SYBR Green Master Kit (Promega, WI, USA) was used to yield a final volume of 20 µL using three different primers: 5'CATCCTTTCTCCCATTTCTC3' (Primer1, Forward); 5'TGGGATTACAGGCGTGATACAG3' (Primer 2, Forward, internal); and 5'ATTTCAGAGCTGGAATAAAA TT3' (Primer 3, Reverse). Primer stock was resuspended and diluted to a working solution of 10 µM. The concentration of primers 1 and 3 is 20 pmol, and the concentration of primer 2 is 40 pmol. The generated fragment sizes were 65bp (Insertion) and 84bp (deletion) and visualized on a 3% agarose gel. Ten percent of the sample was randomly genotyped twice to attest to the genotyping quality. The agreement level was 100%.

2.4 Statistical analysis

All analyses of this study were performed in R version 4.0.2, considering a significance level of 0.05. The verification of the Hardy-Weinberg equilibrium (HWE) was performed using the SNPassoc package. Allelic and genotypic frequency calculations were performed. Logistic regression models were generated to estimate the individual effects of the variables age, sex, RS4646994 polymorphism, and gene expression levels for the Anosmia and Ageusia outcomes.

A logistic regression model was generated to investigate association between clinical and molecular data. We used Ct data of the N gene of SARS-CoV-2 to evaluate whether there was a difference between the viral loads of patients with COVID-19 experiencing anosmia and ageusia vs. those without anosmia and ageusia. Ct values from RNase P (Ribonuclease P) were used for normalization. The results were reported in Table 2 as mean, standard deviation (sd), odds ratio (OR), and confidence interval (CI).

3 Results

Only one patient did not require respiratory support. There were 54 women and 48 men, and the mean duration of hospitalization was 10.2 ± 6.5 days. The death rate was 13.7%, and the mean age of these patients was 55.11 ± 4.6 years. About 25% of patients had diabetes, 55.9% were hypertensive, 13.7% had asthma, and 20.6% were smokers (Table 1).

Hardy Weinberg equilibrium (HWE) analysis was performed separately for case and control groups for the frequency of the *Alu*287bp polymorphism. Anosmia and Ageusia were tested. Both cases were in HWE for the outcome of anosmia and ageusia (p=0.624 and p=0.219, respectively). However, controls for anosmia and ageusia were out of HWE (p=0.021 and p=0.028, respectively). Two individuals could not have their genotypes evaluated (Table 2).

No difference was observed when the variables age and sex were tested in the logistic model for anosmia. Similarly, there were no differences in *ACE1* gene expression in the anosmia. No association was observed between the manifestation of anosmia and the *ACE2* and *TMPRSS2* expression levels (p=0.063 and p=0.068, respectively) (Table 3). No association was observed for the *Alu*287bp polymorphism, testing the codominance, D allele dominance, and I allele dominance models (Table 3).

TABLE 1 Demographic and clinical characteristics of the study sample (n = 102).

Characteristics	Value
Age, mean (sd)	55.1 (14.6)
Hospitalization days, mean (sd)	10.2 (6.5)
Female Sex, N (%)	54 (52.9%)
Death, N (%)	14 (13.7%)
Anosmia, N (%)	18 (17.6%)
Ageusia, N (%)	10 (9.8%)
Respiratory support, N (%)	101 (99%)
Diabetes, N (%)	26 (25.5%)
Obesity N (%)	28 (27.7%)
Smoking N (%)	21 (20.6%)
Hypertension N (%)	57 (55.9%)
Asthma N (%)	14 (13.7%)

sd, standard deviation; No, number; clinical and demographic data from a sample of Covid-19 positive patients admitted to the Eduardo de Menezes hospital, Belo Horizonte, MG. Age, sex, hospitalization days, death and main symptoms.

Age and sex were also not significant when tested in the logistic model for ageusia. There was no difference in *ACE1* gene expression in the ageusia. An association was observed between decreased *ACE2* expression levels and ageusia (OR:1.35; 95%CI: 1.09-1.77). No association for manifestation of ageusia was detected with low *TMPRSS2* gene expression levels (p=0.074) (Table 3). No association was observed for the *Alu*287bp polymorphism, testing the codominance, D allele dominance, and I allele dominance models (Table 3).

No differences were observed for viral load between patients with anosmia and ageusia and the respective controls (p=0.395 and p=0.931, respectively).

4 Discussion

Herein, we evaluated the association of *ACE1*, *ACE2*, and *TMPRSS2* expression with the presence of anosmia and/or ageusia. There was a negative correlation between *ACE2* and ageusia in a sample of hospitalized COVID-19 positive patients. Furthermore, no association was observed between expression of *ACE1* and *TMPRSS2* and the manifestation of ageusia. No association was observed for the three genes and anosmia. In addition, no association was found for the *ALU287pb* polymorphism with the presence of anosmia and/or ageusia,

ACE2 and *TMPRSS2* actively participate in the SARS-Cov-2 infectious process. Some studies have already demonstrated the association of differentiated levels of expression of these genes in the prognosis of COVID-19 (Sardu et al., 2020). For example, the ACE2/TMPRSS2 ratio was associated with the need for respiratory support (Rossi et al., 2021). Although high *ACE2* and *TMPRSS2* expression levels are associated with a severe prognosis of COVID-19, in this study, we evaluated specific clinical symptoms of the disease. Anosmia and ageusia have been observed more frequently in patients with a mild outcome and lower frequency in those with severe disease (Lechien et al., 2020; Aghagoli et al., 2021). The sample used in this study was obtained from patients hospitalized with severe clinical symptoms. In these samples, we found that low *ACE2* gene expression levels correlated with ageusia.

In addition, both genes are highly expressed on the surface of oligodendrocytes, which could explain the proliferation of the virus in nerve tissue cells and subsequent neurological damage and sequelae. *ACE2* is abundantly expressed in the respiratory epithelium and in cells of the oral mucosa tissue, mainly in epithelial cells of the oral mucosa, lips, and tongue, these sites being more susceptible to SARS-CoV-2 invasion compared to other oral anatomical sites, and direct damage to the oral epithelium and the neuroinvasive nature of the virus can lead to taste disturbances (Zhong et al., 2020; Farid et al., 2022). Thus, *ACE2* and *TMPRSS2* expression may be key factors in unveiling neurocognitive consequences of long-COVID-19 syndrome (Huang et al., 2020; Aghagoli et al., 2021).

In animal models, the SARS-CoV-2 virus down-regulates *ACE2* expression leading to an imbalance in the *ACE1/ACE2* cerebrovascular control, resulting in an ACE1 signal mismatch, excessive vasoconstriction, or brain autoregulation disorders

TABLE 2 Genotypic and allelic absolute values for the rs4646994 polymorphism.

Sample		Genotype					p value
	n	DD	DI	II	D	I	
Anosmia case	18	5	11	2	21	15	0.624
Anosmia control	82	35	29	18	99	65	0.021
Ageusia case	10	3	7	0	13	7	0.219
Ageusia control	90	37	33	20	107	73	0.028

Genotypic and allelic absolute values for the rs4646994 polymorphism for case and control groups in two studies: Chance of anosmia and ageusia. Hardy Weinberg equilibrium performed for case and control separately. Yes: case; No: control.

TABLE 3 Logistic regression model for anosmia and ageusia outcomes.

Outcome	Variable	Case		Control		p value	OR CI (95%)
		N	mean (sd) or %	N	mean (sd) or %		
Anosmia	Age	18	55.44 (10.33)	84	54.04 (15.43)	0.916	–
	ACE1 ΔCT	7	11.17 (5.25)	75	10.77 (3.85)	0.835	–
	ACE2 ΔCT	9	15.09 (5.82)	79	13.59 (4.75)	0.063	
	TMPRSS2 ΔCT	9	13.11 (4.99)	79	8.17 (4.59)	0.068	
	Sex (Male)	7	0.39	41	0.49	0.446	
	rs4646994 Codominance DD	5	0.27	35	0.43	–	–
	rs4646994 Codominance DI	11	0.61	29	0.35	0.101	–
	rs4646994 Codominance II	2	0.12	18	0.22	0.777	–
	rs4646994 I allele dominance (DI + II)	13	0.73	47	0.57	0.248	–
	rs4646994 D allele dominance (DD + DI)	16	0.88	64	0.78	0.308	–
Ageusia	Age	10	54.80 (9.41)	92	55.15 (15.11)	0.942	
	ACE1 ΔCT	7	11.14 (6.09)	75	10.81 (3.83)	0.788	
	ACE2 ΔCT	9	17.16 (4.41)	79	13.37 (4.93)	0.012	1.35 (1.098-1.775)
	TMPRSS2 ΔCT	9	13.63 (5.63)	79	8.58 (4.67)	0.074	
	Sex (Male)	4	0.4	44	0.48	0.639	–
	rs4646994 Codominance DD	3	0.3	37	0.41	–	–
	rs4646994 Codominance DI	7	0.7	33	0.37	0.188	–
	rs4646994 Codominance II	0	0	20	0.22	0.994	–
	rs4646994 I allele dominance (DI + II)	7	0.7	53	0.59	0.5	–
	rs4646994 D allele dominance (DD + DI)	10	1	70	0.78	0.991	–

sd, standard deviation; OR, Odds ratio; CI, confidence interval; ΔCT, cycle threshold rate; exploring the variables age, sex rs4646994 polymorphism and ACE1, ACE2 and TMPRSS2 genes expression levels for the presence (yes/case) or absence (no/control) of anosmia or ageusia. The variable "DD +DI" corresponds to the dominance of the D allele and the variable "DI +II" corresponds to the dominance of the I allele.

(Aghagoli et al., 2021). A recent meta-analysis showed that the 287bp deletion in the *ACE1* gene is associated with the prognosis of severe COVID-19 (de Araújo et al., 2022). Nonetheless, the authors have not evaluated long-term health disorders yet. In this study, age and sex did not correlate with onset of anosmia and ageusia. However, age and sex remain important variables in the prognosis of COVID-19. Several studies have shown higher frequencies of disease severity and death in elderly individuals (Izcovich et al., 2020; Izurieta et al., 2020). Sex has also been a factor in COVID-19 prognosis and mortality, mainly affecting male individuals (Ghamrawi and Gunaratne, 2020; Izurieta et al., 2020). A prospective observational cohort study of COVID-19 analyzed 4,182 individuals who self-reported their symptoms in the "COVID Symptom Study app"- a mobile health app developed by Zoe Global (Sudre et al., 2021). In the study, those with long-term COVID were mostly individuals over 70 and more likely to be female.

Currently, evidence indicates that SARS-CoV-2 does not affect only the respiratory tract but also the CNS, which has resulted in symptoms such as anosmia, ageusia, headache, fatigue, nausea, vomiting, acute cerebrovascular disease, and altered consciousness (Conde Cardona et al., 2020; Huang et al., 2020; Meinhardt et al., 2021). Anosmia rates are lower among patients infected by the Gamma and Omicron strains than the original strain. Besides that, no differences were observed between the original strain and the Delta variant (Cardoso et al., 2022).

Here we started to raise the hypothesis and discuss whether there is a bridge linking initial symptoms, such as anosmia and ageusia, modulation of molecular factors expression, to long-COVID, which is the long-term COVID-19 health consequences experienced by an increasing number of patients. There are five types of specialized cells in the olfactory epithelium, namely the sustentacular cells, basal cells, microvillar cells, the olfactory sensory neurons (OSNs), and the ductal cells of Bowman's glands (Riel et al., 2015; Ahmed et al., 2022). The expression of the input factors of SARS-CoV-2 in the olfactory epithelium, resulting in loss of OSNs, may lead to anosmia. Smell and taste disorders are related to our general and mental health and can be early indicators of CNS compromises (Brechbühl et al., 2021; Glezer et al., 2021).

A study investigating viral entry sites and sensory symptoms in mice found that the virus can target chemosensory cells of the gustatory and olfactory systems (Brechbühl et al., 2021). Although the direct action of the virus on these cells is not fully elucidated, mechanisms of cytopathic destruction impact sense of smell and taste, and this impairment could directly contribute to anosmia and ageusia in the long term (Cazzolla

et al., 2020; Brechbühl et al., 2021; Muus et al., 2021). Herein, we have not observed differences in viral load between patients with anosmia and ageusia and the respective controls, suggesting that other mechanisms or factors may be involved in developing long-COVID syndrome.

There are several symptoms related to COVID-associated cognitive impairment, which are persistent and worsen the quality of life of COVID-19 survivors (Becker, 2021; Nasserie et al., 2021). Long-COVID syndrome is associated with impaired concentration, information processing, memory, executive functioning, anxiety, depression, panic syndrome, sleep disorder, and fatigue. COVID-dependent cognitive impairments contribute substantially to reduced global functioning. Long-COVID syndrome has been described to typically last up to 6 to 12 months but can last indefinitely in some individuals (Orrù et al., 2021; Titze-de-Almeida et al., 2022).

In a study (de Paula et al., 2022) performed with 195 individuals with mild COVID-19, 26% had a visuoconstructive deficiency, a typical early manifestation of Alzheimer's disease. There was also increased expression of 11 plasma biomarkers, including chemokines and growth factors. These biomarkers showed a strong positive correlation with the degree of cognitive impairment. The disability has persisted for up to a year after diagnosis. People who had mild COVID-19 and were not hospitalized in the two to ten months before enrollment, and without comorbidities were included. Most of the volunteers are health professionals who work in the hospital region and learned about the study through advertisements made by the institutions. The mean age of the cohort was 38 years (de Paula et al., 2022).

A group from England recently published a robust study involving 785 participants (aged 51–81) with COVID (Douaud et al., 2022), including patients with only mild COVID-19 symptoms. Limbic brain imaging was obtained twice and compared to 384 non-infected controls. They identified a consistent spatial pattern of longitudinal anomalies in limbic brain regions forming a mainly olfactory network, including a greater reduction in global brain size.

The authors hypothesized that the results could represent the hallmarks of the degenerative spread of the disease *via* olfactory pathways, neuroinflammatory events, or loss of sensory input due to anosmia and suggested longer follow-up periods to evaluate these effects. Brain atrophy (due to the loss of input received from the nose) is the only plausible explanation for linking anosmia symptoms in COVID-19 to brain/cognitive symptoms seen in long-COVID Syndrome (Marshall, 2022).

Our group hypothesized that, in addition to viral entry into cells in the CNS, there are signaling pathways activated during the COVID-19 that disrupt the brain homeostasis, thereby leading to long term neurocognitive consequences. As such, anosmia and ageusia could be the early events heralding the neurocognitive changes of long-COVID-19 syndrome. A better understanding of anosmia and ageusia may improve our knowledge of long-lasting cognitive disorders, including long-COVID-19. Future studies will investigate the relative expression of key olfactory and sustentacular cell marker genes in samples collected from post-COVID-19 patients (six months to one year after contracting COVID-19) with or without anosmia and/or ageusia, using neuropsychological tests (de Paula et al., 2022).

To the best of our knowledge, this is the first study utilizing gene expression in nasopharyngeal swab samples of COVID-19 patients to identify expression differences associated with anosmia and ageusia. Future directions include testing a higher number of putative target genes with longer symptom follow-up to obtain better associations between expression differences and long-COVID-19 symptoms and duration. A better understanding of the genes modulated in association with initial anosmia and ageusia may bright light on the signaling pathway alterations that are associated with neurologic symptoms of COVID-19 and the development of long-COVID-19 syndrome and lay the groundwork for pharmacologic therapies that interfere with pathologic signaling changes.

Data availability statement

The original contributions presented in the study are included in the article. Further inquiries can be directed to the corresponding authors.

Ethics statement

The studies involving human participants were reviewed and approved by Certificado de Apresentação de Apreciação Ética: CAAE 32224420.3.0000.0008 and CAAE 31462820.3.0000.5149. The patients/participants provided their written informed consent to participate in this study.

Author contributions

DB and RS conceived the study. IB-P, JA, REA, RS, and DB designed the experiments. IB-P, JA, HA, and RS performed the experiments. IB-P, JA, RSA, RS, and DB interpreted the results and analyzed the data. RSA, RS, and DB contributed with material and analysis tools. REA, GR and MT were responsible for subject's recruitment and clinical follow-up. IB-P, JA, and DB wrote the manuscript. All authors read and approved the final manuscript.

Funding

The authors wish to thank the following funding sources:Rede Corona-ômica BR MCTI/FINEP affiliated to RedeVırus/ ´MCTI (FINEP 01.20.0029.000462/20, CNPq 404096/2020-4),MEC/CAPES (14/2020–23072.211119/2020-10), FINEP (0494/20 01.20.0026.00 and UFMG-NB3 1139/20), FAPEMIG (RPS:APQ-00475-20), FAPERJ (RSA 202.922/2018) and CAPES(88881.506612/2020-0). RPS, RSA, and DB are recipients of CNPq Fellowships.

Acknowledgments

The authors also thank BioMed Proofreading LLC for the English language editing of this manuscript.

Conflict of interest

The authors declare that the research was conducted in the absence of any commercial or financial relationships that could be construed as a potential conflict of interest.

Publisher's note

All claims expressed in this article are solely those of the authors and do not necessarily represent those of their affiliated organizations, or those of the publisher, the editors and the reviewers. Any product that may be evaluated in this article, or claim that may be made by its manufacturer, is not guaranteed or endorsed by the publisher.

References

Aghagoli, G., Gallo Marin, B., Katchur, N. J., Chaves-Sell, F., Asaad, W. F., and Murphy, S. A. (2021). Neurological involvement in COVID-19 and potential mechanisms: A review. *Neurocrit. Care* 34, 1062–1071. doi: 10.1007/s12028-020-01049-4

Ahmed, A. K., Sayad, R., Mahmoud, I. A., EL-Monem, A. M. A., Badry, S. H., Ibrahim, I. H., et al. (2022). "Anosmia" the mysterious collateral damage of COVID-19. *J. Neurovirol.* 28(2), 189–200. doi: 10.1007/s13365-022-01060-9

Becker, R. C. (2021). COVID-19 and its sequelae: A platform for optimal patient care, discovery and training. *J. Thromb. Thrombolysis* 51, 587–594. doi: 10.1007/s11239-021-02375-w

Brechbühl, J., Lopes, A. C., Wood, D., Bouteiller, S., de Vallière, A., Verdumo, C., et al. (2021). Age-dependent appearance of SARS-CoV-2 entry sites in mouse chemosensory systems reflects COVID-19 anosmia-ageusia symptoms. *Commun. Biol.* 4, 1–12. doi: 10.1038/s42003-021-02410-9

Cardoso, C. C., Rossi, Á. D., Galliez, R. M., Faffe, D. S., Tanuri, A., and Castiñeiras, T. M. P. P. (2022). Olfactory dysfunction in patients with mild COVID-19 during gamma, delta, and omicron waves in Rio de Janeiro, Brazil. *JAMA* 328(6), 582–583. doi: 10.1001/jama.2022.11006

Castellon, R., and Hamdi, H. (2007). Demystifying the ACE polymorphism: From genetics to biology. *Curr. Pharm. Des.* 13, 1191–1198. doi: 10.2174/138161207780618902

Cazzolla, A. P., Lovero, R., Lo Muzio, L., Testa, N. F., Schirinzi, A., Palmieri, G., et al. (2020). Taste and smell disorders in COVID-19 patients: Role of interleukin-6. *ACS Chem. Neurosci.* 11, 2774–2781. doi: 10.1021/acschemneuro.0c00447

Choi, J. Y., and Smith, D. M. (2021). SARS-CoV-2 variants of concern. *Yonsei Med. J.* 62, 961–968. doi: 10.3349/ymj.2021.62.11.961

Choudhary, S., Sreenivasulu, K., Mitra, P., Misra, S., and Sharma, P. (2020). Role of genetic variants and gene expression in the susceptibility and severity of COVID-19. *Ann. Lab. Med.* 41, 129–138. doi: 10.3343/alm.2021.41.2.129

Conde Cardona, G., Quintana Pájaro, L. D., Quintero Marzola, I. D., Ramos Villegas, Y., and Moscote Salazar, L. R. (2020). Neurotropism of SARS-CoV 2: Mechanisms and manifestations. *J. Neurol. Sci.* 412, 116824. doi: 10.1016/j.jns.2020.116824

D'ardes, D., Boccatonda, A., Rossi, I., Guagnano, M. T., Santilli, F., Cipollone, F., et al. (2020). COVID-19 and RAS: Unravelling an unclear relationship. *Int. J. Mol. Sci.* 21, 1–8. doi: 10.3390/ijms21083003

de Araújo, J. L. F., Menezes, D., de Aguiar, R. S., and de Souza, R. P. (2022). IFITM3, FURIN, ACE1, and TNF-α genetic association with COVID-19 outcomes: Systematic review and meta-analysis. *Front. Genet.* 13. doi: 10.3389/fgene.2022.775246

de Paula, J. J., Paiva, R. E. R. P., Souza-Silva, N. G., Rosa, D. V., Duran, F. L., de, S., et al. (2022). Selective visuoconstructional impairment following mild COVID-19 with inflammatory and neuroimaging correlation findings. *Mol. Psychiatry*. doi: 10.1038/s41380-022-01632-5

Douaud, G., Lee, S., Alfaro-Almagro, F., Arthofer, C., Wang, C., McCarthy, P., et al. (2022). SARS-CoV-2 is associated with changes in brain structure in UK biobank. *Nature* 604, 697–707. doi: 10.1038/s41586-022-04569-5

Farid, H., Khan, M., Jamal, S., and Ghafoor, R. (2022). Oral manifestations of covid-19-A literature review. *Rev. Med. Virol.* 32, 1–12. doi: 10.1002/rmv.2248

Galisa, S. L. G., Almeida, R. M., de, S., Soares, A. R. A. P., Ribeiro, R. R. A., Pereira, F. R. A., et al. (2021). Influência da suscetibilidade genética na incidência e mortalidade de COVID-19 (SARS-CoV-2). *Res. Soc Dev.* 10, e31810111812. doi: 10.33448/rsd-v10i1.11812

Ghamrawi, R., and Gunaratne, M. (2020). COVID-19 and sex differences. *Mayo Clin. Proc.* 95, 2189–2203. doi: 10.1016/j.mayocp.2020.07.024

Glezer, I., Bruni-Cardoso, A., Schechtman, D., and Malnic, B. (2021). Viral infection and smell loss: The case of COVID-19. *J. Neurochem.* 157, 930–943. doi: 10.1111/jnc.15197

Hopkins, C., Surda, P., Whitehead, E., and Kumar, B. N. (2020). Early recovery following new onset anosmia during the COVID-19 pandemic - an observational cohort study. *J. Otolaryngol. Head Neck Surg.* 49, 1–6. doi: 10.1186/s40463-020-00423-8

Huang, C., Wang, Y., Li, X., Ren, L., Zhao, J., Hu, Y., et al. (2020). Clinical features of patients infected with 2019 novel coronavirus in wuhan, China. *Lancet* 395, 497–506. doi: 10.1016/S0140-6736(20)30183-5

Izcovich, A., Ragusa, M. A., Tortosa, F., Lavena Marzio, M. A., Agnoletti, C., Bengolea, A., et al. (2020). Prognostic factors for severity and mortality in patients infected with COVID-19: A systematic review. *PloS One* 223(6), 945–956. doi: 10.1371/journal.pone.0241955

Izurieta, H. S., Graham, D. J., Jiao, Y., Hu, M., Lu, Y., Wu, Y., et al. (2020). Natural history of coronavirus disease 2019: Risk factors for hospitalizations and deaths among <26 million US Medicare beneficiaries. *J. Infect. Dis.* doi: 10.1093/infdis/jiaa767

Johnson, B. A., Xie, X., Bailey, A. L., Kalveram, B., Lokugamage, K. G., Muruato, A., et al. (2021). Loss of furin cleavage site attenuates SARS-CoV-2 pathogenesis. *Nature* 591, 293–299. doi: 10.1038/s41586-021-03237-4

Lechien, J. R., Chiesa-Estomba, C. M., De Siati, D. R., Horoi, M., Le Bon, S. D., Rodriguez, A., et al. (2020). Olfactory and gustatory dysfunctions as a clinical presentation of mild-to-moderate forms of the coronavirus disease (COVID-19): A multicenter European study. *Eur. Arch. Oto-Rhino-Laryngol.* 277, 2251–2261. doi: 10.1007/s00405-020-05965-1

Marshall, M. (2022). COVID and smell loss: Answers begin to emerge. *Nature*. 606(7915), 631–632. doi: 10.1038/d41586-022-01589-z

Martínez-Gómez, L. E., Herrera-López, B., Martinez-Armenta, C., Ortega-Peña, S., Camacho-Rea, M., del, C., et al. (2022). ACE and ACE2 gene variants are associated with severe outcomes of COVID-19 in men. *Front. Immunol.* 13. doi: 10.3389/fimmu.2022.812940

Meinhardt, J., Radke, J., Dittmayer, C., Franz, J., Thomas, C., Mothes, R., et al. (2021). Olfactory transmucosal SARS-CoV-2 invasion as a port of central nervous system entry in individuals with COVID-19. *Nat. Neurosci.* 24, 168–175. doi: 10.1038/s41593-020-00758-5

Meng, X., and Pan, Y. (2021). COVID-19 and anosmia: The story so far. *Ear Nose Throat J.* 0, 1–9. doi: 10.1177/01455613211048998

Mistry, P., Barmania, F., Mellet, J., Peta, K., Strydom, A., Viljoen, I. M., et al. (2021). SARS-CoV-2 variants, vaccines, and host immunity. *Front. Immunol.* 12. doi: 10.3389/fimmu.2021.809244

Muus, C., Luecken, M. D., Eraslan, G., Sikkema, L., Waghray, A., Heimberg, G., et al. (2021). Single-cell meta-analysis of SARS-CoV-2 entry genes across tissues and demographics. *Nature Medicine*. 27, 546–559 .doi: 10.1038/s41591-020-01227-z

Nasserie, T., Hittle, M., and Goodman, S. N. (2021). Assessment of the frequency and variety of persistent symptoms among patients with COVID-19: A systematic review. *JAMA Netw. Open* 4, 1–19. doi: 10.1001/jamanetworkopen.2021.11417

Orrù, G., Bertelloni, D., Diolaiuti, F., Mucci, F., Di Giuseppe, M., Biella, M., et al. (2021). Long-covid syndrome? A study on the persistence of neurological, psychological and physiological symptoms. *Healthc* 9, 1–15. doi: 10.3390/healthcare9050575

Pedro, N., Silva, C. N., Magalhães, A. C., Cavadas, B., Rocha, A. M., Moreira, A. C., et al. (2021). Dynamics of a dual SARS-CoV-2 lineage Co-infection on a prolonged viral shedding COVID-19 case: Insights into clinical severity and disease duration. *Microorganisms* 9(2), 300. doi: 10.3390/microorganisms9020300

Raman, R., Patel, K. J., and Ranjan, K. (2021). COVID-19: Unmasking emerging SARS-CoV-2 variants, vaccines and therapeutic strategies. *Biomolecules* 11(7), 993. doi: 10.3390/biom11070993

Riel, D., Verdijk, R., and Kuiken, T. (2015). The olfactory nerve: A shortcut for influenza and other viral diseases into the central nervous system. *J. Pathol.* 235, 277–287. doi: 10.1002/path.4461

Rossi, Á. D., de Araújo, J. L. F., de Almeida, T. B., Ribeiro-Alves, M., de Almeida Velozo, C., Almeida, J. M., et al. (2021). Association between ACE2 and TMPRSS2 nasopharyngeal expression and COVID-19 respiratory distress. *Sci. Rep.* 11(1), 9658. doi: 10.1038/s41598-021-88944-8

Saad, H., Jabotian, K., Sakr, C., Mahfouz, R., Akl, I. B., and Zgheib, N. K. (2021). The role of angiotensin converting enzyme 1 Insertion/Deletion genetic polymorphism in the risk and severity of COVID-19 infection. *Front. Med.* 8. doi: 10.3389/fmed.2021.798571

Sardu, C., Gambardella, J., Morelli, M. B., Wang, X., Marfella, R., and Santulli, G. (2020). Hypertension, thrombosis, kidney failure, and diabetes: Is COVID-19 an endothelial disease? A comprehensive evaluation of clinical and basic evidence. *J. Clin. Med.* 9(5), 1417. doi: 10.3390/jcm9051417

Sudre, C. H., Murray, B., Varsavsky, T., Graham, M. S., Penfold, R. S., Bowyer, R. C., et al. (2021). Attributes and predictors of long-COVID. *Nat. Med.* 27, 626–631. doi: 10.1038/s41591-021-01292-y

Titze-de-Almeida, R., da Cunha, T. R., dos Santos Silva, L. D., Ferreira, C. S., Silva, C. P., Ribeiro, A. P., et al. (2022). Persistent, new-onset symptoms and mental health complaints in long-COVID in a Brazilian cohort of non-hospitalized patients. *BMC Infect. Dis.* 22, 1–11. doi: 10.1186/s12879-022-07065-3

Whitcroft, K. L., and Hummel, T. (2020). Olfactory dysfunction in COVID-19: Diagnosis and management. *JAMA J. Am. Med. Assoc.* 323, 2512–2514. doi: 10.1001/jama.2020.8391

Yazdanpanah, N., Saghazadeh, A., and Rezaei, N. (2020). Anosmia: A missing link in the neuroimmunology of coronavirus disease 2019 (COVID-19). *Rev. Neurosci.* 31, 691–701. doi: 10.1515/revneuro-2020-0039

Zawilska, J. B., Lagodzinski, A., and Berezinska, M. (2021). COVID-19: from the structure and replication cycle of SARS-CoV-2 to its disease symptoms and treatment. *J. Physiol. Pharmacol. Off. J. Polish Physiol. Soc* 72(4), 479–501. doi: 10.26402/jpp.2021.4.01

Zhong, M., Lin, B., Pathak, J. L., Gao, H., Young, A. J., Wang, X., et al. (2020). ACE2 and furin expressions in oral epithelial cells possibly facilitate COVID-19 infection *via* respiratory and fecal–oral routes. *Front. Med.* 7. doi: 10.3389/fmed.2020.580796

frontiers | Frontiers in Cellular and Infection Microbiology

TYPE Original Research
PUBLISHED 03 November 2022
DOI 10.3389/fcimb.2022.979641

OPEN ACCESS

EDITED BY
Yu Chen,
State Key Laboratory of Virology,
Wuhan University, China

REVIEWED BY
Anan Jongkaewwattana,
National Center for Genetic Engineering and Biotechnology (BIOTEC), Thailand
Sonia Zuñiga,
National Center for Biotechnology, (CSIC), Spain
Silvia Beatriz Boscardin,
University of São Paulo, Brazil
Bryce Warner,
Public Health Agency of Canada (PHAC), Canada

*CORRESPONDENCE
Michel Klein
michel.klein@umontreal.ca
Ke Wu
ke.wu@bravovax.com

†These authors have contributed equally to this work

SPECIALTY SECTION
This article was submitted to Virus and Host, a section of the journal Frontiers in Cellular and Infection Microbiology

RECEIVED 27 June 2022
ACCEPTED 21 September 2022
PUBLISHED 03 November 2022

CITATION
Wang S, Xu L, Mu T, Qin M, Zhao P, Xie L, Du L, Wu Y, Legrand N, Mouchain K, Fichet G, Liu Y, Yin W, Zhao J, Ji M, Gong B, Klein M and Wu K (2022) Intranasal delivery of a chimpanzee adenovirus vector expressing a pre-fusion spike (BV-AdCoV-1) protects golden Syrian hamsters against SARS-CoV-2 infection.
Front. Cell. Infect. Microbiol. 12:979641.
doi: 10.3389/fcimb.2022.979641

Intranasal delivery of a chimpanzee adenovirus vector expressing a pre-fusion spike (BV-AdCoV-1) protects golden Syrian hamsters against SARS-CoV-2 infection

Shen Wang[1†], Long Xu[2†], Ting Mu[3], Mian Qin[2], Ping Zhao[4], Liang Xie[3], Linsen Du[5], Yue Wu[4], Nicolas Legrand[6], Karine Mouchain[7], Guillaume Fichet[8], Yi Liu[2,9], Wenhao Yin[2], Jin Zhao[4], Min Ji[1], Bo Gong[1], Michel Klein[10,11*] and Ke Wu[10,11*]

[1]Regularoty and Medical Affairs Department, Wuhan BravoVax Co., Ltd., Wuhan, China, [2]Project Management Department, Wuhan BravoVax Co., Ltd., Wuhan, China, [3]Innovative Discovery Department, Wuhan BravoVax Co., Ltd., Wuhan, China, [4]Test Development Department, Wuhan BravoVax Co., Ltd., Wuhan, China, [5]China Office, Voisin Consulting Life Sciences, Shanghai, China, [6]In Vivo Sciences Department, Oncodesign, Centre François Hyafil, Villebon-sur-Yvette, France, [7]DMPK & Bioanalytical Sciences Department, Oncodesign, Centre François Hyafil, Villebon-sur-Yvette, France, [8]In Vitro Sciences Department, Oncodesign, Centre François Hyafil, Villebon-sur-Yvette, France, [9]State Key Laboratory of Biocatalysts and Enzyme Engineering, School of Life Sciences, Hubei University, Wuhan, China, [10]Executive Office, Wuhan BravoVax Co., Ltd., Wuhan, China, [11]Executive Office, Shanghai BravoBio Co., Ltd., Shanghai, China

We evaluated the immunogenicity and protective ability of a chimpanzee replication-deficient adenovirus vectored COVID-19 vaccine (BV-AdCoV-1) expressing a stabilized pre-fusion SARS-CoV-2 spike glycoprotein in golden Syrian hamsters. Intranasal administration of BV-AdCoV-1 elicited strong humoral and cellular immunity in the animals. Furthermore, vaccination prevented weight loss, reduced SARS-CoV-2 infectious virus titers in the lungs as well as lung pathology and provided protection against SARS-CoV-2 live challenge. In addition, there was no vaccine-induced enhanced disease nor immunopathological exacerbation in BV-AdCoV-1-vaccinated animals. Furthermore, the vaccine induced cross-neutralizing antibody responses against the ancestral strain and the B.1.617.2, Omicron(BA.1), Omicron (BA.2.75) and Omicron(BA.4/5) variants of concern. These results demonstrate that BV-AdCoV-1 is potentially a promising candidate vaccine to prevent SARS-CoV-2 infection, and to curtail pandemic spread in humans.

KEYWORDS

Chimpanzee Adenovirus Serotype 68, intranasal, COVID-19 vaccine, challenge study, golden Syrian hamsters

Introduction

Since the end of 2019, more than 600 million people have been infected with SARS-CoV-2 (resource: www.who.int, accessed September 4, 2022), and this number is still increasing as the coronavirus disease 2019 (COVID-19) outbreak and the virus spread globally (Velavan and Meyer, 2020). The approval and emergency usage authorization of COVID-19 vaccines worldwide have been critical in the fight against SARS-CoV-2. So far, the availability of a few licensed COVID-19 vaccines (Huang et al., 2021) has effectively mitigated the pandemic in most countries (Gee et al., 2021; Dagan et al., 2021). In this context, their protective efficacy against COVID-19 has considerably stimulated the interest of the scientific community and the general public.

Among novel approaches to prevent viral infections, the rapidly evolving adenovirus vector-based gene delivery platform has been widely used to engineer vaccines for a wide range of infectious diseases and successfully applied to the production of SARS-CoV-2 vaccines (Koirala et al., 2020). A few recombinant adenovirus-based vaccines have been efficiently administered worldwide and continue to play an important role in controlling and preventing the spread of the pandemic. At present, these vaccines include Convidecia (CanSinoBIO, China), Sputnik V (Gamaleya Institute, Russia), Vaxzevria (Oxford/AstraZeneca, UK), Covishield (India), and AD26.COV2.S (Johnson & Johnson, USA) (Sadoff et al., 2021; Wu et al., 2021; Zare et al., 2021). All adenovirus-based vaccines currently on the market are based on the full-length spike protein (S), are administered intramuscularly and do not induce the mucosal immunity necessary to fully protect against infection and prevent virus shedding and transmission. The SARS-CoV-2 spike which mediates receptor binding and membrane fusion is the primary target for virus neutralization and thus, the immunogen of choice in the design of new-generation COVID-19 vaccines. Viral glycoproteins stabilized in an optimal trimeric prefusion conformation are superior immunogens to their wild-type counterparts (Pallesen et al., 2017; Hsieh et al., 2020). Several vaccines based on SARS-CoV-2 pre-fusion spike have excellent neutralizing activities, including pre-S adjuvanted in ASO3 or alum/CpG (Richmond et al., 2021), delivered with the Ad26 adenovirus vector (Mercado et al., 2020), exposed on nanoparticles (Keech et al., 2020) or encoded by mRNAs (Corbett et al., 2020; Jackson et al., 2020).

Ideally, new-generation vaccines should induce balanced, durable humoral and Th1 T-cell responses as well as mucosal immunity. Mucosal immunization elicits both systemic immune responses and long-lasting protective immunity in the upper and lower respiratory tracts. In contrast to intramuscular vaccination, mucosal immunization is a non-invasive procedure and is the only approach to induce potent and long-lasting secretory IgA responses (sIgA). Robust local immunity at the ports of virus entry should be more efficient at controlling virus infection, replication, shedding and transmission than systemic immunization. Several intranasal and oral vaccines are currently being evaluated in pre-clinical and clinical studies (Kar et al., 2022). They should allow for large-scale vaccination to achieve herd immunity.

The golden Syrian hamster model has been extensively used to study human infectious diseases. *In silico* studies revealed that the angiotensin-converting enzyme 2 (ACE2) receptor of the Syrian hamster is highly homologous to its human counterpart and that it could thus efficiently interact with the SARS-CoV-2 receptor-binding domain (RBD) (Chan et al., 2020; Rosenke et al., 2020) and render animals susceptible to SARS-CoV-2 infection. Indeed, animals challenged intranasally with SARS-CoV-2 isolates consistently showed progressive weight loss, exhibited labored breathing, developed manifestations of disease similar to those of COVID-19 pneumonia observed in humans, as well as other morbidity signs including lethargy, ruffled fur, and hunch posture. Animals may also develop more acute and severe diseases, mimicking severe clinical cases of COVID-19 (O'Donnell et al., 2021; Bednash et al., 2022). Recent results have shown that SARS-CoV can replicate in high titers in both the upper and lower respiratory tracts of infected hamsters that develop pulmonary pathology (Roberts et al., 2005). Thus, golden Syrian hamsters are a valuable model to study the pathogenesis of SARS-CoV-2, evaluate the protective efficacy of COVID-19 vaccines and assess the risk of potential disease enhancement in immune animals challenged with live virus.

We are here reporting that intranasal (IN) delivery of a novel chimpanzee adenovirus vector (Chimpanzee Adenovirus Serotype 68, AdC68) vaccine (BV-AdCoV-1) expressing a stabilized SARS-CoV-2 prefusion spike trimer confers excellent protection in vaccinated golden Syrian hamsters challenged with the ancestral SARS-CoV-2 strain. It also induces cross-neutralizing immunity against the B.1.617.2 (Delta), Omicron (BA.1), Omicron (BA.2.75) and Omicron (BA.4/5) variants of concern (VOCs), indicating that BV-AdCoV-1 could be an efficacious next-generation mucosal COVID-19 vaccine for primary and heterologous booster immunization strategies.

Materials and methods

Vector design, construction and production

The replication-deficient AdC68 derived from the E1/E3 gene-deleted chimpanzee adenovirus type 68 (Suzhou Xiangyi Biotechnology Co., Ltd., China) was engineered to encode a trimeric pre-fusion SARS-CoV-2 spike glycoprotein (pre-S). The spike gene was derived from the SARS-CoV-2 Wuhan-Hu-1 strain. To stabilize the pre-fusion spike conformation (Hsieh et al., 2020), two amino acid residues at positions 986/987 were

mutated to prolines (pre-S-2P) and the furin protease cleavage site (residues 682-685) was replaced with GSAS in the wild-type spike glycoprotein (GeneBank ID: MN908947) (Figure 1A). The transmembrane and intracellular domains (1202-1273) were replaced by the foldon domain of the Phage T4 fibritin protein and the JEV signal peptide fused to the N-terminal was substituted to the original signal peptide. The codon-optimized DNA fragment encoding the modified spike protein was synthesized by Sangon Biotech Co., Ltd. (China), and cloned into the plasmid pAdC68 backbone. The recombinant plasmid containing the expression cassette pAdC68-PreS harboring the pre-fusion spike gene was linearized and transfected into HEK293A cells (Invitrogen, R70507) to rescue the recombinant adenovirus vector (rAdC68-PreS). HEK293A cells were cultured, grown and maintained in DMEM (Gibco, 12100-061) supplemented with 10% FBS in an incubator at 37 °C in 5% CO_2. After plaque purification, the recombinant adenovirus was propagated in HEK293A suspension cell cultures and purified by ion-exchange and size-exclusion chromatography (SEC) to produce BV-AdCoV-1. The number of virus particle (VP) was measured by ultraviolet spectrophotometry, and infectious titers were assessed by immunocytochemistry (ICC).

Expression of trimeric pre-S-2P

To confirm pre-S expression, cell lysates and culture supernatants were mixed with reducing sample buffer [0.25 M Tris HCl (pH 6.8), 40% glycerol, 8% SDS, 5% 2-mercaptoethanol and 0.04% bromophenol blue] and boiled for 10 minutes at 65°C. Proteins resolved by SDS-polyacrylamide gel electrophoresis were transferred to polyvinylidene fluoride membranes, blocked with 5% non-fat powdered milk in PBST (0.5% Tween-20) and probed with rabbit antibodies against SARS-CoV-2 spike RBD (1:2000, Sino Biological, China) at 4°C overnight. Goat Horseradish Peroxidase (HRP)-conjugated secondary antibody

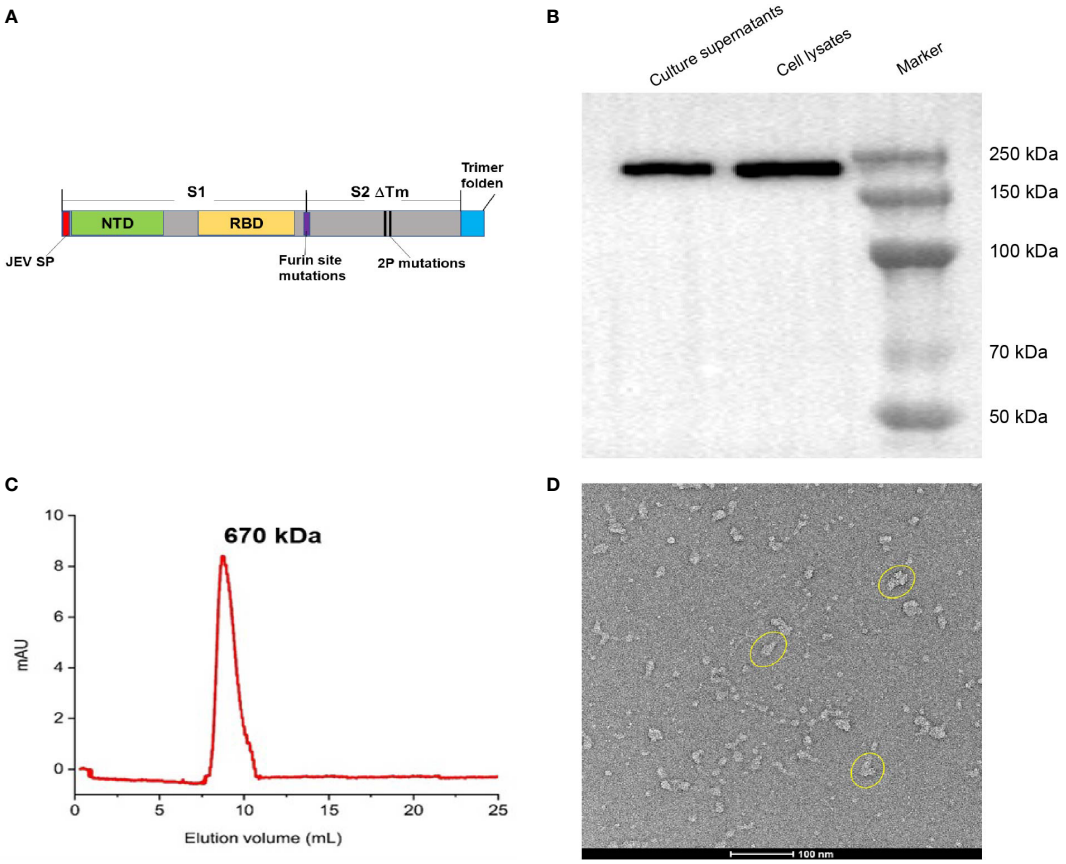

FIGURE 1
Construction and characterization of BV-AdCoV-1. **(A)** Schematic diagram of the DNA sequence coding for the trimeric prefusion spike (Pre-S). The extracellular domain of SARS-COV-2 spike protein (1-1201 aa) was fused to the T4 fibritin trimerization motif, and the original spike's signal peptide was replaced by the Japanese encephalitis virus E protein signal peptide (JEV SP). Mutations in the furin cleavage site and proline substitutions (K986P, V987P) were introduced. **(B)** Western blot analysis of HEK 293 cell lysate and supernatant. **(C)** Pre-S protein elution profile on a calibrated Superdex 200 increase 10/300 GL. **(D)** Cryo-EM picture of purified pre-S protein.

(1:2000, BBI, China) was then added for 1 hour at 37°C. Protein bands were detected using Tanon 5200 Chemiluminescent Imaging System (Tanon, China). Quantity One software was used to calculate molecular weights.

Culture supernatants were further concentrated and purified by anion-exchange chromatography (HiTrap Capto Q 5 × 5mL, Cytiva) followed by size-exclusion chromatography (Superdex 200 increase 10/300 GL, Cytiva) using 0.01 M phosphate buffer, 0.14 M NaCl, pH 7.4 as elution buffer, Purified pre-S was submitted to cryo-electron microscopy (Cryo-EM), and SEC-HPLC analysis. The molecular weight of trimeric pre-S was calculated according to the retention time in the column using Origin software. The purified pre-S protein was negatively stained, deposited onto a copper grid and imaged by 120 kV Cryo-EM (Talos L120C G2).

Immunization and live virus challenge of golden Syrian hamsters

The challenge study in golden Syrian hamsters was performed in a Biosafety Level 3 (BSL-3) laboratory at Oncodesign Biotechnology (France), the animal facility (CFH: Agreement N° B91962106) and BSL-3 facility (Agreement N° D92-032-02). Animal housing and experimental procedures were conducted according to the French and European Regulations and the National Research Council Guide for the Care and Use of Laboratory Animals. All animal procedures (including surgery, anesthesia and euthanasia as applicable) used in the current study were submitted to the Institutional Animal Care and Use Committee of Oncodesign (CNREEA Agreement N° 91) and the CEA (Commissariat à l'Energie Atomique et aux Energies Alternatives Paris-Saclay; Agreement No. CETEA DSV n° 44) approved by French authorities.

Female golden Syrian hamsters at 6-8 weeks of age were purchased from Janvier Labs (France). Animals were randomized into 4 homogeneous groups (n=12) and one negative control group (3 hamsters, non-treated, not infected) according to weight. The 4 homogeneous groups included a Saline intranasal administration group (12 hamsters, Saline), an AdC68-empty vector intranasal administration group (3.4×10^{10} VP/dose, 12 hamsters, AdC68-empty, vector control), a low-dose BV-AdCoV-1 intranasal administration group (3.4×10^{9} VP/dose, 12 hamsters, low-dose vaccine), and a high-dose BV-AdCoV-1 intranasal administration group (3.4×10^{10} VP/dose, 12 hamsters, high-dose vaccine). The details about grouping and vaccination schedule of golden Syrian hamsters are shown in Table 1. The challenge dose for each animal was 10^5 plaque-forming units (PFU) of SARS-CoV-2 (Slovakia/SK-BMC5/2020 isolate which contained the D614G mutation was provided by the European Virus Archive global [EVAg]–GISAIDEPI_ISL_417879, https://www.european-virus-archive.com/virus/sars-cov-2-strain-slovakiask-bmc52020), in a volume of 70 µL (35 µL per nostril). Among the 12 animals in the Saline, AdC68-empty, low-dose vaccine and high-dose vaccine groups, 6 animals were sacrificed 3 days post-challenge, while the remaining 6 animals were sacrificed 7 days post-challenge. The schedule of vaccine administration and virus challenge is shown in Figure 2A.

To explore the cross-neutralizing activity of BV-AdCoV-1 immune sera against VOCs, another immunogenicity study was conducted in China.

Female golden Syrian hamsters at 6-8 weeks of age were purchased from Beijing Vital River Laboratory Animal Technology Co., Ltd. (China). The immunogenicity study was conducted in the Wuhan Myhalic Biotechnological Co., Ltd. (China). The vaccination protocol was approved by the Animal Ethics Committee (No. HLK-20220630-001 for hamsters) of Wuhan Myhalic Biotechnological Co., Ltd.

Animals were randomized into 4 homogeneous groups (n=6). The 4 homogeneous groups included a Saline intranasal administration group (6 hamsters, Saline), an AdC68-empty vector intranasal administration group (3.4×10^{10} VP/dose, 6 hamsters, AdC68-empty, vector control), a low-dose BV-AdCoV-1 intranasal administration group (3.4×10^{9} VP/dose, 6 hamsters, low-dose vaccine), and a high-dose BV-AdCoV-1 intranasal administration group (3.4×10^{10} VP/dose, 6 hamsters, high-dose vaccine). The details about grouping and vaccination schedule of golden Syrian hamsters are shown in Table 2 and Figure 3A.

TABLE 1 Grouping of golden Syrian hamsters and vaccine dose.

Group	No. animals	Test	Injections (intranasal)	Dosage/injection	End point
Negative control	3	–	NA	NA	D49
Saline	6	Saline	NA	NA/70 µL	D45
	6				D49
AdC68-empty	6	AdC68-empty	D0, D28	3.36×10^{10}VP/70 µL	D45
	6				D49
Low-dose vaccine	6	BV-AdCoV-1	D0, D28	3.40×10^{9} VP/70 µL	D45
	6				D49
High-dose vaccine	6	BV-AdCoV-1	D0, D28	3.40×10^{10}VP/70 µL	D45
	6				D49

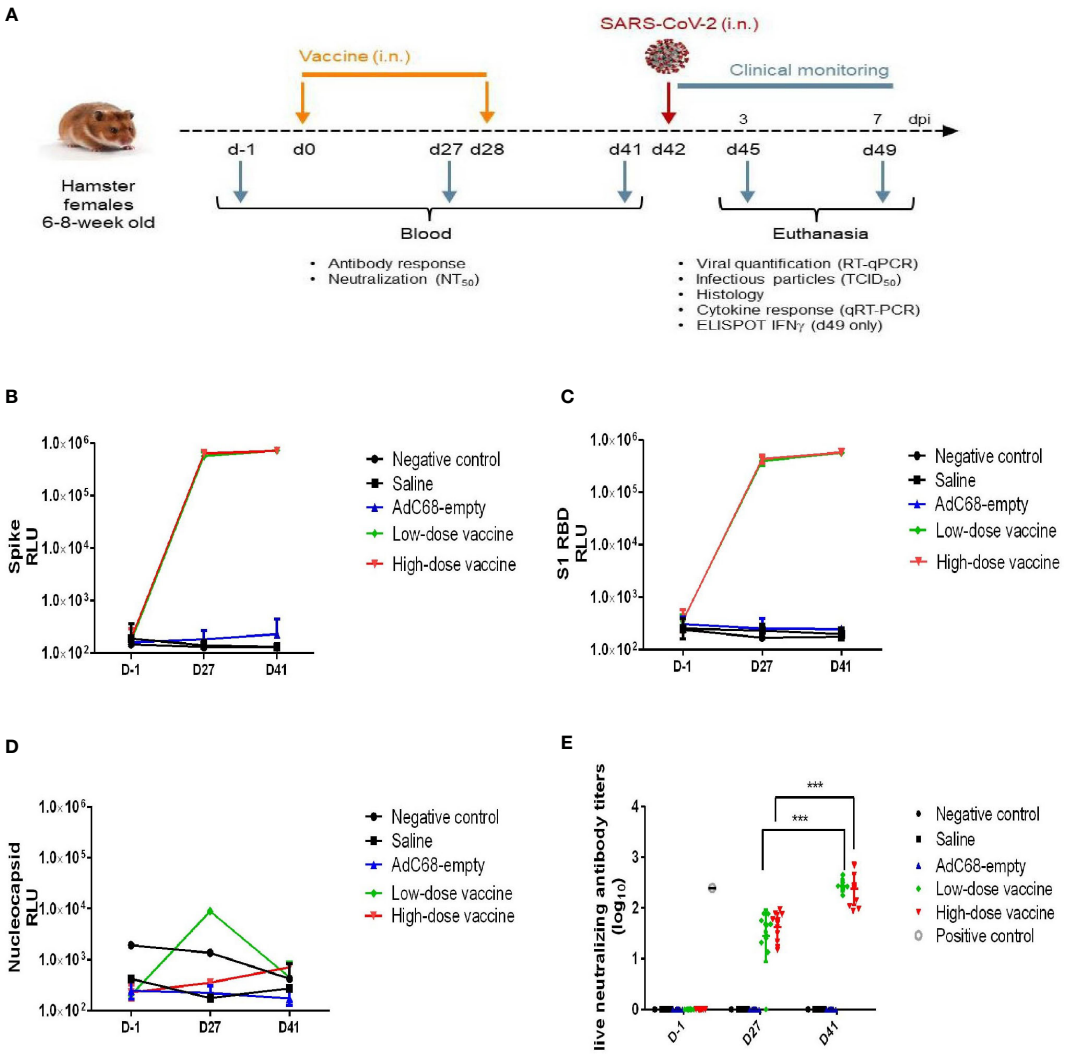

FIGURE 2
Experimental study scheme and anti-SARS-CoV-2 antibody detection. **(A)** Schedule of vaccine administration and virus challenge. dpi (days post-infection). **(B)** Binding anti-spike IgG antibody in golden Syrian hamsters' sera. The antibody level was determined by Multiplex ELISA. **(C)** Binding anti-S1 RBD IgG antibody in golden Syrian hamsters' sera. The antibody levels were determined by Multiplex ELISA. **(D)** Anti-nucleocapsid IgG antibody in golden Syrian hamsters' sera. The antibody level was determined by Multiplex ELISA. **(E)** Live neutralizing antibody titers in golden Syrian hamsters' sera. The neutralizing antibody level was determined by live SARS-CoV-2 cytopathogenicity-based assay. ***$p < 0.001$.

Binding antibody titers determination by Multiplex ELISA in the challenge study

Binding IgG responses against SARS-CoV-2 in hamster sera were analyzed using V-PLEX SARS-CoV-2 Panel 2 plates from Meso Scale Discovery (kit K15383U, USA). Responses to the S, S1 RBD and N antigens were quantified using a multiplex approach. MULTI-SPOT plates were provided with antigens coated on spots in the wells of a 96-well plate. Antibodies bound to the spots were detected using goat anti-Syrian hamster IgG (H and L chains) antibodies (Abcam, reference ab102314) conjugated with MSD SULFO-TAG using the MSD GOLD™ SULFO-TAG TM NHS-Ester kit (MSD, reference R91AO-1). The plates were read on a MESO Quickplex SQ120 imager that measured the light emitted from the MSD SULFO-TAG, and the results were analyzed using the associated software (Discovery Workbench).

Live virus neutralization assay in the challenge study

Sera were inactivated at 56°C for 30 minutes before the neutralization assay. They were diluted with DMEM medium

TABLE 2 Grouping of golden Syrian hamsters and vaccine dose.

Group	No. animals	Test	Injections (intranasal)	Dosage/injection
Saline	6	Saline	NA	NA/70 μL
AdC68-empty	6	AdC68-empty	D0, D28	3.40×10^{10}VP/70 μL
Low-dose vaccine	6	BV-AdCoV-1	D0, D28	3.40×10^{9} VP/70 μL
High-dose vaccine	6	BV-AdCoV-1	D0, D28	3.40×10^{10}VP/70 μL

containing 2% FBS at an initial dilution of 1:5 (v:v), then three-fold diluted to perform the assay. Samples were then mixed (1:1, v:v) with 0.01 MOI per well of SARS-CoV-2 virus (Slovakia/SK-BMC5/2020 isolate) for 30 minutes at room temperature to allow antibody binding to the virus. The virus-antibody mixture (50 μL) was added to Vero E6-TMPRSS2 cells (2×10^4 cells/well) in 200 μL complete growth medium, and further incubated for 2 hours at 37°C, 5% CO_2 to allow viruses to infect target cells. Subsequently, 150 μL of complete cell growth medium (containing 2% FBS) were added to each well. The plates were further incubated for 48 hours at 37°C, in 5% CO_2. After removing 100 μL of supernatant from each well, 100 μL of fresh medium and 20 μL of MTS-PMS reagent (Cell Titer 96®AQueous Non-Radioactive Cell Proliferation Assay, Promega reference G5421) were added for colorimetric determination of the viable cell number. Plates were read using an ELISA plate reader, and data were recorded (acceptance criteria when OD_{450nm} of control cells >1.5). The neutralizing antibody titer (NT_{50}) was defined as the reciprocal of the highest serum dilution that provided ≥50% inhibition of

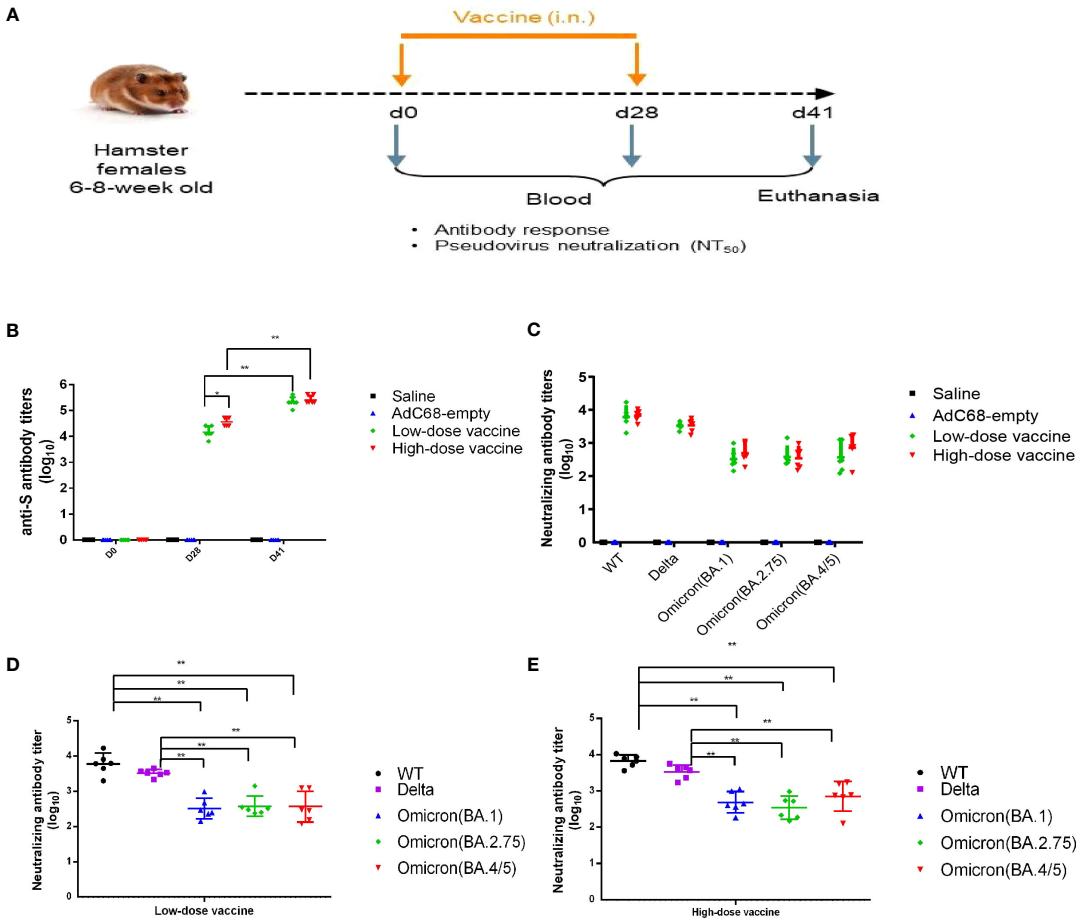

FIGURE 3
Experimental study scheme and cross-neutralizing antibody titers. **(A)** Schedule of vaccine administration. **(B)** Binding anti-spike IgG antibody titers in golden Syrian hamsters' sera. **(C–E)** Cross-neutralizing antibody titers in golden Syrian hamsters' sera. *$p < 0.05$, **$p < 0.01$.

virus infectivity. The NIBSC pooled convalescent serum reference (WHO international standard for anti-SARS-CoV-2 human immunoglobulin, NIBSC reference 20/136) was used as positive control.

Binding antibody titers determination by ELISA in the immunogenicity study

Binding IgG titers in immune sera were measured by ELISA. 96-well plates were coated with 0.05 μg of full-length S protein (Genscript Inc., China) overnight at 4°C and blocked with phosphate-buffered saline (PBS) supplemented with 0.05% Tween-20 (PBST) and 10% NON-Fat Powdered Milk for 2 hours at 37 °C. The microplates were then washed three times with PBST. Sera samples were serially diluted 2-fold and added to the wells. After further incubation for 1 hour at 37°C, plates were washed three times with PBST and 100μL of horseradish peroxidase (HRP)-conjugated goat anti-hamster IgG antibody (1:5000; abcam, ab6892) was added to wells. After incubation for another 1 hour at 37°C, plates were washed three times with PBST and then 100μL of 3,3',5,5 -tetramethylbenzidine (TMB) substrate was added to wells. Following a 12-15 minutes incubation at room temperature in the dark, reactions were stopped with 100μL of 1M sulfuric acid. The optical density was measured at 450 nm. The cutoff value was calculated as 2.1 times the mean $OD_{450\ nm}$ values obtained for samples from non-vaccinated animals. The endpoint titer was calculated as the reciprocal of the highest sample dilution at which the $OD_{450\ nm}$ value was equal to or greater than the cutoff value.

Pseudovirus neutralizing antibody titers determination in the immunogenicity study

Sera were inactivated at 56°C for 30 minutes, 4-fold serially diluted with cell culture medium and added to a 96-well plate at 100 μL/well. Pseudoviruses at 1.3×10^4 $TCID_{50}$/mL were added (50 μL/well) to the plate. The mixtures were incubated at 37°C, 5% CO_2 for 1 hour, along with a negative control and a virus control. 100 μL of Vero cells were added to the 96-well plate at 2×10^4 cells/well. Plates were incubated at 37°C, 5% CO_2 for 24 hours. Finally, the plates were analyzed according to the luciferase assay kit instructions (PerkinElmer, 6066761). The Reed-Muench method was used to calculate the 50% inhibitory concentration (IC_{50}) value.

Pseudoviruses included SARS-CoV-2 ancestral pseudovirus (WT), B.1.617.2 (Delta), Omicron (BA.1), Omicron (BA.2.75) and Omicron (BA.4/5) pseudoviruses. They were purchased from Beijing Yunling Biotechnology Co., Ltd. (China), company related to the China National Institutes for Food and Drug Control.

Enzyme-linked immunospot assay (ELISpot)

T-cell responses against SARS-CoV-2 antigens were evaluated in a hamster ELISpot IFN-γ assay (Mabtech, 3102-2A). The kit was used according to the manufacturer's instructions. Briefly, live immune splenocytes were isolated, counted and re-stimulated with specific 15-mer peptide pools with 11 amino-acid overlap (JPT; PepMix SARS-COV2 S-RBD, reference PM-WCPV-S-RBD-2; PepMix SARS-COV-2 Spike, reference PM-WCPV-S-2; PepMix SARS-COV2 NCAP, reference PM-WCPV-NCAP-2). The ELISpot assay was performed in triplicates at two cell densities (200×10^3 and 60×10^3 cells per well), comparing different conditions: medium only; PMA (20 ng/mL) and ionomycin (1 μM) mix as positive control; peptide pool (2 μg/mL). A lower cell density (10×10^3 cells per well) was used for the PMA/ionomycin positive control. Plates were placed in an incubator at 37 °C in 5% CO_2 for 24 hours after which time cells were removed, and IFN-γ-producing cells were detected as recommended by the manufacturer.

Virus load determination in lung homogenates by RT-qPCR

The extraction of total RNA and its conversion to cDNA were conducted according to the manufacturer's instructions (Macherey nagel Nucleo Spin 96 RNA, 96-well kit, Applied Biosystem Kit). The number of relative levels of RNA (target gene cycle threshold [Ct] value) in the lungs was determined by real-time quantitative PCR (RT-qPCR) after reverse transcription. Quantification of viral loads by RT-qPCR was done using the ORF1ab gene. The primer set for ORF1ab was 5'-CCGCAAGGTTCTTCTTCGTAAG-3', and the probe set for ORF1ab was 5'-TGCTATGTTTAGTGTTCCAGTTTTC-3'. SYBR Green technology was used for PCR product detection and quantification. Results are expressed as a $2^{-\Delta Ct}$ value relative to the γ-actin house-keeping gene for normalization between samples.

Cytokine response profiling by RT-qPCR

Cytokine gene expression in the lungs was determined for 9 target genes: TNF-α, IFN-γ, IL-2, IL-4, IL-5, IL-6, IL-10, IL-12p40, IL-21. The extraction of total RNA and its conversion to cDNA were conducted according to the manufacturer's instructions (NucleoSpin 96 RNA, 96-well kit, Applied Biosystem Kit). cDNA quantification (target gene Ct value) by real-time quantitative PCR was performed with primers targeting the cytokine genes (Table 3). Amplification was performed using a QuantStudio 7 Flex from Applied Biosystem and adjoining software. SYBR Green technology

was used for PCR product detection and quantification. Results are expressed as a $2^{-\Delta Ct}$ value relative to the γ-actin housekeeping gene for normalization between samples.

Virus 50% tissue culture infectious dose ($TCID_{50}$) determination

According to L. J. Reed (Reed and Muench, 1938), Vero E6/TMPRSS2 cells were plated at a density of 2×10^4 cells per well in 200 µL of complete growth medium. Cells were then infected with serial dilutions of the lung homogenates in duplicate for 1 hour at 37°C and fresh medium was added. Two days after cell infection, an MTS/PMS assay was performed according to the manufacturer's instructions (Promega, G5430). $TCID_{50}$ was defined as the amount of pathogen that caused the death of 50% of target cells. Infectivity was expressed as $TCID_{50}$/g of lungs (over 48-hour culture) based on the Spearman-Karber formula. The lower limit of detection of the assay is 520 $TCID_{50}$/g of lung tissue.

Lung histopathology

Left lung lobe specimens were embedded in paraffin. 5 µm-thick sections were cut, mounted on SuperFrost plus glass slides and stained with Hematoxylin-Phloxine to visualize histomorphometric changes. Slides were scanned using the NanoZoomer Digital Pathology System C9600-02.

Histopathology scores were determined for each one of the four sections generated from the collected lobe, as an aggregate of the following parameters: (i) percentage of tissue area showing signs of inflammation (presence of inflammatory leucocyte infiltrates): 0, no pathological change; 1, ≤10% affected area; 2, >10% to <50% affected area; 3, ≥50% affected area; (ii) pulmonary edema (0: absent; 1: present); and (iii) alveolar hemorrhage (0: absent; 1: present) (Imai et al., 2020). The average score for four sections is shown for each individual animal.

TABLE 3 Primer sequences for each target cytokine gene.

Primers and probes	
Name	**Sequences (5'-3')**
TNF-α	Fw : TGAGCCATCGTGCCAATG Rv : AGCCCGTCTGCTGGTATCAC
IFN-γ	Fw : TGTTGCTCTGCCTCACTCAGG Rv : AAGACGAGGTCCCCTCCATTC
IL-2	Fw :CCAGTGCCTGGAAGAAGAACTT Rv : CATCTTCCAAGTGAAAGCTTTTGCT
IL-4	Fw :ACAGAAAAAGGGACACCATGCA Rv : GAAGCCCTGCAGATGAGGTCT
IL-5	Fw : GTTCCTGCACATAAAAATCACC Rv : AACTGCTTCACTCTCCGTC
IL-6	Fw : AGACAAAGCCAGAGTCATT Rv : TCGGTATGCTAAGGCACAG
IL-10	Fw : GGTTGCCAAACCTTATCAGAAATG Rv : TTCACCTGTTCCACAGCCTTG
IL-12p40	Fw : AATGCGAGGCAG CAAATTACTC Rv : CTGCTCTTGACGTTGAACTTCAAG
IL-21	Fw : GGACAGTGGCCCATA AAACAAG Rv : TTCAACACTGTCTATAAGATGACGAAGTC

Statistical analysis

The data were processed using the Graphpad software. Results reported in this study are expressed as means ± standard deviation (SD). Differences were identified using ANOVA and considered to be significant when p <0.05, 0.01, 0.001 and 0.0001.

Results

Generation and characterization of BV-AdCoV-1

We constructed a recombinant AdC68-vectored vaccine (BV-AdCoV-1) to express a trimeric pre-fusion spike in infected cells. The pre-fusion conformation was stabilized by S-2P mutations and the furin cleavage site was mutated. Deletion of the transmembrane and intracellular domains facilitated the secretion of the immunogen. The foldon domain caused the secreted spike protein to form a trimer, in a conformation similar to that of its native state on the surface of the virion. BV-AdCoV-1 was successfully rescued and propagated in HEK293A cell line. Cell lysates and culture supernatants analyzed by SDS PAGE under reducing conditions followed by Western blotting revealed the presence of a 222 kDa monomeric pre-S protein (Figure 1B and Supplementary Material 1). Pre-S was further purified from the culture supernatants of HEK293A cells and shown to be a homogeneous trimer with a molecular mass of 670 kDa according to the retention time measured by analytical size-exclusion chromatography (Figure 1C). The pre-S protein was negatively stained and deposited onto a copper grid and observed by 120 kV Cryo-EM (Figure 1D). Cryo-EM analysis also showed that pre-S formed trimers.

BV-AdCoV-1 elicits robust antibody responses

In the challenge study, BV-AdCoV-1 at both low and high dose elicited very high levels of anti-S, anti-S1 RBD binding IgG antibody responses (Figures 2B, C) on 27 days after a single intranasal administration, while background levels of anti-nucleocapsid binding IgG antibody responses were low in all golden Syrian hamsters (Figure 2D). Binding antibody titers among the two

groups did not differ significantly, which may be related to the high immunogen doses (≥ 3.4×10^9 VP/dose) used for golden Syrian hamsters. Geometric means titer (GMT) of neutralizing antibody titers for the low- and high-dose vaccine groups were 239 and 276, respectively, 41 days after the first vaccination, while the neutralizing antibody titer of the NIBSC reference was 251 (Figure 2E). The neutralizing antibody responses to the low and high vaccine doses were similar and both increased significantly (p <0.001) after the booster administration.

In the immunogenicity study, the levels of anti-S binding IgG antibody titers were very high in the low-dose and high-dose vaccine groups and could be further boosted. There was no significant difference (p >0.05) between the low- and high-dose vaccine groups after a second administration (Figure 3B). Immune sera from the low- and high-dose vaccine groups had high levels of neutralizing antibody titers against pseudoviruses of WT and Delta strains, although neutralizing titers against the Delta strain were slightly lower. GMT of pseudovirus neutralizing antibody titers against WT for the low- and high-dose vaccine groups were 6045 and 6721, respectively, while GMT of neutralizing antibody titers against the Delta pseudovirus were 3289 and 3400, respectively, 41 days after the first vaccination. The neutralizing antibody titers against Omicron (BA.1), Omicron (BA.2.75) and Omicron (BA.4/5) pseudoviruses were 10-20-fold and 4-10-fold reduced (p <0.01) but still substantial, compared to those against the WT and Delta strains, respectively (Figures 3B–E).

Cellular immunity induced by BV-AdCoV-1

In the low- and high-dose vaccine groups (dpi 7, days post-infection 7), IFN-γ signals were significantly higher when

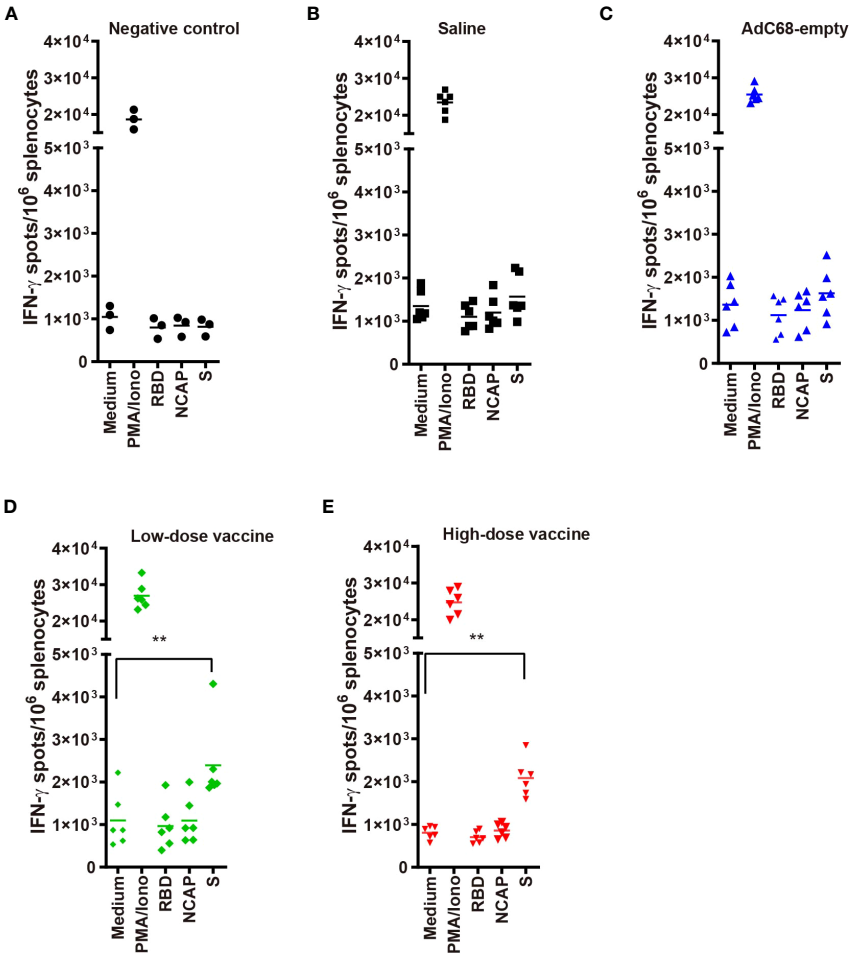

FIGURE 4
(A–E) IFN-γ ELISpots in golden Syrian hamsters' splenocytes re-stimulated with: medium-only (negative control); PMA and ionomycin (positive control); and peptide pools from RBD, nucleocapsid (N) and spike (S). T-cell responses against SARS-CoV-2 antigens were evaluated using a hamster ELISpot IFN-γ kit at dpi 7. **p<0.01.

immune splenocytes were stimulated with a spike peptide cocktail (p <0.01) whereas the IFN-γ signal did not significantly increase when splenocytes were stimulated with either RBD or N peptides compared with medium (Figure 4). In contrast, IFN-γ signals after stimulation with a spike peptide cocktail were similar to that of medium in the Negative control, Saline and AdC68-empty groups. The differences observed between responses to spike and RBD peptide pools could be explained by the lack of strong RBD T-cell epitopes recognized by Syrian hamster MHC haplotypes. The N peptide pool served as a negative control.

Clinical disease in golden Syrian hamsters

Golden Syrian hamsters were infected with 10^5 PFU of SARS-CoV-2 and inspected daily for up to 7 days. Changes in body weight (BWC) decreased in the Saline and AdC68-empty groups from 2 days post infection (dpi 2). Comparative analysis of the negative control group and infected Saline-treated animals clearly showed that infection led to significant body weight losses from days 2 to 7 post infection (dpi 2, dpi 3 and dpi 5 to dpi 7) and those hamsters did not even recover their original weight 7 days post infection. In marked contrast, the BWC pattern in animals vaccinated with BV-AdCoV-1 was similar to that of the negative control group, with body weight changes of ≥100% from dpi 3 to dpi 7 (Figure 5). These data clearly showed that immunization with BV-AdCoV-1 prevented weight loss due to SARS-CoV-2 infection.

Protection against SARS-CoV-2 disease

To assess the protective ability of BV-AdCoV-1 against SARS-CoV-2 disease, relative levels of RNA in the lungs, lung virus infectious doses ($TCID_{50}$) and lung histopathology were examined at dpi 3 and dpi 7. At dpi 3, mean $TCID_{50}$ was similar between the Saline and AdC68-empty groups. In contrast, mean $TCID_{50}$ was dramatically decreased in both the high-dose and low-dose vaccine groups (947 and 583 $TCID_{50}$/g, respectively), representing a 10^5-10^4-fold reduction. This result also indicates that the immune response had already plateaued at the lowest vector dose. Mean $TCID_{50}$ reached a baseline level of 520 $TCID_{50}$/g in all groups at dpi 7 (Figure 6A). At dpi 3, mean viral levels of ORF1 RNA in the high-dose vaccine group (0.04 $2^{-\Delta ct}$) and low-dose vaccine group (0.01 $2^{-\Delta ct}$) were similar and significantly lower (p <0.01) than those in the Saline and AdC68-empty groups. Mean expression reached a baseline level of ≤0.01 $2^{-\Delta ct}$ in all groups at dpi 7 (Figure 6B).

We next assessed the effect of BV-AdCoV-1 on lung inflammation and disease. Several proinflammatory cytokines (TNF-α, IFN-γ, IL-2, IL-4, IL-5, IL-6, IL-10, IL-12p40, IL-17, IL-21) RNA levels were measured in lungs at dpi 3 and dpi 7 (Figures 7, 8). The results were expressed as the relative mean cytokine expression level for each group, as compared to the negative control group. Infection with SARS-CoV-2 induced a significant increase in IFN-γ (p <0.0001), IL-6 (p <0.0001) and IL-10 (p <0.0001) expression in the lung tissue of the Saline group and AdC68-empty group animals at dpi 3, while induction of IL-6 (Saline group: p <0.0001) and IL-10 (Saline group: p <0.0001; AdC68-empty group: p <0.001) at dpi 7 was maintained. In the vaccinated animals (low- and high-dose vaccine groups), IFN-γ, IL-6 and IL-10 levels measured at both time points were not significantly different from those of the negative control group. The levels of IL-2, IL-5, IL-12p40 and IL-21 in animals of the Saline group and AdC68-empty group showed a trend towards increased lung expression at dpi 3, but these values were not statistically significant. The levels of TNF-α, IL-4 and IL-17 did not show any significant sign of induction after SARS-CoV-2 infection.

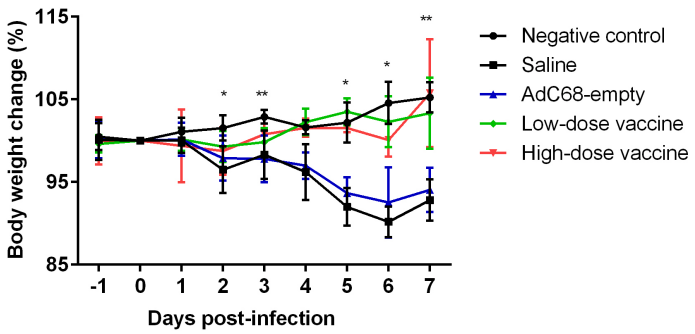

FIGURE 5
Body weight changes in golden Syrian hamsters after live challenge. Data presented as mean ± SD of values. *P<0.05 or **P<0.01 between Negative control and Saline. Intergroup statistical analysis was performed using a two-way ANOVA test, using the infected, saline-treated group as a reference.

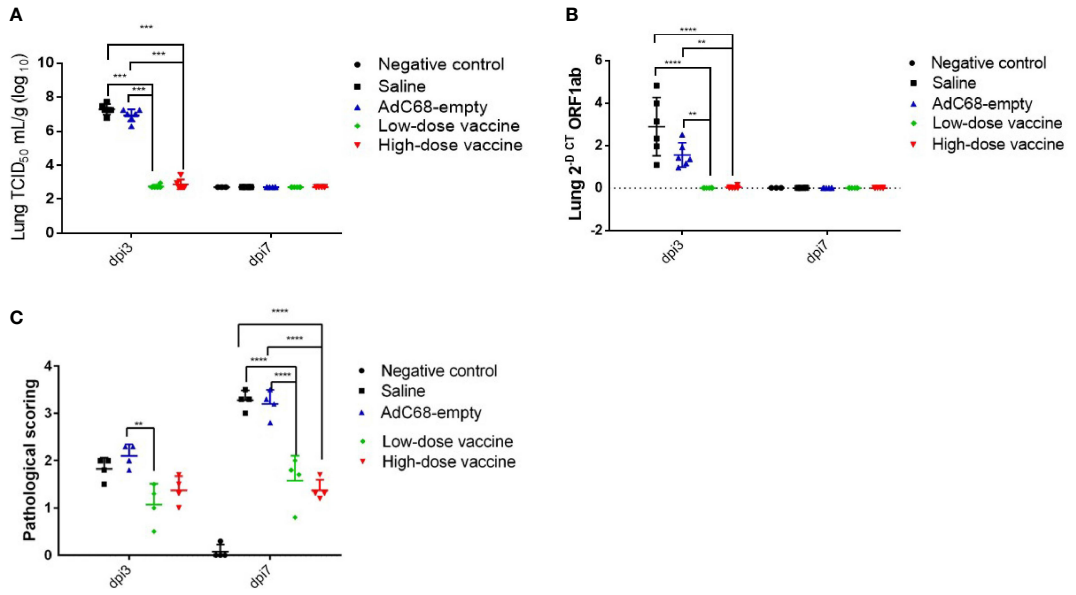

FIGURE 6
Intranasal BV-AdCoV-1 vaccination protects golden Syrian hamsters from SARS-CoV-2 infection. **(A)** SARS-CoV-2 virus infection titers in the lungs of golden Syrian hamsters were defined as the virus 50% tissue culture infectious dose ($TCID_{50}$). **(B)** SARS-CoV-2 relative levels of RNA in the lungs of golden Syrian hamsters. **(C)** Lung histopathology scores in golden Syrian hamsters. Left lung slides were stained with Hematoxylin-Phloxine to visualize histomorphometric changes. Slides were scanned using the NanoZoomer Digital Pathology System C9600-02. $^{**}p < 0.01$, $^{***}p < 0.001$, $^{****}p < 0.0001$.

Moreover, mean histopathology scores ≥3 in animals in the Saline group and AdC68-empty group were dramatically higher than those in the negative control group (mean histopathology score of 3 animals was below 0.1). BV-AdCoV-1 vaccination markedly reduced mean histopathology scores (1.08 and 1.38, respectively) in the lungs of the low-dose and high-dose vaccine groups at dpi 7 (p <0.01), respectively (Figure 6C). BV-AdCoV-1 vaccination reduced lung inflammation (as evidenced by reduced inflammatory leucocyte infiltrates in the lung tissue) and edema (tissue swelling) in golden Syrian hamsters challenged with SARS-CoV-2 (Supplementary Material 2).

Overall, vaccination with BV-AdCoV-1 could protect the lungs of immunized golden Syrian hamsters from an infectious SARS-CoV-2 challenge and induces cross-neutralizing antibody protection against WT, and the Delta, Omicron (BA.1), Omicron (BA.2.75) and Omicron (BA.4/5) variants of concern.

Discussion

In spite of the remarkable efficacy of approved injectable COVID-19 vaccines which induce neutralizing antibodies, elicit polyfunctional T-cell responses and confer protection, new-generations of vaccines stimulating the mucosa-associated lymphoid tissue (MALT) are needed to provide not only systemic responses but also strong long-lasting mucosal immunity to limit virus infection, minimize shedding and prevent transmission (Tiboni et al., 2021). Injectable adenovirus-based SARS-CoV-2 vaccines expressing the full-length spike have efficiently conferred protection in animals and humans (Mendonça et al., 2021). Currently, several adenovirus-vectored SARS-CoV-2 vaccines are being evaluated for their ability to elicit mucosal immunity in the upper and lower respiratory tracts using intranasal administration (Dhama et al., 2022).

In this study, we report that intranasal vaccination of golden Syrian hamsters with BV-AdCoV-1, a chimpanzee adenovirus-vectored vaccine expressing a stabilized SARS-CoV-2 pre-fusion S-2P protein confers immunoprotection against live SARS-CoV-2 challenge and elicits broad cross-neutralizing antibody against prevalent epidemic strains, including the current Omicron (BA.1), Omicron (BA.2.75) and Omicron (BA.4/5) variants of concern. The Syrian hamster model has proved to be a valuable model to evaluate SARS-CoV-2 pre-S and full-length S-based vaccines (Hassan et al., 2020; Doremalen et al., 2021; Lubbe et al., 2021; Boudewijns et al., 2022). A stabilized pre-S spike was used as immunogen since it was reported that the MERS S-2P protein was better expressed and more immunogenic than the S monomer and its wild-type spike counterpart, probably through the preservation of conformational and quaternary

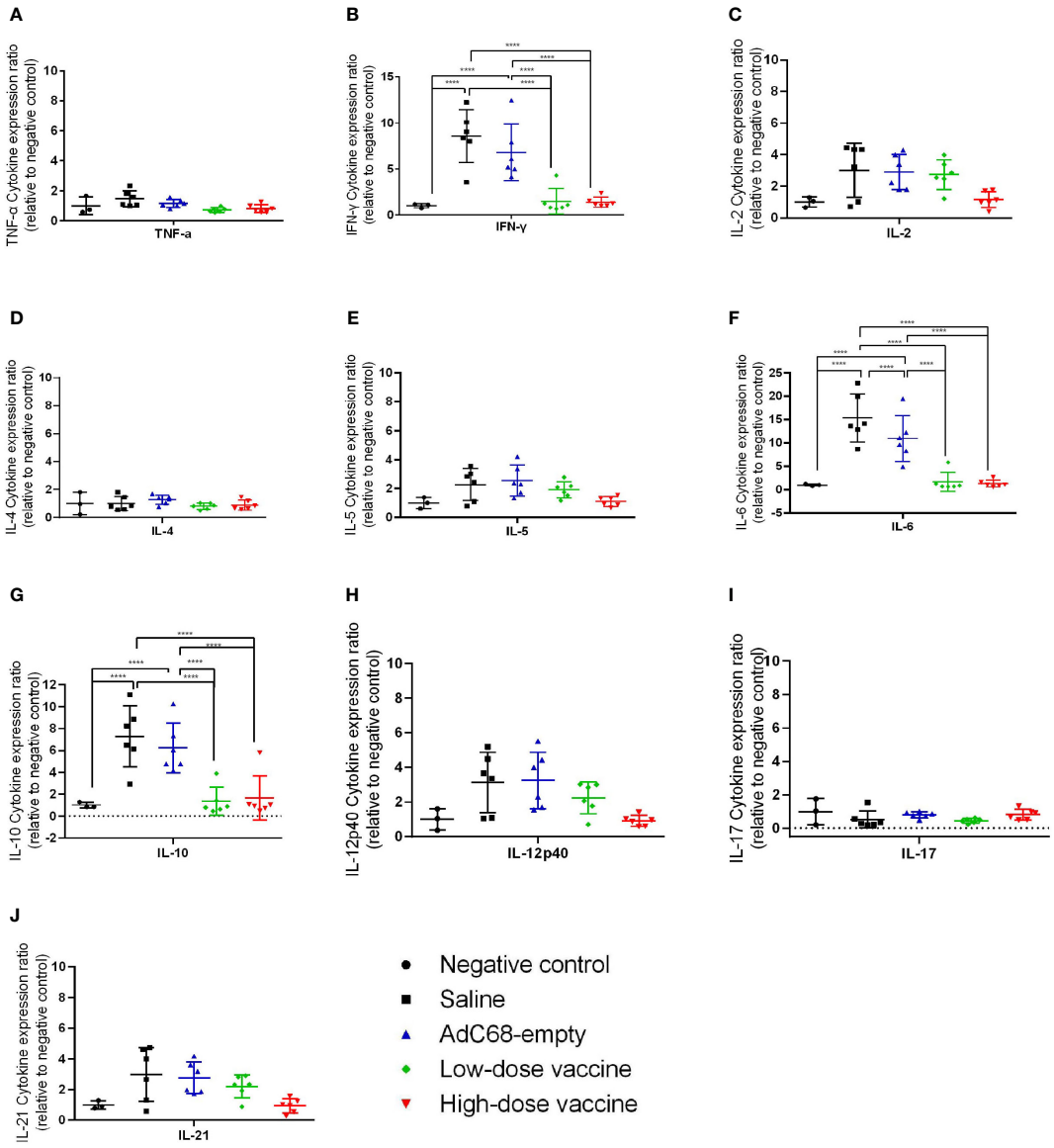

FIGURE 7
Ratios of cytokine expression levels in the lungs of golden Syrian hamsters at dpi 3. The cytokine expression levels in the lungs of golden Syrian hamsters were determined by RT-qPCR at dpi 3. **(A)** Ratios of TNF-α cytokine expression levels in the lungs of golden Syrian hamsters at dpi 3, **(B)** Ratios of IFN-γ cytokine expression levels in the lungs of golden Syrian hamsters at dpi 3, **(C)** Ratios of IL-2 cytokine expression levels in the lungs of golden Syrian hamsters at dpi 3, **(D)** Ratios of IL-4 cytokine expression levels in the lungs of golden Syrian hamsters at dpi 3, **(E)** Ratios of IL-5 cytokine expression levels in the lungs of golden Syrian hamsters at dpi 3, **(F)** Ratios of IL-6 cytokine expression levels in the lungs of golden Syrian hamsters at dpi 3, **(G)** Ratios of IL-10 cytokine expression levels in the lungs of golden Syrian hamsters at dpi 3, **(H)**Ratios of IL-12p40 cytokine expression levels in the lungs of golden Syrian hamsters at dpi 3, **(I)** Ratios of IL-17 cytokine expression levels in the lungs of golden Syrian hamsters at dpi 3, **(J)** Ratios of IL-21 cytokine expression levels in the lungs of golden Syrian hamsters at dpi 3. ****$p < 0.0001$.

neutralization epitopes (Pallesen et al., 2017). This finding was confirmed by Liu et al. (Liu et al., 2021) who showed that a single intranasal injection of a live-attenuated parainfluenza virus-vectored SARS-CoV-2 pre-S-2P induced significantly higher levels of neutralizing antibodies than the SARS-CoV-2 spike. A chimpanzee adenovirus vector was preferred over human adenovirus vectors because of the very low prevalence of pre-existing anti-vector antibodies in humans (Xiang et al., 2006). The results indicated that intranasal delivery of BV-AdCoV-1 elicited robust humoral and cell-mediated responses. Two doses

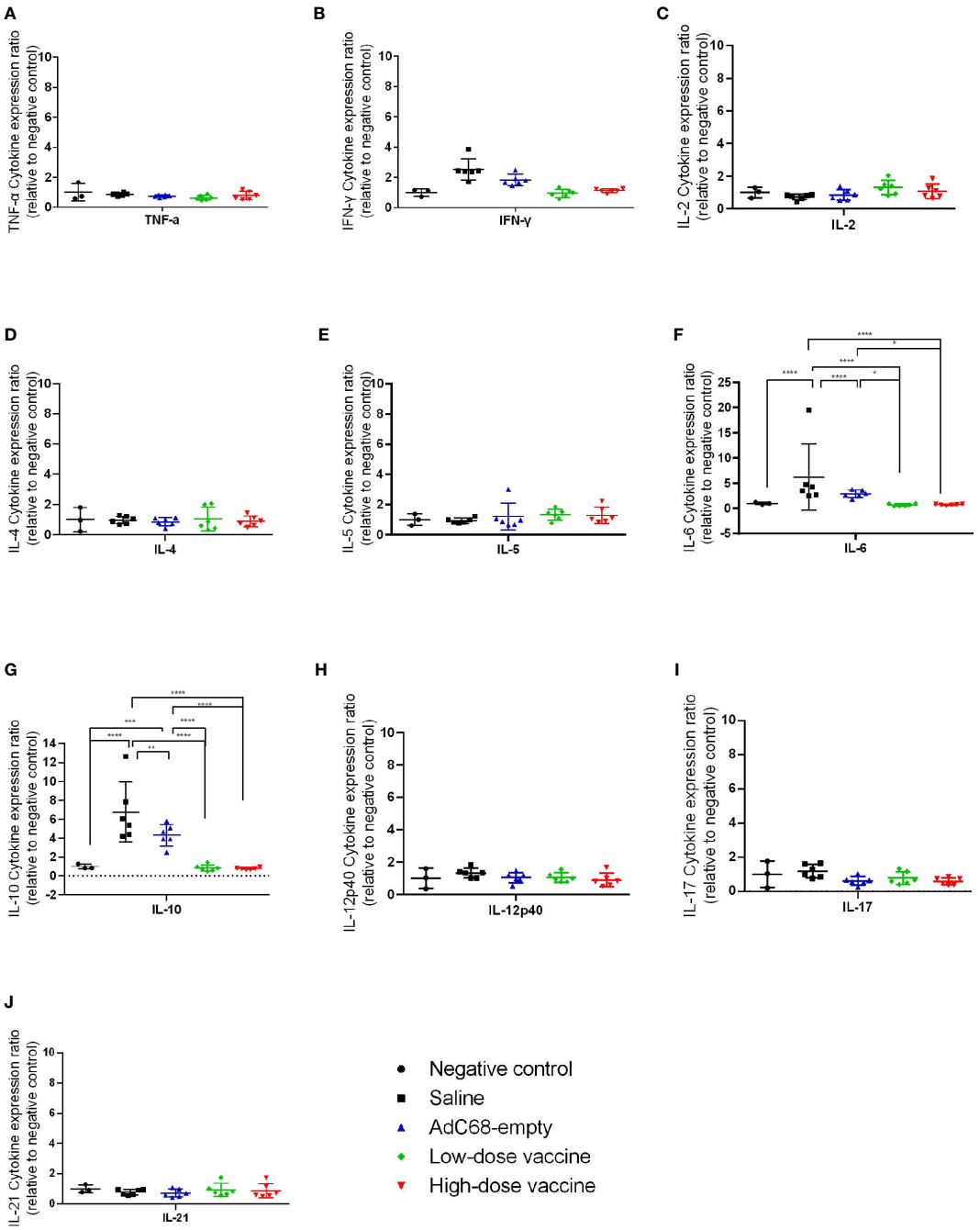

FIGURE 8
Ratios of cytokine expression levels in the lungs of golden Syrian hamsters at dpi 7. The cytokine expression levels in the lungs of golden Syrian hamsters were determined by RT-qPCR at dpi 7. **(A)** Ratios of TNF-α cytokine expression levels in the lungs of golden Syrian hamsters at dpi 7, **(B)** Ratios of IFN-γ cytokine expression levels in the lungs of golden Syrian hamsters at dpi 7, **(C)** Ratios of IL-2 cytokine expression levels in the lungs of golden Syrian hamsters at dpi 7, **(D)** Ratios of IL-4 cytokine expression levels in the lungs of golden Syrian hamsters at dpi 7, **(E)** Ratios of IL-5 cytokine expression levels in the lungs of golden Syrian hamsters at dpi 7, **(F)** Ratios of IL-6 cytokine expression levels in the lungs of golden Syrian hamsters at dpi 7, **(G)** Ratios of IL-10 cytokine expression levels in the lungs of golden Syrian hamsters at dpi 7, **(H)** Ratios of IL-12p40 cytokine expression levels in the lungs of golden Syrian hamsters at dpi 7, **(I)** Ratios of IL-17 cytokine expression levels in the lungs of golden Syrian hamsters at dpi 7, **(J)** Ratios of IL-21 cytokine expression levels in the lungs of golden Syrian hamsters at dpi 7. *$p < 0.05$, **$p < 0.01$, ***$p < 0.001$, ****$p < 0.0001$.

of vaccines induced high levels of S-, S1- and RBD-specific serum antibodies capable of neutralizing SARS-CoV-2 even at the low dose of BV-AdCoV-1 (3.4×10^9 VP). Neutralizing titers were equivalent to those obtained with the NIBSC 20/136 reference or following intranasal immunization of Syrian hamsters with the ChAdOx1 nCoV-19 vaccine which expresses a full-length spike (Doremalen et al., 2021). The results showed that BV-AdCoV-1 could significantly reduce lung viral load (p =0.0067) and pathology (p <0.0001) in immune hamster just as well as the ChAdOx1 nCoV-19 vaccine, that could significantly reduce lung viral load (p =0.0068) while inducing almost no lung pathology. The ChAdOx1 nCoV-19 vaccine also reduced shedding and prevented hamster-to-hamster transmission. A single intranasal dose of another chimpanzee vector expressing the pre-fusion spike induced high levels of neutralizing antibodies, systemic and mucosal IgA responses, as well as T-cell responses and almost prevented infection in mice (Hassan et al., 2020). Furthermore, a recent study comparing the hAd5-nCoV vaccine delivery either through aerosol inhalation or intramuscular administration showed that inhalation was safe and required only a 1/5 to 2/5 of the intramuscular dose to achieve equivalent immunogenicity (Wu et al., 2021).

Moreover, BV-AdCoV-1 elicited S-specific T-cell responses as judged by IFN-γ ELISpot analysis of immune splenocytes. Intranasal vaccination significantly reduced weight loss in animals following SARS-CoV-2 infection. In addition, immunization with BV-AdCoV-1 also markedly reduced relative levels of RNA in the lungs, SARS-CoV-2 infectious titers and lung pathology scored on lung inflammation, edema and hemorrhage. SARS-CoV-2-induced lung pathology in hamsters appeared to be driven by immune pathology, as lung injury at 4 dpi was markedly reduced in STAT2 knockout hamsters (Boudewijns et al., 2020). Chan et al. reported that expression of TNF-α, IFN-γ and other proinflammatory cytokines such as IL-2, IL-5, IL-12p40 and IL-21 usually peaked at dpi 3 in the lungs of infected hamsters (Chan et al., 2020). Here, we observed that IFN-γ, IL-6 and IL-10 RNA levels were significantly reduced in BV-AdCoV-1-immunized animals, going down to baseline levels observed in non-infected animals. Vaccinated golden Syrian hamsters were thus fully protected against a live SARS-CoV-2 challenge. In addition, histopathology results showed that the BV-AdCoV-1 vaccine did not induce enhanced disease nor immunopathological exacerbation.

It has been reported that a single intranasal dose of COVID-19 vaccine could induce neutralizing antibodies and protect against SARS-CoV-2 infection in pre-clinical models (Doremalen et al., 2021; Liu et al., 2021). In this study, both a low and high booster dose of vaccine significantly enhanced virus neutralizing antibody titers, indicating that a two-dose vaccination schedule will yield optimal immunogenicity results.

Compared to systemic immunization, vaccines administered mucosally not only elicit humoral immunity but also local antibodies, including sIgA, and cellular responses that are more efficient at protecting the lower and upper respiratory tracts against infection, limiting shedding and preventing virus transmission. In addition, mucosal vaccine delivery is non-invasive, convenient, easily accessible and thus, represents a promising approach to facilitate mass immunization, overcome vaccine hesitancy and achieve herd immunity. Currently, several mucosal COVID-19 vaccines administered *via* nasal spray or aerosols are being evaluated in particular by Bharat Biotech (India) and Wantai BioPharm (China). Vaccination by inhalation has been successfully used for influenza, MMR (measles, mumps, rubella) and human papillomavirus (HPV) vaccines (Bennett et al., 2002; Nardelli-Haefliger et al., 2005; Amorij et al., 2010).

In our study, no enhanced infection, immunopathology, or disease was observed in immunized Syrian hamsters challenged with live virus. Notably, a two-dose immunization regimen with BV-AdCoV-1 could protect the lungs of immunized hamsters from infectious SARS-CoV-2 challenge and induced broad cross-neutralizing antibody responses against epidemic variants of concern. Based on these preclinical data, we suggest that mucosal delivery *via* nasal spray or aerosolization of BV-AdCoV-1, is a promising platform to safely prevent SARS-CoV-2 infection, disease, and transmission, and warrants further evaluation in humans as a primary or heterologous booster immunization strategy.

Data availability statement

The raw data supporting the conclusions of this article will be made available by the authors, without undue reservation.

Ethics statement

The animal study was reviewed and approved by the Institutional Animal Care and Use Committee of Oncodesign (CNREEA Agreement N° 91) and the CEA (Commissariat à lEnergie Atomique; CETEA DSV n° 44) and Wuhan Myhalic Biotechnological Co., Ltd(No. HLK-20220630-001).

Author contributions

SW, LXu, MQ, and LD designed the experiment protocol. TM and LXi designed and produced BV-AdCoV-1. PZ and YW coordinated the projects. NL, KM, and GF performed the challenge experiments and data analysis. YL and WY identified and analyzed the purified pre-S protein, while JZ, MJ, and BG performed the immunogenicity study in China. SW and LXu wrote the manuscript. MK and KW supervised the

research and finalized the manuscript. All authors contributed to the article and approved the submitted version.

Funding

This work was funded by Wuhan BravoVax Co., Ltd. and Shanghai BravoVax CO., Ltd.

Acknowledgments

The authors wish to thank the innovative discovery department from Wuhan BravoVax Co., Ltd. for designing, engineering and producing BV-AdCoV-1.

Conflict of interest

Author SW, LXu, TM, MQ, PZ, LXi, YW, YL, WY, JZ, MJ, BG, MK, and KW are employed by Wuhan BravoVax Co., Ltd. MK and KW are also employed by Shanghai BravoVax Co., Ltd. Meanwhile, YL is a teacher from Hubei University. LD is employed by Voisin Consulting Life Sciences. NL, KM, and GF are employed by Oncodesign.

The remaining authors declare that the research was conducted in the absence of any commercial or financial relationships that could be construed as a potential conflict of interest.

Publisher's note

Supplementary material

The Supplementary Material for this article can be found online at: https://www.frontiersin.org/articles/10.3389/fcimb.2022.979641/full#supplementary-material

SUPPLEMENTARY MATERIAL 1

Molecular weight of spike. **(A)** Molecular weight of spike secreted in infected HEK293A culture supernatants calculated using the Quantity One software. **(B)** Molecular weight of spike in infected HEK293A cell lysates calculated using the Quantity One software.

SUPPLEMENTARY MATERIAL 2

Histopathological Hematoxylin-Phloxine evaluation of SARS-CoV-2 infection in golden Syrian hamsters (Hematoxylin-Phloxine 10x, scale bar = 250 µm). Pictures are shown for one animal of each group **(A)** Negative control; **(B, C)** Saline; **(D, E)** AdC68-empty; **(F, G)** Low-dose vaccine; and **(H, I)** High-dose vaccine. Arrows show signs of inflammatory leucocyte infiltrates (vertical arrows), pulmonary edema (horizontal arrows) and alveolar hemorrhage (angled arrows). Left lung slides were stained with Hematoxylin-Phloxine to visualize histomorphometric changes. Slides were scanned using the NanoZoomer Digital Pathology System C9600-02.

References

Amorij, J., Hinrichs, W. L., Frijlink, H. W., Wilschut, J. C., and Huckriede, A. (2010). Needle-free influenza vaccination. *Lancet Infect. Dis.* 10 (10), 699–711. doi: 10.1016/S1473-3099(10)70157-2

Bednash, J. S., Kagan, V. E., Englert, J. A., Farkas, D., Tyurina, Y. Y., Tyurin, V. A., et al. (2022). Syrian Hamsters as a model of lung injury with SARS-CoV-2 infection: Pathologic, physiologic, and detailed molecular profiling. *Transl. Res.* 240, 1–16. doi: 10.1016/j.trsl.2021.10.007

Bennett, J. V., Castro, J. F. D., Valdespino-Gomez, J. L., Garcia-Garcia, M. D. L., Islas-Romero, R., Echaniz-Aviles, G., et al. (2002). Aerosolized measles and measles-rubella vaccines induce better measles antibody booster responses than injected vaccines: Randomized trials in Mexican school children. *Bull. W. H. O.* 80 (10), 806–812. doi: 10.1590/S0042-96862002001000009

Boudewijns, R., Pérez, P., Lázaro-Frías, A., Looveren, D. V., Vercruysse, T., Thibaut, H. J., et al. (2022). MVA-CoV2-S vaccine candidate neutralizes distinct variants of concern and protects against SARS-CoV-2 infection in hamsters. *Front. Immunol.* 13. doi: 10.3389/fimmu.2022.845969

Boudewijns, R., Thibaut, H. J., Kaptein, S. J. K., Li, R., Vergote, V., Seldeslachts, L., et al. (2020). STAT2 signaling restricts viral dissemination but drives severe pneumonia in SARS-CoV-2 infected hamsters. *Nat. Commun* 11, 5838. doi: 10.1038/s41467-020-19684-y

Chan, J. F., Zhang, A. J. X., Yuan, S. F., Poon, V. K., Chan, C. C., Lee, A. C., et al. (2020). Simulation of the clinical and pathological manifestations of coronavirus disease 2019 (COVID-19) in a golden Syrian hamster model: Implications for disease pathogenesis and transmissibility. *Clin. Infect. Dis.* 71 (9), 2428–2446. doi: 10.1093/cid/ciaa325

Corbett, K. S., Flynn, B., Foulds, K. E., Francica, J. R., Boyoglu-Barnum, S., Werner, A. P., et al. (2020). Evaluation of the mRNA-1273 vaccine against SARS-CoV-2 in nonhuman primates. *N. Engl. J. Med.* 383 (16), 1544–1555. doi: 10.1056/NEJMoa2024671

Dagan, N., Barda, N., Kepten, E., Miron, O., and Ran, D. B. (2021). BNT162b2 mRNA covid-19 vaccine in a nationwide mass vaccination setting. *N. Engl. J. Med.* 384 (15), 1412–1423. doi: 10.1056/NEJMoa2101765

Dhama, K., Dhawan, M., Tiwari, R., Emran, T. B., Mitra, S., Rabaan, A. A., et al. (2022). COVID-19 intranasal vaccines: Current progress, advantages, prospects, and challenges. *Hum. Vacc. Immunother.*, 18, 1–11. doi: 10.1080/21645515.2022.2045853

Doremalen, N. V., Purushotham, J. N., Schulz, J. E., Holbrook, M. G., Bushmaker, T., Carmody, A., et al. (2021). Intranasal ChAdOx1 nCoV-19/AZD1222 vaccination reduces viral shedding after SARS-CoV-2 D614G challenge in preclinical models. *Sci. Transl. Med.* 13 (607), eabh0755. doi: 10.1126/scitranslmed.abh0755

Gee, J., Marquez, P., Su, J., Calvert, G. M., Liu, R. L., Myers, T., et al. (2021). First month of COVID-19 vaccine safety monitoring - united states, December 14, 2020-January 13, 2021. *MMWR Morb Mortal Wkly Rep.* 70 (8), 283–288. doi: 10.15585/mmwr.mm7008e3

Hassan, A. O., Kafai, N. M., Dmitriev, I. P., Fox, J. M., Smith, B. K., Harvey, I. B., et al. (2020). A single-dose intranasal ChAd vaccine protects upper and lower respiratory tracts against SARS-CoV-2. *Cell* 183 (1), 169–184.e13. doi: 10.1016/j.cell.2020.08.026

Hsieh, C. L., Goldsmith, J. A., Schaub, J. M., DiVenere, A. M., Kuo, H. C., Javanmardi, K., et al. (2020). Structure-based design of prefusion-stabilized SARS-CoV-2 spikes. *Science* 369 (6510), 1501–1505. doi: 10.1126/science.abd0826

Huang, H. Y., Wang, S. H., Tang, Y., Sheng, W., Zuo, C. J., Wu, D. W., et al. (2021). Landscape and progress of global COVID-19 vaccine development. *Hum. Vacc. Immunother.* 17 (10), 3276–3280. doi: 10.1080/21645515.2021.1945901

Imai, M., Iwatsuki-Horimoto, K., Hatta, M., Loeber, S., Halfmann, P. J., Nakajima, N., et al. (2020). Syrian Hamsters as a small animal model for SARS-CoV-2 infection and countermeasure development. *Proc. Natl. Acad. Sci. U. S. A.* 117 (28), 16587–16595. doi: 10.1073/pnas.2009799117

Jackson, L. A., Roberts, P. C., and Graham, B. S. (2020). A SARS-CoV-2 mRNA vaccine - preliminary report. *Reply. N. Engl. J. Med.* 383 (12), 1191–1192. doi: 10.1056/NEJMc2026616

Kar, S., Devnath, P., Emran, T. B., Tallei, T. E., Mitra, S., and Dhama, K. (2022). Oral and intranasal vaccines against SARS-CoV-2: Current progress, prospects, advantages, and challenges. *Immun. Inflamm. Dis.* 10 (4), e604. doi: 10.1002/iid3.604

Keech, C., Albert, G., Cho, I., Robertson, A., Reed, P., Neal, S., et al. (2020). Phase 1-2 trial of a SARS-CoV-2 recombinant spike protein nanoparticle vaccine. *N. Engl. J. Med.* 383 (24), 2320–2332. doi: 10.1056/NEJMoa2026920

Koirala, A., Joo, Y. J., Khatami, A., Chiu, C., and Britton, P. N. (2020). Vaccines for COVID-19: The current state of play. *Paediatr. Respir. Rev.* 35, 43–49. doi: 10.1016/j.prrv.2020.06.010

Liu, X. Q., Luongo, C., Matsuboka, Y., Park, H. S., Santos, C., Yang, L. J., et al. (2021). A single intranasal dose of a live-attenuated parainfluenza virus-vectored SARS-CoV-2 vaccine is protective in hamsters. *PNAS* 118 (50), e2109744118. doi: 10.1073/pnas.2109744118

Lubbe, J. E. M.V.D., Huber, S. K. R., Vijayan, A., Dekking, L., Huizen, E. V., Vreugdenhil, J., et al. (2021). Ad26.COV2.S protects Syrian hamsters against G614 spike variant SARS-CoV-2 and does not enhance respiratory disease. *NPJ Vaccines* 6 (1), 39. doi: 10.1038/s41541-021-00301-y

Mendonça, S. A., Lorincz, R., Boucher, P., and Curiel, D. T. (2021). Adenoviral vector vaccine platforms in the SARS-CoV-2 pandemic. *NPJ Vaccines* 6 (1), 97. doi: 10.1038/s41541-021-00356-x

Mercado, N. B., Zahn, R., Wegmann, F., Loos, C., Chandrashekar, A., Yu, J. Y., et al. (2020). Single-shot Ad26 vaccine protects against SARS-CoV-2 in rhesus macaques. *Nature* 586 (7830), 583–588. doi: 10.1038/s41586-020-2607-z

Nardelli-Haefliger, D., Lurati, F., Wirthner, D., Spertini, F., Schiller, J. T., Lowy, D. R., et al. (2005). Immune responses induced by lower airway mucosal immunisation with a human papillomavirus type 16 virus-like particle vaccine. *Vaccine* 23 (28), 3634–3641. doi: 10.1016/j.vaccine.2005.02.019

O'Donnell, K. L., Pinski, A. N., Clancy, C. S., Gourdine, T., Shifflett, K., Fletcher, P., et al. (2021). Pathogenic and transcriptomic differences of emerging SARS-CoV-2 variants in the Syrian golden hamster model. *EBioMedicine* 73, 103675. doi: 10.1016/j.ebiom.2021.103675

Pallesen, J., Wang, N. S., Corbett, K. S., Wrapp, D., Kirchdoerfer, R. N., Turner, H. L., et al. (2017). Immunogenicity and structures of a rationally designed prefusion MERS-CoV spike antigen. *Proc. Natl. Acad. Sci. U. S. A.* 114 (35), E7348–E7357. doi: 10.1073/pnas.1707304114

Reed, L. J., and Muench, H. (1938). A simple method of estimating fifty per cent endpoints. *Am. J. Epidemiol.* 27 (3), 493–497. doi: 10.1093/oxfordjournals.aje.a118408

Richmond, P., Hatchuel, L., Dong, M., Ma, B., Hu, B., Smolenov, I., et al. (2021). Safety and immunogenicity of s-trimer (SCB-2019), a protein subunit vaccine candidate for COVID-19 in healthy adults: A phase 1, randomised, double-blind, placebo-controlled trial. *Lancet* 397 (10275), 682–694. doi: 10.1016/S0140-6736(21)00241-5

Roberts, A., Vogel, L., Guarner, J., Hayes, N., Murphy, B., Zaki, S., et al. (2005). Severe acute respiratory syndrome coronavirus infection of golden Syrian hamsters. *J. Virol.* 79 (1), 503–511. doi: 10.1128/JVI.79.1.503-511.2005

Rosenke, K., Meade-White, K., Letko, M., Clancy, C., Hansen, F., Liu, Y. N., et al. (2020). Defining the Syrian hamster as a highly susceptible preclinical model for SARS-CoV-2 infection. *Emerg. Microbes Infect.* 9 (1), 2673–2684. doi: 10.1080/22221751.2020.1858177

Sadoff, J., Gray, G., Vandebosch, A., Cárdenas, V., Shukarev, G., Grinsztejn, B., et al. (2021). Safety and efficacy of single-dose Ad26.COV2.S vaccine against covid-19. *N. Engl. J. Med.* 384 (23), 2187–2201. doi: 10.1056/NEJMoa2101544

Tiboni, M., Casettari, L., and Illum, L. (2021). Nasal vaccination against SARS-CoV-2: Synergistic or alternative to intramuscular vaccines? *Int. J. Pharm.* 603, 120686. doi: 10.1016/j.ijpharm.2021.120686

Velavan, T. P., and Meyer, C. G. (2020). The COVID-19 epidemic. *Trop. Med. Int. Health* 25 (3), 278–280. doi: 10.1111/tmi.13383

Wu, S. P., Huang, J. Y., Zhang, Z., Wu, J. J., Zhang, J. L., Hu, H. N., et al. (2021). Safety, tolerability, and immunogenicity of an aerosolised aerosolized adenovirus type-5 vector-based COVID-19 vaccine (Ad5-nCoV) in adults: preliminary report of an open-label and randomised randomized phase 1 clinical trial. *Lancet Infect. Dis.* 21 (12), 1654–1664. doi: 10.1016/S1473-3099(21)00396-0

Xiang, Z. Q., Li, Y., Cun, A., Yang, W., Ellenberg, S., Switzer, W. M., et al. (2006). Chimpanzee adenovirus antibodies in humans, sub-Saharan Africa. *Emerg. Infect. Dis.* 12 (10), 1596–1599. doi: 10.3201/eid1210.060078

Zare, H., Rezapour, H., Mahmoodzadeh, S., and Fereidouni, M. (2021). Prevalence of COVID-19 vaccines (Sputnik V, AZD-1222, and covaxin) side effects among healthcare workers in birjand city, Iran. *Int. Immunopharmacol* 101 (Pt B), 108351. doi: 10.1016/j.intimp.2021.108351

frontiers | Frontiers in Cellular and Infection Microbiology

TYPE Original Research
PUBLISHED 22 November 2022
DOI 10.3389/fcimb.2022.1011672

OPEN ACCESS

EDITED BY
Ke Xu,
Wuhan University, China

REVIEWED BY
Ousman Bajinka,
University of the Gambia, Gambia
Huahao Fan,
Beijing University of Chemical Technology, China

*CORRESPONDENCE
Yajie Wang
wangyajie@ccmu.edu.cn
Ronghua Jin
ronghuajin@ccmu.edu.cn

†These authors have contributed equally to this work and share first authorship

SPECIALTY SECTION
This article was submitted to Virus and Host, a section of the journal Frontiers in Cellular and Infection Microbiology

RECEIVED 04 August 2022
ACCEPTED 28 September 2022
PUBLISHED 22 November 2022

CITATION
Meng H, Wang S, Tang X, Guo J, Xu X, Wang D, Jin F, Zheng M, Yin S, He C, Han Y, Chen J, Han J, Ren C, Gao Y, Liu H, Wang Y and Jin R (2022) Respiratory immune status and microbiome in recovered COVID-19 patients revealed by metatranscriptomic analyses. *Front. Cell. Infect. Microbiol.* 12:1011672. doi: 10.3389/fcimb.2022.1011672

Respiratory immune status and microbiome in recovered COVID-19 patients revealed by metatranscriptomic analyses

Huan Meng[1†], Shuang Wang[1†], Xiaomeng Tang[2], Jingjing Guo[1], Xinming Xu[1], Dagang Wang[1], Fangfang Jin[1], Mei Zheng[1], Shangqi Yin[1], Chaonan He[1], Ying Han[1], Jin Chen[1], Jinyu Han[1], Chaobo Ren[3], Yantao Gao[3], Huifang Liu[3], Yajie Wang[1*] and Ronghua Jin[2*]

[1]Department of Clinical Laboratory, Beijing Ditan Hospital, Capital Medical University, Beijing, China, [2]Beijing Ditan Hospital, Capital Medical University, Beijing, China, [3]Translational R&D Center, Guangzhou Vision Medicals Co. LTD, Guangzhou, China

Coronavirus disease 2019 (COVID-19) is currently a severe threat to global public health, and the immune response to COVID-19 infection has been widely investigated. However, the immune status and microecological changes in the respiratory systems of patients with COVID-19 after recovery have rarely been considered. We selected 72 patients with severe COVID-19 infection, 57 recovered from COVID-19 infection, and 65 with non-COVID-19 pneumonia, for metatranscriptomic sequencing and bioinformatics analysis. Accordingly, the differentially expressed genes between the infected and other groups were enriched in the chemokine signaling pathway, NOD-like receptor signaling pathway, phagosome, TNF signaling pathway, NF-kappa B signaling pathway, Toll-like receptor signaling pathway, and C-type lectin receptor signaling pathway. We speculate that *IL17RD*, CD74, and TNFSF15 may serve as disease biomarkers in COVID-19. Additionally, principal coordinate analysis revealed significant differences between groups. In particular, frequent co-infections with the genera *Streptococcus*, *Veillonella*, *Gemella*, and *Neisseria*, among others, were found in COVID-19 patients. Moreover, the random forest prediction model with differential genes showed a mean area under the curve (AUC) of 0.77, and *KCNK12*, *IL17RD*, *LOC100507412*, *PTPRT*, *MYO15A*, *MPDZ*, *FLRT2*, *SPEG*, *SERPINB3*, and *KNDC1* were identified as the most important genes distinguishing the infected group from the recovered group. *Agrobacterium tumefaciens, Klebsiella michiganensis, Acinetobacter pittii, Bacillus* sp. FJAT.14266, *Brevundimonas naejangsanensis, Pseudopropionibacterium propionicum, Priestia megaterium, Dialister pneumosintes, Veillonella*

rodentium, and *Pseudomonas protegens* were selected as candidate microbial markers for monitoring the recovery of COVID patients. These results will facilitate the diagnosis, treatment, and prognosis of COVID patients recovering from severe illness.

KEYWORDS

coronavirus disease 2019, recovery, metatranscriptome, immune status, microecology

Introduction

Severe acute respiratory syndrome coronavirus 2 (SARS-CoV-2), a highly contagious respiratory pathogen, is a beta-corona virus that causes coronavirus disease 2019 (COVID-19). Previous clinical experience has shown that COVID-19 is highly heterogeneous in symptomatic cases, ranging from mild to severe to lethal (Zhou et al., 2020). Infection with certain respiratory viruses often produces a strong inflammatory response (Huang et al., 2005; de Jong et al., 2006). Deficiencies in immune regulation, known as hypercytokinemia or "cytokine storms," are often associated with deleterious outcomes, such as acute respiratory distress syndrome (ARDS) (de Jong et al., 2006). Most viruses, especially SARS, disrupt the normal immune response of the host, including interferon (IFN) signaling (Shaw et al., 2017; Crosse et al., 2018). The IFN system affects viral replication and downstream antiviral immunity (Costa-Pereira et al., 2002; Grandvaux et al., 2002). The type I interferon (IFN-I) response mainly exerts an antiviral function by inducing the expression of interferon-stimulated genes (ISG), which plays an important role in fighting viral infection (Samuel, 2001). Viral infection and replication lead to differences in the dynamics and magnitude of host responses, which affect the outcome of innate and adaptive immune responses. For example, SARS coronavirus effectively inhibits IFN inducibility and antagonizes IFN effects by utilizing its structural and nonstructural proteins (de Wit et al., 2016). SARS-CoV is unable to elicit strong induction of an IFN response in human macrophages (Cheung et al., 2005; Ziegler et al., 2005) and in SARS patients (Reghunathan et al., 2005). Insufficient IFN responses may lead to progressive increases in viral load with hypercytokinemia and ultimately fatal consequences in patients with SARS. Clinical studies on COVID-19 suggest the presence of severe cytokine MIa (Huang et al., 2020). To date, the mechanisms by which pathogen infection disrupts host immune homeostasis and stimulates excessive inflammation-induced responses remain unknown.

Infectious diseases other than COVID-19 have been identified as post-infection syndromes (Bannister, 1988; Hickie et al., 2006). In a study of COVID-19, Q fever, glandular fever, epidemic polyarthritis, and Legionella were similar to the persistent symptoms of COVID-19 (Hickie et al., 2006; Loenhout et al., 2014). Repeated symptoms include burnout, pain, limited quality of life, and limited health. Therefore, COVID-19 may be a persistent symptom. Additionally, loss of taste and/or smell has not been described in studies of post-infectious syndromes of diseases other than COVID-19; therefore, it is likely to be a persistent symptom of COVID-19. Some patients, even those with COVID-19, still exhibit symptoms after their initial recovery (Greenhalgh et al., 2020; Tenforde et al., 2020). Post-infection syndromes have been identified in many other infectious diseases (Bannister, 1988; Hickie et al., 2006). For example, after a mild SARS-CoV infection, a significant proportion of patients experience residual lung damage (Chan et al., 2003; Zhang et al., 2020). Additionally, some studies have shown that patients infected with SARS-CoV experience psychological symptoms, burnout, health limitations, and a decreased quality of life (Lau et al., 2005; Lee et al., 2007; Lam et al., 2009). Prospective studies have shown burnout, neurocognitive impairment, musculoskeletal pain, and mood disturbances in patients six months after infection. These conditions cannot be extrapolated to patients with COVID-19 (Hickie et al., 2006), but a proportion of patients with COVID-19 are expected to experience physical, cognitive, or psychological distress within three weeks after recovery. However, no studies have described the changes in the immune status of the respiratory tract or changes in the respiratory tract microecology from the perspective of molecular mechanisms in patients with COVID-19 after recovery.

Metatranscriptomic sequencing provides an agnostic approach to detect pathogens that emerge directly from clinical samples (Wilson et al., 2014). Compared with targeted approaches, it also provides valuable information on microbiota composition and may reveal superinfections that may affect disease development and prognosis (Westermann et al., 2012; Avraham et al., 2016). One of the key advantages of metatranscriptomic sequencing is that a snapshot of the patient's microbiome can be obtained at a specific sampling point to detect superinfections and identify other microorganisms that may affect patient outcomes. In addition to evidence of true pathogens, there is growing evidence that the microbiota of the respiratory tract may affect patient health; however, most of the evidence focuses on interactions between bacteria (Kumpitsch et al., 2019). Increasing evidence suggests that analyzing the microbiome makes it possible to predict which patients with respiratory infections are more likely to develop the severe disease (Kumpitsch et al., 2019; Man et al., 2019). Bacterial load and lung microbiota composition may influence the likelihood

of developing acute respiratory distress syndrome (ARDS) in patients with severe artificial respiration (Panzer et al., 2018; Dickson et al., 2020). Metatranscriptomic analysis of COVID-19 offers an opportunity to assess whether the microbiome is beneficial or detrimental to patient outcomes (Li et al., 2019).

In our study, we applied metatranscriptomic sequencing in 194 patients (72 in an infectious period of COVID-19, 57 in a recovery period following COVID-19, and 65 with non-COVID-19 pneumonia) to obtain unbiased, cross-organism transcriptional profiles. We aimed to identify the three core elements of the causative agent of COVID-19–pathogen, respiratory microbiota, and host response–and to apply this information to advance the understanding and diagnosis of COVID-19. This study describes the changes in the immune status and microecology of the respiratory tract after the recovery of patients from the perspective of molecular mechanisms. Also, this study is expected to improve the understanding of the molecular mechanism of the new crown infection process and provide genes and clues for subsequent treatment.

Materials and methods

Participants

A total of 171 patients, balanced for age and sex, were enrolled in this study, including those who were infected with COVID-19 or other pathogens, including human coronavirus, human herpesvirus, rhinovirus, parainfluenza virus, respiratory syncytial virus, *Acinetobacter baumannii*, *Staphylococcus aureus*, and *Klebsiella pneumoniae*, or who were recovering from COVID-19. The samples collected from patients with confirmed COVID-19 and convalescent patients who were recovering from COVID-19 infection were classified into the infected and recovered groups, respectively. The samples from patients infected with other pathogens were classified as the other group. All patients enrolled in the study provided written informed consent approved by the institutional review board of the Beijing Ditan Hospital Capital Medical University.

For the infected group, 65 Consecutive patients older than 18 years with community acquired pneumonia or hospital acquired pneumonia were enrolled. All enrolled patients met the study inclusion and exclusion criteria. Inclusion criteria of patients with community acquired pneumonia: (a) community onset; (b) a new infiltrate, lobar or segment consolidation, ground glass opacity or interstitial images revealed on chest radiograph or CT scan, accompanied by pleural effusion or not; (c) any of the following 4 clinical features: (c1) new occurrence of cough, expectation, or worsen of respiratory symptoms, accompanied by purlurent sputum, chest pain, dyspnea and hemoptysis or not; (c2) fever; (c3) signs of consolidation and/or moist rale on lung auscultation; (c4) peripheral white cell counts $> 10 \times 10^{\wedge}9/L$ or $< 4 \times 10^{\wedge}9/L$. Inclusion criteria of patients with hospital acquired pneumonia:(a) a new or progressive infiltrate, consolidation, or ground glass opacity revealed on chest radiograph or CT scan; (b) two or more of the following 3 criteria: (b1) fever > 38°C; (b2) purulent airway secretions; (b3) peripheral white blood cell count $> 10 \times 10^{\wedge}9/L$ or $< 4 \times 10^{\wedge}9/L$; (c) illness occurs 48 hours or more after admission during hospitalization. Exclusion criteria: (a) patients infected with HIV; (b) pregnant women; (c) patients with an irreversible contraindication for bronchoscopy; (d) patients who were unable to understand the informed consent description or unwilling to sign the informed consent form; (e) patients ultimately diagnosed with a non-infectious disease other than pneumonia.

For the other group, individual who met for the following inclusion criteria and exclusion criteria were enrolled. Inclusion criteria: (a) patients with clinical features such as fever, cough, expectation, pharyngalgia, or diarrhea; (b) peripheral white blood cell count $> 10 \times 10^{\wedge}9/L$ or $< 4 \times 10^{\wedge}9/L$. Exclusion criteria: patients infected with COVID-19 as described above.

Nasopharyngeal (NP) swabs or sputum samples were collected from the participants. NP swabs were collected using a sterile swab. The participants were requested to rinse their mouths with water two or three times and expectorate sputum into a sterilized cup. All samples were immediately sent for RNA extraction or stored at -70°C. A total of 194 samples were obtained, including 72, 57, and 65 samples from the infected, recovered, and other groups, respectively.

Metatranscriptomic sequencing

NP swabs or sputum samples were inactivated using AVL buffer containing guanidinium salts (Vision Medicals, China) and then subjected to RNA extraction (Vision Medicals, China). Library preparation was performed using a Novel coronavirus (2019-nCoV) detection kit (Vision Medicals, China) with 300 µL of the samples, and then 50 bp single-end sequencing was performed with Illumina HiSeq 2500 or MGISEQ-200. Briefly, the extracted RNA was treated with DNase I to remove the contaminating DNA. The mRNAs were purified, fragmented, and rRNA-depleted. RNA was reverse-transcribed and enriched by PCR to construct the final cDNA libraries.

Host transcriptome analysis

Raw sequencing reads were processed using fastp (https://github.com/OpenGene/fastp). Novel coronavirus (2019-nCoV) nucleic acid analysis software (Vision Medicals, China, v1.0) was used to extract the reads from the host, which were then aligned

to the human genome (GRCh38) using HISAT2 v2.1.0. Gene quantification was performed using featureCounts (v2.0.0). DEseq2 v1.32.0 was used to identify significantly differentially expressed genes (|logFC| > 2 and padj < 0.05), which were further subjected to Gene Ontology (GO) (http://www.geneontology.org/) and KEGG (http://www.genome.jp/kegg/) enrichment analyses using clusterProfiler v4.0.5. The expression patterns of 255 immune-related genes from ImmPortDB and 380 interferon-stimulated genes (ISG) (X Wu, 2018 Intrinsic Immunity Shapes Viral Resistance of Stem Cells S0092-8674(17)31365-X) were compared across groups.

Microbiome analysis

After removing the reads from the host, the clean reads were aligned against reference databases, including plasmids, bacteria, fungi, parasites, and viruses. Alpha diversity indices, including richness, ACE, Chao1, Shannon, and Simpson, were calculated for each sample using Vegan (v2.5-7). Principal coordinates analysis (PCoA) was performed using OTU abundances based on the distance of the Jensen-Shannon divergence (JSD). Linear discriminant analysis effect size (LEfSe, v1.0.8) was applied to identify the discriminant bacterial taxa for different sample groups.

Classifier analysis

The random forest model was used to predict patient status, including the infected, recovered, or other groups. The models were trained based on differentially expressed genes, differential microbial taxa, or both, resulting in three kinds of classifiers. The random forest classifier was implemented using Python (version 3.7, Python Software Foundation, https://www.python.org/) with the scikit-learn package (https://github.com/scikit-learn/scikit-learn). Feature (gene or taxa) selection was performed using the SelectFromModel method, and features with low importance (according to mean decrease in accuracy (MDA)) were removed before model construction. The area under the curve (AUC) was calculated as an indicator of model performance. We repeated the experiment 100 times for each type of classifier and measured the mean AUC and standard error of the mean.

Statistical analysis

The Wilcoxon test was used to identify differential genera and species between different groups, and a p-value < 0.05 was considered statistically significant. The Wilcoxon test was also used to compare alpha diversity between groups.

Results

Overview of sequencing data

The average number of total reads was approximately 27.3 million for all the samples (Table S1). The average mapped ratios were 72.13%, 88.11%, and 80.96% of the total reads for the infected, recovered, and other groups, respectively (Table S1). The average proportions of reads mapped to the host were 18.05%, 10.21%, and 50.29% for the infected, recovered, and other groups, respectively (Table S1). The average proportion of reads mapped to plasmids and bacteria was 54.05%, 37.71%, and 70.74% for the infected, recovered, and other groups, respectively, while those mapped to viruses were approximately 0.02%, 0.07%, and <0.01%, respectively (Table S1).

Signatures of host immune response

Differential gene expression analysis was performed between the combinations of infected, recovered, and other groups. A total of 1,982 upregulated and 3,532 downregulated genes were detected between the infected and other groups (Figure 1A), and 79 upregulated and seven downregulated genes were detected between the infected and recovered groups (Figure 1B).

The differentially expressed genes between infected and other groups were enriched in the chemokine signaling pathway, NOD-like receptor signaling pathway, phagosome, TNF signaling pathway, NF-kappa B signaling pathway, Toll-like receptor signaling pathway, and C-type lectin receptor signaling pathway (Figure 2A). However, analysis of the KEGG pathways associated with the differentially expressed genes between the infected and recovered groups did not show any significant enrichment. Interestingly, some upregulated genes in the infected group compared with recovered group were involved in immune-related functions, including *IL17RD* (interleukin 17 receptor D), *CD74* (CD74 molecule), *NTRK2* (neurotrophic receptor tyrosine kinase 2), *NKD1* (NKD inhibitor of WNT signaling pathway 1), *CD180* (CD180 molecule), *TNFSF15* (TNF superfamily member 15), *HLA-DQA1* (major histocompatibility complex, class II, DQ alpha 1), *HLA-DRB1* (major histocompatibility complex, class II, DR beta 1), *CXCL5* (C-X-C motif chemokine ligand 5), *PIGR* (polymeric immunoglobulin receptor), *ILDR2* (immunoglobulin like domain containing receptor 2), *IGSF1* (immunoglobulin superfamily member 1), *ISLR* (immunoglobulin superfamily containing leucine rich repeat), *IGFN1* (immunoglobulin like and fibronectin type III domain containing 1), *ISLR2* (immunoglobulin superfamily containing leucine rich repeat 2), *IGDCC4* (immunoglobulin superfamily DCC subclass member 4), *IGDCC3* (immunoglobulin

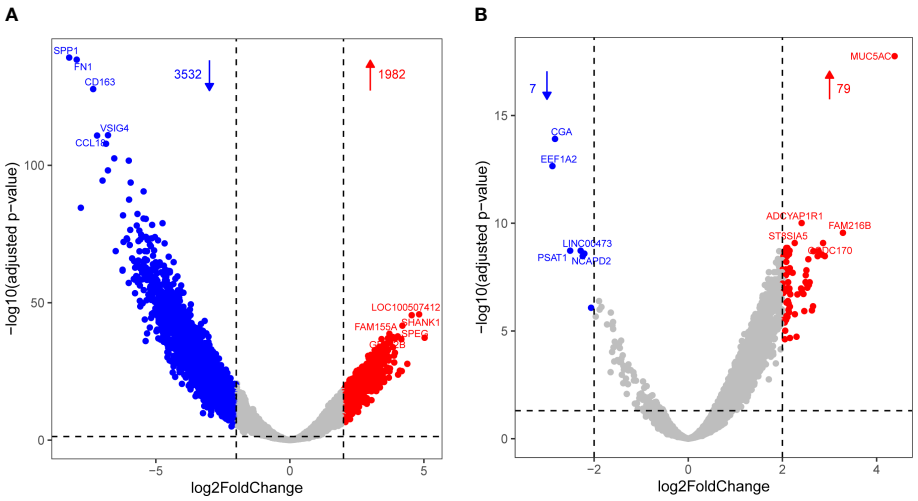

FIGURE 1
Volcano plot showing differential expression with increased DEGs colored in red and decreased DEGs colored in blue for comparisons of infected vs. other **(A)** and infected vs. recovered **(B)** groups, respectively.

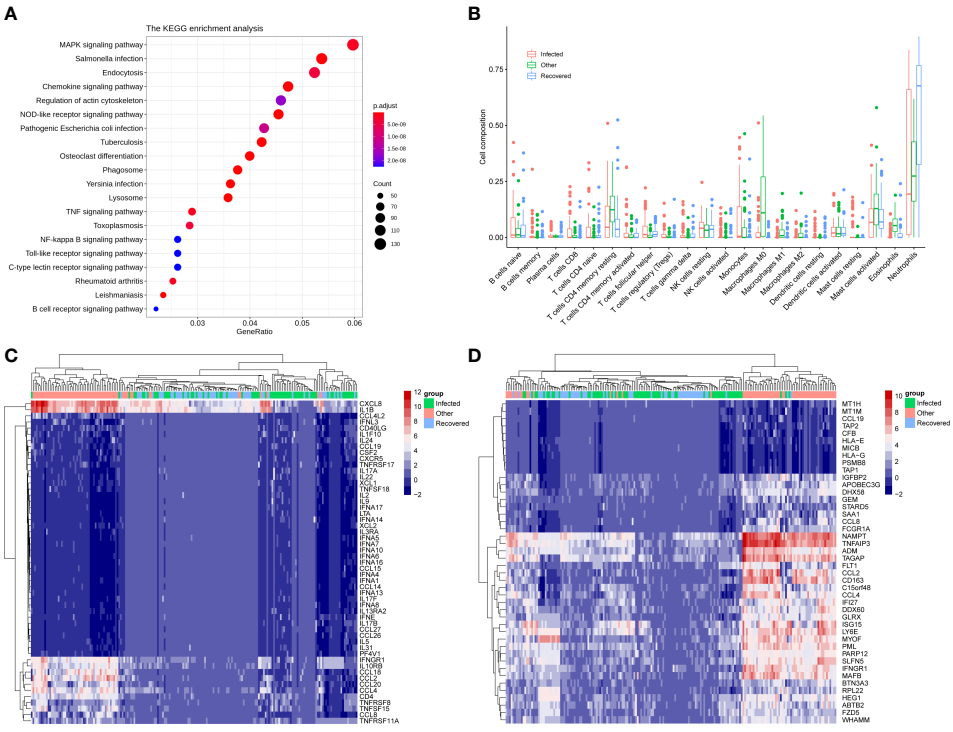

FIGURE 2
Immune signatures associated with differentially expressed genes. **(A)** KEGG enrichment analysis of the differential expressed genes between infected and other groups. **(B)** Cell composition was estimated by the CIBERSORT algorithm of samples for infected, other, and recovered groups. **(C)** Heatmap showing the expression pattern of 53 differential immune genes across groups. **(D)** Heatmap showing the expression pattern of 44 differential interferon-stimulated genes (ISG) across groups.

superfamily DCC subclass member 3), *IGSF9* (immunoglobulin superfamily member 9), and *IGSF22* (immunoglobulin superfamily member 22).

Immune cell abundance was further estimated using the CIBERSORT algorithm, which revealed that neutrophils were the most abundant immune cell subset across groups and showed significant differences for comparisons of the infected vs. recovered and other vs. recovered groups (Figure 2B and Supplementary Figure 1A, *p-value < 0.001*). The abundance of M0, M1, and M2 macrophages in the other group was significantly higher than that in the infected and recovered groups (Figure 2B and Supplementary Figures B, C, *p-value < 0.01*). In addition, 53 immune-related genes (Figure 2C) and 44 interferon-stimulated genes (ISG) (Figure 2D) were significantly differentially expressed between the combinations of infected, recovered, and other groups (*p-value < 0.001*). The above results indicate that patients with COVID-19 infection and recovered COVID-19 patients showed a distinct host immune response compared to other infections.

Changes in the microbiome associated with COVID-19

The microbiome composition in the respiratory tract was evaluated in the three groups. All types of alpha diversity indexes, including richness, ACE, Chao1, Shannon, and Simpson, showed no significant differences between the infected and recovered groups, while those of both these groups showed significant differences when compared with the other group (Figures 3A-E, Wilcoxon test, *p-value* < 0.05). PCoA revealed significant differences between all three groups, especially distinguishing the other group (Figure 3F).

At the genus level, Streptococcus, Veillonella, Gemella, Bacillus, and Neisseria showed the highest abundances (Figure 4A). At the species level, Veillonella parvula, Streptococcus constellatus, Streptococcus pneumoniae, Rothia mucilaginosa, Salmonella enterica, Streptococcus mitis, Gemella haemolysans, Neisseria meningitidis, Lancefieldella parvula, and Prevotella melaninogenica were the most abundant (Figure 4B). However, most of the top 10 abundant genera (Figure 4C) and species (Figure 4D) were observed to be significantly different between all combinations of the above three groups (Wilcoxon test, p-value < 0.05).

Linear discriminant analysis effect size (LEfSe) analysis was performed to further identify microbial taxa as biomarkers for different groups (Figure 5). Specifically, *Human respirovirus 3*, *Pseudomonas aeruginosa*, *Streptococcus pneumoniae*, *Neisseria meningitidis*, *Human orthopneumovirus*, *Acinetobacter baumannii*, *Salmonella enterica*, *Alcaligenes faecalis*, *Lautropia mirabilis*, and *Comamonas thiooxydans* were enriched in the other group (Figure 5D). *Streptococcus constellatus*, *Streptococcus mitis*, *Xanthomonas euvesicatoria*, severe acute respiratory syndrome-related coronavirus, *Streptococcus oralis*, *Streptococcus cristatus*, *Gemella morbillorum*, *Streptococcus koreensis*, *Microbacterium* sp. Y−01, and *Streptococcus parasanguinis* were enriched in the infected group (Figure 5D). In addition, *Veillonella parvula*, *Gemella haemolysans*, *Rothia mucilaginosa*, *Lancefieldella parvula*, *Schaalia odontolytica*, *Haemophilus parainfluenzae*, *Prevotella intermedia*, *Veillonella nakazawae*, *Gemella sanguinis*, and *Neisseria mucosa* were enriched in the recovered group (Figure 5D).

Host transcriptional and microbial classifier associated with COVID-19 recovering

Differential genes, microbial taxa, and combinations of differential genes and microbial taxa were used to train the random forest classifier (Figure 6). The MDA algorithm was performed to select the more reliable features. The random forest prediction model with the differential genes showed a mean AUC of 0.77 (Figure 6B). *KCNK12* (potassium two pore domain channel subfamily K member 12), *IL17RD*, *LOC100507412*, *PTPRT* (protein tyrosine phosphatase receptor type T), *MYO15A* (myosin XVA), *MPDZ* (multiple PDZ domain crumbs cell polarity complex component), *FLRT2* (fibronectin leucine-rich transmembrane protein 2), *SPEG* (striated muscle enriched protein kinase), *SERPINB3* (serpin family B member 3), and *KNDC1* (kinase non-catalytic C-lobe domain containing 1) were identified as the most important genes distinguishing the infected group from the recovered group (Figure 6A). The model with the differential microbial taxa showed a mean AUC of 0.85 (Figure 6D) and severe acute respiratory syndrome-related coronavirus, *Agrobacterium tumefaciens*, *Klebsiella michiganensis*, *Acinetobacter pittii*, *Bacillus* sp. FJAT.14266, *Brevundimonas naejangsanensis*, *Pseudopropionibacterium propionicum*, *Priestia megaterium*, *Dialister pneumosintes*, *Veillonella rodentium*, and *Pseudomonas protegens* were identified as the most important taxa that distinguished the infected group from the recovered group (Figure 6C).

A random forest prediction model with both the differential genes and microbial taxa exhibited better performance than those with differential genes or taxa independently, which achieved AUC of 0.99 ± 0.00, 0.87 ± 0.01, and 0.99 ± 0.00 for comparisons of infected vs. other, infected vs. recovered, and other vs. recovered groups, respectively (Figure 6D and Supplementary Figure 2).

Discussion

In the past two years, COVID-19 has aggressively spread to most countries worldwide and was declared a pandemic by the

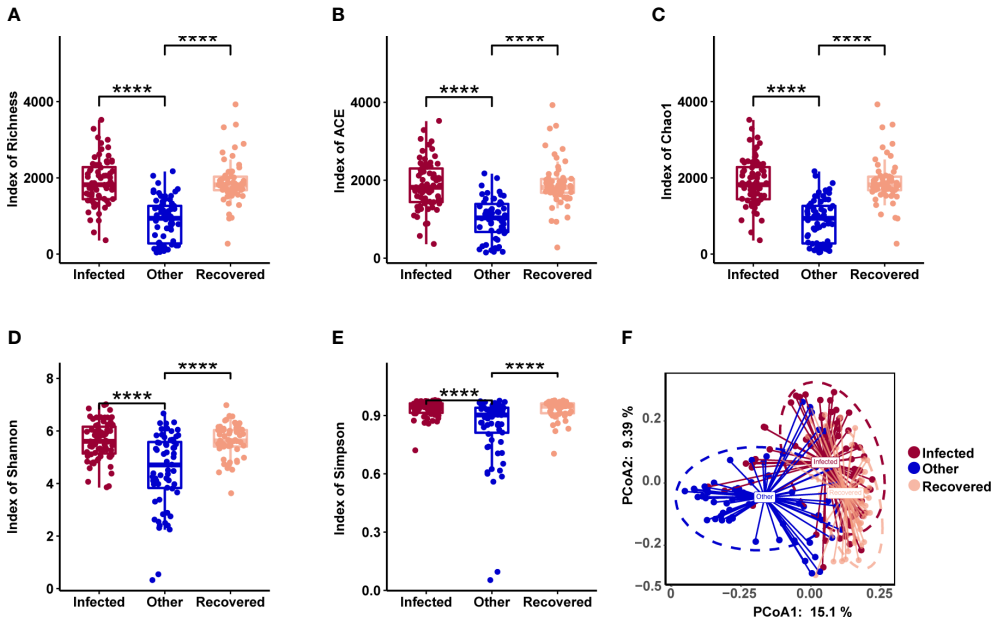

FIGURE 3
Microbial diversity associated with COVID-19. **(A-E)** Alpha diversity includes richness **(A)**, ACE **(B)**, Chao1 **(C)**, Shannon **(D)**, and Simpson **(E)**. **** indicates a *p-value* < 0.0001 (Wilcoxon test). **(F)** Principal coordinates analysis (PCoA) of samples using a Jensen-Shannon Divergence (JSD) distance.

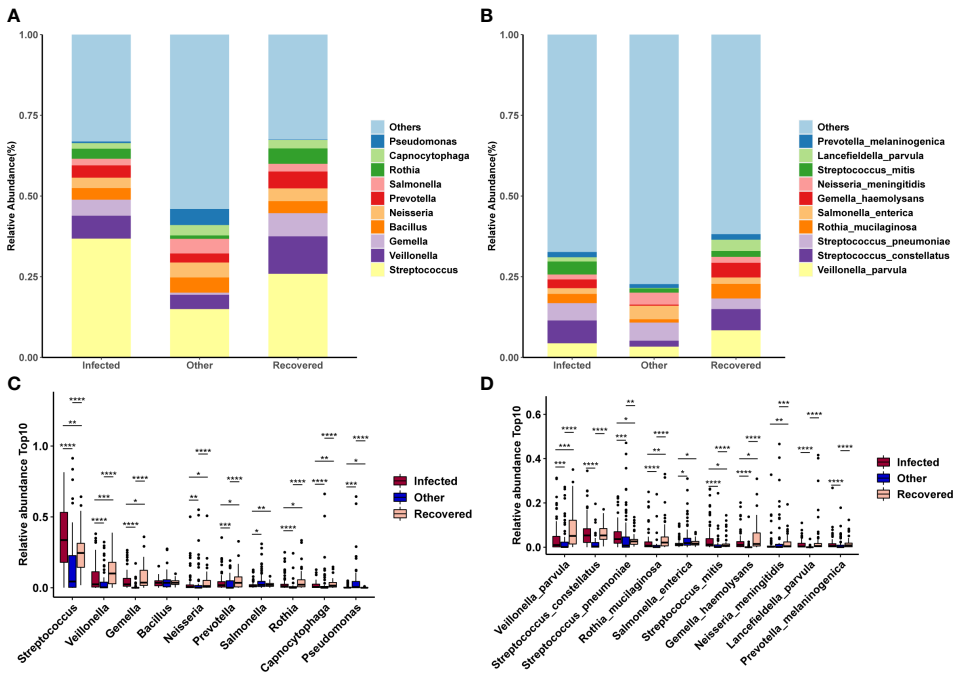

FIGURE 4
Changes in microbial composition across groups. **(A, B)** Microbial composition of the top 10 taxa at the genus **(A)** and species **(B)** levels. **(C, D)** Differences in the microbial composition of the top 10 taxa between groups at the genus **(C)** and species **(D)** levels. *, **, ***, and **** indicates a *p-value* < 0.05, 0.01, 0.001, and 0.0001 (Wilcoxon test), respectively.

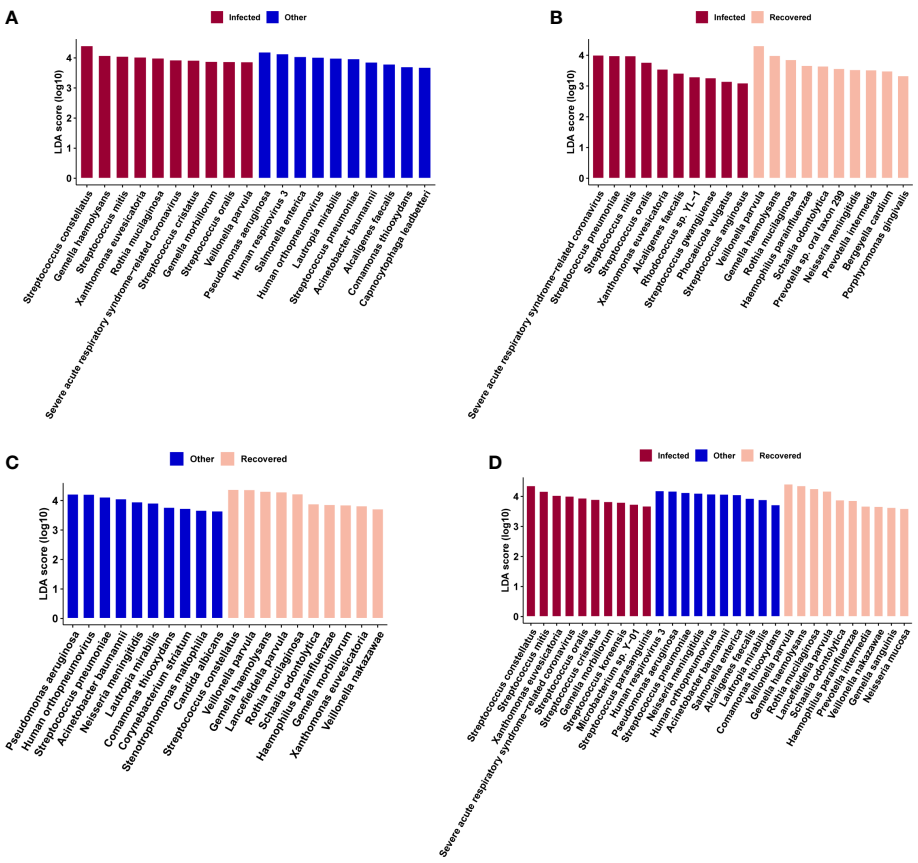

FIGURE 5
Microbial biomarkers identified by linear discriminate analysis effect size (LEfSe) analysis for combinations of infected vs. other **(A)**, infected vs. recovered **(B)**, and other vs. recovered **(C)** groups, and across the above three groups **(D)**, respectively.

WHO in March 2020 (WHO, 2020). SARS-CoV-2 is highly pathogenic and infectious, and the clinical features of COVID-19 differ from those of SARS, Middle East respiratory syndrome (MERS), and seasonal influenza (Huang et al., 2020). The metatranscriptomic characteristics of patients with COVID-19 were reported, and COVID-19 patients have a higher potential for concurrent infection and specific triggers of host immune responses through specific pathways compared with non-COVID-19 pneumonia patients (Zhang et al., 2020). Previous studies have implicated the NF-κB pathway in the etiology of severe COVID-19 phenotypes (Hirano and Murakami, 2020). The NF-κB pathway inhibition has a potential therapeutic role in alleviating severe COVID-19 disease (Hariharan et al., 2021). siRNA depletion of retinoic acid-induced I-like receptor (RLR) or aptamers significantly attenuates cytokine and/or chemokine induction, and RLR signaling also contributes to MERS-CoV-induced inflammation-evoked responses (Zhao et al., 2020). IL1B, P2RX7, IFNB1, IFNB1, TNF, and CASP1 enhance the network connectivity between multiple sclerosis (MS) complex genomes associated with COVID-19 and NOD-like receptor (NLR) signaling. The activity of NLR signaling has been found in COVID-19 and MS, revealing that the NLR signaling pathway plays an important role in COVID-19 disease-associated multiple sclerosis (Qiu et al., 2022). Toll-like receptor (TLRs) pathways, as components of innate immunity, could be involved in the pathogenesis of SARS-CoV-2, and several studies have shown that TLRs play an important role in the pathogenesis of SARS-CoV and MERS-CoV (Khanmohammadi and Rezaei, 2021). Conti et al. found that activation of TLRs during COVID-19 infection may produce inflammation-inducing cytokines such as IL-1β (Conti et al., 2020). Additionally, the immunopathological consequences that lead to death in COVID-19 patients result from interactions between TLRs and virions (Patra et al., 2020). In our study, differentially expressed genes between infected and other groups were enriched in the chemokine signaling pathway, NOD-like receptor signaling pathway, phagosome, TNF signaling pathway, NF-kappa B (NF-κB) signaling pathway, Toll-like receptor signaling pathway, and C-type lectin receptor signaling pathway (Figure 2A).

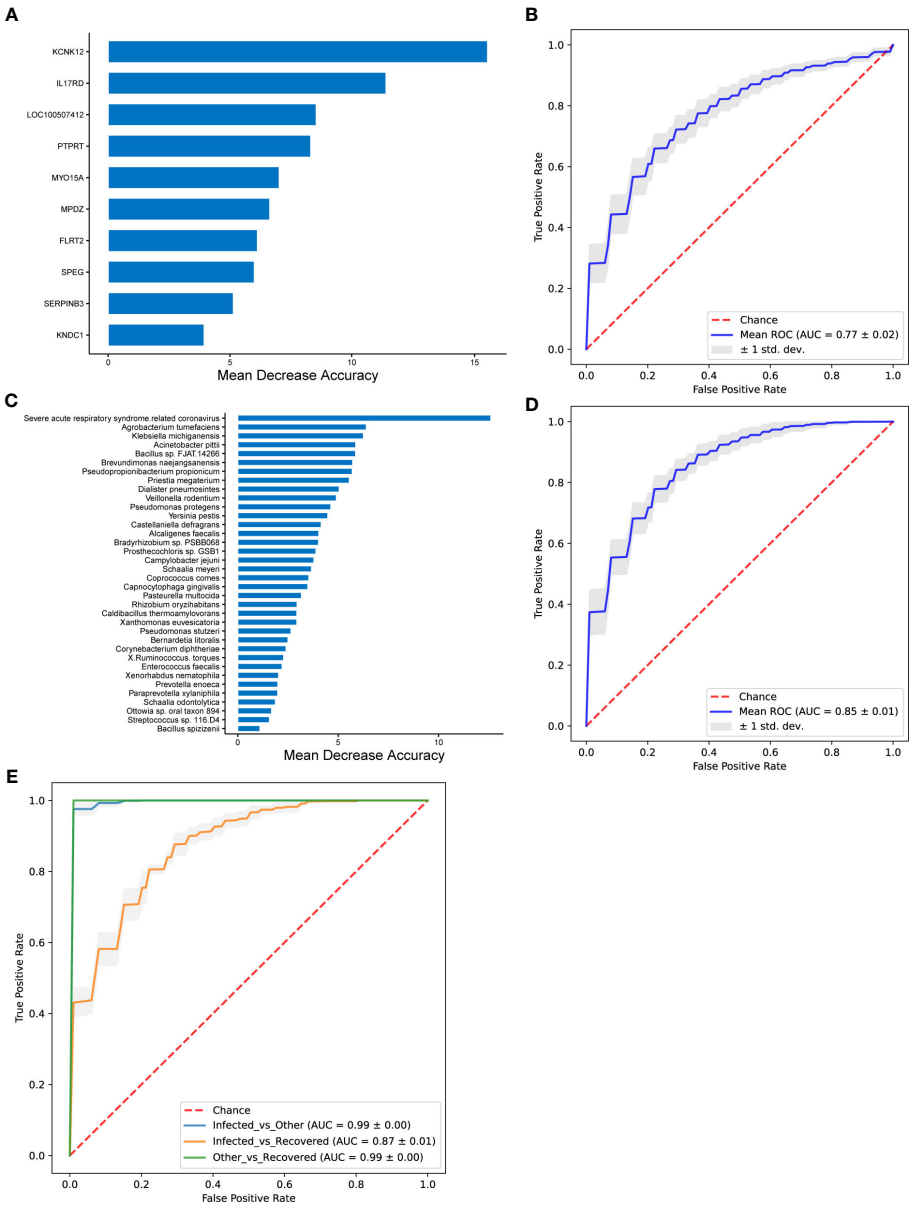

FIGURE 6
The performance of random forest classifier and associated important features. **(A, B)** Performance of random forest model with differential genes for infected vs. recovered groups. **(C, D)** Performance of random forest model with differential microbial taxa for infected vs. recovered groups. **(E)** Performance of random forest model with both differential genes and differential microbial taxa. The important features were selected using MDA (mean decrease in accuracy) algorithm **(A, C)**, and mean ROC curves are shown with ± 1 standard deviation in gray shading **(B, D)**. AUC, area under the curve; ROC, receiver operating characteristic; std. dev., standard deviation.

Based on a previous study, the rate of bacterial co-infection among hospitalized COVID-19 patients has been estimated to be approximately 7% (Lansbury et al., 2020). More seriously, the proportion of patients with bacterial co-infection increases to 14% in the intensive care unit (ICU) (Lansbury et al., 2020). To examine possible concurrent infections in COVID-19 patients, the microbiota community structure at the genus and species levels was analyzed. Our current data reveal frequent co-infection with *Streptococcus* (*Streptococcus constellatus, Streptococcus pneumoniae*, and *Streptococcus mitis*), *Veillonella* (*Veillonella parvula*), *Gemella* (*Gemella haemolysans*) and *Neisseria* (*Neisseria meningitidis*). This result is consistent with those of previous studies (Desai et al., 2020; Brueggemann et al., 2021; Ma et al., 2021). It is strongly believed that *Streptococcus constellatus, Streptococcus pneumonia*, *Streptococcus mitis*, and *Neisseria meningitidis* can cause invasive diseases such as

pyogenic liver abscesses (Kokayi, 2021; Samra et al., 2021), meningitis (Chang et al., 2002; Ostergaard et al., 2005; Kutlu et al., 2008), and pneumonia (Shinzato and Saito, 1995; Catterall, 1999; Glikman et al., 2006). Co-infection can increase the susceptibility of COVID-19 patients to these invasive diseases by decreasing lymphocyte and host immune function and increasing resistance to antibacterial therapy. Thus, the complex nature of pathogen co-infections and host interactions is associated with various clinical symptoms and increases the risk of shock, respiratory failure, prolonged stay in the intensive care unit, and mortality.

However, with an increasing number of patients recovering, it is urgent to focus on the physical status of recovered patients, especially the respiratory immune system. Understanding the changes in the immune status and microbiome of the respiratory tract after recovery is essential for improving diagnosis and treatment. Although analysis of the KEGG pathways associated with the differentially expressed genes between the infected and recovered groups did not show any significant enrichment, some upregulated genes in the infected group compared with the recovered group were involved in immune-related functions (Figure 1B), including *IL17RD* (interleukin 17 receptor D), *CD74* (CD74 molecule), *NTRK2* (neurotrophic receptor tyrosine kinase 2), *NKD1* (NKD inhibitor of WNT signaling pathway 1), *CD180* (CD180 molecule), and *TNFSF15* (TNF superfamily member 15). Previous studies have shown that IL17RD, which is similar to Fgf genes (SEF), acts as a signaling hub that negatively regulates mitogenic signaling pathways, such as the ERK1/2 MAP kinase pathway and innate immune signaling (Girondel et al., 2021). Furthermore, studies have demonstrated that IL-17 can activate NF-κB transcription factors in many cell types (Shabgah et al., 2014). IL-17 in humans is associated with the pathology of numerous autoimmune and inflammatory conditions, such as rheumatoid arthritis (RA) and multiple sclerosis (MS) (Tesmer, 2008). Additionally, transcriptomic analysis of the innate immune signatures of a SARS-CoV-2 protein subunit vaccine ZF2001 and an mRNA vaccine RRV revealed that ZF001 induced MHC class II-related genes, including CD74 and H2-Aa, more expeditiously than did RRV (Wang et al., 2022). A summary data-based Mendelian randomization (SMR) analysis and a transcriptome-wide association study (TWAS) were performed for the severe COVID-19 dataset, and seven novel genes for severe COVID-19 were identified, including CCR5, CCR5AS, IL10RB, TAC4, RMI1, and TNFSF15 (Rao et al., 2021). Thus, we speculate that IL-17RD, CD74, and TNFSF15 might serve as disease biomarkers for COVID-19.

A previous study demonstrated that host transcriptome profiles helped build a host transcriptional classifier (*NFAT-5*, *ZC3H11A*, and *PRRC2C*) for diagnosing lower respiratory tract infections with an AUC of 0.88 (95% CI, 0.75-1.00) (Langelier et al., 2018). These host genes are involved in immune system regulation. The sample size of this study was small, but it still makes a critical contribution to monitoring COVID-19 patients receiving treatment. The MDA algorithm was used to further validate the classifier associated with COVID-19 recovery, which contributed significantly to prediction performance. The predictive model of 10 genes (nine known genes and one uncharacterized gene) revealed remarkable discriminating power and exhibited potential for indicating disease treatment. For example, two-pore domain potassium channels encoded by *KCNK12* enable background leakage of $K^{+,}$ which is important for baseline cellular activity at rest, including membrane potential, calcium homeostasis, and cell volume regulation (Williams et al., 2013). Not only can the gene copy number of *KCNK12* allow it to serve as a molecular biomarker for the early detection of diseases (acute lymphoblastic leukemia (Han and Kang, 2009), non-Hodgkin's lymphoma (Han and Kang, 2009), tubular breast carcinoma (Riener et al., 2008), synovial sarcoma (Heidecker et al., 2010), and malignant peripheral nerve sheath tumors (Nakagawa et al., 2006)) but the expression of these two-pore domain potassium channels also holds promise as an index for therapeutic targets. To the best of our knowledge, this is the first study to identify *KCNK12* as a host classifier for COVID-19. In contrast, severe acute respiratory syndrome-related coronaviruses, *Agrobacterium tumefaciens, Klebsiella michiganensis, Acinetobacter pittii, Bacillus* sp. FJAT.14266, *Brevundimonas naejangsanensis, Pseudopropionibacterium propionicum, Priestia megaterium, Dialister pneumosintes, Veillonella rodentium*, and *Pseudomonas protegens* were selected as candidate microbial markers to trace patient recovery. Ren et al. indicated that *Porphyromonas*, *Haemophilus*, and *Family_XIII_incertae_sedis* carried high levels of oral microbial markers during recovery from COVID-19 (Ren et al., 2021). These similar results indicate that interventions informed by these bacteria may impact patient outcomes. This molecular detection strategy is highly accurate and efficacious. In the future, we might be able to assist physicians in monitoring COVID-19 and predicting disease progression *via* next generation sequencing (NGS).

Conclusion

Although the sample size is small and the sample source is narrow, this study contributes significantly to the exploration of the microbiome which is closely related to COVID-19. We identified compositional and functional alterations in the COVID-19-associated microbiome, identified specific biomarkers in humans, explained the mechanism of co-infection, and developed a diagnostic strategy. The microbiome also plays a vital role in COVID-19 recovery. Therefore, we developed gene-based and microbial-assisted methods to guide antibiotic treatment and monitor patient treatment status. With the progress of NGS and further study of the possible mechanisms by which the microbiome affects

diseases, the use of gene-based and microbial-assisted diagnosis, treatment, and the prognosis is promising for COVID-19.

Data availability statement

The data presented in the study are deposited in the National Genomics Data Center (NGDC) repository, accession number PRJCA012894, https://ngdc.cncb.ac.cn/search/?dbId=bioproject&q=PRJCA012894&page=1.

Ethics statement

The studies involving human participants were reviewed and approved by Beijing Ditan Hospital. The patients/participants provided their written informed consent to participate in this study.

Author contributions

All the authors contributed to the research significantly. RJ and YW conceived and designed the analysis; XX and DW collected the samples; SW and JG tested the samples. HM performed the analysis and CR, YG, HL assist with the bioinformatic analysis; HM wrote the first draft, SW revised the manuscript. All the authors provided critical advice to the revision of the manuscript.

Funding

This work was supported by Beijing Municipal Natural Science Foundation (grant No.2022-2-014) and Beijing high-level public health technical personnel construction project (grant No.M21003).

Conflict of interest

Author CR, YG and HL was employed by the company Guangzhou Vision Medicals Co.LTD. The remaining authors declare that the research was conducted in the absence of any commercial or financial relationships that could be construed as a potential conflict of interest.

Publisher's note

All claims expressed in this article are solely those of the authors and do not necessarily represent those of their affiliated organizations, or those of the publisher, the editors and the reviewers. Any product that may be evaluated in this article, or claim that may be made by its manufacturer, is not guaranteed or endorsed by the publisher.

Supplementary material

The Supplementary Material for this article can be found online at: https://www.frontiersin.org/articles/10.3389/fcimb.2022.1011672/full#supplementary-material

SUPPLEMENTARY FIGURE 1
The differences in immune cell abundance across stages for Neutrophils **(A)**, and Macrophages M0 **(B)**, M1 **(C)**, and M2 **(D)**. The *p values* were calculated using DESeq2.

SUPPLEMENTARY FIGURE 2
The performance of the random forest classifier for the Infected vs. Other **(A, B)** and Other vs. Recovered **(C, D)** groups with differential genes **(A, C)** and differential microbial taxa **(B, D)** as features. Mean ROC curves are shown with ± 1 standard deviation in gray shading. AUC, area under the curve; ROC, receiver operating characteristic; std. dev., standard deviation.

SUPPLEMENTARY TABLE 1
Mapping information of sequencing data.

References

Avraham, R., Haseley, N., Fan, A., Bloom-Ackermann, Z., Livny, J., Hung, D. T., et al. (2016). A highly multiplexed and sensitive rna-seq protocol for simultaneous analysis of host and pathogen transcriptomes. *Nat. Protoc.* 11 (8), 1477. doi: 10.1038/nprot.2016.090

Bannister, B. A. (1988). Post-infectious disease syndrome. *Postgrad. Med. J.* 64 (753), 559–567. doi: 10.1136/pgmj.64.753.559

Brueggemann, A. B., Jansen Van Rensburg, M. J., Shaw, D., Mccarthy, N. D., Jolley, K. A., Maiden, M. C. J., et al. (2021). Changes in the incidence of invasive disease due to streptococcus pneumoniae, haemophilus influenzae, and neisseria meningitidis during the COVID-19 pandemic in 26 countries and territories in the invasive respiratory infection surveillance initiative: a prospective analysis of surveillance data. *Lancet Digit Health* 3, e360–e370. doi: 10.1016/S2589-7500(21)00077-7

Catterall, J. R. (1999). Streptococcus pneumoniae. *Thorax* 54, 929–937. doi: 10.1136/thx.54.10.929

Chang, W. N., Wu, J. J., Huang, C. R., Tsai, Y. C., Chien, C. C., and Lu, C. H. (2002). Identification of viridans streptococcal species causing bacterial meningitis in adults in Taiwan. *Eur. J. Clin. Microbiol. Infect. Dis.* 21, 393–396. doi: 10.1007/s10096-002-0727-z

Chan, K. S., Zheng, J. P., Mok, Y. W., Li, Y. M., Liu, Y. N., Chu, C. M., et al. (2003). SARS: prognosis, outcome and sequelae. *Respirology* 8, 36–40. doi: 10.1046/j.1440-1843.2003.00522.x

Cheung, C. Y., Poon, L. L., Ng, I. H., Luk, W., Sia, S. F., Wu, M. H., et al. (2005). Cytokine responses in severe acute respiratory syndrome coronavirus-infected macrophages *in vitro*: possible relevance to pathogenesis. *J. Virol.* 79, 7819–7826. doi: 10.1128/JVI.79.12.7819-7826.2005

Conti, P., Ronconi, G., Caraffa, A., Gallenga, C., Ross, R., Frydas, I., et al. (2020). Induction of pro-inflammatorycytokines (IL-1and IL-6) and lung inflammation by coronavirus-19(COVI-19 or SARS-CoV-2): anti-inflammatory strategies. *J. Biol. RegulHomeost Agents* 34 (2), 327–331. doi: 10.23812/conti-e

Costa-Pereira, A. P., Williams, T. M., Strobl, B., Watling, D., Briscoe, J., and Kerr, I. M. (2002). The antiviral response to gamma interferon. *J. Virol.* 76 (18), 9060–9068. doi: 10.1128/JVI.76.18.9060-9068.2002

Crosse, K. M., Monson, E. A., Beard, M. R., and Helbig, K. J. (2018). Interferon-stimulated genes as enhancers of antiviral innate immune signaling. *J. Innate Immun.* 10 (2), 85–93. doi: 10.1159/000484258

de Jong, M. D., Simmons, C. P., Thanh, T. T., Hien, V. M., Smith, G. J., Chau, T. N., et al. (2006). Fatal outcome of human influenza a (H5N1) is associated with high viral load and hypercytokinemia. *Nat. Med.* 12, 1203–1207. doi: 10.1038/nm1477

Desai, A., Santonocito, O. G., Caltagirone, G., Kogan, M., Ghetti, F., Donadoni, I., et al. (2020). Effectiveness of streptococcus pneumoniae urinary antigen testing in decreasing mortality of COVID-19 Co-infected patients: A clinical investigation. *Medicina (Kaunas)* 56, 572. doi: 10.3390/medicina56110572

de Wit, E., van Doremalen, N., Falzarano, D., and Munster, V. J. (2016). SARS and MERS: recent insights into emerging coronaviruses. *Nat. Rev. Microbiol.* 14, 523–534. doi: 10.1038/nrmicro.2016.81

Dickson, R. P., Schultz, M. J., van der Poll, T., Schouten, L. R., Falkowski, N. R., Luth, J. E., et al. (2020). Lung microbiota predict clinical outcomes in critically ill patients. *Am. J. Respir. Crit. Care Med.* 201, 555–563. Biomarker Analysis in Septic ICU Patients (BASIC) Consortium. doi: 10.1164/rccm.201907-1487OC

Girondel, C., Lévesque, K., Langlois, M. J., Pasquin, S., Saba-El-Leil, M. K., Rivard, N., et al. (2021). Loss of interleukin-17 receptor d promotes chronic inflammation-associated tumorigenesis. *Oncogene* 40 (2), 452–464. doi: 10.1038/s41388-020-01540-4

Glikman, D., Matushek, S. M., Kahana, M. D., and Daum, R. S. (2006). Pneumonia and empyema caused by penicillin-resistant neisseria meningitidis: a case report and literature review. *Pediatrics* 117, e1061–e1066. doi: 10.1542/peds.2005-1994

Grandvaux, N., tenOever, B. R., Servant, M. J., and Hiscott, J. (2002). The interferon antiviral response: from viral invasion to evasion. *Curr. Opin. Infect. Dis.* 15 (3), 259–267. doi: 10.1097/00001432-200206000-00008

Greenhalgh, T., Knight, M., A'Court, C., Buxton, M., and Husain, L. (2020). Management of post-acute covid-19 in primary care. *BMJ* 370, m3026. doi: 10.1136/bmj.m3026

Han, J., and Kang, D. (2009). TRESK channel as a potential target to treat T-cell mediated immune dysfunction. *Biochem. Biophys. Res. Commun.* 390, 1102–1105. doi: 10.1016/j.bbrc.2009.10.076

Hariharan, A., Hakeem, A. R., Radhakrishnan, S., Reddy, M. S., and Rela, M. (2021). The role and therapeutic potential of NF kappa b pathway in severe COVID 19 patients. *Inflammopharmacology* 29, 91–100. doi: 10.1007/s10787-020-00773-9

Heidecker, B., Lamirault, G., Kasper, E. K., Wittstein, I. S., Champion, H. C., Breton, E., et al. (2010). The gene expression profile of patients with new-onset heart failure reveals important gender-specific differences. *Eur. Heart J.* 31, 1188–1196. doi: 10.1093/eurheartj/ehp549

Hickie, I., Davenport, T., Wakefield, D., Vollmer-Conna, U., Cameron, B., Vernon, S. D., et al. (2006). Dubbo infection outcomes study group. post-infective and chronic fatigue syndromes precipitated by viral and non-viral pathogens: prospective cohort study. *BMJ* 333 (7568), 575. doi: 10.1136/bmj.38933.585764.ae

Hirano, T., and Murakami, M. (2020). COVID-19: a new virus, but a familiar receptor and cytokine release syndrome. *Immunity* 52 (5), 731–733. doi: 10.1016/j.immuni.2020.04.003

Huang, K. J., Su, I. J., Theron, M., Wu, Y. C., Lai, S. K., Liu, C. C., et al. (2005). An interferon-gamma-related cytokine storm in SARS patients. *J. Med. Virol.* 75, 185–194. doi: 10.1002/jmv.20255

Huang, C., Wang, Y., Li, X., Ren, L., Zhao, J., Hu, Y., et al. (2020). Clinical features of patients infected with 2019 novel coronavirus in wuhan, China. *Lancet* 395 (10223), 497–506. doi: 10.1016/S0140-6736(20)30183-5

Khanmohammadi, S., and Rezaei, N. (2021). Role of toll-like receptors in the pathogenesis of COVID-19. *J. Med. Virol.* 93 (5), 2735–2739. doi: 10.1002/jmv.26826

Kokayi, A.Jr. (2021). Septic shock secondary to a pyogenic liver abscess following complicated appendicitis. *Cureus* 13, e18359. doi: 10.7759/cureus.18359

Kumpitsch, C., Koskinen, K., Schöpf, V., and Moissl-Eichinger, C. (2019). The microbiome of the upper respiratory tract in health and disease. *BMC Biol.* 17, 87. doi: 10.1186/s12915-019-0703-z

Kutlu, S. S., Sacar, S., Cevahir, N., and Turgut, H. (2008). Community-acquired streptococcus mitis meningitis: a case report. *Int. J. Infect. Dis.* 12, e107–e109. doi: 10.1016/j.ijid.2008.01.003

Lam, M. H., Wing, Y. K., Yu, M. W., Leung, C. M., Ma, R. C., Kong, A. P., et al. (2009). Mental morbidities and chronic fatigue in severe acute respiratory syndrome survivors: long-term follow-up. *Arch. Intern. Med.* 169 (22), 2142–2147. doi: 10.1001/archinternmed.2009.384

Langelier, C., Kalantar, K. L., Moazed, F., Wilson, M. R., Crawford, E. D., Deiss, T., et al. (2018). Integrating host response and unbiased microbe detection for lower respiratory tract infection diagnosis in critically ill adults. *Proc. Natl. Acad. Sci. U.S.A.* 115, E12353–E12362. doi: 10.1073/pnas.1809700115

Lansbury, L., Lim, B., Baskaran, V., and Lim, W. S. (2020). Co-Infections in people with COVID-19: a systematic review and meta-analysis. *J. Infect.* 81, 266–275. doi: 10.1016/j.jinf.2020.05.046

Lau, H. M., Lee, E. W., Wong, C. N., Ng, G. Y., Jones, A. Y., and Hui, D. S. (2005). The impact of severe acute respiratory syndrome on the physical profile and quality of life. *Arch. Phys. Med. Rehabil.* 86 (6), 1134–1140. doi: 10.1016/j.apmr.2004.09.025

Lee, A. M., Wong, J. G., McAlonan, G. M., Cheung, V., Cheung, C., Sham, P. C., et al. (2007). Stress and psychological distress among SARS survivors 1 year after the outbreak. *Can. J. Psychiatry* 52 (4), 233–240. doi: 10.1177/070674370705200405

Li, N., Ma, W. T., Pang, M., Fan, Q. L., and Hua, J. L. (2019). The commensal microbiota and viral infection: a comprehensive review. *Front. Immunol.* 10, 1551. doi: 10.3389/fimmu.2019.01551

Loenhout, J. A., Tiel, H. H., den Heuvel, J., Vercoulen, J. H., Bor, H., der Velden, K., et al. (2014). Serious long-term health consequences of q-fever and legionnaires' disease. *J. Infect.* 68 (6), 527–533. doi: 10.1016/j.jinf.2014.01.004

Man, W. H., Houten, M. A., van Mérelle, M. E., Vlieger, A. M., Chu, M. L. J. N., Jansen, N. J. G., et al. (2019). Bacterial and viral respiratory tract microbiota and host characteristics in children with lower respiratory tract infections: a matched case-control study. *Lancet Respir. Med.* 7, 417–426. doi: 10.1016/S2213-2600(18)30449-1

Ma, S., Zhang, F., Zhou, F., Li, H., Ge, W., Gan, R., et al. (2021). Metagenomic analysis reveals oropharyngeal microbiota alterations in patients with COVID-19. *Signal Transduct Target Ther.* 6, 191. doi: 10.1038/s41392-021-00614-3

Nakagawa, Y., Yoshida, A., Numoto, K., Kunisada, T., Wai, D., Ohata, N., et al. (2006). Chromosomal imbalances in malignant peripheral nerve sheath tumor detected by metaphase and microarray comparative genomic hybridization. *Oncol. Rep.* 15, 297–303. doi: 10.3892/or.15.2.297

Ostergaard, C., Konradsen, H. B., and Samuelsson, S. (2005). Clinical presentation and prognostic factors of streptococcus pneumoniae meningitis according to the focus of infection. *BMC Infect. Dis.* 5, 93. doi: 10.1186/1471-2334-5-93

Panzer, A. R., Lynch, S. V., Langelier, C., Christie, J. D., McCauley, K., Nelson, M., et al. (2018). Lung microbiota is related to smoking status and to development of acute respiratory distress syndrome in critically ill trauma patients. *Am. J. Respir. Crit. Care Med.* 197, 621–631. doi: 10.1164/rccm.201702-0441OC

Patra, R., Chandra Das, N., and Mukherjee, S. (2020). Targeting human TLRs tocombat COVID-19: A solution? *J. Med. Virol.* 93, 615–617. doi: 10.1002/jmv.26387

Qiu, D., Zhang, D., Yu, Z., Jiang, Y., and Zhu, D. (2022). Bioinformatics approach reveals the critical role of the NOD-like receptor signaling pathway in COVID-19-associated multiple sclerosis syndrome. *J. Neural Transm (Vienna)* 1, 1–8. doi: 10.1007/s00702-022-02518-0

Rao, S., Baranova, A., Cao, H., Chen, J., Zhang, X., and Zhang, F. (2021). *Genetic mechanisms of COVID-19 and its association with smoking and alcohol consumption* Vol. 22 (Beijing, China: Brief Bioinform), bbab357.

Reghunathan, R., Jayapal, M., Hsu, L. Y., Chng, H. H., Tai, D., Leung, B. P., et al. (2005). Expression profile of immune response genes in patients with severe acute respiratory syndrome. *BMC Immunol.* 6, 2. doi: 10.1186/1471-2172-6-2

Ren, Z., Wang, H., Cui, G., Lu, H., Wang, L., Luo, H., et al. (2021). Alterations in the human oral and gut microbiomes and lipidomics in COVID-19. *Gut* 70, 1253–1265. doi: 10.1136/gutjnl-2020-323826

Riener, M. O., Nikolopoulos, E., Herr, A., Wild, P. J., Hausmann, M., Wiech, T., et al. (2008). Microarray comparative genomic hybridization analysis of tubular breast carcinoma shows recurrent loss of the CDH13 locus on 16q. *Hum. Pathol.* 39, 1621–1629. doi: 10.1016/j.humpath.2008.02.021

Samra, G. S., Randhawa, J. S., Patel, D., and Sabri, R. (2021). Asymptomatic incidental pyogenic hepatic abscess in an obese adult. *Cureus* 13, e17626. doi: 10.7759/cureus.17626

Samuel, C. E. (2001). Antiviral actions of interferons. *Clin. Microbiol. Rev.* 14, 778–809. doi: 10.1128/CMR.14.4.778-809.2001

Shabgah, A. G., Fattahi, E., and Shahneh, F. Z. (2014). Interleukin-17 in human inflammatory diseases. *Postepy Dermatol. Alergol.* 31 (4), 256–261. doi: 10.5114/pdia.2014.40954

Shaw, A. E., Hughes, J., Gu, Q., Behdenna, A., Singer, J. B., Dennis, T., et al. (2017). Fundamental properties of the mammalian innate immune system revealed by multispecies comparison of type I interferon responses. *PLoS Biol.* 15 (12), e2004086. doi: 10.1371/journal.pbio.2004086

Shinzato, T., and Saito, A. (1995). The streptococcus milleri group as a cause of pulmonary infections. *Clin. Infect. Dis.* 21 Suppl 3, S238–S243. doi: 10.1093/clind/21.Supplement_3.S238

Tenforde, M. W., Kim, S. S., Lindsell, C. J., Billig, R. E., Shapiro, N. I., Files, D. C., et al. (2020). IVY network investigators; CDC COVID-19 response team; IVY network investigators. symptom duration and risk factors for delayed return to usual health among outpatients with COVID-19 in a multistate health care systems network - united states, march-June 2020. *MMWR Morb Mortal Wkly Rep.* 69 (30), 993–998. doi: 10.15585/mmwr.mm6930e1

Tesmer, M. (2008). Th17 cells in human disease. *Immunol. Rev.* 223, 87–113. doi: 10.1111/j.1600-065X.2008.00628.x

Wang, Q., Song, Z., Yang, J., He, Q., Mao, Q., Bai, Y., et al. (2022). Transcriptomic analysis of the innate immune signatures of a SARS-CoV-2 protein subunit vaccine ZF2001 and an mRNA vaccine RRV. *Emerg. Microbes Infect.* 11 (1), 1145–1153. doi: 10.1080/22221751.2022.2059404

Westermann, A. J., Gorski, S. A., and Vogel, (2012). Dual RNA-seq of pathogen and host. *Nat. Rev. Microbiol.* 10 (9), 618–630. doi: 10.1038/nrmicro2852

WHO *WHO characterizes COVID-19 as a pandemic.* 2020. Available at: https://www.who.int.

Williams, S., Bateman, A., and O'kelly, I. (2013). Altered expression of two-pore domain potassium (K2P) channels in cancer. *PloS One* 8, e74589. doi: 10.1371/journal.pone.0074589

Wilson, M. R., Naccache, S. N., Samayoa, E., Biagtan, M., Bashir, H., Yu, G., et al. (2014). Actionable diagnosis of neuroleptospirosis by next-generation sequencing. *N Engl. J. Med.* 370 (25), 2408–2417. doi: 10.1056/NEJMoa1401268

Zhang, P., Li, J., Liu, H., Han, N., Ju, J., Kou, Y., et al. (2020). Long-term bone and lung consequences associated with hospital-acquired severe acute respiratory syndrome: a 15-year follow-up from a prospective cohort study. *Bone Res.* 8, 8. doi: 10.1038/s41413-020-0084-5

Zhao, X., Chu, H., Wong, B. H., Chiu, M. C., Wang, D., Li, C., et al. (2020). Activation of c-type lectin receptor and (RIG)-I-Like receptors contributes to proinflammatory response in middle East respiratory syndrome coronavirus-infected macrophages. *J. Infect. Dis.* 221 (4), 647–659. doi: 10.1093/infdis/jiz483

Zhou, Z., Ren, L. L., Zhang, L., Zhong, J., Xiao, Y., Jia, Z., et al. (2020). Heightened innate immune responses in the respiratory tract of COVID-19 patients. *Cell Host Microbe* 27, 883–890. doi: 10.1016/j.chom.2020.04.017

Ziegler, T., Matikainen, S., Ro¨ nkko¨, E., Osterlund, P., Sillanpa€a, M., Sire € ´ n, J., et al. (2005). Severe acute respiratory syndrome coronavirus fails to activate cytokine-mediated innate immune responses in cultured human monocyte-derived dendritic cells. *J. Virol.* 79, 13800–13805. doi: 10.1128/JVI.79.21.13800-13805.2005

frontiers | Frontiers in Cellular and Infection Microbiology

TYPE Original Research
PUBLISHED 07 February 2023
DOI 10.3389/fcimb.2022.1035711

OPEN ACCESS

EDITED BY
Ke Xu,
Wuhan University, China

REVIEWED BY
Haiyan Zhao,
Wuhan University, China
Fei Yu,
Hebei Agricultural University, China

*CORRESPONDENCE
You Li
zhonghualiyou@163.com

†These authors have contributed equally to the work

SPECIALTY SECTION
This article was submitted to Virus and Host, a section of the journal Frontiers in Cellular and Infection Microbiology

RECEIVED 03 September 2022
ACCEPTED 13 December 2022
PUBLISHED 07 February 2023

CITATION
Zhang L, Zhang Y, Wang R, Liu X, Zhao J, Tsuda M and Li Y (2023) SARS-CoV-2 infection of intestinal epithelia cells sensed by RIG-I and DHX-15 evokes innate immune response and immune cross-talk. *Front. Cell. Infect. Microbiol.* 12:1035711. doi: 10.3389/fcimb.2022.1035711

SARS-CoV-2 infection of intestinal epithelia cells sensed by RIG-I and DHX-15 evokes innate immune response and immune cross-talk

Lijuan Zhang[1†], Yize Zhang[2†], Ruiqin Wang[3], Xiaoning Liu[1], Jinmeng Zhao[4], Masato Tsuda[5] and You Li[1,3*]

[1]School of Medicine, Huanghe Science and Technology College, Zhengzhou, China, [2]Precision Medicine Center, Gene Hospital of Henan Province, The First Affiliated Hospital of Zhengzhou University, Zhengzhou, China, [3]School of Life Science and Technology, Tongji University, Shanghai, China, [4]School of Life Science, Zhengzhou University, Zhengzhou, China, [5]School of Medicine, Niigata University, Niigata, Japan

SARS-CoV-2 causes a spectrum of clinical symptoms from respiratory damage to gastrointestinal disorders. Intestinal infection of SARS-CoV-2 triggers immune response. However, the cellular mechanism that how SARS-CoV-2 initiates and induces intestinal immunity is not understood. Here, we exploited SARS-CoV-2-GFP/ΔN trVLP pseudo-virus system and demonstrated that RIG-I and DHX15 are required for sensing SARS-CoV-2 and inducing cellular immune response through MAVS signaling in intestinal epithelial cells (IECs) upon SARS-CoV-2 infection. NLRP6 also engages in the regulation of SARS-CoV-2 immunity by producing IL-18. Furthermore, primary cellular immune response provoked by SARS-CoV-2 in IECs further cascades activation of MAIT cells and produces cytotoxic cytokines including IFN-γ, granzyme B *via* an IL-18 dependent mechanism. These findings taken together unveil molecular basis of immune recognition in IECs in response to SARS-CoV-2, and provide insights that intestinal immune cross-talk with other immune cells triggers amplified immunity and probably contributes to immunopathogenesis of COVID-19.

KEYWORDS

SARS-CoV-2, IECs, RIG-I, DHX15, MAIT, IL-18

Introduction

The severe acute respiratory syndrome coronavirus 2 (SARS-CoV-2) pandemic has caused over 500 million infections and more than 6 million deaths worldwide (WHO, 2022). Infection with SARS-CoV-2 results in a spectrum of clinical presentations of varying severity. Besides the common respiratory symptoms, growing studies have reported a substantial proportion of gastrointestinal (GI) manifestations, such as nausea, abdominal pain, vomiting and diarrhoea at the onset of the disease (Xiao et al., 2020; Guo et al., 2021). Although the accurate mechanism of GI symptom is still unclear, intestinal organ-specific immune response has been proposed to link GI symptom in SARS-CoV-2-infected patient (Chen et al., 2022).

Clinical evidence shows that human intestine is susceptible to SARS-CoV-2 infection (Jin et al., 2020; Livanos et al., 2021). Intestinal enterocytes enrich ACE2 entry receptors and accessory proteinase TMPRSS2 which promotes SARS-CoV-2 virus efficiently infecting enterocytes in human intestinal organoids (Shang et al., 2020; Zang et al., 2020). Gastrointestinal tract provides the first line of host innate immune response for pathogenic microorganism invasion (Wu and Wu, 2012). *Ex vivo* studies of SARS-CoV-2 with human colon organoids or intestinal enteroids demonstrate that SARS-CoV-2 infection initiates antiviral innate immune response by producing type I interferon (IFN) and type III IFN (Stanifer et al., 2020; Zhou et al., 2020). While well-coordinated immune response induced by virus infection of epithelial cells leads to viral clearance, exuberant response and hyperactivation can contribute to disease exacerbation reversely. Patients infected with SARS-CoV-2 are also accompanied with aggressive inflammatory response and release of a large amount of pro-inflammatory cytokines (Divij et al., 2020; Laing et al., 2020; Leticia et al., 2020). In a nonhuman primate model, SARS-CoV-2 infection results in dynamic inflammation profile and inflammatory cytokines release including IL-1β, IL-1ra, MCP-1, IL-12, MIP-1β as disease progress in gastrointestinal tissue (Jiao et al., 2021). Of note, IL18 is upregulated at the onset of infection (dpi 1, 4), which is corresponding to that IL-18 is increased upon fever onset and remains highly elevated in the acute phase of SARS-CoV-2 infection in patients (Rodrigues et al., 2020a; Tao et al., 2020b; Flament et al., 2021; Ashrafzadeh-Kian et al., 2022). Thus, intestinal infection and replication of SARS-CoV-2 triggers antiviral or inflammatory response. Nonetheless, it remains unveiled that how SARS-CoV-2 infection initiates and induces immune response in intestine, and whether and how intestinal immunity participates in cross-talk in local immune response and even contributes to system cytokines production.

SARS-CoV-2 is a positive-sense, single-stranded RNA beta-coronavirus that produce double-stranded RNA (dsRNA) intermediates during genome replication and virion propagation (van Dorp et al., 2020; Wu et al., 2020). As in other coronavirus, dsRNA intermediates can be recognized by varied cytosolic RNA sensors, such as RIG-I, MDA5, DHX-15, LGP-2 which signals through MAVS and initiates antiviral innate immune response (Lu et al., 2014; Kell and Gale, 2015; Hur, 2019). Notably, the specific virus sensor that involves in different RNA viral defense is cell type dependent. In lung epithelial cells, MDA5 governs the innate immunity in response to SARS-CoV-2; while in macrophage, RIG-I dominates the immune response (Kato et al., 2006; Takeshi et al., 2007; Bruns et al., 2014; Kenta et al., 2014; Kell and Gale, 2015). Intestinal epithelia cells, the most abundant cell type in gut, are likewise equipped with various RNA sensors to defense viral invasion (Adrish et al., 2012; Lazear et al., 2015). It remains unclear whether SARS-CoV-2 immunity is subject to a similar sensor mechanism in intestinal epithelial cells and by which sensor virus are sensed to initiate immune response.

In viral infections, the crucial role of inflammasome in control of immune response and viral infections has been elucidated. NLRP3 inflammasome activation in infected macrophages/monocyte has been reported to contribute to SARS-CoV-2 related inflammation (Pan et al., 2021). A prominent role of Nlrp6 in the regulation of antiviral immune responses by interacting with dsRNA sensor DHX15 has also been documented recently (Xing et al., 2021). Nlrp6 exhibits cell-type specific higher expression in intestinal epithelial cells (Elinav et al., 2011) and mediates intestinal immunity. It is intriguing to investigate whether intestinal Nlrp6 inflammasome participates in SARS-CoV-2 related immune response in intestine.

Nlrp6 activation signals proinflammatory cytokine IL-18 production (Levy et al., 2015). In SARS-CoV-2 infected patients, IL-18 levels are markedly increased either in serum or faecal samples, which correlates with disease severity (Tao et al., 2020a). Furthermore, IL-18 mediated cell cross-talk in SARS-CoV-2 immunity subsequently cascades further immune response, and is associated with poor clinical outcome (Rodrigues et al., 2020a; Flament et al., 2021).

Here, we exploited SARS-CoV-2-GFP/ΔN trVLP system, as previously described (Ju et al., 2021), to infect intestinal epithelial cell line Caco-2 and investigated virus-enterocytes interaction to understand the mechanisms by which SARS-CoV-2 is recognized and induces immune response in intestinal epithelial cells. We found that RIG-I and DHX-15 are the required sensors for intestinal epithelial cells to recognize SARS-CoV-2 invasion and to induce IFNs and inflammatory cytokine production, particularly IL18. Coculture of SARS-CoV-2 infected intestinal epithelial cells with human PBMC results in activation of mucosal-associated invariant T cells and cytotoxic cytokine release such as IFN-γ, Granzyme B, TNF-α by MAIT in an IL-18 dependent manner. Given the elevated IL18 levels in relation to disease severity of COVID-19 patients, we proposed to link IL18 production to immunopathogenic response during SARS-CoV-2 infection.

Result

Entry receptor expression and permissiveness of intestinal epithelial cells to SARS-CoV-2 pseudo-virus

Intestinal epithelial cells (IECs) are highly permissive for SARS-CoV-2 infection due to high expression of entry receptor ACE2 and TMPRSS serine protease which facilitates virus entry into host cells (Zang et al., 2020). Recently, CD147-spike interaction was reported as an alternative entry route for SARS-CoV-2 infection (Wang et al., 2020). We screened related proteins expression in the frequently used intestinal epithelial cell lines, including T84, HT-29 and Caco-2, and primary IECs to seek an effective model for further investigation. Basically, all intestinal cell lines displayed constitutively high expression of ACE2, TMPRSS2, but not Vero E6. Of note, compared with T84 and HT-29, Caco-2 presented relative higher expression of ACE2 in mRNA and comparable CD147 (Figures 1A, B), corresponding to that Caco-2 is naturally permissive for SARS-CoV-2 infection and effective for viral replication (Stanifer et al., 2020). To determine the relative permissiveness of these intestinal cell lines to SARS-CoV-2 viral entry, we used a VSV-based SARS-CoV-2 pseudo-virus, designated as VSV-SARS-CoV-2, in which the backbone was provided by rVSV-ΔG-luciferase pseudotypes and the glycoprotein (G) gene was replaced with SARS-CoV-2 spike protein (Nie et al., 2020). Intestinal epithelial cell lines were inoculated with VSV-SARS-CoV-2 entry virus respectively and luciferase activity was analyzed at 24h post infection. The results largely correlated with ACE2 expression and Caco-2 presented highest luciferase activity after VSV-SARS-CoV-2 infection (Figure 1C), indicating the relatively higher permissiveness. Thus, we selected Caco-2 for further investigation. Given much higher ACE2 level in primary IECs, we enhanced ACE2 expression in Caco-2 by stable transduction, designated Caco-2-ACE2 (Figure S1). Permissiveness of Caco-2-ACE2 was measured with VSV-SARS-CoV-2 infection. Caco-2-ACE2 showed much higher luciferase activity than Caco-2 after 24h VSV-SARS-CoV-2 inoculation (Figure 1D).

Establish pseudo-SARS-CoV-2 infection system in IECs mimicking viral life cycle

Though VSV backbone-based SARS-CoV-2 pseudo-viruses have been broadly used to study SARS-CoV-2 entry and drug discovery (Hoffmann et al., 2020; Ou et al., 2020), these types of pseudo-virus are not applicable for simulating entire life cycle of SARS-CoV-2 since vesicular stomatitis virus (VSV) possesses divergent replication mechanism. Thus, we established an alternative pseudo-SARS-CoV-2 infection model in IECs to simulate viral life cycle, such as infection, replication and virion propagation, by exploiting transcription and replication-competent SARS-CoV-2 virus-like-particles (trVLP) system as previously described (Ju et al., 2021)with minor refinement. Briefly, reverse genetic viral genome fragments of SARS-CoV-2 were assembled as SARS-CoV-2-GFP/ΔN trVLP in which viral nucleocapsid gene (N domain) was replaced with GFP reporter; separately, viral N domain gene was stably assembled *via* lentiviral transduction into Caco-2-ACE2 cell (Figure 2A). The newly constructed cell line, designated as Caco-2-ACE2-N, and SARS-CoV-2-GFP/ΔN trVLP constituted the pseudo-SARS-CoV-2 infection model. Of note, the viral replication and complete life cycle of pseudo-SARS-CoV-2 was exclusively achieved in Caco-2-ACE2-N cells due to lacking of nucleocapsid gene in pseudo-SARS-CoV-2 genome. Thus, this system only required Biosafety level-2 environment. To validate the efficacy of infection and propagation of pseudo-SARS-CoV-2 system, *in vitro* transcribed SARS-CoV-2-GFP/ΔN mRNA was electroporated into Caco-2-ACE2-N cells to produce SARS-CoV-2-GFP/ΔN trVLP. The supernatant containing SARS-CoV-2-GFP/ΔN trVLP was collected and further inoculated Caco-2-ACE2 or Caco-2-ACE2-N cells respectively. SARS-CoV-2 GFP/ΔN trVLP infection developed increasing number of GFP+ Caco-2-ACE2-N cells over time, but barely GFP+ Caco-2-ACE2 cells were detected (Figure 2B). Concurrently, distinguishable replication kinetics were observed in Caco-2-ACE2-N cells and viral RNA multiplied and peaked at 60h dpi (Figure 2C). In contrast, GFP + cells or viral RNA was barely detectable or retain at low level in Caco-2 or Caco-2-ACE2 cells throughout the process (Figures 2B, C), which was in line with previously described. For sake of abbreviation, we used pseudo-SARS-CoV-2 or CoV-2 referring to SARS-CoV-2-GFP/ΔN trVLP below.

Pseudo-SARS-CoV-2 infection induces innate immune response in intestinal epithelial cells

Next, using the pseudo-SARS-CoV-2 infection system, we investigated the cellular immune response profile of Caco-2-ACE2-N cells to SARS-CoV-2 GFP/ΔN trVLP infection. Virus invasion basically initiates antiviral immune defense by producing interferons. We noticed that viral mRNA was declined over 72h post infection (Figure 2C). Thus, we measured the mRNA levels of IFNs over the course of infection by qRT-PCR first. As shown in Figure S2A, mRNA of IFN-λ2, IFN-λ3 was induced and peaked at 48-60h post infection, which was coordinated with time course of virus RNA levels. Two categories of immune factor genes containing antiviral IFNs and inflammatory cytokines/chemokines commonly observed in COVID-19 patients were further determined. The mRNA expression of IFN-α, IFN-β, IFN-λ1, IFN-λ2/3, IFN-γ, TNF-α, IL-1β, CCL5, IP-10, IL-18, IL-6, IL-8, IFIT2, ISG15, CXCL1 was quantified at 48h post-infection. Generally, Caco-2-ACE2-N presented moderate immune response profile in response to pseudo-SARS-CoV-2 infection, which was in accordance with that reported in intestinal enteroids (Stanifer et al., 2020).

10.3389/fcimb.2022.1035711

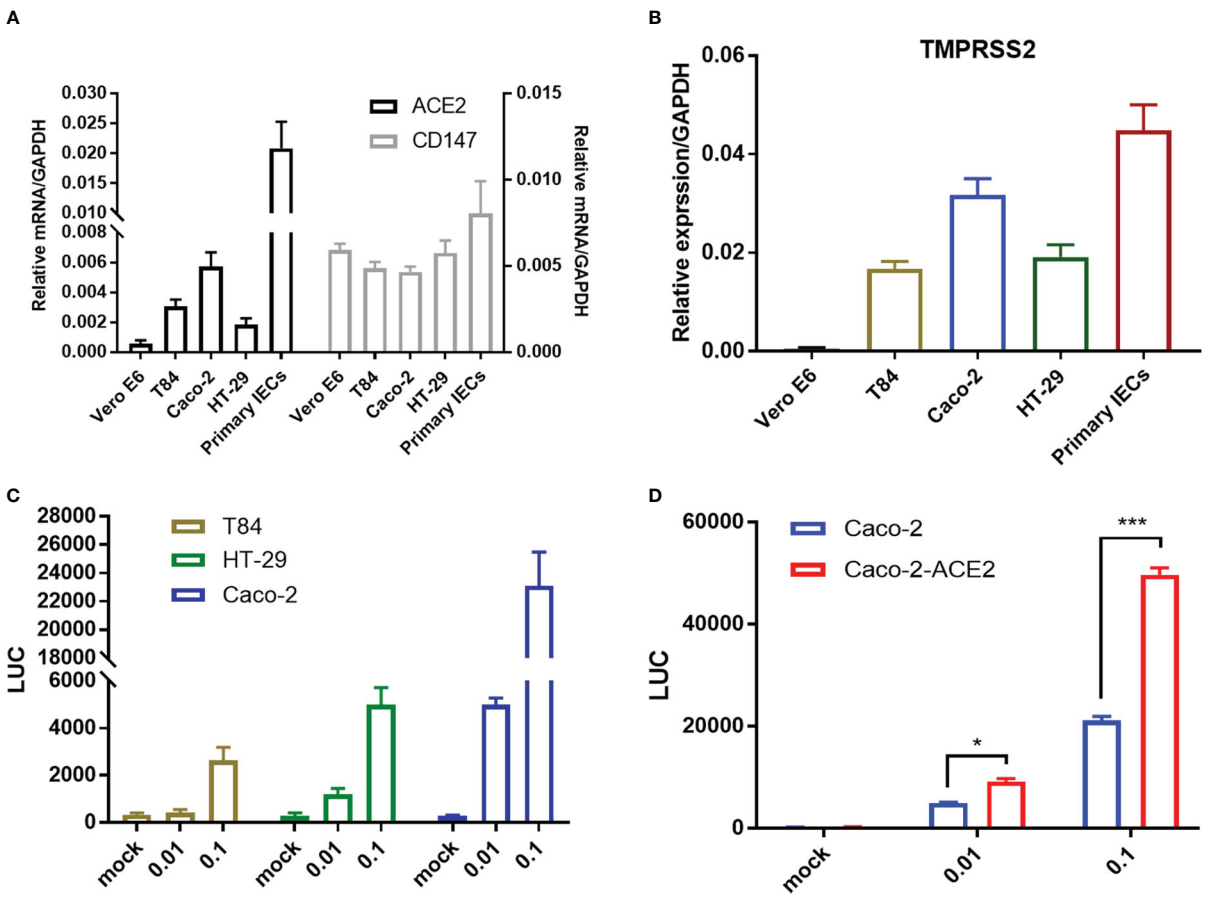

FIGURE 1
Entry receptor expression and permissiveness of intestinal epithelial cells to SARS-CoV-2 pseudo-virus. mRNA expression of SARS-CoV-2 entry receptor ACE2, CD147 **(A)** and coreceptor TMPRSS2 **(B)** on Vero E6, multiple epithelial cell lines and primary epithelial cells respectively. **(C)** Indicated intestinal epithelial cell lines ($1x10^5$) were infected with VSV-SARS-CoV-2 pseudo-virus at increasing MOIs (0.01, 0.1). Luciferase activity was determined at 24 hpi. **(D)** Luciferase activity in ACE2 overexpressed Caco-2 cells (Caco-2-ACE2) at 24 hpi of VSV-SARS-CoV-2 pseudo-virus with increasing MOIs (0.01, 0.1). Data are represented as mean ± SEM. Statistical significance is indicated (*p<0.05, ***p<0.001, one-way ANOVA).

Compared with non-infected cells, IFN-λ2, IFN-λ3, IL-18, IL-1β, ISG15 and CXCL1 were substantially induced by pseudo-SARS-CoV-2 infection in infected cells, while IFN-β, TNF-α, IP-10, IL-6, IFIT2 were moderately increased; other anti-viral cytokine IFN-α, IFN-λ1, as well as IFN-γ, CCL5, IP-10 were not induced significantly (Figure 3A). Furthermore, the immune response was aborted by Remdesivir which is incorporated into the viral RNA to inhibit RNA replication, suggesting that viral RNA replication may contribute to the induction of cellular immune response (Figure 3B). To further confirm the immune response induction at protein level, the elevated cytokines at protein level were measured by ELISA at 48h and 72h post-infection. IFN-λ2, IFN-λ3, IL-18, CXCL1 and TNF-α in Caco-2-ACE2-N cells was observed increased after exposure to pseudo-SARS-CoV-2 (Figures S2B, C). To address whether SARS-CoV-2 components themselves contribute to immune response, SARS-CoV-2-GFP/ΔN trVLP was irradiated by gamma ray and the incompetent virus were inoculated into Caco-2-ACE2-N cells for cytokine induction in IECs. The incompetent virus was not capable of inducing IFN-λ2, IFN-λ3, IL-18, CXCL1 and TNF-α production (Figures S2B, C). Collectively, these results indicated that pseudo-SARS-CoV-2 infection and propagation but not viral components themselves induced innate immune response in intestinal epithelial cells.

RIG-I and DHX15 are required for cellular immune response in IECs upon SARS-CoV-2 infection

SARS-CoV-2 propagation produce double-stranded RNA (dsRNA) intermediates. Numerous viral RNA sensors have been reported to sense viral RNAs and initiate cellular

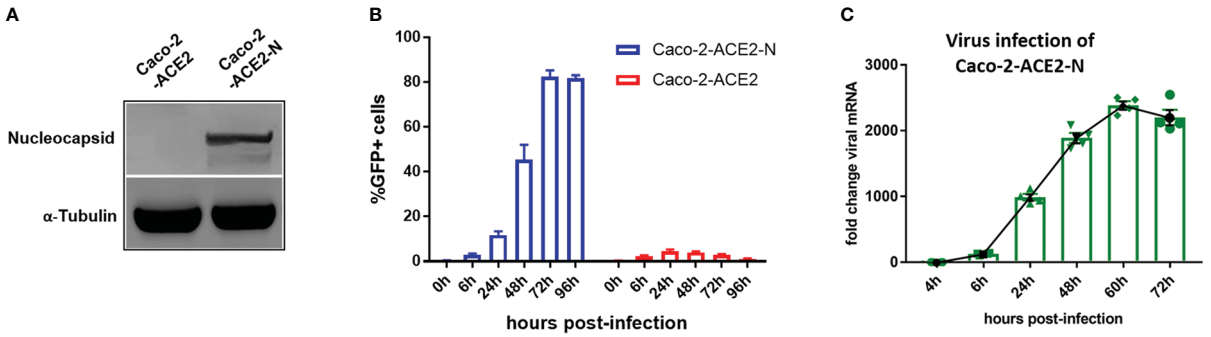

FIGURE 2
Establishment of pseudo-SARS-CoV-2 infection system in epithelial cell lines mimicking viral life cycle. **(A)** Caco-2-ACE2 cells were stably transfected with nucleocapsid. Western blot showed overexpression of nucleocapsid in Caco-2-ACE2-N cells. **(B)** Caco-2-ACE2 or Caco-2-ACE2-N cells ($2x10^5$) were inoculated and infected with SARS-CoV-2 GFP/ΔN trVLP. GFP+ cell percentage was quantified by flow cytometry at indicated time points. **(C)** Replication kinetics of SARS-CoV-2 GFP/ΔN trVLP in Caco-2-ACE2-N cell was quantified with viral RNA expression by RT-PCR after inoculation.

immune response, of which RIG-I, MDA5, DHX-15, LGP-2 were demonstrated responsible for recognizing several enteric viruses, such as rotavirus, reovirus, EMCV. To identify the specific sensors that involve in recognizing SARS-CoV-2 RNA and contribute to immunity induction in intestinal epithelial cells, we established RNA sensors RIG-I, MDA5, DHX15, LGP-2, TLR3 deficient models with CRISPR-Cas9 knockout respectively in basis of Caco-2-ACE2-N cell line. In addition, the key adapter MAVS responsible for IFNs induction was also depleted efficiently for use (Figure 4A).

First, we exploit dsRNA analog poly I:C as a stimulus to investigate the immune response in RIG-I, MDA5, DHX-15, LGP -2, TLR3, MAVS depletion cell lines. Poly I:C stimulation of Caco-2-ACE2-N IEC engaged in immune response, presenting remarkably elevated IFNλ2, IFNβ, and CCL5. Depletion of RIG-I, MDA5 or DHX15 reduced the cytokine production with different extent in Caco-2-ACE2-N IECs, whereas depletion of LGP-2 or TLR3 had no effect on immune response (Figures 4B, C). These data implied critical role of RIG-I, MDA5 and DHX15 in recognizing RNA and regulating cellular immune response in Caco-2-ACE2-N IECs.

To investigate whether these findings are applicable in SARS-CoV-2-induced immune response, RIG-I, MDA5, DHX-15, LGP-2 or MAVS- knockout or control Caco-2-ACE2-N IECs

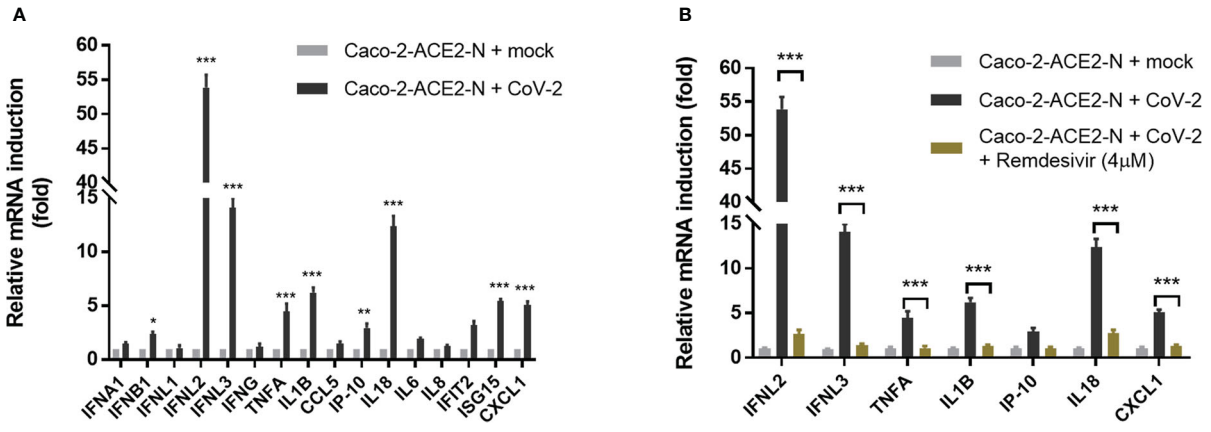

FIGURE 3
Immune response profile of Caco-2-ACE2-N cells to SARS-CoV-2 GFP/ΔN trVLP infection. **(A)** Caco-2-ACE2-N cells ($2x10^5$) were infected with SARS-CoV-2 GFP/ΔN trVLP (CoV-2) with MOI = 0.25. At 48h post infection, mRNA induction of immune cytokines and chemokines response to CoV-2 infection was determined by qRT-PCR. Data were presented with fold change relative to mock infection. Four replicates were performed in the experiment. **(B)** With or without RNA replication inhibitor Remdesivir, the mRNA induction of immune cytokines and chemokines response to CoV-2 infection. Data are represented as mean ± SEM of four replicates. Statistical significance is indicated (*p<0.05, **p<0.01 ***p<0.001, unpaired t test).

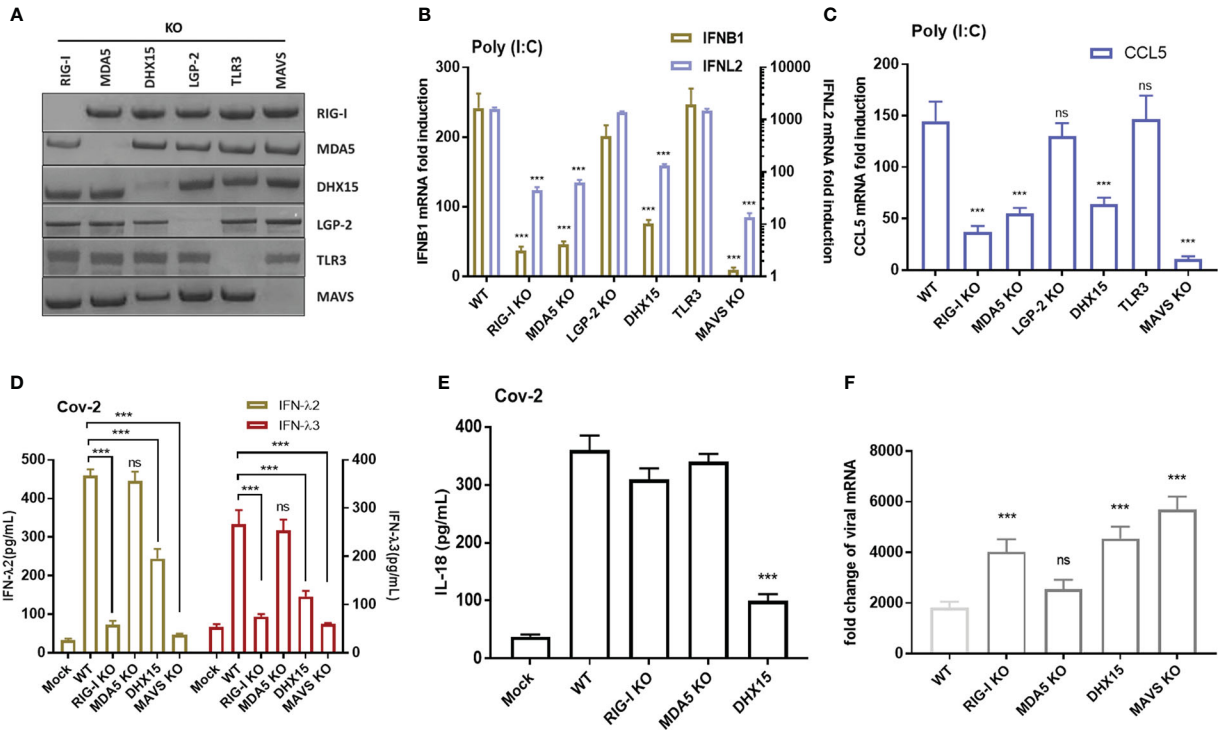

FIGURE 4
RIG-I and DHX15 are required for cellular immune response in IECs upon SARS-CoV-2 infection. **(A)** Western blot showing the knockout efficiency of multiple RNA sensors with CRISPR-Cas9 system in Caco-2-ACE2-N cells. The right indicated targeted immunoblot proteins. The top showed targeted knockout. **(B, C)** Cellular immune response to dsRNA analog poly I:C in RNA sensor knockout Caco-2-ACE2-N cells. The knockout cells were transfected with 5 μg/mL poly (I:C) to induce cellular immune response. After 16h post transfection, mRNA expression of IFNB1, IFNL2, CCL5 were quantified by qRT-PCR. Data are represented with fold changes relative to mock group. **(D, E)** Cellular immune response to CoV-2 infection in RNA sensor knockout Caco-2-ACE2-N cells . The knockout cells were infected with CoV-2 at 0.5 MOI. At 60h post infection, supernatants of cell infection culture were collected. IFNλ2, IFNλ3 and IL-18 were determined by ELISA in sensor knockout cells respectively. **(F)** Infected cells were also harvested; viral mRNA was quantified by qPCR. Fold change of viral RNA relative to mock group (no CoV-2 infection) was presented. Data are represented as mean ± SEM of four replicates. Statistical significance is indicated. (ns, not significant, ***p<0.001, unpaired t test and One-way ANOVA).

were infected with SARS-CoV-2-GFP/ΔN-trVLP (MOI=0.5) and cytokine production was measured by ELISA. As shown in Figures 4D, E, depletion of RNA sensing adaptor RIG-I or DHX-15 diminished cytokine production in response to pseudo-SARS-CoV-2. IFN-λ2, IFN-λ3 expression were dramatically attenuated in RIG-I-KO Caco-2-ACE2-N IEC cells. DHX15-KO also impeded these cytokines production with slight but significant extent (Figure 4D). Notably, substantial IL-18 reduction was only observed in DHX15-KO Caco-2-ACE2-N IEC cells (Figure 4E). Depletion of MAVS, the key adaptor downstream of RIG-I or DHX-15, virtually abolished innate immune response to CoV-2 infection. In contrast, depletion of sensor MDA5 had little effect on cytokine production. These results indicated that RNA sensors RIG-I and DHX15 are required for cellular immune response to SARS-CoV-2 infection in Caco-2-ACE2-N IEC cells, and DHX15 is inferred to be responsible for IL-18 induction. Given the critical role of IFNs in viral inhibition, we investigated viral load in each group at 60h post inoculation. Viral replication and proliferation were derepressed in RIG-I or DHX15 -KO Caco-2-ACE2-N IECs, presenting higher level of viral mRNA in these cells compared to WT counterpart (Figure 4F).

NLRP6 participated in the regulation of CoV-2 induced cellular immunity in IECs

Recently, NLRP6 was demonstrated to mediate cellular immunity in intestinal epithelia cells in response to enteric RNA virus infection, by interacting with DHX15. In addition, activation of NLRP6 inflammasome accounts for IL18 maturation and production. To determine whether NLRP6 engages in the regulation of SARS-CoV-2 immunity in IECs, we established NLRP6 knockout cell line in basis of Caco-2-ACE2-N IECs and evaluated the cytokine production with SARS-CoV-2 GFP/ΔN-trVLP infection. We confirmed

constitutive expression of NLRP6 in Caco-2-ACE2-N IECs, and found SARS-CoV-2 infection. Incompetent SARS-CoV-2 virus were incapable of increasing NLRP6 expression (Figure S3) intriguingly upregulated NLRP6 expression (Figures 5A, B). In the context of SARS-CoV-2 GFP/ΔN-trVLP infection, cytokine production of IFNλ2/3, IL-18 (Figure 5C) was reduced in NLRP6-knockout Caco-2-ACE2-N IECs compared with parallel control either at mRNA or protein level, suggesting a pivotal role of NLRP6 in regulating SARS-CoV-2 immunity and induction of IFNλ2/3, IL-18 cytokine. To further define the role of caspase-1 which is downstream of NLRP6 inflammasome signaling, we evaluated cytokine production in Casp1-KO Caco-2-ACE2-N IECs. Only IL-18 production but not IFNs or CXCL1 were virtually disturbed in Casp1-KO Caco-2-ACE2-N IECs upon SARS-CoV-2 GFP/ΔN-trVLP infection, demonstrating that NLRP6-caspase1 axis is responsible for IL18 regulation in Caco-2-ACE2-N IECs (Figure 5C).

Cross-talk between CoV-2-infected epithelial cells and immune cells provoked MAIT activation and exacerbated inflammation

The host's immune system plays a pivotal role in determination of the course of disease of COVID-19. Primary immune response is required for pathogen elimination during onset stage, while overbalanced immune response is deleterious and contributes to systemic hyperinflammation and local damage. To better understand immune dysregulation and immunopathogenesis in COVID-19, we established an *in vitro* coculture system in which Caco-2-ACE2-N IECs were exposed to SARS-CoV-2 GFP/ΔN-trVLP for 48h; supernatants were replaced with fresh medium suitable for PBMCs; the infected IECs were then cocultured for 16h with human peripheral blood mononuclear cells (PBMCs) in Transwells. Transcriptional

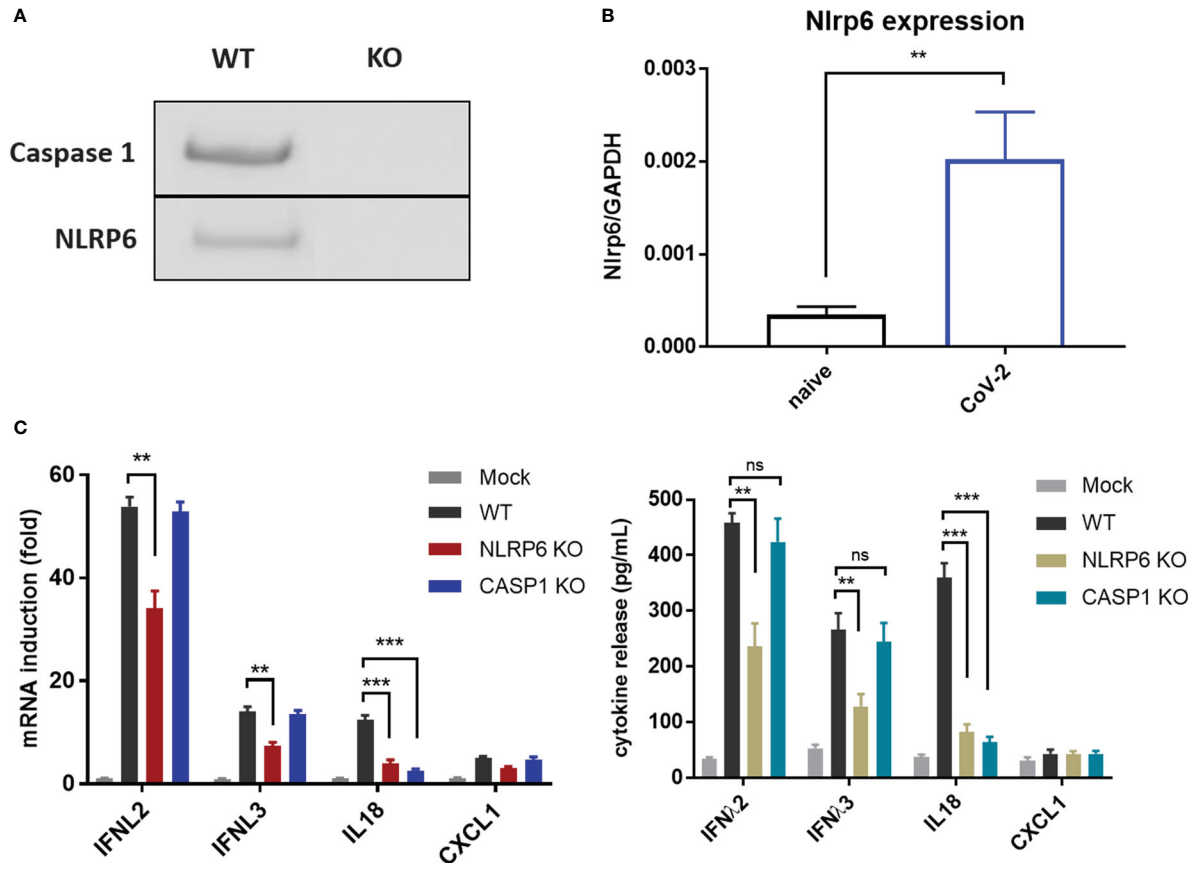

FIGURE 5
NLRP6 participated in the regulation of CoV-2 induced cellular immunity in IECs. **(A)** NLRP6 is constitutively expressed in Caco-2-ACE2-N cells. Western blot showing knockout efficiency of Caspase1 or NLRP6 by CRISPR-Cas9 system in Caco-2-ACE2-N cells. **(B)** Caco-2-ACE2-N cells were infected with CoV-2 at 0.5 MOI. At 16 hpi, mRNA level of nlrp6 was quantified by qRT-PCR. **(C)** The immune response profile of Nlrp6 or Casp1 knockout Caco-2-ACE2-N cells infected with CoV-2 for 48h. mRNA expression of anti-viral and inflammatory cytokines were determined by qPCR. Anti-viral and inflammatory cytokine release were confirmed at protein level by ELSIA. Data are represented as mean ± SEM of four replicates. Statistical significance is indicated. (ns, not significant, **p<0.01 ***p<0.001, unpaired t test).

change of immunity related genes was profiled with RT2 Profiler PCR Array Gene Expression Analysis. We found that CoV-2 epithelia-immunocytes coculture induced a profound inflammatory response in immunocytes, distinct from the immunological profile of Caco-2-ACE2-N cells infected with SARS-CoV-2 (Figure 6A). Of note, in PBMC immunocytes, anti-viral genes or interferon induced genes, such as ISG15, IFIT1, IFIT2, IFIT3, MX1, OAS3, OAS1, were substantially elevated by the coculture. Inflammatory cytokines, such as IL10, IL6, CCL3, IL1B, IFNG, GZMB or receptors, IL2RA, IL1RN were as well activated in PBMC by coculture. These data suggested that cellular cross-talk contributed to further immune response and magnification. Recent study reported mucosal-associated invariant T (MAIT) cells in particularly are highly activated in COVID-19 patients, and corelated with cytotoxicity by producing IFN-γ, Granzyme B, TNF-α cytokines, and with the severity and mortality of SARS-CoV-2 (Flament et al., 2021). Proinflammatory cytokines, notably interleukin (IL)-18, was associated with MAIT activation. Given the fact that IL-18 receptor is highly expressed on MAIT cells, and high level of IL-18 was induced in intestinal epithelia cell in response to SARS-CoV-2 infection, we sought to examine whether SARS-CoV-2 infection of IECs contributes to MAIT activation and potentiate further inflammatory response. Flow cytometry analysis showed that after coculture with CoV-2 infected Caco-2-ACE2-N cells, CD69 was upregulated in CD161 +Vα7.2+ MAIT cells, but not in other T cell subtypes (Figure 6B). CoV-2 infection of IECs stimulated robust IFN-γ, Granzyme B, TNF-α production in MAIT cells (Figures 6C, D). Additionally, substantial IFN-γ induction was also observed in NK cells (Figure 6C). Exposure to the conditional medium from infected IECs presented a similar activation profile in MAIT, suggesting that some factors in conditional medium activated PBMCs and MAIT. We speculated that IL-18, originally named IFN-γ inducing factor, contributed to MAIT activation and IFN-γ production. Indeed, depletion of IL-18 from conditional medium with αIL-18 failed to induce IFN-γ production in MAIT cells. However, recombinant IL-18 alone was incapable of activating MAIT cells, suggesting that IL-18 is required but not sufficient for MAIT activation (Figure 6E). Taken together, these data indicated that SARS-CoV-2 infection initiates primary cellular immune response in IECs, which cascades further activation of PBMCs and MAIT cells to produce inflammatory cytokines including IFN-γ, granzyme B *via* an IL-18 dependent mechanism.

Discussion

Infection with SARS-CoV-2 causes a spectrum of clinical symptoms of varying severity from respiratory damage to gastrointestinal disorders. Although studies have evidenced that human intestine is highly susceptible to SARS-CoV-2 infection, the mechanism how SARS-CoV-2 is sensed by intestinal cell host and induces cellular response is unclear. Innate immune response is pivotal for viral elimination at onset stage by producing IFN and proinflammatory cytokines. However, overbalanced immune response instead contributes to pathogenesis of COVID-19, such as acute lung injury, GI symptoms and even systemic inflammatory response syndrome (SIRS) (Polidoro et al., 2020; Sherwani and Khan, 2020). Gastrointestinal system, as an immune organ, have been proposed to play a crucial role in SARS-CoV-2 immunity. Therefore, it is urgent and indispensable to investigate the signaling pathways and mechanisms that contribute to cellular immune response in intestinal cells upon SARS-CoV-2 infection.

Manipulating infectious pathogenic virus is strictly restricted in BSL-3 laboratories, which hinders broad experimental research. Reverse genetics have profoundly advanced experimental viral study. Recently, several reverse genetics systems have been successfully created to produce fully infectious recombinant SARS-CoV-2 virus and replicons, providing powerful tools for broader study on SARS-CoV-2 beyond clinical isolates (Shang et al., 2020; Zang et al., 2020). In this concept, Ju et al. (2021) developed a trans-complementary system modeling SARS-CoV-2 life cycle (Ju et al., 2021), which only required biosafety 2 level environment. We exploited the trans-complementary system to mimic SARS-CoV-2 infection in intestinal cells and investigated the underlying mechanism of immunity.

In this study, we found that unlike lung epithelial cells, intestinal epithelial cell line Caco-2 presented relatively moderate immune response upon SARS-CoV-2 infection. Specifically, canonical anti-virus IFN, IFN-β, was not significantly induced, whereas IFNλ was dominant in anti-virus cellular immune response, which is coordinated with the findings in colon enteroid studies in response to SARS-CoV-2. The moderate anti-viral IFN production may partially explain why human colon epithelial cell line Caco-2 can support extensive viral replication and produce large amounts of viral particles in infection. ISG gene activation indicated inflammatory immune response. Of the induced proinflammatory cytokines, IL-18 was substantially increased. TNF-α, CXCL1, IP-10 were also mounted in the context of SARS-CoV-2 infection at variant timepoints. Thus, SARS-CoV-2 infection induces moderate but considerable anti-virus and inflammatory immune response in intestinal epithelial cells. The recently epidemic Omicron variant displayed less pathogenic in clinical. Research study reported that unlike previous SARS-COV-2 variant, Omicron isolates present less replication and lower viral load in Caco-2 cell when infected, and are highly sensitive to interferon treatment (Bojkova et al., 2022). This suggested sufficient IFNs were produced by intestinal epithelial cells to control virus, in agreement with less GI symptoms and less severe disease in omicron infected patients.

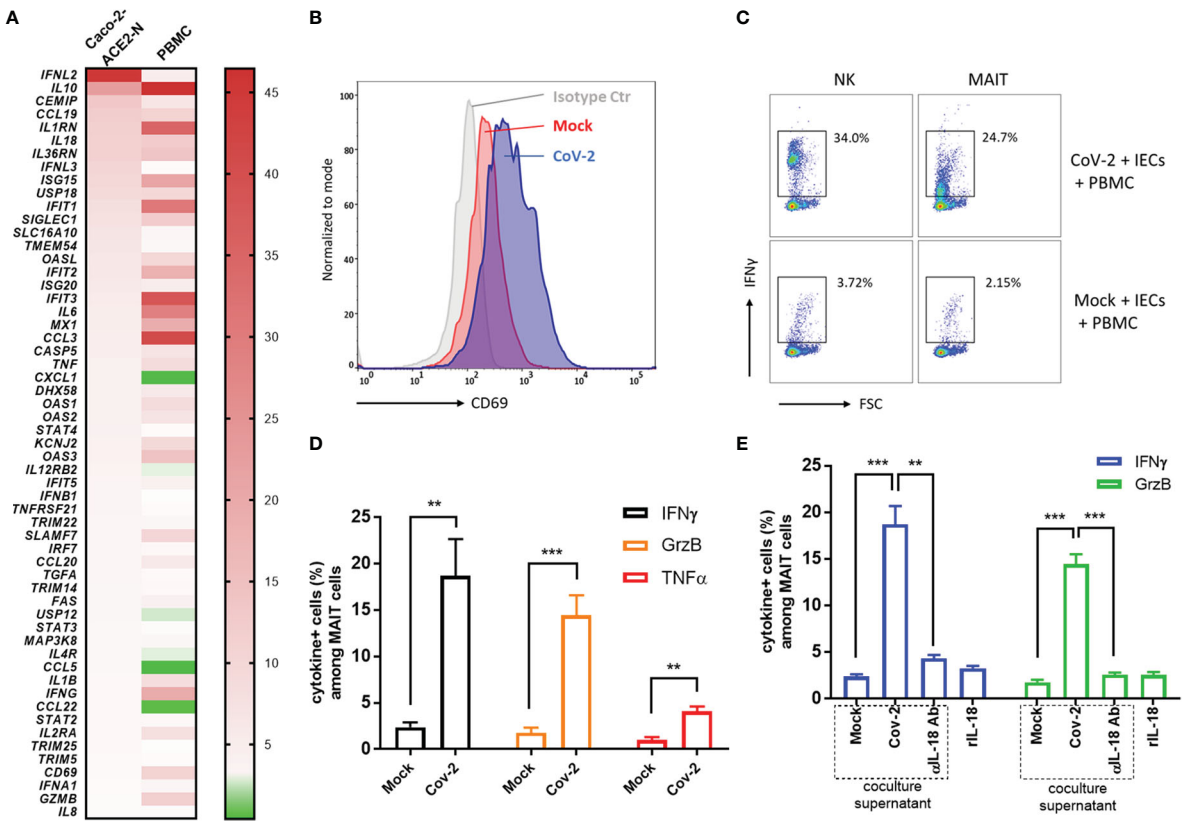

FIGURE 6
Cross-talk between CoV-2-infected epithelial cells and immune cells activated MAIT and exacerbated inflammation. **(A)** Heatmap of immunological profile of Caco-2-ACE2-N cells infected with CoV-2 and PBMC cocultured with CoV-2-infected Caco-2-ACE2-N cells. mRNA fold change of immune genes was profiled by RT2 Profiler PCR Array Gene Expression Analysis. Left panel indicated group of CoV-2-infected Caco-2-ACE2-N cells, shortly named with "Caco-2 ACE2-N"; data were presented with mRNA fold change relative to Mock-treated Caco-2-ACE2-N cells. Right panel indicated group of PBMCs cocultured with CoV-2-infected Caco-2-ACE2-N cells, shortly named with "PBMC"; data were presented with mRNA fold change relative to control PBMCs cocultured with Mock-treated Caco-2-ACE2-N cells. **(B)** CD69 expression profile on MAIT cells in various coculture groups. "Isotype ctr" indicated isotype antibody staining; "Mock" group indicated MAIT cells cocultured with Mock-treated IECs (Caco-2-ACE-2-N); "CoV-2" group indicated MAIT cells cocultured with CoV-2-infected IECs. **(C)** Representative flow cytometry dot plot of IFNγ expression in NK and MAIT cells after coculture with either Mock or CoV-2 infected IECs (Caco-2-ACE-2-N). **(D)** Inflammatory cytokine (IFNγ, GrzB, TNFα) expression in MAIT cells determined by FACS with positive population percentage. "Mock" indicated group of MAIT cells cocultured with Mock-treated IECs; "CoV-2" indicated group of MAIT cells cocultured with CoV-2-infected IECs **(E)** Depletion of IL18 by adding αIL18 Ab into medium at the beginning of coculture. Cytokine expression in MAIT with depletion of IL18 in coculture or with rIL18 addition alone in PBMC culture medium. All data are represented as mean ± SEM of three replicates. Statistical significance is indicated. (ns, not significant, **p<0.01 ***p<0.001, unpaired t test or One-way ANOVA).

SARS-CoV-2 is a positive-sense RNA virus belonging to the β-coronavirus genus. The innate immune system defense against RNA virus infection by developing multiple RNA recognizing mechanisms to induce numerous host defense molecules, including type I and type III interferons and proinflammatory cytokines and chemokines. The RLRs are commonly identified sensors that recognize viral RNA in the cytosol and are essential for triggering the innate immune response to RNA viruses in most cell types (Loo and Gale, 2011; Chow et al., 2018). The RLRs include MDA5, LGP2 and RIG-I. Recently, MDA5 and RIG-I was shown to sense SARS-CoV-2 and trigger IFN production in lung epithelial cells (Yin et al., 2021; Antoine et al., 2022). Several members of the DExD/H-box helicases other than the RLRs have emerged as important for innate immune signaling and control of virus infection. DHX15 has been characterized as a sensor for several enteric RNA viruses and control production of IFN-β, IFN-λ3, and IL-18 in IECs (Kenta et al., 2014; Lu et al., 2014; Xing et al., 2021). Recent study identified DHX16 recognizes specific viral RNA to trigger RIG-I-dependent IFN-β production (Hage et al., 2022).

We also demonstrated that RIG-I and DHX15 were required for sensing SARS-CoV-2 and inducing cellular immune response through MAVS signaling in intestinal epithelial cells upon SARS-CoV-2 infection. Of note, RIG-I was mainly responsible for antiviral immunity and inflammatory cytokine production, while DHX15 also participated in regulation of IFNs

but was specifically responsible for IL-18 production. The overlapping but distinctive contribution to SARS-CoV-2 immunity suggested interaction between DHX15 and RIG-I signaling. DHX15 appeared to interact with both K63- and K48-poly-Ub (Hage et al., 2022). Unanchored K63-linked poly-Ub (K63-poly-Ub) promotes the activation of RIG-I for optimal production of IFNs and pro-inflammatory cytokines (Zeng et al., 2010; Jiang et al., 2012). These clues hint that DHX15 may interact with K63-poly-Ub and partner with RIG-I for antiviral IFNs production and ISG expression. Depletion of MAVS shut down the immune response, implying a vital role of MAVS in the signaling.

Furthermore, we found that NLRP6 engaged in the regulation of SARS-CoV-2 immunity in IECs. Depletion of NLRP6 diminished the immune response and cytokine production, especially IL-18. It has been reported that DHX15–NLRP6 sense RNA and subsequently regulate IFNs and IL-18 secretion in the control of intestinal viral infections (Xing et al., 2021). However, another study showed that loss of DHX15 has no impact on inflammasome activation during virus infection, suggesting a DHX15-independent manner of NLRP6 inflammasome activation (Shen et al., 2021). Thus, it remains unclear whether DHX15 links to NLRP6 and how NLRP6 achieves roles in SARS-CoV-2 immunity in IECs. Notably, recombinant IFN-L2 treatment induces Nlrp6 mRNA expression in IECs (Penghua et al., 2015). It is possible that RIG-I- and DHX15-MAVS signaling produces type III IFNs, which further induces Nlrp6 expression and results in Nlrp6 inflammasome activation.

Infection of SARS-CoV-2 potentially provokes excessive production of proinflammatory cytokines and even systemic hyperinflammation, resulting in multiorgan failure to lethal damage. A few research studies have emphasized that immune dysregulation contributes to SARS-CoV-2 immunopathogenesis, dissecting the molecular mechanism that profound alteration in myeloid cells, T cells drives hyperinflammation and severe clinical manifestations (le Bert et al., 2020; Lu et al., 2021). In our study, SARS-CoV-2 infection of intestinal epithelial cells is characterized with excessive IL-18 production. Using coculture system, we investigated the interaction between SARS-CoV-2 infected intestinal epithelial cell Caco-2 and PBMCs. SARS-CoV-2 infected IECs directly produced mixed antiviral and inflammatory cytokines. MAIT cells in PBMCs was activated when cocultured with infected IECs in an IL-18-dependent mode and subsequently amplified the immune response by producing IFN-γ, TNF-α and granzyme B. As data showed, blocking IL-18 in SARS-CoV-2 infected IECs conditional medium with IL-18 antibody interrupted MAIT activation, while recombinant IL-18 alone could not activate MAIT, suggesting that IL-18 is required for MAIT activation but not sufficient and other supernatant factors or cell interactions are required in IECs- immunocytes cross-talk for MAIT activation. Granzyme B was reported to activate cell pyroptosis (Verdonck et al., 2022). Recent study demonstrated that IFN-γ and TNF-α combination triggers Inflammatory Cell Death, Tissue Damage, and Mortality in SARS-CoV-2 Infection and Cytokine Shock Syndromes (Karki et al., 2021). Given the prominence of MAIT cells in human peripheral blood (1–10%) and in tissue sites of inflammation (Dusseaux et al., 2011; Fergusson et al., 2016), MAIT activation may considerably account for systemic hyperinflammation and local damage in SARS-CoV-2 infection. Our data provides insights that cell cross-talk in SARS-CoV-2 infection triggers cascade and amplified immunity and contributes to immunopathogenesis of COVID-19.

In summary, this work unveils the molecular basis of immune recognition of the SARS-CoV-2 virus, depicts mechanism of cellular response in IECs, and provides insights that intestinal immune cross-talk with other immune cells triggers amplified immunity (Figure 7). Nevertheless, the viral immunity driven by innate and adaptive immune response balances host immunopathogenesis and protective effect with great complexity. DHX-15-MAVS signaling pathway cross-talks with NLRP6 related inflammasome in IECs; IECs transmit immune response to mucosal and peripheral immune cells, resulting in overall response. We propose further studies to dissect the specific mechanism that links viral sensor DHX-15 with NLRP6 signaling pathway. Also, it is critical to fully understand the immune cross-talk between distinct immune cell types, such as MAIT, NK, monocytes, and T cells, in which various cytokines besides IL-18 involved. These insights would benefit COVID-19 prevention and therapeutics development.

Method

Cell culture

Human colon carcinoma cell line T84 (ATCC CCL-248) and human intestinal epithelial cells (IECs) line HT-29 (ATCC HTB-38) were maintained in DMEM/F12 medium supplemented with 10% fetal bovine serum (FBS) and 1% penicillin/streptomycin. Human colorectal adenocarcinoma Caco-2 (ATCC HTB-37) and Vero E6 (ATCC CRL 1586) were maintained in DMEM supplemented with 10% FBS and 1% penicillin/streptomycin.

Mouse primary intestinal epithelial cells (IECs) were isolated from 6-week-old C57BL/6 mouse intestines. Briefly, intestines were cut into pieces and digested with 0.72mg/mL Dispase and 2.5mg/mL Collagenase IV for 30min. Cell suspension was collected and separated by Percoll gradient (GE Health). Purified IECs were cultured in DMEM, supplemented with 10% FBS, 4mM glutamine, 20mM HEPES, and 1% penicillin/streptomycin. After culture, the purity of IECs was confirmed by flow cytometry with PE-anti-E-Cadherin antibody and FITC-anti-Cytokeratin 18 antibody.

Caco-2 cells stably expressing ACE2 and nucleocapsid were generated by transduction with lentivirus containing ACE2/

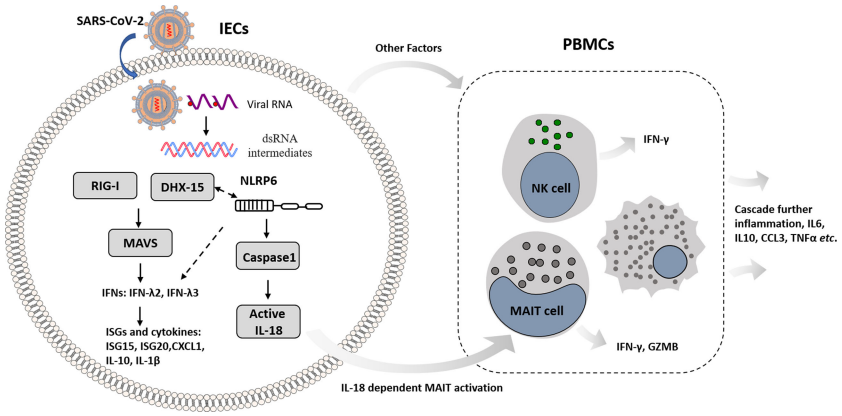

FIGURE 7
Schematic overview of mechanism basis of innate immunity in IECs response to SARS-CoV-2 infection and immune cross-talk with other immune cells in intestinal context.

IRES-puro or nucleocapsid/IRES-G418 vector. Stably transduced cells were maintained in corresponding culture medium with 1μg/ml puromycin, and/or 1 mg/ml G418.

For CRISPR-Cas9-mediated gene disruption, Caco-2-ACE2-N cells were transduced with Cas9 and sgRNA LentiVector and selected with antibiotics for at least 10 days. cells were subcloned and then lysed for western blot to identify knockout clones.

Pseudo-SARS-CoV-2 entry virus infections

To determine permissiveness of intestinal cell lines to SARS-CoV-2 viral entry, pseudo-typed virus VSV-SARS-CoV-2 with luciferase was used for infection assay. Cells were seeded in 96 well plates. VSV-SARS-CoV-2 was added at the indicated MOI. At 24 hpi, cells were harvested for luciferase assays following the Luciferase Assay System protocol (E1501, Promega). Luminescence was detected by Perkinelmer EnSight Microplate Reader.

Virus titration assay

Viral titers in cell culture supernatant were determined by a modified plaque-forming assay with Caco-ACE2-N cells. Briefly, $5x10^5$ Caco-ACE2-N cells were seeded in 12-well plates overnight. Harvested culture supernatants from infected Caco-ACE2-N cells were 10-fold serially diluted with fresh medium. Seeded cells were inoculated with diluted supernatants respectively. After 1h infection, 1 mL of 0.6% microcrystalline cellulose (MCC, Sigma 435244) was added. The plates were incubated for another 3 days in incubator. On day 4, MCC was removed. 4% formalin was used to fix the cells. Plaques were quantified and recorded as PFU/mL.

Quantitative reverse-transcription-PCR

Total cellular RNA was isolated using Qiagen RNeasy Mini Kit according to the manufacturer's instructions. Reverse transcription was performed using iScript™ cDNA Synthesis Kit (Bio-Rad). The primers for viral RNA were as follows: Vprimer1-CGAAAGGTAAGATGGAGAGCC and Vprimer2-TGTTGACGTGCCTCTGATAAG. Real-time qPCR was performed in 96-well plates in triplicates using SYBR Green Supermix (Bio-Rad) and StepOne Plus system (Applied Biosystems). For other immune genes detection, Taqman probes, GAPDH (Hs99999905_m1), ISG15 (Hs01921425_s1), OAS1 (Hs00973637_m1), IFITM3 (Hs03057129_s1), IFNB1 (Hs01077958_s1), IFNL1 (Hs00601677_g1), and IFNL2 (Hs00820125_g1), etc. were used for quantification of mRNA expression.

RT2 profiler

The RT2 first strand kit (Qiagen) was used for the synthesis of the cDNA strand using 500ng of total RNA from samples extracted using the RNeasy kit (Qiagen). The customized RT2 Profiler PCR array kit was used for profiling immunological genes expression according to the manufacturer's instructions. The average of the threshold cycle (CT) values from mock controls were used to normalize gene expression. Fold changes of mRNA expression between the noninfected and the infected conditions were analyzed using the ΔΔCT values.

ELISA

The supernatant from different groups were collected and cytokines were measured by human IFN-λ2, IFN-λ3, IL-18, CXCL1 and TNF-α ELISA kit (Biolegend) following manufacturer's instructions.

Coculture of CoV-2 infected IECs with PBMC

Human PBMC were purchased from SAILY Bio. $1x10^6$ PBMCs were cocultured with $2×10^5$ SARS-CoV-2 GFP/ΔN trVLP-infected (MOI=0.5) or mock Caco-2-ACE2-N cells in a 96-well U-bottomed plate and incubated for 16 h with the addition of brefeldin A at 10 h. After 16h coculture, cells were harvested and fixed with Fixation Buffer (Biolegend) for FACS staining.

For Transwell coculture, Caco-2-ACE2-N cells were inoculated and infected with mock control or pseuo-SARS-CoV-2. After 48h inoculation, supernatants were replaced with fresh medium suitable for PBMC. Then CoV-2-infected or mock Caco-2-ACE2-N cells were replated onto Transwell inserts. PBMCs were placed into the bottom chamber for 16h of coculture. After that, PBMC were harvested for immune genes profiling with customized RT2 Profiler PCR Array Gene Expression Kit (Qiagen). Cocultures were performed with at least three biological replicates per condition. For depletion assay, 20μg/mL αIL-18 neutralizing antibody was added at the start of the coculture. For conditional medium assay, conditional medium of Caco-2-ACE2-N cells with 60h CoV-2 infection was added into PBMC with 1:1 ratio of PBMC culture medium. After 16h culturing, PBMC were harvested and MAIT cells were analyzed by flow cytometry. For rIL18 addition, 10ng/mL rIL18 was added into PBMC culture for 16hs.

Flow cytometry

Flow cytometry was exploited for analysis of cytokine expression after coculture. Surface staining was performed as follows. MAIT cells were defined by anti-CD3-FITC (BioLegend), anti-CD161-APC/Cy7 (BD Pharmingen) and anti-Vα7.2-APC (BD Pharmingen). NK cells were identified by anti-CD56-BV421 (BioLegend). After surface staining, cells were aliquoted into 3 parts and incubated with anti-IFNγ-PE (clone B27), anti-TNFα-PE (clone MAb11), or anti-GzB-PE (clone GB11) for intracellular staining at 4°C for 30min. Dead cells were excluded with 7-AAD. Cells were acquired on BD Lyric analyzer (BD Biosciences) and analyzed with FlowJo software.

Western blot

Cells were washed twice with PBS on ice and lysed with lysis buffer (50 mM Tris-HCl, 1 mM EDTA, 150 mM NaCl, 1.0% NP-40) containing protease inhibitor Cocktail (ThermoFisher Scientific) for immunoblot analysis. Protein samples were dissolved in SDS sample buffer. After electrophoresis, separated proteins were transferred onto PVDF membrane. The membrane was then blocked with 5% nonfat milk. After incubation with specific primary antibody, HRP-conjugated secondary antibody was applied. The membranes were scanned by an enhanced chemiluminescence system (ThermoFisher Scientific).

Quantification and statistical analysis

All data were presented as means ± SEM as indicated and analyzed by GraphPad PRISM software. Unpaired t test, Student's paired t test, one-way ANOVA with multiple comparisons were used. *$p < 0.05$; **$p < 0.01$; ***$p < 0.001$.

Data availability statement

The original contributions presented in the study are included in the article/Supplementary Material. Further inquiries can be directed to the corresponding authors.

Author contributions

YL designed the experiments and wrote the manuscript. LZ, YZ and RW mainly designed and conducted the experiment. LZ and YZ contributed to equal work. RW conducted flow cytometry, qPCR and cell culture. XL completed molecular construction and provided plasmids. JZ performed western blot and ELISA, MT helped to revise the manuscript. All authors contributed to the article and approved the submitted version.

Conflict of interest

The authors declare that the research was conducted in the absence of any commercial or financial relationships that could be construed as a potential conflict of interest.

Publisher's note

Supplementary material

The Supplementary Material for this article can be found online at: https://www.frontiersin.org/articles/10.3389/fcimb.2022.1035711/full#supplementary-material

References

Adrish, S., Michael, R., Gourab, M., Ningguo, F., Tomer, K., Nitya, N., et al. (2012). Innate immune response to homologous rotavirus infection in the small intestinal villous epithelium at single-cell resolution. *Proc. Natl. Acad. Sci.* 109, 20667–20672. doi: 10.1073/pnas.1212188109

Antoine, R., Luiza, C. V. A., Marine, T., Ghizlane, M., Boris, B., Joe, M., et al. (2022). SARS-CoV-2 triggers an MDA-5-Dependent interferon response which is unable to control replication in lung epithelial cells. *J. Virol.* 95, e02415–e02420. doi: 10.1128/JVI.02415-20

Ashrafzadeh-Kian, S., Campbell, M. R., Jara Aguirre, J. C., Walsh, J., Kumanovics, A., Jenkinson, G., et al. (2022). Role of immune mediators in predicting hospitalization of SARS-CoV-2 positive patients. *Cytokine* 150, 155790. doi: 10.1016/j.cyto.2021.155790

Bojkova, D., Rothenburger, T., Ciesek, S., Wass, M. N., Michaelis, M., and Cinatl, J. (2022). SARS-CoV-2 omicron variant virus isolates are highly sensitive to interferon treatment. *Cell Discovery* 8, 42. doi: 10.1038/s41421-022-00408-z

Bruns, A. M., Leser, G. P., Lamb, R. A., and Horvath, C. M. (2014). The innate immune sensor LGP2 activates antiviral signaling by regulating MDA5-RNA interaction and filament assembly. *Mol. Cell* 55, 771–781. doi: 10.1016/j.molcel.2014.07.003

Chen, T.-H., Hsu, M.-T., Lee, M.-Y., and Chou, C.-K. (2022). Gastrointestinal involvement in SARS-CoV-2 infection. *Viruses* 14, 1188. doi: 10.3390/v14061188

Chow, K. T., Gale, M., and Loo, Y.-M. (2018). RIG-I and other RNA sensors in antiviral immunity. *Annu. Rev. Immunol.* 36, 667–694. doi: 10.1146/annurev-immunol-042617-053309

Divij, M., Josephine, R. G., Amy, E. B., Derek, A. O., Allison, R. G., Jennifer, E. W., et al. (2020). Deep immune profiling of COVID-19 patients reveals distinct immunotypes with therapeutic implications. *Science* 369, eabc8511. doi: 10.1126/science.abc8511

Dusseaux, M., Martin, E., Serriari, N., Péguillet, I., Premel, V., Louis, D., et al. (2011). Human MAIT cells are xenobiotic-resistant, tissue-targeted, CD161hi IL-17–secreting T cells. *Blood* 117, 1250–1259. doi: 10.1182/blood-2010-08-303339

Elinav, E., Strowig, T., Kau, A. L., Henao-Mejia, J., Thaiss, C. A., Booth, C. J., et al. (2011). NLRP6 inflammasome regulates colonic microbial ecology and risk for colitis. *Cell* 145, 745–757. doi: 10.1016/j.cell.2011.04.022

Fergusson, J. R., Hühn, M. H., Swadling, L., Walker, L. J., Kurioka, A., Llibre, A., et al. (2016). CD161intCD8+ T cells: A novel population of highly functional, memory CD8+ T cells enriched within the gut. *Mucosal Immunol.* 9, 401–413. doi: 10.1038/mi.2015.69

Flament, H., Rouland, M., Beaudoin, L., Toubal, A., Bertrand, L., Lebourgeois, S., et al. (2021). Outcome of SARS-CoV-2 infection is linked to MAIT cell activation and cytotoxicity. *Nat. Immunol.* 22, 322–335. doi: 10.1038/s41590-021-00870-z

Guo, M., Tao, W., Flavell, R. A., and Zhu, S. (2021). Potential intestinal infection and faecal–oral transmission of SARS-CoV-2. *Nat. Rev. Gastroenterol. Hepatol.* 18, 269–283. doi: 10.1038/s41575-021-00416-6

Hage, A., Bharaj, P., van Tol, S., Giraldo, M. I., Gonzalez-Orozco, M., Valerdi, K. M., et al. (2022). The RNA helicase DHX16 recognizes specific viral RNA to trigger RIG-i-dependent innate antiviral immunity. *Cell Rep.* 38, 110434. doi: 10.1016/j.celrep.2022.110434

Hoffmann, M., Kleine-Weber, H., Schroeder, S., Krüger, N., Herrler, T., Erichsen, S., et al. (2020). SARS-CoV-2 cell entry depends on ACE2 and TMPRSS2 and is blocked by a clinically proven protease inhibitor. *Cell* 181, 271–280.e8. doi: 10.1016/j.cell.2020.02.052

Hur, S. (2019). Double-stranded RNA sensors and modulators in innate immunity. *Annu. Rev. Immunol.* 37, 349–375. doi: 10.1146/annurev-immunol-042718-041356

Jiang, X., Kinch, L. N., Brautigam, C. A., Chen, X., Du, F., Grishin, N., et al. (2012). Ubiquitin-induced oligomerization of the RNA sensors RIG-I and MDA5 activates antiviral innate immune response. *Immunity* 36, 959–973. doi: 10.1016/j.immuni.2012.03.022

Jiao, L., Li, H., Xu, J., Yang, M., Ma, C., Li, J., et al. (2021). The gastrointestinal tract is an alternative route for SARS-CoV-2 infection in a nonhuman primate model. *Gastroenterology* 160, 1647–1661. doi: 10.1053/j.gastro.2020.12.001

Jin, X., Lian, J.-S., Hu, J.-H., Gao, J., Zheng, L., Zhang, Y.-M., et al. (2020). Epidemiological, clinical and virological characteristics of 74 cases of coronavirus-infected disease 2019 (COVID-19) with gastrointestinal symptoms. *Gut* 69, 1002–1009. doi: 10.1136/gutjnl-2020-320926

Ju, X., Zhu, Y., Wang, Y., Li, J., Zhang, J., Gong, M., et al. (2021). A novel cell culture system modeling the SARS-CoV-2 life cycle. *PloS Pathog.* 17, e1009439. doi: 10.1371/journal.ppat.1009439

Karki, R., Sharma, B. R., Tuladhar, S., Williams, E. P., Zalduondo, L., Samir, P., et al. (2021). Synergism of TNF-α and IFN-γ triggers inflammatory cell death, tissue damage, and mortality in SARS-CoV-2 infection and cytokine shock syndromes. *Cell* 184, 149–168.e17. doi: 10.1016/j.cell.2020.11.025

Kato, H., Takeuchi, O., Sato, S., Yoneyama, M., Yamamoto, M., Matsui, K., et al. (2006). Differential roles of MDA5 and RIG-I helicases in the recognition of RNA viruses. *Nature* 441, 101–105. doi: 10.1038/nature04734

Kell, A. M., and Gale, M. (2015). RIG-I in RNA virus recognition. *Virology* 479–480, 110–121. doi: 10.1016/j.virol.2015.02.017

Kenta, M., Yusuke, S., Seiko, I.-K., Kazuo, K., Tetsuo, N., Atsushi, M., et al. (2014). The DEAH-box RNA helicase DHX15 activates NF-κB and MAPK signaling downstream of MAVS during antiviral responses. *Sci. Signal* 7, ra40–ra40. doi: 10.1126/scisignal.2004841

Laing, A. G., Lorenc, A., del Molino del Barrio, I., Das, A., Fish, M., Monin, L., et al. (2020). A dynamic COVID-19 immune signature includes associations with poor prognosis. *Nat. Med.* 26, 1623–1635. doi: 10.1038/s41591-020-1038-6

Lazear, H. M., Nice, T. J., and Diamond, M. S. (2015). Interferon-λ: Immune functions at barrier surfaces and beyond. *Immunity* 43, 15–28. doi: 10.1016/j.immuni.2015.07.001

le Bert, N., Tan, A. T., Kunasegaran, K., Tham, C. Y. L., Hafezi, M., Chia, A., et al. (2020). SARS-CoV-2-specific T cell immunity in cases of COVID-19 and SARS, and uninfected controls. *Nature* 584, 457–462. doi: 10.1038/s41586-020-2550-z

Leticia, K.-C., Betina, P. M., Wenzhao, M., Aaron, M. R., Caroline, A. G. I., Ariel, R. W., et al. (2020). Comprehensive mapping of immune perturbations associated with severe COVID-19. *Sci. Immunol.* 5, eabd7114. doi: 10.1126/sciimmunol.abd7114

Levy, M., Thaiss, C. A., Zeevi, D., Dohnalová, L., Zilberman-Schapira, G., Mahdi, J. A., et al. (2015). Microbiota-modulated metabolites shape the intestinal microenvironment by regulating NLRP6 inflammasome signaling. *Cell* 163, 1428–1443. doi: 10.1016/j.cell.2015.10.048

Livanos, A. E., Jha, D., Cossarini, F., Gonzalez-Reiche, A. S., Tokuyama, M., Aydillo, T., et al. (2021). Intestinal host response to SARS-CoV-2 infection and COVID-19 outcomes in patients with gastrointestinal symptoms. *Gastroenterology* 160, 2435–2450.e34. doi: 10.1053/j.gastro.2021.02.056

Loo, Y.-M., and Gale, J. M. (2011). Immune signaling by RIG-i-like receptors. *Immunity* 34, 680–692. doi: 10.1016/j.immuni.2011.05.003

Lu, Q., Liu, J., Zhao, S., Gomez Castro, M. F., Laurent-Rolle, M., Dong, J., et al. (2021). SARS-CoV-2 exacerbates proinflammatory responses in myeloid cells through c-type lectin receptors and tweety family member 2. *Immunity* 54, 1304–1319.e9. doi: 10.1016/j.immuni.2021.05.006

Lu, H., Lu, N., Weng, L., Yuan, B., Liu, Y., and Zhang, Z. (2014). DHX15 senses double-stranded RNA in myeloid dendritic cells. *J. Immunol.* 193, 1364. doi: 10.4049/jimmunol.1303322

Nie, J., Li, Q., Wu, J., Zhao, C., Hao, H., Liu, H., et al. (2020). Establishment and validation of a pseudovirus neutralization assay for SARS-CoV-2. *Emerg. Microbes Infect.* 9, 680–686. doi: 10.1080/22221751.2020.1743767

Ou, X., Liu, Y., Lei, X., Li, P., Mi, D., Ren, L., et al. (2020). Characterization of spike glycoprotein of SARS-CoV-2 on virus entry and its immune cross-reactivity with SARS-CoV. *Nat. Commun.* 11, 1620. doi: 10.1038/s41467-020-15562-9

Pan, P., Shen, M., Yu, Z., Ge, W., Chen, K., Tian, M., et al. (2021). SARS-CoV-2 n protein promotes NLRP3 inflammasome activation to induce hyperinflammation. *Nat. Commun.* 12, 4664. doi: 10.1038/s41467-021-25015-6

Penghua, W., Shu, Z., Long, Y., Shuang, C., Wen, P., Ruaidhri, J., et al. (2015). Nlrp6 regulates intestinal antiviral innate immunity. *Sci. (1979)* 350, 826–830. doi: 10.1126/science.aab3145

Polidoro, R. B., Hagan, R. S., de Santis Santiago, R., and Schmidt, N. W. (2020). Overview: Systemic inflammatory response derived from lung injury caused by SARS-CoV-2 infection explains severe outcomes in COVID-19. *Front. Immunol.* 11. doi: 10.3389/fimmu.2020.01626

Ricardo-Lax, I., Luna, J. M., Thi Nhu Thao, T., le Pen, J., Yu, Y., Hoffmann, H.-H., et al. *Replication and single-cycle delivery of SARS-CoV-2 replicons*. Available at: https://www.science.org.

Rodrigues, T. S., de Sá, K. S. G., Ishimoto, A. Y., Becerra, A., Oliveira, S., Almeida, L., et al. (2020a). Inflammasomes are activated in response to SARS-CoV-2 infection and are associated with COVID-19 severity in patients. *J. Exp. Med.* 218, e20201707. doi: 10.1084/jem.20201707

Shang, J., Wan, Y., Luo, C., Ye, G., Geng, Q., Auerbach, A., et al. (2020) Cell entry mechanisms of SARS-CoV-2. *Proceedings of the National Academy of Sciences* 117, 11727–11734 doi: 10.1073/pnas.2003138117/-/DCSupplemental

Shen, C., Li, R., Negro, R., Cheng, J., Vora, S. M., Fu, T.-M., et al. (2021). Phase separation drives RNA virus-induced activation of the NLRP6 inflammasome. *Cell* 184, 5759–5774.e20. doi: 10.1016/j.cell.2021.09.032

Sherwani, S., and Khan, M. W. A. (2020). Cytokine response in SARS-CoV-2 infection in the elderly. *J. Inflammation Res.* 13, 737–747. doi: 10.2147/JIR.S276091

Stanifer, M. L., Kee, C., Cortese, M., Zumaran, C. M., Triana, S., Mukenhirn, M., et al. (2020). Critical role of type III interferon in controlling SARS-CoV-2 infection in human intestinal epithelial cells. *Cell Rep.* 32, 107863. doi: 10.1016/j.celrep.2020.107863

Takeshi, S., Reiko, H., Yueh-Ming, L., David, O., Cynthia, L. J., Sangita, C. S., et al. (2007). Regulation of innate antiviral defenses through a shared repressor domain in RIG-I and LGP2. *Proc. Natl. Acad. Sci.* 104, 582–587. doi: 10.1073/pnas.0606699104

Tao, W., Zhang, G., Wang, X., Guo, M., Zeng, W., Xu, Z., et al. (2020a). Analysis of the intestinal microbiota in COVID-19 patients and its correlation with the inflammatory factor IL-18. *Med. Microecology* 5, 100023. doi: 10.1016/j.medmic.2020.100023

Tao, W., Zhang, G., Wang, X., Guo, M., Zeng, W., Xu, Z., et al. (2020b). Analysis of the intestinal microbiota in COVID-19 patients and its correlation with the inflammatory factor IL-18 and SARS-CoV-2-specific IgA. *medRxiv* 2020, 8.12.20173781. doi: 10.1101/2020.08.12.20173781

van Dorp, L., Acman, M., Richard, D., Shaw, L. P., Ford, C. E., Ormond, L., et al. (2020). Emergence of genomic diversity and recurrent mutations in SARS-CoV-2. *Infection Genet. Evol.* 83, 104351. doi: 10.1016/j.meegid.2020.104351

Verdonck, S., Nemegeer, J., Vandenabeele, P., and Maelfait, J. (2022). Viral manipulation of host cell necroptosis and pyroptosis. *Trends Microbiol.* 30, 593–605. doi: 10.1016/j.tim.2021.11.011

Wang, K., Chen, W., Zhang, Z., Deng, Y., Lian, J. Q., Du, P., et al. (2020). CD147-spike protein is a novel route for SARS-CoV-2 infection to host cells. *Signal Transduct Target Ther.* 5, 283. doi: 10.1038/s41392-020-00426-x

WHO (2022). *dashboard. WHO coronavirus disease (COVID-19)*. Available at: https://covid19.who.int/.

Wu, H.-J., and Wu, E. (2012). The role of gut microbiota in immune homeostasis and autoimmunity. *Gut Microbes* 3, 4–14. doi: 10.4161/gmic.19320

Wu, F., Zhao, S., Yu, B., Chen, Y.-M., Wang, W., Song, Z.-G., et al. (2020). A new coronavirus associated with human respiratory disease in China. *Nature* 579, 265–269. doi: 10.1038/s41586-020-2008-3

Xiao, F., Tang, M., Zheng, X., Liu, Y., Li, X., and Shan, H. (2020). Evidence for gastrointestinal infection of SARS-CoV-2. *Gastroenterology* 158, 1831–1833.e3. doi: 10.1053/j.gastro.2020.02.055

Xie, X., Muruato, A., Lokugamage, K. G., Narayanan, K., Zhang, X., Zou, J., et al. (2020). An infectious cDNA clone of SARS-CoV-2. *Cell Host Microbe* 27, 841–848.e3. doi: 10.1016/j.chom.2020.04.004

Xing, J., Zhou, X., Fang, M., Zhang, E., Minze, L. J., and Zhang, Z. (2021). DHX15 is required to control RNA virus-induced intestinal inflammation. *Cell Rep.* 35, 109205. doi: 10.1016/j.celrep.2021.109205

Yin, X., Riva, L., Pu, Y., Martin-Sancho, L., Kanamune, J., Yamamoto, Y., et al. (2021). MDA5 governs the innate immune response to SARS-CoV-2 in lung epithelial cells. *Cell Rep.* 34, 108628. doi: 10.1016/j.celrep.2020.108628

Zang, R., Florencia Gomez Castro, M., Mccune, B. T., Zeng, Q., Rothlauf, P. W., Sonnek, N. M., et al. (2020) *TMPRSS2 and TMPRSS4 promote SARS-CoV-2 infection of human small intestinal enterocytes*. Available at: https://www.science.org.

Zeng, W., Sun, L., Jiang, X., Chen, X., Hou, F., Adhikari, A., et al. (2010). Reconstitution of the RIG-I pathway reveals a signaling role of unanchored polyubiquitin chains in innate immunity. *Cell* 141, 315–330. doi: 10.1016/j.cell.2010.03.029

Zhou, J., Li, C., Liu, X., Chiu, M. C., Zhao, X., Wang, D., et al. (2020). Infection of bat and human intestinal organoids by SARS-CoV-2. *Nat. Med.* 26, 1077–1083. doi: 10.1038/s41591-020-0912-6

frontiers | Frontiers in Cellular and Infection Microbiology

TYPE Review
PUBLISHED 29 March 2023
DOI 10.3389/fcimb.2023.1098712

OPEN ACCESS

EDITED BY
You Zhou,
Cardiff University, United Kingdom

REVIEWED BY
Aftab Alam,
University at Buffalo, United States
Larissa Langhi Prata,
Mayo Clinic, United States

*CORRESPONDENCE
Chengliang Zhu
zhuchengliang@whu.edu.cn
Xuan Xiao
xiaoxuan1111@whu.edu.cn

†These authors have contributed equally to this work and share first authorship

SPECIALTY SECTION
This article was submitted to Virus and Host, a section of the journal Frontiers in Cellular and Infection Microbiology

RECEIVED 15 November 2022
ACCEPTED 06 March 2023
PUBLISHED 29 March 2023

CITATION
Li Z, Tian M, Wang G, Cui X, Ma J, Liu S, Shen B, Liu F, Wu K, Xiao X and Zhu C (2023) Senotherapeutics: An emerging approach to the treatment of viral infectious diseases in the elderly. *Front. Cell. Infect. Microbiol.* 13:1098712. doi: 10.3389/fcimb.2023.1098712

Senotherapeutics: An emerging approach to the treatment of viral infectious diseases in the elderly

Zhiqiang Li[1†], Mingfu Tian[2†], Guolei Wang[1†], Xianghua Cui[1†], Jun'e Ma[1], Siyu Liu[2], Bingzheng Shen[3], Fang Liu[2], Kailang Wu[2], Xuan Xiao[1*] and Chengliang Zhu[1*]

[1]Department of Clinical Laboratory, Institute of Translational Medicine, Renmin Hospital of Wuhan University, Wuhan, China, [2]State Key Laboratory of Virology, College of Life Sciences, Wuhan University, Wuhan, China, [3]Department of Pharmacy, Renmin Hospital of Wuhan University, Wuhan, China

In the context of the global COVID-19 pandemic, the phenomenon that the elderly have higher morbidity and mortality is of great concern. Existing evidence suggests that senescence and viral infection interact with each other. Viral infection can lead to the aggravation of senescence through multiple pathways, while virus-induced senescence combined with existing senescence in the elderly aggravates the severity of viral infections and promotes excessive age-related inflammation and multiple organ damage or dysfunction, ultimately resulting in higher mortality. The underlying mechanisms may involve mitochondrial dysfunction, abnormal activation of the cGAS-STING pathway and NLRP3 inflammasome, the role of pre-activated macrophages and over-recruited immune cells, and accumulation of immune cells with trained immunity. Thus, senescence-targeted drugs were shown to have positive effects on the treatment of viral infectious diseases in the elderly, which has received great attention and extensive research. Therefore, this review focused on the relationship between senescence and viral infection, as well as the significance of senotherapeutics for the treatment of viral infectious diseases.

KEYWORDS

senescence, virus, COVID-19, cGAS-STING, NLRP3 inflammasome, senotherapeutics

1 Introduction

Although the increasing aging population worldwide indicates that the average life expectancy of humans has lengthened, a simultaneous increase in age-related chronic diseases has also been observed. Simultaneously, there has been unprecedented interest in aging-related research, especially during the global COVID-19 pandemic, in which the elderly were found to suffer from higher morbidity and mortality compared to other age groups (Grasselli et al., 2020; Onder et al., 2020).

Age is considered a critical risk for the severity of COVID-19 disease (Zhou et al., 2020; Wang et al., 2020a). Data from China showed that the case fatality rate (CFR) of COVID-19 increased with age, and the CFR for patients aged 40 years or younger was ≤0.4%, but rose to 8.0% in patients aged 70 to 79 years, and 14.8% in patients aged ≥80 years (The Novel Coronavirus Pneumonia Emergency Response Epidemiology Team, 2020). Similarly, data from Italy revealed that CFR was also ≤0.4% for patients aged ≤40 years and, rose to 12.8% and 20.2% in patients aged 70 - 79 years and ≥80 years, respectively (Onder et al., 2020). In addition, a retrospective study on 5256 COVID-19 patients in the United States found that old age, male sex and impaired physical or cognitive function were independent risk factors for 30-day mortality (Panagiotou et al., 2021). Overall, current epidemiological evidence suggests that elderly COVID-19 patients (age ≥80 years) have a significantly higher risk of death than younger patients (Ackermann et al., 2020; Akbar and Gilroy, 2020). Moreover, higher mortality rates have also been reported in the elderly with influenza virus and respiratory syncytial virus infections (Thompson et al., 2003).

Thus, there are several unanswered questions between viral infections and senescence, such as: why do older people have higher morbidity and mortality from viral infections or how do viral infections and senescence interact and influence each other? To answer these questions, this review focuses on the relationship between senescence and viral infections and discusses the significance of senescence-targeted drugs for the treatment of viral infectious diseases, so as to provide insights for better understanding the role of senescence in disease development.

2 Characteristics of senescence

A basic feature of aged organisms is the accumulation of senescent cells. Senescence is a permanent status of cell cycle arrest in normal proliferating cells, described back in the 1960s when Hayflick and Moorhead found that the proliferation ability of cultured human diploid cells was limited and that cells stopped proliferating after serial passage *in vitro* (Hayflick and Moorhead, 1961; Hayflick, 1965; Lynch et al., 2021). Since then, biologists have gained a more comprehensive understanding on the characteristics associated with senescence.

2.1 Inducing factors of senescence

Cellular senescence is caused by repeated cell divisions and cellular stressors (Kelley et al., 2020). Replicative senescence results from repeated cellular divisions and has been confirmed to be related to the gradual shortening of telomeres during cell division (Shay, 2016; Lynch et al., 2021). Stress-induced senescence arises from cellular stressors, such as oncogene activation, DNA damage, reactive oxygen species (ROS), mitochondrial dysfunction and epigenetic stress (Hernandez-Segura et al., 2018), which may result from irradiation, chemotherapeutic drugs, pathogen infections, long-term exposure to pollutants (cigarette smoke) and certain aging syndromes such as progeria (Nyunoya et al., 2006; Nyunoya et al., 2009; Wheaton et al., 2017; Kelley et al., 2020; Di Micco et al., 2021) (Figure 1). Therefore, cells from both young and aged hosts may exhibit senescent properties (Kelley et al., 2020).

Activation of DNA damage response (DDR) signaling cascades initiated by nucleus DNA double-strand breaks (DSBs) is considered to be a common factor to induce cellular senescence (Di Micco et al., 2021). Specifically, there are two kinases upstream of DDR, known as ataxia telangiectasia mutated (ATM) and ATM- and Rad3-Related (ATR) protein kinases, they are respectively activated by the MRE11-RAD50-NBS1 (MRN) complex at DSBs and the TopBP1 or ETAA1 at replication protein A coated ssDNA

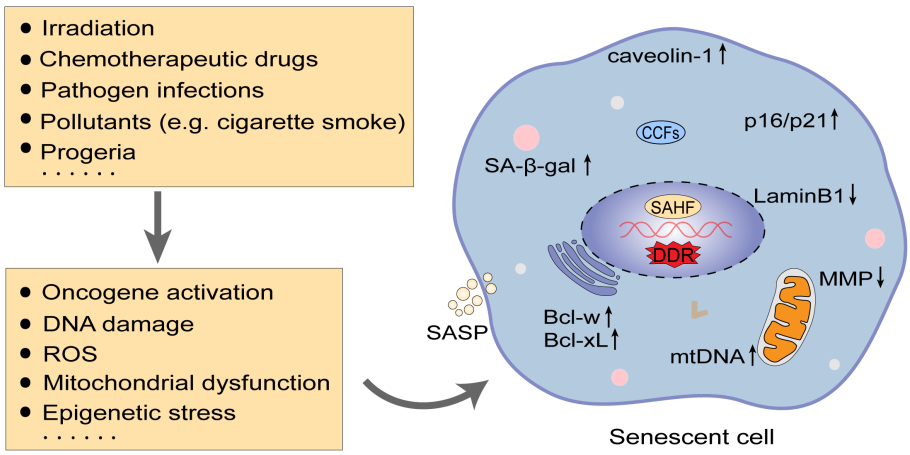

FIGURE 1
Inducing factors and characteristics of senescence. In addition to replicative senescence induced by telomere shortening, numerous factors such as irradiation, chemotherapeutic drugs, and pathogenic infections can evoke senescence by impacting oncogene activation, DNA damage, mitochondrial dysfunction, etc. DNA damage response (DDR) is an essential mechanism in triggering senescence. Cellular senescence features altered cell morphology and structure, arrest of the cell cycle (upregulation of p16/p21), and enhanced resistance to apoptosis (upregulation of Bcl-xL and Bcl-w), along with detectable nuclear senescence-associated heterochromatin foci (SAHFs), increased senescence-associated β-galactosidase (SA-β-gal) activity, and secretion of senescence-associated secretory phenotype (SASP). ROS, reactive oxygen species; MMP, membrane potential; CCFs, cytoplasmic chromatin fragments; mtDNA, mitochondrial DNA.

(RPA-ssDNA). Activated ATR and ATM can further phosphorylate the downstream kinases CHK1 and CHK2, respectively, which in turn activate the p53 pathway, leading to cell cycle arrest (Blackford and Jackson, 2017; Di Micco et al., 2021). Importantly, factors that can cause DNA damage, such as telomere shortening, oncogene activation and ROS, would ultimately be involved in activating the DDR pathway(van Deursen, 2014). If DNA damage from various causes persists, prolonged DDR signaling and proliferation arrest can invoke the onset of cellular senescence (Fumagalli et al., 2014). In addition, studies have reported that IFN-β secreted by senescent cells can stimulate DDR through ROS and generate senescence-like cell cycle arrest in human fibroblasts, which can trigger positive feedback activation of DDR and further amplify the senescence phenotype (Yu et al., 2015).

2.2 Hallmarks of senescence

Senescent cells have various characteristics (Hernandez-Segura et al., 2018) (Figure 1): (1) Morphologically, senescent cells are abnormally enlarged and flattened, with a disproportionate increase in the cytoplasm and nuclei (Bent et al., 2016; Druelle et al., 2016; Cormenier et al., 2018; Di Micco et al., 2021); changes in the composition of the plasma membrane, such as caveolin-1 protein upregulation (Dasari et al., 2006; Chrétien et al., 2008; Althubiti et al., 2014); increased lysosome content and some proteins (Cho and Hwang, 2012); accumulated mitochondria and decreased membrane potential (MMP) (Passos et al., 2007; Korolchuk et al., 2017; Tai et al., 2017); nuclear membrane structural protein loss, such as the downregulation of LaminB1 protein and presence of nuclear senescence-associated heterochromatin foci (SAHFs) with detectable dense 4',6-diamidino-2-phenylindole (DAPI)-positive nuclear structural features (Di Micco et al., 2011; Sadaie et al., 2013); (2) Elevated senescence-associated β-galactosidase (SA-β-gal) activity: SA-β-gal is a lysosomal-derived enzyme that is regarded as a surrogate marker for increased lysosomal content in senescent cells and is one of the most common markers of senescence (Dimri et al., 1995; Kurz et al., 2000; Lee et al., 2006); (3) Accumulation of cyclin-dependent kinase inhibitors (CDKis): Senescence-related cell cycle arrest is primarily driven by CDKis encoded at *CDKN2A* ($p16^{INK4a}$ or p16), *CDKN2B* ($p15^{INK4b}$ or p15) and *CDKN1A* ($p21^{CIP1}$ or p21) loci. p21 and p16 maintain the tumor suppressor protein pRb in an inactive hypophosphorylated state, thereby preventing the transcription factor E2F from transcribing genes that promote cell cycle progression, and both are often used as unique senescence hallmarks to identify senescent cells in tissues and cultured cells (Narita et al., 2003; Baker et al., 2011; Di Micco et al., 2021); (4) Senescence-associated secretory phenotype (SASP): SASP consists of various cytokines, chemokines and some enzymes involved in extracellular matrix remodeling, mainly including IL-1α/β, IL-6, IL-8, TNF-α, TGF-β, monocyte chemotactic protein 1 (MCP1, also known as CCL-2) and matrix metalloproteinases (MMPs). SASP is thought to be the main mechanism by which senescent cells exert their pleiotropic biological functions and can also induce paracrine senescence (Freund et al., 2010; Acosta et al., 2013; Tchkonia et al., 2013; Gorgoulis et al., 2019); (5) Enhanced apoptosis resistance: Senescent cells stimulate a wide range of pro-survival factors, such as BCL-2 family members, particularly Bcl-xL and Bcl-w, which can be resistant to apoptosis and favor the survival of senescent cells (Childs et al., 2014; Yosef et al., 2016).

Defects associated with aging of the immune system are another feature of aging, termed "immunosenescence" (Kelley et al., 2020). It is characterized by decreased proliferation of hematopoietic stem cells, dysfunction of innate immunity, degeneration of the thymus and reduced numbers of naïve T and B cells, as well as accumulation of memory T and B cells, and decline in T and B cell functions (Kelley et al., 2020; Xu et al., 2020). Immunosenescence is associated with increased susceptibility to various diseases, such as infections, cancer, cardiovascular diseases, hypertension, diabetes, neurological dysfunction, and autoimmune diseases (Xu et al., 2020).

3 Virus-induced senescence

Virus infections can prematurely stimulate cellular senescence, known as virus-induced senescence (VIS). Studies have shown that some viruses, such as the human immunodeficiency virus (HIV), measles virus (MV), respiratory syncytial virus (RSV) and influenza virus, can induce cell fusion and form multinucleated cells upon infecting the organism as a mechanism for expanding its spread in the infected organisms (Chen and Olson, 2005; Duelli and Lazebnik, 2007; Sapir et al., 2008; Delpeut et al., 2012). MV infection has been proven to induce p53 and p16-pRb pathway-dependent cellular senescence *via* cell fusion (Chuprin et al., 2013). Epstein–Barr virus (EBV), Kaposi sarcoma herpesvirus (KSHV) and human RSV infections can trigger DNA damage-mediated cellular senescence through replicative stress or induction of mitochondrial ROS (Koopal et al., 2007; Martínez et al., 2016; Hafez and Luftig, 2017). Some viral proteins, such as NS1 of influenza A virus (IAV) (Yan et al., 2017), HBx of hepatitis B virus (HBV) (Idrissi et al., 2016) and IE2 of human cytomegalovirus (CMV) (Noris et al., 2002), were found to induce senescence by increasing the inducible NO synthase (iNOS) expression and NO release and regulating the p21 and p16 pathways, respectively. HIV Tat and Nef proteins can provoke bone marrow mesenchymal stem cells senescence through either enhanced inflammation or reduced autophagy (Beaupere et al., 2015), and HIV Tat can also trigger microglia senescence upon miR-505-SIRT3 axis-mediated mitochondrial oxidative stress (Thangaraj et al., 2021) (Table 1).

The occurrence of VIS was assessed in a basic research study (Lee et al., 2021), which found that human diploid fibroblast models exposed to high-titer retrovirus exhibited typical characteristics of senescence and the activated cyclic GMP-AMP synthase-stimulator of interferon genes (cGAS-STING) pathway after the fifth day of infection. Consistently, VIS was detectable in human lung carcinoma cells and non-malignant epithelial cells upon infection with lentivirus, adeno-associated virus (AAV), vesicular stomatitis virus (VSV) and the low-pathogenic human alphacoronavirus NL63 (HCoV-NL63). In parallel, canonical cellular senescence phenotype were found in SARS-CoV-2-infected human primary nasal epithelial cells (HNEpc), alveolar epithelial cells (AEC),

TABLE 1 Virus-induced senescence and potential mechanism.

Virus	Mechanism	Refs
Measles virus	Cell fusion and induction of p53 and p16-pRb pathways	(Chuprin et al., 2013)
Respiratory syncytial virus	Mitochondrial ROS production and DNA damage response	(Martínez et al., 2016)
Kaposi sarcoma herpesvirus	Oncogene activation and DNA damage response	(Koopal et al., 2007)
Epstein-Barr virus	Replicative stress and DNA damage response	(Hafez and Luftig, 2017)
Influenza A virus	NS1 protein increases the iNOS expression and NO release; SASP-related paracrine senescence	(Yan et al., 2017; Lv et al., 2022; Schmitt et al., 2022)
Hepatitis B virus	HBx C-terminal mutants of HBV regulate the p21 and p16 pathways	(Idrissi et al., 2016)
Cytomegalovirus	IE2 protein regulates the p53 and p16 pathways	(Noris et al., 2002)
Human immunodeficiency virus	Induction of immunosenescence; HIV Tat protein augments miR-505-SIRT3 axis-mediated mitochondrial oxidative stress and enhances inflammation; HIV Nef protein reduces autophagy	(Beaupere et al., 2015; Blanco et al., 2021; Thangaraj et al., 2021; Chauvin and Sauce, 2022)
SARS-CoV-2	Activation of DNA damage response; SASP-related paracrine senescence	(Lee et al., 2021; Evangelou et al., 2022; Lv et al., 2022; Schmitt et al., 2022)
Herpes simplex virus 1	Activation of p53/p16 pathways and NLRP3	(Sivasubramanian et al., 2022)

ROS, reactive oxygen species; iNOS, inducible nitric oxide synthase; NO, nitric oxide.

normal human bronchus epithelial (NHBE) cells and macrophages, and COVID-19 patients also displayed marked signs of senescence in their nasopharyngeal and lung tissue specimens and elevated serum levels of SASP factors, suggesting that SASP-mediated effects are pivotal factors in secondary paracrine senescence, lung disease, hyperinflammation, tissue damage, and coagulation disorders of patients infected with SARS-CoV-2 (Wiley et al., 2019; Ackermann et al., 2020; Lee et al., 2021; Evangelou et al., 2022; Schmitt et al., 2022). Likewise, a recent study (Lv et al., 2022) also indicated that aged mice deficient in telomerase RNA ($Tere^{-/-}$) were extremely sensitive to IAV, SARS-CoV-2 and other respiratory virus infections. $Tere^{-/-}$ mice showed typical features of cellular senescence and aberrant activation of the cGAS-STING pathway and NOD-like receptor family pyrin domain containing 3 (NLRP3) inflammasome mediated by leaked mitochondrial DNA (mtDNA), which could contribute to an excessive inflammatory response, particularly following viral exposure, thereby were more likely to develop severe viral pneumonia in non-fatal respiratory virus infections and abnormally increased mortality for $Tere^{-/-}$ mice (Ackermann et al., 2020; Akbar and Gilroy, 2020; Decout et al., 2021; Sanchez-Vazquez et al., 2021; Xian et al., 2021; Lv et al., 2022). Further, latent herpes simplex virus 1 (HSV-1) infection in the key brainstem regions of female mice induces senescence by activating the p53/p16 pathway and NLRP3, resulting in neuroinflammation and neurodegeneration (Sivasubramanian et al., 2022).

HIV infection can also induce a senescent phenotype with the same characteristics as normal senescence (Appay et al., 2007). Owing to antiretroviral therapy (ART), the life expectancy of HIV-infected persons (PLWH) has increased (Wandeler et al., 2016). However, there is still persistent immune activation and inflammation in PLWH even though the virus is effectively suppressed, thus contributing to premature aging (Blanco et al., 2021; Chauvin and Sauce, 2022).

Acquired immune deficiency syndrome (AIDS) patients are often co-infected with the herpes virus (CMV, EBV and HSV), HBV and hepatitis C virus (HCV), of which CMV is the most common chronic infection (Blanco et al., 2021). Chronic CMV infection is highly prevalent in the HIV-negative general elderly population and nearly universal in the HIV-positive elderly population, enabling T-cell clonal expansion and leading to immunosenescence and chronic low-grade inflammation (Khan et al., 2002; Koch et al., 2007; Leng and Margolick, 2020), whereas CMV and HIV co-infection can cause further adverse effects (Leng and Margolick, 2020). Interestingly, AIDS patients have reduced levels of Kupffer cells and $CD4^+$ T cells in the presence of HIV and HCV co-infection, which can lead to a decrease in the clearance of microbial products and an increase in the levels of soluble CD14 (sCD14), lipopolysaccharide (LPS), peptidoglycan, and ribosomal DNA in the blood *via* microbial translocation (Ancuta et al., 2008; Sandler and Douek, 2012; Blanco et al., 2021). These microbial products can bind to pattern recognition receptors (PRRs) and trigger signaling cascades that favor chronic immune activation and inflammation (Sandler and Douek, 2012; Vázquez-Castellanos et al., 2015; Dillon et al., 2016). At the same time, a reduction in the number of $CD4^+$ T cells during HIV infection may promote the replication of HCV, resulting in $CD8^+$ T cells being continuously activated. This reciprocates the cycle of viral replication and immune activation, showing signs of activation, exhaustion, and immunosenescence (Appay and Kelleher, 2016; Hoffmann et al., 2016; Blanco et al., 2021).

PLWH has similar features as natural immunosenescence. For instance, PLWH is associated with decreased numbers and impaired proliferative capacity of circulating $CD34^+$ hematopoietic progenitor cells (HPCs), thymic degeneration, reduced initial T cells and an accumulation of memory T cells. They also have reduced $CD56^+$

$^{+}$NK cells and CD14^{++}CD16^{-}classical monocytes while increased CD14^{++} CD16^{+} intermediate and CD14^{+} CD16^{++} non-classical monocytes (Hakim et al., 2005; Seidler et al., 2010; Sauce et al., 2011; Hearps et al., 2012; Naranbhai et al., 2013; Massanella et al., 2015; Chauvin and Sauce, 2022). These factors can increase the risk of various age-related diseases in PLWH, such as cardiovascular diseases, renal failure, liver diseases, osteoporosis, cancer and cognitive dysfunctions (Deeks et al., 2013; Gallant et al., 2017).

4 Consequences of senescence

With an increase in age, organisms tend to turn into a pro-inflammatory state characterized by low levels of circulating pro-inflammatory factors and perpetuate chronic inflammation in the elderly population (Franceschi et al., 2000; Xu et al., 2020). However, in the event of viral infections, virus-induced senescence combined with an existing senescence in aged or vulnerable hosts may trigger a more intense inflammatory cascade response, leading to more severe symptoms and multi-organ damage or even dysfunction in the elderly infected population, and thus a higher mortality rate (Figure 2).

4.1 Excessive inflammation and tissue damage associated with aging

As aging occurs, cumulative senescent cells accelerate chronic inflammation through senescence-associated secretory phenotype (SASP), whereby SASP demonstrates a double-edged sword role (Hernandez-Segura et al., 2017). On the one hand, short-term SASP secretion promotes tissue repair and wound healing (Jun and Lau, 2010; Demaria et al., 2014) and enhances immune surveillance to inhibit tumor progression and pathological fibrosis (Xue et al., 2007; Krizhanovsky et al., 2008; Kang et al., 2011; Sagiv et al., 2016), while on the other hand, prolonged SASP secretion contributes to the development of age-related chronic inflammatory diseases by triggering over-recruitment of immune cells (Muñoz-Espín and Serrano, 2014; Childs et al., 2015; He and Sharpless, 2017). Excessive SASP can also recruit immature myeloid cells to favor tumorigenesis and tumor progression in a paracrine manner and affect tissue regeneration by limiting the proliferative potential of stem and progenitor cells (Yoshimoto et al., 2013; Di Mitri et al., 2014; Eggert et al., 2016; Gonzalez-Meljem et al., 2017; Di Micco et al., 2021). The mechanisms of excessive inflammation and tissue damage caused by aging may involve the abnormal activation of the mtDNA/CCFs-cGAS-STING pathway and NLRP3 inflammasome, the role of pre-activated macrophages and over-recruited immune cells and the accumulation of innate immune cells with trained immunity (Figure 2).

4.1.1 Abnormal activation of the mtDNA/CCFs-cGAS-STING pathway and NLRP3 inflammasome

Aging-related mitochondrial dysfunction is identified as a potential mechanism leading to increased inflammation. Mitochondria are extremely important organelles involved in a wide range of cellular activities, such as oxidative phosphorylation, ATP synthesis, apoptosis, autophagy and immune responses (Nunnari and Suomalainen, 2012; Mills et al., 2017; Lv et al., 2022). Thus, complete mitochondrial structure and function are

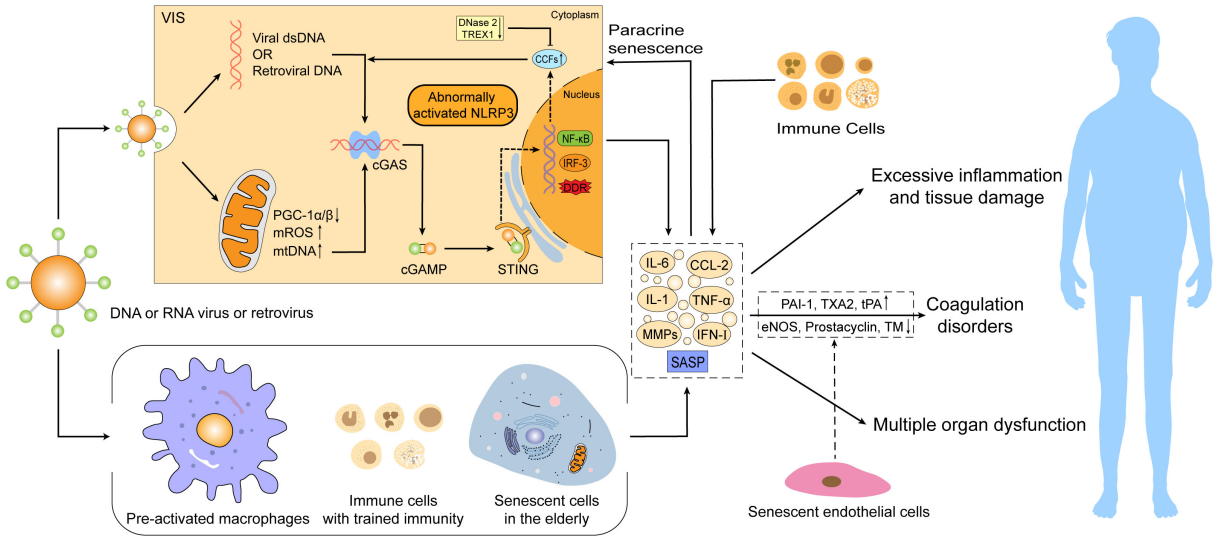

FIGURE 2
Virus-induced senescence (VIS) combined with an existing senescence in the elderly intensifies the severity of viral infections. Senescence can promote the development of viral infectious diseases *via* abnormal activation of the mtDNA/CCFs-cGAS-STING pathway and NLRP3 inflammasome, pre-activated macrophages, over-recruited immune cells, and accumulation of innate immune cells with "trained immunity" characteristics. These alterations can trigger excessive SASP production and secondary paracrine senescence, resulting in hyperinflammation, tissue damage, coagulation disorders, and even multiple organ dysfunction, thus leading to a higher mortality risk. SASP, senescence-associated secretory phenotype; cGAMP, cyclic GMP–AMP; CCFs, cytoplasmic chromatin fragments; DDR, DNA damage response; eNOS, endothelial NO synthase; PAI-1, plasminogen activator inhibitor-1; TXA2, thromboxane A2; TM, thrombomodulin; ROS, reactive oxygen species.

essential for maintaining cellular homeostasis and physiological function (Nunnari and Suomalainen, 2012). However, the adaptability and integrity of mitochondria gradually deteriorate with age, thereby provoking a decline in oxidative phosphorylation efficiency, decrease in MMP, impairment in ATP generation, increase in ROS production and altered autophagic activity, ultimately prompting the leakage of mtDNA from dysfunctional mitochondria (López-Otín et al., 2013; Korolchuk et al., 2017; Hopfner and Hornung, 2020; Lv et al., 2022). Importantly, mtDNA can be recognized by the cGAS-STING system to trigger immune and inflammatory responses (Hopfner and Hornung, 2020; Lv et al., 2022). Specifically, cGAS can directly bind to DNA released into the cytoplasm and subsequently synthesize cyclic GMP–AMP (cGAMP) from GTP and ATP. STING is bound and activated by cGAMP, which activates the NF-κB and IRF3 pathways, thus inducing the production of type I interferon and pro-inflammatory cytokines such as IL-1 and IL-6 (Hopfner and Hornung, 2020; Yang et al., 2021).

In addition to mitochondrial-derived mtDNA, there is evidence that age-related reduction of the LaminB1 protein compromises nuclear envelope integrity and causes the accumulation of cytoplasmic chromatin fragments (CCFs), which can also activate the cGAS-STING pathway and intensify the production of pro-inflammatory factors (Ivanov et al., 2013; Shah et al., 2013; Dou et al., 2017; Glück et al., 2017). Likewise, increased DNA in the cytoplasm caused by telomere dysfunction can be detected by cGAS (Chen et al., 2017; Nassour et al., 2019). The cumulation of nuclear DNA in the cytoplasm is associated with the downregulation of DNases involved in cytoplasmic DNA degradation in senescent cells, such as DNase 2 and TREX1 (Takahashi et al., 2018). Moreover, senescence-related impairment of autophagy, which delays the clearance of activated STING and other cellular debris, can also lead to further accumulation of cytoplasmic DNA and amplify the cGAS-STING pathway and inflammation (Paul et al., 2021).

It was previously reported (Lv et al., 2022) that Tere$^{-/-}$ aged mice were more sensitive to respiratory viral infections such as IAV and SARS-CoV-2, exhibiting excessive inflammatory responses, typical senescence features and increased mortality, which further abnormally activated the cGAS-STING pathway and NLRP3 inflammasome by a process that is mainly mediated by leaked mtDNA. Compared with normal controls, the mitochondria in Tere$^{-/-}$ macrophages showed a swollen shape, irregular rarefied cristae and compromised ATP generation, as well as increased mROS stress. Consistently, there was an elevated amount of cytoplasmic mtDNA in Terc$^{-/-}$ macrophages upon IAV infection, while less mtDNA was retained in mitochondria. Of note, the above phenotypes were more visible following viral infection. However, targeted inhibition of mtDNA release *via* VBIT-4 significantly weakened the abnormal activation of the cGAS-STING pathway in Tere$^{-/-}$ macrophages relative to controls (Lv et al., 2022), suggesting the importance of aging-related mitochondrial dysfunction in response to viral infection in triggering exaggerated inflammatory responses and causing severe organ damage. Further effects of viral infection on mitochondrial function through the induction of more VIS may play a vital role in the higher levels of mtDNA liberation, leading to stronger inflammatory responses.

An increasing number of research showed that aberrant activation of the aging-associated cGAS-STING pathway and NLRP3 inflammasome underlies the increased lethality of SARS-CoV-2 infection in the elderly, and activation of the NLRP3 inflammasome may be mediated *via* the cGAS-STING pathway (Lara et al., 2020; Wang et al., 2020b; Lv et al., 2022). Specifically, telomere dysfunction in the elderly stimulates p53-mediated cellular responses and inhibits major regulators of mitochondrial function such as PGC-1α and PGC-1β, conducing to impaired mitochondrial function, enhanced oxidative stress and mtDNA accumulation. Higher levels of mtDNA can generate sustained activation of the cGAS-STING pathway and NLRP3 inflammasome, as well as elevated levels of pro-inflammatory factors. When viral infection occurs, VIS further boosts these pathways and facilitates more production of pro-inflammatory factors, inflicting greater damage to the organism (Kang et al., 2018; Lara et al., 2020; Lv et al., 2022). In addition to SARS-CoV-2 and IAV, when exposed to a series of RNA or DNA viruses or viral products such as human rhinovirus, dengue virus, adenovirus, HCV, MV, RSV, HIV and HSV, organisms demonstrate antiviral effects by activating inflammasomes, such as NLRP3 and AIM2 (Shrivastava et al., 2016), and PRRs, such as Toll-like receptors and RIG-I-like receptors, which are important for recognizing viruses in addition to cGAS (Kawai and Akira, 2008; Wilkins and Gale, 2010). Thereinto, the toll-like receptor-3 (TLR-3) proved to exacerbate SASP secretion of human senescent cells upon SARS-CoV-2 infection (Tripathi et al., 2021). The Toll-like receptor 2 (TLR2) and its partner TLR10 were shown to be key mediators of senescence *in vitro* and in murine models during oncogene-induced senescence (OIS). TLR2 can promote cell cycle arrest by regulating tumor suppressors p53-p21, p16 and p15 and modulate the SASP production by inducing acute-phase serum amyloids A1 and A2 (Hari et al., 2019). However, little is known about whether antiviral responses induced by other PRRs or inflammasomes are linked to aging or aging-related excessive inflammation and tissue damage.

Notably, RNA viruses such as IAV and SARS-CoV-2 are thought to be recognized by RNA receptors such as Toll-like receptors and RIG-I rather than cGAS, a DNA receptor, upon infections (Liu et al., 2016). In this regard, as previously described, for non-DNA virus infection, the infectious agent may indirectly trigger cGAS-STING activation by directly or indirectly inducing mitochondrial stress to leak mtDNA (Hanada et al., 2020; Hopfner and Hornung, 2020). Such a situation applies to the dengue virus and HSV. Dengue virus is a single positive-stranded RNA virus whose infection generates an endogenous source of cytoplasmic DNA through the release of mtDNA, which drives cGAS to produce cGAMP, with the latter subsequently binding and activating STING, which in return activate the NF-κB and IRF3 pathways and trigger an innate immune antiviral response (Ha et al., 2011; Aguirre et al., 2017; Sun et al., 2017). Although HSV is a DNA virus, its infection can also stimulate the liberation of mtDNA and activate the cGAS-STING pathway (West et al., 2015). Additionally, intracellular accumulation of retrotransposable elements can be

reactivated during aging in somatic tissues to drive cGAS-dependent type I interferon responses and contribute to the maintenance of age-related inflammation (De Cecco et al., 2019). For example, HIV, a retrovirus, can trigger cGAS-STING reaction with its reverse-transcribed HIV DNA, and inhibitors of HIV reverse transcriptase can block the induction of interferon response by this virus (Gao et al., 2013). The binding of cGAS to HIV DNA is assisted by the host factor NONO, a multifunctional protein that binds nucleic acids and HIV capsid proteins in the nucleus. NONO is thought to directly recognize HIV DNA by nuclear-localized cGAS (Lahaye et al., 2018). In addition to NONO, host proteins such as PQBP1 (Yoh et al., 2015), ZCCHC3 (Lian et al., 2018) and G3BP1 (Liu et al., 2019) can also contribute to cGAS sensing of reverse-transcribed DNA.

4.1.2 Pre-activated macrophages and over-recruitment of immune cells

It was found that compared to resting macrophages in the lungs of young mice, resident pulmonary macrophages from old mice were in an activated state and more likely to be activated in response to infections. Moreover, these aged lung macrophages harbored higher basal levels of circulating pro-inflammatory cytokines, such as IL-1β, IL-6 and TNF-α (Canan et al., 2014). Saskia L Smits et al. previously reported that SARS-CoV-infected aged macaques developed more severe pathology and higher lethality with a stronger host response than young adult animals, even though viral replication levels were similar and the mRNA levels of IFN-β were negatively correlated with gross pathology. However, treatment with type I interferon significantly diminished the expression of pro-inflammatory genes and attenuated the pathological response in old macaques (Smits et al., 2010). This could be explained by the role of pre-activated macrophages and higher basal levels of pro-inflammatory factors in aged individuals, and also to some extent by the fact that fatal viral infections in the elderly are often associated with exuberant inflammatory cell infiltration and delayed interferon production (Arunachalam et al., 2020).

In addition, previous studies showed that aging could increase mortality from influenza virus infection (Thompson et al., 2003). Senescent alveolar epithelial cells recruit excessive neutrophils (PMNs) in old mice by secreting higher levels of chemokines CXCL1 and CXCL2 upon influenza virus infection (Kulkarni et al., 2019). More importantly, activated PMNs can also generate more pro-inflammatory factors, further recruiting immune cells and leading to more severe inflammatory responses and tissue damage relative to young mice (Peiró et al., 2018; Kulkarni et al., 2019). However, the depletion of PMNs following viral infection can substantially improve the survival of aged mice without altering viral clearance (Kulkarni et al., 2019).

Collectively, the pre-existing inflammatory state and the over-recruitment of immune cells in response to viral infections in older individuals can precipitate increased inflammatory responses to external pathogens, resulting in a massive release of inflammatory mediators and potentially causing widespread tissue damage in common and non-fatal infections for the elderly.

4.1.3 Role of immune cells with trained immunity

Immune memory is traditionally regarded as an exclusive hallmark of adaptive immunity. However, activation of the innate immune system can also lead to an enhanced response to secondary infections, termed “trained immunity”, which is actually a form of innate immune memory (Netea et al., 2020a). Maojun You et al. revealed the establishment of trained immunity in COVID-19 convalescent individuals *via* the single-cell epigenomic landscape of peripheral immune cells, showing that trained and activated states of $CD14^+$ and $CD16^+$ monocytes were dominantly enriched in individuals recovering from COVID-19 (You et al., 2021). These observations indicate that innate immune cells can form a non-specific but stable immune memory after initial infection, although it may be transient compared to classical T and B cells (Netea et al., 2020a; You et al., 2021). Furthermore, this epigenomic regulation of the innate immune memory response may not be specific to SARS-CoV-2 but also be elicited following other infections such as SARS-CoV-1, MERS, HIV, or vaccination, which is deemed to be a fundamental characteristic of host defense of multicellular organisms, including mammals (Netea et al., 2020a; You et al., 2021; Sviridov et al., 2022).

Evidence accumulated in recent years suggests that trained immunity caused by epigenetic and metabolic reprogramming is a double-edged sword. Although it enables a rapid and efficient host immune response to reinfected pathogens, it can also induce chronic inflammatory diseases (Netea et al., 2020a; Netea et al., 2020b; You et al., 2021). In the elderly, the accumulation of immune cells with trained immunity in the body may promote excessive inflammation and cause more severe tissue damage in the event of reinfection. Thus, appropriate targeting of immune cells with trained immunity in elderly individuals might be beneficial to relieve inflammation (You et al., 2021; Lv et al., 2022).

4.2 Aging-related multi-organ dysfunction

The effects of viral infections on the organism often involve multiple systems and organs. For example, SARS-CoV-2, a respiratory virus, in addition to causing lung infection, the virus can also replicate in cells of the intestine, liver and kidney, thus causing a variety of clinical symptoms other than the respiratory tract, such as gastrointestinal disorders, liver and kidney dysfunction (Chu et al., 2020) and even multi-organ failure (Chen et al., 2020). However, there is growing evidence supporting the role of aging in multi-organ dysfunction caused by viral infections (Figure 2).

Coagulation abnormalities and thrombosis can occur in the late stages in patients with viral infections and are often associated with poor prognosis (Nehme et al., 2020). Several factors, however, including aging, have been shown to be risk factors for vascular dysfunction (Nehme et al., 2020). On the one hand, senescent cells can secrete large amounts of SASP pro-inflammatory mediators that may trigger endothelial injury and favor thrombosis. On the other hand, together with inflammatory factors, senescent endothelial cells can shift the balance between pro- and

anticoagulant pathways towards an elevated risk for thrombosis *via* the upregulation of factors that induce platelet aggregation such as plasminogen activator inhibitor-1 (PAI-1), thromboxane A2 (TXA2) and von Willebrand factor (vWF), while downregulating factors that inhibit platelet aggregation such as endothelial NO synthase (eNOS), prostacyclin and thrombomodulin (Bochenek et al., 2016; Wiley et al., 2019; Nehme et al., 2020). Therefore, the elderly may develop more severe coagulation disorders if infected by SARS-CoV, MERS-CoV, H1N1, HIV or other viruses (Obi et al., 2019; Ackermann et al., 2020; de Magalhães et al., 2020; Giannis et al., 2020). It was found that compared with young controls, aged hamsters exhibited prolongation of PT, intravascular clotting and acute kidney damage upon SARS-CoV-2 infection (Ohno et al., 2021). These changes are often present in patients with COVID-19 and strongly associated with disease severity and higher mortality (Helms et al., 2020; Porfidia et al., 2020; Loo et al., 2021). In addition, H1N1 acute respiratory distress syndrome (ARDS) patients possessed a 23.3-fold higher risk for pulmonary embolism and a 17.9-fold increased risk for venous thromboembolism (Obi et al., 2019). Simultaneously, in HIV-infected patients, endothelial dysfunction caused by HIV replication may also lead to a hypercoagulable state (Kuller et al., 2008; Armah et al., 2012), while aging-related inflammation and cellular changes may further contribute to coagulation dysfunction (de Magalhães et al., 2020).

Additionally, due to abnormal immune responses and excessive inflammation associated with aging, the elderly are more prone to complications such as liver and kidney dysfunction, myocardial injury, and neurological symptoms in the event of viral infections such as SARS-CoV-2. In particular, the massive secretion of SASP may generate fibrosis or cause injuries in organs other than the lungs, such as the liver, kidney and cardiovascular system (Cai et al., 2020; George et al., 2020; Napoli et al., 2020; Sharma et al., 2020; D'Agnillo et al., 2021). A decline in the blood-brain barrier function with aging may also cause infection of the central nervous system, leading to neurological symptoms (Yamazaki et al., 2016; Mao et al., 2020; Propson et al., 2021).

4.3 Dual role of aging antiviral response

Presently, it is believed that aging may cause dual effects during antiviral infection. Primarily, SASP cytokines and chemokines from senescent cells and accordingly recruited innate immune cells such as PMNs may predispose virus-induced senescence to become a part of the antiviral immune response (Baz-Martínez et al., 2016). This antiviral mechanism may enable the secretion of SASP factors by virus-induced senescent cells to restrict virus replication in neighboring cells and avoid its spread (Kelley et al., 2020). Moreover, the human papillomavirus (HPV), HBV, EBV and KSHV have evolved various mechanisms that can specifically combat cellular senescence (Yang et al., 2000; Oishi et al., 2007; Leidal et al., 2012; Zhi et al., 2015; Estêvão et al., 2019), indirectly suggesting that senescence may lead to antiviral defense in certain circumstances (Kelley et al., 2020).

Conversely, it was documented that senescence is conducive to the pathophysiology of viral infections and may promote viral replication and mutagenesis (Kelley et al., 2020; Evangelou et al., 2022). For instance, RSV infection can alter human airway epithelial differentiation and trigger the senescence of lung epithelial cells both *in vivo* and *in vitro* by generating ROS and causing DNA damage, thereby contributing to airway tissue remodeling and the severity and long-term consequences of RSV infections (Persson et al., 2014; Martínez et al., 2016). The influenza and varicella-zoster viruses can replicate more efficiently in senescent human bronchial epithelial cells and senescent human dermal fibroblasts, respectively, compared with non-senescent cells (Kim et al., 2016). The possible reasons for this phenomenon are the downregulation of type I interferon induction upon senescence and the defective mitochondrial dynamics of senescent cells, which consequently inhibit interferon expression and early interferon responses, thus favoring viral replication (Kim et al., 2016; Kelley et al., 2020). However, Baz-Martínez M et al. found that primary or chemotherapy-induced senescence reduces VSV replication (Baz-Martínez et al., 2016), suggesting that senescence plays a different role in response to diverse viral infections under distinguishing conditions. Remarkably, recent studies revealed that infected senescent cells might be a source of apolipoprotein B mRNA-editing (APOBEC) enzyme-mediated SARS-CoV-2 mutations (Evangelou et al., 2022).

Taken together, the effects of senescence on the body's antiviral immune response are multifaceted (Figure 3). In this regard, it has been hypothesized from the perspective of acute respiratory viral infections that aging may play different roles in viral infections depending on host resilience (Kelley et al., 2020). In young hosts, VIS may enhance antiviral immunity by recruiting PMNs and other immune cells *via* SASP, thereby promoting viral clearance and tissue repair. However, in old or vulnerable hosts, VIS coupled with an existing senescence condition may lead to excessive immune responses with high levels of SASP cytokines and chemokines, resulting in secondary senescence and over-recruitment of immune cells, eliciting severe tissue damage and multi-organ failure (Kelley et al., 2020; Camell et al., 2021).

5 Significance of senotherapeutics in viral infectious diseases

In the presence of viral infections, VIS plus naturally occurring senescence are pivotal in precipitating excessive inflammatory responses, severe organ damage, and higher mortality in the elderly. Hence, senotherapeutics seem to be of great importance in alleviating clinical symptoms and organ damage and influencing disease regression in elderly individuals with viral infections.

Actually, for viral infectious diseases in aged people, there are currently two main areas of research in senotherapeutics (Table 2). The first one is the targeted removal of senescent cells, termed "senolytics", mainly by propping up apoptosis of senescent cells, such as quercetin and fisetin (natural flavonoids), navitoclax (an inhibitor of BCL-2 pro-survival family) and dasatinib (a tyrosine

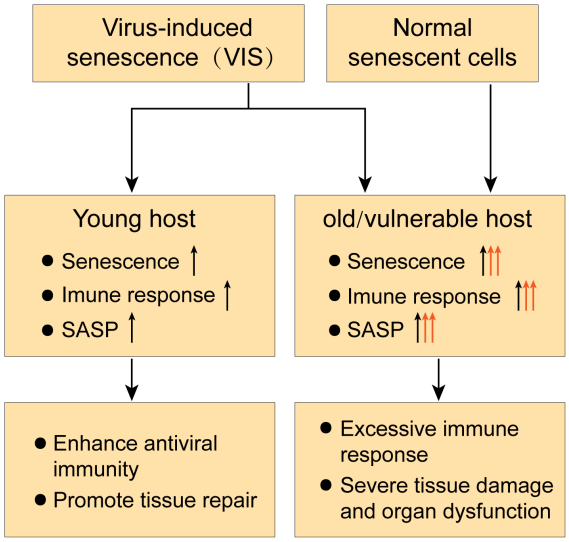

FIGURE 3
Dual role of senescence in antiviral immune responses.

kinase inhibitor). The second one is the inhibition of diverse components of SASP or inflammatory pathways involved in SASP synthesis, known as "senomorphics", such as targeted inhibition of the cGAS-STING and NF-κB pathways or IL-1 and IL-6 cytokines. Intriguingly, available evidence implies a positive effect on mitigating aging-related diseases by eliminating senescent cells or inhibiting SASP secretion, and various clinical studies on senotherapeutics applied to viral infectious diseases are ongoing or have been completed (Table 3).

5.1 Senolytics

The most widely studied therapeutic strategy for the targeted elimination of senescent cells by senolytics is the combination therapy of dasatinib (D) with quercetin (Q). "D+Q" treatment was shown to reduce the cellular stress of aged mice, lessen vascular sclerosis, strengthen vasodilatory functions and impel lung function in mice with pulmonary fibrosis, thus improving the health status and lifespan of elderly mice (Roos et al., 2016;

TABLE 2 Senescence-targeted therapeutics of viral infectious diseases.

Drugs	Main targets	Effect of treatment	Refs
Senolytics			
Quercetin	PI3K	Reduce the burden of senescent cells and major SASP factors, improving health	(Camell et al., 2021; Lee et al., 2021; Di Pierro et al., 2021a; Di Pierro et al., 2021b; Lv et al., 2022)
Fistein	PIK3/AKT	Alleviate cellular senescence features and mitochondrial damage, inhibit abnormal activation of cGAS-STING pathway and NLRP3 inflammasome	(Camell et al., 2021; Lee et al., 2021; Lv et al., 2022)
Dasatinib	Tyrosine kinases	Reduce the burden of senescent cells and major SASP factors, improving health	(Camell et al., 2021; Lee et al., 2021; Lv et al., 2022)
Navitoclax	Bcl-2, Bcl-xL, Bcl-w	Alleviate cellular senescence features and improve prognosis	(Chang et al., 2016; Lee et al., 2021)
Senomorphics			
Rapamycin	mTOR	Inhibit SASP generation, enhance antiviral activity and prolong healthy lifespan	(Wilkinson et al., 2012; Mannick et al., 2014; Wang et al., 2014; Herranz et al., 2015; Kindrachuk et al., 2015; Husain and Byrareddy, 2020)
Metformin	NF-κB	Inhibit the NF-κB pathway and pro-inflammatory factors production, resulting in a significant reduction in mortality	(Valencia et al., 2017; Crouse et al., 2020; Li et al., 2020; Luo et al., 2020; Xian et al., 2021)
Anakinra	IL-1R	Relieve clinical symptoms of viral infection and improve prognosis	(Cauchois et al., 2020; Huet et al., 2020)
Tocilizumab	IL-6R	Relieve clinical symptoms of viral infection and reduce mortality	(Group, 2021; Gupta et al., 2021)

Lehmann et al., 2017; Xu et al., 2018). Likewise, preliminary clinical trials have demonstrated that "D+Q" therapy significantly improved the physical function of elderly patients with pulmonary fibrosis, reduced the burden of senescent cells in diabetic patients with chronic kidney disease, decreased the levels of major circulating SASP factors, and slowed disease progression (Hickson et al., 2019; Justice et al., 2019).

In terms of viral infectious diseases, Camell et al. discovered that human endothelial senescent cells initiated excessive inflammation upon exposure to SARS-CoV-2, which was accompanied by enhanced SASP expression and a pronounced increase in cellular senescence, inflammation and mortality among aged mice with similar β-coronavirus infection (Camell et al., 2021). However, the use of fisetin or the "D+Q" therapy with senescence-targeted ability selectively combated senescent cells, substantially reduced the signs of senescence and the levels of inflammatory markers and decreased viral infections-related mortality (Camell et al., 2021). In a recent study (Lee et al., 2021), SARS-CoV-2 virus infection and the subsequent VIS were determined to be driving factors in modulating COVID-19-related cytokine storm and tissue damage.

TABLE 3 Clinical studies on senotherapeutics applied to viral infectious diseases.

Main targets	Agents	NCT Number	Conditions	Phase	Status	Dates	
						First Posted	Last Update Posted
PI3K	Quercetin	NCT05601180	Long COVID	-	Recruiting	2022-11-01	2022-11-01
		NCT05037240	COVID-19	-	Completed	2021-09-08	2021-09-08
		NCT04861298	COVID-19	-	Completed	2021-04-27	2022-02-07
		NCT04853199	COVID-19	I	Completed	2021-04-21	2023-01-04
		NCT04578158	COVID-19	III	Completed	2020-10-08	2021-04-22
		NCT04377789	COVID-19	-	Completed	2020-05-06	2021-02-18
		NCT04851821	COVID-19	I	Completed	2021-04-20	2023-01-04
		NCT01438320	Chronic Hepatitis C	I	Completed	2011-09-22	2015-03-20
NF-κB	&Curcumin	NCT05130671	COVID-19	-	Completed	2021-11-23	2022-01-28
PI3K/AKT	Fistein	NCT04771611	COVID-19	II	Enrolling by invitation	2021-02-25	2023-01-18
		NCT04537299	COVID-19	II	Enrolling by invitation	2020-09-03	2023-01-25
		NCT04476953	COVID-19	II	Enrolling by invitation	2020-07-20	2023-01-25
TKI	Dasatinib	NCT05527418	HIV-1 Infection	II	Not yet recruiting	2022-09-02	2022-09-02
NF-κB	Isoquercetin	NCT04536090	COVID-19	II	Not yet recruiting	2020-09-02	2021-08-23
TKI	&Masitinib	NCT04622865	COVID-19	II	Recruiting	2020-11-10	2022-06-22
mTOR	Rapamycin	NCT04948203	COVID-19/Long COVID	II/III	Recruiting	2021-07-01	2022-11-22
		NCT04461340	COVID-19	II	Unknown	2020-07-08	2020-09-09
		NCT04341675	COVID-19	II	Unknown	2020-04-10	2020-05-20
	RTB101	NCT04584710	COVID-19	II	Active, not recruiting	2020-10-14	2021-02-09
		NCT04409327	COVID-19	II	Terminated	2020-06-01	2021-02-10
NF-κB	Metformin	NCT04625985	COVID-19	II	Completed	2020-11-12	2021-08-08
IL-1R	Anakinra	NCT05611710	Dengue	II	Not yet recruiting	2022-11-10	2022-11-10
		NCT04680949	COVID-19	III	Completed	2020-12-23	2022-09-06
		NCT04643678	COVID-19	II/III	Completed	2020-11-25	2022-08-16
		NCT04462757	COVID-19	II	Terminated	2020-07-08	2021-04-30
		NCT04443881	COVID-19	II/III	Completed	2020-06-23	2021-06-01
		NCT04364009	COVID-19	III	Terminated	2020-04-27	2021-01-15
		NCT04362111	COVID-19	III	Active, not recruiting	2020-04-24	2023-01-26
		NCT04357366	COVID-19	II	Active, not recruiting	2020-04-22	2023-01-13
		NCT04341584	COVID-19	II	Completed	2020-04-10	2021-02-01
IL-6R	&Tocilizumab	NCT04412291	COVID-19	II	Unknown	2020-06-02	2021-02-18
		NCT04339712	COVID-19	II	Completed	2020-04-09	2021-01-11
IFN-γ	&Emapalumab	NCT04324021	COVID-19	II/III	Terminated	2020-03-27	2022-03-10
JAK	&Baricitinib	NCT04362943	COVID-19	-	Completed	2020-04-27	2021-07-28
JAK1/2	&Ruxolitinib	NCT04366232	COVID-19	II	Terminated	2020-04-28	2020-12-16
IL-6R JAK1/2	&Tocilizumab and Ruxolitinib	NCT04424056	COVID-19	III	Unknown	2020-06-09	2020-06-23
IL-6R IL-6	&Tocilizumab and Siltuximab	NCT04330638	COVID-19	III	Completed	2020-04-01	2021-09-29
IL-6R	Tocilizumab	NCT05164133	COVID-19	I	Recruiting	2021-12-20	2023-01-18
		NCT05057962	COVID-19	-	Completed	2021-09-27	2022-05-17
		NCT04924829	COVID-19	-	Recruiting	2021-06-14	2021-06-14
		NCT04893031	COVID-19	-	Completed	2021-05-19	2021-05-20
		NCT04730323	COVID-19	IV	Completed	2021-01-29	2021-01-29

(Continued)

TABLE 3 Continued

Main targets	Agents	NCT Number	Conditions	Phase	Status	Dates	
						First Posted	Last Update Posted
		NCT04479358	COVID-19	II	Recruiting	2020-07-21	2022-05-18
		NCT04445272	COVID-19	II	Completed	2020-06-24	2021-06-02
		NCT04412772	COVID-19	III	Unknown	2020-06-02	2020-11-17
		NCT04403685	COVID-19	III	Terminated	2020-05-27	2020-08-26
		NCT04377750	COVID-19	IV	Unknown	2020-05-06	2020-05-06
		NCT04377659	COVID-19	II	Terminated	2020-05-06	2022-11-02
		NCT04372186	COVID-19	III	Active, not recruiting	2020-05-01	2021-09-27
		NCT04363853	COVID-19	II	Unknown	2020-04-27	2020-11-30
		NCT04363736	COVID-19	II	Completed	2020-04-27	2022-08-31
		NCT04359667	COVID-19	-	Unknown	2020-04-27	2020-11-12
		NCT04356937	COVID-19	III	Completed	2020-04-22	2021-07-27
		NCT04346355	COVID-19	II	Terminated	2020-04-15	2020-06-22
		NCT04335071	COVID-19	II	Terminated	2020-04-06	2020-10-14
		NCT04332913	COVID-19	-	Unknown	2020-04-03	2020-04-13
		NCT04332094	COVID-19	II	Recruiting	2020-04-02	2021-05-06
		NCT04331795	COVID-19	II	Completed	2020-04-02	2022-06-09
		NCT04320615	COVID-19	III	Completed	2020-03-25	2021-06-30
		NCT04317092	COVID-19	II	Unknown	2020-03-20	2021-03-03
		NCT04315480	COVID-19	II	Unknown	2020-03-19	2020-04-13
JAK	&Baricitinib	NCT05082714	COVID-19	-	Recruiting	2021-10-19	2022-04-13

PI3K, PhosphoInositide-3 Kinase; TKI, tyrosine kinase inhibitor; IL, interleukin; IL-1R, interleukin-1 receptor; IL-6R, interleukin-6 receptor; JAK, Janus kinase; mTOR, mammalian target of rapamycin; NF-κB, nuclear factor-κB.

However, the targeted removal of senescent cells with senescence-targeted drugs such as navitoclax, D+Q and fisetin lead to a significant reduction in senescent cells and a marked attenuation of senescence-related traits, both *in vitro* and in the respiratory epithelium of hamster models. Further, COVID-19-related lung diseases, inflammation, tissue damage and coagulation disorders significantly subsided (Lee et al., 2021). Additionally, in senescent macrophages exposed to IAV or SARS-CoV-2 (Lv et al., 2022), fisetin prominently suppressed the aberrant activation of the cGAS-STING pathway, NLRP3 inflammasome and the resultant excessive inflammatory responses in senescent macrophages *via* the induction of apoptosis and reduction of dysfunctional mitochondrial load. In the Tere$^{-/-}$ aged mice model, fisetin was also found to dampen pathogenic inflammation mediated by the cGAS-STING pathway and NLRP3 inflammasome by lowering senescent cells-related burden and improving mitochondrial integrity, thus providing a considerable improvement in the survival rate of Tere$^{-/-}$ mice infected with IAV. Comparable results were obtained upon validation using the "D+Q" combination treatment (Lv et al., 2022).

In prospective randomized controlled clinical trials among patients with COVID-19, quercetin appeared to be effective in decreasing viral load and relieving clinical symptoms during the early application of viral infection in combination with standardized care, which offered protection against serious complications and conferred a high safety profile (Di Pierro et al., 2021a; Di Pierro et al., 2021b). Correspondingly, a systematic review of quercetin revealed that quercetin and its derivatives were associated with significantly reduced mean viral load and generation of pro-inflammatory cytokines, chemokines, reactive oxygen species, mucus and airway resistance in animals infected with respiratory viruses such as influenza virus and human rhinovirus. These observations were associated with a significant reduction in infected animal fatality and were considered a potential strategy for treating lower respiratory tract viral diseases (Brito et al., 2021).

5.2 Senomorphics

The mammalian target of rapamycin (mTOR) pathway has been demonstrated to facilitate SASP production in recent years by regulating the translation of mRNA subsets, including those encoding IL-1α (Herranz et al., 2015; Laberge et al., 2015). Rapamycin can target the mTOR pathway to inhibit the activity of the mTORC1 complex, which is known to regulate mRNA translation, leading to reduced mRNA levels of cytokines such as IL-6 and IL-10 and selective inhibition of the translation of IL-1α. This creates a drop in SASP production and reduces the risk of age-related cognitive decline and cardiac or hepatic dysfunction, eventually extending the lifespan of mice and improving immune functions in the elderly (Majumder et al., 2012; Wilkinson et al., 2012; Flynn et al., 2013; Mannick et al., 2014; Laberge et al., 2015). More importantly, the application of rapamycin can potentiate antiviral activity in the event of SARS-CoV-2, MERS-CoV, H1N1 and other viral infections, which can be conducive to attenuating the severity of diseases (Wang et al., 2014; Kindrachuk et al., 2015; Husain and Byrareddy, 2020). Currently, ongoing clinical trials are assessing the safety and efficacy of rapamycin in the treatment or prevention of COVID-19 (Geier and Perl, 2021).

In addition, metformin, a biguanide that combats age-related diseases to extend health span, is the first drug for age-targeted effects in a large clinical trial (Kulkarni et al., 2020). Available evidence supports that metformin can dampen aging-related

features directly or indirectly through multiple pathways, such as improving nutrient perception, inhibiting the NF-κB pathway and pro-inflammatory factors production, enhancing cellular autophagy and intercellular communication, regulating mitochondrial function, modulating gut microbiota, delaying stem cell aging, curtailing telomere attrition, and attenuating cellular senescence (Kulkarni et al., 2020). It was reported that metformin could extend the lifespan of mice by inhibiting the production of pro-inflammatory factors and diminishing DNA damage (Martin-Montalvo et al., 2013; Moiseeva et al., 2013; Valencia et al., 2017). It could also decrease age-related chronic inflammation and the risk of cardiovascular diseases, cancer, neurodegenerative diseases and cognitive dysfunction, ultimately exerting a constructive effect on improving the overall health status and prolonging the lifespan of aged persons (Barzilai et al., 2016; Campbell et al., 2017; Markowicz-Piasecka et al., 2017; Campbell et al., 2018; Tizazu et al., 2019).

Data from China revealed that the metformin treatment was associated with lower mortality in hospital patients with COVID-19 (Li et al., 2020; Luo et al., 2020) and fewer COVID-19-related heart failure and inflammation compared with other anti-diabetic agents (Cheng et al., 2020). Similarly, metformin could also cause an almost 11-fold reduction in the odds ratio of death among COVID-19 African-American patients with T2DM (Crouse et al., 2020). A recent study confirmed that metformin inhibited mtDNA synthesis and cytoplasmic Ox-mtDNA production in macrophages, thereby suppressing NLRP3 inflammasome activation, IL-1β generation and IL-6 secretion and relieving lung inflammation in human ACE2 transgenic mice infected with SARS-CoV-2 (Xian et al., 2021). Such protective effects were independent of glycemic control and correlated with the anti-inflammatory properties of metformin (Valencia et al., 2017; Marcucci et al., 2020). Nevertheless, it should also be noted that metformin use is linked to a high incidence of acidosis, especially in severe COVID-19 cases (Cheng et al., 2020), and careful consideration should be made on tackling the complications during clinical administration.

Anakinra, an IL-1 receptor antagonist, was shown to cause a rapid decrease in inflammatory and febrile symptoms, lower oxygen requirements, increase the duration of non-invasive mechanical ventilation and improve various clinical conditions when administered early in COVID-19 patients (Cauchois et al., 2020). In parallel, another cohort study also concluded that therapy with Anakinra was associated with fewer needs for invasive mechanical ventilation, lowered the mortality of patients with severe COVID-19, and, importantly, did not cause serious side effects (Huet et al., 2020). Moreover, a multicenter cohort study enrolling 3924 COVID-19 patients suggested that treatment with a monoclonal antibody of the IL-6 receptor (Tocilizumab) during the first 2 days of patient admission to the ICU could significantly reduce the risk of in-hospital mortality (Gupta et al., 2021). A randomized controlled clinical trial from the United Kingdom also demonstrated that Tocilizumab lowered the probability of invasive mechanical ventilation needs and 28-day mortality in patients with COVID-19 (Group, 2021). Further, a Bruton tyrosine kinase (BTK) inhibitor was also found to reduce BTK-dependent activation of NF-κB and NLRP3 inflammasome, which suppressed pro-inflammatory factors production and COVID-19 cytokine storm, thereby improving the prognosis of COVID-19 patients (Roschewski et al., 2020).

Altogether, these findings not only further illustrate the critical role of SASP components in the development of viral infectious diseases such as COVID-19 but also demonstrate the high interest in targeting SASP components or the inflammatory pathways involved in their synthesis for the treatment of aging-related viral infectious diseases.

6 Conclusion and outlook

Senescence and viral infections interact in a reciprocal relationship. In general, viral infections can induce senescence and increase the susceptibility and severity of viral infections *via* multiple mechanisms, such as immunodeficiency, mitochondrial dysfunction, SASP secretion, pre-activated macrophages, over-recruitment of immune cells, and accumulation of innate immune cells with trained immunity. In the elderly, virus-induced senescence, in addition to their pre-existing senescent condition, is believed to aggravate the underlying disease outcomes, but could be counteracted by senotherapeutics, which was shown to mitigate the severity of viral infections.

Undeniably, well-controlled senescence onset may positively enhance antiviral immunity, yet excessive inflammatory responses by accumulated senescent cells are critical factors underlying the development of multiple aging-related diseases. However, the relationship between viral infections and senescence should be further clarified, because it remains undetermined whether the effects are fully compatible between virus-induced senescence and naturally occurred senescence on the antiviral responses of hosts, the exact mechanisms of virus-induced senescence are not fully clear, the optimal doses of anti-senescence therapeutic drugs remain investigational, and the specific adverse events are not yet fully known. Thus, further research and clinical trials are needed to prolong a healthy lifespan of the elderly.

Author contributions

ZL, MT, and CZ conceptualized and designed this study. ZL, MT, and GW wrote the original draft and prepared the diagrams. XC, J'eM, and SL researched data and collected the references. XC and BS reviewed and edited the manuscript. CZ, XX, KW, and FL critically revised the manuscript. All authors contributed to the article and approved the submitted version.

Funding

This work was supported by the Fundamental Research Funds for the Central Universities (No.2042022kf1215), the Special Funds for Innovation in Scientific Research Program of Zhongshan under Grant 2020AG024, Chinese Foundation for Hepatitis Prevention and Control-Tian Qing Liver Disease Research Fund Subject (TGQB20210109), the Open Funds of Key Laboratory of Diagnosis and Treatment of Digestive System Tumors of Zhejiang Province (KFJJ-202005, KFJJ-201907), the Open Research Program of the State Key Laboratory of Virology of China (2021KF002, 2021KF006) and the Key Research and Development Project of Hubei Province (2022BCA009).

Conflict of interest

The authors declare that the research was conducted in the absence of any commercial or financial relationships that could be construed as a potential conflict of interest.

Publisher's note

References

Ackermann, M., Verleden, S. E., Kuehnel, M., Haverich, A., Welte, T., Laenger, F., et al. (2020). Pulmonary vascular endothelialitis, thrombosis, and angiogenesis in covid-19. *N Engl. J. Med.* 383 (2), 120–128. doi: 10.1056/NEJMoa2015432

Acosta, J. C., Banito, A., Wuestefeld, T., Georgilis, A., Janich, P., Morton, J. P., et al. (2013). A complex secretory program orchestrated by the inflammasome controls paracrine senescence. *Nat. Cell Biol.* 15 (8), 978–990. doi: 10.1038/ncb2784

Aguirre, S., Luthra, P., Sanchez-Aparicio, M. T., Maestre, A. M., Patel, J., Lamothe, F., et al. (2017). Dengue virus NS2B protein targets cGAS for degradation and prevents mitochondrial DNA sensing during infection. *Nat. Microbiol.* 2, 17037. doi: 10.1038/nmicrobiol.2017.37

Akbar, A. N., and Gilroy, D. W. (2020). Aging immunity may exacerbate COVID-19. *Science* 369 (6501), 256–257. doi: 10.1126/science.abb0762

Althubiti, M., Lezina, L., Carrera, S., Jukes-Jones, R., Giblett, S. M., Antonov, A., et al. (2014). Characterization of novel markers of senescence and their prognostic potential in cancer. *Cell Death Dis.* 5 (11), e1528. doi: 10.1038/cddis.2014.489

Ancuta, P., Kamat, A., Kunstman, K. J., Kim, E. Y., Autissier, P., Wurcel, A., et al. (2008). Microbial translocation is associated with increased monocyte activation and dementia in AIDS patients. *PloS One* 3 (6), e2516. doi: 10.1371/journal.pone.0002516

Appay, V., Almeida, J. R., Sauce, D., Autran, B., and Papagno, L. (2007). Accelerated immune senescence and HIV-1 infection. *Exp. Gerontol* 42 (5), 432–437. doi: 10.1016/j.exger.2006.12.003

Appay, V., and Kelleher, A. D. (2016). Immune activation and immune aging in HIV infection. *Curr. Opin. HIV AIDS* 11 (2), 242–249. doi: 10.1097/coh.0000000000000240

Armah, K. A., McGinnis, K., Baker, J., Gibert, C., Butt, A. A., Bryant, K. J., et al. (2012). HIV Status, burden of comorbid disease, and biomarkers of inflammation, altered coagulation, and monocyte activation. *Clin. Infect. Dis.* 55 (1), 126–136. doi: 10.1093/cid/cis406

Arunachalam, P. S., Wimmers, F., Mok, C. K. P., Perera, R., Scott, M., Hagan, T., et al. (2020). Systems biological assessment of immunity to mild versus severe COVID-19 infection in humans. *Science* 369 (6508), 1210–1220. doi: 10.1126/science.abc6261

Baker, D. J., Wijshake, T., Tchkonia, T., LeBrasseur, N. K., Childs, B. G., van de Sluis, B., et al. (2011). Clearance of p16Ink4a-positive senescent cells delays ageing-associated disorders. *Nature* 479 (7372), 232–236. doi: 10.1038/nature10600

Barzilai, N., Crandall, J. P., Kritchevsky, S. B., and Espeland, M. A. (2016). Metformin as a tool to target aging. *Cell Metab.* 23 (6), 1060–1065. doi: 10.1016/j.cmet.2016.05.011

Baz-Martínez, M., Da Silva-Álvarez, S., Rodríguez, E., Guerra, J., El Motiam, A., Vidal, A., et al. (2016). Cell senescence is an antiviral defense mechanism. *Sci. Rep.* 6, 37007. doi: 10.1038/srep37007

Beaupere, C., Garcia, M., Larghero, J., Fève, B., Capeau, J., and Lagathu, C. (2015). The HIV proteins tat and nef promote human bone marrow mesenchymal stem cell senescence and alter osteoblastic differentiation. *Aging Cell* 14 (4), 534–546. doi: 10.1111/acel.12308

Bent, E. H., Gilbert, L. A., and Hemann, M. T. (2016). A senescence secretory switch mediated by PI3K/AKT/mTOR activation controls chemoprotective endothelial secretory responses. *Genes Dev.* 30 (16), 1811–1821. doi: 10.1101/gad.284851.116

Blackford, A. N., and Jackson, S. P. (2017). ATM, ATR, and DNA-PK: The trinity at the heart of the DNA damage response. *Mol. Cell* 66 (6), 801–817. doi: 10.1016/j.molcel.2017.05.015

Blanco, J. R., Negredo, E., Bernal, E., and Blanco, J. (2021). Impact of HIV infection on aging and immune status. *Expert Rev. Anti Infect. Ther.* 19 (6), 719–731. doi: 10.1080/14787210.2021.1848546

Bochenek, M. L., Schütz, E., and Schäfer, K. (2016). Endothelial cell senescence and thrombosis: Ageing clots. *Thromb. Res.* 147, 36–45. doi: 10.1016/j.thromres.2016.09.019

Brito, J. C. M., Lima, W. G., Cordeiro, L. P. B., and da Cruz Nizer, W. S. (2021). Effectiveness of supplementation with quercetin-type flavonols for treatment of viral lower respiratory tract infections: Systematic review and meta-analysis of preclinical studies. *Phytother. Res.* 35 (9), 4930–4942. doi: 10.1002/ptr.7122

Cai, Q., Huang, D., Yu, H., Zhu, Z., Xia, Z., Su, Y., et al. (2020). COVID-19: Abnormal liver function tests. *J. Hepatol.* 73 (3), 566–574. doi: 10.1016/j.jhep.2020.04.006

Camell, C. D., Yousefzadeh, M. J., Zhu, Y., Prata, L., Huggins, M. A., Pierson, M., et al. (2021). Senolytics reduce coronavirus-related mortality in old mice. *Science* 373 (6552). doi: 10.1126/science.abe4832

Campbell, J. M., Bellman, S. M., Stephenson, M. D., and Lisy, K. (2017). Metformin reduces all-cause mortality and diseases of ageing independent of its effect on diabetes control: A systematic review and meta-analysis. *Ageing Res. Rev.* 40, 31–44. doi: 10.1016/j.arr.2017.08.003

Campbell, J. M., Stephenson, M. D., de Courten, B., Chapman, I., Bellman, S. M., and Aromataris, E. (2018). Metformin use associated with reduced risk of dementia in patients with diabetes: A systematic review and meta-analysis. *J. Alzheimers Dis.* 65 (4), 1225–1236. doi: 10.3233/jad-180263

Canan, C. H., Gokhale, N. S., Carruthers, B., Lafuse, W. P., Schlesinger, L. S., Torrelles, J. B., et al. (2014). Characterization of lung inflammation and its impact on macrophage function in aging. *J. Leukoc. Biol.* 96 (3), 473–480. doi: 10.1189/jlb.4A0214-093RR

Cauchois, R., Koubi, M., Delarbre, D., Manet, C., Carvelli, J., Blasco, V. B., et al. (2020). Early IL-1 receptor blockade in severe inflammatory respiratory failure complicating COVID-19. *Proc. Natl. Acad. Sci. U.S.A.* 117 (32), 18951–18953. doi: 10.1073/pnas.2009017117

Chang, J., Wang, Y., Shao, L., Laberge, R. M., Demaria, M., Campisi, J., et al. (2016). Clearance of senescent cells by ABT263 rejuvenates aged hematopoietic stem cells in mice. *Nat. Med.* 22 (1), 78–83. doi: 10.1038/nm.4010

Chauvin, M., and Sauce, D. (2022). Mechanisms of immune aging in HIV. *Clin. Sci. (Lond)* 136 (1), 61–80. doi: 10.1042/cs20210344

Chen, E. H., and Olson, E. N. (2005). Unveiling the mechanisms of cell-cell fusion. *Science* 308 (5720), 369–373. doi: 10.1126/science.1104799

Chen, Y. A., Shen, Y. L., Hsia, H. Y., Tiang, Y. P., Sung, T. L., and Chen, L. Y. (2017). Extrachromosomal telomere repeat DNA is linked to ALT development *via* cGAS-STING DNA sensing pathway. *Nat. Struct. Mol. Biol.* 24 (12), 1124–1131. doi: 10.1038/nsmb.3498

Chen, N., Zhou, M., Dong, X., Qu, J., Gong, F., Han, Y., et al. (2020). Epidemiological and clinical characteristics of 99 cases of 2019 novel coronavirus pneumonia in wuhan, China: a descriptive study. *Lancet* 395 (10223), 507–513. doi: 10.1016/s0140-6736(20)30211-7

Cheng, X., Liu, Y. M., Li, H., Zhang, X., Lei, F., Qin, J. J., et al. (2020). Metformin is associated with higher incidence of acidosis, but not mortality, in individuals with COVID-19 and pre-existing type 2 diabetes. *Cell Metab.* 32 (4), 537–547.e533. doi: 10.1016/j.cmet.2020.08.013

Childs, B. G., Baker, D. J., Kirkland, J. L., Campisi, J., and van Deursen, J. M. (2014). Senescence and apoptosis: Dueling or complementary cell fates? *EMBO Rep.* 15 (11), 1139–1153. doi: 10.15252/embr.201439245

Childs, B. G., Durik, M., Baker, D. J., and van Deursen, J. M. (2015). Cellular senescence in aging and age-related disease: From mechanisms to therapy. *Nat. Med.* 21 (12), 1424–1435. doi: 10.1038/nm.4000

Cho, S., and Hwang, E. S. (2012). Status of mTOR activity may phenotypically differentiate senescence and quiescence. *Mol. Cells* 33 (6), 597–604. doi: 10.1007/s10059-012-0042-1

Chrétien, A., Piront, N., Delaive, E., Demazy, C., Ninane, N., and Toussaint, O. (2008). Increased abundance of cytoplasmic and nuclear caveolin 1 in human diploid fibroblasts in H(2)O(2)-induced premature senescence and interplay with p38alpha (MAPK). *FEBS Lett.* 582 (12), 1685–1692. doi: 10.1016/j.febslet.2008.04.026

Chu, H., Chan, J. F., Yuen, T. T., Shuai, H., Yuan, S., Wang, Y., et al. (2020). Comparative tropism, replication kinetics, and cell damage profiling of SARS-CoV-2 and SARS-CoV with implications for clinical manifestations, transmissibility, and laboratory studies of COVID-19: An observational study. *Lancet Microbe* 1 (1), e14–e23. doi: 10.1016/s2666-5247(20)30004-5

Chuprin, A., Gal, H., Biron-Shental, T., Biran, A., Amiel, A., Rozenblatt, S., et al. (2013). Cell fusion induced by ERVWE1 or measles virus causes cellular senescence. *Genes Dev.* 27 (21), 2356–2366. doi: 10.1101/gad.227512.113

Cormenier, J., Martin, N., Deslé, J., Salazar-Cardozo, C., Pourtier, A., Abbadie, C., et al. (2018). The ATF6α arm of the unfolded protein response mediates replicative senescence in human fibroblasts through a COX2/prostaglandin E(2) intracrine pathway. *Mech. Ageing Dev.* 170, 82–91. doi: 10.1016/j.mad.2017.08.003

Crouse, A. B., Grimes, T., Li, P., Might, M., Ovalle, F., and Shalev, A. (2020). Metformin use is associated with reduced mortality in a diverse population with COVID-19 and diabetes. *Front. Endocrinol. (Lausanne)* 11. doi: 10.3389/fendo.2020.600439

D'Agnillo, F., Walters, K. A., Xiao, Y., Sheng, Z. M., Scherler, K., Park, J., et al. (2021). Lung epithelial and endothelial damage, loss of tissue repair, inhibition of fibrinolysis, and cellular senescence in fatal COVID-19. *Sci. Transl. Med.* 13 (620), eabj7790. doi: 10.1126/scitranslmed.abj7790

Dasari, A., Bartholomew, J. N., Volonte, D., and Galbiati, F. (2006). Oxidative stress induces premature senescence by stimulating caveolin-1 gene transcription through p38 mitogen-activated protein kinase/Sp1-mediated activation of two GC-rich promoter elements. *Cancer Res.* 66 (22), 10805–10814. doi: 10.1158/0008-5472.Can-06-1236

De Cecco, M., Ito, T., Petrashen, A. P., Elias, A. E., Skvir, N. J., Criscione, S. W., et al. (2019). L1 drives IFN in senescent cells and promotes age-associated inflammation. *Nature* 566 (7742), 73–78. doi: 10.1038/s41586-018-0784-9

Decout, A., Katz, J. D., Venkatraman, S., and Ablasser, A. (2021). The cGAS-STING pathway as a therapeutic target in inflammatory diseases. *Nat. Rev. Immunol.* 21 (9), 548–569. doi: 10.1038/s41577-021-00524-z

Deeks, S. G., Lewin, S. R., and Havlir, D. V. (2013). The end of AIDS: HIV infection as a chronic disease. *Lancet* 382 (9903), 1525–1533. doi: 10.1016/s0140-6736(13)61809-7

Delpeut, S., Noyce, R. S., Siu, R. W., and Richardson, C. D. (2012). Host factors and measles virus replication. *Curr. Opin. Virol.* 2 (6), 773–783. doi: 10.1016/j.coviro.2012.10.008

de Magalhães, M. C., Sánchez-Arcila, J. C., Lyra, A. C. B., Long, L. F. B., Vasconcellos de Souza, I., Ferry, F. R. A., et al. (2020). Hemostasis in elderly patients with human immunodeficiency virus (HIV) infection-cross-sectional study. *PloS One* 15 (2), e0227763. doi: 10.1371/journal.pone.0227763

Demaria, M., Ohtani, N., Youssef, S. A., Rodier, F., Toussaint, W., Mitchell, J. R., et al. (2014). An essential role for senescent cells in optimal wound healing through secretion of PDGF-AA. *Dev. Cell* 31 (6), 722–733. doi: 10.1016/j.devcel.2014.11.012

Dillon, S. M., Frank, D. N., and Wilson, C. C. (2016). The gut microbiome and HIV-1 pathogenesis: A two-way street. *AIDS* 30 (18), 2737–2751. doi: 10.1097/qad.0000000000001289

Di Micco, R., Krizhanovsky, V., Baker, D., and d'Adda di Fagagna, F. (2021). Cellular senescence in ageing: From mechanisms to therapeutic opportunities. *Nat. Rev. Mol. Cell Biol.* 22 (2), 75–95. doi: 10.1038/s41580-020-00314-w

Di Micco, R., Sulli, G., Dobreva, M., Liontos, M., Botrugno, O. A., Gargiulo, G., et al. (2011). Interplay between oncogene-induced DNA damage response and heterochromatin in senescence and cancer. *Nat. Cell Biol.* 13 (3), 292–302. doi: 10.1038/ncb2170

Di Mitri, D., Toso, A., Chen, J. J., Sarti, M., Pinton, S., Jost, T. R., et al. (2014). Tumour-infiltrating gr-1+ myeloid cells antagonize senescence in cancer. *Nature* 515 (7525), 134–137. doi: 10.1038/nature13638

Dimri, G. P., Lee, X., Basile, G., Acosta, M., Scott, G., Roskelley, C., et al. (1995). A biomarker that identifies senescent human cells in culture and in aging skin *in vivo*. *Proc. Natl. Acad. Sci. U.S.A.* 92 (20), 9363–9367. doi: 10.1073/pnas.92.20.9363

Di Pierro, F., Derosa, G., Maffioli, P., Bertuccioli, A., Togni, S., Riva, A., et al. (2021a). Possible therapeutic effects of adjuvant quercetin supplementation against early-stage COVID-19 infection: A prospective, randomized, controlled, and open-label study. *Int. J. Gen. Med.* 14, 2359–2366. doi: 10.2147/ijgm.S318720

Di Pierro, F., Iqtadar, S., Khan, A., Ullah Mumtaz, S., Masud Chaudhry, M., Bertuccioli, A., et al. (2021b). Potential clinical benefits of quercetin in the early stage of COVID-19: Results of a second, pilot, randomized, controlled and open-label clinical trial. *Int. J. Gen. Med.* 14, 2807–2816. doi: 10.2147/ijgm.S318949

Dou, Z., Ghosh, K., Vizioli, M. G., Zhu, J., Sen, P., Wangensteen, K. J., et al. (2017). Cytoplasmic chromatin triggers inflammation in senescence and cancer. *Nature* 550 (7676), 402–406. doi: 10.1038/nature24050

Druelle, C., Drullion, C., Deslé, J., Martin, N., Saas, L., Cormenier, J., et al. (2016). ATF6α regulates morphological changes associated with senescence in human fibroblasts. *Oncotarget* 7 (42), 67699–67715. doi: 10.18632/oncotarget.11505

Duelli, D., and Lazebnik, Y. (2007). Cell-to-cell fusion as a link between viruses and cancer. *Nat. Rev. Cancer* 7 (12), 968–976. doi: 10.1038/nrc2272

Eggert, T., Wolter, K., Ji, J., Ma, C., Yevsa, T., Klotz, S., et al. (2016). Distinct functions of senescence-associated immune responses in liver tumor surveillance and tumor progression. *Cancer Cell* 30 (4), 533–547. doi: 10.1016/j.ccell.2016.09.003

Estêvão, D., Costa, N. R., Gil da Costa, R. M., and Medeiros, R. (2019). Hallmarks of HPV carcinogenesis: The role of E6, E7 and E5 oncoproteins in cellular malignancy. *Biochim. Biophys. Acta Gene Regul. Mech.* 1862 (2), 153–162. doi: 10.1016/j.bbagrm.2019.01.001

Evangelou, K., Veroutis, D., Paschalaki, K., Foukas, P. G., Lagopati, N., Dimitriou, M., et al. (2022). Pulmonary infection by SARS-CoV-2 induces senescence accompanied by an inflammatory phenotype in severe COVID-19: Possible implications for viral mutagenesis. *Eur. Respir. J.* 60 (2). doi: 10.1183/13993003.02951-2021

Flynn, J. M., O'Leary, M. N., Zambataro, C. A., Academia, E. C., Presley, M. P., Garrett, B. J., et al. (2013). Late-life rapamycin treatment reverses age-related heart dysfunction. *Aging Cell* 12 (5), 851–862. doi: 10.1111/acel.12109

Franceschi, C., Bonafè, M., Valensin, S., Olivieri, F., De Luca, M., Ottaviani, E., et al. (2000). Inflamm-aging. an evolutionary perspective on immunosenescence. *Ann. N Y Acad. Sci.* 908, 244–254. doi: 10.1111/j.1749-6632.2000.tb06651.x

Freund, A., Orjalo, A. V., Desprez, P. Y., and Campisi, J. (2010). Inflammatory networks during cellular senescence: Causes and consequences. *Trends Mol. Med.* 16 (5), 238–246. doi: 10.1016/j.molmed.2010.03.003

Fumagalli, M., Rossiello, F., Mondello, C., and d'Adda di Fagagna, F. (2014). Stable cellular senescence is associated with persistent DDR activation. *PloS One* 9 (10), e110969. doi: 10.1371/journal.pone.0110969

Gallant, J., Hsue, P. Y., Shreay, S., and Meyer, N. (2017). Comorbidities among US patients with prevalent HIV infection-a trend analysis. *J. Infect. Dis.* 216 (12), 1525–1533. doi: 10.1093/infdis/jix518

Gao, D., Wu, J., Wu, Y. T., Du, F., Aroh, C., Yan, N., et al. (2013). Cyclic GMP-AMP synthase is an innate immune sensor of HIV and other retroviruses. *Science* 341 (6148), 903–906. doi: 10.1126/science.1240933

Geier, C., and Perl, A. (2021). Therapeutic mTOR blockade in systemic autoimmunity: Implications for antiviral immunity and extension of lifespan. *Autoimmun Rev.* 20 (12), 102984. doi: 10.1016/j.autrev.2021.102984

George, P. M., Wells, A. U., and Jenkins, R. G. (2020). Pulmonary fibrosis and COVID-19: the potential role for antifibrotic therapy. *Lancet Respir. Med.* 8 (8), 807–815. doi: 10.1016/s2213-2600(20)30225-3

Giannis, D., Ziogas, I. A., and Gianni, P. (2020). Coagulation disorders in coronavirus infected patients: COVID-19, SARS-CoV-1, MERS-CoV and lessons from the past. *J. Clin. Virol.* 127, 104362. doi: 10.1016/j.jcv.2020.104362

Glück, S., Guey, B., Gulen, M. F., Wolter, K., Kang, T. W., Schmacke, N. A., et al. (2017). Innate immune sensing of cytosolic chromatin fragments through cGAS promotes senescence. *Nat. Cell Biol.* 19 (9), 1061–1070. doi: 10.1038/ncb3586

Gonzalez-Meljem, J. M., Haston, S., Carreno, G., Apps, J. R., Pozzi, S., Stache, C., et al. (2017). Stem cell senescence drives age-attenuated induction of pituitary tumours in mouse models of paediatric craniopharyngioma. *Nat. Commun.* 8 (1), 1819. doi: 10.1038/s41467-017-01992-5

Gorgoulis, V., Adams, P. D., Alimonti, A., Bennett, D. C., Bischof, O., Bishop, C., et al. (2019). Cellular senescence: Defining a path forward. *Cell* 179 (4), 813–827. doi: 10.1016/j.cell.2019.10.005

Grasselli, G., Zangrillo, A., Zanella, A., Antonelli, M., Cabrini, L., Castelli, A., et al. (2020). Baseline characteristics and outcomes of 1591 patients infected with SARS-CoV-2 admitted to ICUs of the Lombardy region, Italy. *JAMA* 323 (16), 1574–1581. doi: 10.1001/jama.2020.5394

Group, R. C. (2021). Tocilizumab in patients admitted to hospital with COVID-19 (RECOVERY): A randomised, controlled, open-label, platform trial. *Lancet* 397 (10285), 1637–1645. doi: 10.1016/s0140-6736(21)00676-0

Gupta, S., Wang, W., Hayek, S. S., Chan, L., Mathews, K. S., Melamed, M. L., et al. (2021). Association between early treatment with tocilizumab and mortality among critically ill patients with COVID-19. *JAMA Intern. Med.* 181 (1), 41–51. doi: 10.1001/jamainternmed.2020.6252

Ha, T. T., Huy, N. T., Murao, L. A., Lan, N. T., Thuy, T. T., Tuan, H. M., et al. (2011). Elevated levels of cell-free circulating DNA in patients with acute dengue virus infection. *PloS One* 6 (10), e25969. doi: 10.1371/journal.pone.0025969

Hafez, A. Y., and Luftig, M. A. (2017). Characterization of the EBV-induced persistent DNA damage response. *Viruses* 9 (12). doi: 10.3390/v9120366

Hakim, F. T., Memon, S. A., Cepeda, R., Jones, E. C., Chow, C. K., Kasten-Sportes, C., et al. (2005). Age-dependent incidence, time course, and consequences of thymic renewal in adults. *J. Clin. Invest.* 115 (4), 930–939. doi: 10.1172/jci22492

Hanada, Y., Ishihara, N., Wang, L., Otera, H., Ishihara, T., Koshiba, T., et al. (2020). MAVS is energized by mff which senses mitochondrial metabolism *via* AMPK for acute antiviral immunity. *Nat. Commun.* 11 (1), 5711. doi: 10.1038/s41467-020-19287-7

Hari, P., Millar, F. R., Tarrats, N., Birch, J., Quintanilla, A., Rink, C. J., et al. (2019). The innate immune sensor toll-like receptor 2 controls the senescence-associated secretory phenotype. *Sci. Adv.* 5 (6), eaaw0254. doi: 10.1126/sciadv.aaw0254

Hayflick, L. (1965). The limited *in vitro* lifetime of human diploid cell strains. *Exp. Cell Res.* 37, 614–636. doi: 10.1016/0014-4827(65)90211-9

Hayflick, L., and Moorhead, P. S. (1961). The serial cultivation of human diploid cell strains. *Exp. Cell Res.* 25, 585–621. doi: 10.1016/0014-4827(61)90192-6

He, S., and Sharpless, N. E. (2017). Senescence in health and disease. *Cell* 169 (6), 1000–1011. doi: 10.1016/j.cell.2017.05.015

Hearps, A. C., Martin, G. E., Angelovich, T. A., Cheng, W. J., Maisa, A., Landay, A. L., et al. (2012). Aging is associated with chronic innate immune activation and dysregulation of monocyte phenotype and function. *Aging Cell* 11 (5), 867–875. doi: 10.1111/j.1474-9726.2012.00851.x

Helms, J., Tacquard, C., Severac, F., Leonard-Lorant, I., Ohana, M., Delabranche, X., et al. (2020). High risk of thrombosis in patients with severe SARS-CoV-2 infection: A multicenter prospective cohort study. *Intensive Care Med.* 46 (6), 1089–1098. doi: 10.1007/s00134-020-06062-x

Hernandez-Segura, A., de Jong, T. V., Melov, S., Guryev, V., Campisi, J., and Demaria, M. (2017). Unmasking transcriptional heterogeneity in senescent cells. *Curr. Biol.* 27 (17), 2652–2660.e2654. doi: 10.1016/j.cub.2017.07.033

Hernandez-Segura, A., Nehme, J., and Demaria, M. (2018). Hallmarks of cellular senescence. *Trends Cell Biol.* 28 (6), 436–453. doi: 10.1016/j.tcb.2018.02.001

Herranz, N., Gallage, S., Mellone, M., Wuestefeld, T., Klotz, S., Hanley, C. J., et al. (2015). mTOR regulates MAPKAPK2 translation to control the senescence-associated secretory phenotype. *Nat. Cell Biol.* 17 (9), 1205–1217. doi: 10.1038/ncb3225

Hickson, L. J., Langhi Prata, L. G. P., Bobart, S. A., Evans, T. K., Giorgadze, N., Hashmi, S. K., et al. (2019). Senolytics decrease senescent cells in humans: Preliminary report from a clinical trial of dasatinib plus quercetin in individuals with diabetic kidney disease. *EBioMedicine* 47, 446–456. doi: 10.1016/j.ebiom.2019.08.069

Hoffmann, M., Pantazis, N., Martin, G. E., Hickling, S., Hurst, J., Meyerowitz, J., et al. (2016). Exhaustion of activated CD8 T cells predicts disease progression in primary HIV-1 infection. *PloS Pathog.* 12 (7), e1005661. doi: 10.1371/journal.ppat.1005661

Hopfner, K. P., and Hornung, V. (2020). Molecular mechanisms and cellular functions of cGAS-STING signalling. *Nat. Rev. Mol. Cell Biol.* 21 (9), 501–521. doi: 10.1038/s41580-020-0244-x

Huet, T., Beaussier, H., Voisin, O., Jouveshomme, S., Dauriat, G., Lazareth, I., et al. (2020). Anakinra for severe forms of COVID-19: A cohort study. *Lancet Rheumatol* 2 (7), e393–e400. doi: 10.1016/s2665-9913(20)30164-8

Husain, A., and Byrareddy, S. N. (2020). Rapamycin as a potential repurpose drug candidate for the treatment of COVID-19. *Chem. Biol. Interact.* 331, 109282. doi: 10.1016/j.cbi.2020.109282

Idrissi, M. E., Hachem, H., Koering, C., Merle, P., Thénoz, M., Mortreux, F., et al. (2016). HBx triggers either cellular senescence or cell proliferation depending on cellular phenotype. *J. Viral Hepat* 23 (2), 130–138. doi: 10.1111/jvh.12450

Ivanov, A., Pawlikowski, J., Manoharan, I., van Tuyn, J., Nelson, D. M., Rai, T. S., et al. (2013). Lysosome-mediated processing of chromatin in senescence. *J. Cell Biol.* 202 (1), 129–143. doi: 10.1083/jcb.201212110

Jun, J. I., and Lau, L. F. (2010). The matricellular protein CCN1 induces fibroblast senescence and restricts fibrosis in cutaneous wound healing. *Nat. Cell Biol.* 12 (7), 676–685. doi: 10.1038/ncb2070

Justice, J. N., Nambiar, A. M., Tchkonia, T., LeBrasseur, N. K., Pascual, R., Hashmi, S. K., et al. (2019). Senolytics in idiopathic pulmonary fibrosis: Results from a first-in-human, open-label, pilot study. *EBioMedicine* 40, 554–563. doi: 10.1016/j.ebiom.2018.12.052

Kang, T. W., Yevsa, T., Woller, N., Hoenicke, L., Wuestefeld, T., Dauch, D., et al. (2011). Senescence surveillance of pre-malignant hepatocytes limits liver cancer development. *Nature* 479 (7374), 547–551. doi: 10.1038/nature10599

Kang, Y., Zhang, H., Zhao, Y., Wang, Y., Wang, W., He, Y., et al. (2018). Telomere dysfunction disturbs macrophage mitochondrial metabolism and the NLRP3 inflammasome through the PGC-1α/TNFAIP3 axis. *Cell Rep.* 22 (13), 3493–3506. doi: 10.1016/j.celrep.2018.02.071

Kawai, T., and Akira, S. (2008). Toll-like receptor and RIG-i-like receptor signaling. *Ann. N Y Acad. Sci.* 1143, 1–20. doi: 10.1196/annals.1443.020

Kelley, W. J., Zemans, R. L., and Goldstein, D. R. (2020). Cellular senescence: Friend or foe to respiratory viral infections? *Eur. Respir. J.* 56 (6). doi: 10.1183/13993003.02708-2020

Khan, N., Shariff, N., Cobbold, M., Bruton, R., Ainsworth, J. A., Sinclair, A. J., et al. (2002). Cytomegalovirus seropositivity drives the CD8 T cell repertoire toward greater clonality in healthy elderly individuals. *J. Immunol.* 169 (4), 1984–1992. doi: 10.4049/jimmunol.169.4.1984

Kim, J. A., Seong, R. K., and Shin, O. S. (2016). Enhanced viral replication by cellular replicative senescence. *Immune Netw.* 16 (5), 286–295. doi: 10.4110/in.2016.16.5.286

Kindrachuk, J., Ork, B., Hart, B. J., Mazur, S., Holbrook, M. R., Frieman, M. B., et al. (2015). Antiviral potential of ERK/MAPK and PI3K/AKT/mTOR signaling modulation for middle East respiratory syndrome coronavirus infection as identified by temporal kinome analysis. *Antimicrob. Agents Chemother.* 59 (2), 1088–1099. doi: 10.1128/aac.03659-14

Koch, S., Larbi, A., Ozcelik, D., Solana, R., Gouttefangeas, C., Attig, S., et al. (2007). Cytomegalovirus infection: A driving force in human T cell immunosenescence. *Ann. N Y Acad. Sci.* 1114, 23–35. doi: 10.1196/annals.1396.043

Koopal, S., Furuhjelm, J. H., Järviluoma, A., Jäämaa, S., Pyakurel, P., Pussinen, C., et al. (2007). Viral oncogene-induced DNA damage response is activated in kaposi sarcoma tumorigenesis. *PloS Pathog.* 3 (9), 1348–1360. doi: 10.1371/journal.ppat.0030140

Korolchuk, V. I., Miwa, S., Carroll, B., and von Zglinicki, T. (2017). Mitochondria in cell senescence: Is mitophagy the weakest link? *EBioMedicine* 21, 7–13. doi: 10.1016/j.ebiom.2017.03.020

Krizhanovsky, V., Yon, M., Dickins, R. A., Hearn, S., Simon, J., Miething, C., et al. (2008). Senescence of activated stellate cells limits liver fibrosis. *Cell* 134 (4), 657–667. doi: 10.1016/j.cell.2008.06.049

Kulkarni, A. S., Gubbi, S., and Barzilai, N. (2020). Benefits of metformin in attenuating the hallmarks of aging. *Cell Metab.* 32 (1), 15–30. doi: 10.1016/j.cmet.2020.04.001

Kulkarni, U., Zemans, R. L., Smith, C. A., Wood, S. C., Deng, J. C., and Goldstein, D. R. (2019). Excessive neutrophil levels in the lung underlie the age-associated increase in influenza mortality. *Mucosal Immunol.* 12 (2), 545–554. doi: 10.1038/s41385-018-0115-3

Kuller, L. H., Tracy, R., Belloso, W., De Wit, S., Drummond, F., Lane, H. C., et al. (2008). Inflammatory and coagulation biomarkers and mortality in patients with HIV infection. *PloS Med.* 5 (10), e203. doi: 10.1371/journal.pmed.0050203

Kurz, D. J., Decary, S., Hong, Y., and Erusalimsky, J. D. (2000). Senescence-associated (beta)-galactosidase reflects an increase in lysosomal mass during replicative ageing of human endothelial cells. *J. Cell Sci.* 113 (Pt 20), 3613–3622. doi: 10.1242/jcs.113.20.3613

Laberge, R. M., Sun, Y., Orjalo, A. V., Patil, C. K., Freund, A., Zhou, L., et al. (2015). MTOR regulates the pro-tumorigenic senescence-associated secretory phenotype by promoting IL1A translation. *Nat. Cell Biol.* 17 (8), 1049–1061. doi: 10.1038/ncb3195

Lahaye, X., Gentili, M., Silvin, A., Conrad, C., Picard, L., Jouve, M., et al. (2018). NONO detects the nuclear HIV capsid to promote cGAS-mediated innate immune activation. *Cell* 175 (2), 488–501.e422. doi: 10.1016/j.cell.2018.08.062

Lara, P. C., Macías-Verde, D., and Burgos-Burgos, J. (2020). Age-induced NLRP3 inflammasome over-activation increases lethality of SARS-CoV-2 pneumonia in elderly patients. *Aging Dis.* 11 (4), 756–762. doi: 10.14336/ad.2020.0601

Lee, B. Y., Han, J. A., Im, J. S., Morrone, A., Johung, K., Goodwin, E. C., et al. (2006). Senescence-associated beta-galactosidase is lysosomal beta-galactosidase. *Aging Cell* 5 (2), 187–195. doi: 10.1111/j.1474-9726.2006.00199.x

Lee, S., Yu, Y., Trimpert, J., Benthani, F., Mairhofer, M., Richter-Pechanska, P., et al. (2021). Virus-induced senescence is a driver and therapeutic target in COVID-19. *Nature* 599 (7884), 283–289. doi: 10.1038/s41586-021-03995-1

Lehmann, M., Korfei, M., Mutze, K., Klee, S., Skronska-Wasek, W., Alsafadi, H. N., et al. (2017). Senolytic drugs target alveolar epithelial cell function and attenuate experimental lung fibrosis ex vivo. *Eur. Respir. J.* 50 (2). doi: 10.1183/13993003.02367-2016

Leidal, A. M., Cyr, D. P., Hill, R. J., Lee, P. W., and McCormick, C. (2012). Subversion of autophagy by kaposi's sarcoma-associated herpesvirus impairs oncogene-induced senescence. *Cell Host Microbe* 11 (2), 167–180. doi: 10.1016/j.chom.2012.01.005

Leng, S. X., and Margolick, J. B. (2020). Aging, sex, inflammation, frailty, and CMV and HIV infections. *Cell Immunol.* 348, 104024. doi: 10.1016/j.cellimm.2019.104024

Li, J., Wei, Q., Li, W. X., McCowen, K. C., Xiong, W., Liu, J., et al. (2020). Metformin use in diabetes prior to hospitalization: Effects on mortality in covid-19. *Endocr. Pract.* 26 (10), 1166–1172. doi: 10.4158/ep-2020-0466

Lian, H., Wei, J., Zang, R., Ye, W., Yang, Q., Zhang, X. N., et al. (2018). ZCCHC3 is a co-sensor of cGAS for dsDNA recognition in innate immune response. *Nat. Commun.* 9 (1), 3349. doi: 10.1038/s41467-018-05559-w

Liu, Z. S., Cai, H., Xue, W., Wang, M., Xia, T., Li, W. J., et al. (2019). G3BP1 promotes DNA binding and activation of cGAS. *Nat. Immunol.* 20 (1), 18–28. doi: 10.1038/s41590-018-0262-4

Liu, J., Qian, C., and Cao, X. (2016). Post-translational modification control of innate immunity. *Immunity* 45 (1), 15–30. doi: 10.1016/j.immuni.2016.06.020

Loo, J., Spittle, D. A., and Newnham, M. (2021). COVID-19, immunothrombosis and venous thromboembolism: biological mechanisms. *Thorax* 76 (4), 412–420. doi: 10.1136/thoraxjnl-2020-216243

López-Otín, C., Blasco, M. A., Partridge, L., Serrano, M., and Kroemer, G. (2013). The hallmarks of aging. *Cell* 153 (6), 1194–1217. doi: 10.1016/j.cell.2013.05.039

Luo, P., Qiu, L., Liu, Y., Liu, X. L., Zheng, J. L., Xue, H. Y., et al. (2020). Metformin treatment was associated with decreased mortality in COVID-19 patients with diabetes in a retrospective analysis. *Am. J. Trop. Med. Hyg* 103 (1), 69–72. doi: 10.4269/ajtmh.20-0375

Lv, N., Zhao, Y., Liu, X., Ye, L., Liang, Z., Kang, Y., et al. (2022). Dysfunctional telomeres through mitostress-induced cGAS/STING activation to aggravate immune senescence and viral pneumonia. *Aging Cell* 21 (4), e13594. doi: 10.1111/acel.13594

Lynch, S. M., Guo, G., Gibson, D. S., Bjourson, A. J., and Rai, T. S. (2021). Role of senescence and aging in SARS-CoV-2 infection and COVID-19 disease. *Cells* 10 (12). doi: 10.3390/cells10123367

Majumder, S., Caccamo, A., Medina, D. X., Benavides, A. D., Javors, M. A., Kraig, E., et al. (2012). Lifelong rapamycin administration ameliorates age-dependent cognitive deficits by reducing IL-1β and enhancing NMDA signaling. *Aging Cell* 11 (2), 326–335. doi: 10.1111/j.1474-9726.2011.00791.x

Mannick, J. B., Del Giudice, G., Lattanzi, M., Valiante, N. M., Praestgaard, J., Huang, B., et al. (2014). mTOR inhibition improves immune function in the elderly. *Sci. Transl. Med.* 6 (268), 268ra179. doi: 10.1126/scitranslmed.3009892

Mao, L., Jin, H., Wang, M., Hu, Y., Chen, S., He, Q., et al. (2020). Neurologic manifestations of hospitalized patients with coronavirus disease 2019 in wuhan, China. *JAMA Neurol.* 77 (6), 683–690. doi: 10.1001/jamaneurol.2020.1127

Marcucci, F., Romeo, E., Caserta, C. A., Rumio, C., and Lefoulon, F. (2020). Context-dependent pharmacological effects of metformin on the immune system. *Trends Pharmacol. Sci.* 41 (3), 162–171. doi: 10.1016/j.tips.2020.01.003

Markowicz-Piasecka, M., Sikora, J., Szydłowska, A., Skupień, A., Mikiciuk-Olasik, E., and Huttunen, K. M. (2017). Metformin - a future therapy for neurodegenerative diseases : Theme: Drug discovery, development and delivery in alzheimer's disease guest Editor: Davide brambilla. *Pharm. Res.* 34 (12), 2614–2627. doi: 10.1007/s11095-017-2199-y

Martínez, I., García-Carpizo, V., Guijarro, T., García-Gomez, A., Navarro, D., Aranda, A., et al. (2016). Induction of DNA double-strand breaks and cellular senescence by human respiratory syncytial virus. *Virulence* 7 (4), 427–442. doi: 10.1080/21505594.2016.1144001

Martin-Montalvo, A., Mercken, E. M., Mitchell, S. J., Palacios, H. H., Mote, P. L., Scheibye-Knudsen, M., et al. (2013). Metformin improves healthspan and lifespan in mice. *Nat. Commun.* 4, 2192. doi: 10.1038/ncomms3192

Massanella, M., Gómez-Mora, E., Carrillo, J., Curriu, M., Ouchi, D., Puig, J., et al. (2015). Increased ex vivo cell death of central memory CD4 T cells in treated HIV infected individuals with unsatisfactory immune recovery. *J. Transl. Med.* 13, 230. doi: 10.1186/s12967-015-0601-2

Mills, E. L., Kelly, B., and O'Neill, L. A. J. (2017). Mitochondria are the powerhouses of immunity. *Nat. Immunol.* 18 (5), 488–498. doi: 10.1038/ni.3704

Moiseeva, O., Deschênes-Simard, X., St-Germain, E., Igelmann, S., Huot, G., Cadar, A. E., et al. (2013). Metformin inhibits the senescence-associated secretory phenotype by interfering with IKK/NF-κB activation. *Aging Cell* 12 (3), 489–498. doi: 10.1111/acel.12075

Muñoz-Espín, D., and Serrano, M. (2014). Cellular senescence: from physiology to pathology. *Nat. Rev. Mol. Cell Biol.* 15 (7), 482–496. doi: 10.1038/nrm3823

Napoli, C., Tritto, I., Benincasa, G., Mansueto, G., and Ambrosio, G. (2020). Cardiovascular involvement during COVID-19 and clinical implications in elderly patients. a review. *Ann. Med. Surg. (Lond)* 57, 236–243. doi: 10.1016/j.amsu.2020.07.054

Naranbhai, V., Altfeld, M., Karim, S. S., Ndung'u, T., Karim, Q. A., and Carr, W. H. (2013). Changes in natural killer cell activation and function during primary HIV-1 infection. *PloS One* 8 (1), e53251. doi: 10.1371/journal.pone.0053251

Narita, M., Nũnez, S., Heard, E., Narita, M., Lin, A. W., Hearn, S. A., et al. (2003). Rb-Mediated heterochromatin formation and silencing of E2F target genes during cellular senescence. *Cell* 113 (6), 703–716. doi: 10.1016/s0092-8674(03)00401-x

Nassour, J., Radford, R., Correia, A., Fusté, J. M., Schoell, B., Jauch, A., et al. (2019). Autophagic cell death restricts chromosomal instability during replicative crisis. *Nature* 565 (7741), 659–663. doi: 10.1038/s41586-019-0885-0

Nehme, J., Borghesan, M., Mackedenski, S., Bird, T. G., and Demaria, M. (2020). Cellular senescence as a potential mediator of COVID-19 severity in the elderly. *Aging Cell* 19 (10), e13237. doi: 10.1111/acel.13237

Netea, M. G., Domínguez-Andrés, J., Barreiro, L. B., Chavakis, T., Divangahi, M., Fuchs, E., et al. (2020a). Defining trained immunity and its role in health and disease. *Nat. Rev. Immunol.* 20 (6), 375–388. doi: 10.1038/s41577-020-0285-6

Netea, M. G., Giamarellos-Bourboulis, E. J., Domínguez-Andrés, J., Curtis, N., van Crevel, R., van de Veerdonk, F. L., et al. (2020b). Trained immunity: a tool for reducing susceptibility to and the severity of SARS-CoV-2 infection. *Cell* 181 (5), 969–977. doi: 10.1016/j.cell.2020.04.042

Noris, E., Zannetti, C., Demurtas, A., Sinclair, J., De Andrea, M., Gariglio, M., et al. (2002). Cell cycle arrest by human cytomegalovirus 86-kDa IE2 protein resembles premature senescence. *J. Virol.* 76 (23), 12135–12148. doi: 10.1128/jvi.76.23.12135-12148.2002

Nunnari, J., and Suomalainen, A. (2012). Mitochondria: In sickness and in health. *Cell* 148 (6), 1145–1159. doi: 10.1016/j.cell.2012.02.035

Nyunoya, T., Monick, M. M., Klingelhutz, A. L., Glaser, H., Cagley, J. R., Brown, C. O., et al. (2009). Cigarette smoke induces cellular senescence *via* werner's syndrome protein down-regulation. *Am. J. Respir. Crit. Care Med.* 179 (4), 279–287. doi: 10.1164/rccm.200802-320OC

Nyunoya, T., Monick, M. M., Klingelhutz, A., Yarovinsky, T. O., Cagley, J. R., and Hunninghake, G. W. (2006). Cigarette smoke induces cellular senescence. *Am. J. Respir. Cell Mol. Biol.* 35 (6), 681–688. doi: 10.1165/rcmb.2006-0169OC

Obi, A. T., Tignanelli, C. J., Jacobs, B. N., Arya, S., Park, P. K., Wakefield, T. W., et al. (2019). Empirical systemic anticoagulation is associated with decreased venous thromboembolism in critically ill influenza a H1N1 acute respiratory distress syndrome patients. *J. Vasc. Surg. Venous Lymphat Disord.* 7 (3), 317–324. doi: 10.1016/j.jvsv.2018.08.010

Ohno, M., Sasaki, M., Orba, Y., Sekiya, T., Masum, M. A., Ichii, O., et al. (2021). Abnormal blood coagulation and kidney damage in aged hamsters infected with severe acute respiratory syndrome coronavirus 2. *Viruses* 13 (11). doi: 10.3390/v13112137

Oishi, N., Shilagardi, K., Nakamoto, Y., Honda, M., Kaneko, S., and Murakami, S. (2007). Hepatitis b virus X protein overcomes oncogenic RAS-induced senescence in human immortalized cells. *Cancer Sci.* 98 (10), 1540–1548. doi: 10.1111/j.1349-7006.2007.00579.x

Onder, G., Rezza, G., and Brusaferro, S. (2020). Case-fatality rate and characteristics of patients dying in relation to COVID-19 in Italy. *JAMA* 323 (18), 1775–1776. doi: 10.1001/jama.2020.4683

Panagiotou, O. A., Kosar, C. M., White, E. M., Bantis, L. E., Yang, X., Santostefano, C. M., et al. (2021). Risk factors associated with all-cause 30-day mortality in nursing home residents with COVID-19. *JAMA Intern. Med.* 181 (4), 439–448. doi: 10.1001/jamainternmed.2020.7968

Passos, J. F., Saretzki, G., Ahmed, S., Nelson, G., Richter, T., Peters, H., et al. (2007). Mitochondrial dysfunction accounts for the stochastic heterogeneity in telomere-dependent senescence. *PloS Biol.* 5 (5), e110. doi: 10.1371/journal.pbio.0050110

Paul, B. D., Snyder, S. H., and Bohr, V. A. (2021). Signaling by cGAS-STING in neurodegeneration, neuroinflammation, and aging. *Trends Neurosci.* 44 (2), 83–96. doi: 10.1016/j.tins.2020.10.008

Peiró, T., Patel, D. F., Akthar, S., Gregory, L. G., Pyle, C. J., Harker, J. A., et al. (2018). Neutrophils drive alveolar macrophage IL-1β release during respiratory viral infection. *Thorax* 73 (6), 546–556. doi: 10.1136/thoraxjnl-2017-210010

Persson, B. D., Jaffe, A. B., Fearns, R., and Danahay, H. (2014). Respiratory syncytial virus can infect basal cells and alter human airway epithelial differentiation. *PloS One* 9 (7), e102368. doi: 10.1371/journal.pone.0102368

Porfidia, A., Valeriani, E., Pola, R., Porreca, E., Rutjes, A. W. S., and Di Nisio, M. (2020). Venous thromboembolism in patients with COVID-19: Systematic review and meta-analysis. *Thromb. Res.* 196, 67–74. doi: 10.1016/j.thromres.2020.08.020

Propson, N. E., Roy, E. R., Litvinchuk, A., Köhl, J., and Zheng, H. (2021). Endothelial C3a receptor mediates vascular inflammation and blood-brain barrier permeability during aging. *J. Clin. Invest.* 131 (1). doi: 10.1172/jci140966

Roos, C. M., Zhang, B., Palmer, A. K., Ogrodnik, M. B., Pirtskhalava, T., Thalji, N. M., et al. (2016). Chronic senolytic treatment alleviates established vasomotor dysfunction in aged or atherosclerotic mice. *Aging Cell* 15 (5), 973–977. doi: 10.1111/acel.12458

Roschewski, M., Lionakis, M. S., Sharman, J. P., Roswarski, J., Goy, A., Monticelli, M. A., et al. (2020). Inhibition of bruton tyrosine kinase in patients with severe COVID-19. *Sci. Immunol.* 5 (48). doi: 10.1126/sciimmunol.abd0110

Sadaie, M., Salama, R., Carroll, T., Tomimatsu, K., Chandra, T., Young, A. R., et al. (2013). Redistribution of the lamin B1 genomic binding profile affects rearrangement of heterochromatic domains and SAHF formation during senescence. *Genes Dev.* 27 (16), 1800–1808. doi: 10.1101/gad.217281.113

Sagiv, A., Burton, D. G., Moshayev, Z., Vadai, E., Wensveen, F., Ben-Dor, S., et al. (2016). NKG2D ligands mediate immunosurveillance of senescent cells. *Aging (Albany NY)* 8 (2), 328–344. doi: 10.18632/aging.100897

Sanchez-Vazquez, R., Guío-Carrión, A., Zapatero-Gaviria, A., Martínez, P., and Blasco, M. A. (2021). Shorter telomere lengths in patients with severe COVID-19 disease. *Aging (Albany NY)* 13 (1), 1–15. doi: 10.18632/aging.202463

Sandler, N. G., and Douek, D. C. (2012). Microbial translocation in HIV infection: causes, consequences and treatment opportunities. *Nat. Rev. Microbiol.* 10 (9), 655–666. doi: 10.1038/nrmicro2848

Sapir, A., Avinoam, O., Podbilewicz, B., and Chernomordik, L. V. (2008). Viral and developmental cell fusion mechanisms: conservation and divergence. *Dev. Cell* 14 (1), 11–21. doi: 10.1016/j.devcel.2007.12.008

Sauce, D., Larsen, M., Fastenackels, S., Pauchard, M., Ait-Mohand, H., Schneider, L., et al. (2011). HIV Disease progression despite suppression of viral replication is associated with exhaustion of lymphopoiesis. *Blood* 117 (19), 5142–5151. doi: 10.1182/blood-2011-01-331306

Schmitt, C. A., Tchkonia, T., Niedernhofer, L. J., Robbins, P. D., Kirkland, J. L., and Lee, S. (2022). COVID-19 and cellular senescence. *Nat. Rev. Immunol.* 1-13. doi: 10.1038/s41577-022-00785-2

Seidler, S., Zimmermann, H. W., Bartneck, M., Trautwein, C., and Tacke, F. (2010). Age-dependent alterations of monocyte subsets and monocyte-related chemokine pathways in healthy adults. *BMC Immunol.* 11, 30. doi: 10.1186/1471-2172-11-30

Shah, P. P., Donahue, G., Otte, G. L., Capell, B. C., Nelson, D. M., Cao, K., et al. (2013). Lamin B1 depletion in senescent cells triggers large-scale changes in gene expression and the chromatin landscape. *Genes Dev.* 27 (16), 1787–1799. doi: 10.1101/gad.223834.113

Sharma, P., Uppal, N. N., Wanchoo, R., Shah, H. H., Yang, Y., Parikh, R., et al. (2020). COVID-19-Associated kidney injury: A case series of kidney biopsy findings. *J. Am. Soc. Nephrol.* 31 (9), 1948–1958. doi: 10.1681/asn.2020050699

Shay, J. W. (2016). Role of telomeres and telomerase in aging and cancer. *Cancer Discov* 6 (6), 584–593. doi: 10.1158/2159-8290.Cd-16-0062

Shrivastava, G., León-Juárez, M., García-Cordero, J., Meza-Sánchez, D. E., and Cedillo-Barrón, L. (2016). Inflammasomes and its importance in viral infections. *Immunol. Res.* 64 (5-6), 1101–1117. doi: 10.1007/s12026-016-8873-z

Sivasubramanian, M. K., Monteiro, R., Harrison, K. S., Plakkot, B., Subramanian, M., and Jones, C. (2022). Herpes simplex virus type 1 preferentially enhances neuro-inflammation and senescence in brainstem of female mice. *J. Virol.* 96 (17), e0108122. doi: 10.1128/jvi.01081-22

Smits, S. L., de Lang, A., van den Brand, J. M., Leijten, L. M., van, I. W. F., Eijkemans, M. J., et al. (2010). Exacerbated innate host response to SARS-CoV in aged non-human primates. *PloS Pathog.* 6 (2), e1000756. doi: 10.1371/journal.ppat.1000756

Sun, B., Sundström, K. B., Chew, J. J., Bist, P., Gan, E. S., Tan, H. C., et al. (2017). Dengue virus activates cGAS through the release of mitochondrial DNA. *Sci. Rep.* 7 (1), 3594. doi: 10.1038/s41598-017-03932-1

Sviridov, D., Miller, Y. I., and Bukrinsky, M. I. (2022). Trained immunity and HIV infection. *Front. Immunol.* 13. doi: 10.3389/fimmu.2022.903884

Tai, H., Wang, Z., Gong, H., Han, X., Zhou, J., Wang, X., et al. (2017). Autophagy impairment with lysosomal and mitochondrial dysfunction is an important characteristic of oxidative stress-induced senescence. *Autophagy* 13 (1), 99–113. doi: 10.1080/15548627.2016.1247143

Takahashi, A., Loo, T. M., Okada, R., Kamachi, F., Watanabe, Y., Wakita, M., et al. (2018). Downregulation of cytoplasmic DNases is implicated in cytoplasmic DNA accumulation and SASP in senescent cells. *Nat. Commun.* 9 (1), 1249. doi: 10.1038/s41467-018-03555-8

Tchkonia, T., Zhu, Y., van Deursen, J., Campisi, J., and Kirkland, J. L. (2013). Cellular senescence and the senescent secretory phenotype: therapeutic opportunities. *J. Clin. Invest.* 123 (3), 966–972. doi: 10.1172/jci64098

Thangaraj, A., Chivero, E. T., Tripathi, A., Singh, S., Niu, F., Guo, M. L., et al. (2021). HIV TAT-mediated microglial senescence: Role of SIRT3-dependent mitochondrial oxidative stress. *Redox Biol.* 40, 101843. doi: 10.1016/j.redox.2020.101843

The Novel Coronavirus Pneumonia Emergency Response Epidemiology Team (2020). The epidemiological characteristics of an outbreak of 2019 novel coronavirus diseases (COVID-19) - China 2020. *China CDC Wkly* 2 (8), 113–122. doi: 10.46234/ccdcw2020.032

Thompson, W. W., Shay, D. K., Weintraub, E., Brammer, L., Cox, N., Anderson, L. J., et al. (2003). Mortality associated with influenza and respiratory syncytial virus in the united states. *JAMA* 289 (2), 179–186. doi: 10.1001/jama.289.2.179

Tizazu, A. M., Nyunt, M. S. Z., Cexus, O., Suku, K., Mok, E., Xian, C. H., et al. (2019). Metformin monotherapy downregulates diabetes-associated inflammatory status and impacts on mortality. *Front. Physiol.* 10. doi: 10.3389/fphys.2019.00572

Tripathi, U., Nchioua, R., Prata, L., Zhu, Y., Gerdes, E. O. W., Giorgadze, N., et al. (2021). SARS-CoV-2 causes senescence in human cells and exacerbates the senescence-associated secretory phenotype through TLR-3. *Aging (Albany NY)* 13 (18), 21838–21854. doi: 10.18632/aging.203560

Valencia, W. M., Palacio, A., Tamariz, L., and Florez, H. (2017). Metformin and ageing: improving ageing outcomes beyond glycaemic control. *Diabetologia* 60 (9), 1630–1638. doi: 10.1007/s00125-017-4349-5

van Deursen, J. M. (2014). The role of senescent cells in ageing. *Nature* 509 (7501), 439–446. doi: 10.1038/nature13193

Vázquez-Castellanos, J. F., Serrano-Villar, S., Latorre, A., Artacho, A., Ferrús, M. L., Madrid, N., et al. (2015). Altered metabolism of gut microbiota contributes to chronic immune activation in HIV-infected individuals. *Mucosal Immunol.* 8 (4), 760–772. doi: 10.1038/mi.2014.107

Wandeler, G., Johnson, L. F., and Egger, M. (2016). Trends in life expectancy of HIV-positive adults on antiretroviral therapy across the globe: comparisons with general population. *Curr. Opin. HIV AIDS* 11 (5), 492–500. doi: 10.1097/coh.0000000000000298

Wang, C. H., Chung, F. T., Lin, S. M., Huang, S. Y., Chou, C. L., Lee, K. Y., et al. (2014). Adjuvant treatment with a mammalian target of rapamycin inhibitor, sirolimus, and steroids improves outcomes in patients with severe H1N1 pneumonia and acute respiratory failure. *Crit. Care Med.* 42 (2), 313–321. doi: 10.1097/CCM.0b013e3182a2727d

Wang, L., He, W., Yu, X., Hu, D., Bao, M., Liu, H., et al. (2020a). Coronavirus disease 2019 in elderly patients: Characteristics and prognostic factors based on 4-week follow-up. *J. Infect.* 80 (6), 639–645. doi: 10.1016/j.jinf.2020.03.019

Wang, W., Hu, D., Wu, C., Feng, Y., Li, A., Liu, W., et al. (2020b). STING promotes NLRP3 localization in ER and facilitates NLRP3 deubiquitination to activate the inflammasome upon HSV-1 infection. *PloS Pathog.* 16 (3), e1008335. doi: 10.1371/journal.ppat.1008335

West, A. P., Khoury-Hanold, W., Staron, M., Tal, M. C., Pineda, C. M., Lang, S. M., et al. (2015). Mitochondrial DNA stress primes the antiviral innate immune response. *Nature* 520 (7548), 553–557. doi: 10.1038/nature14156

Wheaton, K., Campuzano, D., Ma, W., Sheinis, M., Ho, B., Brown, G. W., et al. (2017). Progerin-induced replication stress facilitates premature senescence in Hutchinson-gilford progeria syndrome. *Mol. Cell Biol.* 37 (14). doi: 10.1128/mcb.00659-16

Wiley, C. D., Liu, S., Limbad, C., Zawadzka, A. M., Beck, J., Demaria, M., et al. (2019). SILAC analysis reveals increased secretion of hemostasis-related factors by senescent cells. *Cell Rep.* 28 (13), 3329–3337.e3325. doi: 10.1016/j.celrep.2019.08.049

Wilkins, C., and Gale, M.Jr (2010). Recognition of viruses by cytoplasmic sensors. *Curr. Opin. Immunol.* 22 (1), 41–47. doi: 10.1016/j.coi.2009.12.003

Wilkinson, J. E., Burmeister, L., Brooks, S. V., Chan, C. C., Friedline, S., Harrison, D. E., et al. (2012). Rapamycin slows aging in mice. *Aging Cell* 11 (4), 675–682. doi: 10.1111/j.1474-9726.2012.00832.x

Xian, H., Liu, Y., Rundberg Nilsson, A., Gatchalian, R., Crother, T. R., Tourtellotte, W. G., et al. (2021). Metformin inhibition of mitochondrial ATP and DNA synthesis abrogates NLRP3 inflammasome activation and pulmonary inflammation. *Immunity* 54 (7), 1463–1477.e1411. doi: 10.1016/j.immuni.2021.05.004

Xu, M., Pirtskhalava, T., Farr, J. N., Weigand, B. M., Palmer, A. K., Weivoda, M. M., et al. (2018). Senolytics improve physical function and increase lifespan in old age. *Nat. Med.* 24 (8), 1246–1256. doi: 10.1038/s41591-018-0092-9

Xu, W., Wong, G., Hwang, Y. Y., and Larbi, A. (2020). The untwining of immunosenescence and aging. *Semin. Immunopathol.* 42 (5), 559–572. doi: 10.1007/s00281-020-00824-x

Xue, W., Zender, L., Miething, C., Dickins, R. A., Hernando, E., Krizhanovsky, V., et al. (2007). Senescence and tumour clearance is triggered by p53 restoration in murine liver carcinomas. *Nature* 445 (7128), 656–660. doi: 10.1038/nature05529

Yamazaki, Y., Baker, D. J., Tachibana, M., Liu, C. C., van Deursen, J. M., Brott, T. G., et al. (2016). Vascular cell senescence contributes to blood-brain barrier breakdown. *Stroke* 47 (4), 1068–1077. doi: 10.1161/strokeaha.115.010835

Yan, Y., Du, Y., Zheng, H., Wang, G., Li, R., Chen, J., et al. (2017). NS1 of H7N9 influenza a virus induces NO-mediated cellular senescence in Neuro2a cells. *Cell Physiol. Biochem.* 43 (4), 1369–1380. doi: 10.1159/000481848

Yang, B., Dan, X., Hou, Y., Lee, J. H., Wechter, N., Krishnamurthy, S., et al. (2021). NAD(+) supplementation prevents STING-induced senescence in ataxia telangiectasia by improving mitophagy. *Aging Cell* 20 (4), e13329. doi: 10.1111/acel.13329

Yang, X., He, Z., Xin, B., and Cao, L. (2000). LMP1 of Epstein-Barr virus suppresses cellular senescence associated with the inhibition of p16INK4a expression. *Oncogene* 19 (16), 2002–2013. doi: 10.1038/sj.onc.1203515

Yoh, S. M., Schneider, M., Seifried, J., Soonthornvacharin, S., Akleh, R. E., Olivieri, K. C., et al. (2015). PQBP1 is a proximal sensor of the cGAS-dependent innate response to HIV-1. *Cell* 161 (6), 1293–1305. doi: 10.1016/j.cell.2015.04.050

Yosef, R., Pilpel, N., Tokarsky-Amiel, R., Biran, A., Ovadya, Y., Cohen, S., et al. (2016). Directed elimination of senescent cells by inhibition of BCL-W and BCL-XL. *Nat. Commun.* 7, 11190. doi: 10.1038/ncomms11190

Yoshimoto, S., Loo, T. M., Atarashi, K., Kanda, H., Sato, S., Oyadomari, S., et al. (2013). Obesity-induced gut microbial metabolite promotes liver cancer through senescence secretome. *Nature* 499 (7456), 97–101. doi: 10.1038/nature12347

You, M., Chen, L., Zhang, D., Zhao, P., Chen, Z., Qin, E. Q., et al. (2021). Single-cell epigenomic landscape of peripheral immune cells reveals establishment of trained immunity in individuals convalescing from COVID-19. *Nat. Cell Biol.* 23 (6), 620–630. doi: 10.1038/s41556-021-00690-1

Yu, Q., Katlinskaya, Y. V., Carbone, C. J., Zhao, B., Katlinski, K. V., Zheng, H., et al. (2015). DNA-Damage-induced type I interferon promotes senescence and inhibits stem cell function. *Cell Rep.* 11 (5), 785–797. doi: 10.1016/j.celrep.2015.03.069

Zhi, H., Zahoor, M. A., Shudofsky, A. M., and Giam, C. Z. (2015). KSHV vCyclin counters the senescence/G1 arrest response triggered by NF-κB hyperactivation. *Oncogene* 34 (4), 496–505. doi: 10.1038/onc.2013.567

Zhou, F., Yu, T., Du, R., Fan, G., Liu, Y., Liu, Z., et al. (2020). Clinical course and risk factors for mortality of adult inpatients with COVID-19 in wuhan, China: a retrospective cohort study. *Lancet* 395 (10229), 1054–1062. doi: 10.1016/s0140-6736(20)30566-3

Frontiers in
Cellular and Infection Microbiology

Investigates how microorganisms interact with their hosts

Explores bacteria, fungi, parasites, viruses, endosymbionts, prions and all microbial pathogens as well as the microbiota and its effect on health and disease in various hosts.

Discover the latest Research Topics

See more →

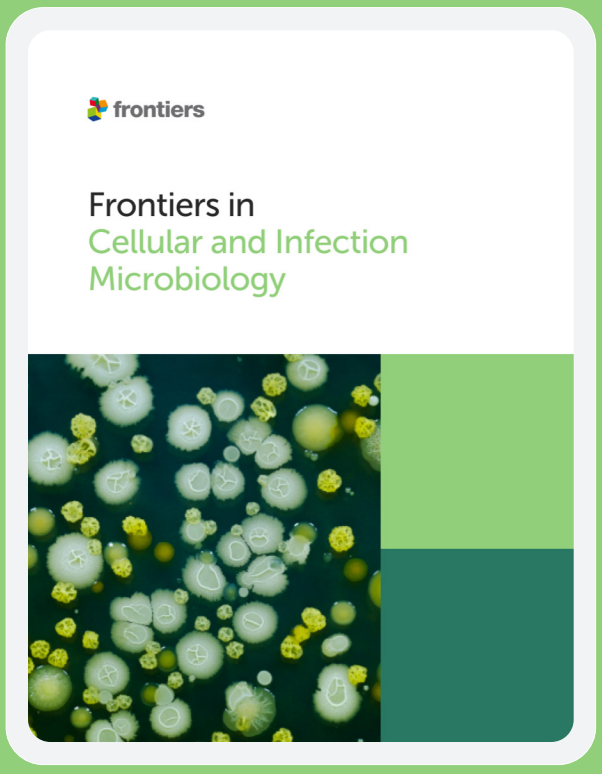

Frontiers

Avenue du Tribunal-Fédéral 34
1005 Lausanne, Switzerland
frontiersin.org

Contact us

+41 (0)21 510 17 00
frontiersin.org/about/contact